Adaptive and Resilient Electricity Grid Management with Smart Buildings

Zur Erlangung des akademischen Grades eines
Doktors der Ingenieurwissenschaften

(Dr.-Ing.)

von der KIT-Fakultät für Wirtschaftswissenschaften
des Karlsruher Instituts für Technologie (KIT)

genehmigte

DISSERTATION

von

Mischa Ahrens, M.Sc.

Tag der mündlichen Prüfung:	16. März 2026
Referent:	Prof. Dr. Hartmut Schmeck
Korreferent:	Prof. Dr.-Ing. Sven Tomforde

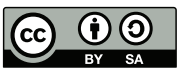

Abstract

The transition from large power plants to decentralized and mostly renewable energy generation as well as the electrification of the transportation and heating sectors entail new challenges for electricity distribution grids. Issues such as the overloading of grid lines and transformers as well as voltage range deviations can become more common, as existing grids were designed for smaller, unidirectional, and less synchronous loads.

One way to reduce the burden on distribution grids is to utilize the energy flexibility of modern residential buildings. In the context of buildings, energy flexibility is the possibility of changing the profile of energy consumption and generation by adjusting the settings and run times of controllable or programmable devices. Building energy management systems and distribution grids enhanced with information and communication technology (ICT), called *smart grids*, can make the flexibility of a building usable for grid support. While smart grids provide comprehensive and detailed monitoring and control options, they also make electricity grids subject to ICT disturbances, such as communication disruptions or cyberattacks. The existing literature with regard to ICT disturbances in smart grids only addresses specific issues. It lacks comprehensive approaches for achieving resilient distribution grid operation in the presence of diverse ICT disturbances.

The main contribution of this thesis is the development and evaluation of an *adaptive grid management system*. This system provides resilience with regard to both electrical as well as ICT disturbances by leveraging the energy flexibility and intelligence of smart residential buildings. We implement it by extending the building energy management system *Organic Smart Home*, which is based on the *Observer/Controller* architecture stemming from the research initiative *Organic Computing*. This allows for the self-organization of the system participants. To build and evaluate the system, we develop a resilience definition and resilience quantification metrics for smart electricity distribution grids as well as appropriate countermeasures to a range of electrical and ICT disturbances. Newly developed voltage maintenance, adaptive photovoltaic system curtailment, and active power flexibility use algorithms provide resilience against voltage-, transformer-, and grid-line-related disturbances. To achieve resilience against ICT disturbances, the system participants switch between newly developed centralized, distributed, and decentralized grid management strategies in a self-organized manner to mitigate the effects of communication disruption, participant misconduct (system-internal or due to cyberattacks), and sensor failure.

After comprehensive parameter studies, we conduct a comparative evaluation of the developed grid management measures and strategies as well as individual studies evaluating the performance of the system with regard to mitigating communication disruption and

participant misconduct. Our evaluation results show that the developed grid management system and each individual grid management strategy fully prevents electricity outages and equipment damage even in extreme scenarios if undisturbed ICT infrastructure is assumed. The employed grid management measures are effective in limiting the need for load curtailment. By switching between the three strategies, the grid management system is able to uphold grid operation in almost all evaluated communication disruption and participant misconduct scenarios. However, misconduct by multiple buildings at once can only be compensated by the remaining buildings up to a certain point.

In conclusion, the presented and evaluated adaptive grid management system not only adds to the research area concerned with resilient smart grids, but also contributes to the research fields Organic Computing and *Energy Informatics*.

Zusammenfassung

Die Energiewende von großen Kraftwerken hin zu dezentralisierter und meist erneuerbarer Energieerzeugung sowie die Elektrifizierung der Verkehrs- und Wärmesektoren stellen Stromverteilnetze vor neue Herausforderungen. Probleme wie die Überlastung von Netzleitungen und Transformatoren sowie Spannungsbandabweichungen können hierdurch häufiger auftreten, da die bestehenden Netze für kleinere Lasten ausgelegt wurden.

Eine Möglichkeit die Belastung von Stromverteilnetzen zu senken ist die Nutzung der energetischen Flexibilität moderner Wohngebäude. Im Gebäudekontext beschreibt energetische Flexibilität die Möglichkeit zur Anpassung des Energieerzeugungs- und -verbrauchsprofils durch die Anpassung von Einstellungen und Laufzeiten steuer- oder programmierbarer Geräte und Anlagen. Gebäudeenergiemanagementsysteme und mit Informations- und Kommunikationstechnologie (IKT) aufgewertete Stromverteilnetze (*Smart Grids*) können diese Flexibilität auch zur Netzunterstützung abrufbar machen. Smart Grids bieten umfangreiche Überwachungs- und Steuerungsmöglichkeiten, machen die Stromnetze allerdings auch anfällig für IKT-Störungen, wie Kommunikationsabbrüche und Cyberangriffe. In der existierenden Literatur fehlen umfassende Ansätze zur Erreichung eines resilienten Stromverteilnetzbetriebs trotz störungsanfälliger IKT-Infrastruktur.

Der wesentliche Beitrag dieser Arbeit ist die Entwicklung und Evaluation eines *adaptiven Stromnetzmanagementsystems*. Durch die Nutzung der energetischen Flexibilität und Intelligenz von Wohngebäuden mit Gebäudeenergiemanagementsystemen schafft dieses System Resilienz sowohl gegenüber elektrischen als auch IKT-Störungen. Das System wird durch Erweiterung des Gebäudeenergiemanagementsystems *Organic Smart Home* implementiert, welches auf der *Observer/Controller*-Architektur aus dem *Organic Computing* basiert und die Selbstorganisation der Systemteilnehmer erlaubt. Um das System erstellen und evaluieren zu können, werden eine Definition der Resilienz von intelligenten Stromverteilnetzen, Metriken zur Quantifizierung dieser Resilienz sowie geeignete Maßnahmen gegen elektrische und IKT-Störungen entwickelt. Neuentwickelte Algorithmen zur Spannungshaltung, adaptiven Photovoltaikabregelung, und Nutzung von Wirkleistungsflexibilität schaffen Resilienz gegen Spannungs-, Transformator-, und Leitungs-basierte Störungen. Um Resilienz gegen IKT-Störungen zu erzielen, werden zentralisierte, verteilte und dezentralisierte Netzmanagementstrategien entwickelt, zwischen denen die Systemteilnehmer selborganisiert wechseln, falls Kommunikationsabbrüche, Teilnehmerfehlverhalten (systemintern oder durch Cyberangriffe) oder Sensorausfälle auftreten.

Nach umfassenden Parameterstudien, werden sowohl eine vergleichende Evaluation der verschiedenen Netzmanagementstrategien und -maßnahmen, als auch individuelle Studien zur Bewertung der Leistung des Systems bei Auftreten von IKT-Störungen durchgeführt.

Die Ergebnisse der Evaluation zeigen, dass das entwickelte Netzmanagementsystem und jede Netzmanagementstrategie für sich Stromausfälle und Schäden an den Netzbetriebsmitteln sogar in extremen Lastszenarien vollständig verhindert, sofern eine ungestörte IKT-Infrastruktur angenommen wird. Die verwendeten Netzmanagementmaßnahmen limitieren die Notwendigkeit zur Lastabregelung zudem effektiv. Durch den Wechsel zwischen den drei Strategien, kann das Netzmanagementsystem den Netzbetrieb in fast allen evaluierten Szenarien zu Kommunikationsabbrüchen und Teilnehmerfehlerverhalten aufrechterhalten. Allerdings kann das Fehlverhalten mehrerer Gebäude nur bis zu einem gewissen Punkt durch die übrigen Gebäude kompensiert werden.

Zusammenfassend erweitern die Entwicklung und Evaluation des vorgestellten adaptiven Netzmanagementsystems nicht nur die Forschung im Kontext resilienter Smart Grids, sondern auch die Forschungsfelder Organic Computing und *Energieinformatik*.

Acknowledgments

I would first like to express my sincere gratitude to my supervisor Prof. Dr. Hartmut Schmeck for giving me the opportunity to pursue this research as well as for his continuous guidance and valuable advice throughout the preparation of this thesis. I am also grateful to my co-supervisor Prof. Dr.-Ing. Sven Tomforde for his interest in my work as well as for his insightful comments and suggestions. I would furthermore like to thank Prof. Dr. Andreas Oberweis and Prof. Dr. Orestis Terzidis for their helpful advice and for serving on the examination committee.

My sincere thanks also go to the students and my former colleagues at the *Institute of Applied Informatics and Formal Description Methods* at the *Karlsruhe Institute of Technology* and at the department *Intelligent Information and Communication in Technical Systems* at the *FZI Research Center for Information Technology* for their constructive feedback, for the fruitful academic exchange, and for the foundational work on which parts of this thesis build.

Finally, I would like to thank my friends, my parents Gabriele and Ulrich, my sister Theresa, and my partner Laura for their constant support and encouragement throughout my studies and academic career.

The author acknowledges support by the state of Baden-Württemberg through bwHPC.

The author gratefully acknowledges the support of the *German Federal Ministry of Education and Research* (BMBF), which partially funded the research presented in this thesis through the project *Ein Organic-Computing-basierter Ansatz zur Sicherstellung und Verbesserung der Resilienz in technischen und IKT-Systemen* (OCTIKT, English: An Organic Computing-based Approach for Ensuring and Improving Resilience in Technical and ICT Systems) under grant number 01IS18064A.

Contents

List of Figures

List of Tables

List of Abbreviations

BDEW Bundesverband der Energie- und Wasserwirtschaft e. V. (English: German Association of Energy and Water Industries).

BEMS Building energy management system.

BESS Battery energy storage system.

BEV Battery electric vehicle.

CAL Communication abstraction layer.

CHP Cogeneration of heat and power.

CLS Controllable local system.

DER Distributed energy resource.

DoS Denial of service.

DSM Demand side management.

DSO Distribution system operator.

EA Evolutionary algorithm.

EAL Entity abstraction layer.

EEG Erneuerbare-Energien-Gesetz (English: German Renewable Energy Sources Act).

EMS Energy management system.

EMT Externer Marktteilnehmer (English: External market participant).

ENTSO-E European Network of Transmission System Operators for Electricity.

EnWG Energiewirtschaftsgesetz (English: German Energy Industry Act).

ESC Energy simulation core.

EU European Union.

EV Electric vehicle.

FDIA False data injection attack.

GAI Generative artificial intelligence.

GCP Grid connection point.

GWA Smart meter gateway administrator.

HAN Home area network.

HEMS Home energy management system.

HP Heat pump.

HVAC High-voltage alternating current.

HVDC High-voltage direct current.

ICT Information and communication technology.

IDE Integrated development environment.

IDS Intrusion detection system.

IECSA Integrated Energy and Communication Systems Architecture.

IoT Internet of Things).

IPP Interdependent problem part.

LLM Large language model.

LMN Local metrological network.

MITM Man in the middle.

O/C Observer/controller.

OC Organic Computing.

OSH Organic Smart Home.

PV Photovoltaic(s).

REMS Regional energy management system.

RTU Remote terminal unit.

SCADA Supervisory control and data aquisition.

SESAM Selbstorganisation und Spontaneität in liberalisierten und harmonisierten Märkten (English: Self-Organization and Spontaneity in Liberalized and Harmonized Markets).

SGAM Smart Grid Architecture Model.

SGIRM Smart grid interoperability reference model.

SMGW Smart meter gateway.

SoC State of charge.

SuOC System under observation and control.

TAF Tariff use case.

TSO Transmission system operator.

VRDT Voltage regulated distribution transformer.

WAN Wide area network.

1. Introduction

This chapter provides an introduction to the topic of this thesis. After detailing our motivation for the development of an adaptive grid management system, we state the considered problem and derive corresponding research questions. Subsequently, we list our assumptions for the development and application of the system and clarify its scope and limitations. Finally, we list the main contributions and findings of this thesis and give an overview of its structure.

Some text passages of this chapter are transferred verbatim from one of our own publications [1]. For a summary of this publication, its relation to this thesis, and its mapping to our research questions, see Section 1.4.

1.1. Motivation

The transition from large power plants to decentralized and mostly renewable energy generation as well as the electrification of the transportation and heating sectors entail new challenges for electricity distribution grids. Issues such as the overloading of grid lines and transformers as well as voltage range deviations can become more common, as existing grids were designed for smaller, unidirectional, and less synchronous loads [2].

One way to reduce the burden on distribution grids is to utilize the energy flexibility that can be provided by distributed energy resources (DERs) in modern residential buildings, such as intelligent appliances as well as energy generation and storage devices. In the context of buildings, energy flexibility is the possibility of changing the profile of energy consumption and generation by adjusting the settings and run times of controllable or programmable devices. Building or home energy management systems (BEMSs/HEMSs), which are typically utilized to increase the self-consumption of locally generated energy, to reduce energy costs and to partake in demand response, can also make the energy flexibility of a building exploitable for grid support [3].

Information and communication technology (ICT), such as a smart meter infrastructure [4], enables the use of the energy flexibility of residential buildings for grid-supportive purposes. An electricity grid enhanced by such ICT infrastructure is commonly called *smart grid* [5]. While smart grids provide comprehensive and detailed monitoring and control options on the distribution grid level [6, 7], they also make electricity grids subject to ICT disturbances, such as communication disruptions or cyberattacks [8–14].

The existing research with regard to ICT disturbances in smart electricity distribution grids, such as [15–25], only addresses specific issues. None of the publications we became aware of provides comprehensive approaches for achieving resilient distribution grid operation in the presence of diverse ICT disturbances.

To address both the aforementioned grid operation challenges resulting from the energy transition as well as the challenges introduced by the use of ICT infrastructure on the distribution grid level, we develop and evaluate an adaptive grid management system. This system leverages the energy flexibility and intelligence of smart residential buildings to provide comprehensive countermeasures to diverse electrical and ICT disturbances and prioritizes less invasive over more invasive measures to minimize the necessity of curtailing loads in critical situations.

1.2. Problem Statement and Research Questions

The adaptive grid management system developed in this thesis addresses the following challenges.

Challenge 1 The increasing amount of decentralized electricity generation, the increased electricity consumption of residential buildings due to the home charging of battery electric vehicles (BEVs), and the electrification of the heating sector introduce problems with regard to the operation of electricity distribution grids. The increased generation and consumption of electricity in distribution grids that were not designed with these new loads in mind can lead to deviations from the admissible voltage range as well as the overloading of lines and transformers. As a consequence, solutions are needed that increase the resilience of distribution grids against these types of problems. Smart buildings with BEMSs can potentially mitigate these problems by providing energy flexibility in situations that require a decrease in load to ensure resilient grid operation [26].

Challenge 2 Most approaches to solving or preventing congestion in electricity distribution grids presuppose a central observation and control unit as well as functioning communication infrastructure that enable the respective control systems to operate correctly. This not only introduces a single point of failure but also a secondary infrastructure that may itself be susceptible to technical failures. A failure of the central observation and control unit or the disruption of communication infrastructure could potentially prevent control systems from ensuring reliable grid operation (see also Section 2.7.4). Consequently, systems that are designed to increase the resilience of distribution grids have to handle communication disruption as well.

Challenge 3 If a grid management strategy uses sensor data to determine the grid status and appropriate measures against electrical disturbances, the electrical resilience of the grid can be compromised if one or more sensors fail. Therefore, systems implemented to address Challenges 1 and 2 have to be able to adapt to sensor failure as well (see also Sections 2.7.4 and 3).

Challenge 4 Communication disruption, incorrect or missing sensor data, and erroneous control actions may not only be caused by failures of technical components. Participant misconduct can introduce such problems as well. Participant misconduct can either be system-internal and willingly performed by participants of the grid management system, that is, buildings inhabitants/owners or distribution system operator (DSO) personnel, or induced by outsiders through cyberattacks (see also Sections 2.7.4 and 3). As a consequence, participant misconduct should be considered as well when designing systems to increase distribution grid resilience.

Challenge 5 Approaches addressing Challenge 1 that do not presuppose functioning communication infrastructure, often utilize fixed, "one size fits all" requirements. An example would be limiting the feed-in of electricity to 70 % of the peak power a local PV system can generate [27, 28]. On the one hand, this can lead to preventable losses due to the curtailment of PV generation in scenarios where this is not necessary. On the other hand, the fixed requirements may not be sufficient to ensure resilient grid operation in other scenarios. To enable appropriate measures in all conceivable scenarios, the implemented systems have to be able to adapt to the current grid status.

The following research questions arise from the presented challenges.

Research Question 1 Can the use of energy flexibility provided by smart buildings improve the resilience of distribution grids?

This research question encompasses multiple issues that have to be addressed. It is therefore split into the following sub-questions.

Sub-Question 1.1 How can resilience be defined in the context of smart electricity distribution grids?

To evaluate the influence of the grid-supportive use of the energy flexibility of smart buildings on distribution grids, resilience in the context of such grids has to be defined. Such a definition has to cover different aspects. It is not only important to consider resilience with regard to electrical disturbances but also with regard to disturbances of the ICT infrastructure used to facilitate the measures aimed at improving the electrical resilience. Another aspect of the resilience of a distribution grid is the invasiveness of

the deployed countermeasures to electrical disturbances, such as the curtailment of PV-generated electricity. To give a drastic example - if the active power feed-in of all PV systems in a given grid is curtailed to 0 W at all times, no PV-induced disturbances would occur. This would however defeat the purpose of making distribution grids more resilient in the context of increasing decentralized electricity generation.

Sub-Question 1.2 How can the resilience of a smart electricity distribution grid be quantified?

The evaluation of the effects of a certain management strategy on the resilience of a distribution grid requires this resilience to be quantified. Since the resilience of distribution grids touches multiple aspects, as discussed in the context of Sub-Question 1.1, multiple quantitative metrics are needed as well. Metrics are needed to quantify the improvement of grid operation with respect to electrical disturbances as well as the invasiveness of the deployed countermeasures to electrical disturbances.

Sub-Question 1.3 Which evaluation scenarios are representative of realistic situations that require an increase in distribution grid resilience?

To measure the impact of a management strategy on the resilience of a distribution grid, scenarios have to be chosen, in which an increase in resilience is required. Such scenarios should represent realistic situations as well, so that the results of simulation studies are applicable to real-world situations.

Sub-Question 1.4 To what extent can electrical disturbances be mitigated by smart buildings in the chosen evaluation scenarios, assuming undisturbed ICT infrastructure?

This sub-question only considers resilience with regard to electrical disturbances. Resilience with regard to communication disruption, participant misconduct, and sensor failure as well as the invasiveness of the deployed countermeasures to electrical disturbances are considered separately in the following (sub-)questions. To answer this sub-question, the resilience quantification metrics developed to answer Sub-Question 1.2 and the scenarios established to answer Sub-Question 1.3 can be used to perform simulation studies evaluating the ability of smart buildings to mitigate electrical disturbances.

Sub-Question 1.5 To what extent can the necessity of load curtailment be reduced in the chosen evaluation scenarios by utilizing adaptive and less invasive measures for achieving grid-supportive operation of smart buildings, assuming undisturbed ICT infrastructure?

This sub-question addresses the aspect of the invasiveness of the utilized countermeasures to electrical disturbances mentioned in the context of Sub-Question 1.1. The main aim of this thesis is to facilitate better integration of decentralized energy generation, electric mobility, and electric heating into distribution grids by preventing problems caused by these developments. Better integration also means that these problems should preferably

not be addressed by substantially curtailing the amount of energy that can be generated or consumed. The resilience quantification metrics developed to answer Sub-Question 1.2 also cover the invasiveness of the deployed countermeasures to electrical disturbances. Consequently, the simulation studies performed to answer Sub-Question 1.4 can be evaluated with regard to this aspect as well.

Research Question 2 How do distributed or decentralized grid management strategies compare to a centralized grid management strategy?

As mentioned in the context of Sub-Question 1.1, potential disturbances of the utilized ICT infrastructure have to be considered when managing a distribution grid. If the communication infrastructure or sensors fail or if participant misconduct occurs, electrical disturbances may not be mitigated appropriately. Distributed or decentralized grid management strategies can reduce the dependence on undisturbed ICT infrastructure and may provide further benefits such as better scalability and the avoidance of a single point of failure. However, there may be advantages and disadvantages to each strategy.

Sub-Question 2.1 How do the different strategies compare with regard to mitigating electrical disturbances in the chosen evaluation scenarios, assuming undisturbed ICT infrastructure?

To answer this sub-question, the resilience quantification metrics developed to answer Sub-Question 1.2 and the scenarios established to answer Sub-Question 1.3 can be used to perform comparative simulation studies.

Sub-Question 2.2 How do the different strategies compare with regard to the invasiveness of the deployed countermeasures to electrical disturbances, assuming undisturbed ICT infrastructure?

The resilience quantification metrics developed to answer Sub-Question 1.2 also cover the invasiveness of the deployed countermeasures to electrical disturbances. Consequently, the comparative simulation studies performed to answer Sub-Question 2.1 can be evaluated with regard to this aspect as well.

Sub-Question 2.3 Are there additional advantages or disadvantages to each strategy?

Evaluating the different strategies only with regard to Sub-Questions 2.1 and 2.2 may be misleading. Therefore, other aspects that can potentially influence the applicability of each strategy have to be considered as well.

Research Question 3 Can grid operation be upheld during communication disruption, sensor failure, or participant misconduct?

The centralized, distributed and decentralized grid management strategies evaluated to answer Research Question 2 can be combined to form an adaptive grid management system. This system adapts its management strategy when communication disruption, sensor failure, or participant misconduct occurs. To develop and evaluate such a system, the following sub-questions have to be answered.

Sub-Question 3.1 Which communication disruption, participant misconduct, and sensor failure scenarios should be considered?

There are different conceivable types and magnitudes of communication disruption, participant misconduct, and sensor failure that have to be considered. An example would be that the central observation and control unit of a DSO fails to communicate appropriate commands to mitigate electrical disturbances.

Sub-Question 3.2 How can communication disruption, participant misconduct, and sensor failure be mitigated?

For the grid management system to be able to adapt its management strategy to mitigate communication disruption, participant misconduct, and sensor failure, the smart buildings in the distribution grid have to autonomously react to such events. Otherwise an automatic transition from a centralized to a distributed or decentralized strategy or the mitigation of the misconduct by other participants is not possible. Different types and magnitudes of communication disruption, participant misconduct, and sensor failure require different strategies to be implemented. An appropriate strategy has to be chosen for each communication disruption, participant misconduct, and sensor failure scenario determined in the answer to Sub-Question 3.1.

Sub-Question 3.3 Is the adaptive grid management system able to handle the considered communication disruption, participant misconduct, and sensor failure scenarios?

The communication disruption, participant misconduct, and sensor failure scenarios determined in the answer to Sub-Question 3.1 can be simulated to evaluate the ability of the adaptive grid management system to mitigate the effects of such events.

1.3. Assumptions and Limitations

We make the following assumptions for the development and evaluation of the grid management system presented in this thesis:

- While the system is only evaluated by simulation, we assume that it can be applied in the real world as well, since its basis, the BEMS *Organic Smart Home* (OSH, see also Section 2.4.2) has been successfully used to manage the energy-related devices of real buildings, such as the *KIT Energy Smart Home Lab* [29] and the *FZI House of Living Labs* [30] in Karlsruhe.
- We further assume that the solar irradiance profile is approximately the same for buildings connected to the same transformer and therefore do not utilize qualitatively different PV generation profiles for individual buildings.
- For the system to work correctly, we assume that each building connected to the grid is equipped with a smart meter that can measure voltage, active power, and reactive power at the grid connection point (GCP) of a building with a temporal resolution of at maximum one minute. Furthermore, each building is assumed to be equipped with a BEMS, such as the OSH, but at least with the functionality outlined in [31], that can be extended with the functionality presented in this thesis.
- As in [32], all power-flow studies performed by the DSO and the buildings are conducted using a single-phase representation, assuming an even load distribution across all three phases.
- We assume that the grids managed by the system employ fuses that behave according to the characteristic curves for *Niederspannungs-Hochleistungs* (NH, English: low-voltage-high-performance) fuses given in [325] and are not already excessively worn.
- Since the system requires communication infrastructure to enable the communication between the DSO, the transformer, and the buildings for applying the centralized and distributed grid management strategies, we assume that some type of communication infrastructure is present and usable when the system is deployed. It is important to note that this infrastructure does not have to be fail-safe, because the system is able to adapt to and still function during communication disruption, participant misconduct, and sensor failure.
- Another key assumption is that if the developed system can completely prevent electricity outages and equipment damage in the extreme scenarios chosen for the evaluation, it can also prevent electricity outages and equipment damage in less extreme scenarios.

The following limitations apply to the developed grid management system:

- In its current form, the system can not react to sub-minute fluctuations of the grid status and does not consider problems related to harmonics, an unequal load distribution across the three phases, or the physical destruction of grid equipment.
- The system does not feature predictive maintenance, frequency control, islanded operation, or physical load shedding.
- While certain aspects of the system may be applied to electricity transmission grids as well, its designated area of application is distribution grids.

- While the system is able to mitigate participant misconduct, which can be introduced by internal decisions or external attacks, it does not encompass explicit cybersecurity measures to avoid external attacks in the first place.
- The system currently does not consider bidirectional BEV charging or grid topologies other than radial ones. However, it could be extended in future work to incorporate this functionality without substantial effort.
- While the system is able to mitigate sensor failure and participant misconduct with regard to the communication of false sensor data to a large extent, the mitigation measures could be further enhanced in future work by explicitly detecting false sensor data and replacing the affected measurements with estimated values based on historical and/or predicted data.

1.4. Own Publications Directly Related to this Thesis

During the preparation of this thesis, we published preliminary versions of some of the presented aspects, concepts, and results after peer review. Some text passages contained in this thesis are transferred verbatim from these publications. We indicate in the chapter or section introductions whether the respective chapters or sections contain such transferred text passages. In Table 1.1, we give an overview of our publications directly related to this thesis, explain their concrete relation, and provide a mapping to the research questions posed and answered by this thesis. An overview of all publications by the author of this thesis as of the beginning of 2026 is given in Appendix A.1.

Table 1.1: Overview of the publications by the author directly related to this thesis. The given abstracts are quoted verbatim from the respective publications.

2021 — Mischa Ahrens, Fabian Kern, and Hartmut Schmeck. "Strategies for an Adaptive Control System to Improve Power Grid Resilience with Smart Buildings". In: *Energies* 14.15 (2021). ISSN: 1996-1073. DOI: 10.3390/en14154472. [33]

Abstract

Low-voltage distribution grids face new challenges through the expansion of decentralized, renewable energy generation and the electrification of the heat and mobility sectors. We present a multi-agent system consisting of the energy management systems of smart buildings, a central grid controller, and the local controller of a transformer. It can coordinate the provision of ancillary services for the local grid in a centralized way, coordinated by the central controller, and in a decentralized way, where each building makes independent control decisions based on locally measurable data. The presented system and the different control strategies provide the foundation for a fully adaptive grid control system we plan to implement in the future, which does not only provide resilience against electricity outages but also against communication failures by appropriate switching of strategies. The decentralized strategy, meant to be used during communication failures, could also be used exclusively if communication infrastructure is generally unavailable. The strategies are evaluated in a simulated scenario designed to represent the most extreme load conditions that might occur in low-voltage grids in the future. In the tested scenario, they can substantially reduce voltage range deviations, transformer temperatures, and line congestions.

Relation to this thesis

This publication presents some of the preliminary work for this thesis in that it introduces the centralized and decentralized grid management strategies, early versions of the reactive-power-based voltage maintenance algorithms and active power flexibility use approach, as well as some preliminary evaluation results comparing the two strategies.

Mapping to research questions

Consequently, the publication partially and preliminarily addresses Sub-Questions 1.2, 1.3, and 1.4 of Research Question 1 as well as Sub-Questions 2.1 and 2.3 of Research Question 2.

Continued on next page

Table 1.1: Overview of the publications by the author directly related to this thesis. The given abstracts are quoted verbatim from the respective publications (continued).

2022 — Mischa Ahrens. “Increasing Power Grid Resilience with a Multi-Agent System of Smart Buildings”. In: *Organic Computing - Doctoral Dissertation Colloquium 2021*. Edited by Sven Tomforde and Christian Krupitzer. kassel university press, 2022, pp. 15–31. DOI: 10.17170/kobra-202202215780. [1]

Abstract

The flexibility of buildings with energy generation and storage capacities, intelligent appliances, and energy management systems can be utilized to prevent or reduce critical situations in electricity grids arising from the ongoing adaptation of decentralized energy generation and electric vehicles. This work outlines a multi-agent system that determines and coordinates the responses of multiple buildings to such situations to increase the resilience of the local grid. The utilized methods are designed to be resilient against communication failures as well. The energy management systems used to facilitate the proposed methods are based on the Observer/Controller-architecture. This enables them to work adaptively using centralized, cooperative, or autonomous control schemes depending on the availability of communication infrastructure.

Relation to this thesis

This book chapter lays out the planned functionality of the adaptive grid management system presented in this thesis, presents an approach to answer earlier versions of the corresponding research questions, and provides some evaluation results for earlier versions of the centralized and distributed strategies. Resilience against participant misconduct and sensor failure as well as adaptive PV curtailment are not considered yet.

Mapping to research questions

The book chapter partially and preliminarily addresses Sub-Questions 1.1, 1.2, 1.3, and 1.4 of Research Question 1, Sub-Questions 2.1 and 2.3 of Research Question 2, as well as Sub-Question 3.3 of Research Question 3.

Continued on next page

Table 1.1: Overview of the publications by the author directly related to this thesis. The given abstracts are quoted verbatim from the respective publications (continued).

2025 Mischa Ahrens and Hartmut Schmeck. “Organic Computing for Adaptive and Resilient Electricity Grid Management”. In: *Go Where the Bugs Are: Essays Dedicated to Wolfgang Reif on the Occasion of His 65th Birthday*. Edited by Gidon Ernst et al. Cham: Springer Nature Switzerland, 2025, pp. 242–261. ISBN: 978-3-031-92196-4. DOI: 10.1007/978-3-031-92196-4_12. [34]

Abstract

The motivation behind the research initiative "Organic Computing” has been the need for system architectures supporting the self-organized response of decentralized technical application systems to changing requirements and disturbances in their operational environment, while respecting functional objectives as defined by their users. Such a property is strongly resembling the notion of system resilience. In this paper, we report some results on the achievement of resilience in energy systems by an adaptive system for regional management of electricity grids. This system mitigates physical disturbances of the grid in different ways, depending on the availability of information on the current status of the relevant entities, such as the distribution system operator, grid equipment, and (active) buildings. Our approach is based on an extension of the Organic Smart Home, a software framework for energy system management, simulation, and optimization, which has been strongly influenced by the observer/controller architecture, which emerged as a core generic architectural concept for organic computing systems. Depending on the current availability of communication infrastructure, the adaptive grid management switches between centralized, distributed, and completely decentralized derivation of control decisions in response to undesired deviations of voltages at grid connection points, high transformer temperatures, or high line currents. Based on power profiles from real-life studies and simulation models, our evaluation shows that even the completely decentralized strategy is still capable of guaranteeing the desired resilience.

Relation to this thesis

This publication provides a substantially updated overview of the adaptive grid management system presented in this thesis and first evaluation results for the management strategy adaptation in response to communication disruption.

Mapping to research questions

The publication partially and preliminarily addresses all sub-questions of Research Question 3.

1.5. Declaration of Tool Use

In the following, we list the tools used during the creation of this thesis. We put a special focus on how we used generative artificial intelligence (GAI).

1.5.1. Tool Use

Table 1.2 lists the tools used during the creation of this thesis.

Table 1.2: Tools used during the creation of this thesis.

Tool	Usage
TeXstudio [35]	LaTeX-editor to write the thesis
MiKTeX [36]	TeX-distribution and package manager
LaTeX template for dissertations of the Software Design and Quality research group at the Karlsruhe Institute of Technology (KIT) [37]	LaTeX template for the thesis
Zotero [38]	Reference management
Adobe Acrobat Reader [39]	Viewing and reading PDF-files
Briss 0.9 [40]	Cropping PDF-files
Microsoft Word [41]	Final proofreading of the thesis
Microsoft Excel [42]	Table and diagram creation and editing
Microsoft PowerPoint [43]	Figure creation
Microsoft Windows Snipping Tool [44]	Taking screenshots
OpenOffice Calc [45]	Table and diagram creation and editing
Draw.io desktop [46]	Figure creation
Eclipse Integrated Development Environment (IDE) [47]	IDE for Java development
PyCharm [48]	IDE for Python development
GAI tools [49–51] and DeepL translator [52]	See Section 1.5.2

1.5.2. Declaration of Generative Artificial Intelligence Use

Between January 2025 and May 2026, the author used GAI for various aspects during the creation of this thesis. The used GAI tools include the *large language models* (LLMs) *ChatGPT o3/o4(-mini)* and *ChatGPT 5/5.1/5.2/5.3/5.4/5.5 (Thinking)* provided by *OpenAI* [49,

50] as well as *Gemini 2.5 Pro Preview* provided by *Google* [51]. Between 2018 and May 2026, the artificial-intelligence-based *DeepL* translator by *DeepL SE* [52] was occasionally used to help with English wording. The listed LLMs and translator were used for the following aspects:

- Identifying potentially outdated factual information in Sections 2.2 and 2.6.3 previously written by the author and suggesting candidate literature sources for updating data and/or extending the coverage of the section
  - The sections were analyzed by an LLM with the request to suggest appropriate sources for more current data or additional background references on the topics mentioned.
  - All proposed sources were independently accessed, validated, selected, and interpreted by the author.
  - When a source was deemed appropriate, the relevant information was gathered directly from the original source, integrated into the respective section, and appropriately cited by the author.
- Initial scoping steps for parts of Sections 2.4.1 and 2.6.2
  - An LLM was tasked with suggesting lists of candidate open-source energy management systems and smart grid frameworks.
  - The existence and relevant characteristics of each suggested entry were independently confirmed by the author.
  - The author independently identified relevant entries and wrote descriptions of the selected systems and frameworks based on primary sources, which are appropriately cited.
- Gathering feedback on factual and grammatical correctness as well as understandability and consistency for Sections 2.6.3 and 3.2, selected sections in Chapter 4, as well as Section 5.3.1 previously written by the author
  - All feedback received by the LLMs was carefully reviewed by the author and only acted upon if sensible.
  - When feedback was deemed sensible, appropriate changes were entirely determined and implemented by the author.
- Formatting of text, tables, notation, equations, algorithms, and bibliography entries throughout the thesis
  - LLMs were occasionally used to aid in improving the formatting of text, tables, notation, equations, algorithms, and bibliography entries.
- Grammar, spelling, and phrasing checks throughout the thesis
  - LLMs and the DeepL translator were occasionally used to aid in correcting grammar and spelling as well as to suggest more concise and idiomatic terminology, phrasing, and translations.
  - Suggested changes were carefully reviewed by the author and only implemented when appropriate.

The author did *not* use GAI for programming, creating figures, nor to generate the scientific content (ideas, methods, evaluation, results, interpretation) presented in this thesis. GAI was exclusively used to suggest edits with regard to language, formatting, understandability, and consistency, to flag potential factual issues for the author to verify, and to suggest candidate sources, systems, and frameworks for subsequent manual review. No substantial

passages of GAI-generated text were copied verbatim into the thesis. Individual words and short phrases may coincide with GAI-suggested edits, even after critical review and, if necessary, revision by the author. The final content, phrasing, and structure of the thesis were entirely determined by the author, who takes full responsibility for them.

1.6. Contributions and Main Findings

Our thesis makes the following contributions:

- Development of an adaptive grid management system that leverages the energy flexibility of smart buildings to increase the resilience of electricity distribution grids with regard to
  - electrical disturbances comprising voltage-, transformer-, and line-related problems
  - ICT disturbances comprising or entailing communication disruption, participant misconduct (system-internal or externally induced through cyberattacks), and sensor failure
- Development of a resilience definition and resilience quantification metrics for smart electricity distribution grids that encompass
  - the operation of the electrical grid
  - the handling of the effects of ICT disturbances
  - the invasiveness of the utilized grid management measures
- Evaluation of the developed system to answer the following research questions:
  1. Can the use of energy flexibility provided by smart buildings improve the resilience of distribution grids?
  2. How do distributed or decentralized grid management strategies compare to a centralized grid management strategy?
  3. Can grid operation be upheld during communication disruption, sensor failure, or participant misconduct?

Our main findings with regard to our research questions are the following:

1. Assuming undisturbed ICT infrastructure, the grid management system fully prevents electricity outages and equipment damage in the evaluated scenarios by leveraging the energy flexibility of smart buildings. The employed grid management measures are effective in limiting the need for load curtailment.

2. All developed grid management strategies fully prevent electricity outages and potential equipment failure in the evaluated scenarios that assume undisturbed ICT infrastructure. While the centralized and distributed strategies show the exact same performance, the decentralized strategy incurs higher losses of potentially generatable active energy due to PV curtailment, as it uses a more conservative curtailment approach.
3. The grid management system prevents electricity outages and equipment damage for almost all evaluated communication disruption and participant misconduct scenarios, which implicitly cover sensor failure as well. The only exception is a scenario, in which the misconduct by too many buildings can not be fully compensated for by the correctly acting buildings anymore.

1.7. Overview of the Thesis

The thesis starts with an introduction to the topic in Chapter 1. After delineating our motivation for the development of an adaptive grid management system, we state the challenges and resulting research questions this thesis addresses. Subsequently, we list the assumptions made for the development of the system and clarify its scope by detailing its limitations. We then clarify that some of the content in this thesis is transferred from previous, peer-reviewed publications by the author and declare how we used GAI during the preparation of the thesis. After a brief description of our contributions and main findings, we conclude the chapter with an overview of the thesis.

Chapter 2 introduces the relevant fundamentals on which the developed grid management system is based. It starts with an introduction to the research initiative *Organic Computing*, which provided the basis for the development of the OSH, an open-source BEMS. Afterwards, we detail different types of DER commonly found in modern residential buildings, provide data on their current prevalence and projected expansion, as well as an assessment of the grid-supportive operational flexibility they can provide. We then outline the general functionality and use cases of BEMSs, including the methods they employ to optimize energy flows, and give examples of open-source energy management systems (EMSs) before discussing the development and functionality of the OSH. Following this, we give an overview of the operating principles of electricity distribution and smart grids. We end the chapter by discussing different resilience definitions established in the literature and potential disturbances occurring in actively managed distribution grids.

Chapter 3 provides an overview of the existing research related to our thesis. We first analyze literature studying the impacts of cyberattacks and failing or lossy communication on the operation of actively managed distribution grids with DERs to assess the need for appropriate counter measures or fallback strategies. Following that, we give an overview of cyberattack detection methods in the context of distribution grids proposed in the literature. Finally, we address and compare literature most closely related to our own research. This covers publications that not only provide insights with regard to impacts and detection, but also provide strategies to uphold stable grid operation during and

after communication disruption, participant misconduct (that is, cyberattacks), or sensor failure.

Chapter 4 presents the methodology employed to develop the adaptive grid management system. After introducing the typographic conventions and time scales utilized in this thesis, we provide our own definition of resilience in the context of smart electricity distribution grids. Subsequently, we present three different grid management strategies that provide the basis for the adaptation of the grid management system during communication disruption, participant misconduct, or sensor failure. We then provide the criteria that signal different types of electrical disturbances in the grid as well as the countermeasures employed by the developed system to mitigate these disturbances. Building on the previously introduced grid management strategies, we explain the strategy adaptation functionality of the system. After describing the architecture and concrete implementation of the grid management system, we briefly discuss the transferability of the system to different BEMSs than the OSH. We then provide details on a visual demonstrator developed in the context of the thesis. After establishing the evaluation scenarios and metrics for assessing the performance of the system, we conclude the chapter with comprehensive parameter studies for all relevant parameters to ensure the system performs optimally, at least within the tested value ranges.

The evaluation results are presented and discussed in Chapter 5. The chapter starts with a comparative evaluation of the three grid management strategies available to the adaptive grid management system and an array of different grid management configurations. We compare the strategies and configurations with respect to their ability to prevent electricity outages and equipment damage as well as the resulting losses of active energy potentially generatable by PV systems due to PV curtailment. All strategies and configurations are evaluated for three different distribution grids and three seasons, covering a wide range of possible scenarios. Subsequently, we evaluate the ability of the system to adapt to communication disruption and participant misconduct, which implicitly covers sensor failure as well. We evaluate different scenarios to isolate the responses of the system to different types of problems that can be introduced by the dependence of a smart electricity distribution grid on information and communication technology infrastructure. The chapter concludes with a summary of the evaluation results.

We end the thesis by drawing conclusions from our findings, explicitly answering every posed research question, and giving an outlook to possible future work in Chapter 6.

2. Fundamentals

The following chapter introduces the relevant fundamentals on which the developed adaptive grid management system is based. It starts with an introduction to the research initiative *Organic Computing* (OC), which provided the basis for the development of the *Organic Smart Home* (OSH) energy management system and simulation framework. Afterwards, we detail different types of distributed energy resources (DERs) commonly found in modern buildings, provide data on their current prevalence and projected expansion, as well as an assessment of the grid-supportive operational flexibility they can provide. We then outline the general functionality and uses cases of building energy management systems (BEMSs), including the methods they employ to optimize energy flows, and give examples of open-source energy management systems (EMSs) before discussing the development and functionality of the OSH. Following this, we give an overview of the operating principles of electricity distribution and smart grids. We end the chapter by discussing different resilience definitions established in the literature and potential disturbances occurring in actively managed distribution grids.

2.1. Organic Computing

The development and use of often interconnected, increasingly complex (referring to description complexity) as well as intelligent computational devices and software makes it progressively harder or even impossible for humans to fully comprehend and maintain the resulting systems. The OC research initiative aims at reducing the adverse effects of incomprehensible computational systems by developing and providing system design principles and methods that enable the self-organization of systems with minimal need for human interaction. These principles are aimed at enabling computational systems to behave in an organic manner and consequently possess so-called *self-*-properties*, such as self-healing and self-adaptation, similar to living things [53].

We start the section by giving an overview of the historical context of the OC initiative. Subsequently we present the basic principles of OC as well as the *Observer/Controller* (O/C) architecture developed by the OC community. We conclude the section by introducing *evolutionary algorithms* (EAs), which are often used in the context of OC, since our adaptive grid management system makes use of an EA to optimize the energy flows of residential buildings.

2.1.1. Historical Context

The term *Organic Computing* arose independently in two different contexts in 2001 and 2002. The 2001 coining of the term refers to a combination of neuro sciences, molecular biology, and software engineering, while the 2002 coining refers to the research initiative introduced in this section. Almost simultaneously, the closely related *Autonomic Computing* initiative and *Organic IT* strategy emerged independently. Both initiatives have been driven by corporations, such as *International Business Machines Corporation* (IBM), Microsoft, and HP. While Organic IT proposes adaptive system architectures, Autonomic Computing aims at creating self-organizing large-scale computing and data center infrastructures [54].

The term *Organic Computing*, as it is used in this thesis, was chosen as the headline of a position paper summarizing the results of a 2002 workshop on predicting future technical developments in computer science. The workshop was organized by the special interest group *Fachausschuss ARCS - Architektur von Computer-Systemen* (English: Computer Architecture) of the *Gesellschaft für Informatik* (English: German Informatics Society). The OC initiative was subsequently carried forward in the *Priority Programme 1183*, which was funded by the *Deutsche Forschungsgemeinschaft* (English: German Research Foundation) from 2005 to 2011 [55], as well as the *OC perspectives* workshop series in 2013 and 2014. Afterwards, the OC community established the *The International Workshop on Self-Optimisation in Autonomic and Organic Computing Systems* (SAOS), the *International Workshop on Self-Improving System Integration* (SISSY), as well as the *Organic Computing Doctoral Dissertation Colloquium* (OC-DDC) [54]. The yearly installments of SISSY and OC-DDC are still ongoing as of 2026.

2.1.2. Basic Principles

The central concepts that relate to OC are self-organization, emergence, robustness, and autonomy. These terms are described in the following.

Self-organization In the context of OC, self-organization is the ongoing process in which a system is organized from within and by its subsystems. There are different degrees of self-organization. While a fully self-organized system achieves its objectives without external control, less self-organized systems require some degree of external control [53].

A quantification method for self-organization is proposed in [56]. The authors measure the self-organization of a system composed of autonomous agents by utilizing a probabilistic model that estimates distributions of messages exchanged between the agents over a fixed time period. They compare the current distribution of messages to a reference distribution estimated for the same system but for an earlier, equally long time period. Differences between these two distributions indicate self-organization, as the communication pattern between the agents has changed without external interference. The authors conclude

that the degree of self-organization is proportional to the difference between the two distributions.

Self-*-properties Inherent self-*-properties give a (partially) self-organized system the adaptivity needed to stay functional when its environment or objectives change and to learn from previous situations or internally performed simulations. Self-*-properties, which are sometimes called self-x-properties, encompass but are not limited to self-organization, self-adaptation, self-configuration, self-optimization, self-healing, self-protection, and self-explanation [57].

Self-*-properties were first introduced in the context of the Autonomic Computing initiative (see also Section 2.1.1). The original properties were self-configuration, self-optimization, self-healing, and self-protection [58].

Flexibility Flexibility in OC is the ability of a system to change its behavior in response to external changes or new objectives [59].

Different approaches to allow for the flexibility of systems designed according to the *Multi-Level Observer/Controller* framework [60] are discussed and evaluated in [61].

Robustness Robustness describes the ability of a system to adapt its behavior to maintain the required system functionality despite of certain internal or external disturbances. One prerequisite for achieving robustness is that a system has some degree of flexibility [59].

An approach to quantify the robustness of self-adapting and self-organizing systems was developed and evaluated in [62] and [63]. The approach utilizes the area enclosed by the constant utility target line and the actual graph of the utility of a system over time during external disturbances as a measure for the robustness of the system. The authors evaluate this approach in three application scenarios, namely wireless sensor networks, an open, distributed Multi-agent system with applied trust metrics, and urban traffic management. They find that the approach is expressive but subject to limitations that require further research.

Emergence The concept of emergence is based on self-organization. It is defined as the transition from a less ordered state to a more ordered state that is achieved by a self-organizing system without external control. Since not every emergent behavior of a system is desired, OC methods are aimed at achieving controlled emergence. This means that a balance is struck between complete external and complete internal control to achieve desired system behavior while not suppressing unforeseen but beneficial behavior [53].

Emergent behavior of a system can be measured by observing the system and extracting characteristic attributes. If the probability that a system displays a certain attribute changes over time, this indicates emergent behavior [64]. In [64], the authors propose several emergence measures for technical systems based on non-parametric or model-based

probability density estimation methods. These methods can be used for systems with categorical or continuous attributes as well as systems with multiple categorical and/or continuous attributes. They can quantify the degree of emergence of a system and detect concept drift as well as disappearing or newly emerging processes. The authors evaluate the developed measures on artificial data sets as well as an intrusion detection data set comprised of real data. They find that the measures can be applied to real data as well.

Autonomy Autonomy is a measure for the extent of the self-organization of a system. The degree of its autonomy is determined by the complexity reduction achieved by a system. In general, this complexity reduction is the difference between the external and internal configuration spaces. The external configuration space is composed of the different objective parameters that can be set from outside the system and the different values each parameter can assume. The internal configuration space comprises all types of control signals the system can be configured with by internal controllers and their respective value ranges. In OC, two types of autonomy have been established. The static degree of autonomy is determined by the complexity reduction in relation to the full internal and external state spaces. Here, all possible combinations of objective parameter values an external entity can set are compared to all possible configuration states the system can take. In contrast, for the dynamic degree of autonomy, the complexity reduction only considers the actual control actions taken by internal controllers and external entities in a certain time period [53].

2.1.3. Observer/Controller-Architecture

The generic O/C architecture stems from the OC research initiative and was first proposed in [65]. It provides a generic system design framework aimed at enabling controlled self-organization and emergence in technical systems. In the O/C architecture, a system is managed via closed loop-control performed by an O/C-*unit* composed of an *observer* and a *controller* [66]. A schematic of the O/C architecture is shown in Figure 2.1.

System Under Observation and Control The system that is managed by the O/C-unit is called the *system under observation and control* (SuOC) [66]. Since the O/C architecture is generic, such a system can have various forms and sizes. In the context of electricity grids, an SuOC could be the entire interconnected grid of a continent, a local distribution grid, a building, a single device or anything in between. The requirements an SuOC has to fulfill are the observability of its behavior and environmental conditions, the measurability of its performance with respect to one or more external objectives, and the dynamic adaptability of certain parameters that influence its performance at run-time [68].

Observer The observer is used to measure, analyze, and process the current state of the SuOC via the available sensors. These tasks are internally distributed over different components. The *monitor* is used to sample the state of the SuOC using a specified rate

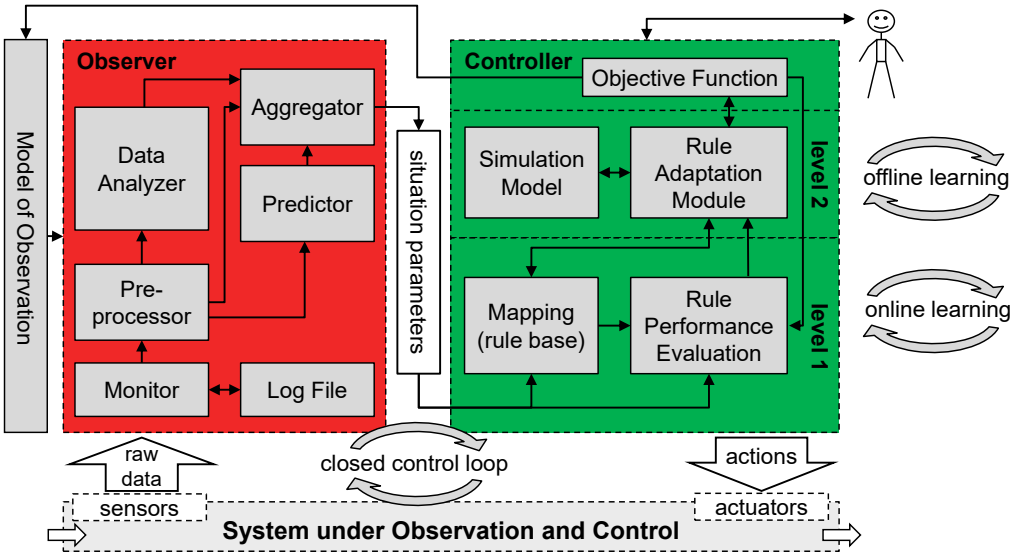

Figure 2.1: The generic Observer/Controller architecture. Image reproduced from [67]. Based on an image first published in [57].

and to store the acquired data in a log file. Afterwards, a *pre-processor* pre-processes the currently sampled data for the following analysis. The *data analyzer* then generates a description of the current system state in a structure than depends on the type of the observed system. In parallel, a *predictor* is used to provide a prognosis of the SuOCs future behavior and conditions to enable the controller to make control decisions based on current as well as predicted future system states. Finally, an *aggregator* merges the data from the pre-processor, the data analyzer, and the predictor into suitable situation parameters that can be used by the controller. A *model of observation* can be used by the controller to change the situation parameters provided by the observer [68].

Controller The controller is used to control the SuOC using the data provided by the observer. The control objective can be set and modified by an external entity via an *objective function*. The situation parameters communicated by the observer are used in a rule-based *mapping* component as well as a *rule performance evaluation* component. The former stores mappings of previous states to actions performed in reaction to these states and performs control actions to influence the SuOC based on its current state. The latter evaluates the performance of previous actions based on the resulting states with regard to the objective function and updates the situation-action mappings accordingly, using the *rule adaptation module*. The task of the rule adaptation module is to generate new situation-action mappings based on the performance evaluation of real situations as well as internal simulations performed by a *simulation model* of the SuOC [68].

2.1.4. Evolutionary Algorithms

The following descriptions of EAs are based on the explanations provided in [69]. EAs are a subset of stochastic optimization methods. Notable examples of EAs are genetic algorithms, evolution strategies, evolutionary programming, and genetic programming. The EA utilized in this thesis is a genetic algorithm.

In the application of EAs, principles of natural evolution are transferred to optimization problems to achieve good approximations of exact solutions to these problems. The different steps of an EA are stochastic in nature. This is especially useful for optimization problems that would take substantial amounts of time to solve exactly.

In an EA, a population of multiple individuals, which are solution candidates for the considered optimization problem, is usually initialized randomly. The solution candidates can take different forms depending on the optimization problem and the selected representation as an individual in the population. A typical form of representation is a string of bits, which is used by genetic algorithms. The representation of a solution candidate as an individual in the population of an EA is called genotype, while the structure of the search space, that is, the space of concrete operations to be searched, is called phenotype. A decoding function is used to map the genotype of a solution candidate to its corresponding phenotypical manifestation. An evaluation function determines the quality, often called fitness, of a solution candidate in the phenotype space.

After the initialization of the population, a fitness-based selection process determines which solution candidates are recombined to new, potentially improved solution candidates. There are different options for selecting solution candidates for recombination. In fitness proportionate selection, solution candidates are chosen based on individual probabilities computed from their individual fitness values and the cumulative fitness value of the entire population. A method with usually lower computation time is tournament selection where a small subset of the population is chosen randomly. The individual with the highest fitness value in this subset is selected for recombination. This process is repeated until the desired number of solution candidates is selected. In contrast to fitness proportionate selection (also called roulette wheel selection), tournament selection does not require computationally intensive probability computations. Tournament selection can mitigate other problems of fitness proportionate selection as well, such as the domination of the selection process by particularly fit solution candidates, which can hinder the exploration of the search space. Different recombination methods can be used, such as one-point crossover, n-point crossover, and uniform crossover. The number of solution candidates recombined to one or more new solution candidates can vary depending on the utilized algorithm. A mutation operator can then be applied to new solution candidates, which randomly alters one or more parts of their genotype according to a predefined mutation rate to explore the search space more comprehensively. Subsequently, the new solution candidates are evaluated using the evaluation function and integrated into the population via so-called environmental selection. In the environmental selection, the old or new solution candidates with the highest fitness are selected to form the new population. The population size is usually limited. Consequently, the least fit solution candidates are

discarded. Some EAs may just replace the entire old population with newly determined solution candidates. The described process is repeated until a termination criterion is met. Such a criterion may be a maximum number of generations, that is, the number of the number of successive populations, or a minimum improvement of the average fitness of a new generation over the previous generation. An overview of the functionality of an EA according to [70] is shown in Figure 2.2.

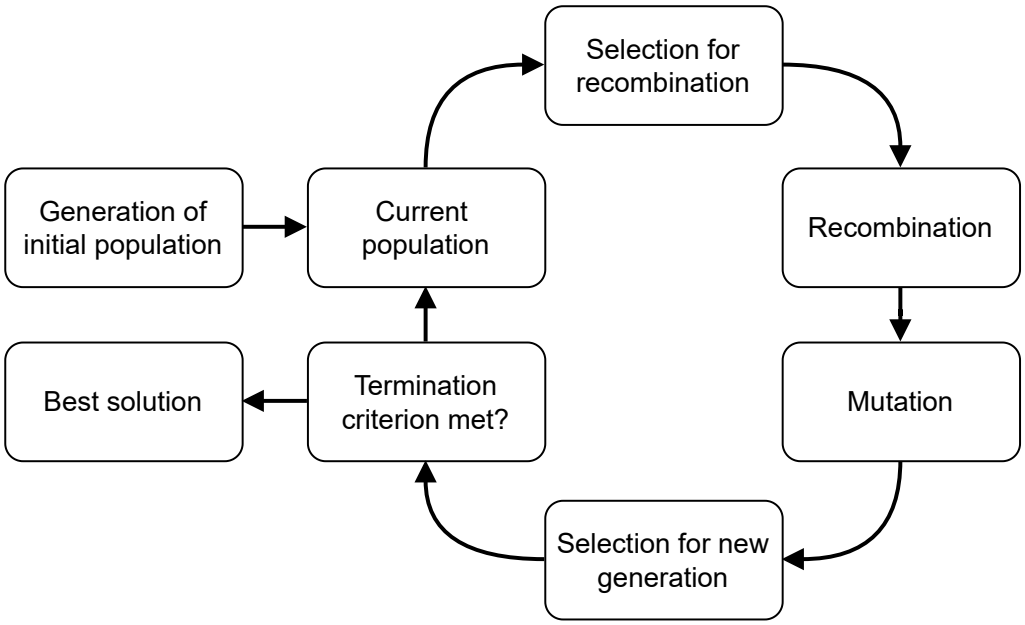

Figure 2.2: Overview of the functionality of an EA. Reproduced and translated from [70]. Partly based on a figure in [69].

2.2. Decentralized Electricity Generation and Consumption

This section introduces DERs that can be found in modern residential buildings. While the considered DERs consume or generate relatively large amounts of energy compared to inflexible consumers such as lighting, televisions, computers, or cooking devices, each of them provides some form of operational flexibility that can be used by BEMSs to optimize the energy flows of a building with regard to different objectives. The operational flexibility of each DER introduced in this section is discussed in Section 2.3. Wind turbines are not considered, since this thesis focuses on devices that can regularly be found in residential buildings. At least in Germany, as of 2025, small wind turbines up to 80 kW are almost irrelevant, with a total capacity of only 8.9 MW [71]. We assume the capacity directly connected to residential buildings in low-voltage grids to be even substantially lower.

2.2.1. Photovoltaic Systems

Photovoltaic (PV) systems convert solar radiation to electrical energy. Typical PV systems are made up of multiple solar panels, each made up of multiple solar cells [72].

In Germany, PV systems provided 74.1 TWh of electrical energy in 2024, which amounted to 14.2 % of the gross electricity consumption of the entire country [73]. The total installed PV capacity in Germany at the end of 2024 was 99.8 GW_p [73], which was distributed over more than 4.8 million [74] individual PV systems. These systems are most often situated on residential buildings and consequently connected to low-voltage distribution grids. A 2025 report stated that, by the end of 2024, 3.97 million PV systems where installed on residential buildings in Germany [75].

PV generation is on the rise internationally as well. According to [76], the world-wide cumulative installed PV capacity grew to over 2.2 TW by the end of 2024, with the global annual PV installations rising from 40 GW_p in 2014 to 602 GW_p in 2024.

The German *Gesetz zu Sofortmaßnahmen für einen beschleunigten Ausbau der erneuerbaren Energien und weiteren Maßnahmen im Stromsektor* (English: Law on Immediate Measures for the Accelerated Expansion of Renewable Energies and Further Measures in the Electricity Sector) [77] determines an updated solar energy expansion path for the 2023 revision of the German *Erneuerbare-Energien-Gesetz* (EEG, English: Renewable Energy Sources Act) [27, 78]. Among the targets to be reached are 215 GW of installed PV capacity by 2030 and 400 GW by 2040. Since this equates to an increase by a factor of four by 2040 over the installed capacity in 2024, it can be assumed that PV systems on residential buildings will become much more commonplace in Germany and that the capacity per building will increase as well. A diagram of the planned solar energy expansion path, which was published in [79], is provided in Figure 2.3.

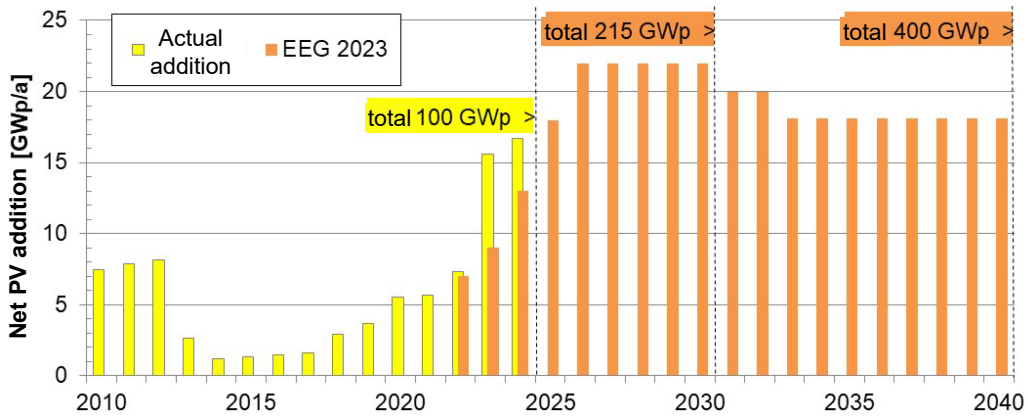

Figure 2.3: Planned net expansion of the installed PV capacity in Germany according to [79]. "EEG 2023": net PV addition up to 2040 according to [78]. Image reproduced and translated from [79].

The EEG [27], up to 2022, mandated that PV systems with a capacity of up to 25 kW_p had to either provide the possibility of remotely regulating their generation or that the feed-in of active power by the systems had to be curtailed to a maximum of 70 % of their peak

power. This was done to prevent grid congestion during periods of high PV generation [28]. However, this rule was lifted for all PV systems build in Germany on or after January 1, 2023 [77]. This date of repeal was subsequently brought forward to September 14, 2022. Furthermore, the rule was lifted for existing systems up to 7 kW_p from January 1, 2023 as well. For existing systems with more than 7 kW_p capacity, the rule expires as soon as an associated smart meter is installed [80].

2.2.2. Heat Pumps

A heat pump (HP) converts thermal energy from a reservoir with low energy into usable heat with higher energy using technical work. The most common type of HP used to heat residential buildings is the electrically driven compression HP. In such a HP, a gaseous refrigerant is compressed and fed to a heat exchanger, which liquifies it and transfers the condensation heat to a room or a water circuit. Afterwards, the refrigerant is expanded and, consequently, cooled. An evaporator then transfers heat from a reservoir to the refrigerant, leading to the evaporation of the latter. Different types of reservoir, such as the ambient air around a building, can be used for this purpose. Subsequently, the process is repeated [81].

HPs generated 17.88 TWh of the renewable heat consumed by German households in 2024. This corresponds to a share of 4.1 % of the final energy consumption in relation to heat and cold of German households in 2024 [82]. The progression of this share from 2005 to 2024 is given in Figure 2.4. It is important to note that more than 4.1 % of the total amount of heat consumed by households was generated by HPs, because this share only includes renewably generated heat. The utilized HPs predominantly consume electricity and part of this electricity is still produced non-renewably, for example, in coal-fired power plants. Therefore, an increase in the share of renewably generated electricity would increase the share of renewably generated heat by HPs as well, even without increasing the number of HPs [83]. Furthermore, the share would be even higher if the total heat generated by HPs for households could be brought in relation to the final energy consumption of households exclusively related to heat instead of heat *and* cold. We could not find a definitive value for the 2024 share of heat generated for households by HPs. However, [84] notes that, in 2022, the share of HPs among the total number of heat generators in existing buildings (not only residential) was 7.3 %. Furthermore, [85] states that 69.4 % of newly constructed residential buildings used HPs as their primary heat source in 2024.

According to [86], the German government planned to create the conditions to increase the yearly installations from 154,000 HPs in 2021 to at least 500,000 HPs from 2024 onward. Starting from the total number of installed HPs in Germany of just over one million in 2021, this would have represented a substantial expansion. To accomplish this goal, the German government wanted to create incentives to increase the production and installation of HPs and reduce regulatory and funding-related impediments. At the same time, the manufacturers pledged to increase production capacities and develop HP systems that are easier and more efficient to install. The associated specialist trade wanted to extend the qualification of professionals, make the corresponding jobs more appealing, reorient

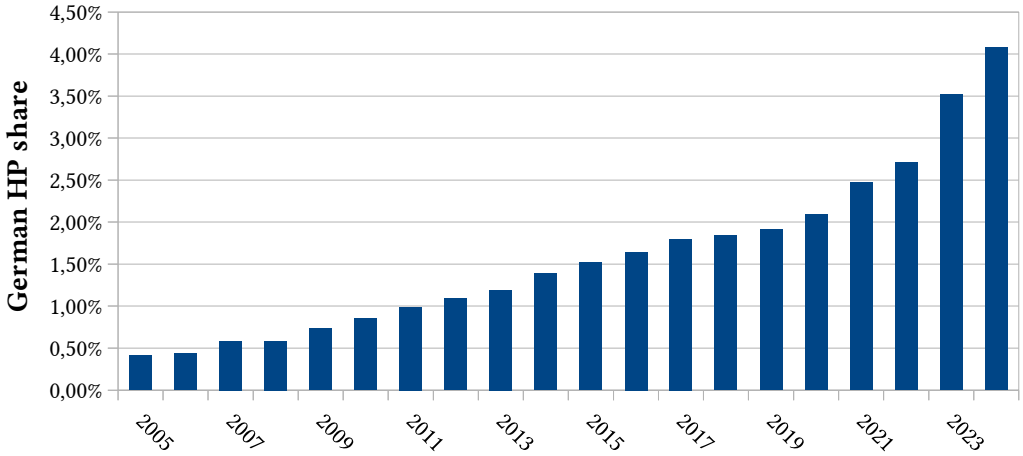

Figure 2.4: Progression of the share of renewable heat produced by heat pumps (HPs) of the German final energy consumption by households in relation to heat and cold from 2005 to 2024 according to [82].

businesses away from fossil fuel based to renewable solutions, and improve customer consulting. Another measure, which is especially relevant in the context of this thesis, is the stabilization of electricity grids and the grid-supportive flexibilization of HP use to reliably provide the required electricity. This falls in the area of responsibility of energy providers and grid operators. Since [86] was released, yearly sales of HPs rose to 236,000 in 2022 and 356,000 in 2023 but then fell to only 193,000 in 2024 [87]. Consequently, the further progression of HP sales and installations in Germany is uncertain as of 2025.

The international situation is similar to the one in Germany, with an increasing share of HPs for building heating. 10 % of the global heat consumption of buildings was supplied by HPs in 2023 with a 3 % decrease in sales over 2022 after significant increases in 2021 and 2022 [88].

2.2.3. Cogeneration of Heat and Power

Cogeneration of heat and power (CHP) is the simultaneous generation of usable thermal and mechanical energy from different forms of energy using a technical system. The generated mechanical energy is predominantly converted to electricity. CHP plants that produce electricity as well as heat are divided into CHP plants using Otto, Diesel, or Stirling engines, fuel cell CHP plants, CHP stations based on gas turbines with downstream waste heat boilers or combined cycle plants, and CHP stations using steam boilers as well as steam turbines or engines. Fuel cell CHP plants are a newer type of CHP plant, which can reach higher efficiencies with respect to electricity generation than combustion based CHP plants if driven with renewably produced hydrogen [89].

In 2024, 103.5 TWh of the net electricity generation and 196.8 TWh of the net heat generation in Germany were generated using CHP (preliminary information). For the German net electricity generation, this corresponded to a share of 21.5 % [90]. This includes all types of CHP plants and stations. Small CHP plants, which are used for space heating as

well as hot water supply and more likely to be deployed in residential buildings, had been typically combustion- or Stirling-engine-based in the past. Then, up to 2020, fuel cell CHP plants had been increasingly dominating the market for CHP plants with a rated electrical power of 3 kW or less [91]. However, while the shares of electricity and heat generated using CHP by and for residential buildings are not explicitly given, the yearly installations of smaller CHP plants ($\leq 10\,kW_{el}$) in Germany fell sharply after 2021 according to [92]. Compared to the yearly installations of HPs (see Section 2.2.2), they are several orders of magnitude lower. The progressions of newly installed CHP plants and stations in Germany with rated electrical powers of up to $2\,kW_{el}$, greater than $2\,kW_{el}$ and up to $10\,kW_{el}$, as well as those with a rated electrical power greater than $10\,kW_{el}$ from 2009 to 2024 according to [92] are given in Figure 2.5.

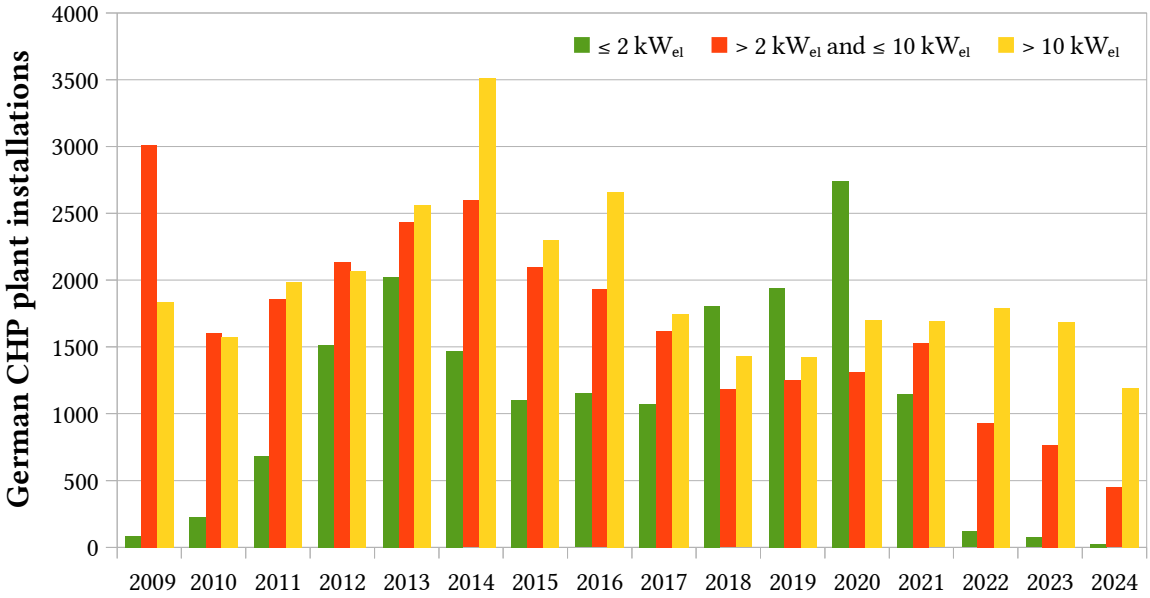

Figure 2.5: Progression of the new installations of CHP plants and stations per year in Germany from 2009 to 2024 according to [92].

According to [93], the future development of CHP in the supply of buildings in Germany is uncertain and depends on the design of the corresponding regulatory system. Small CHP plants for building supply are in direct competition with renewable heat production and connections to district heating networks, but provide emission savings compared to fossil fuel boilers as well as possibilities for flexible, grid-supportive electricity generation. For the development of CHP in Germany overall, [93] cites studies that indicate that a further increase in the use of CHP is possible up to 2030, but sees a decline in favor of renewable heat production in subsequent years as very likely. Newer German publications note regulatory uncertainty as an obstacle for the further deployment of CHP in general [94] and a low relevance of CHP for the direct heat supply of buildings going forward [95].

Internationally, direct heat supply of buildings by small CHP plants is a niche as well [96], with most of the deployment of small fuel cell CHP plants concentrated in Japan and Europe [97].

2.2.4. Intelligent Appliances

Some household appliances, such as washing machines, tumble dryers, and dish washers, can provide energy flexibility by shifting their operation within the day, temporarily interrupting their operation, and changing their mode of operation [67]. To exploit their flexibility, appliances have to be controllable to an appropriate extent. In the context of this thesis, appliances that provide some form of controllability ex works, such that they can be integrated into a BEMS, are called intelligent appliances.

In Germany, 13 % of households used one or more intelligent appliances, such as vacuum cleaning robots, refrigerators, or washing machines, at the beginning of 2022 [98]. Although it did not explicitly consider intelligent appliances, a newer study found that 46 % of the surveyed German households used smart home applications in 2024, which represents a significant uptrend from 26 % in 2018 [99].

When considering the international situation, [100] noted in 2024 that smart appliances, such as dish washers and washing machines, are moving closer to capturing the global mass market. According to [101], 38 % of consumers indicate that they will pay more for smart variants of major domestic appliances (tumble dryers, washing machines, dishwashers, cooling, built-in hobs). This is reflected in the sales figures as well, since roughly 40 % of tumble dryers, washing machines, and dishwashers sold globally in the first half of 2024 had smart functionality, even though smart variants were significantly more expensive than their non-smart counterparts [101]. In the US, a 2022 survey found that 21 % of US-citizens owned one large smart appliance or more [102]. A 2024 survey stated that sales of smart washing machines accounted for over 50 % of washing machines sold in the UK between August 2023 and July 2024 [103].

Another key factor in the use of the flexibility intelligent appliances can provide is user acceptance. A 2014 PhD thesis [104] analyzed the results of a German field test tracking the reactions of electricity customers to dynamic electricity price signals. This field test was performed in the research project *MeRegio* and ran from November 2009 to December 2011. The author found that the test customers shifted their load considerably in response to price signal changes and slightly reduced their overall consumption. The initiated load changes were found to be dependent on the time of day, the day of the week, and the season. While the author notes that reactions to price signal changes were more pronounced at the beginning of the field test, a stable and significant level of participation was reached soon after. A 2021 survey among 195 Romanian, Hungarian and Serbian citizens found that 81 % of the participants were willing to take part in demand response programs aimed at reducing CO_2 emissions and global warming [105]. A larger Finish study conducted in 2023 found that the willingness to participate in demand response programs was higher for heating and electrical appliances than for electric vehicles, younger consumers were more willing to participate than older ones, and financial compensation was a bigger incentive than emission reductions [106]. A 2023 report stated that 40 % of French households already use the delayed start functionality of appliances, such as dishwashers and washing machines, with about half of them incentivized by variable electricity tariffs [107].

2.2.5. Battery Energy Storage Systems

Battery energy storage systems (BESSs) can be used in conjunction with PV systems to substantially increase the self-consumption of locally generated electricity. For this use case, the BESS is charged with surplus PV-generated electricity, for example, around noon, and discharged during times when electricity is needed, but not locally generated, such as in the evening and night hours. The BESS types most often used for this purpose are lead-gel- and lithium-ion-based BESSs. Lead-gel-based BESSs have been used in the past due to their relatively low cost. Higher specific energy densities and longer life cycles make lithium-ion-based BESSs a suitable, but more expensive alternative [108]. In the past decade, the cost of lithium-ion-based BESSs has dropped sharply, which indicates that their usage will increase further in the future. From 2023 to 2024 alone, lithium-ion battery pack prices decreased by 20 % [109]. In the same time frame, levelized costs for utility-scale battery storage projects decreased by 33 % [110], with an 86 % drop from 2014 to 2024.

In Germany, the number of installed BESSs has been exponentially increasing in the last decade [111]. According to [112], 580,000 residential BESSs were installed in 2024, which corresponded to roughly a third of all residential systems installed at the end of 2024. These newly installed systems had an average capacity of 8.5 kWh. 80 % of newly installed PV systems were coupled with a BESS. The progression of the yearly BESSs installations in Germany, including the distributions over different capacity classes, from 2014 to 2023 according to [111] is shown in Figure 2.6.

Key drivers for the use of BESSs in Germany are the diminishing feed-in remuneration for PV-generated electricity [113, 114] as well as the abolition of the *EEG-Umlage* (English: EEG-surcharge) on self-consumption [115], which make the consumption of PV-generated electricity directly on-site more attractive.

Internationally, installations of residential BESSs are on the rise as well. [116] estimated a global installed residential BESS capacity of 34 GWh at the end of 2023, with 88 % of this capacity concentrated in Germany, Italy, Japan, the US and Australia. Almost all of this installed capacity was installed from 2019 to 2023, with the yearly added capacity increasing from roughly 2.5 GWh in 2020 to 12 GWh in 2023.

2.2.6. Battery Electric Vehicles

The German *Nationaler Entwicklungsplan Elektromobilität der Bundesregierung* (English: National Electromobility Development Plan of the German Federal Government) [117] defines five categories of vehicles that use electric motors, which are given in Table 2.1.

According to [117], electric engines for vehicles have multiple advantages over classical combustion engines. They are more efficient (approximately by a factor of three compared to diesel engines [118]), they reduce the dependency on potentially scarce energy carriers, such as crude oil, and they can contribute substantially to the reduction of CO_2- and pollutant-emissions if they are driven with electricity from renewable energy sources.

Figure 2.6: Progression of the yearly BESSs installations in Germany, including the distributions over different capacity classes, from 2014 to 2023. "Anteil Anlagenzubau": Share of new plant construction. "Jahre": years. "Tsd.": thousand. Image reproduced from [111].

Another key benefit is the inherent flexibility provided by the batteries of battery electric vehicles (BEVs). The flexibility in charging and discharging rates and times can be utilized to lessen the impacts of the fluctuating energy supply from renewables on electricity grids.

In Germany, the share of electric vehicles among the total new registrations of passenger cars was 29 % for the first three quarters of 2025. This corresponds to an increase of 47.2 % or 9.2 percentage points compared to the same period of the previous year. The share of newly registered BEVs increased by 39.4 % or 5.1 percentage points to 18.4 % when comparing the same periods [119].

On July 1, 2025, the total number of registered passenger cars with alternative drive systems (including hybrid without plug-in capability, hydrogen-based drives, and unspecified drive systems) in Germany was still relatively small at 6,169,212, of which only 1,835,578 were

Table 2.1: Categories of vehicles that use electric motors. Defined by the *Nationaler Entwicklungsplan Elektromobilität der Bundesregierung* (English: National Electromobility Development Plan of the German Federal Government) [117]. Table reproduced, shortened and translated from [117].

Vehicle type	Characteristics
Battery electric vehicle	• Electric engine with grid rechargeable battery • Cars or two wheeled vehicles • High potential for reduction of CO_2-emissions through use of renewable energy
Range extended electric vehicle	• Electric engine with grid rechargeable battery • Modified low power combustion engine or fuel cell
Plug-in hybrid electric vehicle	• Electric engine with grid rechargeable battery • Combination of combustion engine and electric engine • Passenger or utility cars
Hybrid electric vehicle	• Combination of combustion engine and electric engine • Battery charging by recovering braking energy • Passenger or utility cars
Fuel cell hybrid electric vehicle	• Electric engine with a fuel cell as the energy supply

BEVs. Since the total number of registered vehicles in Germany was 49,525,608 at the time, the share of BEVs corresponded to 3.71 %. Compared to the share of BEVs one year earlier (July 1, 2024) this corresponds to an increase of 20.06 % [120]. The progression of the German BEV share in three month intervals is shown in Figure 2.7.

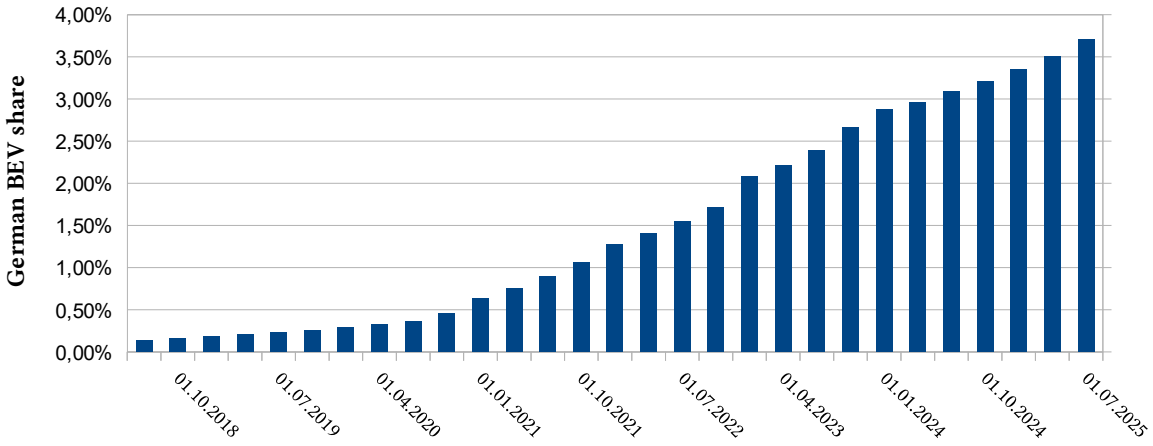

Figure 2.7: Progression of the share ofBEVs in Germany from July 1, 2018 to July 1, 2025 according to [120].

Until 2030, the German federal government aims to increase the number of BEVs in Germany to 15 million [121]. Using the number of all registered vehicles in Germany on July 1, 2025 as a basis, this would correspond to a BEV share of roughly 30 %. Considering the current progression of the BEV share shown in Figure 2.7, this is a highly ambitious goal. The number of BEVs in Germany would have to increase more than eightfold in only five years, which means that the yearly registrations of BEVs would have to grow exponentially instead of the rather linear growth currently observed.

According to [122], global sales of electric vehicles (not specified whether only BEVs were considered) exceeded 17 million in 2024 and are estimated to reach over 20 million in 2025, with China and Europe expected to lead the electrification of the mobility sector. The global share of electric vehicles among overall car sales is estimated to exceed 40 % in 2030.

2.3. Energy Flexibility

In this thesis, we use the term *energy flexibility* to describe the ability of an energy consuming or generating device or a combination of such devices to change its operation such that a change in its electric load profile is achieved. For the sake of simplicity, the term *flexibility* is used in the following. All devices introduced in Section 2.2 can provide some form of flexibility. The flexibility of each device type is described in the following. Figure 2.8 visualizes the effects of energy flexibility on load profiles according to [123] and [124].

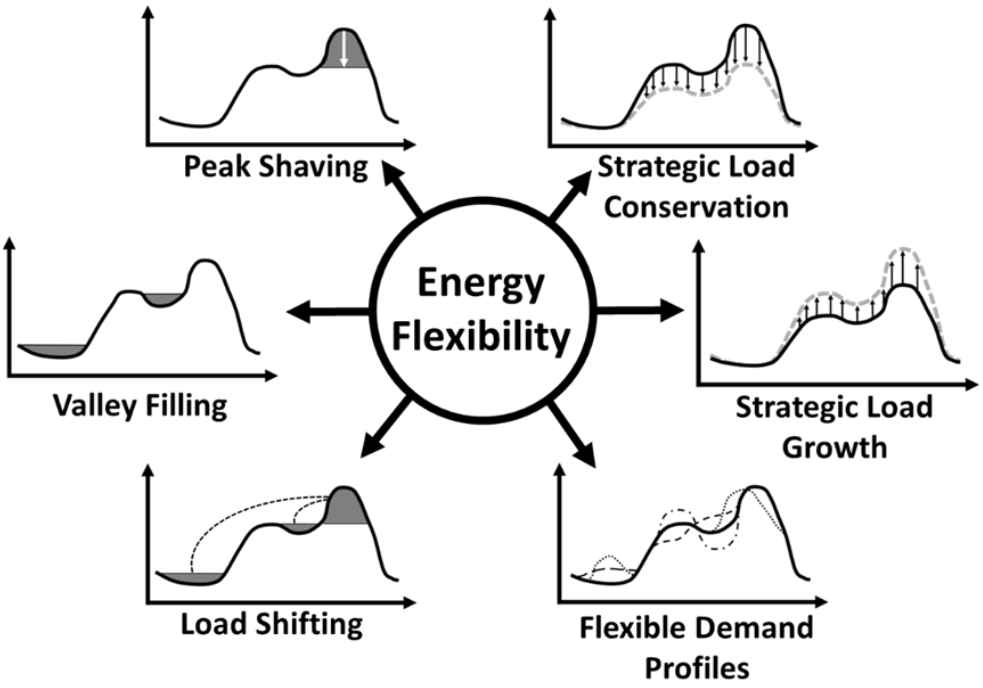

Figure 2.8: An image from [123] adapted by [124] illustrating how energy flexibility can impact load profiles.

Photovoltaic Systems To connect a PV system to the electricity grid of a building as well as the distribution grid, a PV inverter is needed. It converts the direct current a PV system generates to alternating current, which is commonly used in electricity grids. Furthermore, PV inverters provide functionality that can be used for grid congestion prevention and voltage maintenance [72]. PV inverters can absorb or inject reactive power in addition to converting active power. In the context of grid congestion, reactive power compensation can be useful. Here, the capability of a PV inverter to absorb or inject reactive power is used to compensate for the current reactive power absorption or injection of other devices. This decreases or eliminates the reactive power that has to be transferred by the adjacent electricity grid and, consequently, reduces the load the latter has to carry. Reactive power can also be leveraged to decrease or increase voltages in an electricity grid, which makes it an effective tool for voltage maintenance. The absorption or injection of reactive power decreases or increases voltages, respectively, which is especially useful in low-voltage grids with decentralized power feed-in [125]. Furthermore, inverters, such as those manufactured by *SMA Solar Technology AG*, can be used to curtail the active power generated by PV systems [126].

Heat pumps HPs can provide flexibility by utilizing the thermal inertia of buildings to shift their operating time within a certain time span while maintaining a room or water temperature within a desired temperature range. The achievable time shift can be substantially increased by utilizing thermal buffering tanks and high quality building insulation [127]. Since HPs that are used to heat buildings typically require electricity to run [81], a shift of their operating time results in a shift of electricity consumption.

Cogeneration of heat and power Similar to HPs, CHP plants offer flexibility in the form of temporally shifting their operating times when connected to hot water storage tanks [93]. However, in contrast to HPs, CHP plants generate rather than consume electricity during heat generation. This means that a shift of the operating time of a CHP plant results in a shift of electricity generation.

Intelligent appliances As mentioned in Section 2.2.4, intelligent appliances offer flexibility by changing their operation mode, interrupting their operation, or shifting their operation time. Naturally, this flexibility is limited by the preferences and requirements of building inhabitants and their general willingness to consider external goals in their appliance usage.

Battery energy storage systems Of all devices considered in this section, BESSs offer the most flexibility, since their operation can not only be shifted temporally and is not substantially limited by user behavior and preferences. Adjustable charging and discharging rates can be utilized to achieve a wide range of load profiles [128]. The achievable flexibility is limited by the capacity of the particular BESS, the minimum and maximum charging and discharging rates, as well as the granularity of the adjustment range.

Battery Electric vehicles The batteries of BEVs theoretically offer similar flexibility to BESSs. However, due to their primary purpose of driving the electric engines of BEVs, their flexibility is limited by user behavior and preferences, similar to intelligent appliances. The flexibility of the battery of a BEV is only available if the BEV is present and connected to the electricity grid. To discharge the battery, appropriate *vehicle to grid* [118] equipment has to be installed and the user has to agree to this type of use. Furthermore, the user has to input the expected time of departure and desired state of charge (SoC) so that optimized charging and discharging schedules can be determined accordingly.

2.4. Building Energy Management Systems

This section describes the functionality and areas of application of BEMSs and provides several examples of open-source EMSs that can be utilized as BEMSs. We put a special focus on the OSH [129, 130], which we use as the basis for developing the adaptive grid management system presented in this thesis.

2.4.1. Functionality, Use Cases, and Examples

It is important to note that, in the context of this thesis, *energy management* should not be understood in the sense of energy management and energy management systems as defined, for example, in the ISO 50001 [131]. Standards like the ISO 50001 provide organizations with tools to create processes and systems to improve energy efficiency, energy use, and energy consumption by means of creating energy awareness and policies. In contrast, the terms EMS and BEMS used in this thesis describe software systems that utilize the flexibility of energy-related devices to automatically optimize energy flows with regard to certain objectives.

BEMSs in the context of residential buildings, which this thesis focuses on, are often also called *home energy management systems* (HEMSs). According to [3], HEMSs are systems that can be deployed in residential buildings to monitor, optimize, and control the energy consumption and generation of the devices in the building. Devices commonly managed by a HEMS are energy generators, such as PV systems, energy storages, such as BESSs and BEVs, heating, ventilation, and air conditioning systems, as well as appliances. A typical HEMS comprises multiple components, such as a central controller that enables the optimization and control of the energy flows in the building and communication technology to interact with the devices in the building, external entities, and building inhabitants. HEMSs are often able to optimize the energy flows of a building by monitoring and analyzing sensor data and intelligently scheduling and controlling device operation based on different objectives, constraints, and predictions. It can factor in variable energy tariffs, weather conditions and predictions, learned behavioral patterns and preferences of building inhabitants, as well as electricity-grid-related aspects. HEMSs often support user interaction as well by providing user interfaces for data visualization and system configuration based on user preferences.

The optimization algorithms employed by BEMSs are diverse and often depend on the particular use case. The utilized algorithms comprise mathematical programming approaches such as linear or dynamic programming, heuristic approaches such as Markov decision processes or back tracking search, metaheuristic approaches such as genetic algorithms or simulated annealing, and other approaches such as fuzzy optimization techniques or stochastic programming [132].

There are various use cases for BEMSs and different objectives depending on the particular stakeholder. From the end user perspective, a typical optimization objective is the maximization of the self-consumption of locally generated energy for financial reasons or to achieve a higher degree of self-sufficiency [133]. In the presence of time-variable energy tariffs, the optimization objective can be to minimize the energy costs over the time horizon in which future energy prices are known [67]. Instead of or in addition to using variable tariffs set by energy providers, energy customers deploying BEMSs can also participate directly in dedicated markets [134]. Other common objectives are the improvement of energy efficiency [135] or the minimization of greenhouse gas emissions [136]. From the point of view of energy providers, BEMSs can be used in the context of *demand side management* (DSM) [137], where incentives, requirements, or commands are communicated to energy consumers or prosumers, with the goal of facilitating a better balancing of energy generation and consumption. Additionally, distribution system operators (DSOs) may use the flexibility harnessed by BEMSs to prevent local congestion in distribution grids [32].

While we use the OSH (see also Section 2.4.2), there is a plethora of other EMSs, which have been developed by different institutions and for different use cases. Besides numerous proprietary systems, there are several EMSs that are open source like the OSH as well:

BEMOSS The *Building Energy Management Open Source Software* (BEMOSS) is an open-source software platform developed in the US that improves the monitoring and control of energy-related systems in commercial buildings. It can interact with different load control devices and supports various communication protocols [138, 139].

OpenEMS *Open Energy Management System* (OpenEMS) is a German open-source BEMS that is actively developed and maintained by multiple institutions. Users can draw on its documentation and community forum for support. Its developers describe OpenEMS as an *Internet of Things* (IoT) stack that provides fast control of devices, expandability, modularity, as well as device-independent control algorithms and supports a wide range of devices. The IoT stack consists of three main components. *OpenEMS Edge* runs locally and enables communication with the monitored and controlled devices. *OpenEMS Backend* runs on a server and connects multiple different OpenEMS Edge instances for remote aggregation, monitoring, and control. *OpenEMS UI* is a user interface that connects to OpenEMS Edge and/or OpenEMS Backend and enables data tracking and visualization [140, 141].

OGEMA 2.0 The *Open Gateway Energy Management* (OGEMA 2.0) is an open-source framework for energy management systems developed by the *Fraunhofer Institute for Integrated Circuits IIS* in Germany. It has a modular architecture and provides functionality for smart industry, smart building, and smart living applications. Like OpenEMS, it is modular, hardware-independent, and already integrates various communication interfaces to enable interoperability between different processes, services, and technologies. However, in contrast to OpenEMS or the OSH it represents a middleware rather than a full EMS [142, 143].

VOLTTRON *VOLTTRON* is an open-source data, device, and system integration platform for sensing and control applications. While it is application-agnostic and not explicitly marketed as an EMS, it can be used to enable the monitoring and control of buildings in the context of energy management. Like the previously mentioned systems, it supports a wide range of communication protocols and focuses on interoperability and modularity [144–147].

BEMServer *BEMServer* is an internationally developed modular open-source building energy management platform that can run different energy management modules. While the platform itself is free, the modules are often paid and can be selected in a modules store depending on the particular application and stakeholder [148, 149].

OpenEnergyMonitor *OpenEnergyMonitor* is an open-source hardware and software system developed in Wales that can monitor electricity consumption and generation, temperature, and humidity. The utilized hardware is based on the Arduino [150] and Raspberry Pi [151] platforms. While it can be classified as an EMS, it does not provide intrinsic device control capabilities [152].

openHAB The *open Home Automation Bus* (openHAB) is a widely used open-source home automation platform. Similar to VOLTTRON, it does not focus specifically on energy management applications, but can be used for such application as well. Like most of the other platforms previously mentioned, it is modular and supports a wide range of devices and communication protocols to facilitate monitoring and control [153].

Home Assistant Similar to openHAB, *Home Assistant* is a widely used, modular, open-source home automation platform. It supports a plethora of different modules, called "integrations" in the Home Assistant terminology, which enable the communication with different IoT- and energy-related devices and services. In contrast to BEMServer-modules, the integrations are typically open source as well [154].

MyEMS *MyEMS* is a Chinese, open-source EMS that builds on the ISO 50001 [131] standard. It supports the logging, monitoring, and visualization of energy data collected by different sensors and meters. While the documentation mentions forecasting and device control as well, the system is focused on data collection, processing, and visualization [155, 156].

While the EMSs listed above vary greatly in their function range, they often provide some form of controllability for energy-related devices in buildings. However, they usually lack the proactive and comprehensive energy flow optimization capabilities provided, for example, by the OSH.

A major reason for choosing the OSH for the implementation of our grid management system is its co-simulation capabilities (multi-building and power-flow), which we need to develop and evaluate the system. The following section provides an overview of the OSH, including these capabilities.

2.4.2. Organic Smart Home

Some text passages of this section are transferred verbatim from one of our own publications [34]. For a summary of this publication, its relation to this thesis, and its mapping to our research questions, see Section 1.4.

The open-source BEMS used to implement and evaluate the adaptive grid management system developed in this thesis is the OSH, which has been developed in Germany at the *Institute of Applied Informatics and Formal Description Methods* (AIFB) at the *Karlsruhe Institute of Technology* (KIT) and the *FZI Research Center for Information Technology* (FZI). OSH Version 4.0, released in 2016, is available under GNU General Public License 3.0 at [130]. We choose the OSH over the other open-source (B/H)EMSs listed in Section 2.4.1 due to its comprehensive functionality, modularity, expandability, and integrated simulation capabilities, which enable the extensive functionality expansion presented in this thesis as well as its simulative evaluation.

To enable an appropriate degree of self-organization for the devices managed by the OSH, it is based on a hierarchical implementation of the O/C architecture (see Section 2.1.3). Here, each device has its own customized, local O/C-unit that is responsible for appropriate low-level observation and control as well as the communication of relevant data to and the implementation of commands from higher levels. The local O/C-units are themselves observed and controlled by a global O/C-unit that is responsible for the energy management of the building. It aggregates the data communicated from the lower levels and retrieves external signals, such as variable electricity tariffs and user inputs, to make optimized control decisions using an EA (see Section 2.1.4). The resulting control sequences are subsequently communicated to and implemented by the local O/C-units [70]. An overview of the OSH architecture for the development status in [70] is shown in Figure 2.9.

Based on extensions of the OSHs architecture introduced in [157], the OSH was significantly enhanced in [158] and [67] to become a multi-modal BEMS. An energy-related degree of

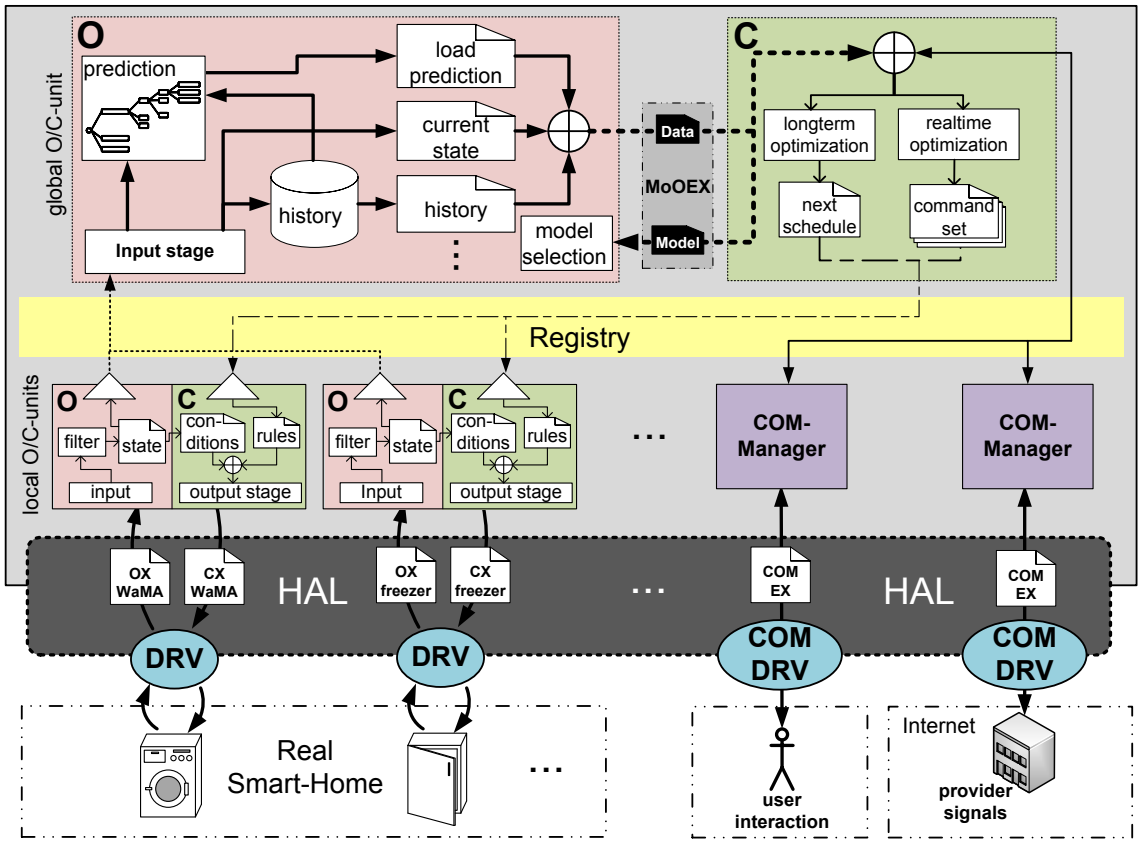

Figure 2.9: Overview of the OSH for the development status in [70]. "DRV": driver. "HAL": hardware abstraction layer. "OX": observation exchange object. "CX": control exchange object. "COM EX": communication exchange object. "O": observer. "C": controller. "COM-Manager": communication manager. "MoOEX": model of observation exchange. Reproduced from [70].

freedom was added to form a multi-commodity simulation and optimization that allows switching energy carriers for hybrid home appliances whenever feasible and advantageous. Furthermore, simulation models for several interruptible and hybrid appliances, adsorption chillers, trigeneration systems, gas boilers, and electrical insert heating elements were integrated into the OSH. In addition to the new simulation models, the previous models or load profiles of appliances, the CHP plant, the PV system and the simulated hot water consumption were reworked to more accurately represent their real-world counterparts. The possibility of simulating and optimizing BESSs was added in [128] and extended in [159]. Figure 2.10 shows the updated OSH architecture for the development status in [67].

To facilitate the aforementioned enhancements of the OSH as well as to enable a more flexible and generalized hierarchical approach to the different entities that can make up the observed and controlled system, the architecture was revised to include multiple abstraction layers and *interdependent problem parts* (IPPs) as shown in Figure 2.10. The *entity abstraction layers* (EALs) provide standardized interfaces that abstract the local O/C-units from the sub-ordinate entities via entity drivers. Consequently, EALs are situated

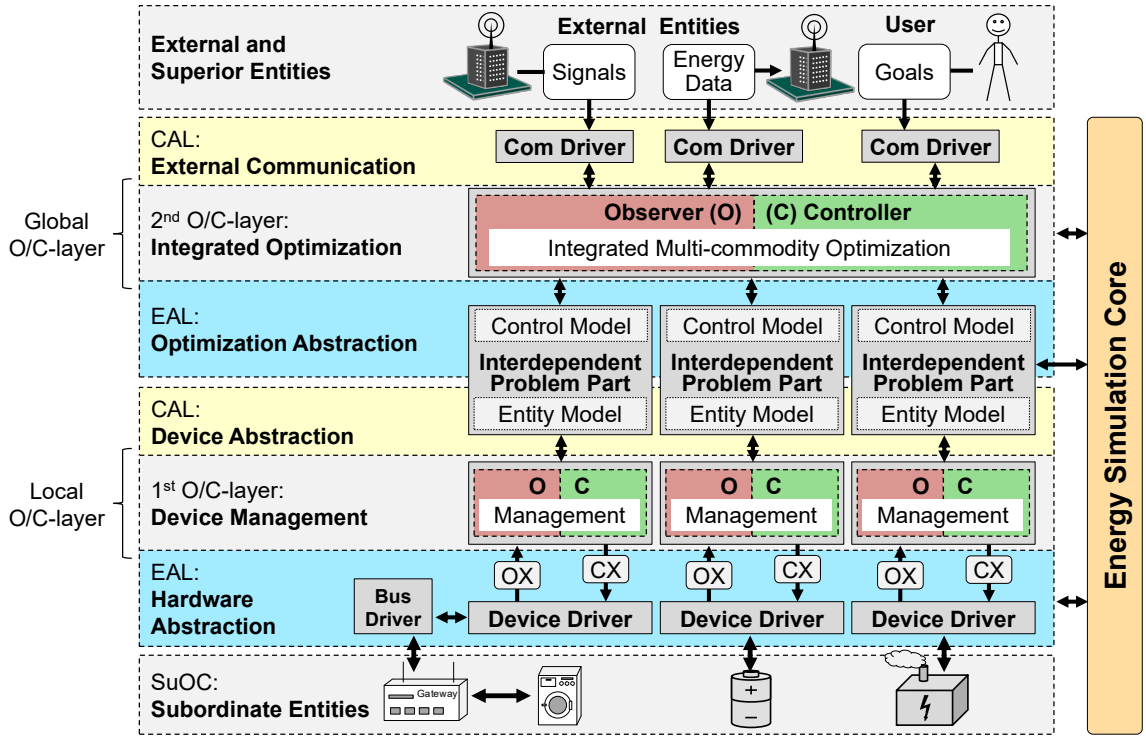

Figure 2.10: Overview of the Organic Smart Home (OSH) for the development status in [67]. "CAL": communication abstraction layer. "Com": communication. "EAL": entity abstraction layer. "OX": observation exchange object. "CX": control exchange object. "SuOC": system under observation and control. Reproduced from [67] (original image partially based on [158]).

between the local O/C-units and the managed devices as well as between the local O/C-units and the global O/C-unit. The *communication abstraction layers* (CALs) manage and abstract the properties and thereby the observability and controllability of entities using communication drivers. They are utilized for the communication with superior entities, for example, to receive and implement variable energy tariffs in the case of the communication of the global O/C-unit with an energy provider or to exchange IPPs in the case of the communication of local O/C-units with the global O/C-unit. The IPPs represent the different entities that are managed by the OSH and enable a fully modular optimization, even if one entity is dependent on another or vice versa. An example of the interdependency of different entities would be a heating system comprising a CHP plant and a hot water storage tank. Whereas before the introduction of IPPs, such a system was treated as a single part of the optimization problem, the use of IPPs enables the separate modeling of the involved entities. This modularity, in turn, enables their integrated simulation and optimization in combination with additional entities, such as adsorption chillers and chilled water storage tanks. To achieve this, each IPP comprises an *entity model*, which contains relevant information about the behavior and specifications of the entity, as well as a *control model*, which provides possible control sequences and interactions with other entities. The entity model functions as an agent in a multi-agent energy simulation that is used to evaluate the quality of solution candidates provided by the optimization algorithm. Concretely, the entity model provides permissible load profiles

based on the control sequences encoded in the solution candidates. In contrast, the control model provides possible options for external control, parameters and interactions with interdependent entities, which are encoded as a bit string. When a new solution candidate in the form of a bit string is provided by the optimization algorithm, the control model interprets it to determine the underlying control sequence to be evaluated [67].

To evaluate the solution candidates provided by the optimization algorithm, the *energy simulation core* (ESC) uses the IPPs as agents and additional information about physical connections and interdependencies in a time discrete multi-agent energy simulation. This results in so-called *ancillary commodity load profiles*, which represent the different use cases and sources of the present energy carriers. An example of an ancillary commodity is the self-consumption of active power generated by a PV system. This partitioning enables the calculation of energy costs and feed-in remuneration for differently priced or remunerated energy flows. The feed-in remuneration, for example, can differ for active power generated by a PV system or a CHP plant. The ESC can be used in two contexts. The first use case is the simulation of the future behavior of the entities in a building to determine appropriate control sequences in the optimization of real or simulated buildings. The second use case is the detailed simulation of entire virtual buildings that utilize the OSH. Different temporal resolutions can be set for these two use cases. In [67], a resolution of one second was used for the simulation of the virtual buildings and a resolution of one minute for the optimizations performed by the buildings. The usage of the ESC in the optimization process is shown in Figure 2.11 [67].

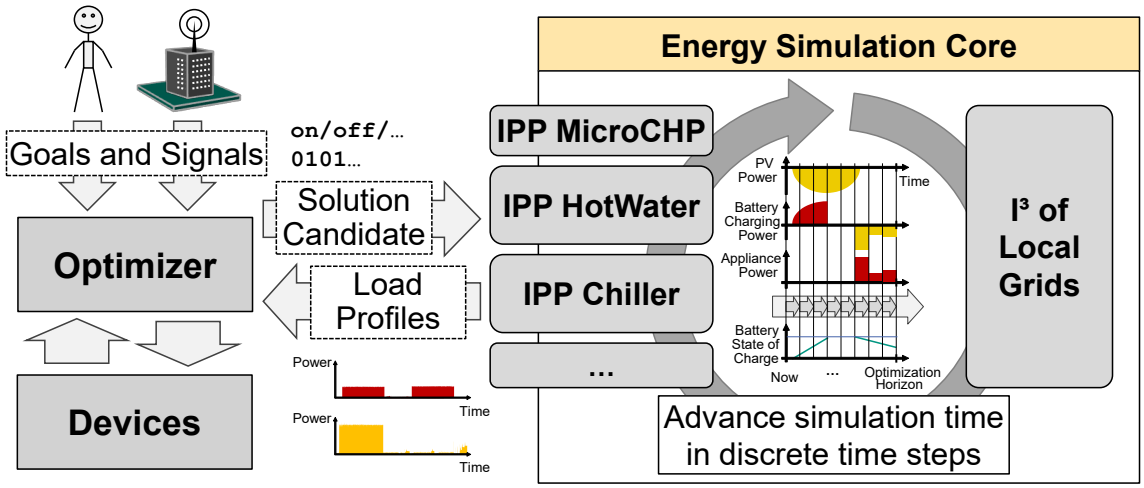

Figure 2.11: Utilization of the ESC for the energy flow optimization by the OSH. I^3: interdependency and interconnection information. Reproduced from [67].

The energy flow optimization is facilitated by an EA with a rolling optimization horizon. Each time a relevant change in device configurations, user objectives or a difference between predicted and actual behavior is detected, a new optimization is performed for the given time horizon, which starts when a new optimization is triggered [67].

Based on the aforementioned advancements on the building level, the OSH was further developed in [32] to include co-simulation capabilities. These enable the simulation of

multiple buildings simultaneously and their interactions with a simulated low-voltage distribution grid including conventional or voltage regulated distribution transformers (VRDTs), which were integrated in [160]. Furthermore, a *software-in-a-hardware-loop*-environment was created, in which real components such as a smart building can be attached to the co-simulation environment. These new options were used to implement and evaluate a *regional energy management system* (REMS) that coordinates the use of the flexibility of simulated or real buildings in a grid-supportive manner. To achieve this, the REMS possesses a dedicated O/C-unit, which is superior to the global O/C-units of the buildings and the O/C-units of grid equipment such as VRDTs. The *REMS global observer* receives data measured and calculated by buildings and grid equipment as well as information gathered from power-flow studies and generates a comprehensive evaluation of the current grid status. Here, a newly developed formulation of the *BDEW*[1] *Smart Grid Traffic Light Concept* [161] (see also Section 2.6.2) is used to determine different traffic light phases based on the given grid topology, voltages, line currents, and transformer temperatures. The REMS ascribes an individual traffic light phase to each building, depending on the type and magnitude of the occurring problems and the potential influence of a building on the situation. Based on the traffic light phase assigned to a building, the *REMS global controller* determines measures to be taken according to a cascade of measures. If the congestion can be resolved by the DSO using grid equipment, this step is taken first. If the congestion can not be resolved, the use of reactive power is preferred before using active power flexibility. To achieve a change in building behavior when necessary, the REMS global controller communicates price incentives, which are superimposed on existing electricity tariffs and aimed at reducing reactive power absorption or injection and active power consumption or generation for a certain amount of time depending on the cause of the congestion. In the yellow traffic light phase, the REMS only uses tariff changes that are financially beneficial for the addressed buildings compared to the default tariffs. In the red traffic light phase, tariffs that are not beneficial are used as well so that the available flexibility is exploited more comprehensively. The architecture of the REMS for the development status in [32] is shown in Figure 2.12.

The power-flow simulation capabilities are implemented as quasi-stationary power-flow studies that are periodically performed using the Newton-Raphson method with a configurable temporal resolution. In the power-flow studies, the voltages at the grid nodes and the currents on the grid lines are calculated from the active and reactive powers communicated by the buildings. To evaluate the co-simulation environment as well as the newly developed REMS, multiple reference scenarios were presented and used to parameterize the power-flow and building simulations. The power-flow simulation can be parameterized according to the reference grids (*rural*, *village*, and *suburban*). The analyzed building configurations (*today*, *tomorrow*, and *the day after tomorrow*) affect the equipment present in the buildings, for example, the prevalence and capacity of PV installations [32, 162]. An overview of the introduced reference grids is given in Table 2.2.

[1] *Bundesverband der Energie- und Wasserwirtschaft e. V.* (English: German Association of Energy and Water Industries)

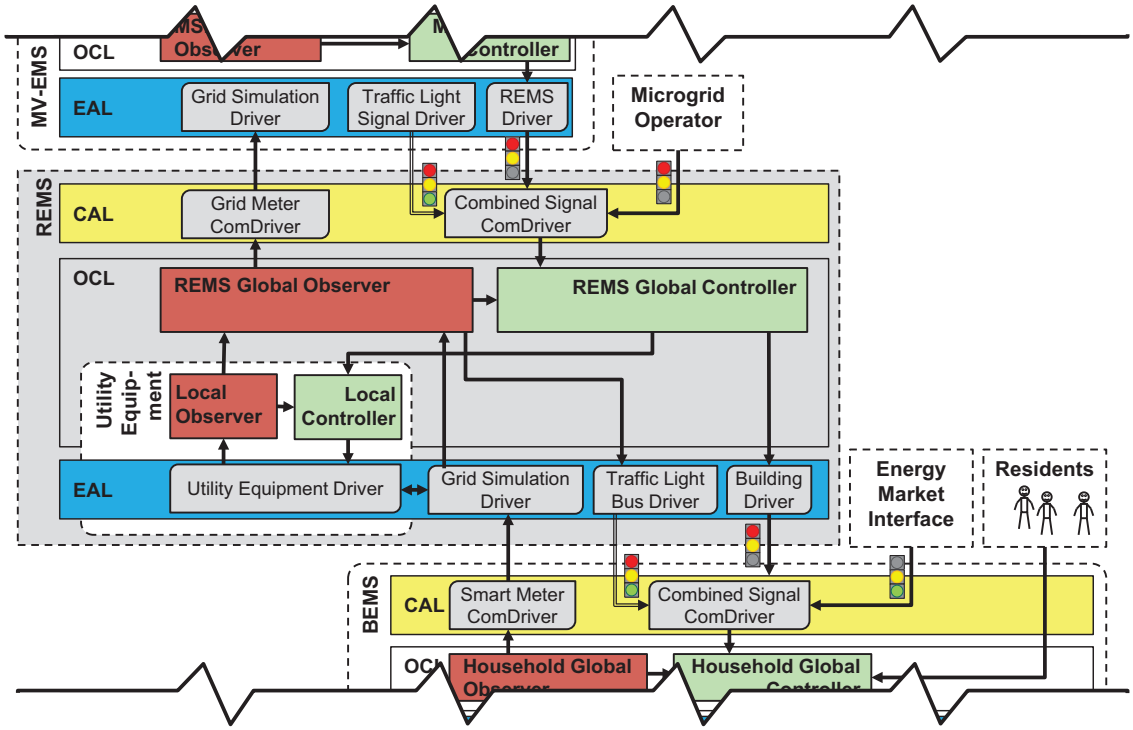

Figure 2.12: Overview of the REMS architecture utilizing the extended generic O/C architecture [32]. "MV-EMS": Medium voltage energy management system. "OCL": Observer/Controller layer. "EAL": entity abstraction layer. "CAL": communication abstraction layer. Reproduced from [32].

Using the different reference scenarios, the effect of the REMS on grid operation was evaluated. The results showed that uncoordinated optimization with regard to user objectives already had a small positive effect on the grid status. The REMS, however, could resolve red traffic light phases to a large extent and reduce the occurrence of yellow traffic light phases [32].

2.5. Electricity Grid Operation

This section introduces the basics of electricity transmission and distribution before focusing on the components, specifications, as well as the control technology and mechanisms specific to distribution grids.

2.5.1. Electricity Grid Levels

Besides a growing number of long-range high-voltage direct current (HVDC) links ([163]), European electricity grids usually utilize alternating current and are divided into four voltage levels, namely *extra high voltage*, *high voltage*, *medium voltage* and *low voltage*. Extra high voltage (380 kV or 220 kV) is used in transmission grids, which transfer electricity

Table 2.2: Overview of the characteristics of the reference grids in [32]. GCP: grid connection point, corresponds to the number of connected buildings. Reproduced and translated from [32].

	Rural grid	**Village grid**	**Suburban grid**
		Topology	
Topology	Radial	Radial	(Open) rings, radial
Feeders	2	5	8
Nodes	14	62	136
GCPs	11	55	130
Distributing cabinets	1	5	4
Secondary lines	1	5	5
		Lines	
Connections	Overhead line	Buried cable	Buried cable
Line type	70-AL1/11-ST1A	NAYY 4x150 SE	NAYY 4x150 SE
Average length	53 m	34 m	15 m
		Transformer	
Type	VRDT	VRDT	VRDT
Nominal power	250 kVA	400 kVA	630 kVA

over long distances using meshed topologies. These grids are fed by thermal power plants and large wind parks and feed the downstream high voltage grids. High voltage (110 kV) grids are subtransmission grids that are fed by upstream extra high voltage grids and transfer electricity to DSOs and other large customers, such as industrial companies, hospitals, or universities. They mostly use radial topologies and have a similar function as medium- and low-voltage grids, but for longer distances. Medium voltage (10 kV or 20 kV) is used in primary and secondary distribution grids, which are fed by upstream high voltage grids and transfer electricity from substations that transform high into medium voltage to distribution and load-center substations as well as industrial customers. Low-voltage (0.4 kV or 0.6 kV) distribution grids transfer electricity between medium voltage grids and final customers [7].

Transmission and distribution grids usually use three-phase alternating current, due to several advantages over single-phase alternating or direct current. Alternating current instead of direct current enables transformability as well as simpler switch technology. The transformability is exploited to transfer electricity using high voltages and low currents, which enables low energy losses. To achieve this, power transformers are utilized to connect the different voltage levels and transform higher to lower voltage and vice versa. Three phases instead of a single phase enable the construction and use of robust and

inexpensive asynchronous motors, the generation and transmission of constant active power, the saving of conductor material, and lower energy losses. Another advantage are the two different achievable voltages levels (230 V and 400 V) in distribution grids, which can be used for different use cases [7]. However, for very long-range electricity transmission, high-voltage direct current (HVDC) transmission can be more efficient than high-voltage alternating current (HVAC) transmission. HVDC incurs lower energy losses as it is not affected by capacitive and reactive charging effects, which occur for HVAC and have to be compensated by additional grid equipment. HVDC also requires fewer cables and smaller cross-sectional areas for these cables. HVDC incurs higher fixed costs compared to HVAC due to the expensive rectifier and inverter stations needed to convert alternating current to direct current and vice versa. However, these fixed costs become less relevant the longer the transmission lines are, while the additional grid equipment needed to keep losses low for HVAC becomes costlier for longer lines [163]. German examples of long-range HVDC links are Nordlink [164] and Südlink [165]. Nordlink is a HVDC connection between Germany and Norway with a capacity of 1.4 GW at 525 kV. It was commissioned in 2021 and is composed of 54 km of buried cable as well 516 km of undersea cable. Südlink is an inner-German HVDC connection between the south and north of the country. It will carry 2 GW at 525 kV and be composed of 693 km of buried cable. It is currently under construction with its commission planned for 2028.

2.5.2. Low-Voltage Electricity Distribution Grid Topologies, Equipment, and Specifications

Low-voltage electricity distribution grids for residential areas can have radial, ring or meshed topologies. The latter provide advantages with regard to voltage maintenance, load balancing, and security of supply. However, currently, mostly radial topologies are used due to their clear and simple operating mode [7].

Electricity grids are made up of different interconnected equipment. Low-voltage distribution grids comprise transformers, lines, distributing cabinets, as well as protection and control equipment, such as circuit breakers, VRDTs, and linear regulators [7].

Distribution transformers transform electricity supplied by medium voltage grids (10 or 20 kV) to low voltage (230 V or 400 V) utilized by buildings. In general, transformers leverage electromagnetic induction to transform voltages according to the ratio of the respective number of turns of the primary and secondary windings. If the number of turns of the primary windings is higher than that of the secondary windings, the voltage on the secondary windings is lower or vice versa. If the transformer is voltage-regulated, the transmission ratio can be changed to different discrete values inside a certain range around the transmission ratio for the nominal voltages. This is done via tap changers, which enable the tapping of different turns of the primary and secondary windings [7].

[166] specifies maximum temperatures and currents for distribution transformers. The specified limits for normal cyclical load are given in Table 2.3.

Table 2.3: Current and temperature limits for distribution transformers under normal cyclical load according to [166]. Reproduced, shortened, and translated from [166].

Limit type	Value
Current (relative to rated current)	1.5
Hot-spot temperature of the winding and of metal parts, which are in contact with cellulosic insulation	120 °C
Hot-spot temperature of other metal parts (in contact with oil, aramide paper, fiberglass)	140 °C
Temperature of the top oil layer	105 °C

According to [167], the voltage in low-voltage distribution grids has to stay inside a range of +/-10 % around the nominal voltage at all times. [168] further specifies that, during undisturbed operation of the grid, the amount of slow voltage change caused by all electricity generation and storage devices with grid connection points (GCPs) within a particular low-voltage grid must not exceed 3 % at any node in this grid compared to the voltage without electricity generation and storage devices. However, the DSO can permit deviations from this value, for example, if a voltage-regulated distribution transformer is used.

Distribution grid lines are either deployed as overhead or buried lines and typically follow the streets connecting the local buildings [7]. For lines, the rated currents are specified by the manufacturer and vary among different types and dimensionings.

2.5.3. Grid Management in Distribution Grids

To ensure reliable grid operation and to comply with the permitted voltage ranges, load and temperature limits referenced in Section 2.5.2, different measures can be taken by DSOs.

In the context of the ongoing integration of decentralized electricity generation, voltage maintenance, which, before the start of the energy transition, was almost exclusively handled on the higher grid levels, becomes increasingly important on the low-voltage level as well. In distribution grids, voltage maintenance can be handled using VRDTs (see also Section 2.5.2), linear regulators, the absorption or injection of reactive power, as well as electricity consumption and generation management. Since the absorption or injection of reactive power is linked to the node voltages of a grid, it can be used to keep the voltage inside the acceptable range. This can be done using dedicated reactive power systems, but also by utilizing the reactive power provision capabilities of modern PV inverters (see also Section 2.3) [7].

Different modes of operation are possible when it comes to the absorption or injection of reactive power by PV inverters. The most commonly implemented mode is a static ratio of the active and reactive power provided by an inverter determined by the power factor $\cos(\varphi)$. The use of a voltage depended reactive power control, often called *Q(U)*-control, where a *Q(U)*-curve is used to determine the reactive power to be absorbed or injected depending on the local node voltage, is possible as well. Since the node voltages differ depending on the position in the grid, this leads to a situation in which some inverters have to provide more reactive power than others. Another option is the absorption or injection of reactive power according to a $\cos(\varphi)(P)$-curve, where the $\cos(\varphi)$ is determined according to the currently generated active power [168].

Especially generation and consumption management require the presence of a sufficient number of sensors in the managed grid, which allow the calculation of the grid status with the necessary accuracy. An appropriate smart meter infrastructure (see also Section 2.6.3) can provide the information needed to achieve comprehensive knowledge about the grid utilization at all times [7]. While the term DSM is often used for electricity consumption management, for example, in [7], in the context of this thesis, the DSM definition given in [67] is used, which includes generation management as well. This definition comprises all measures that can be taken to influence the consumption and generation behavior of the electricity demand side. It includes static measures such as energy taxes, dynamic measures such as time-variable electricity tariffs, as well as more invasive measures such as load curtailment, load shedding, and direct load control. In this thesis, the definition is extended by the implementation of target load profiles, which can be seen as more invasive than time-variable tariffs, but less invasive than direct load control. In the context of distribution grid management, DSM can make use of the flexibility provided by devices such as the ones described in Section 2.3 to stabilize the discrepancy between local electricity generation and consumption (also called *residual load*) and thereby prevent or reduce grid congestion. Highly invasive measures such as load curtailment or shedding should only be used if other options have already been exploited without fully resolving a critical grid status [7]. Another way to remedy grid congestion is reactive power compensation, which we describe in Section 2.3.

2.6. Smart Grids

The enhancement of an electricity grid with information and communication technology (ICT) for the purpose of facilitating the effective integration of (renewable) energy generation on the distribution grid level creates a system that is commonly called *smart grid* [5]. In the following, the differences between the related concepts of conventional electricity grids, smart grids, microgrids, and nanogrids are explained before the functionality and use cases of smart grids and smart meter infrastructures are detailed.

2.6.1. Differentiation

Before the energy transition, electricity distribution grids were relatively simple to operate. Unidirectional energy flows and almost exclusively consumption-based load required only rough monitoring and simplified load forecasting. Voltage maintenance and congestion prevention were tasks that were limited to transmission grids and realized by redispatching conventional thermal power plants and switching operations using *supervisory control and data acquisition* (SCADA) as well as power plant and network control technology. The increasing installation of DERs as well as the electrification of the mobility and heating sectors drastically change the load characteristics of distribution grids, which entails an increasing need for monitoring, control, and communication infrastructure on the lower voltage levels as well [7].

To meet the aforementioned challenges, distribution grids have to be equipped with sensors as well as ICT and thus transformed into smart grids. The additional system intelligence can be used to gather comprehensive knowledge on the grid status and implement appropriate DSM (see also Section 2.5.3) measures. Furthermore, the data collected by a smart grid can enable electricity customers to gain useful information on their electricity profile and, consequently, provide them with possibilities to change their behavior with the goal of reducing their electricity costs [6].

Another concept in the context of smart grids is the *microgrid*. Microgrids are small scale distribution grids that comprise various distributed electricity consuming and generating components that are locally managed so that they behave as single entities from the points of view of both the market and the superordinate grid. A key differentiating factor compared to conventional grids and the broader concept of smart grids is the ability of a microgrid to operate in a grid connected as well as an islanded mode, where local consumption and generation are fully balanced [169].

Another term, which is related to the concept of microgrids, is the *nanogrid*. According to the definition given in [170], a nanogrid has the same characteristics as a microgrid, but is confined to an individual building, such as a single family home. Consequently, a microgrid can comprise multiple nanogrids.

2.6.2. Use Cases and Frameworks

The transition of conventional electricity grids to smart grids provides a plethora of new capabilities to increase the efficiency, safety, quality, and resilience of the energy system as well as the necessary prerequisites for the energy transition to renewable energy sources. By utilizing ICT, a smart grid makes power flows visible even at the lowest levels, which enables customers to make informed decisions about their electricity consumption and generation and partake in electricity markets, for example, by enabling the implementation and accounting of time-variable electricity tariffs. It accommodates large power plants as well as decentralized generation and storage by allowing the active management of electricity supply and demand according to the current needs of electricity consumers and

availability of electricity generation and storage capacities. The information provided by a smart grid can be used to reduce peak loads and congestion as well, by enabling customers to shift parts of their consumption to times of lower electricity demand. Smart grids also provide the requisites for timely and even predictive maintenance by continuously gathering equipment data, which increases the reliability of the electrical infrastructure and reduces its operating costs. Electricity costs can be decreased by appropriately controlling equipment to reduce energy losses, while power quality can be adjusted to the specific needs of different end customers. Furthermore, smart grids make it possible to react quickly to problematic internal events, such as equipment faults, and external events, such as lightning. The timely detection of such events enables the reconfiguration of grids to prevent larger outages [171].

There have been several initiatives in different regions of the world proposing frameworks and architectures for the implementation of smart grid infrastructure.

In the US, the *Electric Power Research Institute* and the *Electricity Innovation Institute* released the *Integrated Energy and Communication Systems Architecture* (IECSA) in 2003, spanning four volumes [172–175]. Although it did not yet use the term smart grid, the IECSA provides plans and concepts aimed at integrating information infrastructure into the energy system to enable distributed and renewable electricity generation, customer participation, as well as comprehensive grid automation, monitoring and control measures. In 2008, *The GridWise Architecture Council* released the *GridWise Interoperability Context-Setting Framework* to provide a basis for discussing interoperability issues between different entities of the energy system in the context of smart grid implementation [176]. The *IEEE Guide for Smart Grid Interoperability of Energy Technology and Information Technology Operation with the Electric Power System (EPS), End-Use Applications, and Loads* was released in 2011 [177]. Among other things, it establishes the smart grid interoperability reference model (SGIRM), a design tool giving architectural direction for the implementation of smart grids considering the three perspectives *power systems*, *communications*, and *information technology*. Starting in 2017, the *U. S. Department of Energy* released the four-volume *Modern Distribution Grid* report [178–181]. It is aimed at providing a consistent understanding of the requirements of a modern distribution grid. While it does not mention the term smart grid often, its scope is consistent with typical smart grid characteristics, such as situational awareness, controllability, management of DERs, and resilience. First released in 2010 and updated to its latest version 4.0 in 2021, the *NIST Framework and Roadmap for Smart Grid Interoperability Standards* by the *National Institute of Standards and Technology* provides a conceptual model, an ontology, and implementation methods for smart grids aimed at achieving interoperability, cybersecurity, and a common language between stakeholders [182, 183].

In China, similar frameworks to promote and aid smart grid development have been released over the previous decade. In 2015, *Guidelines on the Promotion of Smart Grids Development* where released by the *National Development and Reform Commission* (NDRC) and the *National Energy Administration* (NEA) [184]. They give instructions on how to implement smart grids to achieve improved efficiency, automation, reliability, safety, and integration of renewables and storage in transmission as well as distribution grids.

The NDRC, the NEA, and the *Ministry of Industry and Information Technology* released *Guidelines for Promoting 'Internet+' Smart Energy Development* in 2016 [185]. In addition to promoting smart grid implementation, these guidelines lay out an *Energy Internet*, which represents a deep integration of the energy system and the Internet. A strategic study of the *Chinese Academy of Engineering*, the *Theoretical Framework and Key Technologies of Transparent Power Grid*, was published in 2022 [186]. The study extends on the 'Internet+' Smart Energy concept and proposes the *Transparent Power Grid*, which is built on the four architecture layers *perception* (that is, measurements), *network*, *platform*, and *application*.

In Europe, the *CEN-CENELEC-ETSI Smart Grid Coordination Group* released a series of documents from 2012 to 2014 providing support for smart grid implementation and standardization [187–194]. One of the main achievements of this initiative was the creation of the *Smart Grid Architecture Model* (SGAM) framework (see also Figure 2.13). The SGAM comprises the three dimensions *interoperability layers*, *domains*, and *zones*, with several layers each. This enables categorizing the processes, products, and operations in the energy system as well as highlighting their potential interdependencies and aligning them with the corresponding standards.

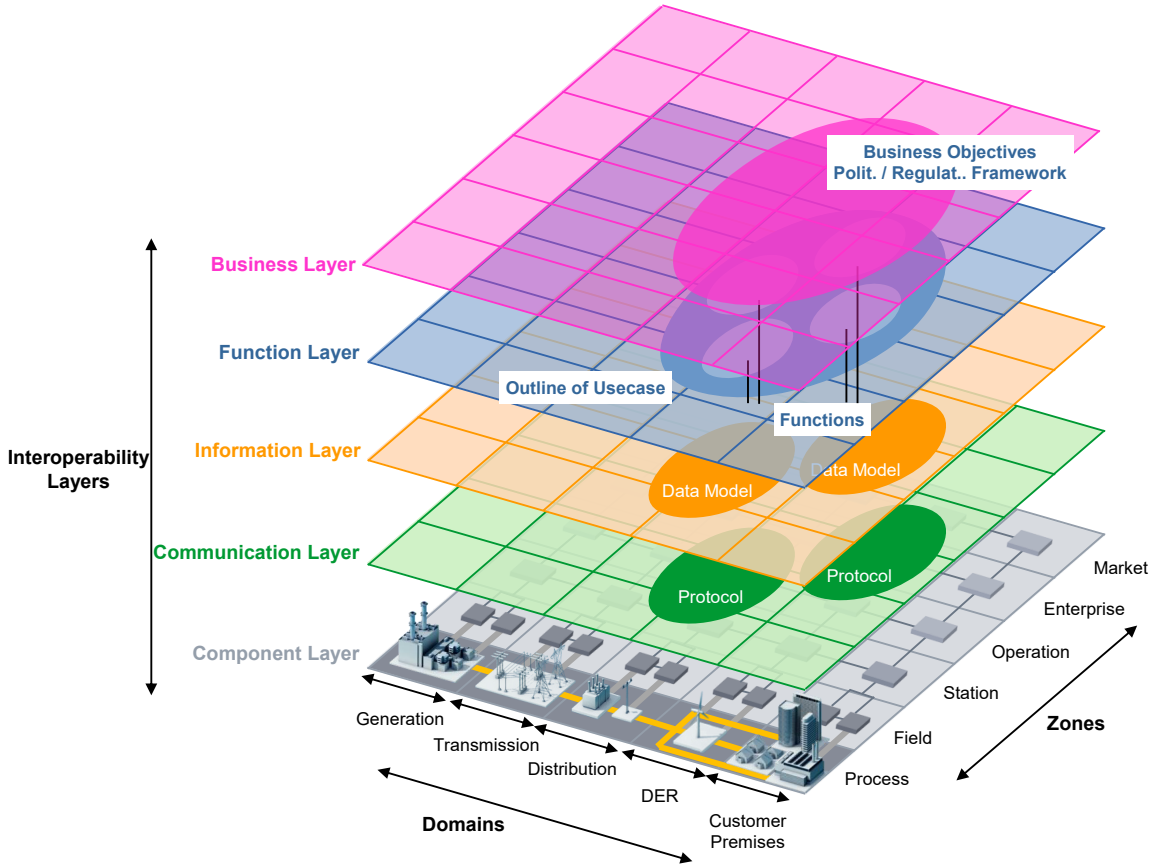

Figure 2.13: Diagram of the Smart Grid Architecture Model (SGAM) framework. Reproduced from [187].

Using the SGAM as a point of reference, the adaptive grid management system developed in this thesis maps to the component, communication, information, and function layers

on the interoperability dimension. In the domains dimension, the system touches the distribution, DER, and customer premises layers. Furthermore, it can be placed in the process, field, station, and operation layers in the zones dimension.

For the European Union (EU) specifically, the *EU DSO Entity* has been established in 2021 [195]. Similar to the *European Network of Transmission System Operators for Electricity* (ENTSO-E, [196]) for transmission system operators (TSOs), the EU DSO Entity is an EU-mandated organization of European DSOs of all sizes. Its main objectives are the development of network codes and guidelines for distribution grids, the strengthening of DSO-TSO cooperation, and the sharing of best practices among DSOs. Together with the ENTSO-E, it submitted the *Joint Network Code on Demand Response* to facilitate access of DERs to electricity markets, to guide the development of common rules, and to define market-based mechanisms to extract demand side flexibility [197]. Furthermore, the two organizations launched the data platform *Joint Working Group Data Interoperability Repository*, which provides a repository of national practices, reference models, and development support for harmonized data models across Europe [198]. Both of these efforts are essential for the implementation of coherent European smart grids.

In Germany, the *traffic light concept* was introduced by the BDEW in 2013 [199] and formalized as the *BDEW Smart Grid Traffic Light Concept* in 2015 [161]. It was subsequently used by other European initiatives, such as the *Universal Smart Energy Framework* [200]. The concept aims at coordinating the responses of DSOs to predicted or actual distribution grid congestion and comprises three traffic light phases. In the green phase, unconstrained market-based energy flexibility use is the modus operandi. In the yellow/amber phase, a DSO predicts future grid congestion and leverages the flexibility of DERs to prevent it, preferably in the most cost-efficient manner. In the red phase, the grid status is already critical, so that a DSO has to resort to more drastic measures, such as consumption or generation curtailment, to prevent the grid status from deteriorating further. Although not explicitly linked to the traffic light concept by German law makers, §14c and §14a of the newest iteration of the German *Energiewirtschaftsgesetz* (EnWG, English: Energy Industry Act) [201] provide a legal basis for DSOs to implement the previously described measures for the yellow/amber and red traffic light phases respectively.

The work by Kochanneck [32], on which this thesis partially builds, proposes its own formulation of the traffic light concept. In this formulation, the yellow/amber phase involves temporary, end-consumer-favorable electricity tariff adjustments to incentivize grid-supportive behavior, while the red phase allowed for unfavorable tariff adjustments as well (see also Section 2.4.2). Our approach with regard to the traffic light concept differs from the one utilized in [32], in that we do not explicitly differentiate between yellow/amber and red traffic light phases. We prefer the use of less invasive measures, such as reactive power and active power flexibility use, over more invasive measures, such as PV curtailment, as well. However, we partially uphold grid-topology- and grid-equipment-specific apparent power limits for PV curtailment even during times that could be considered green or yellow/amber phases, to prevent sudden violations of grid equipment or user device specifications, which can be caused by spikes in PV generation. Nevertheless, these apparent power limits only affect PV system operation in situations, in

which the grid status would become critical otherwise. Furthermore, we do not directly use electricity tariff adjustments to incentivize grid-supportive building behavior. However, we do employ short-term feed-in remuneration adjustments after grid-supportive active power flexibility use. These temporary adjustments incentivize buildings to discharge their BESS, which increases the usable active power flexibility for the next critical grid status. For detailed information on our approach see Section 4.5.

2.6.3. Smart Meter Infrastructure

A key element in the implementation of smart grids is the smart meter. A smart meter is a digital electricity meter that collects electrical data with a relatively high temporal resolution (minutely to hourly) and provides interfaces for the communication of this data to different stakeholders, such as DSOs, energy providers, and electricity customers. It may also provide bidirectional communication, so that external information such as time-variable electricity tariffs can be received as well. Smart meters are installed for multiple, partly overlapping reasons. They make the status of distribution grids visible with a high accuracy and resolution, enable the implementation of DSM measures (see also Section 2.5.3), provide detailed electrical load profiles to customers, and enable the market participation of small electricity prosumers [4]. The architecture of a smart meter according to [4] is shown in Figure 2.14.

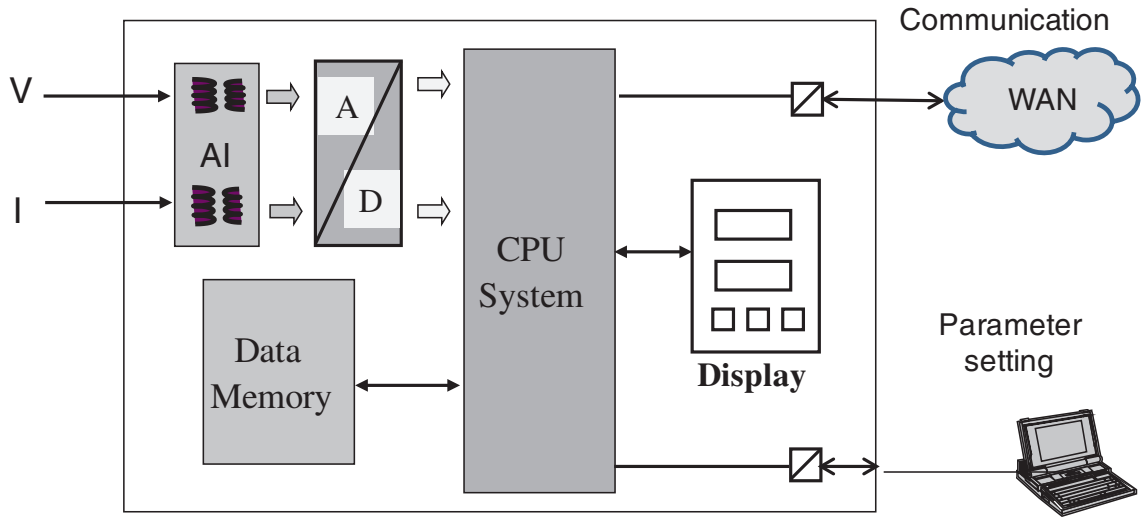

Figure 2.14: Architecture of a smart meter according to [4]. V: voltage, I: current. Reproduced from [4].

The adoption of smart meters varies substantially among different countries. In Europe, countries such as Germany [202] still have relatively low adoption rates, while the prevalence of smart meters is already relatively high in other countries, such as Italy [203], Estonia [204], and Scandinavia [205]. According to [205], smart meters achieved a penetration of 43 % of the global electricity meter market in late 2023. The North American

region had the most mature market at 77 %, followed by the Asia-Pacific region at 49 %, largely driven by roll-outs in China and Japan, and Europe at 47 %. The global smart meter adoption for the fourth quarter of 2023 according to [205] is shown in Figures 2.15 and 2.16.

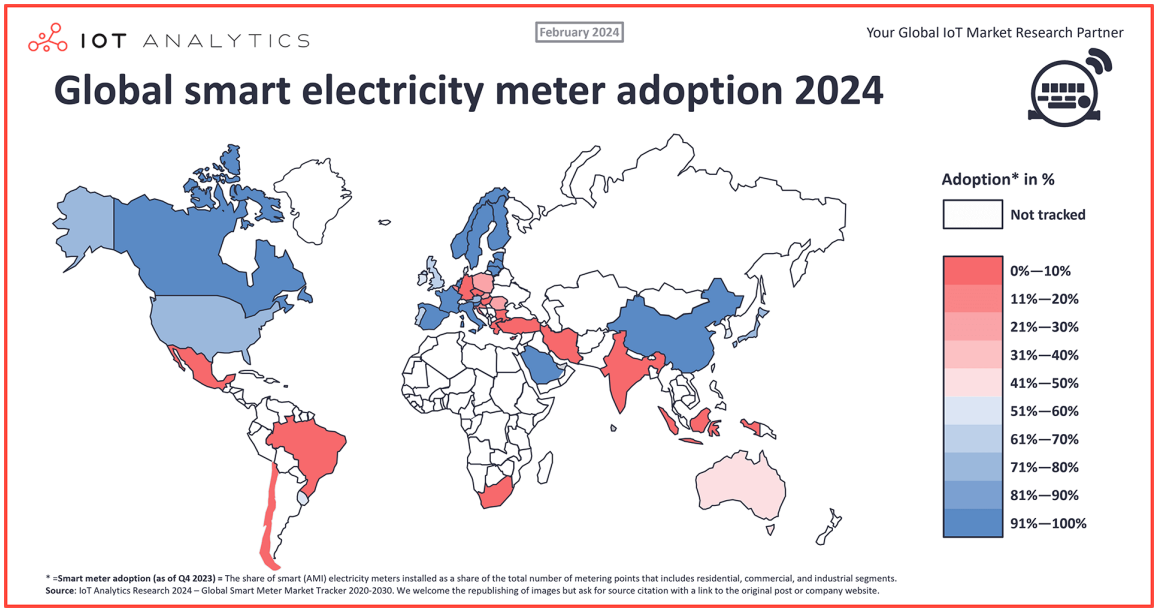

Figure 2.15: "Global smart electricity meter adoption 2024" [205]. Reproduced from [205].

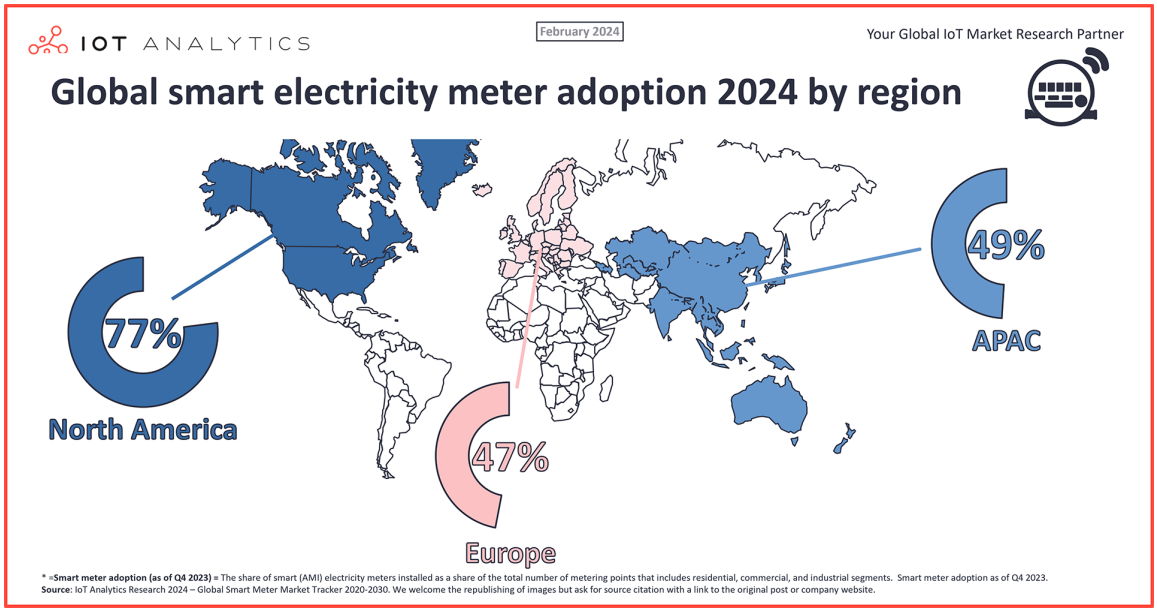

Figure 2.16: "Global smart electricity meter adoption 2024 by region" [205]. Reproduced from [205].

In the future, the adoption of smart meters is expected to increase substantially. According to [206], Europe is expected to reach a smart meter penetration of up to 80 % by 2029. In the US and Canada, smart meter penetration is expected to reach 94 % and 96 %, respectively, in 2029 [207].

The German smart meter infrastructure puts a significant emphasis on security, data protection, and interoperability. Consequently, one or more smart meters can be combined with *smart meter gateways* (SMGWs). Together they form the *intelligentes Messsystem* (iMSys, English: smart metering system), in which the smart meters are the energy data gathering components and the SMGW is the communication component. The latter has to be certified by the *Bundesamt für Sicherheit in der Informationstechnik* (English: German Federal Office for Information Security) to ensure its compliance with security- and interoperability-related, as well as technical requirements [208].

The SMGW communicates via the local metrological network (LMN), the home area network (HAN), and the wide area network (WAN) [209]:

- **LMN**: The LMN comprises the smart meters, not only for electricity, but also for gas, water, and thermal energy if present.
- **HAN**: The HAN comprises local communication adapters and control systems for controllable energy consuming or generating devices, EMSs, or other value-added services. Such devices, systems, and services are denoted as *controllable local systems* (CLSs). Service technicians and end customers can use the HAN to communicate with the SMGW as well.
- **WAN**: The WAN enables the communication with *external market participants* (EMTs, German: externe Marktteilnehmer) and the *smart meter gateway administrator* (GWA). EMTs can be DSOs, energy providers, metering point operators, or other authorized service providers.

A diagram of the processing of meter measurements by an SMGW according to [210] is given in Figure 2.17.

Until the release of the technical guideline *BSI TR-03109-1, Version 2.0*[2] German SMGWs were primarily mandated to implement the tracking of active energy in 15-minute intervals according to *TAF7*[3] [209, 211, 212]. SMGWs certified according to version 2.0 are also mandated to support *TAF10*[4], among others [209]. This TAF enables the handling and communication of instantaneous measurement values for active power, phase angle (which enables the calculation of reactive power), voltage, and others at temporal resolutions ≤ 60s. The underlying smart meters are capable of measuring and providing these values if they implement optional, so called *Grid-Funktionen* (English: grid functions) [213]. This means the German smart meter infrastructure can potentially provide the necessary data points and resolutions to enable the implementation of the adaptive grid management system presented in this thesis. However, if the smart meter does not support grid functions, it would have to be upgraded or replaced. Furthermore, if the SMGW is an older model, the

[2] Technische Richtlinie BSI TR-03109-1: Anforderungen an die Interoperabilität der Kommunikationseinheit eines intelligenten Messsystems (English: Technical Guideline BSI TR-03109-1: Requirements for the Interoperability of the Communication Unit of a Smart Metering System)

[3] Tarifanwendungsfall 7 “Zählerstandsgangmessung” (TAF7, English: Tariff use case 7 "Meter reading profile")

[4] TAF10 “Abruf von Netzzustandsdaten” (English: "Retrieval of grid status data")

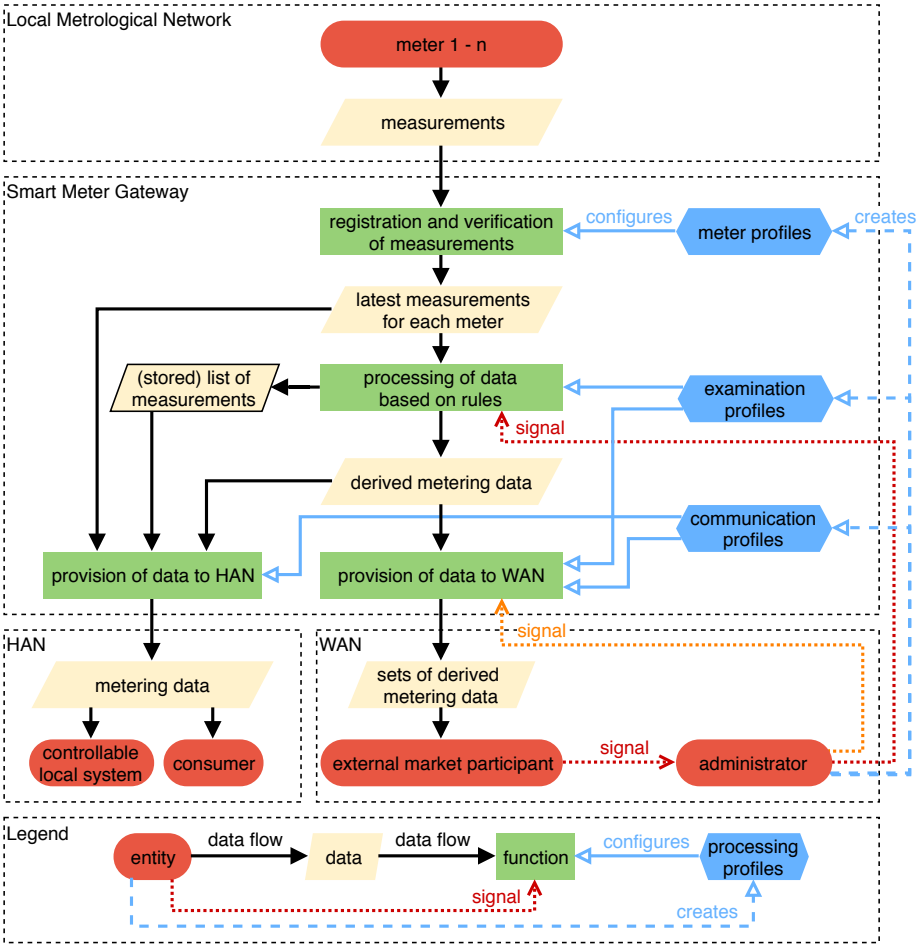

Figure 2.17: "The processing of meter measurements by a Smart Meter Gateway" [210]. "HAN": home area network, "WAN": wide area network. Reproduced from [210], based on [211].

communication of the relevant data points with a high resolution according to TAF10 may not be possible. In this case, the real-world implementation of the presented system may require the direct readout of smart meters via their optical ports and the communication of the gathered data without using an SMGW. Alternatively, the SMGW could be upgraded with a firmware update or replaced with a newer model.

2.7. Resilient Infrastructure

In this section, we introduce different resilience definitions from the literature for technical systems in general as well as for electricity grids specifically. Subsequently, an overview of potential disturbances in electricity grids as well as the associated ICT infrastructures is given. It is important to note that terms, such as resilience, robustness, and stability, can be defined differently in different disciplines and areas of research. For example, the research initiative Organic Computing utilizes a specific robustness definition (see also

Section 2.1), which can deviate from the electricity-grid-specific definitions cited in the following.

2.7.1. Technical Systems

The concept of resilience touches many different areas of life and research. The following general definition of resilience is given in [214]:

> *Numerous definitions of resilience exist within different research traditions, disciplines, and fields such as sociology, psychology, medicine, engineering, economics, ecology, political science [7–11]*[[215–219]]. *The common use of the resilience concept relates to the ability of an entity, individuals [sic], community, or system to return to normal condition or functioning after the occurrence of an event that disturbs its state.*

The articles quoted by [214] ([215–219]) collect numerous definitions of resilience in various contexts from the literature. However, the definition given by Erik Hollnagel, which he describes as a "logical continuation" of different definitions developed during his extensive work in the field of resilience engineering and is "not yet documented in a book" [220], fits closely to the scope of this thesis:

> *A system is resilient if it can adjust its functioning prior to, during, or following events (changes, disturbances, and opportunities), and thereby sustain required operations under both expected and unexpected conditions.*

2.7.2. Electricity Grids

While the resilience definitions given in Section 2.7.1 can be applied to electricity grids as well, there are many different definitions specific to electricity grids and energy systems in the literature. The term resilience is often used in the context of low probability, high impact events, such as natural disasters [221–223] and cyber or physical attacks [224–226], their impacts on power grids, as well as suitable mitigation and recovery strategies.

A definition of cyber-physical resilience in power systems that accounts for the interdependencies between electricity grids and ICT infrastructure (see also Section 2.6) is given in [227]:

> *Power system cyber-physical resilience is the system's ability to maintain continuous electricity flow to customers given a certain load prioritization scheme. A resilient power system responds to cyber-physical disturbances in real-time or semi real-time, avoiding interruptions of critical services. A resilient power system alters its structure, loads, and resources in an agile way.*

For power systems, Arghandeh et al. [227] distinguish between resilience, reliability, robustness, and stability. Their respective definitions for the latter three concepts are given in the following:

> *Robustness is the ability of a system to cope with a given set of disturbances and maintain its functionality.*
>
> *Reliability is the ability of the power system to deliver electricity to customers with acceptable quality and in the amount desired while maintaining grid functionality even when failures occur [50,51]*[[228],[229]].
>
> *Stability is the ability of a system to remain intact after being subjected to small perturbations [54]*[[230]].

Considering these definitions, it is not clear, which of these concepts fit best into the context of this thesis. The adaptive use of different grid management strategies in response to disruption of the utilized ICT infrastructure or participant misconduct falls explicitly into the given definition of power system cyber-physical resilience. However, the assignment of the utility provided by the individual grid management strategies in this thesis to one of the presented definitions is less intuitive. Since the goal of all grid management strategies we utilize is the continuous adherence to given temperature or current limits as well as voltage ranges and the types and causes of the considered electrical disturbances are known, the definitions of robustness, reliability, or stability appear more fitting. However, Arghandeh et al. [227] also mention that:

> *Robustness and resilience belong to two different design philosophies. Robustness is concerned with strength, whereas resilience is concerned with flexibility.*

Since our grid management strategies preferentially use energy flexibility to mitigate electrical disturbances and prevent electricity outages as well as equipment damage without extending or strengthening existing grids, resilience would be a better match from this perspective. Arghandeh et al. [227] further determine that:

> *Discussions of resilience often center around a system survivability that leverages load shedding, generation outages, and other actions. Reliability is a measure of the system's ability to serve all loads. The system's ability to serve loads is traditionally referred to as service availability, which falls under the power systems definition of reliability.*

From this point of view, the individual management strategies developed in this thesis provide increased reliability rather than resilience. Concerning the differentiation between stability and resilience or robustness, Arghandeh et al. [227] write that:

> *In power systems, stability for a given initial operating condition means the system will regain operation equilibrium state after small perturbations. [...] In order to be robust and resilient, the electric grid has to be able to cope with small disturbances as well as major equipment failures, man-made attacks, and natural disasters [54]*[[230]].

If congestion scenarios that originate from within the electricity grid are viewed as small perturbations, which is not clear from the descriptions given in [227], the concept of stability would also fit the functionality of the individual grid management strategies in this thesis.

Given the aforementioned definitions and descriptions, our grid management system increases the resilience of electricity distribution grids against internal or external events that disturb their adjacent ICT infrastructure or entail participant misconduct. It furthermore improves grid operation with respect to electrical disturbances stemming from within a given grid. Since the latter includes the use of energy flexibility and emergency measures, such as PV generation curtailment, to prevent equipment failure and electricity outages, but does not consider the recovery after previous outages, the system touches resilience, reliability, as well as stability.

2.7.3. Electrical Disturbances

Some text passages of this section are transferred verbatim from one of our own publications [33]. For a summary of this publication, its relation to this thesis, and its mapping to our research questions, see Section 1.4.

The types of electrical disturbance considered in this thesis are the imminent overloading of lines, the imminent overheating of transformers, and voltages that threaten to exceed or fall below the permitted range. Respective specifications for the relevant quantities are given in Section 2.5.2. Overheating due to prolonged exceedance of the rated power of a transformer decreases the working life of the transformer. This can entail financial losses and even electricity outages caused by premature equipment failure [166]. Violations of the permitted voltage range can entail electricity outages and damage to devices connected to the grid [231]. The congestion of lines can trigger protective equipment, such as fuses, which can result in electricity outages and the need for manual repair [7].

Other types of disturbances, such as frequency-, flicker-, transient-, symmetry-, and harmonic-related problems [7], are not considered, as they are either not fully addressable from within a distribution grid or require grid monitoring and control with substantially higher spatial and temporal resolutions and responsiveness than typical smart meters and BEMSs can provide.

Electricity outages and electricity grid equipment damage caused directly by extreme weather events and accidental or deliberate physical destruction are out of scope for this thesis as well. Such damage would have to be manually repaired, which falls outside the capabilities of a software-based grid management system. However, disruptions of the ICT infrastructure, which can be caused by the aforementioned events, are considered. Furthermore, a grid management system such as the one presented can improve the detection of such events and consequently speed up the following restoration of grid operation.

2.7.4. Disturbances of Information and Communication Technology

The implementation of smart grid applications depends on ICT (see also Section 2.6), which may be error-prone and subject to different types of attacks. As a consequence, the reliable operation of electricity grids increasingly does not only depend on sufficiently dimensioned grid equipment, but on continuously available and undisturbed ICT infrastructure, which facilitates appropriate monitoring and control strategies, as well. Due to this, a new research area has emerged, which deals with disturbances and disruptions of the ICT infrastructure utilized to improve the operation of power systems, their effects on power system reliability, and mitigation strategies.

As described in [8], problematic data loss in smart grids can have numerous reasons, such as malfunctioning hardware and software systems or bandwidth and interference related problems.

In [9], the authors mention the possibility of cascading power failures affecting large grid areas due to communication errors in smaller regions. They give examples for ICT-induced or -magnified power system failures as well. Namely, a 2003 blackout in London caused by faulty alarm data [232], malfunctioning relay protection devices in the Chinese transmission grid in 2009 due to high latency and bit errors [233], and another 2003 power outage in the US and Canada, which was propagated due to the interruption of communications [234].

Thadikemalla et al. [10] emphasize the negative impact communication issues, such as radio interference, large transmission distances, and hardware malfunction, can have on state estimation in smart grids that are operated using wireless communication and provide a corresponding data loss mitigation mechanism.

A literature review on internet outages, not explicitly in the context of smart grids, was conducted in [235]. Among other things, the authors identify natural causes, human-oriented causes, and logical failures as the reasons for network outages. Given examples of natural causes are thunderstorms, hurricanes, and earth quakes. Power shortages are identified as a further possible reason. Human oriented causes can be censorship, unintentional misconduct, as well as physical and cyberattacks by terrorist or military organizations. The authors furthermore determine that:

> *Internet outages are inevitable, frequent, opaque, expensive, and poorly understood. They are inevitable because the perfect system is not achievable in practice since issues and threats can not be completely prevented, or their prevention can be economically unfeasible.*

They also identify a major challenge in the study of internet outages, which can potentially be transferred to any type of privately owned and operated ICT infrastructure:

> *[...] our understanding of Internet outages is severely weakened by the lack of data, information and collaboration from the network operators for which network outages represent a sensitive topic critical to their business.*

This makes it impossible to determine how prevalent failures in ICT infrastructures actually are, but enables the assumption that they occur more frequently than is currently known.

Liu et al. [11] put a focus on *quality of service* in the context of smart grid operation, which can potentially influence and compromise decision making processes. They further categorize cyber events in the ICT infrastructure, which can be intentionally introduced by malicious actors or occur due to hardware and software errors, into events concerning physical equipment, communication channels, applications, or data.

A review of research concerning the impacts of ICT malfunctions on power systems is provided in [12]. The authors identify several ICT-related challenges with regard to digitalized power systems. They determine that failures of individual ICT elements can lead to an inability to execute external commands, or provide information on the current system status, while network failures can hinder the communication of such commands or information, despite functioning ICT elements. Such ICT failures entail a loss of situational awareness and controllability, which increases the probability of failures in the power system. Besides technical malfunctions, the authors identify cyberattacks as well as environmental conditions as possible causes of failure in smart grids. As an example of an environmental influence, they mention increased noise levels in information transmission mediums due to topological and meteorological conditions. They identify denial of service attacks, false data injection, intrusion, phishing, sabotage, and terrorism as relevant in the context of attacks on the ICT infrastructure of smart grids.

Simou et al. [13] note that the increasing dependence of critical infrastructures, such as the energy system, on ICT makes these infrastructures more vulnerable to cyberattacks. They also refer to legislation aimed at increasing the cyber security of critical infrastructures, such as the European *Network and Information Security (NIS) Directive* [236] and the German *IT Security Act* [237].

An overview of possible cyberattacks on smart grids is provided in [14]. Here, different steps (reconnaissance, scanning, exploitation, and maintaining access) of the implementation of cyberattacks on smart grids are described in detail. Techniques such as traffic analysis, social engineering, viruses, denial of service attacks, replay attacks, and the implementation of backdoors are analyzed regarding their likelihood and effects on information security. Furthermore, possible attack detection methods, countermeasures, and forensic techniques to identify attackers are proposed.

2.8. Summary

With Organic Computing (OC), we first introduced the basic design philosophy for the adaptive grid management system developed in this thesis. We detailed the principles of OC, including the Observer/Controller (O/C) architecture, which enables our system to self-organize and self-adapt without external control. Subsequently, we presented the distributed energy resources (DERs) commonly found in modern residential buildings and discussed the respective energy flexibility each of them can provide when managed

by a building energy management system (BEMS). We then explained how and why a BEMS manages such DERs, gave several examples of open-source energy management systems, and detailed the Organic Smart Home (OSH), which is the BEMS we extend in Section 4 to implement the new grid management system. The OSH is based on a hierarchical implementation of the O/C architecture. After describing the way electricity grids are generally structured and managed, we introduced the concept of the smart grid. Among other things, smart grids enable the grid-supportive use of the flexibility provided by the DERs of residential buildings through the use of information and communication technology (ICT) but also make electricity grids vulnerable to ICT disturbances. The latter requires grid management systems to not only provide resilience with regard to electrical but ICT disturbances as well. We therefore concluded the section by providing an overview of existing definitions for resilient technical systems in general as well as resilient electricity grids in particular and analyzing the problems that can occur in electricity grids. The latter includes disturbances introduced by the mechanics of grid operation and use as well as disturbances of the adjacent ICT infrastructure utilized by a smart grid. While the discussed definitions provide the basis for our own definition of resilience inside the narrower scope of smart electricity distribution grids, the presented problems inform the development of the corresponding countermeasures our grid management system can utilize.

3. Related Work

The adaptive grid management system developed in this thesis combines two aspects. It provides measures against electrical disturbances using distributed energy resources (DERs) in smart buildings to prevent electricity outages and equipment failure in distribution grids. Furthermore, it employs grid management strategy adaptation to mitigate the effects of communication disruption, participant misconduct (system-internal or external due to cyberattacks), and sensor failure. This is why we limit the scope of this chapter to literature that meets all of the following conditions:

- Focus on distribution grids with at least partial DER penetration
- Consideration of (some) grid constraints (admissible voltage ranges, line capacities, or transformer capacities/temperatures)
- Consideration of failing communication, cyberattacks/misconduct, or sensor failure during grid operation

We do not consider literature with an explicit focus on any of the following topics:

- Transmission grids
- Islanded/off-grid microgrids
- Direct-current-grids
- Grid frequency control
- Islanding/electricity outage detection
- Strategies to perform cyberattacks
- Wind energy
- Load forecasting/prediction
- Grid status estimation with sparsely distributed sensors
- Electricity grid/communication network planning or construction
- Determination of vulnerable grid equipment, controllers, or sensors without providing problem detection or mitigation measures

We first analyze literature studying the impacts of cyberattacks and failing or lossy communication on the operation of actively managed distribution grids with DERs in Section 3.1 to assess the need for appropriate counter measures or fallback strategies. Following that, we give an overview of cyberattack detection methods in the context of distribution grids proposed in the literature in Section 3.2. Finally, we address and compare literature most closely related to our own research in Section 3.3. This covers publications that not only provide insights with regard to impacts and detection, but also provide strategies to uphold stable grid operation during and after communication disruption, cyberattacks/misconduct, or sensor failure. Part of the literature that could be classified as somewhat related to our thesis is already analyzed in Sections 2.4.2, 2.6.2, and 2.7 and therefore not discussed again in this section.

3.1. Impacts of Cyberattacks and Communication or Sensor Failure on Grid Operation

This section focuses on the potential impacts of cyberattacks and communication or sensor failure on the operation of actively managed distribution grids with DER penetration.

Most of the research regarding such grids concentrates on cyberattacks, while there are only few publications on the specific impact of communication or sensor problems, such as [238–240]. Chaojun et al. [238] address the impacts of communication disruption on the monitoring and control of electricity grids using remote terminal units (RTUs) in a supervisory control and data acquisition (SCADA) system. They note loss of observability, loss of load, overload of generators or transmission lines, and cascading effects through larger parts of the grid as possible impacts of communication disruption and suggest upgrading old communication equipment in RTUs as a mitigation measure. Dutton et al. [239] show that communication disruption in the context of the energy flow optimization of buildings with controllable DERs can lead to increases in energy costs for end consumers. Baptista et al. [240] find that communication or DER failure in the context of battery energy storage system (BESS) scheduling can cause degraded voltage conformity in distribution grids.

A substantially larger part of the existing research considers the impacts of cyberattacks on actively managed distribution grids. The most considered cyberattack type are false data injection attacks (FDIAs). Some publications focus on FDIAs exclusively [241–252]. Others also consider denial of service (DoS) attacks [253–259], attacks giving full access to DER control systems [260, 261], botnet attacks [262], jamming attacks [259], man in the middle (MITM) attacks [253, 254, 258, 259, 263–265], hijacking attacks [266], or multiple different attack types [253–256, 258, 259, 263, 266].

In the surveyed literature, voltage problems are the most commonly stated effects of cyberattacks on the monitoring and control infrastructure in electricity grids. These problems range from deviations from the nominal voltage that could potentially impact grid operation [241, 249, 251, 260], over phase imbalances [243], to violations of the

permitted voltage range [248, 257, 259, 261–263, 265], or even total system deterioration in the context of grid forming inverters [252] or microgrids [244].

The second most commonly noted impacts of cyberattacks are economical. The possible impacts comprise increased energy costs for end consumers [242], economic losses due to excessive power curtailment [263], increased demand response program costs for utilities or aggregators [245, 249], financial penalties to battery electric vehicle (BEV) charging cluster operators [266], and higher financial benefits generated with attacker-operated DERs by ignoring given restrictions [246].

Further impacts of cyberattacks stated in the literature encompass:

- Electricity outages [247, 258, 261, 264]
- Damage to equipment or triggering of protective equipment [258, 259, 261, 264]
- Frequency destabilization in microgrids [244, 245, 252, 259]
- Line congestion [255, 260, 262]
- Increased tap-changing operations of voltage-regulated transformers [243, 263, 265]
- Emergency load shedding [250, 255]
- Cascading failures [258]
- Reactive power imbalances [265]
- Concealment of congestion [242]
- Energy theft [258]
- Diminished performance of optimal power flow algorithms [249]
- Load profile alterations [253]
- Increases in power and energy demand [256]
- Wrong zone temperatures for smart buildings [256]

The diversity of possible cyberattacks and communication problems as well as their often substantial and sometimes catastrophic impacts on electricity grid operation strongly underline the need for cyber- and failure-resilient grid management systems such as the one presented and evaluated in this work.

3.2. Detection of Cyberattacks on Electricity Grids

During our search for publications related to our thesis, we found that a significant portion of the literature that matches the criteria presented at the beginning of this chapter is focused on detecting cyberattacks rather than providing methods to mitigate their effects. While this does not go as far as our approach, which provides such mitigation measures, the detection focused research is sufficiently closely related to our thesis to warrant a dedicated analysis. After carefully checking the publications gathered during our literature search with regard to their scope, we identified 25 publications that focus only on cyberattack detection. Note that this is not an exhaustive list.

To cluster the detection-focused publications, we searched for highly cited (100 citations or higher) surveys that may provide category suggestions for the presented detection methods. The authors of [267] cluster detection methods for FDIAs broadly into model-based and data-driven algorithms. They further separate model-based algorithms into estimation-based algorithms, either static or dynamic, and "others". The authors separate data-driven algorithms into machine learning methods, either supervised or unsupervised, data mining, and "others". In [268], machine learning methods for detecting FDIAs are clustered into classic supervised learning, classic unsupervised learning, and deep/reinforcement learning. The authors of [269] differentiate between host-based, network-based, and physics-based intrusion detection systems (IDSs). A host-based IDS detects attacks based on anomalies (for example in event logs) or signature problems on host systems such as servers or workstations. A network-based IDS detects attacks based on network-related information such as IP addresses or traffic volumes. Most relevant in the context of this thesis are the physics-based IDSs, which the authors cluster into data-driven, model-based, as well as data and model blended IDSs.

We analyzed the 25 collected detection-focused publications based on the aforementioned surveys and classified the presented detection methods into the following categories, which we loosely based on the category suggestions provided in the surveys. Note that these categories are non-exhaustive and that there may be other categorization approaches. Some publications fit into more than one category as they present hybrid or combined methods and are therefore cited multiple times.

Perturbation- or watermarking-based detection Control signals are slightly modified before their communication, either deterministically in perturbation-based detection [270, 271] or stochastically in watermarking-based detection [272, 273]. The modifications are only known to the defender, for example, a distribution system operator (DSO), and therefore hidden from the attacker. Using a physics-based model of the observed system, such as a linearized model of a microgrid [272], the corresponding system status can be estimated based on the modified control signal. If the estimated system status deviates from the measured system status by more than a predefined threshold, an attack can be assumed. The major advantage of these detection methods is that they do not require knowledge or training data on the performed attacks.

Statistical unsupervised anomaly detection Under normal operation, grid status data, such as voltages, follow a certain statistical distribution that can be estimated from historical measurements. These distributions provide thresholds that are used to determine whether a specific measurement is within a normal range or outside of it. If a measurement falls outside the normal range, a potential attack can be assumed. The methods in the literature are either model-based, where thresholds are derived from the statistical distribution of the differences between values predicted by the model and the actual measurements, or model-free, where thresholds are derived entirely from historical data [274–276]. Other methods learn what normal grid operation looks like using unsupervised anomaly models and assume attacks when an anomaly score exceeds a certain threshold [277]. The main advantage of these detection methods is that they do not require labeled training data. However, a skilled attacker may be able to modify measurements such that they do not deviate from historical value ranges but still have adverse effects on grid operation.

Supervised machine learning classifiers Machine learning classifiers, such as decision trees, support vector machines, or neural networks, are trained to differentiate between grid status data, such as node voltages, in attack scenarios as well as normal operation using labeled training data sets. The classifier regularly checks new measurements and flags any detected potential attack. The performance of these methods is highly dependent on the quality and comprehensiveness of the available data sets [278–286].

Deep learning reconstruction A deep neural network is trained to learn how grid status data behaves spatially and temporally under normal operation. The network encodes the input data and then decodes it so that the output data matches the input data as closely as possible. If a trained network receives grid status data obtained under an attack that modifies the measurements, the reproduction error becomes large since it is assumed that the network can only reproduce data obtained under normal operation. A large reproduction error is thus used as an indicator for a potential attack [287–289]. An advantage of this approach over supervised machine learning classifiers is that no data on attack scenarios is needed to train the neural networks.

Asset-specific detection Several publications present detection methods tailored to detect cyberattacks on specific devices, equipment, or applications. Basumatary et al. [276] use a nonlinear autoregressive exogenous input neural network to detect FDIAs that mimic the natural behavior of electric vehicle (EV) charging processes to circumvent other detection methods. Liu et al. [290] propose a detection framework for cyberattacks manipulating electricity prices for smart homes based on partially observable Markov decision processes. Abedi et al. [291] focus on cyber security and FDIA detection via model- and signal-based intrusion detection in the context of EV charging. Youssef et al. [292] present a detection method for load-altering attacks in the context of peak shaving with electric water heaters using a time-delay neural network. Warraich et al. [293] provide a machine-learning-based method to detect DoS attacks targeting ancillary service provision by EV fast charging stations. Yi et al. [294] propose a detection strategy based on complete ensemble empirical

mode decomposition with adaptive noise and a broad learning system for FDIAs against EV charging stations.

As the overview provided in this section shows, the cyberattack detection methods proposed in the literature are generally focused on specific measurements, assets, applications, attack types, or control signals. Furthermore, they usually rely on assumptions about the performed attacks, such as that the attack changes measurements in a way that makes them deviate from certain statistical distributions, or that they are the same as or similar to attacks already contained in training data. If distribution grid operation should be resilient to any cyberattack, regardless of the attack type, goal, or detectability, an adaptive and resilient grid management system, such as the one developed and evaluated in this thesis, is needed.

3.3. Cyber- and Failure-Resilient Active Distribution Grid Management

We used the *Scopus* database [295] to search for any publications meeting the conditions given in the beginning of this chapter. Based on the titles and abstracts of the search results, we preselected 202 publications that met our conditions at first glance. Subsequently, we analyzed the gathered publications in more detail and assigned them to the categories "impact only", "detection only", "loosely related", and "closely related". While we discarded the "loosely related" publications, we used the publications in the "impact only"-category as a basis for Section 3.1 and those in the "detection only"-category for Section 3.2. This left us with 52 "closely related" publications for further analysis based on the following ten questions:

Does the publication focus on actively managed distribution grids? *(Must have)*

Does the publication incorporate *(Must have at least one)*

- voltage maintenance/control/regulation?
- line current control/regulation?
- transformer load control/regulation?

Does the publication consider *(Must have at least one)*

- communication disruption?
- participant misconduct/cyberattacks?
- sensor failure?

Does the publication *(Nice to have)*

- consider multiple different DER types?

- leverage the flexibility of smart buildings/homes?
- feature automatic switching between multiple grid management strategies in response to communication disruption, cyberattacks/misconduct, or sensor failure?

After carefully checking each publication using the above questionnaire, we discarded another 22 publications previously categorized as "closely related". Most of the discarded publications either did not focus on distribution grids, did not consider grid constraints, such as admissible voltage ranges, at all, or did neither consider misconduct/cyberattacks nor failing communication/sensors. Some publications were discarded for other reasons, such as a focus on direct current grids, grid planning, or single devices without a broader grid context. The remaining 30 publications are the work most closely related to our thesis we became aware of during our literature search. It should be noted that this list of publications is non-exhaustive. A classification of the remaining publications with regard to the questionnaire above is given in Table 3.1. In the table, we omit the column for the *(must have)* question whether the publication focuses on actively managed distribution grids, as all listed publications fulfill this requirement. The publications in the table are sorted from top to bottom from most to least closely related.

Table 3.1: Overview of the publications most closely related to this thesis.

Publication	Voltage	Line current	Transformer load	Communication disruption	Misconduct/ Cyberattacks	Sensor failure	Multiple DER types	Building flexibility	Strategy adaptation
This thesis	✓	✓	✓	✓	✓	✓	✓	✓	✓
[15]	✓	✓	✓	✓	✗	✗	✓	✓	✓
[16]	✓	✗	✗	✓	✓	✗	✓	✓	✗
[17]	✗	✓	✗	✗	✓	✗	✓	✓	✓
[18]	✗	✓	✓	✓	✓	✗	✗	✗	✓
[19]	✓	✗	✗	✗	✓	✗	✓	✗	✓
[20]	✓	✓	✗	✗	✓	✗	✓	✗	✗
[21, 22]	✓	✓	✗	✓	✗	✗	✓	✗	✗
[23]	✓	✗	✗	✓	✗	✗	✓	✗	✓
[24]	✓	✓	✗	✓	✗	✗	✗	✗	✓
[25]	✓	✓	✗	✗	✓	✗	✗	✗	✓
[296–298]	✓	✗	✗	✓	✓	✗	✗	✗	✗
[299–302]	✓	✗	✗	✗	✓	✗	✓	✗	✗
[303]	✓	✗	✓	✓	✗	✗	✗	✗	✗
[304]	✗	✗	✓	✓	✓	✗	✗	✗	✗
[305–311]	✓	✗	✗	✗	✓	✗	✗	✗	✗
[312–314]	✓	✗	✗	✓	✗	✗	✗	✗	✗

As can be seen in Table 3.1, even among the closely related publications, there are substantial differences in the congruence with our thesis. Therefore, we only take the eleven publications comprising at least four of the nine features listed in Table 3.1 into account for the following deeper analysis.

Ipach et al. [15] build on previous work [315] introducing a centralized operation management scheme to optimize the power flows in a distribution grid with different types of DER (PV, BEV, heat pumps (HPs)) to maximize the sum of the utility values of the DER owners. The authors determine the individual utility of DERs by assigning a different priority to each DER that is then multiplied with a quadratic function of the active power generation or consumption of the DER. In [15], they redevelop this algorithm to take distribution grid constraints (voltage level constraints, thermal limit currents for grid lines and the substation transformer) into account. Furthermore, to make the operation management scheme more flexible and robust in context of controller or communication link failure, they redesign the management scheme from the previous centralized approach to a distributed approach. The distributed approach is similar to the distributed strategy employed in this thesis. Each prosumer is equipped with an intelligent node controller that communicates locally measured grid status data to other intelligent node controllers in the grid. This data is used to perform state estimation for the current grid status. The state estimation results and each prosumer's utility function are then used by an optimization algorithm that is run locally and only for the DERs belonging to the particular prosumer. This way, if controllers or communication links of some prosumers fail, the rest of the prosumers can still achieve satisfying optimization performance and counteract the changed grid status introduced by the failures up to a certain point. The authors also briefly address a fallback strategy that intelligent node controllers with failing communication can utilize. In the fallback strategy, the intelligent node controllers apply relatively high power consumption limits to the affected DERs to maintain rudimentary service quality. This differs from our approach in the decentralized strategy, which sets conservative limits to preempt any adverse effects on grid operation. The authors evaluate their approach on a simulated distribution grid interspersed with the DERs mentioned earlier and determine it to be robust with regard to communication delays and controller failure in the considered scenarios.

To our knowledge, [15] is the publication most closely related to our thesis. Like our thesis, the authors propose a distributed operation management scheme to achieve resilience against failing communication while taking the same grid constraints into account. However, in contrast to our adaptive grid management system, their system does not allow switching between centralized and distributed or decentralized strategies to maximize the data basis for maintaining stable grid operation and their decentralized backup strategy does not take grid operation into account. Like us, the authors employ multiple different DER types. However, the range of DERs is limited compared to our studies, lacking combined heat and power plants, intelligent appliances, and BESSs. Furthermore, robustness or resilience is only considered and demonstrated against communication and controller failure, while our system takes participant misconduct, either internal or externally caused

by cyberattacks, and sensor failure into account as well. Additionally, unlike us, the authors do not deploy reactive-power-based voltage maintenance to preserve more of the active power flexibility of DERs for other purposes, such as congestion prevention or energy cost reduction.

Iacovella et al. [16] propose a novel decentralized droop control voltage maintenance algorithm for buildings equipped with multiple DERs (PV, smart appliances, EVs, electric hot water boilers) and local controllers that functions without a communication network. The authors note that the lack of communication makes the approach resilient with regard to communication disruption and cyberattacks. The droop control algorithm not only accommodates DERs with freely-adjustable power setpoints, but also DERs that provide only on/off-flexibility, such as a smart appliance. Each building controls its own devices according to the voltage measured at its grid connection point, contributing to the overall voltage maintenance for the grid. The algorithm is evaluated through Monte Carlo experiments involving two distribution feeders equipped with the DERs listed above. The authors find that it substantially lowers the occurrence of over- and undervoltage on average in the considered scenarios, but caution that this effect can not be guaranteed due to the low temporal resolution of measurements and control actions as well as the absence of communication.

What makes [16] closely related to our thesis is its focus on diversely equipped buildings that control their operation in a completely decentralized and grid-supportive manner. However, unlike our thesis, the publication does not take sensor failure or line- and transformer-related problems into account. Furthermore, it does not feature grid management strategy adaptation, which could take advantage of the wealth of grid status data available if communication between participants is possible. Additionally, the presented droop control algorithm is constrained to utilizing active power flexibility, while the significant voltage maintenance potential of reactive power is neglected.

Ansari et al. [17] present a two-level decentralized framework to detect and mitigate FDIAs causing line congestion. On the lower level, microgrid operators detect false measurements using a Kalman filter that decides whether the value of a measurement varies too far from an estimated value. When the filter flags a possible FDIA, the corresponding measurement is replaced with an estimated value to minimize the impact on operation. On the upper level, a market mechanism called *Cyberattack-based Congestion Prevention Market* is established, in which demand response aggregators can sell their remaining energy flexibility to prevent line congestion caused by cyberattacks. The framework is evaluated using a distribution grid interspersed with a relatively diverse range of DERs, including smart homes, PV, Diesel generators, EVs, and wind turbines. The evaluation results show that the presented framework can prevent line congestion during cyberattacks in the considered scenarios.

[17] has in common with our thesis that it utilizes the flexibility of diverse DERs to mitigate the impacts of cyberattacks utilizing different strategies depending on the situation.

However, the authors tackle only line congestion, while neglecting transformer overheating and voltage maintenance. Furthermore, the presented approach only provides increased resilience against FDIAs on measurements, while other types of cyberattack, such as attacks on DER controllers, as well as communication or sensor failure are neither detected nor mitigated. While [17] combines different strategies, the market mechanism to prevent line congestion is centralized without a backup strategy that achieves at least acceptable performance when the market is unreachable or compromised.

Gümrükcü et al. [18] develop a distributed capacity sharing solution for bidirectional EV charging clusters to prevent line and transformer overloading during communication disruption affecting the DSO, caused either by hardware faults or cyberattacks. During normal operation the DSO communicates capacity constraints that determine how much active power may be used for charging by each charging cluster. When the communication to the DSO is disrupted, the charging clusters use predetermined, conservative capacity constraints. Furthermore, the clusters communicate with each other to share potential capacity surpluses among each other, so that each cluster remains below its particular conservative capacity constraint after optimizing their charging or discharging processes to accommodate the targeted EV states of charge and departure times. The authors evaluate their capacity sharing solution on a simulated distribution grid with multiple EV charging clusters and find that it substantially improves charging service continuity in the considered scenario.

[18] has similarities to our thesis in that it uses DER flexibility in a distributed fallback strategy to prevent line- and transformer overloading during communication disruption affecting the DSO. However, it has a much narrower scope, as it does not consider voltage maintenance, sensor failure, cyberattacks that cause participant misconduct, or communication disruption affecting participants other than the DSO itself. Furthermore, the publication is focused only on EVs, while our research covers a wide range of DERs.

Jain et al. [19] propose a two-tiered system to detect and mitigate cyberattacks that modify the command signals sent by DER management systems and can introduce severe violations of the admissible voltage range in distribution grids. The upper tier is a centralized cyber layer that uses cryptographic measures to flag and drop suspicious command packets. The lower tier becomes active when a DER controller is already compromised so that would receive and accept malicious commands without further countermeasures. Linearized expressions to determine expected control command values based on locally available power and weather data are created using multivariate linear regression. These expressions enable local DER controllers to assess the validity of incoming control commands with low computational effort. The authors evaluate the proposed system using two different distribution grid models interspersed with PV systems and BESSs and find that their attack detection and mitigation strategy can prevent damaging voltage range violations, which would otherwise be caused by the considered cyberattacks.

[19] is related to our thesis in that it provides a centralized as well as a decentralized strategy to mitigate the effects of cyberattacks on voltage maintenance in distribution grids. However, the authors neither consider line- or transformer congestion, nor measures to uphold reliable grid operation during communication or sensor failure. Furthermore, unlike our thesis, which covers a wide range of DERs, they evaluate their approach by simulating only PV systems and BESSs. Another significant difference is the reliance on centralized cryptographic and potentially inaccurate local measures to explicitly detect cyberattacks, while our adaptive grid management system is designed to uphold reliable grid operation even in the case of undetected cyberattacks.

Naderi et al. [20] present a moving target defense mechanism to detect and mitigate FDIAs on sensor measurements in microgrids to prevent voltage range and line current violations. The mechanism involves generating multiple copies of each measurement using separate sensors and randomly sending a measurement from a pool of copies, which reduces the attack surface. Incoming measurements are then verified on the receiver-side by comparing them to reference values generated by a recurrent neural network based on historical and weather data. If the deviation is too large, the corresponding measurement is dropped. They evaluate their approach with a physical, lab-scale microgrid comprising PV systems, wind turbines, and BESSs and find that it prevents voltage and current violations in the selected scenarios.

[20] is related to our thesis, because it provides measures for mitigating the adverse effects of certain cyberattacks on grid operation in the presence of DERs. However, the authors apply their approach to a microgrid instead of a conventional distribution grid and consequently focus on currents and voltages, while not considering transformer load. Furthermore, they do not consider the effects of communication and sensor failure or cyberattacks with different targets than measurements and thus do not provide different situation-dependent strategies that could be used in an adaptive grid management system, such as the one presented in this thesis.

Zhang et al. [21] propose a distributed optimization algorithm for voltage regulation in distribution grids using the reactive and active power flexibility of DERs. The optimization problem is formulated as a convexified, semidefinite programming problem, which is solved in a distributed manner to minimize the voltage-dependent power losses in the grid. Each grid node solves its own local version of the optimization problem and then communicates with its neighboring nodes to eliminate voltage angle differences with its neighbors by iteratively adjusting their problem solutions. The authors evaluate their approach on two distribution grid topologies with a PV system and electrical energy storage capacity at every connected bus and find that it keeps voltages inside the reference range while respecting the thermal limits of grid lines even during communication link failures, which are modeled as packet drops.

Like our thesis, [21] proposes a distributed strategy to regulate voltages and line currents in a way that is robust to communication disruption. However, the authors do not consider

the thermal limits of transformers, longer-term communication disruption, sensor failure, or cyberattacks/misconduct. Furthermore, they do not provide different grid management strategies that enable adaptability in response to different problems and only consider two DER types in their evaluation.

Yuan et al. [22] develop a similar distributed optimization algorithm as [21], which aims at minimizing the operating costs for the distribution grid as well as the connected microgrids. The presented relaxed alternating direction method of multipliers algorithm adheres to voltage and line power flow limits and provides robust performance even during communication disruption. The algorithm is evaluated on a simulated distribution grid interspersed with a low number of not further specified distributed generators and distributed energy storages. The authors find that the algorithm converges even for high probabilities of random packet dropouts and transmission delays.

Like [21], [22] is related to our thesis, because it provides a distributed grid management strategy that is robust against communication disruption and respects voltage and current limits. However, like [21], the publication does not cover transformer-related problems, more comprehensive communication disruption, sensor failure, cyberattacks/misconduct, or strategy adaptation. Unlike in our approach, the DERs simulated for the evaluation are generic and lack diversity.

Zamora et al. [23] present a novel modified droop-based control algorithm to regulate voltages, frequencies, and power sharing of islanded, grid-connected, or networked microgrids. It works in a decentralized manner and is activated when communication disruption within a microgrid occurs. During normal operation, each microgrid is controlled by a *microgrid central controller* that derives control commands for the local controllers of DERs from communicated sensor data. During communication disruption, the local DER controllers deploy the decentralized droop-based control algorithm, which only relies on data that can be locally measured at the particular DER. It handles dispatchable, that is, fully controllable, distributed generators as well as partially controllable distributed generation, such as combinations of PV systems and BESSs. The algorithm is evaluated by simulating an islanded and a grid-connected microgrid as well as two networked microgrids. Each of the microgrids comprises a hybrid PV-BESS system as well as a dispatchable distributed generator. The authors find that the control algorithm provides satisfactory performance in the performed simulation studies.

While [23] has some similarities to our approach, since it employs a decentralized backup strategy to regulate voltages and frequencies in the case of communication disruption, it differs significantly in other areas. The publication puts a strong focus on the different operating modes of microgrids, where local frequency control is often necessary, while our thesis targets more conventional distribution grids with very limited influence on the grid frequency of the larger electricity grid. Consequently, the presented approach does not consider transformer load. Cyberattacks/misconduct and sensor failure are not covered either, although we would assume that the proposed backup strategy could provide some

resilience against such problems as well. While the simulated DERs cover part of the flexibility that can be provided by DERs, the evaluation scenarios considered by the authors lack the detailed and diverse DER models employed in this thesis.

Liu et al. [24] propose an optimization algorithm that determines active power generation limits for DERs to be decentrally applied if the communication with a central controller fails. The particle-swarm-optimization-based algorithm is run offline before grid operation and takes grid parameters as well as the uncertainties of communication disruption, power generation, and power consumption into account to determine generation limits that minimize voltage range deviations and overcurrent risk. During normal operation, control commands for the DERs are determined and communicated by a central control center. If one or more communication links fail, the affected DERs are locally controlled using their individual, predetermined generation limits. In this case, DERs with still functioning communication links are still managed by the control center. The authors evaluate their algorithm by simulating a distribution grid interspersed with controllable PV systems. They find that the individually optimized generation limits reduce the voltage deviation and overcurrent risk compared to rudimentary strategies using fixed and homogenous generation limits for all DERs in the case of communication disruption.

A notable similarity between [24] and our thesis is the use of predetermined generation limits for PV systems to keep grid operation stable during communication disruption. In our case, these limits are learned during normal operation, while they are determined via offline optimization before the grid starts operating in [24]. This means that the employed approach requires more prior knowledge than ours and may be less adaptable. Furthermore, the approach does not take reactive power into account, although this could alleviate the need for active power curtailment to prevent voltage range deviations. Unlike our thesis, the publication does not cover transformer load, sensor failure, or cyberattacks/misconduct and the performed evaluation studies utilize only a single type of DER.

Majumdar et al. [25] develop a multi-strategy approach to detect and mitigate FDIAs on sensor measurements in the context of power loss minimization in distribution grids with controllable DERs. The DSO first uses a regression-analysis-based method presented in earlier work of the authors [316] to identify maliciously modified measurements. If all measurements are good, it can then determine optimal reactive power setpoints for each DER based on the received data. If the DSO detects bad measurements, it can decide to use a stochastic optimization method utilizing probability density curves constructed from historical or forecasted power data. This method determines optimal reactive power setpoints for each DER as well, while respecting the admissible voltage range and the thermal capacities of grid lines. The DSO can also decide to use a backup strategy, where DERs are controlled by their local controllers based on predetermined reactive power setpoints designed for a worst case scenario. Since this strategy only takes voltage maintenance into account, it represents a sub-optimal solution. The authors do not clarify how the DSO decides whether to use the stochastic optimization method or the backup strategy. The approach is evaluated on a simulated distribution grid with two connected PV systems

and the results show that voltage ranges are not violated and power losses are minimized in the two considered test cases. The authors also state improvements in voltages, voltage angles, reactive and active power compared to a 1500-sample Monte Carlo simulation. Since the authors do not further specify the Monte Carlo simulations or what exactly constitutes an improvement, we assume that these simulations represent grid operation without any measures against electrical disturbances or cyberattacks.

[25] is related to our thesis in that it provides different strategies to mitigate the effects of cyberattacks on voltage and current control. However, the presented approach strictly focuses on reactive power control with PV systems and does not consider active power curtailment, active power flexibility, or the wide range of DERs utilized in this thesis. Furthermore, the publication does not cover transformer load, communication disruption, sensor failure, or different cyberattack types than FDIAs on sensor measurements. While the authors propose different control strategies based on the current situation, they do not provide a mechanism to decide on strategies after measurements are compromised.

As can be seen in Table 3.1, most of the remaining, less closely related publications (17 out of 19) focus on voltage maintenance exclusively. Notable exceptions are [303], which considers both voltages and transformer load, and [304], which focuses on transformer load exclusively. The majority of the less closely related publications (11 out of 19) considers cyberattacks only. Exceptions are [296–298, 304], which cover both cyberattacks as well as communication disruption and [303, 312–314], which only take communication disruption into account. None of the less closely related publications covers line currents, sensor failure, utilizing the energy flexibility of buildings, or grid management strategy adaptation in response to problems originating from the information and communication infrastructure. Only few of these publications (4 out of 19) [299–302] consider multiple types of DER in their approaches or evaluations.

Even the most closely related publications analyzed in this section exhibit only partial overlap with our thesis and the presented approaches consequently lack the comprehensive resilience provided by our adaptive grid management system. All publications we are aware of address only specific aspects, such as cyberattacks in the context of voltage maintenance or only use individual countermeasures to electrical disturbances, such as active power flexibility or reactive-power-based voltage maintenance. While some authors evaluate their approaches using multiple different DER types, resilient grid management enabled by smart buildings with local building energy management systems and a diverse range of DERs is still lacking in the existing literature. These findings substantiate the need for a comprehensive grid management system, such as the one presented in this thesis.

3.4. Summary

We analyzed the literature related to our thesis, and found that only a part of it provides concrete measures to mitigate electrical disturbances in electricity distribution grids as well as the effects of disturbances of the adjacent information and communication technology (ICT) infrastructure. We first discussed research focused on the impacts of communication disruption and cyberattacks in smart distribution grids and found that such incidents can have a wide range of significant and even catastrophic consequences. Afterwards, we analyzed literature focused on the detection of cyberattacks and clustered the corresponding publications according to the functionality of the utilized detection methods. Finally, we analyzed the literature most closely related to our thesis, that is, publications that provide some measures to mitigate the effects of communication disruption, sensor failure, or cyberattacks in the context of actively managed distributions grids interspersed with distributed energy resources (DERs). While some of these publications have a somewhat significant overlap with our thesis, most of them only cover a small part of the topics we consider. None of the methods and strategies proposed in the publications we became aware of during our literature analysis provide the comprehensive resilience our adaptive grid management system achieves for electricity distribution grids.

Only three of the analyzed publications take the flexibility provided by smart buildings into account and none use the wide range of DERs considered in this thesis to evaluate the resilience improvement achievable through utilizing their energy flexibility for grid-supportive purposes. This motivates us to answer Research Question 1.

While seven publications propose multiple strategies for different situations, none of them thoroughly compares centralized, distributed, and decentralized grid management strategies with regard to their performance as well as other aspects, such as necessary prior knowledge. Usually, related publications only present a backup strategy and evaluate its ability to assist certain aspects of grid operation during ICT disturbances. This underlines the importance of answering Research Question 2.

None of the related publications explicitly considers sensor failure or system-internal participant misconduct and very few cover more than a single type of electrical or ICT disturbance. This justifies addressing Research Question 3.

4. Methodology

This chapter presents the methodology employed to develop the adaptive grid management system. After introducing the typographic conventions and time scales utilized in this thesis, we provide our own definition of resilience in the context of smart electricity distribution grids. Subsequently, we present three different grid management strategies that provide the basis for the adaptation of the grid management system during communication disruption, participant misconduct, or sensor failure. We then provide the criteria that signal different types of electrical disturbances in the grid as well as the countermeasures employed by the developed system to mitigate these disturbances. Building on the previously introduced grid management strategies, we explain the strategy adaptation functionality of the system next. After describing the architecture and concrete implementation of the grid management system, we briefly discuss the transferability of the system to different building energy management systems (BEMSs) than the *Organic Smart Home* (OSH). We then provide details on a visual demonstrator developed in the context of the thesis. After establishing the evaluation scenarios and metrics for assessing the performance of the system, we conclude the chapter with comprehensive parameter studies for all relevant parameters to ensure the system performs optimally, at least within the tested value ranges.

4.1. Typographic Conventions and Time Scales

We present the typography conventions for the symbols used in equations and algorithms throughout Chapter 4 in Table 4.1.

We use three time scales. The first is used for building simulations, which are performed with discrete simulation steps t_{sim} and a simulation step size $\Delta t_{\text{sim}} = 1\,\text{s}$. In a real-world application, this would correspond to measurement instants of building-internal sensors. The second time scale is used by the grid management system presented in the following sections. It uses management intervals t with a duration $\Delta t = 1\,\text{min}$. At the start of each management interval, power-flow studies are run by the system participants based on the measurement data (simulated in this thesis) received during the previous interval. Based on the power-flow studies, the participants implement different grid management measures, depending on whether the grid status is critical and its cause. The third time scale is used by the building energy flow optimizations run by each building. The optimizations produce device operation schedules over the optimization horizon. These schedules use

Table 4.1: Typography conventions for the symbols used in Chapter 4. GCP: grid connection point, VRDT: voltage regulated distribution transformer, PV: photovoltaic.

Scope	Convention	Example(s)
Variables / parameters	*Italic*	Reactive power: Q Normalized line current threshold for active power flexibility: i_{P}
Units	Upright	Watt: W
Indices	*Italic subscripts*	Voltage at the GCP of building b in management interval t: $u_{b,t}$
Context selectors	Upright subscripts	Initial normalized apparent power limit for line/transformer disturbances: $s_{\mathrm{L}}^{\mathrm{ini}}/s_{\mathrm{T}}^{\mathrm{ini}}$ Upper voltage boundary for reactive-power-/VRDT-based voltage maintenance: $u_{\mathrm{Q}}^{\mathrm{upp}}/u_{\mathrm{V}}^{\mathrm{upp}}$
Roles / states / operations	Upright superscripts	Normalized reactive power setpoint for the PV inverter of building b in management interval t: $q_{b,t}^{\mathrm{PV,set}}$ Upper voltage boundary for building b in the decentralized strategy: $u_b^{\mathrm{upp,dec}}$
Physical quantities	Dimensioned: uppercase Normalized: lowercase	Reactive power: Q Normalized reactive power: q
Differences / step sizes / increments	Denoted by Δ	Management interval duration: Δt Voltage deadband for VRDT-based voltage maintenance: $\Delta u_{\mathrm{V}}^{\mathrm{dea}}$
Arrays	***Bold & italic***	Ranking of buildings by flexibility in management interval t: $\boldsymbol{R}_t$
Sets	**Bold & upright**	Set of all buildings in the grid: $\mathbf{B}$

scheduling time slots τ with a duration $\Delta\tau = 5\,\mathrm{min}$. We give more detail on the mentioned processes in the following sections. Equation 4.1 relates the three different time scales:

$$\Delta\tau = 5\,\Delta t = 300\,\Delta t_{\mathrm{sim}} \tag{4.1}$$

All voltages and currents appearing in Chapters 4 and 5 are given as effective values. Voltages are given in pu, which stands for *per unit* and constitutes a normalization of the voltage by the nominal voltage of a given grid. Line currents are normalized as well. Lines usually consist of multiple segments connecting grid connection points, the transformer,

and branch points. Therefore, we normalize each line segment current to the rated current of the respective line segment.

Although the word *load* is often used to refer to electricity consumption exclusively, we use *load* to refer to both electricity consumption as well as generation.

4.2. Resilience Definition for Smart Electricity Distribution Grids

To evaluate the performance of the developed adaptive grid management system to improve the operation of smart electricity distribution grids, a specific definition of resilience for such grids is needed. Providing such a definition answers Sub-Question 1.1 of Research Question 1 and thereby provides a basis to answer Sub-Question 1.2 as well. Based on the definitions introduced in Section 2.7, we define the resilience of smart electricity distribution grids as follows:

The resilience of a smart electricity distribution grid can be defined as the capability of the grid to operate within the technical specifications of the grid equipment and the devices powered by the grid even in the presence of electrical disturbances as well as disturbances of the utilized information and communication technology and without curtailing connected loads (that is, power generation or consumption) more than necessary.

This definition combines aspects of the resilience definition for technical systems given in [220] (see Section 2.7.1) and the cyber-physical resilience, stability, and reliability definitions given in [227] (see Section 2.7.2). However, it is specific to smart electricity distributed grids, while the aforementioned definitions consider a broader context and are therefore less suitable for the scope of this work. Furthermore, our definition considers the invasiveness of power generation curtailment, which is lacking in the aforementioned definitions. Our resilience definition provides the basis for the measures to quantify the resilience provided by the adaptive grid management system presented in this thesis (see also Section 4.11).

Possible electrical disturbances, including those considered in this thesis, are given in Section 2.7.3. It is important to note that the considered electrical disturbances can also be viewed in the context of reliability or stability (see also Section 2.7.2). However, for the sake of simplicity, the term resilience is used exclusively in the following sections and chapters. In the context of this thesis, the term electrical disturbance is used to describe situations in which one or more grid status values, such as the voltage at a particular grid connection point (GCP), reaches a critical value. The grid can still be functional with a critical status, but may require the implementation of measures to prevent a further deterioration of the grid status that ultimately leads to electricity outages or equipment damage.

Numerous information and communication technology (ICT) disturbances that can affect the resilience of a smart grid are detailed in Section 2.7.4. Our adaptive grid management

system implicitly considers ICT disturbances that comprise or entail (partial) communication disruption between participants, sensor failure, or participant misconduct (system-internal or externally caused by cyberattacks). An example of such an ICT disturbance is a cyberattack that shuts down a server that is used to host a communication platform for the exchange of locally measured grid status data between buildings, a transformer, and a distribution system operator (DSO), which results in a disruption of all associated communication links. Another example is a Cyberattack that forces participant misconduct by modifying the control actions determined by the DSO or a building. The different handling of electrical and ICT disturbances in the context of this thesis should be noted. Electrical disturbances are detected directly based on measured or calculated grid status data and countermeasures are taken immediately to prevent electricity outages and equipment damage. In contrast, ICT disturbances, are not handled directly. If an ICT disturbance occurs, measures are only taken to mitigate the resulting problems (for example communication disruption), which may otherwise lead to electricity outages or equipment damage due to limited observability and controllability. Our focus is on providing strategies and methods for the resilient grid-supportive use of smart buildings, rather than preventive measures or countermeasures to phenomena such as cyberattacks, ICT errors, or inherent limitations of communication media. Our goal is to keep the electricity grid fully operational even if direct measures against ICT disturbances have already failed.

4.3. Grid Management Strategies

Some text passages of this section are transferred verbatim from two of our own publications [1, 34]. For summaries of these publications, their relation to this thesis, and their mapping to our research questions, see Section 1.4.

A grid management system requires functioning ICT infrastructure among the participants to exchange grid status data, information on implemented grid management measures, and commands. Furthermore, it presumes the compliance of its participants. This makes grid management systems susceptible to ICT disturbances resulting in communication disruption, participant misconduct, or sensor failure. To ensure resilient grid operation during such events, we propose the adaptive use of different grid management strategies depending on the current situation. In this section, we introduce these strategies and thereby create some of the prerequisites for answering all sub-questions of Research Questions 2 as well as Sub-Question 3.2 and 3.3 of Research Question 3. The strategies are visualized in Figure 4.1. The adaptive use of the strategies depending on the current situation is described in Section 4.6. However, we introduce our electrical disturbance criteria (Section 4.4) and the countermeasures to electrical disturbances (Section 4.5) first, since the strategy adaptation often relates to the latter.

4.3.1. Centralized Strategy

This strategy is only used when the DSO is able to regularly receive data from buildings connected to a low-voltage distribution grid and the transformer supplying it. Furthermore, the DSO has to be able to send commands to the buildings, when an electrical disturbance occurs that can potentially lead to electricity outages or equipment damage. The grid is operated by the observer/controller (O/C)-unit of the DSO based on the data communicated by the connected buildings as well as the transformer and additional data calculated in regularly performed power-flow studies using part of the received data as inputs. The data communicated by the buildings comprises voltages, active and reactive powers at their GCPs, measured by smart meters, as well as information on currently implemented and potentially implementable countermeasures to electrical disturbances. The data communicated by the transformer comprises its load factor, hot-spot temperature, transmission ratio and primary voltage. The data calculated in the power-flow studies are the currents on all lines and all GCP voltages. The latter can be compared to the respective measured voltages, to assess the accuracy of the power-flow studies (see also Section 4.6.1). If the DSO detects an electrical disturbance, it derives countermeasures and sends corresponding commands to the global O/C-units of the buildings.

It is important to note that the centralized strategy can still work during partial communication disruption, participant misconduct, or sensor failure. If the current grid status can still be observed with sufficient accuracy, commands for buildings that behave and communicate normally can still be determined when an electrical disturbance is detected. If the BEMS of a building that can not communicate anymore is still operational, such a building uses the decentralized strategy, which is described later in this section, while other buildings still operate according to the centralized strategy.

4.3.2. Distributed Strategy

This strategy is used if the DSO communicates incorrect commands or none at all, while a sufficient number of the communication links between the buildings and the transformer are still intact and enough sensors still provide accurate data. This could, for example, be the case if the DSO is subject to a cyberattack, which prevents it from communicating or forces it to communicate malicious commands. The distributed strategy can also be used as a default in combination with the decentralized strategy, which is described in the following section. The use of the centralized strategy is not required, even if no communication disruption, sensor failure, or participant misconduct occurs. In the distributed strategy, each building sends the same data it would send to the DSO in the centralized strategy to all other buildings and the transformer. Similarly, the transformer communicates the data it would send to the DSO to all buildings as well. Based on the data received from other buildings and the transformer as well as its own measured data, each building regularly performs power-flow studies to gain a complete understanding of the current grid status. This is achievable without excessive computational power. As a point of reference, for the 55-node village grid described in Section 4.10, one power-flow calculation, which is

performed once every minute by each building, takes approximately 2 ms on a single core processor. In doing so, each building has the same information as all other buildings and knows whether and how it should react to a certain electrical disturbance. Since all buildings have the same knowledge base, each building can determine its own capability to improve the grid status and, if necessary, communicate this to all others. This means that the observation of the grid and the determination of countermeasures is shifted from the DSO to the buildings and the transformer. Each building uses the same algorithms the DSO would use to autonomously determine appropriate countermeasures to electrical disturbances.

Just as with the centralized strategy, the distributed strategy can still be applied if partial communication disruption, participant misconduct, or sensor failure occurs, as long as the current grid status can still be observed with sufficient accuracy. In such a situation, all buildings that still behave and communicate normally use the distributed strategy, while buildings that can not communicate but behave normally otherwise switch to the decentralized strategy.

To enable the buildings to seamlessly switch from the centralized to the distributed strategy if necessary, the same communication of data and information among the buildings and the transformer implemented in the distributed strategy is also implemented when the centralized strategy is used. This way, the buildings can detect communication disruption or DSO misconduct immediately.

4.3.3. Decentralized Strategy

This strategy is applied by buildings that currently can not communicate with other buildings or the transformer, or for which the current grid status can not be observed with the required accuracy, due to a lack of sufficient or accurate grid status data received by other participants. If the grid status can not be observed with sufficient accuracy and the buildings switch from another strategy to the decentralized strategy, the transformer, if it is a voltage regulated distribution transformer (VRDT), switches back to the neutral transmission ratio. This is done to prevent additional electrical disturbances potentially caused by switching actions based on incorrect grid status data. It does so in a stepwise manner, to give the buildings time to adjust their reactive power setpoints to the resulting increase or decrease in voltages measured at their own GCPs. Each building then has to detect and improve electrical disturbances on its own and without full knowledge of the current grid status. Here, the only grid status data available to a building are the active power consumption or feed-in, the reactive power absorption or injection, as well as the voltage at its GCP. If a building detects a local deviation from a predetermined voltage range, which is varied depending on the distance between the building and the transformer, it determines countermeasures based on the magnitude of the deviation and, if applicable, already implemented measures. Although the buildings can only measure local voltage range deviations, there are synergies with other electrical disturbances. If the local voltage is critical, it is likely that voltages at other points on the same line are critical as well. Furthermore, as long as all grid equipment is intact, problematic voltages are usually

caused by high magnitudes of simultaneous active power feed-in [317] or consumption [318], which also causes high currents that can overload grid equipment [319]. Therefore, countermeasures such as reducing active power feed-in or consumption triggered by local voltage problems can prevent the overloading of lines or the transformer as well. The physical countermeasures to electrical disturbances in the decentralized strategy are the same as for the other strategies. However, the corresponding algorithms and electrical disturbance criteria are modified so that countermeasures can be implemented solely based on the local GCP voltage, the position of a building in the grid, and previously implemented countermeasures (see also Sections 4.4 and 4.5).

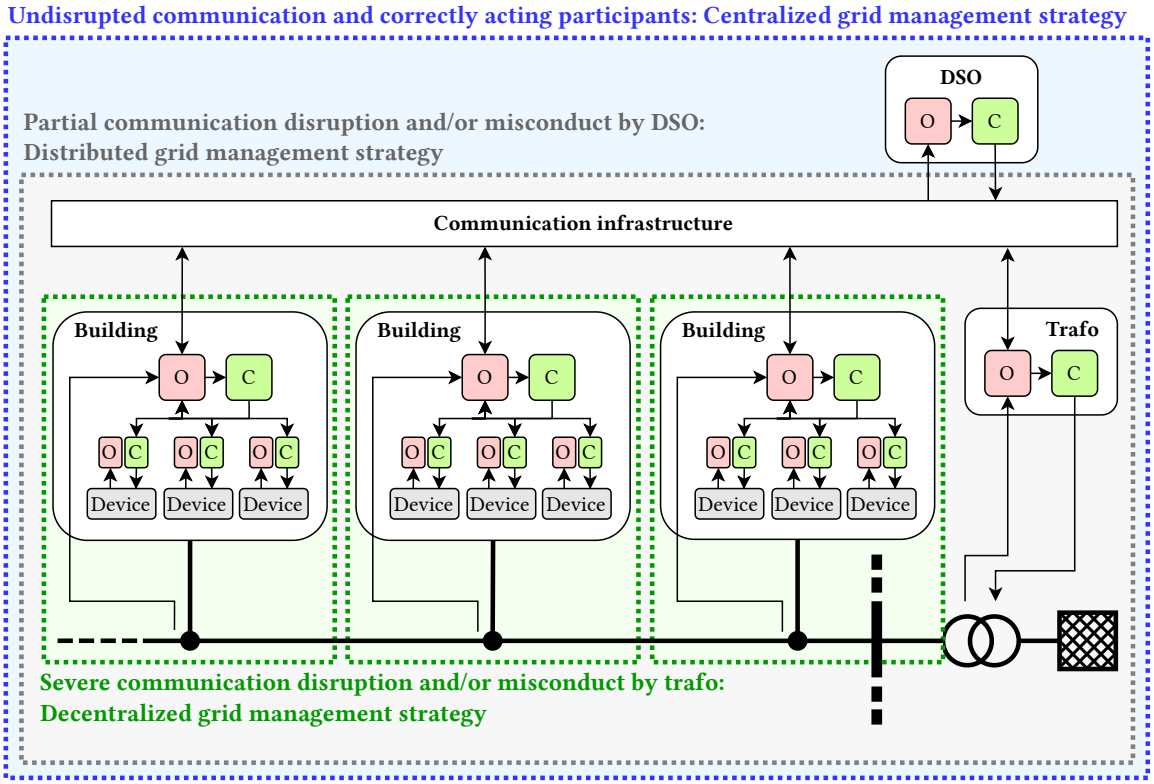

Figure 4.1: Visualization of the centralized, distributed, and decentralized grid management strategies, O: Observer, C: Controller, DSO: distribution system operator, Trafo: transformer, image based on [33]

4.4. Electrical Disturbance Criteria

Some text passages of this section are transferred verbatim from two of our own publications [33, 34]. For summaries of these publications, their relation to this thesis, and their mapping to our research questions, see Section 1.4.

We consider three types of electrical disturbance that are relevant in low-voltage grids. Preventing or alleviating these disturbances can consequently substantially increase the resilience of a given grid [2]. We explain in Section 2.7.3 why we do not consider other types of electrical disturbance. The electrical disturbance criteria established in this section

are necessary for answering Sub-Questions 1.2, 1.4, and 1.5 of Research Question 1 as well as Sub-Questions 2.1 and 2.2 of Research Question 2.

The first type of disturbances is critical voltages. As mentioned in Section 2.5.2, voltages in low-voltage grids have to stay within a range of ±10 % around the nominal voltage [167]. The specifications given in [168], which are described in Section 2.5.2 as well, are assumed not to be relevant in the context of this thesis, since a DSO can allow deviations from them, for example, if a VRDT is used. For grids that are not supplied by a VRDT, but rather by a conventional transformer with a fixed transmission ratio, the strategies and methods presented in this thesis can provide, among other things, a similar effect as a VRDT would. The utilized reactive-power-based voltage maintenance algorithms described in Section 4.5.3 are designed to ensure adherence to the permitted voltage range as defined in [167] at all times.

To prevent voltage range deviations due to sudden spikes in power consumption or feed-in, we propose more narrow voltage ranges than ±10 % to trigger the activation of grid management measures. Kochanneck [32] proposes ranges of -5 % to +3 % and -8 % to +7 % around the nominal voltage, outside of which yellow or red grid traffic light signals are triggered, respectively. This enables timely responses to voltages running up to critical values, even if countermeasures entailing significant time delays, such as optimization, are utilized. Different from [32], we do not differentiate between yellow and red traffic light signals. [32] proposes a system that financially incentivizes buildings to act in a grid-supportive manner. While this is potentially more attractive for the building inhabitants, it does not ensure reliable grid operation at all times and does not take into account the potentially generatable active energy lost due to photovoltaic (PV) curtailment. The system proposed in this thesis is designed to fully prevent the occurrence of electrical outages while maximizing the amount of energy that can be generated by PV systems utilizing the capabilities of the present grid as much as possible with specific commands and actions. It is useful to differentiate between different grid status (yellow, red) in general when deciding on the magnitude of the financial incentives proposed in [32]. However, for our system, the incorporation of a yellow grid status, which already entails countermeasures, despite being far from resulting in electricity outages, would effectively hinder the maximization of energy generated by PV systems. Instead, we use different disturbance criteria, depending on the particular countermeasure to be utilized and the particular grid management strategy used. These criteria are introduced in the following. Their specific numeric values are determined by the parameter studies presented in Section 4.12.

The upper and lower voltage boundaries that trigger voltage maintenance are varied depending on the utilized management strategy and voltage maintenance method. The centralized and distributed strategies use the boundaries $u_{\mathrm{Q}}^{\mathrm{upp}}$ and $u_{\mathrm{Q}}^{\mathrm{low}}$ or $u_{\mathrm{V}}^{\mathrm{upp}}$ and $u_{\mathrm{V}}^{\mathrm{low}}$, depending on whether reactive power (see Section 4.5.3) or a VRDT (see Section 4.5.1) is used for voltage maintenance, respectively. The decentralized strategy, which functions without comprehensive knowledge on the current grid status, has to utilize different boundaries than the centralized and distributed strategies, for which this information is available. Otherwise, only buildings that measure very high or low local voltages in the decentralized strategy would implement countermeasures. This may not be sufficient

to prevent voltage problems that could be prevented if more buildings implemented countermeasures. Consequently, in the decentralized strategy, the voltage boundaries are varied depending on the position of a building on the line feeding it. The closer a building is positioned to the transformer, the narrower the voltage range becomes. This is done because of the voltage drop or increase that occurs along lines, depending on whether the line exhibits low voltages due to high power consumption or high voltages due to high power feed-in of the connected buildings, respectively. If, for example, the voltages on a line are high due to the simultaneous active power feed-in of multiple buildings with PV systems, the voltage at the GCP of the building situated at the opposing end of the line relative to the transformer will be the highest of all buildings connected to the line. The upper and lower voltage boundaries for a particular building in the decentralized strategy are thus calculated according to Equations 4.2 and 4.3:

$$u_b^{\text{upp,dec}} = u_{\text{Q}}^{\text{upp}} - \Delta u_{\text{Q}}^{\text{coe}} \cdot \left(1 - \frac{d_b}{d_{l(b)}}\right) \tag{4.2}$$

$$u_b^{\text{low,dec}} = u_{\text{Q}}^{\text{low}} + \Delta u_{\text{Q}}^{\text{coe}} \cdot \left(1 - \frac{d_b}{d_{l(b)}}\right) \tag{4.3}$$

In Equations 4.2 and 4.3, $u_b^{\text{upp,dec}}$ and $u_b^{\text{low,dec}}$ are the upper and lower voltage boundaries for building b that trigger reactive-power-based voltage maintenance in the decentralized strategy. $\Delta u_{\text{Q}}^{\text{coe}}$ is a voltage coefficient for the term $\left(1 - \frac{d_b}{d_{l(b)}}\right)$. d_b is the total length of all line segments between the transformer and building b. $d_{l(b)}$ is the total length of all line segments between the transformer and the building that is situated at the end of line $l(b)$ feeding building b. This means that only the building at the end of a line uses the full voltage range, while all other buildings fed by the line use narrower ranges according to their positions. If the grid topology changes through construction measures or switching operations, d_b and $d_{l(b)}$ have to be redetermined for the new topology. This can either be done by DSO who then communicates the updated values to the buildings or by the buildings themselves after they receive the updated topology from the DSO.

We define any deviation from the voltage ranges applicable in a given situation as a voltage disturbance. Furthermore, we define any voltage outside of these ranges as a critical voltage.

In addition to the upper and lower voltage boundaries, criteria for the implementation of preventive measures due to voltage jumps are used as well. Since a voltage jump can indicate a further voltage rise in the following management interval, which could already violate the admissible voltage range, it can be useful to implement countermeasures, even if the voltage range outside of which countermeasures are triggered is not yet violated. Voltages in low-voltage grids fluctuate substantially more in the upper than in the lower range. The active power generation of spatially close PV systems is highly synchronized, which is common for systems connected to the same low-voltage grid. Since cloud movement strongly influences this synchronized generation, the resulting

voltage fluctuations can be substantial. Because the feed-in of PV systems causes voltage increases on the lines they feed, we only consider voltage jumps within the range above the nominal voltage. Sudden voltage drops within the range below the nominal voltage are considerably smaller and far less likely to increase further in the next management interval, since they are caused by increases in active power consumption, which is substantially less synchronized than the active power generation of PV systems. Countermeasures are triggered if the voltage jumps by at least $\Delta u_{\mathrm{Q}}^{\mathrm{jum}}$ (for reactive-power-based voltage maintenance) or $\Delta u_{\mathrm{V}}^{\mathrm{jum}}$ (for VRDT-based voltage maintenance) between two management intervals in the centralized and distributed strategies. An additional requirement that has to be met, is the minimum voltage that has to result from a voltage jump $u_{\mathrm{Q}}^{\mathrm{jum,min}}$ or $u_{\mathrm{V}}^{\mathrm{jum,min}}$. In the decentralized strategy, the necessary voltage jump and the resulting voltage are varied depending on the position of a building on the line as well. The respective parameters for a particular building in the decentralized strategy are calculated according to Equations 4.4 and 4.5:

$$\Delta u_b^{\mathrm{jum,dec}} = \Delta u_{\mathrm{Q}}^{\mathrm{jum}} \cdot \frac{u_b^{\mathrm{upp,dec}} - 1\,\mathrm{pu}}{u_{\mathrm{Q}}^{\mathrm{upp}} - 1\,\mathrm{pu}} \tag{4.4}$$

$$u_b^{\mathrm{jum,min,dec}} = 1\,\mathrm{pu} + \left(u_{\mathrm{Q}}^{\mathrm{jum,min}} - 1\,\mathrm{pu}\right) \cdot \frac{u_b^{\mathrm{upp,dec}} - 1\,\mathrm{pu}}{u_{\mathrm{Q}}^{\mathrm{upp}} - 1\,\mathrm{pu}} \tag{4.5}$$

Combining Equation 4.2 with Equations 4.4 and 4.5 results in Equations 4.6 and 4.7:

$$\Delta u_b^{\mathrm{jum,dec}} = \Delta u_{\mathrm{Q}}^{\mathrm{jum}} \cdot \frac{u_{\mathrm{Q}}^{\mathrm{upp}} - \Delta u_{\mathrm{Q}}^{\mathrm{coe}} \cdot \left(1 - \frac{d_b}{d_{l(b)}}\right) - 1\,\mathrm{pu}}{u_{\mathrm{Q}}^{\mathrm{upp}} - 1\,\mathrm{pu}} \tag{4.6}$$

$$u_b^{\mathrm{jum,min,dec}} = 1\,\mathrm{pu} + \left(u_{\mathrm{Q}}^{\mathrm{jum,min}} - 1\,\mathrm{pu}\right) \cdot \frac{u_{\mathrm{Q}}^{\mathrm{upp}} - \Delta u_{\mathrm{Q}}^{\mathrm{coe}} \cdot \left(1 - \frac{d_b}{d_{l(b)}}\right) - 1\,\mathrm{pu}}{u_{\mathrm{Q}}^{\mathrm{upp}} - 1\,\mathrm{pu}} \tag{4.7}$$

We determine appropriate values for the parameters $u_{\mathrm{Q}}^{\mathrm{upp}}$, $u_{\mathrm{Q}}^{\mathrm{low}}$, $u_{\mathrm{V}}^{\mathrm{upp}}$, $u_{\mathrm{V}}^{\mathrm{low}}$, $\Delta u_{\mathrm{Q}}^{\mathrm{coe}}$, $\Delta u_{\mathrm{Q}}^{\mathrm{jum}}$, $\Delta u_{\mathrm{V}}^{\mathrm{jum}}$, $u_{\mathrm{Q}}^{\mathrm{jum,min}}$, and $u_{\mathrm{V}}^{\mathrm{jum,min}}$ in parameter studies (see Section 4.12).

The second considered type of electrical disturbance is the imminent congestion of lines due to excessive power transfer entailing currents that may exceed the rated current of a line in subsequent management intervals. The use of active power flexibility (see Section 4.5.5) of buildings fed by a particular line is triggered if the current on the line exceeds i_{P}. Exceeding i_{P} triggers reactive power compensation (see Section 4.5.2) by the fed buildings as well if their PV inverters are not currently used for reactive-power-based voltage maintenance. Adaptive PV curtailment (see Section 4.5.4) is triggered if the current exceeds i_{S}, which is higher than i_{P}, since PV curtailment is a more invasive measure than using active power flexibility. The two current thresholds are only applicable

for the centralized and distributed strategies. In the decentralized strategy, a building can only measure the voltage at its GCP and its own power generation or consumption. Therefore, countermeasures against potential line congestion have to be triggered based on the locally measured voltage as well as building-specific apparent power limits for PV curtailment learned while using the centralized and distributed strategies. As described in Section 4.3.3, problematic voltages have the same causes as high currents that can overload lines. Therefore, countermeasures such as using active power flexibility to reduce active power feed-in or consumption, triggered by local voltage problems, can prevent the congestion of lines as well. As mentioned before, the voltage at the GCP of a building not only depends on grid utilization, but also on the position of the building on the line relative to the transformer. Therefore, we use voltage as well as position-based disturbance criteria to trigger the use of reactive power compensation and active power flexibility in the decentralized strategy. These criteria are given in Equations 4.8 and 4.9:

$$u_{b,t} > 1\,\mathrm{pu} + \Delta u^{\mathrm{off}} + \Delta u_{\mathrm{P}}^{\mathrm{coe}} \cdot \frac{d_b}{d_{l(b)}} \tag{4.8}$$

$$u_{b,t} < 1\,\mathrm{pu} - \Delta u^{\mathrm{off}} - \Delta u_{\mathrm{P}}^{\mathrm{coe}} \cdot \frac{d_b}{d_{l(b)}} \tag{4.9}$$

In Equations 4.8 and 4.9, $u_{b,t}$ is the voltage at the GCP of building b in management interval t. Each building b using the decentralized strategy independently checks both conditions at the start of management interval t. Δu^{off} is a base voltage offset. $\Delta u_{\mathrm{P}}^{\mathrm{coe}}$ is a voltage coefficient of the term $\frac{d_b}{d_{l(b)}}$. d_b and $d_{l(b)}$ are the same as in Equations 4.2 and 4.3. Hence, buildings that are closer to the transformer trigger reactive power compensation and active power flexibility use outside of narrower voltage ranges as buildings situated farther away.

If reactive-power-based voltage maintenance is currently active, the adjusted parameters $\Delta u^{\mathrm{off,Q}}$ and $\Delta u_{\mathrm{P}}^{\mathrm{coe,Q}}$ are used according to Equations 4.10 and 4.11 to compensate for the distorted voltage level.

$$u_{b,t} > 1\,\mathrm{pu} + \Delta u^{\mathrm{off,Q}} + \Delta u_{\mathrm{P}}^{\mathrm{coe,Q}} \cdot \frac{d_b}{d_{l(b)}} \tag{4.10}$$

$$u_{b,t} < 1\,\mathrm{pu} - \Delta u^{\mathrm{off,Q}} - \Delta u_{\mathrm{P}}^{\mathrm{coe,Q}} \cdot \frac{d_b}{d_{l(b)}} \tag{4.11}$$

For PV curtailment, the decentralized strategy uses static apparent power limits, which are learned during time periods in which the centralized or distributed strategies can be used. Consequently, there is no separate disturbance criterion to trigger PV curtailment in the decentralized strategy.

As for the parameters related to the voltage disturbance criteria, we determine appropriate values for the parameters i_{P}, i_{S}, Δu^{off}, $\Delta u_{\mathrm{P}}^{\mathrm{coe}}$, $\Delta u^{\mathrm{off,Q}}$, and $\Delta u_{\mathrm{P}}^{\mathrm{coe,Q}}$ in parameter studies (see Section 4.12).

The third considered type of electrical disturbance is the overheating of the transformer that supplies a particular grid due to congestion. [32] proposes transformer hot-spot temperatures of 70 °C and 80 °C to trigger yellow and red grid traffic light phases respectively. In contrast, we use different disturbance criteria to trigger different temperature-lowering measures instead of differentiating between different traffic light phases. When the load factor of the transformer exceeds k_{P}, reactive power compensation and active power flexibility use are triggered. We prefer this method, as the temperature of the transformer is a lagging indicator of congestion due to the thermal inertia of the transformer oil. Deploying less invasive measures earlier, such as active power flexibility use, can reduce the need for PV curtailment later. PV curtailment is only triggered if the hot-spot temperature exceeds θ^{upp} or if it exceeds θ^{mid} and the temperature in the current management interval is higher than in the last management interval. We differentiate between these two temperature thresholds, to prevent curtailment from being implemented too late. θ^{upp} is set near the maximum admissible hot-spot temperature given in [166]. θ^{mid} is set lower to prevent overshooting the maximum admissible temperature during fast temperature increases over multiple management intervals. We set both of these temperature thresholds substantially higher than the temperatures that trigger yellow and red traffic light phases in [32]. This still complies with the temperature limits given in [166], while it reduces the amount of potentially generatable active energy that is lost due to PV curtailment. As with the parameters related to the voltage and line disturbance criteria, we determine appropriate values for the parameters k_{P}, θ^{upp}, and θ^{mid} in parameter studies (see Section 4.12).

As for line-related disturbances, the aforementioned criteria can only be applied in the centralized or distributed strategies, which enable the communication of transformer data to the DSO and buildings. For the decentralized strategy, the transformer disturbance criteria that trigger reactive power compensation and active power flexibility use are the same as for line-related disturbances (see Equations 4.8 to 4.11). We do this because transformer disturbances have the same reasons as line disturbances. As with line disturbances, static apparent power limits learned in the centralized or distributed strategies are used for PV curtailment in the decentralized strategy.

All defined disturbance criteria are given in Table 4.3. The quantities and parameters used for these criteria are explained in Table 4.2. Transformer hot-spot temperatures are given in °C. Voltages are given in pu, which stands for *per unit* and constitutes a normalization of the voltage to the nominal voltage of a given grid. Line currents are normalized as well. Lines usually consist of multiple segments connecting GCPs, the transformer, and branch points. Therefore, we normalize each line segment current to the rated current of the respective line segment. Since segment currents generally accumulate along the line in the direction of the transformer, the maximum of the normalized magnitudes of the line segment currents is the relevant quantity to observe for detecting line disturbances.

Table 4.2: Symbol descriptions for the electrical disturbance criteria.

Symbol	Description
$u_t^{\max/\min}$	Max./min. voltage in the grid in management interval t [pu]
$u_{\mathrm{V}}^{\mathrm{upp/low}}$	Upper/lower voltage boundary for VRDT-based voltage maintenance [pu]
$u_{\mathrm{V}}^{\mathrm{jum,min}}$	Minimum voltage to consider voltage jumps for VRDT-based voltage maintenance [pu]
$\Delta u_{\mathrm{V}}^{\mathrm{jum}}$	Minimum voltage jump for VRDT-based voltage maintenance [pu]
$u_{l(b),t}^{\max/\min}$	Max./min. voltage on the line l feeding building b in man. interval t [pu]
$u_{\mathrm{Q}}^{\mathrm{upp/low}}$	Upper/lower voltage boundary for reactive-power-based voltage maintenance [pu]
$u_{\mathrm{Q}}^{\mathrm{jum,min}}$	Minimum voltage to consider voltage jumps for reactive-power-based voltage maintenance [pu]
$\Delta u_{\mathrm{Q}}^{\mathrm{jum}}$	Min. voltage jump for reactive-power-based voltage maintenance [pu]
$u_{b,t}$	Voltage at the GCP of building b in management interval t [pu]
d_b	Total length of line segments between the transformer and building b [m]
$d_{l(b)}$	Total length of line segments between the transformer and the building that is situated at the end of line l feeding building b [m]
$\Delta u_{\mathrm{Q}}^{\mathrm{coe}}$	Voltage coefficient used in the position-based voltage disturbance criteria for the decentralized strategy [pu]
$i_{l(b),t}$	Maximum of the normalized magnitudes of the line segment currents on line l feeding building b in management interval t [-]
i_{P}	Normalized line current threshold for active power flexibility [-]
i_{S}	Normalized line current threshold for PV curtailment [-]
$\Delta u^{\mathrm{off}(,\mathrm{Q})}$	Voltage offset used in the voltage- and position-based transformer/line disturbance criteria for the decentralized strategy if reactive-power-based voltage maintenance is currently inactive (active) [pu]
$\Delta u_{\mathrm{P}}^{\mathrm{coe}(,\mathrm{Q})}$	Voltage coefficient used in the voltage- and position-based transformer/line disturbance criteria for the decentralized strategy if reactive-power-based voltage maintenance is currently inactive (active) [pu]
k_t	Transformer load factor in management interval t [-]
k_{P}	Transformer load factor threshold for active power flexibility [-]
θ_t	Transformer hot-spot temperature in management interval t [°C]
$\theta^{\mathrm{upp/mid}}$	Upper/mid transformer hot-spot temperature for PV curtailment [°C]

Table 4.3: Electrical disturbance criteria that trigger countermeasures, partially based on [32].

Electrical disturbance	Disturbance criterion
Imminent deviations from admissible voltage range	Centralized and distributed strategies with VRDT: $u_t^{\max} > u_{\mathrm{V}}^{\mathrm{upp}} \ \vee \ u_t^{\min} < u_{\mathrm{V}}^{\mathrm{low}} \ \vee \ u_t^{\max} > u_{\mathrm{V}}^{\mathrm{jum,min}} \ \wedge \ u_t^{\max} - u_{t-1}^{\max} > \Delta u_{\mathrm{V}}^{\mathrm{jum}}$ Centralized and distributed strategies without VRDT: $u_{l(b),t}^{\max} > u_{\mathrm{Q}}^{\mathrm{upp}} \ \vee \ u_{l(b),t}^{\min} < u_{\mathrm{Q}}^{\mathrm{low}} \ \vee$ $u_{l(b),t}^{\max} > u_{\mathrm{Q}}^{\mathrm{jum,min}} \ \wedge \ u_{l(b),t}^{\max} - u_{l(b),t-1}^{\max} > \Delta u_{\mathrm{Q}}^{\mathrm{jum}}$ Decentralized strategy: $u_{b,t} > u_{\mathrm{Q}}^{\mathrm{upp}} - \Delta u_{\mathrm{Q}}^{\mathrm{coe}} \cdot \left(1 - \frac{d_b}{d_{l(b)}}\right) \ \vee \ u_{b,t} < u_{\mathrm{Q}}^{\mathrm{low}} + \Delta u_{\mathrm{Q}}^{\mathrm{coe}} \cdot \left(1 - \frac{d_b}{d_{l(b)}}\right) \ \vee$ $u_{b,t} > 1\,\mathrm{pu} + \left(u_{\mathrm{Q}}^{\mathrm{jum,min}} - 1\,\mathrm{pu}\right) \cdot \frac{u_{\mathrm{Q}}^{\mathrm{upp}} - \Delta u_{\mathrm{Q}}^{\mathrm{coe}} \cdot \left(1 - \frac{d_b}{d_{l(b)}}\right) - 1\,\mathrm{pu}}{u_{\mathrm{Q}}^{\mathrm{upp}} - 1\,\mathrm{pu}} \ \wedge$ $u_{b,t} - u_{b,t-1} > \Delta u_{\mathrm{Q}}^{\mathrm{jum}} \cdot \frac{u_{\mathrm{Q}}^{\mathrm{upp}} - \Delta u_{\mathrm{Q}}^{\mathrm{coe}} \cdot \left(1 - \frac{d_b}{d_{l(b)}}\right) - 1\,\mathrm{pu}}{u_{\mathrm{Q}}^{\mathrm{upp}} - 1\,\mathrm{pu}}$
Imminent line congestion	Centralized and distributed strategies (reactive power compensation and active power flexibility): $i_{l(b),t} > i_{\mathrm{P}}$ Centralized and distributed strategies (PV curtailment): $i_{l(b),t} > i_{\mathrm{S}}$ Decentralized strategy, reactive-power-based voltage maintenance inactive (reactive power compensation and active power flexibility): $u_{b,t} > 1\,\mathrm{pu} + \Delta u^{\mathrm{off}} + \Delta u_{\mathrm{P}}^{\mathrm{coe}} \cdot \frac{d_b}{d_{l(b)}} \ \vee \ u_{b,t} < 1\,\mathrm{pu} - \Delta u^{\mathrm{off}} - \Delta u_{\mathrm{P}}^{\mathrm{coe}} \cdot \frac{d_b}{d_{l(b)}}$ Decentralized strategy, reactive-power-based voltage maintenance active (active power flexibility): $u_{b,t} > 1\,\mathrm{pu} + \Delta u^{\mathrm{off,Q}} + \Delta u_{\mathrm{P}}^{\mathrm{coe,Q}} \cdot \frac{d_b}{d_{l(b)}} \ \vee \ u_{b,t} < 1\,\mathrm{pu} - \Delta u^{\mathrm{off,Q}} - \Delta u_{\mathrm{P}}^{\mathrm{coe,Q}} \cdot \frac{d_b}{d_{l(b)}}$
Imminent transformer overheating	Centralized and distributed strategies (reactive power compensation and active power flexibility): $k_t > k_{\mathrm{P}}$ Centralized and distributed strategies (PV curtailment): $\theta_t > \theta^{\mathrm{upp}} \ \vee \ \theta_t > \theta_{t-1} \ \wedge \ \theta_t > \theta^{\mathrm{mid}}$ Decentralized strategy: Same as for imminent line congestion

4.5. Countermeasures to Electrical Disturbances

This section presents the countermeasures to electrical disturbances utilized in the context of this thesis. Section 4.5.1 introduces the algorithm used to control a VRDT if one is present. Sections 4.5.2 and 4.5.3 describe the use of reactive power to reduce congestion and to regulate voltages, respectively. After introducing algorithms that adaptively curtail the active power generation of a PV system to achieve a specific apparent power limit at the GCP of a building in Section 4.5.4, the use of active power flexibility to reduce line and transformer disturbances as well as the need for PV curtailment is detailed in Section 4.5.5. The countermeasures to electrical disturbances established in this section provide a part of the basis for answering Sub-Questions 1.4 and 1.5 of Research Question 1 as well as Sub-Questions 2.1 and 2.2 of Research Question 2.

Some text passages of this section are transferred verbatim from two of our own publications [33, 34]. For summaries of these publications, their relation to this thesis, and their mapping to our research questions, see Section 1.4.

4.5.1. Voltage Regulated Distribution Transformer

If the low voltage grid is connected to the higher voltage level via a VRDT, the latter is capable of changing its transmission ratio for voltage maintenance. We prefer this over using reactive-power-based voltage maintenance (see Section 4.5.3), as it entails lower additional load on the grid. The control algorithm used for the VRDT is partially based on the control algorithm developed and implemented in [160]. The original algorithm only considers voltages exceeding an upper boundary. For this thesis, the algorithm is extended to also cover voltages that fall below a lower boundary. Furthermore, it is extended to consider voltage jumps occurring due to rapid movement of clouds above the PV systems installed in the grid. These can otherwise lead to late responses by the VRDT. This can entail momentary exceedances of the permitted upper voltage boundary and, consequently, potentially cause electricity outages. The transmission ratio can only be increased due to voltage jumps after a minimum waiting period of three management intervals since the management interval in which the transmission ratio was last decreased. This avoids the misinterpretation of previous VRDT switching operations as voltage jumps induced by PV generation. To prevent unnecessary switching operations, only voltage jumps to voltages above a minimum voltage $u_{\mathrm{V}}^{\mathrm{jum,min}}$ are considered. The control variable n_t, that is, the tap position index in management interval t is bounded to $[n^{\mathrm{min}}, n^{\mathrm{max}}]$ and can only be changed in discrete increments once each management interval. This respects the limits of the VRDT, prevents saturation effects, and mitigates oscillations. A voltage deadband $\Delta u_{\mathrm{V}}^{\mathrm{dea}}$ is used to reduce oscillations of the transmission ratio further. As an additional oscillation mitigation measure, we introduce a delay T_{V} before switching to a more neutral transmission ratio when the relevant voltage (the maximum voltage in the grid for a high and the minimum voltage for a low transmission ratio) is within the uncritical range and outside the deadband again. Algorithm 1 shows the VRDT control algorithm, which implements the voltage disturbance criteria introduced in Section 4.4

as well as the additional measures described above. As with the parameters from the disturbance criteria, the values of the newly introduced parameters T_{V}, and $\Delta u_{\mathrm{V}}^{\mathrm{dea}}$ are determined in parameter studies (see Section 4.12).

4.5.2. Reactive Power Compensation

Reactive power can be used to mitigate different types of electrical disturbance. In the context of line or transformer congestion, reactive power compensation can be useful. Here, the capability of an inverter to absorb or inject reactive power is used to compensate for the current reactive power absorption or injection of a building. This decreases or eliminates the amount of reactive power that has to be transmitted through the line feeding the building and through the transformer. This can be especially useful in situations where the equipment utilization is already high due to high amounts of transferred active power [125].

According to the *VDE-AR-N 4105:2018-11* [168], PV inverters are required to be able to operate at least down to a power factor ($\cos \varphi^{\mathrm{req}}$) of 0.9 for a total rated generator apparent power above 4.6 kVA at the GCP and 0.95 for smaller connections. The earlier *VDE-AR-N 4105:2011-08* [320] gave 13.8 kVA as a threshold. In practice, DSOs determine the actual operating characteristics [321, 322]. For our simulations in Chapter 5, we still use the 13.8 kVA threshold of the 2011 edition of the VDE-AR-N 4105 to set the reactive power capability of the PV inverters. We do this to avoid overstating the reactive power headroom of older and smaller inverters, which, given the longevity of PV systems, might be less capable than inverters dimensioned according to the 2018 edition of the VDE-AR-N 4105. In theory, this makes our simulation results conservative with regard to the congestion relief achievable through reactive power compensation. However, in practice, this does not affect the results, since the amount of reactive power that has to be compensated in the simulated buildings is insignificant in comparison with the reactive power capabilities of the inverters. For the scenarios considered in this thesis, all PV inverters are dimensioned so that they are able to operate at least down to their respective required power factors even at the peak active powers of the attached PV systems. In a scenario where this is not the case, the maximum magnitude of the reactive power setpoint would have to be dynamically adjusted or, alternatively, the active power generation would have to be dynamically curtailed. We furthermore assume symmetric inductive and capacitive reactive power capability for all inverters. Given these prerequisites and assumptions, we can calculate the applicable maximum magnitude of the reactive power setpoint for each inverter by combining Equations 4.12 and 4.13 into Equation 4.14:

$$\left(Q_b^{\mathrm{PV,max}}\right)^2 + \left(P_b^{\mathrm{PV,max}}\right)^2 = \left(S_b^{\mathrm{PV,max}}\right)^2 \tag{4.12}$$

$$P_b^{\mathrm{PV,max}} = S_b^{\mathrm{PV,max}} \cdot \cos \varphi^{\mathrm{req}} \tag{4.13}$$

$$Q_b^{\mathrm{PV,max}} = S_b^{\mathrm{PV,max}} \cdot \sqrt{1 - \left(\cos \varphi^{\mathrm{req}}\right)^2} \tag{4.14}$$

Data:

t	Management interval index [-]
Δt	Management interval duration [min]
t^{up}	Management interval index of the last tap increase [-]
$n^{\text{max/min}}$	Maximum/minimum tap position (neutral tap index is 0) [-]
$u_t^{\text{max/min}}$	Maximum/minimum voltage in the grid in management interval t [pu]
$u_{\text{V}}^{\text{upp/low}}$	Upper/lower voltage boundary for VRDT-based voltage maintenance [pu]
$\Delta u_{\text{V}}^{\text{jum}}$	Minimum voltage jump for VRDT-based voltage maintenance [pu]
$u_{\text{V}}^{\text{jum,min}}$	Min. voltage to consider voltage jumps for VRDT-based volt. maint. [pu]
$c^{\text{upp/low}}$	Counters for delayed switching to a more neutral transmission ratio [-]
$T_{\text{V}}/N_{\text{V}}$	Delay before switching to a more neutral transmission ratio in minutes/management intervals [min]/[-]
$\Delta u_{\text{V}}^{\text{dea}}$	Voltage deadband for VRDT-based voltage maintenance [pu]
Δr	Per-tap ratio increment (we use 0.025) [-]

Result:

n_t	Tap position index in management interval t [-]
r_t	Transmission ratio in management interval t [-]

Initialization (once, if undefined):

$n_{t-1} \leftarrow 0$; $c^{\text{upp}} \leftarrow 0$; $c^{\text{low}} \leftarrow 0$; $N_{\text{V}} \leftarrow \frac{T_{\text{V}}}{\Delta t}$; $t^{\text{up}} \leftarrow t - 3$

Each management interval:

$n_t \leftarrow n_{t-1}$

if $n_t > n^{\min} \wedge \left(u_t^{\max} > u_{\text{V}}^{\text{upp}} \vee u_t^{\max} - u_{t-1}^{\max} > \Delta u_{\text{V}}^{\text{jum}} \wedge u_t^{\max} > u_{\text{V}}^{\text{jum,min}} \wedge t - t^{\text{up}} > 2\right)$ **then**

  $n_t \leftarrow n_t - 1$; $c^{\text{upp}} \leftarrow 0$; $c^{\text{low}} \leftarrow 0$

else if $n_t < 0 \wedge u_t^{\max} < u_{\text{V}}^{\text{upp}} - \Delta u_{\text{V}}^{\text{dea}}$ **then**

  $c^{\text{upp}} \leftarrow c^{\text{upp}} + 1$

  if $c^{\text{upp}} = N_{\text{V}}$ **then**

    $n_t \leftarrow n_t + 1$; $t^{\text{up}} \leftarrow t$; $c^{\text{upp}} \leftarrow 0$

else if $n_t < n^{\max} \wedge u_t^{\min} < u_{\text{V}}^{\text{low}}$ **then**

  $n_t \leftarrow n_t + 1$; $t^{\text{up}} \leftarrow t$; $c^{\text{low}} \leftarrow 0$; $c^{\text{upp}} \leftarrow 0$

else if $n_t > 0 \wedge u_t^{\min} > u_{\text{V}}^{\text{low}} + \Delta u_{\text{V}}^{\text{dea}}$ **then**

  $c^{\text{low}} \leftarrow c^{\text{low}} + 1$

  if $c^{\text{low}} = N_{\text{V}}$ **then**

    $n_t \leftarrow n_t - 1$; $c^{\text{low}} \leftarrow 0$

else

  $c^{\text{upp}} \leftarrow 0$; $c^{\text{low}} \leftarrow 0$

$r_t \leftarrow \frac{1}{1+n_t \cdot \Delta r}$

Algorithm 1: VRDT control algorithm. Partially based on the control algorithm developed in [160]. Applied autonomously by the VRDT in the centralized and distributed strategies. Not utilized in the decentralized strategy or if the transformer is not a VRDT.

In Equations 4.12 to 4.14, $S_b^{\mathrm{PV,max}}$ is the rated apparent power of the PV inverter of building b. $P_b^{\mathrm{PV,max}}$ is the maximum active power at which the PV inverter of building b is still able to operate at the required power factor $\cos\varphi^{\mathrm{req}}$. $Q_b^{\mathrm{PV,max}}$ is the maximum magnitude of the reactive power setpoint for the PV inverter of building b that still meets the required power factor $\cos\varphi^{\mathrm{req}}$ at its rated apparent power $S_b^{\mathrm{PV,max}}$. For the purpose of reactive power compensation, we do not apply fixed power factors. However, the magnitude of the reactive power setpoint has to stay below or at the calculated maximum magnitude of the reactive power setpoint. Each building commanded to compensate its reactive power by the DSO in the centralized strategy or autonomously deciding to use reactive power compensation in the distributed or decentralized strategies calculates its own reactive power setpoint according to Equation 4.15:

$$Q_{b,t_{\mathrm{sim}}}^{\mathrm{PV,set}} = \begin{cases} Q_b^{\mathrm{PV,max}} & , \quad Q_{b,t_{\mathrm{sim}}-1}^{\mathrm{PV}} - Q_{b,t_{\mathrm{sim}}-1} \geq Q_b^{\mathrm{PV,max}} \\ Q_{b,t_{\mathrm{sim}}-1}^{\mathrm{PV}} - Q_{b,t_{\mathrm{sim}}-1} & , \quad -Q_b^{\mathrm{PV,max}} < Q_{b,t_{\mathrm{sim}}-1}^{\mathrm{PV}} - Q_{b,t_{\mathrm{sim}}-1} < Q_b^{\mathrm{PV,max}} \\ -Q_b^{\mathrm{PV,max}} & , \quad -Q_b^{\mathrm{PV,max}} \geq Q_{b,t_{\mathrm{sim}}-1}^{\mathrm{PV}} - Q_{b,t_{\mathrm{sim}}-1} \end{cases} \tag{4.15}$$

In Equation 4.15, $Q_{b,t_{\mathrm{sim}}}^{\mathrm{PV,set}}$ denotes the new reactive power setpoint to be implemented by the inverter of building b at simulation step t_{sim}. $Q_{b,t_{\mathrm{sim}}-1}^{\mathrm{PV}}$ is the reactive power absorbed or injected by the inverter of building b at the previous simulation step. $Q_{b,t_{\mathrm{sim}}-1}$ is the reactive power absorbed from or injected into the grid at the GCP of building b at the previous simulation step. In a real-world deployment, the reactive power setpoint would be recalculated at measurement instants instead of simulation steps. Positive values for the reactive power Q in this context denote absorption (inductive reactive power) and negative values injection (capacitive reactive power), except when referring to magnitudes. When reactive power compensation is triggered according to the transformer and line disturbance criteria presented in Section 4.4, we set the duration for which the reactive power compensation stays active to one hour. During this time, the reactive power setpoint is adjusted at every simulation step. When the hour has passed, the need for reactive power compensation is checked again and its use is extended if necessary.

4.5.3. Reactive-Power-Based Voltage Maintenance

Besides reactive power compensation, reactive power can also be leveraged to decrease or increase voltages in a grid, which makes it an effective tool for voltage maintenance [125]. If voltages are critical according to the boundaries introduced in Section 4.4 and assigned values in Section 4.12, we always prefer the use of reactive power for voltage maintenance over reactive power compensation since voltage range deviations generally result in damaged equipment faster [231] than congestion [166, 323]. Therefore, if reactive power compensation is used when grid voltages require reactive-power-based voltage maintenance, the former is deactivated.

We utilize reactive-power-based voltage maintenance algorithms that are designed to limit the additional load on the grid introduced by the increased transfer of reactive

power. If a situation requires no or less reactive power transfer than fixed power factors, *Q(U)*-control, or $\cos(\varphi)$*(P)*-control (see also Section 2.5.3) would entail, the load on the grid is lessened, which reduces congestion. Furthermore, our algorithms prevent voltage oscillations that can occur when using *Q(U)*-control [324]. *Q(U)*-control changes the reactive power absorption or injection as a direct function of the measured voltage and thereby changes the voltage itself, which can cause subsequent changes in the reactive power absorption or injection in the opposite direction. We circumvent this oscillation effect by adjusting the reactive power setpoint in small and discrete increments only once each management interval, keeping the setpoint constant when voltages are inside a predefined deadband, and utilizing waiting times before relaxing the setpoint when the grid status is uncritical again. We respect the limits of the particular inverter and prevent saturation effects by bounding the control variable $Q_{b,t}^{\mathrm{PV,set}}$, that is, the reactive power setpoint for building b in management interval t to $[-Q_b^{\mathrm{PV,max}}, Q_b^{\mathrm{PV,max}}]$.

The prerequisites and assumptions with regard to inverter dimensioning and capabilities given for reactive power compensation in Section 4.5.2 apply to reactive-power-based voltage maintenance as well. This includes the 13.8 kVA threshold for the total rated generator apparent power at the GCP above which the PV inverters are required to be able to operate at least down to a power factor ($\cos\varphi^{\mathrm{req}}$) of 0.9 according to the *VDE-AR-N 4105:2011-08* [320]. Since the *VDE-AR-N 4105:2018-11* [168] lowered this threshold to 4.6 kVA, the simulation results shown in Chapter 5 are slightly conservative with regard to the voltage maintenance capabilities of the simulated buildings. Buildings with a total rated generator apparent power at their GCPs between 4.6 kVA and 13.8 kVA would have more reactive power headroom and thus better voltage maintenance capability if the inverters were dimensioned according to the VDE-AR-N 4105:2018-11. However, as mentioned in Section 4.5.2, given the longevity of PV systems, in a real-world scenario there might still be PV inverters dimensioned according to the 2011 version of the VDE-AR-N 4105. As a consequence, we use the 2011 threshold to avoid overstating the voltage maintenance capability. The results in Chapter 5 show that, even with our conservative assumptions and for the most extreme evaluation scenarios, the reactive power headroom is still sufficient to prevent all deviations from the admissible voltage range.

Algorithm 2 is utilized by the DSO *for* each building in the centralized strategy or *by* each building in the distributed strategy. Algorithm 2 not only determines reactive power setpoints for buildings with a critical voltage at their own GCPs but also for buildings fed by the same line as other buildings with critical voltages at their GCPs. The maximum or minimum node voltage on the line l feeding building b is referred to as $u_{l(b),t}^{\mathrm{max/min}}$. The algorithm considers voltage jumps as well. However, as in the VRDT control algorithm (Algorithm 1), sudden voltage drops are not considered, since the simultaneity of PV generation and the resulting voltage jumps are much more pronounced than the voltage drops occurring due to device usage. For the same reason, we use two different step sizes to step up the reactive power setpoint, while using only the smaller step size when stepping it down. Which step size is used for stepping up the reactive power setpoint depends on the previous reactive power setpoint. When the previous setpoint already exceeds a certain threshold, but the voltage is still critical, the small step size is used to

prevent overcorrections. For the same reason, voltage jumps no longer trigger reactive power setpoint increases once the setpoint is above this threshold. Before decreasing the reactive power absorption or injection of the PV inverter again, $u_{l(b),t}^{\max/\min}$ has to stay inside the uncritical range, which is further constrained by a voltage deadband $\Delta u_{\mathrm{Q}}^{\mathrm{dea}}$, for the duration T_{Q}. We do this to prevent a premature reduction of reactive power absorption or injection in the context of highly fluctuating voltages, for example, due to rapid passing by of clouds above a PV system. The condition can be bypassed if the previously critical voltage crosses the nominal voltage in the opposite direction. The reactive power setpoint is recalculated at the beginning of each management interval t when new power-flow study results are available. This differs from the recalculation of the reactive power setpoint when reactive power compensation is active, which is done at every simulation step in the case of our simulations or at every building-internal measurement instance in a real-world deployment. Table 4.4 provides descriptions for the symbols used in Algorithms 2 and 3. As with the parameters used in the disturbance criteria, the values of the newly introduced parameters $q^{\mathrm{lar|sma}}$, Δq^{lar}, Δq^{sma}, T_{Q}, and $\Delta u_{\mathrm{Q}}^{\mathrm{dea}}$ are determined in parameter studies (see Section 4.12).

Algorithm 3 is used by each building in the decentralized strategy. It is similar to Algorithm 2, which is used in the centralized and distributed strategies. However, there are some key differences. Due to the lack of communication among buildings and the DSO, Algorithm 3 considers only the voltage $u_{b,t}$ at the GCP of a building b, instead of the most critical voltage on the line feeding building b. To compensate for this, the position of the building on the line (see also Section 4.4) is considered as well when determining whether a reactive power setpoint should be used and its appropriate value.

In the centralized strategy, the DSO only communicates changed setpoints to the buildings. As long as a building does not receive a new setpoint in the centralized strategy, it uses the last setpoint previously received. In the distributed and decentralized strategies, each building implements new reactive power setpoints autonomously.

4.5.4. Adaptive Photovoltaic Generation Curtailment

As described in Section 2.3, PV inverters can curtail the active power generation of attached PV systems. This functionality can be used to implement algorithms that dynamically adjust the generated active power depending on the current grid status and the available active power flexibility of the other devices in the building. We do not use curtailment algorithms for devices other than PV systems, as all other high-power devices that can be present in a residential building provide some flexibility in their operation without curtailment that can be leveraged to prevent or counteract disturbances according to the methods described in Section 4.5.5. Aside from PV systems, the devices in residential buildings typically showing the highest consumption or generation of active power are battery electric vehicles (BEVs), battery energy storage systems (BESSs), heat pumps (HPs) and cogeneration of heat and power (CHP) plants. While the active power consumption or

Table 4.4: Symbols used in Algorithms 2 and 3. Normalized reactive powers are normalized to $Q_b^{\mathrm{PV,max}}$.

Symbol	Description
t	Management interval index [-]
Δt	Management interval duration [min]
b	Building index [-]
l	Line index [-]
$q_{b,t}^{\mathrm{PV,set}}$	Normalized reactive power setpoint for the PV inverter of building b in management int. t [-]
$u_{l(b),t}^{\mathrm{max/min}}$	Max./min. voltage on line l feeding building b in man. interval t [pu]
$u_{\mathrm{Q}}^{\mathrm{upp/low}}$	Upper/lower voltage disturbance boundary for reactive-power-based voltage maintenance [pu]
$u_{\mathrm{Q}}^{\mathrm{jum,min}}$	Minimum voltage for considering voltage jumps for reactive-power-based voltage maintenance [pu]
$\Delta u_{\mathrm{Q}}^{\mathrm{jum}}$	Min. voltage jump for reactive-power-based voltage maint. [pu]
$q^{\mathrm{lar\|sma}}$	Normalized reactive power threshold for step size switching [-]
$\Delta q^{\mathrm{lar/sma}}$	Normalized reactive power large/small step [-]
$c_b^{\mathrm{upp/low}}$	Counters for delayed reduction of reactive power absorption/injection for building b [-]
$T_{\mathrm{Q}}/N_{\mathrm{Q}}$	Delay for the reduction of reactive power absorption or injection in minutes/management intervals [min]/[-]
$\Delta u_{\mathrm{Q}}^{\mathrm{dea}}$	Voltage deadband for reactive-power-based voltage maint. [pu]
d_b	Total length of line segments between the transformer and building b [m]
$d_{l(b)}$	Total length of line segments between the transformer and the building that is situated at the end of line l feeding building b [m]
$\Delta u_{\mathrm{Q}}^{\mathrm{coe}}$	Voltage coefficient used in the position-dependent voltage disturbance criteria for the decentralized strategy [pu]
$u_b^{\mathrm{upp/low,dec}}$	Upper/lower voltage disturbance boundary for building b for reactive-power-based voltage maintenance in the dec. strategy [pu]
$u_b^{\mathrm{jum,min,dec}}$	Minimum voltage for considering voltage jumps for building b for reactive-power-based voltage maintenance in the dec. strategy [pu]
$\Delta u_b^{\mathrm{jum,dec}}$	Minimum voltage jump for building b for reactive-power-based voltage maintenance in the decentralized strategy [pu]
$\Delta u_b^{\mathrm{dea,dec}}$	Voltage deadband for building b for reactive-power-based voltage maintenance in the decentralized strategy [pu]
$u_{b,t}$	Voltage at the GCP of building b in management interval t [pu]
$Q_b^{\mathrm{PV,max}}$	Maximum magnitude of the reactive power setpoint for the inverter of building b [var]

Data: See Table 4.4

Result:

$Q_{b,t}^{\mathrm{PV,set}}$ Reactive power setpoint for building b in management interval t [var]

Initialization (once, if undefined): $q_{b,t-1}^{\mathrm{PV,set}} \leftarrow 0$; $c_b^{\mathrm{upp}} \leftarrow 0$; $c_b^{\mathrm{low}} \leftarrow 0$; $N_{\mathrm{Q}} \leftarrow \dfrac{T_{\mathrm{Q}}}{\Delta t}$

Each management interval:

$q_{b,t}^{\mathrm{PV,set}} \leftarrow q_{b,t-1}^{\mathrm{PV,set}}$
if $q_{b,t}^{\mathrm{PV,set}} \geq 0$ **then**
  if $u_{l(b),t}^{\max} > u_{\mathrm{Q}}^{\mathrm{upp}} \vee u_{l(b),t}^{\max} > u_{\mathrm{Q}}^{\mathrm{jum,min}} \wedge u_{l(b),t}^{\max} - u_{l(b),t-1}^{\max} > \Delta u_{\mathrm{Q}}^{\mathrm{jum}}$ **then**
    if $q_{b,t}^{\mathrm{PV,set}} \leq q^{\mathrm{lar|sma}}$ **then** $q_{b,t}^{\mathrm{PV,set}} \leftarrow q_{b,t}^{\mathrm{PV,set}} + \Delta q^{\mathrm{lar}}$
    else if $u_{l(b),t}^{\max} > u_{\mathrm{Q}}^{\mathrm{upp}}$ **then** $q_{b,t}^{\mathrm{PV,set}} \leftarrow q_{b,t}^{\mathrm{PV,set}} + \Delta q^{\mathrm{sma}}$
  else if $u_{l(b),t}^{\max} \geq u_{\mathrm{Q}}^{\mathrm{upp}} - \Delta u_{\mathrm{Q}}^{\mathrm{dea}}$ **then** $c_b^{\mathrm{upp}} \leftarrow 0$
  else if $q_{b,t}^{\mathrm{PV,set}} > 0$ **then**
    $c_b^{\mathrm{upp}} \leftarrow c_b^{\mathrm{upp}} + 1$
    if $c_b^{\mathrm{upp}} \geq N_{\mathrm{Q}} \vee u_{l(b),t}^{\max} < 1\,\mathrm{pu}$ **then** $q_{b,t}^{\mathrm{PV,set}} \leftarrow q_{b,t}^{\mathrm{PV,set}} - \Delta q^{\mathrm{sma}}$
    if $q_{b,t}^{\mathrm{PV,set}} < 0$ **then** $q_{b,t}^{\mathrm{PV,set}} \leftarrow 0$
  if $q_{b,t}^{\mathrm{PV,set}} > 1$ **then** $q_{b,t}^{\mathrm{PV,set}} \leftarrow 1$
if $q_{b,t}^{\mathrm{PV,set}} \leq 0$ **then**
  if $u_{l(b),t}^{\min} < u_{\mathrm{Q}}^{\mathrm{low}}$ **then** $q_{b,t}^{\mathrm{PV,set}} \leftarrow q_{b,t}^{\mathrm{PV,set}} - \Delta q^{\mathrm{sma}}$
  else if $u_{l(b),t}^{\min} \leq u_{\mathrm{Q}}^{\mathrm{low}} + \Delta u_{\mathrm{Q}}^{\mathrm{dea}}$ **then** $c_b^{\mathrm{low}} \leftarrow 0$
  else if $q_{b,t}^{\mathrm{PV,set}} < 0$ **then**
    $c_b^{\mathrm{low}} \leftarrow c_b^{\mathrm{low}} + 1$
    if $c_b^{\mathrm{low}} \geq N_{\mathrm{Q}} \vee u_{l(b),t}^{\min} > 1\,\mathrm{pu}$ **then** $q_{b,t}^{\mathrm{PV,set}} \leftarrow q_{b,t}^{\mathrm{PV,set}} + \Delta q^{\mathrm{sma}}$
    if $q_{b,t}^{\mathrm{PV,set}} > 0$ **then** $q_{b,t}^{\mathrm{PV,set}} \leftarrow 0$
  if $q_{b,t}^{\mathrm{PV,set}} < -1$ **then** $q_{b,t}^{\mathrm{PV,set}} \leftarrow -1$
$Q_{b,t}^{\mathrm{PV,set}} \leftarrow q_{b,t}^{\mathrm{PV,set}} \cdot Q_b^{\mathrm{PV,max}}$

Algorithm 2: Determination of reactive power setpoints for reactive-power-based voltage maintenance. Used by the DSO for each building in the centralized strategy or by each building in the distributed strategy. Positive setpoints denote absorption and negative setpoints injection of reactive power. For the symbol descriptions see Table 4.4.

Data: See Table 4.4

Result:

$Q_{b,t}^{\mathrm{PV,set}}$ Reactive power setpoint for building b in management interval t [var]

Initialization (once, if undefined):

$q_{b,t-1}^{\mathrm{PV,set}} \leftarrow 0$; $c_b^{\mathrm{upp}} \leftarrow 0$; $c_b^{\mathrm{low}} \leftarrow 0$; $N_\mathrm{Q} \leftarrow \dfrac{T_\mathrm{Q}}{\Delta t}$

$u_b^{\mathrm{upp,dec}} \leftarrow u_\mathrm{Q}^{\mathrm{upp}} - \Delta u_\mathrm{Q}^{\mathrm{coe}} \cdot \left(1 - \frac{d_b}{d_{l(b)}}\right)$; $u_b^{\mathrm{low,dec}} \leftarrow u_\mathrm{Q}^{\mathrm{low}} + \Delta u_\mathrm{Q}^{\mathrm{coe}} \cdot \left(1 - \frac{d_b}{d_{l(b)}}\right)$

$u_b^{\mathrm{jum,min,dec}} \leftarrow 1\,\mathrm{pu} + \left(u_\mathrm{Q}^{\mathrm{jum,min}} - 1\,\mathrm{pu}\right) \cdot \frac{u_b^{\mathrm{upp,dec}} - 1\,\mathrm{pu}}{u_\mathrm{Q}^{\mathrm{upp}} - 1\,\mathrm{pu}}$; $\Delta u_b^{\mathrm{jum,dec}} \leftarrow \Delta u_\mathrm{Q}^{\mathrm{jum}} \cdot \frac{u_b^{\mathrm{upp,dec}} - 1\,\mathrm{pu}}{u_\mathrm{Q}^{\mathrm{upp}} - 1\,\mathrm{pu}}$

$\Delta u_b^{\mathrm{dea,dec}} \leftarrow \Delta u_\mathrm{Q}^{\mathrm{dea}} \cdot \frac{u_b^{\mathrm{upp,dec}} - 1\,\mathrm{pu}}{u_\mathrm{Q}^{\mathrm{upp}} - 1\,\mathrm{pu}}$

Each management interval:

$q_{b,t}^{\mathrm{PV,set}} \leftarrow q_{b,t-1}^{\mathrm{PV,set}}$

if $q_{b,t}^{\mathrm{PV,set}} \geq 0$ **then**

- **if** $u_{b,t} > u_b^{\mathrm{upp,dec}} \vee u_{b,t} > u_b^{\mathrm{jum,min,dec}} \wedge u_{b,t} - u_{b,t-1} > \Delta u_b^{\mathrm{jum,dec}}$ **then**
  - **if** $q_{b,t}^{\mathrm{PV,set}} \leq q^{\mathrm{lar|sma}}$ **then** $q_{b,t}^{\mathrm{PV,set}} \leftarrow q_{b,t}^{\mathrm{PV,set}} + \Delta q^{\mathrm{lar}}$
  - **else if** $u_{b,t} > u_b^{\mathrm{upp,dec}}$ **then** $q_{b,t}^{\mathrm{PV,set}} \leftarrow q_{b,t}^{\mathrm{PV,set}} + \Delta q^{\mathrm{sma}}$
- **else if** $u_{b,t} \geq u_b^{\mathrm{upp,dec}} - \Delta u_b^{\mathrm{dea,dec}}$ **then** $c_b^{\mathrm{upp}} \leftarrow 0$
- **else if** $q_{b,t}^{\mathrm{PV,set}} > 0$ **then**
  - $c_b^{\mathrm{upp}} \leftarrow c_b^{\mathrm{upp}} + 1$
  - **if** $c_b^{\mathrm{upp}} \geq N_\mathrm{Q} \vee u_{b,t} < 1\,\mathrm{pu}$ **then** $q_{b,t}^{\mathrm{PV,set}} \leftarrow q_{b,t}^{\mathrm{PV,set}} - \Delta q^{\mathrm{sma}}$
  - **if** $q_{b,t}^{\mathrm{PV,set}} < 0$ **then** $q_{b,t}^{\mathrm{PV,set}} \leftarrow 0$
- **if** $q_{b,t}^{\mathrm{PV,set}} > 1$ **then** $q_{b,t}^{\mathrm{PV,set}} \leftarrow 1$

if $q_{b,t}^{\mathrm{PV,set}} \leq 0$ **then**

- **if** $u_{b,t} < u_b^{\mathrm{low,dec}}$ **then** $q_{b,t}^{\mathrm{PV,set}} \leftarrow q_{b,t}^{\mathrm{PV,set}} - \Delta q^{\mathrm{sma}}$
- **else if** $u_{b,t} \leq u_b^{\mathrm{low,dec}} + \Delta u_b^{\mathrm{dea,dec}}$ **then** $c_b^{\mathrm{low}} \leftarrow 0$
- **else if** $q_{b,t}^{\mathrm{PV,set}} < 0$ **then**
  - $c_b^{\mathrm{low}} \leftarrow c_b^{\mathrm{low}} + 1$
  - **if** $c_b^{\mathrm{low}} \geq N_\mathrm{Q} \vee u_{b,t} > 1\,\mathrm{pu}$ **then** $q_{b,t}^{\mathrm{PV,set}} \leftarrow q_{b,t}^{\mathrm{PV,set}} + \Delta q^{\mathrm{sma}}$
  - **if** $q_{b,t}^{\mathrm{PV,set}} > 0$ **then** $q_{b,t}^{\mathrm{PV,set}} \leftarrow 0$
- **if** $q_{b,t}^{\mathrm{PV,set}} < -1$ **then** $q_{b,t}^{\mathrm{PV,set}} \leftarrow -1$

$Q_{b,t}^{\mathrm{PV,set}} \leftarrow q_{b,t}^{\mathrm{PV,set}} \cdot Q_b^{\mathrm{PV,max}}$

Algorithm 3: Determination of reactive power setpoints for reactive-power-based voltage maintenance. Used by each building currently operating with the decentralized strategy. Positive setpoints denote absorption and negative setpoints injection of reactive power. For the symbol descriptions see Table 4.4.

generation of BEVs and BESSs can be adjusted without curtailment, the time of operation of HPs and CHP plants can be shifted within the day (see also Section 2.3).

Since different types of electrical disturbances require adjusted algorithms, we use different algorithms for PV curtailment, depending on whether the occurring disturbance is line- or transformer-related. For voltage disturbances, we do not require a PV curtailment algorithm, since these can be fully addressed using reactive-power-based voltage maintenance or a VRDT if available. The PV curtailment algorithms introduced in the following are utilized in the centralized strategy by the DSO for each building or in the distributed strategy by each building. The appropriate curtailment settings learned by these algorithms are saved to be applied in the decentralized strategy if needed. Consequently, there is no separate PV curtailment algorithm for the decentralized strategy.

While the algorithm for transformer disturbances is fully dynamic, that is, PV curtailment is adjusted every time a transformer disturbance occurs or fades, the algorithm for line disturbances learns individual curtailment settings for each line, which are constantly applied to each building fed by it. This distinction is made to account for the thermal inertia of transformers, which allows the exceedance of their rated power for a certain amount of time until a critical temperature is reached. In contrast, lines can only be overloaded for a relatively short duration until protective equipment is triggered and electricity outages occur [325].

The algorithms do not directly limit the active power produced by a PV system, but the apparent power at the GCP of the building on which the PV system is installed, since this is the actual power that determines line and transformer loading. This means that the active power flexibility of the buildings can be used to lessen the impact of PV curtailment. The actual PV generation is only curtailed as far as is necessary to satisfy the apparent power limit for the GCP. The basis for the curtailment is the rated apparent power of the PV inverter. As an example, an apparent power limit of 50 % of the rated apparent power of the inverter would entail that this apparent power can be fed into the grid at any given time, regardless of whether the actual active power generated by the PV system is currently higher or lower than 50 % of its peak active power. For instance, the PV system could currently generate 70 % of its peak active power, while the inverter implements reactive power compensation, and the other devices in the building consume 20 % of the peak power of the PV system. In this case, the active power generation of the PV system is not curtailed, while the apparent power limit at the GCP is still met. An example in the opposite direction for the same apparent power limit could be a situation in which the PV system could currently generate 50 % of its peak active power, but the inverter currently implements reactive-power-based voltage maintenance while all other devices in the building are switched off and consume no active power. In this case, the active power generation of the PV system has to be curtailed to below 50 % of its peak active power to satisfy the apparent power limit.

The symbol descriptions for Algorithms 4 and 5 are given in Table 4.5. The values of the newly introduced parameters $s_{\mathrm{L}}^{\mathrm{ini}}$, $s_{\mathrm{L}}^{\mathrm{lar|sma}}$, $\Delta s_{\mathrm{L}}^{\mathrm{lar}}$, $\Delta s_{\mathrm{L}}^{\mathrm{sma}}$, $s_{\mathrm{T}}^{\mathrm{ini}}$, $s_{\mathrm{T}}^{\mathrm{lar|sma}}$, $\Delta s_{\mathrm{T}}^{\mathrm{lar}}$, $\Delta s_{\mathrm{T}}^{\mathrm{sma}}$, and $\Delta s_{\mathrm{T}}^{\mathrm{off}}$ are determined in parameter studies (see Section 4.12.)

Table 4.5: Symbol descriptions for Algorithms 4 and 5. Line segment currents are normalized to the rated current of the applicable line segment. Normalized apparent powers (symbol s) are normalized to the rated apparent power of the PV inverter of the respective building.

Symbol	Description
t	Management interval index [-]
b	Building index [-]
$s_{b,t}^{\text{lim}}$	Normalized apparent power limit at the GCP of building b in management interval t [-]
t_b^{lim}	Management interval of the last apparent power limit change for building b [-]
$i_{l(b),t}$	Maximum of the normalized magnitudes of the line segment currents on line l feeding building b in management interval t [-]
i_{S}	Normalized line current threshold for PV curtailment [-]
$s_{\text{L}}^{\text{ini}}$	Initial normalized apparent power limit for line disturbances [-]
$s_{\text{L}}^{\text{lar\|sma}}$	Normalized apparent power level for step size switching for line disturbances [-]
$\Delta s_{\text{L}}^{\text{lar/sma}}$	Normalized apparent power large/small step for line disturbances [-]
$s_{l(b)}^{\text{lim}}$	Learned normalized apparent power limit for line disturbances on the line l feeding building b [-]
$s_{\text{T}}^{\text{lim}}$	Learned normalized apparent power limit for transformer disturbances [-]
$s_b^{\text{lim,dec}}$	Learned normalized apparent power limit for the decentralized strategy for building b [-]
$S_b^{\text{PV,max}}$	Rated apparent power of the PV inverter of building b [VA]
b'	Building index for iterating over all buildings in the grid [-]
$\mathbf{B}$	Set of all buildings in the grid [-]
θ_t	Transformer hot-spot temperature in management interval t [°C]
$\theta^{\text{upp/mid/low}}$	Upper/mid/lower transformer hot-spot temperature threshold for PV curtailment [°C]
$s_{\text{T}}^{\text{ini}}$	Initial normalized apparent power limit for transformer disturbances [-]
$s_{\text{T}}^{\text{lar\|sma}}$	Normalized apparent power level for step size switching for transformer disturbances [-]
$\Delta s_{\text{T}}^{\text{lar/sma}}$	Normalized apparent power large/small step for transformer disturbances [-]
$\Delta s_{\text{T}}^{\text{off}}$	Normalized apparent power offset for $s_{\text{T}}^{\text{lim}}$ [-]

The PV curtailment algorithm for line disturbances is given in Algorithm 4.

Data: See Table 4.5

Result:

$S_{b,t}^{\text{lim}}$ Apparent power limit at the GCP of building b in man. interval t [VA]

Initialization (once, if undefined):

$s_{b,t-1}^{\text{lim}}, s_{\text{T}}^{\text{lim}}, s_{b}^{\text{lim,dec}} \leftarrow 1$; $t_{b}^{\text{lim}} \leftarrow t-1$

Each management interval:

$s_{b,t}^{\text{lim}} \leftarrow s_{b,t-1}^{\text{lim}}$

if $i_{l(b),t} > i_{\text{S}} \wedge t_{b}^{\text{lim}} \neq t$ **then**

- **if** $s_{b,t}^{\text{lim}} > s_{\text{L}}^{\text{ini}}$ **then** $s_{b,t}^{\text{lim}} \leftarrow s_{\text{L}}^{\text{ini}}$
- **else if** $s_{b,t}^{\text{lim}} > s_{\text{L}}^{\text{lar|sma}}$ **then**
  - **if** $s_{b,t}^{\text{lim}} \bmod \left(\Delta s_{\text{L}}^{\text{lar}}\right) > 0$ **then** $s_{b,t}^{\text{lim}} \leftarrow s_{b,t}^{\text{lim}} - s_{b,t}^{\text{lim}} \bmod \left(\Delta s_{\text{L}}^{\text{lar}}\right)$
  - **else** $s_{b,t}^{\text{lim}} \leftarrow s_{b,t}^{\text{lim}} - \Delta s_{\text{L}}^{\text{lar}}$
- **else if** $s_{b,t}^{\text{lim}} \bmod \left(\Delta s_{\text{L}}^{\text{sma}}\right) > 0$ **then** $s_{b,t}^{\text{lim}} \leftarrow s_{b,t}^{\text{lim}} - s_{b,t}^{\text{lim}} \bmod \left(\Delta s_{\text{L}}^{\text{sma}}\right)$
- **else** $s_{b,t}^{\text{lim}} \leftarrow s_{b,t}^{\text{lim}} - \Delta s_{\text{L}}^{\text{sma}}$
- $t_{b}^{\text{lim}} \leftarrow t$; $s_{l(b)}^{\text{lim}} \leftarrow s_{b,t}^{\text{lim}}$; $s_{b}^{\text{lim,dec}} \leftarrow \min\left(s_{l(b)}^{\text{lim}}, s_{\text{T}}^{\text{lim}}\right)$

if $s_{b,t}^{\text{lim}} < 0$ **then** $s_{b,t}^{\text{lim}} \leftarrow 0$

$S_{b,t}^{\text{lim}} \leftarrow s_{b,t}^{\text{lim}} \cdot S_{b}^{\text{PV,max}}$

Algorithm 4: PV curtailment algorithm for line disturbances. Executed by the DSO for each building in the centralized strategy or by each building in the distributed strategy. "mod" denotes the real remainder. In the decentralized strategy, each building uses its learned limit $s_{b}^{\text{lim,dec}}$ determined while using the other strategies. $s_{b',t}^{\text{lim}} = 1$ means that no curtailment is applied.

After setting an initial normalized apparent power limit $s_{\text{L}}^{\text{ini}}$ when a line disturbance first occurs, the normalized apparent power limit $s_{b,t}^{\text{lim}}$ is only lowered gradually to prevent excessive PV curtailment. $s_{b,t}^{\text{lim}}$ is only lowered as far as is necessary to remedy the line disturbance. Initially, a larger normalized apparent power step size $\Delta s_{\text{L}}^{\text{lar}}$ is used until a predefined normalized apparent power level $s_{\text{L}}^{\text{lar|sma}}$ is reached. From then on, a smaller step size $\Delta s_{\text{L}}^{\text{sma}}$ is used, again, to prevent excessive PV curtailment. Before $s_{b,t}^{\text{lim}}$ is lowered, we check if the current limit is a multiple of the step size to be used. If it is not, the corresponding residual is subtracted from $s_{b,t}^{\text{lim}}$ instead. This is done to ensure that the algorithm for line disturbances and the algorithm for transformer disturbances do not interfere with each other in the case of simultaneous line and transformer disturbances. Another measure to avoid such interference is to save the time when a limit was last set t_{b}^{lim}, so that $s_{b,t}^{\text{lim}}$ is not lowered twice in one management interval. Each lower limit is saved as the learned normalized apparent power limit to prevent line disturbances

$s_{l(b)}^{\text{lim}}$. Subsequently, $s_{l(b)}^{\text{lim}}$ is compared to the learned normalized apparent power limit to prevent transformer disturbances $s_{\text{T}}^{\text{lim}}$ and the lower of the two values is saved as the learned normalized apparent power limit for the decentralized strategy for building b $s_b^{\text{lim,dec}}$. Finally, $s_{b,t}^{\text{lim}}$ is multiplied by the rated apparent power of the PV inverter of building b $S_b^{\text{PV,max}}$ to determine the (non-normalized) apparent power limit at the GCP of building b in management interval t $S_{b,t}^{\text{lim}}$. It is important to note that $S_{b,t}^{\text{lim}}$ can only be lowered in response to line disturbances, but not increased again. When the final $S_{b,t}^{\text{lim}}$ that prevents all potential line-related outages is found, it is upheld indefinitely, unless the physical grid configuration changes.

The algorithm permits short-term and moderate exceedance of rated line currents while learning the appropriate $s_{l(b)}^{\text{lim}}$, which is the same for all buildings connected to a particular line. We allow this to exploit the rated currents of all lines as much as possible so that no active energy potentially generatable by the PV systems is wasted. This is unproblematic for the lines and the utilized fuses, as long as the magnitude and duration of the exceedances stay within certain ranges. This is explained in more detail in Section 4.11. The algorithm also ensures that rated line currents are never exceeded due to PV-generated active power after the appropriate normalized apparent power limit for each line has been learned.

In Algorithm 4, the control variable $S_{b,t}^{\text{lim}}$ is bounded to $[0, S_b^{\text{PV,max}}]$ and can only be lowered in discrete increments once each management interval. This respects the limits of the particular inverter and prevents saturation effects. Measures to reduce oscillations are not needed in this algorithm, since $S_{b,t}^{\text{lim}}$ can only be lowered and not increased again.

The PV curtailment algorithm for transformer disturbances is given in Algorithm 5.

The PV curtailment algorithm for transformer disturbances is similar to the one for line disturbances. However, there are some key differences.

Instead of the single disturbance criterion used for line disturbances, three different temperature thresholds are utilized.

If the measured transformer temperature θ_t is above the upper threshold θ^{upp}, the normalized apparent power limit $s_{b,t}^{\text{lim}}$ can be lowered regardless of whether θ_t is lower or higher than the measured temperature in the previous management interval θ_{t-1}. This prevents the temperature from slowly rising over time if a currently sufficient $s_{b,t}^{\text{lim}}$ is set that is insufficient to prevent the temperature from rising in the future. To illustrate this point: if the current temperature is 118 °C and the previously measured temperature is 119 °C, $s_{b,t}^{\text{lim}}$ would not be lowered. In the next management interval, the temperature could now rise to 121 °C, so that only then a new limit would be set. However, the maximum admissible temperature of 120 °C (see also Section 2.5.2) would already have been exceeded.

If the transformer temperature is currently below θ^{upp}, but above the mid temperature threshold θ^{mid}, $s_{b,t}^{\text{lim}}$ can only be lowered if θ_t is higher than θ_{t-1}. This is done to prevent excessive PV curtailment, which may not be needed to keep the temperature inside the admissible range. Due to the thermal inertia of the transformer oil, the transformer takes a certain time to cool down. This means that a decreased $s_{b,t}^{\text{lim}}$ may not take full effect

Data: See Table 4.5

Result:

$S_{b,t}^{\text{lim}}$ Apparent power limit at the GCP of building b in management interval t [VA]

Initialization (once, if undefined):

foreach $b' \in \mathbf{B}$ **do**

  $s_{b',t-1}^{\text{lim}} \leftarrow 1$

$s_{b,t-1}^{\text{lim}}, s_{\text{T}}^{\text{lim}}, s_{l(b)}^{\text{lim}}, s_{b}^{\text{lim,dec}} \leftarrow 1$; $t_b^{\text{lim}} \leftarrow t-1$

Each management interval:

$s_{b,t}^{\text{lim}} \leftarrow s_{b,t-1}^{\text{lim}}$

if $\left(\theta_t > \theta^{\text{upp}} \vee \theta_t > \theta^{\text{mid}} \wedge \theta_t \geq \theta_{t-1}\right) \wedge t_b^{\text{lim}} \neq t \wedge s_{b,t}^{\text{lim}} = \max_{b' \in \mathbf{B}} \left(s_{b',t-1}^{\text{lim}}\right)$ **then**

  if $s_{b,t}^{\text{lim}} > s_{\text{T}}^{\text{ini}}$ **then** $s_{b,t}^{\text{lim}} \leftarrow s_{\text{T}}^{\text{ini}}$

  else if $s_{b,t}^{\text{lim}} > s_{\text{T}}^{\text{lar|sma}}$ **then**

    if $s_{b,t}^{\text{lim}} \bmod \left(\Delta s_{\text{T}}^{\text{lar}}\right) > 0$ **then** $s_{b,t}^{\text{lim}} \leftarrow s_{b,t}^{\text{lim}} - s_{b,t}^{\text{lim}} \bmod \left(\Delta s_{\text{T}}^{\text{lar}}\right)$

    else $s_{b,t}^{\text{lim}} \leftarrow s_{b,t}^{\text{lim}} - \Delta s_{\text{T}}^{\text{lar}}$

  else if $s_{b,t}^{\text{lim}} \bmod \left(\Delta s_{\text{T}}^{\text{sma}}\right) > 0$ **then** $s_{b,t}^{\text{lim}} \leftarrow s_{b,t}^{\text{lim}} - s_{b,t}^{\text{lim}} \bmod \left(\Delta s_{\text{T}}^{\text{sma}}\right)$

  else $s_{b,t}^{\text{lim}} \leftarrow s_{b,t}^{\text{lim}} - \Delta s_{\text{T}}^{\text{sma}}$

  $t_b^{\text{lim}} \leftarrow t$

  if $s_{b,t}^{\text{lim}} + \Delta s_{\text{T}}^{\text{off}} < s_{\text{T}}^{\text{lim}} \wedge \theta_t \geq \theta_{t-1}$ **then**

    $s_{\text{T}}^{\text{lim}} \leftarrow s_{b,t}^{\text{lim}} + \Delta s_{\text{T}}^{\text{off}}$; $s_{b}^{\text{lim,dec}} \leftarrow \min\left(s_{l(b)}^{\text{lim}}, s_{\text{T}}^{\text{lim}}\right)$

else if $\theta_t \leq \theta^{\text{low}} \wedge s_{b,t}^{\text{lim}} < 1 \wedge t_b^{\text{lim}} \neq t \wedge s_{b,t}^{\text{lim}} < s_{l(b)}^{\text{lim}}$ **then**

  $s_{b,t}^{\text{lim}} \leftarrow s_{b,t}^{\text{lim}} + \Delta s_{\text{T}}^{\text{sma}}$; $t_b^{\text{lim}} \leftarrow t$; **if** $s_{b,t}^{\text{lim}} > s_{l(b)}^{\text{lim}}$ **then** $s_{b,t}^{\text{lim}} \leftarrow s_{l(b)}^{\text{lim}}$

if $s_{b,t}^{\text{lim}} > 1$ **then** $s_{b,t}^{\text{lim}} \leftarrow 1$

else if $s_{b,t}^{\text{lim}} < 0$ **then** $s_{b,t}^{\text{lim}} \leftarrow 0$

$S_{b,t}^{\text{lim}} \leftarrow s_{b,t}^{\text{lim}} \cdot S_{b}^{\text{PV,max}}$

Algorithm 5: PV curtailment algorithm for transformer disturbances. Executed by the DSO for each building in the centralized strategy or by each building in the distributed strategy. "mod" denotes the real remainder. Normalized apparent power limits $s_{b',t}^{\text{lim}}$ are communicated among buildings. In the decentralized strategy, each building uses its learned limit $s_{b}^{\text{lim,dec}}$ determined while using the other strategies. $s_{b',t}^{\text{lim}} = 1$ means that no curtailment is applied.

immediately, which would prompt a further, but unnecessary limit decrease in the next management interval if the temperature trend is not considered.

All buildings with PV systems in the grid contribute to transformer loading when their PV systems generate active power, but some buildings may already implement an apparent power limit to prevent disturbances on the line that feeds them, while others require no or a less restrictive apparent power limit for their particular line. To increase the fairness when curtailing PV systems in response to transformer disturbances, we only decrease the apparent power limits of a building if its $s_{b,t}^{\mathrm{lim}}$ currently corresponds to the maximum normalized apparent power limit among all buildings $\max_{b' \in \mathbf{B}} \left(s_{b',t-1}^{\mathrm{lim}} \right)$. Note that this can still include a large number of buildings.

We add a normalized apparent power offset $\Delta s_{\mathrm{T}}^{\mathrm{off}}$ to the normalized apparent power limit when assigning a new value to the learned normalized apparent power limit to prevent transformer disturbances $s_{\mathrm{T}}^{\mathrm{lim}}$. We do this because of the thermal inertia of the transformer oil. In the centralized and distributed strategies, the apparent power limit is lowered and increased dynamically to enable timely reactions to potential overheating, but curtailing the active power generation of PV systems as little as possible. In many situations, this leads to apparent power limits that are relatively low for short time periods until the transformer temperature decreases below a certain threshold. When applying this relatively low learned normalized apparent power limit continuously in the decentralized strategy, the transformer heats up substantially less than in the other strategies, staying far below the maximum admissible temperature. The applied offset mitigates this effect. As in Algorithm 4, $s_{\mathrm{T}}^{\mathrm{lim}}$ is compared to the learned normalized apparent power limit to prevent line disturbances $s_{l(b)}^{\mathrm{lim}}$ and the lower of the two values is saved as the learned normalized apparent power limit for the decentralized strategy $s_b^{\mathrm{lim,dec}}$.

Only if the transformer temperature is below or equal to the lower temperature threshold θ^{low}, $s_{b,t}^{\mathrm{lim}}$ is increased again. The increase is stopped if θ^{low} is exceeded again or if $s_{l(b)}^{\mathrm{lim}}$ is reached. In contrast to Algorithm 4, here, it is useful to increase $s_{b,t}^{\mathrm{lim}}$ if θ_t is below θ^{low}, as the thermal inertia of the transformer allows for higher apparent power transfer until θ^{low} is reached.

As in Algorithm 4, the control variable $S_{b,t}^{\mathrm{lim}}$ is bounded to $[0, S_b^{\mathrm{PV,max}}]$ to respect the limits of the particular inverter and prevent saturation effects. The temperature range between θ^{low} and θ^{mid} acts as a deadband to reduce oscillations. Oscillations are further mitigated by only adjusting $S_{b,t}^{\mathrm{lim}}$ in discrete increments once each management interval. We do not use a time delay before increasing $S_{b,t}^{\mathrm{lim}}$ when the temperature falls below θ^{low}, since the thermal inertia of the transformer oil already has a dampening effect, and further delays would increase the losses of potentially generatable active energy due to PV curtailment.

After Algorithms 4 and 5 determine a new $S_{b,t}^{\mathrm{lim}}$, the building implements it by determining the maximum active power the PV system is allowed to generate $P_{b,t_{\mathrm{sim}}}^{\mathrm{PV,min}}$ in the next simulation step t_{sim} based on power data observed in the previous simulation step $t_{\mathrm{sim}} - 1$. Note that we use *min* instead of *max* in the symbol for this power, since we use a positive

sign for active power consumption and a negative sign for active power generation. In a real-world deployment, the allowed active power generation would be recalculated between measurement instants instead of simulation steps.

The approximate (since it is not exactly known yet) apparent power at the GCP of building b at simulation step t_{sim} can be calculated using Equation 4.16:

$$\left(S_{b,t_{\text{sim}}}\right)^2 = \left(P_{b,t_{\text{sim}}}\right)^2 + \left(Q_{b,t_{\text{sim}}}\right)^2 \tag{4.16}$$

In Equation 4.16, $S_{b,t_{\text{sim}}}$, $P_{b,t_{\text{sim}}}$, and $Q_{b,t_{\text{sim}}}$ denote the approximate apparent, active, and reactive power at the GCP of building b at simulation step t_{sim}, respectively. It should be noted that these powers can deviate from the actual powers at t_{sim}, since the latter are also subject to unpredictable changes between simulation steps resulting from the behavior of building inhabitants and the load profiles of the devices in the building. We assume such changes to be small in comparison to the power produced by the PV system and thus disregard them for PV curtailment.

$P_{b,t_{\text{sim}}}$ can be calculated according to Equation 4.17:

$$P_{b,t_{\text{sim}}} = P_{b,t_{\text{sim}}-1} + P^{\text{PV}}_{b,t_{\text{sim}}} - P^{\text{PV}}_{b,t_{\text{sim}}-1} + P^{\text{bat,cha}\star}_{b,t_{\text{sim}}} - P^{\text{bat,cha}}_{b,t_{\text{sim}}-1} \tag{4.17}$$

Here, $P^{\text{PV}}_{b,t_{\text{sim}}}$ is the approximate active power generated by the PV system of building b at simulation step t_{sim}. $P^{\text{PV}}_{b,t_{\text{sim}}-1}$ is the (actual) active power generated at the previous simulation step. As mentioned previously, we define consumed power to have a positive sign and generated power to have a negative sign. This means that $P^{\text{PV}}_{b,t_{\text{sim}}}$ can only be negative or zero, since the PV system can only generate and not consume active power, with the exception of the active power needed to run the PV inverter. The latter is considered and part of the (actual) active power at the GCP of building b at the previous simulation step $P_{b,t_{\text{sim}}-1}$. $P^{\text{bat,cha}\star}_{b,t_{\text{sim}}}$ is the optimized maximum charging power of the BESS of building b applicable at simulation step t_{sim} determined by the optimization algorithm of the BEMS. $P^{\text{bat,cha}}_{b,t_{\text{sim}}-1}$ is the (actual) charging power of the BESS at the previous simulation step. The inclusion of the term $P^{\text{bat,cha}\star}_{b,t_{\text{sim}}} - P^{\text{bat,cha}}_{b,t_{\text{sim}}-1}$ is important, since the actual charging power of the BESS not only depends on the optimized maximum charging power, but also on the active power currently available for charging, that is, the active power that would otherwise be fed into the distribution grid and depends on $P^{\text{PV}}_{b,t_{\text{sim}}}$. If the term $P^{\text{bat,cha}\star}_{b,t_{\text{sim}}} - P^{\text{bat,cha}}_{b,t_{\text{sim}}-1}$ is not considered when determining $P^{\text{PV,min}}_{b,t_{\text{sim}}}$, while still satisfying $S^{\text{lim}}_{b,t}$, the fraction of $P^{\text{PV}}_{b,t_{\text{sim}}}$ that could be used to charge the BESS instead of being fed into the grid would not be generated.

$Q_{b,t_{\text{sim}}}$ can be calculated according to Equation 4.18:

$$Q_{b,t_{\text{sim}}} = Q^{\text{PV,set}}_{b,t_{\text{sim}}} + Q_{b,t_{\text{sim}}-1} - Q^{\text{PV}}_{b,t_{\text{sim}}-1} \tag{4.18}$$

Here, $Q^{\mathrm{PV,set}}_{b,t_{\mathrm{sim}}}$ is the reactive power setpoint for the PV inverter applicable at simulation step t_{sim} determined according to Equation 4.15, Algorithm 2, or Algorithm 3. $Q_{b,t_{\mathrm{sim}}-1}$ is the (actual) reactive power at the GCP of building b at the previous simulation step. $Q^{\mathrm{PV}}_{b,t_{\mathrm{sim}}-1}$ is the (actual) reactive power absorbed or injected by the PV inverter at the previous simulation step.

Equations 4.16, 4.17, and 4.18 can be combined to form Equation 4.19:

$$\left(S_{b,t_{\mathrm{sim}}}\right)^2 = \left(P_{b,t_{\mathrm{sim}}-1} + P^{\mathrm{PV}}_{b,t_{\mathrm{sim}}} - P^{\mathrm{PV}}_{b,t_{\mathrm{sim}}-1} + P^{\mathrm{bat,cha}\star}_{b,t_{\mathrm{sim}}} - P^{\mathrm{bat,cha}}_{b,t_{\mathrm{sim}}-1}\right)^2 + \left(Q^{\mathrm{PV,set}}_{b,t_{\mathrm{sim}}} + Q_{b,t_{\mathrm{sim}}-1} - Q^{\mathrm{PV}}_{b,t_{\mathrm{sim}}-1}\right)^2 \quad (4.19)$$

Solving Equation 4.19 for $P^{\mathrm{PV}}_{b,t_{\mathrm{sim}}}$, replacing $P^{\mathrm{PV}}_{b,t_{\mathrm{sim}}}$ with $P^{\mathrm{PV,min}}_{b,t_{\mathrm{sim}}}$, and $S_{b,t_{\mathrm{sim}}}$ with the apparent power limit for the current management interval $S^{\mathrm{lim}}_{b,t}$ results in Equation 4.20:

$$P^{\mathrm{PV,min}}_{b,t_{\mathrm{sim}}} = P^{\mathrm{PV}}_{b,t_{\mathrm{sim}}-1} + P^{\mathrm{bat,cha}}_{b,t_{\mathrm{sim}}-1} - P^{\mathrm{bat,cha}\star}_{b,t_{\mathrm{sim}}} - P_{b,t_{\mathrm{sim}}-1} \pm \sqrt{\left(S^{\mathrm{lim}}_{b,t}\right)^2 - \left(Q^{\mathrm{PV,set}}_{b,t_{\mathrm{sim}}} + Q_{b,t_{\mathrm{sim}}-1} - Q^{\mathrm{PV}}_{b,t_{\mathrm{sim}}-1}\right)^2} \quad (4.20)$$

Since there are two solutions to Equation 4.19, we have to determine the correct solution for the problem at hand. In Equation 4.20, the term under the square root must not be smaller than zero, since $P^{\mathrm{PV,min}}_{b,t_{\mathrm{sim}}}$ has to be a real number. As mentioned earlier, $P^{\mathrm{PV}}_{b,t_{\mathrm{sim}}}$ can only be negative or zero. For the solution in which the square root term is added, $P^{\mathrm{PV,min}}_{b,t_{\mathrm{sim}}}$ increases as $S^{\mathrm{lim}}_{b,t}$ increases. This is not the desired behavior, as a higher (that is, less restrictive) $S^{\mathrm{lim}}_{b,t}$ should entail higher (more negative $P^{\mathrm{PV,min}}_{b,t_{\mathrm{sim}}}$) and not lower (positive or less negative $P^{\mathrm{PV,min}}_{b,t_{\mathrm{sim}}}$) PV generation. Consequently, we use the solution where the square root term is subtracted.

Following the previous explanations, $P^{\mathrm{PV,min}}_{b,t_{\mathrm{sim}}}$, which is set using the PV inverter, to achieve a given $S^{\mathrm{lim}}_{b,t}$ is calculated according to Equations 4.21 to 4.24 in all three management strategies:

$$A = P^{\mathrm{PV}}_{b,t_{\mathrm{sim}}-1} + P^{\mathrm{bat,cha}}_{b,t_{\mathrm{sim}}-1} - P^{\mathrm{bat,cha}\star}_{b,t_{\mathrm{sim}}} - P_{b,t_{\mathrm{sim}}-1} \quad (4.21)$$

$$B = \left(S^{\mathrm{lim}}_{b,t}\right)^2 \quad (4.22)$$

$$C = \left(Q^{\mathrm{PV,set}}_{b,t_{\mathrm{sim}}} + Q_{b,t_{\mathrm{sim}}-1} - Q^{\mathrm{PV}}_{b,t_{\mathrm{sim}}-1}\right)^2 \quad (4.23)$$

$$P_{b,t_{\text{sim}}}^{\text{PV,min}} = \begin{cases} A - \sqrt{B - C} & , \quad A \leq \sqrt{B - C} \wedge B \geq C \\ A & , \quad A \leq 0 \wedge B < C \\ 0 & , \quad \text{otherwise} \end{cases} \tag{4.24}$$

For better readability, Equations 4.21 to 4.24 are not combined into a single equation. Equation 4.24 considers three different cases. In the first case, $S_{b,t}^{\text{lim}}$ is larger than or equal to the expected magnitude of the reactive power at the GCP of building b. This means that the square root term $\sqrt{B - C}$ always leads to $P_{b,t_{\text{sim}}}^{\text{PV,min}}$ being a real number and thus can be used. For this case to be used, A must be smaller or equal to $\sqrt{B - C}$ as well, since $P_{b,t_{\text{sim}}}^{\text{PV,min}}$ would become positive otherwise, which is not physically possible. The second case is only used if the square root term is not usable and thus dropped, but the calculated $P_{b,t_{\text{sim}}}^{\text{PV,min}}$ is still negative or zero. Dropping the square root term means that $S_{b,t}^{\text{lim}}$ has already been reached or exceeded by the reactive power absorbed or injected at the GCP alone, and therefore there is no clearance that allows for further feed-in of active power at the GCP. Using only term A entails controlling $P_{b,t_{\text{sim}}}^{\text{PV,min}}$ in a way that keeps the active power at the GCP at approximately zero. The third case is only used, when both other cases can not be used, that is, if $P_{b,t_{\text{sim}}}^{\text{PV,min}}$ would receive a positive or complex value. In this case, the active power generation of the PV system is always curtailed to zero. If $P_{b,t_{\text{sim}}}^{\text{PV,min}}$ is not saturated by the actual active power generated by the PV system, the latter is not curtailed at simulation step t_{sim}.

Note that Equations 4.21 to 4.24 allow for exceeding a given $S_{b,t}^{\text{lim}}$ if the latter is smaller than the magnitude of $Q_{b,t_{\text{sim}}}$. This could only be avoided by curtailing the reactive power absorbed or injected by the PV system as well. However, this would restrict reactive-power-based voltage maintenance (see also Section 4.5.3), which is prioritized since voltage range deviations generally result in damaged equipment faster [231] than congestion [166, 323].

4.5.5. Active Power Flexibility

The flexibility of a building in adjusting its active power consumption or feed-in can be used for voltage maintenance as well as reducing the utilization of lines and transformers [32]. This can be especially useful in situations with a high simultaneity of load, for example, arising from PV generation around noon or BEV charging in the evening. In the context of this thesis, we do not directly use active power flexibility for voltage maintenance, as voltage maintenance is already achieved using reactive power or a VRDT (see also Sections 4.5.3 and 4.5.1). The active power flexibility provided by the buildings can thus be fully utilized to combat line and transformer disturbances. However, this can positively influence voltages as well, since the load profiles of the buildings are flattened by the use of active power flexibility against line and transformer disturbances. This in turn can reduce the need for reactive power, which further decreases the load on lines and the transformer.

If PV curtailment is active, that is, an apparent power limit is set (see also Section 4.5.4) and the current apparent power at the GCP of a building equals this limit, active power flexibility is not directly used to prevent disturbances. However, since this limit applies to the GCP of the building, the use of active power flexibility can reduce the actual curtailment of the PV system's active power generation.

We consider two different methods to achieve the use of active power flexibility for grid-supportive purposes. The first method uses active power targets to be achieved by utilizing the active power flexibility of a building, which can be set by the DSO in the centralized or by the buildings themselves in the distributed and decentralized grid management strategies. The second method factors in the PV curtailment during the determination of energy cost optimized device operation schedules for a building.

The first method is loosely based on the load shifting method implemented in [32]. This includes the flexibility calculation, flexibility ranking, and group-wise flexibility calls described in the following. However, our method is substantially adjusted with the aim of exploiting the available active power flexibility of the buildings more directly and comprehensively. Furthermore, it allows the grid-supportive use of active power flexibility without a central planner in the distributed and decentralized grid management strategies, while [32] focuses on centralized grid management. We determine appropriate values for the utilized parameters in parameter studies (see Section 4.12) to improve the flexibility exploitation further. Our method requires the BEMSs to allow for scheduling based on a given active power target. In the case of the OSH, the already implemented evolutionary algorithm and device models are used in conjunction with a new objective function that was implemented in [324]. The corresponding optimization problem is given in Equations 4.25 and 4.26:

$$N^{\mathrm{opt},\tau} = \frac{T^{\mathrm{opt}}}{\Delta\tau} \tag{4.25}$$

$$\boldsymbol{P}_{b,t}^{\mathrm{tar}\star} \in \underset{\boldsymbol{P}_{b,t}\in \mathbf{X}_{b,t}}{\arg\min} \sum_{\tau=1}^{N^{\mathrm{opt},\tau}} \left(P_{b,t,\tau} - P_b^{\mathrm{tar}}\right)^2 \tag{4.26}$$

In Equation 4.25, τ is the scheduling time slot index. $N^{\mathrm{opt},\tau}$ is the number of scheduling time slots in the active power target optimization horizon T^{opt}. $\Delta\tau$ is the duration of one scheduling time slot. In Equation 4.26, $\boldsymbol{P}_{b,t}^{\mathrm{tar}\star}$ is the target-optimized load profile for building b over the optimization horizon beginning in management interval t. $P_{b,t,\tau}$ is the average active power at the GCP of building b over scheduling time slot τ for the optimization horizon beginning in management interval t. $\boldsymbol{P}_{b,t}$ is a feasible load profile for building b over the optimization horizon beginning in management interval t, with components $P_{b,t,\tau}$ for $\tau = 1, \ldots, N^{\mathrm{opt},\tau}$. $\mathbf{X}_{b,t}$ is the set of all feasible load profiles for building b over the optimization horizon beginning in management interval t. $\mathbf{X}_{b,t}$ contains only load profiles that satisfy all constraints, such as the predicted PV generation profile, the predicted base load profile, user preferences, or device dimensioning and capabilities. These constraints

are the same as for the optimization with regard to energy costs, which predates this thesis. For an explanation of the optimization functionality of the OSH, see Section 2.4.2 as well as the publications referenced there. P_b^{tar} is the active power target. The terms in Equation 4.26 are squared to favor flatter load profiles over ones with more peaks. This is advantageous since new load peaks introduced by rescheduling can potentially intensify disturbances, despite the new load profile being very close to P_b^{tar} on average. It is important to note that the target-optimized load profile is a prediction. Scheduling inputs, such as the predicted PV generation profile, may deviate from their actual values, so that the actual load profile at the GCP of the building may deviate from the one determined by the optimization as well.

In contrast to the PV curtailment, we do not use an apparent power limit here, since reactive power is not relevant in this case. The reactive power absorbed or injected by devices in the building other than the PV system can be compensated by the PV inverter (see also Section 4.5.2) if necessary and if reactive-power-based voltage maintenance (see also Section 4.5.3) is currently not needed. If reactive-power-based voltage maintenance is used, Algorithms 2 and 3 adjust the reactive power setpoints for all relevant buildings, such that the appropriate amount of reactive power is absorbed from or injected into the grid to keep voltages inside the admissible range. This compensates for the reactive power absorbed or injected by devices other than PV systems as well.

To start the use of active power flexibility, the criteria introduced in Section 4.4 have to be met. If this is the case, all buildings that can potentially influence the particular disturbance determine and communicate their current active power flexibility to all other buildings and the DSO in the centralized and distributed strategies. In the centralized strategy, this process is initiated by the DSO. In the distributed strategy, each building initiates the process by itself if it detects a disturbance it can potentially influence. In the decentralized strategy, each building calculates its flexibility if the criteria defined for this strategy are met. However, since the communication of the calculated flexibility value to the other participants may not be possible due to the circumstances that prompted the building to switch to the decentralized strategy, successful communication is not assumed when using this strategy. Therefore, the building does not consider the flexibilities of other buildings when determining whether to use active power flexibility in the decentralized strategy.

To calculate its flexibility, each building first schedules its device operation according to its current optimization objective. In this thesis, this is the minimization of energy costs over the energy cost optimization horizon of 24 hours. The resulting cost-optimized load profile is saved. The particular temporal resolution for the optimized load profiles used for the evaluation in this thesis is five minutes. Higher resolutions substantially increase the computational cost and do not significantly improve the optimization [326]. After the cost-optimized load profile is determined, the building schedules its device usage again, but this time solving the active-power-target-based optimization problem given in Equation 4.26. When the target-optimized load profile is determined, it is compared to the cost-optimized load profile and the active power flexibility is calculated using Equation 4.27:

$$F_{b,t} = \sum_{\tau=1}^{N^{\mathrm{opt},\tau}} \left(\left(P_{b,t,\tau}^{\mathrm{cost}\star} - P_b^{\mathrm{tar}} \right)^2 - \left(P_{b,t,\tau}^{\mathrm{tar}\star} - P_b^{\mathrm{tar}} \right)^2 \right) \tag{4.27}$$

In Equation 4.27, $F_{b,t}$ is the active power flexibility of building b for the active power target optimization horizon beginning in management interval t. $P_{b,t,\tau}^{\mathrm{cost}\star}$ and $P_{b,t,\tau}^{\mathrm{tar}\star}$ are the cost-optimized and target-optimized average active powers at the GCP of building b over scheduling time slot τ for the optimization horizon beginning in management interval t, respectively. The other variables and parameters are the same as in Equation 4.26. It is important to note that $N^{\mathrm{opt},\tau}$ does not have to be equal to the number of scheduling time slots in the energy cost optimization horizon. Only overlapping scheduling time slots are compared. Both terms inside the sum are squared so that higher deviations from the active power target are weighted higher than lower deviations for both the cost-optimized as well as the target-optimized load profile. As in the active-power-target-based optimization problem in Equation 4.26, this is aimed at reducing load peaks, which lead to especially high load on lines and the transformer as well as voltage fluctuations. An $F_{b,t}$ of zero or below means that the implementation of the target-optimized load profile would not improve the grid status and the building should continue acting as if it was uncritical. An $F_{b,t}$ below zero can occur due to the functionality of the utilized evolutionary algorithm, which is aimed at finding good solutions within a short time as opposed to finding optimal solutions. This functionality is utilized because, in real applications, building optimization algorithms often have to run on low-cost, low-energy computers and repeatedly throughout the day. Furthermore, the uncertainty associated with the optimization of the energy flows of a building diminishes the advantages of optimal over good solutions [158]. However, this can lead to certain cost-optimized load profiles being nearer to an active power target on average than certain target-optimized load profiles by accident, especially if the current flexibility of the building is low. If this happens, the current flexibility of a building is assumed to be zero. A positive $F_{b,t}$ indicates that the building can improve the grid status and enables a comparison with the flexibility of other buildings.

When the buildings have calculated their respective flexibilities in the centralized or distributed strategies, they communicate them to the DSO and all other buildings. In the centralized strategy, the DSO then ranks all buildings with a positive flexibility according to their flexibility and calls the flexibility of the group of the most flexible buildings by commanding them to implement their respective target-optimized load profiles. We define the flexibility group size as a fraction of the total number of nodes in the grid, which is determined in the parameter studies in Section 4.12. We use the number of nodes as a reference rather than the number of buildings to scale the flexibility group to the electrical size and impedance of the grid. This better captures branching and stays topology-agnostic across different grids. In the distributed strategy, each building performs the same ranking process for itself and all other buildings that have communicated their flexibilities. Based on this ranking, each building can determine if it is among the group of the most flexible buildings and implement its target-optimized load profile accordingly. If the grid status is still critical after the first group of buildings have started to implement their target-optimized load profiles, the flexibility of the next group of buildings is called. This process

repeats until the disturbance is resolved or all relevant buildings are already implementing target-optimized load profiles.

In the decentralized strategy, the flexibility ranking and calling process is not possible due to lacking communication among buildings. Therefore, each building implements a target-optimized load profile as soon as the relevant disturbance criteria for the decentralized strategy are met and its calculated flexibility is larger than zero.

To limit the need for PV curtailment as much as possible, we aim to fully exploit the flexibility of each building whose flexibility has been called. Consequently, we always set P_b^{tar} to 0 W, which ensures that the active power consumption or feed-in of the building is reduced as much as possible for the duration of the active power target optimization horizon. In scenarios where a very large amount of flexibility is available, for example, when optimizing the use of groups of generators or standalone BESSs, it may be advantageous to set active power targets smaller or larger than 0 W to not waste this flexibility. However, for the use case considered in this thesis, where flexibility is relatively limited, this would likely not lead to better performance.

To further enhance grid-supportive flexibility exploitation, we permit the BESS to feed active power into the distribution grid for twice the duration of the active power target optimization horizon as soon as the grid-supportive flexibility use starts. Additionally, we double the feed-in remuneration for all feed-in-capable devices in the building for a period equal to the optimization horizon, starting when this horizon ends. These measures incentivize the BEMS to discharge the BESS to the grid after providing grid-supportive flexibility, rather than retaining energy for the following day or further charging it using local generation. We do this because we expect the considered electrical disturbances to be overwhelmingly caused by excessive active power feed-in from PV systems, at least in the grids evaluated in this thesis. Our evaluation results in Section 5 confirm this expectation. Consequently, having an empty BESS at the onset of PV generation the following day is highly beneficial when trying to minimize PV curtailment. The feed-in of active power by the BESS is permitted during the optimization horizon as well, since it can be beneficial to discharge the BESS at the start of the optimization horizon to more effectively reduce predicted load peaks later in the day.

The algorithms that determine whether active power flexibility should be used are given in Algorithm 6 and 7. They are based on the electrical disturbance criteria given in Section 4.4, the mechanisms described in this section, as well as deadbands and waiting periods introduced to avoid premature flexibility use deactivations and redundant flexibility calculations. Algorithm 6 is used by the DSO for each building in the centralized and by each building in the distributed grid management strategy. Algorithm 7 is used by each building in the decentralized strategy. The symbol descriptions for Algorithms 6 and 7 are given in Tables 4.6 and 4.7. Appropriate values for the newly introduced parameters T^{opt}, T^{cal}, T^{unc}, $\Delta k_{\mathrm{P}}^{\mathrm{dea}}$, Δi^{dea}, and $\Delta u_{\mathrm{P}}^{\mathrm{dea}}$ are determined in parameter studies (see also Section 4.12). In Algorithms 6 and 7, we use the symbol $F_{b,t}^{\mathrm{str}}$ instead of $F_{b,t}$. While the latter denotes the active power flexibility of building b for the optimization horizon beginning in management interval t, the former is the active power flexibility value stored in management interval t. $F_{b,t}^{\mathrm{str}}$ receives the flexibility value calculated in management

interval t and stores it until the flexibility is activated or the delay between flexibility calculations T^{cal} has passed. When the flexibility is activated or when the delay has passed and the grid is uncritical again, $F^{\text{str}}_{b,t}$ is set to zero. When the flexibility has not been activated, the delay has passed, and the grid is still critical, the flexibility is recalculated for the current management interval and its value assigned to $F^{\text{str}}_{b,t}$. Since we determine an appropriate value for T^{cal} in our parameter studies, we assume that the flexibility value stays sufficiently accurate for this duration, even if the beginning of the optimization horizon for which the flexibility value was determined has already passed.

The second method to utilize the active power flexibility of buildings is implemented by factoring in the apparent power limit for the GCP of a building, which is set using the PV curtailment algorithms (Algorithm 4 and 5), during the cost-optimized scheduling of device operation. To achieve this, a building uses Equations 4.21 to 4.24 to determine the maximum admissible PV generation for each scheduling time slot depending on the operation schedules of the other devices. Since PV generation lost due to PV curtailment results in higher electricity costs, the evolutionary algorithm (EA) tries to maximize the active power produced by the PV system while factoring in the apparent power limit. The functionality of the second method is the same for all strategies, as it is always performed locally by the building and without coordination among buildings and the DSO. It is only effective if a detected disturbance is caused by excessive active power feed-in by PV systems and a corresponding apparent power limit has already been set. If a disturbance is caused by excessive power feed-in or consumption by other devices or if no apparent power limit has been set, the first method is used as a backup. It is important to note that we do not use the two methods in combination. Already implicitly using the flexibility for grid-supportive purposes by utilizing the second method would defeat the purpose of implementing target-optimized load profiles according to the first method. They represent different options for achieving similar goals and are tested separately in the evaluation in Chapter 5.

4.5.6. Cascade of Measures

While the main objective of the adaptive grid management system is to prevent electricity outages and equipment failure, its secondary objective is to minimize the losses of active energy potentially generatable by PV systems caused by the implementation of grid management measures. To accommodate this secondary objective, among other things, we use a cascade of measures similar to the one employed in [32]. For each grid management strategy this cascade of measures starts with the least invasive countermeasure to electrical disturbances and ends with the most invasive. Less invasive measures, which restrict the normal operation of the buildings less, are applied first, while more invasive measures, which restrict building operation more, are applied last.

The least invasive countermeasures to electrical disturbances are the voltage maintenance measures introduced in the previous sections, because they entail neither changes in the optimization objective used by a building nor losses of potentially generatable active energy.

Table 4.6: Symbol descriptions for Algorithm 6. "Active power flexibility" is shortened to "flexibility" for brevity. In the centralized strategy, CalcF() includes the communication of a command from the DSO to the building to trigger the procedure.

Symbol	Description
t	Management interval index [-]
b	Building index [-]
Δt	Management interval duration [min]
$\chi_{\mathrm{P},b}$	Boolean: flexibility use active for building b (true = active) [-]
$F_{b,t}^{\mathrm{str}}$	Active power flexibility value of building b stored in management interval t [W²]
t_b^{act}	Management interval of the last flexibility activation for building b [-]
t_b^{cal}	Management interval of the last flexibility calculation for building b [-]
T^{opt}	Active power target optimization horizon in minutes [min]
$N^{\mathrm{opt,t}}$	Active power target optimization horizon in management intervals [-]
T^{cal}	Delay between flexibility calculations in minutes [min]
N^{cal}	Delay between flexibility calculations in management intervals [-]
T^{unc}	Minimum uncritical duration for flexibility deactivation in minutes [min]
N^{unc}	Minimum uncritical duration for flexibility deactivation in management intervals [-]
c_b^{unc}	Counter of consecutive uncritical steps for building b [-]
k_t	Transformer load factor in management interval t [-]
k_{P}	Transformer load factor threshold for flexibility [-]
$\Delta k_{\mathrm{P}}^{\mathrm{dea}}$	Transformer load factor deadband for flexibility [-]
$i_{l(b),t}$	Maximum of the normalized magnitudes of the line segment currents on line l feeding building b in management interval t [-]
i_{P}	Normalized line current threshold for flexibility [-]
Δi^{dea}	Normalized line current deadband for flexibility [-]
$\boldsymbol{R}_{t-1}$	Ranking of buildings by flexibility in management interval $t-1$ (array of building identifiers sorted by flexibility in descending order) [-]
g	Building group size for flexibility (fraction of total number of grid nodes) [-]
N^{nod}	Total number of grid nodes [-]
CalcF()	Determine cost-optimized load profile, determine target-optimized load profile (Equation 4.26), calculate flexibility (Equation 4.27), assign the calculated flexibility value to $F_{b,t}^{\mathrm{str}}$, communicate $F_{b,t}^{\mathrm{str}}$ to DSO and other buildings for ranking if possible [W²]

Data: See Table 4.6

Result:

$\chi_{\mathrm{P},b}$ Boolean: flexibility use active for building b (true = active) [-]

$F^{\mathrm{str}}_{b,t}$ Active power flexibility value of building b stored in management interval t [W²]

Initialization (once, if undefined):

$\chi_{\mathrm{P},b} \leftarrow \mathrm{false}$; $c^{\mathrm{unc}}_b \leftarrow 0$; $N^{\mathrm{unc}} \leftarrow \frac{T^{\mathrm{unc}}}{\Delta t}$; $N^{\mathrm{opt,t}} \leftarrow \frac{T^{\mathrm{opt}}}{\Delta t}$; $N^{\mathrm{cal}} \leftarrow \frac{T^{\mathrm{cal}}}{\Delta t}$; $\boldsymbol{R}_{t-1} \leftarrow \emptyset$

$t^{\mathrm{act}}_b \leftarrow -N^{\mathrm{opt,t}} - 1$; $t^{\mathrm{cal}}_b \leftarrow -N^{\mathrm{cal}} - 1$; $F^{\mathrm{str}}_{b,t-1} \leftarrow 0$

Each management interval:

$F^{\mathrm{str}}_{b,t} \leftarrow F^{\mathrm{str}}_{b,t-1}$

if $\chi_{\mathrm{P},b}$ **then**

  if $k_t \geq k_{\mathrm{P}} - \Delta k^{\mathrm{dea}}_{\mathrm{P}} \ \vee \ i_{l(b),t} \geq i_{\mathrm{P}} - \Delta i^{\mathrm{dea}}$ **then** $c^{\mathrm{unc}}_b \leftarrow 0$

  else

    $c^{\mathrm{unc}}_b \leftarrow c^{\mathrm{unc}}_b + 1$

    if $c^{\mathrm{unc}}_b \geq N^{\mathrm{unc}}$ **then**

      $\chi_{\mathrm{P},b} \leftarrow \mathrm{false}$; $c^{\mathrm{unc}}_b \leftarrow 0$

  if $t - t^{\mathrm{act}}_b > N^{\mathrm{opt,t}}$ **then**

    $\chi_{\mathrm{P},b} \leftarrow \mathrm{false}$; $c^{\mathrm{unc}}_b \leftarrow 0$

if $\neg\chi_{\mathrm{P},b} \ \wedge \ \left(k_t > k_{\mathrm{P}} \ \vee \ i_{l(b),t} > i_{\mathrm{P}}\right)$ **then**

  if $b \in \boldsymbol{R}_{t-1}\left[0{:}\max\left(1, \min\left(\left\lfloor g \cdot N^{\mathrm{nod}} \right\rceil, \ |\boldsymbol{R}_{t-1}|\right)\right)\right)$ **then**

    $\chi_{\mathrm{P},b} \leftarrow \mathrm{true}$; $t^{\mathrm{act}}_b \leftarrow t$; $c^{\mathrm{unc}}_b \leftarrow 0$; $F^{\mathrm{str}}_{b,t} \leftarrow 0$

  else if $t - t^{\mathrm{cal}}_b > N^{\mathrm{cal}}$ **then**

    $F^{\mathrm{str}}_{b,t} \leftarrow$ CalcF(); $t^{\mathrm{cal}}_b \leftarrow t$

else if $F^{\mathrm{str}}_{b,t} \neq 0 \wedge t - t^{\mathrm{cal}}_b > N^{\mathrm{cal}}$ **then** $F^{\mathrm{str}}_{b,t} \leftarrow 0$

Algorithm 6: Algorithm for triggering active power flexibility ranking, calculation, activation, and deactivation. Used by the DSO for each building in the centralized and by each building in the distributed grid management strategy. The $\lfloor ... \rceil$-symbols denote commercial rounding. For the symbol descriptions see Table 4.6.

Data: See Tables 4.6 and 4.7

Result:

$\chi_{\mathrm{P},b}$ Boolean: flexibility use active for building b (true = active) [-]

$F_{b,t}^{\mathrm{str}}$ Active power flexibility value of building b stored in management interval t [W²]

Initialization (once, if undefined):

$\chi_{\mathrm{P},b} \leftarrow \mathrm{false}$; $c_b^{\mathrm{unc}} \leftarrow 0$; $N^{\mathrm{unc}} \leftarrow \frac{T^{\mathrm{unc}}}{\Delta t}$; $N^{\mathrm{opt,t}} \leftarrow \frac{T^{\mathrm{opt}}}{\Delta t}$; $N^{\mathrm{cal}} \leftarrow \frac{T^{\mathrm{cal}}}{\Delta t}$; $t_b^{\mathrm{act}} \leftarrow -N^{\mathrm{opt,t}} - 1$
$t_b^{\mathrm{cal}} \leftarrow -N^{\mathrm{cal}} - 1$; $F_{b,t-1}^{\mathrm{str}} \leftarrow 0$

Each management interval:

$F_{b,t}^{\mathrm{str}} \leftarrow F_{b,t-1}^{\mathrm{str}}$

if $\chi_{\mathrm{P},b}$ **then**

  if $\left(\begin{array}{l} Q_{b,t}^{\mathrm{PV,set}} = 0 \ \wedge \ \left(u_{b,t} \le 1\,\mathrm{pu} + \Delta u^{\mathrm{off}} + \left(\Delta u_{\mathrm{P}}^{\mathrm{coe}} - \Delta u_{\mathrm{P}}^{\mathrm{dea}}\right) \cdot \frac{d_b}{d_{l(b)}} \right. \\ \qquad\qquad \vee \quad u_{b,t} \ge 1\,\mathrm{pu} - \Delta u^{\mathrm{off}} - \left(\Delta u_{\mathrm{P}}^{\mathrm{coe}} - \Delta u_{\mathrm{P}}^{\mathrm{dea}}\right) \cdot \frac{d_b}{d_{l(b)}} \Big) \vee \\ Q_{b,t}^{\mathrm{PV,set}} \neq 0 \ \wedge \ \left(u_{b,t} \le 1\,\mathrm{pu} + \Delta u^{\mathrm{off,Q}} + \left(\Delta u_{\mathrm{P}}^{\mathrm{coe,Q}} - \Delta u_{\mathrm{P}}^{\mathrm{dea}}\right) \cdot \frac{d_b}{d_{l(b)}} \right. \\ \qquad\qquad \vee \quad u_{b,t} \ge 1\,\mathrm{pu} - \Delta u^{\mathrm{off,Q}} - \left(\Delta u_{\mathrm{P}}^{\mathrm{coe,Q}} - \Delta u_{\mathrm{P}}^{\mathrm{dea}}\right) \cdot \frac{d_b}{d_{l(b)}} \Big) \end{array}\right)$ **then**

    $c_b^{\mathrm{unc}} \leftarrow 0$

  else

    $c_b^{\mathrm{unc}} \leftarrow c_b^{\mathrm{unc}} + 1$

    if $c_b^{\mathrm{unc}} \ge N^{\mathrm{unc}}$ **then**

      $\chi_{\mathrm{P},b} \leftarrow \mathrm{false}$; $c_b^{\mathrm{unc}} \leftarrow 0$

  if $t - t_b^{\mathrm{act}} > N^{\mathrm{opt,t}}$ **then**

    $\chi_{\mathrm{P},b} \leftarrow \mathrm{false}$; $c_b^{\mathrm{unc}} \leftarrow 0$

if $\left(\begin{array}{l} \neg\chi_{\mathrm{P},b} \ \wedge \ \left(Q_{b,t}^{\mathrm{PV,set}} = 0 \ \wedge \ \left(u_{b,t} > 1\,\mathrm{pu} + \Delta u^{\mathrm{off}} + \Delta u_{\mathrm{P}}^{\mathrm{coe}} \cdot \frac{d_b}{d_{l(b)}} \right. \right. \\ \qquad\qquad\qquad\qquad \vee \quad u_{b,t} < 1\,\mathrm{pu} - \Delta u^{\mathrm{off}} - \Delta u_{\mathrm{P}}^{\mathrm{coe}} \cdot \frac{d_b}{d_{l(b)}} \Big) \vee \\ \qquad\qquad Q_{b,t}^{\mathrm{PV,set}} \neq 0 \ \wedge \ \left(u_{b,t} > 1\,\mathrm{pu} + \Delta u^{\mathrm{off,Q}} + \Delta u_{\mathrm{P}}^{\mathrm{coe,Q}} \cdot \frac{d_b}{d_{l(b)}} \right. \\ \qquad\qquad\qquad\qquad \vee \quad u_{b,t} < 1\,\mathrm{pu} - \Delta u^{\mathrm{off,Q}} - \Delta u_{\mathrm{P}}^{\mathrm{coe,Q}} \cdot \frac{d_b}{d_{l(b)}} \Big)\Big) \end{array}\right)$ **then**

  if $t - t_b^{\mathrm{cal}} > N^{\mathrm{cal}}$ **then**

    $F_{b,t}^{\mathrm{str}} \leftarrow \textsc{CalcF}()$; $t_b^{\mathrm{cal}} \leftarrow t$

    if $F_{b,t}^{\mathrm{str}} > 0$ **then**

      $\chi_{\mathrm{P},b} \leftarrow \mathrm{true}$; $t_b^{\mathrm{act}} \leftarrow t$; $c_b^{\mathrm{unc}} \leftarrow 0$; $F_{b,t}^{\mathrm{str}} \leftarrow 0$

else if $F_{b,t}^{\mathrm{str}} \neq 0 \wedge t - t_b^{\mathrm{cal}} > N^{\mathrm{cal}}$ **then** $F_{b,t}^{\mathrm{str}} \leftarrow 0$

Algorithm 7: Algorithm for triggering active power flexibility calculation, activation, and deactivation. Used by each building in the decentralized grid management strategy. For the symbol descriptions see Tables 4.6 and 4.7.

Table 4.7: Symbol descriptions specific to Algorithm 7. "Active power flexibility" is shortened to "flexibility" for brevity. For descriptions of the other symbols in Algorithm 7 see Table 4.6.

Symbol	Description
$Q_{b,t}^{\mathrm{PV,set}}$	Reactive power setpoint for building b in management interval t [var]
$u_{b,t}$	Voltage at the GCP of building b in management interval t [pu]
$\Delta u^{\mathrm{off}(,\mathrm{Q})}$	Voltage offset used in the voltage- and position-based transformer/line disturbance criteria for the decentralized strategy if reactive-power-based voltage maintenance is currently inactive (active) [pu]
$\Delta u_{\mathrm{P}}^{\mathrm{coe}(,\mathrm{Q})}$	Voltage coefficient used in the voltage- and position-based transformer/line disturbance criteria for the decentralized strategy if reactive-power-based voltage maintenance is currently inactive (active) [pu]
$\Delta u_{\mathrm{P}}^{\mathrm{dea}}$	Voltage deadband for flexibility [pu]
d_b	Total length of line segments between the transformer and building b [m]
$d_{l(b)}$	Total length of line segments between the transformer and the building that is situated at the end of line l feeding building b [m]

If the particular grid is supplied by a VRDT, the latter is used for voltage maintenance (Algorithm 1) instead of reactive power, since changes of the transformer transmission ratio put substantially less additional load on the grid than additional absorption or injection of reactive power by PV inverters. Only if the transformer supplying the grid is not a VRDT or if a VRDT is not able to operate correctly (see also Section 4.6), reactive-power-based voltage maintenance is applied (Algorithms 2 and 3). As already stated in Section 4.5.3, we prefer the use of reactive power for voltage maintenance over reactive power compensation, since voltage range deviations generally result in damaged equipment faster [231] than congestion [166, 323].

The second least invasive countermeasures are reactive power compensation (Equations 4.15) and active power flexibility use (Algorithms 6 and 7), as the latter requires changing the optimization objective of a building. This might increase electricity costs or reduce feed-in remuneration, depending on whether and how the grid-supportive flexibility provision is financially compensated. Reactive power compensation by itself is even less invasive than reactive-power-based voltage maintenance, as the magnitudes of reactive power absorbed or injected by the PV inverters of buildings are generally substantially lower for reactive power compensation. However, we always activate reactive power compensation and active power flexibility use simultaneously, since the impact of reactive power compensation by itself is generally small when it comes to mitigating line and transformer disturbances or reducing the need for PV curtailment. This is strongly indicated by the simulation results shown in Chapter 5.

The second most invasive countermeasure is PV curtailment for line disturbances. While it entails losses of active energy potentially generatable by PV systems, these losses are limited to buildings on lines with critical currents.

The most invasive countermeasure is PV curtailment for coping with transformer disturbances. It results in losses of potentially generatable active energy for all buildings in the grid equipped with PV systems, because every building supplied by the same transformer contributes to its hot-spot temperature progression.

The general cascades of measures are very similar for all grid management strategies. They are the same for the centralized and distributed strategies. However, in the decentralized strategy, the electrical disturbance criteria differ from the ones employed in the centralized and distributed strategies due to very limited observability of the current grid status (see also Section 4.4). For the same reason, there is no differentiation between line and transformer disturbances in the decentralized strategy.

Figure 4.2 visualizes our employed cascades of measures for each grid management strategy.

4.6. Adaptive Grid Management

The three grid management strategies, introduced in Section 4.3, are used depending on the current situation and allow the adaptation of the grid management system to ICT disturbances resulting in communication disruption, participant misconduct, and sensor failure. In the following, we describe how the system participants determine the necessity of switching strategies in response to occurring events. Thereby, we answer Sub-Questions 3.1 and 3.2 of Research Question 3 and provide a part of the basis for answering Sub-Question 3.3.

4.6.1. Communication Disruption

Some text passages of this section are transferred verbatim from one of our own publications [1]. For a summary of this publication, its relation to this thesis, and its mapping to our research questions, see Section 1.4.

For the following descriptions, the centralized strategy (see also Section 4.3.1) is assumed to be the default strategy. To be able to adapt their behavior in the case of communication disruption, the buildings and the transformer have to detect this autonomously. The buildings achieve this by continuously monitoring the grid status at their respective GCPs and communicating relevant data not only to the DSO, but to all other buildings and the transformer as well. The transformer also communicates relevant data to the buildings. Based on the locally measured data and the data received by other buildings and the transformer, each building regularly performs its own power-flow studies and is consequently aware of the current status of the entire low-voltage grid it is connected to.

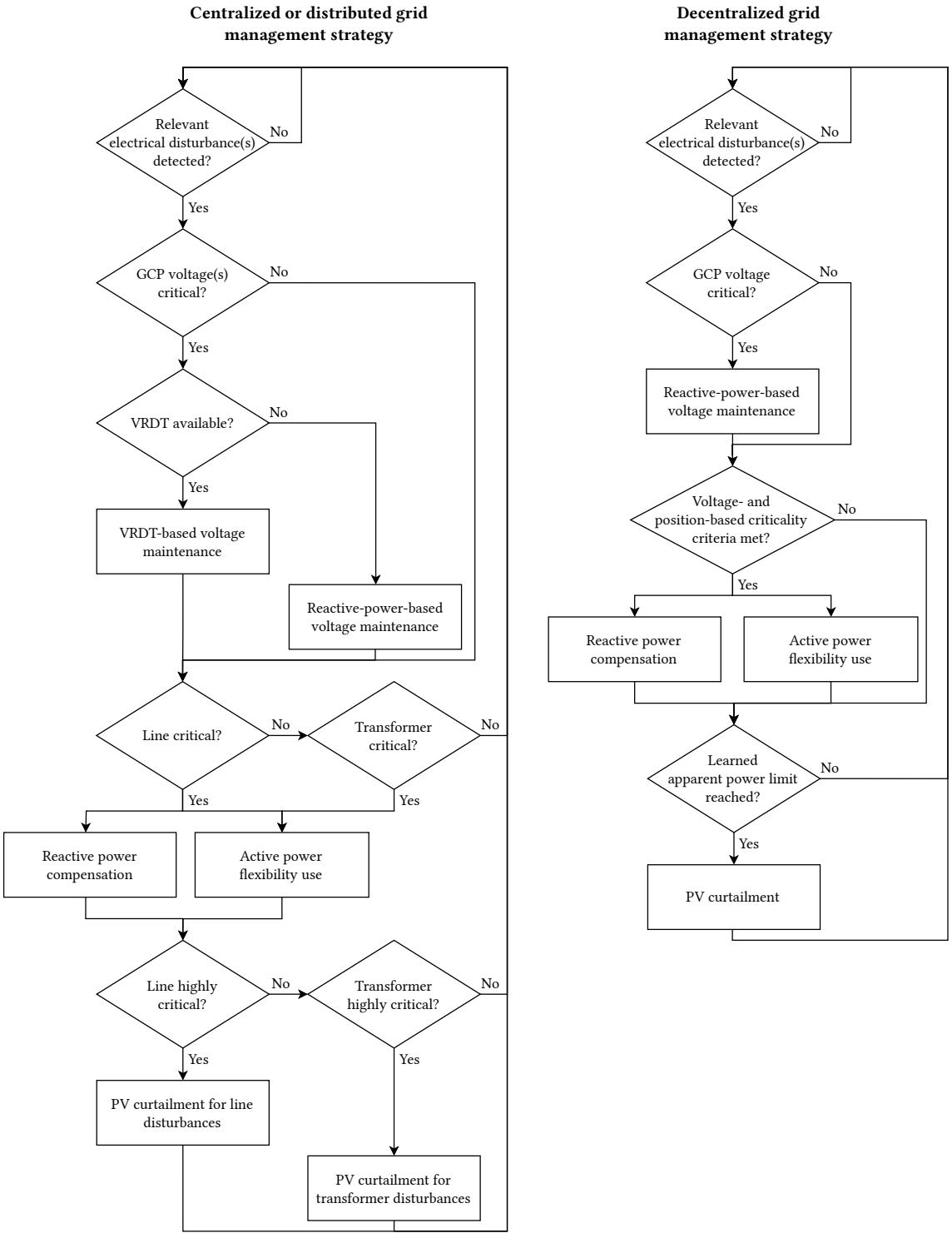

Figure 4.2: Cascades of measures for the centralized, distributed, and decentralized grid management strategies. The cascades of measures are run through in each management interval. The particular cascade of measures is run through for each building in the centralized strategy and by each building in the distributed and decentralized strategies.

If a building detects a critical grid status that requires a countermeasure and no command is received from the DSO, the building starts to implement appropriate countermeasures based on the data received from the transformer and the other buildings as well as the current results of its own power-flow studies. This behavior corresponds to the distributed strategy (see also Section 4.3.2). The transformer does not require dedicated measures to detect communication disruption to the DSO. If it is a VRDT, it already autonomously decides on switching measures in the centralized strategy, purely based on the data communicated by the buildings. If it is not a VRDT, it has no ability to implement commands from the DSO and thus is not impaired by communication disruption to the DSO.

Since the described method for detecting communication disruption to the DSO entails continuous communication among the buildings and the transformer, an even more comprehensive disruption that also disrupts the communication among these entities is easily detectable. If no data is received from other buildings anymore, a building can immediately adapt by switching to the decentralized strategy (see also Section 4.3.3) and exclusively act based on locally measured data, its own position in the grid, and previously learned apparent power limits for PV curtailment. If no data is received from the transformer anymore, a building switches to the decentralized strategy as well, since the communicated hot-spot temperature, load factor, and voltage data are essential to determine appropriate countermeasures in the centralized and distributed strategies. The transformer, if it is a VRDT and does not receive data from the buildings anymore, gradually switches back to the neutral tap position. This changes the voltages in the grid, which prompts the buildings to implement reactive-power-based voltage maintenance.

The decentralized strategy can be deployed selectively as well if the DSO still receives data from some buildings in the centralized strategy or some buildings can still communicate with each other in the distributed strategy. This is possible as long as reacting to unreliable grid status data calculated from insufficiently current input data can be avoided. In the centralized and distributed strategies, the power-flow studies are performed using the sensor data received from still communicating buildings and the last communicated data of buildings that do not communicate anymore. The latter may be sufficient in many, but not all situations. For example, in a situation where only two buildings on a line that feeds 15 buildings in total can still communicate, the real grid status will increasingly deviate from the grid status calculated by the still communicating buildings based on mostly old data. Therefore, the reliability of the power-flow studies is regularly checked using the calculated and measured GCP voltages. While the reliability of line current data is not determined directly, deviations between measured and calculated voltages indicate unreliable calculated line current data as well. In the centralized strategy, each building whose measured GCP voltage deviates from the corresponding GCP voltage calculated in the power-flow studies by more than 0.005 pu does not receive commands from the DSO anymore and switches to the decentralized strategy, even if it can still communicate. All buildings regularly calculate their own voltage deviation as well and therefore can also switch to the decentralized strategy coming from the distributed strategy if necessary. Buildings whose calculated GCP voltages differ by 0.005 pu or less from their measured GCP voltages continue using the centralized or distributed strategies if they can

still communicate. If a VRDT is used for voltage maintenance, the reliability of the grid status data is relevant for the transformer as well. Therefore, the buildings communicate whether they determine the current calculated grid status to be reliable or not. If one or more buildings determine the calculated data to be unreliable, the transformer gradually switches back to the neutral tap position and gives the buildings clearance to deploy reactive-power-based voltage maintenance (see also Section 4.5.3). It also does this if more than 20 % of the buildings in the particular grid have stopped communicating. We assume this value to be quite conservative, since this is an additional measure to the regular reliability checks performed by the buildings. The value may be set higher, especially if further measures are taken, such as estimating missing GCP voltages based on the available measured voltages at other GCPs on the particular line, which is out of scope for this thesis.

When the communication to the other buildings is restored after a disruption and the deviation between the measured and calculated GCP voltages is acceptable, a building switches back to the distributed or centralized strategy, depending on whether it receives commands from the DSO again as well. When a building is currently using the distributed strategy but receives one or more commands from the DSO, it switches back to the centralized strategy. The transformer, if it is a VRDT, starts to decide on switching operations again, as soon as at least 80 % of the buildings communicate again and all communicating buildings determine the current calculated grid status to be reliable.

The described decision processes are summarized in Figure 4.3.

4.6.2. Participant Misconduct

Participant misconduct can be caused either by system-internal decisions or by external attacks. An example for an external attack is a cyberattack that modifies control decisions or communicated sensor measurements. An example for an internal decision is a building owner that modifies their PV system controller to disregard apparent power limits for PV curtailment to receive a higher feed-in remuneration. Note that this perspective differs from the related work presented in Chapter 3, which generally focuses on cyberattacks but does not explicitly consider the possibility of malicious, system-internal decisions. In the following, we present mitigation strategies for misconduct by the DSO, the transformer, as well as the buildings connected to the grid.

4.6.2.1. Distribution System Operator Misconduct

There are two relevant misconduct options that can be taken by a malicious actor that has access to the O/C-unit of the DSO. The first is the communication of inappropriate reactive power setpoints (see also Section 4.5.3) aimed at inducing electricity outages by increasing or decreasing voltages above or below the admissible voltage range. The second option is the communication of inappropriate apparent power limits for PV curtailment (see also Section 4.5.4) to induce electricity outages by increasing the load on the grid.

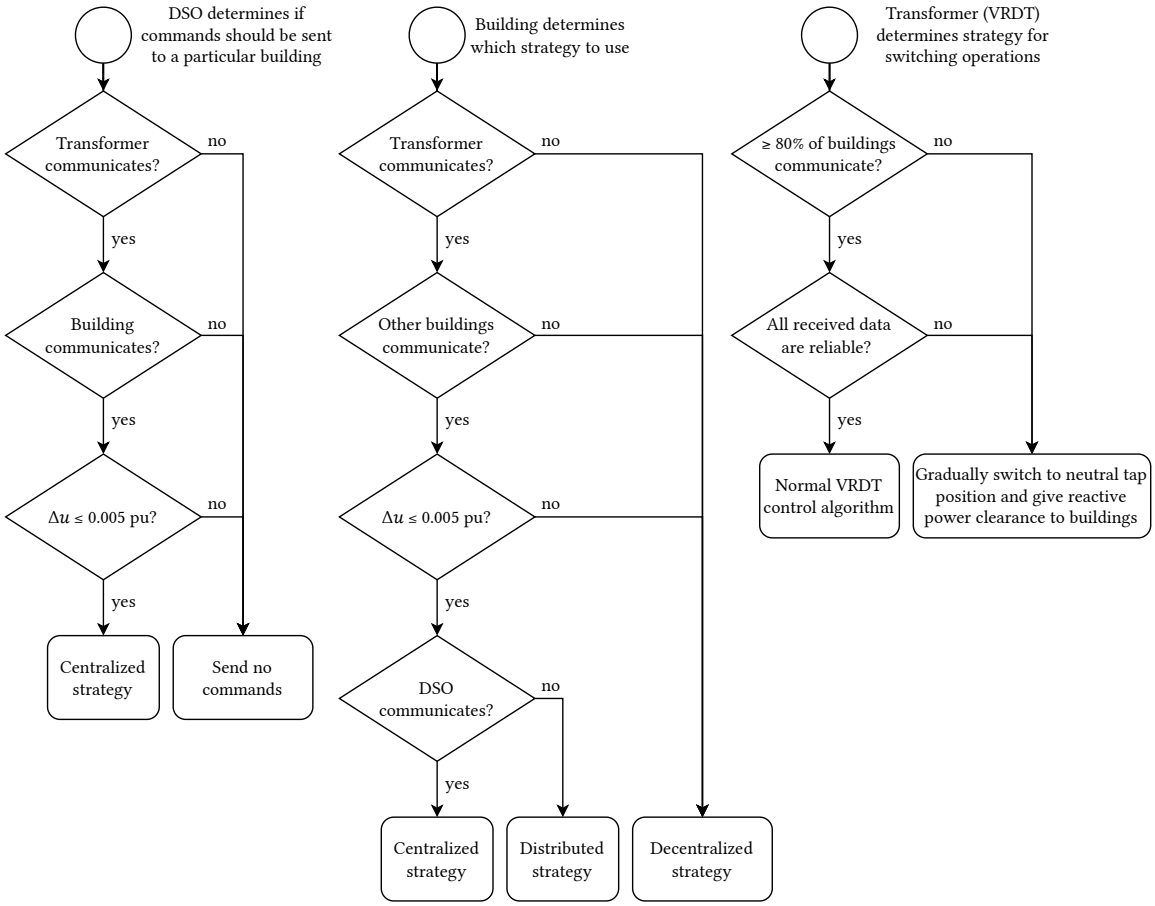

Figure 4.3: Decision processes for determining the appropriate grid management strategy in response to communication disruption from the perspectives of the DSO (left), a building (middle), and the transformer (right). Δu: difference between the measured voltage and the voltage calculated in the power-flow studies at the GCP of a building.

This can cause violations of the maximum admissible transformer hot-spot temperature, rated line currents, and the admissible voltage range.

Neither the use of active power flexibility (see also Section 4.5.5) nor reactive power compensation (see also Section 4.5.2) are considered in this context, since these methods can not cause electricity outages or equipment failure by themselves. A maliciously set active power target would be counteracted by adjusting the curtailment of PV systems. An unnecessary activation of reactive power compensation would only lessen the load on the grid, while a premature deactivation would be counteracted by PV curtailment adjustments as well.

To implement appropriate countermeasures, the buildings have to detect misconduct by the DSO. This is achieved by checking the communicated commands for correctness.

Before implementing a reactive power setpoint communicated by the DSO, a building first executes the algorithm to determine reactive power setpoints based on the current grid status data and the currently implemented setpoint (Algorithm 2). In this case, the

algorithm is executed without updating the utilized counters. The latter would disturb the regular functionality of the algorithm, which is the determination of setpoints that will actually be implemented. It then compares the resulting setpoint to the setpoint communicated by the DSO. If both setpoints are the same, it implements the communicated setpoint. However, if the setpoints deviate from each other, the building assumes misconduct by the DSO and switches to the distributed strategy. Subsequent commands from the DSO are ignored until they correspond to the correct measures for the current grid status again. This fully prevents the implementation of malicious reactive power setpoints, as long as the global O/C-unit of the building is working correctly.

The decision process before implementing or denying an apparent power limit for PV curtailment communicated by the DSO is very similar to the one for communicated reactive power setpoints. The building first executes Algorithms 4 and 5 without updating the learned apparent power limits to prevent line and transformer disturbances, and compares the result to the apparent power limit communicated by the DSO. The limit is only implemented if it is correct. If it is not, the building switches to the distributed strategy.

The described decision processes are summarized in Figure 4.4.

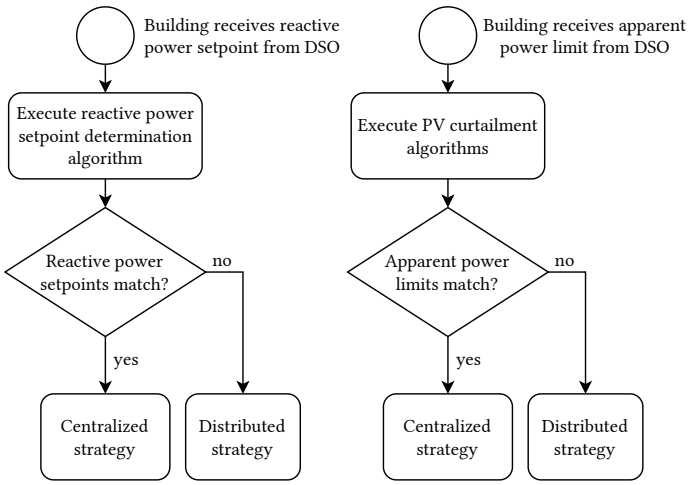

Figure 4.4: Decision processes a building uses before implementing or denying reactive power setpoints and apparent power limits communicated by the DSO in the centralized strategy. The executed reactive power setpoint determination algorithm corresponds to Algorithm 2. The executed PV curtailment algorithms correspond to Algorithms 4 and 5.

4.6.2.2. Transformer Misconduct

There are different types of misconduct that can be initiated by a malicious actor who can access the O/C-unit of the transformer, depending on whether it is a VRDT or not. The first type applies to both VRDTs as well as to transformers without voltage maintenance capabilities. Since the DSO or the buildings decide on countermeasures to electrical disturbances based on the transformer hot-spot temperature, among other things, a communicated false

temperature can cause transformer overheating and consequently equipment failure and electricity outages. Communicated false load factor and secondary voltage data do not have to be mitigated explicitly. The communicated load factor is only used to decide on active power flexibility use and reactive power compensation, which are non-essential for upholding grid operation. The secondary voltage is used in the power-flow studies conducted by the DSO and the buildings. Communicated false secondary voltages thus decrease the accuracy of the power-flow study results, which is already mitigated by the measures presented in Section 4.6.1. The second type of misconduct only applies to VRDTs. A malicious actor could switch the transmission ratio of a VRDT to increase or decrease voltages outside of the admissible voltage range and consequently cause electricity outages or device damage.

To detect possible misconduct by the transformer with regard to its hot-spot temperature, each time a new temperature is communicated by the transformer, the DSO and each building check its plausibility according to the conditions given in Equations 4.28 and 4.29.

$$|\theta_t - \theta_{t-1}| > 7\,^{\circ}\mathrm{C} \tag{4.28}$$

In Equation 4.28, θ_t and θ_{t-1} are the transformer hot-spot temperatures in the current and previous management intervals respectively. A temperature jump or drop by more than 7 °C does not occur naturally in the one-minute time frame between measurements and management intervals in the simulations performed for this thesis.

$$\lfloor \theta_t \cdot 10000 \rceil = \lfloor \theta_{t-1} \cdot 10000 \rceil = \lfloor \theta_{t-2} \cdot 10000 \rceil \tag{4.29}$$

The condition in Equation 4.29 checks whether the temperature has not changed to the fourth decimal place over three consecutive management intervals (which also correspond to the measurement frequency). In our simulations, even under steady conditions, the hot-spot temperature did not remain constant to the fourth decimal place over three consecutive minutes. The $\lfloor \ldots \rceil$-symbols denote commercial rounding.

If one of the conditions in Equations 4.28 and 4.29 is fulfilled, this indicates probable misconduct by the transformer and the buildings switch to the decentralized strategy, regardless of whether the centralized or the distributed strategy was used before. If the centralized strategy was used before, the DSO stops sending commands.

The buildings and the DSO only switch back to the distributed or centralized strategies if the communicated temperature changes again according to the condition in Equation 4.30 and if none of the conditions in Equations 4.28 and 4.29 are met.

$$\lfloor \theta_t \cdot 10000 \rceil \neq \lfloor \theta_{t-1} \cdot 10000 \rceil \tag{4.30}$$

The described decision processes are summarized in Figure 4.5.

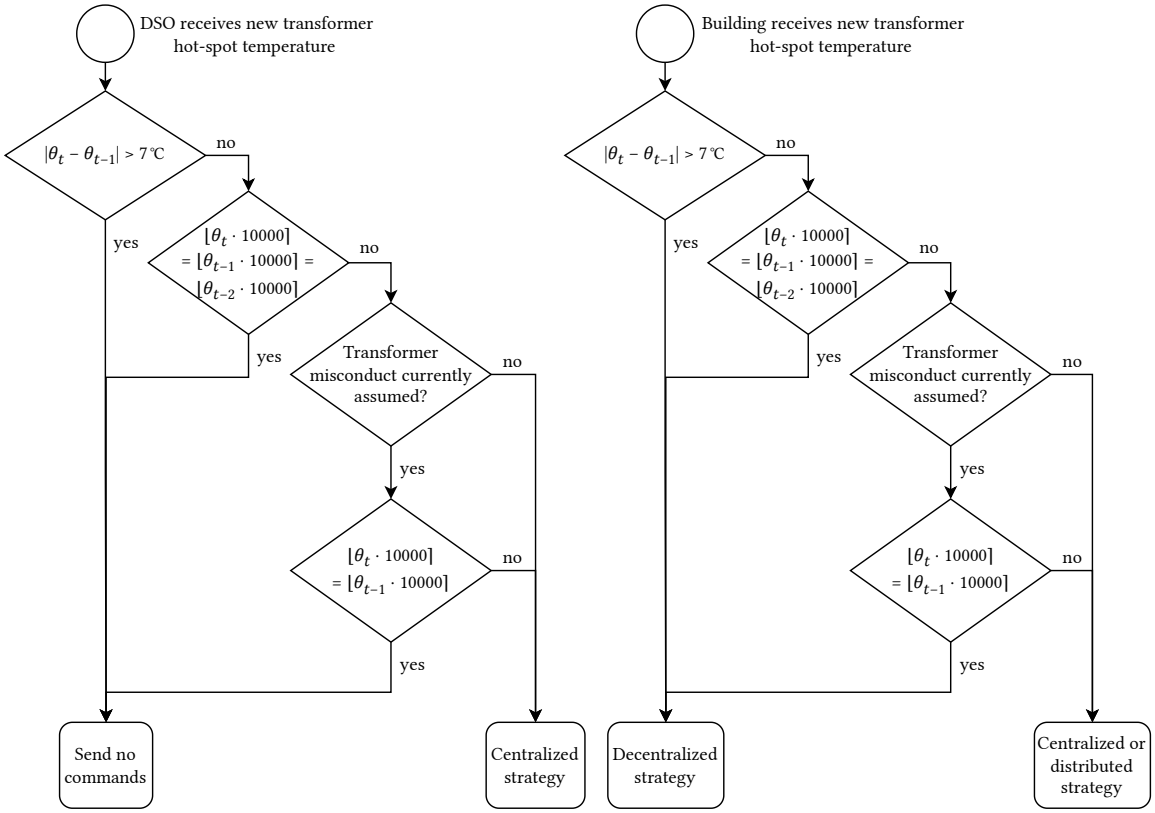

Figure 4.5: Decision processes before implementing measures in response to newly communicated transformer hot-spot temperatures, from the perspectives of the DSO (left) and a building (right). θ_t, θ_{t-1}, θ_{t-2}: Transformer hot-spot temperatures communicated in the current, previous, and penultimate management intervals respectively.

The most obvious way to provoke electricity outages and equipment failures is the repeated communication of a low temperature that does not change. This is why the presented conditions should catch the overwhelming majority of maliciously communicated false transformer hot-spot temperatures if the transformer hot-spot temperature behaves like in our simulations and is communicated with a very high accuracy. We use these conditions in our evaluation in Section 5.

However, there are more sophisticated methods to maliciously communicate false temperatures that circumvent these conditions, especially if an attacker is aware of these conditions. As an example, the communicated temperatures could be decreased gradually by 1 or 2 °C at a time, to circumvent the condition in Equation 4.28. When the target temperature is reached, the communicated temperatures could then be increased and decreased by 1 °C periodically to circumvent the condition in Equation 4.29. Furthermore, as previously mentioned, the conditions in Equations 4.28, 4.29, and 4.30 are very specific to our simulations and may consequently be insufficient for a real-world application. This means that a more practical condition is required for many scenarios. The buildings and the DSO have the capability to determine the approximate load factor of the transformer k^{app} by summing up the communicated apparent powers at the GCPs of all buildings

and dividing by the rated apparent power of the transformer. This enables checking the condition in Equation 4.31:

$$1 < k_{t-1}^{\text{app}} < k_t^{\text{app}} \wedge \theta_{t-1} > \theta_t \tag{4.31}$$

In Equation 4.31, k_t^{app} and k_{t-1}^{app} are the approximate transformer load factors in the current and previous management intervals respectively. This should not be confused with the load factor k communicated by the transformer itself. While the buildings and the DSO also receive this load factor from the transformer, it would not be reasonable to use this communicated load factor when determining transformer misconduct, as the transformer could communicate false load factors as well. The condition also includes the requirement that the load factor has to be greater than one. This is a conservative value that substantially reduces the possibility of erroneous misconduct detection, as the transformer hot-spot temperature can fall even if the load factor increases if the general load level is low enough that environmental conditions can outweigh the heat input of the current on the transformer windings. Furthermore, a load factor equal to or smaller than one means that the transformer is not overloaded and the possibility of transformer overheating is negligible, even if the transformer communicates false hot-spot temperatures. In contrast to the previous misconduct conditions, Equation 4.31 does not depend on the number of available decimal places. It works even if the temperature is communicated as an integer. However, the higher the accuracy of the communicated hot-spot temperature, the earlier potential misconduct can be detected.

When having determined transformer misconduct using Equation 4.31, the buildings and the DSO only switch back to the distributed or centralized strategies if the communicated temperature changes again according to the condition in Equation 4.32 and if the condition in Equation 4.31 is not met.

$$\theta_{t-1} \neq \theta_t \tag{4.32}$$

The described decision processes are summarized in Figure 4.6.

As the first method of hot-spot-temperature-related transformer misconduct detection, the second method can be circumvented as well. A possible course of action could be for an attacker to start repeating the last hot-spot temperature indefinitely before the hot-spot temperature becomes critical, which would not trigger the condition in Equation 4.31. Attacks, such as the ones described for each of the presented methods, could only be counteracted by using more sophisticated detection methods. Corresponding approaches are presented in Chapter 3 but are outside the scope of this thesis.

When a VRDT maliciously switches its transmission ratio to bring voltages outside of the admissible range, switching to another grid management strategy does not improve the situation. However, the changed transmission ratio can be counteracted with reactive-power-based voltage maintenance. To detect misconduct by a VRDT with regard to switching operations, the DSO as well as the buildings observe the most critical GCP

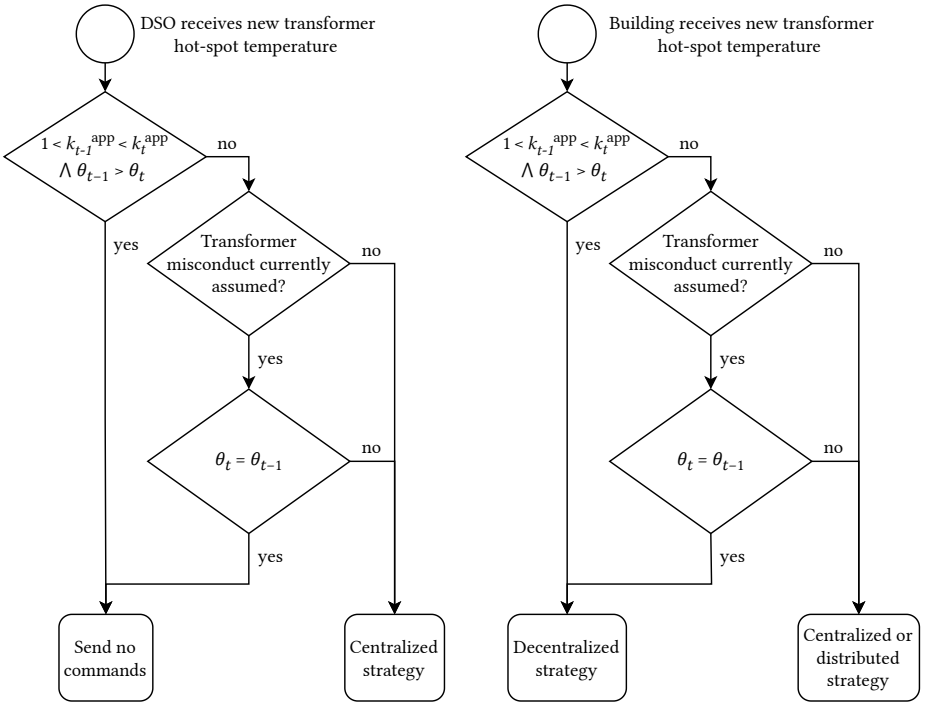

Figure 4.6: Alternative decision processes before implementing measures in response to newly communicated transformer hot-spot temperatures, from the perspectives of the DSO (left) and a building (right). k_t^{app}, k_{t-1}^{app}: Approximate transformer load factors calculated in the current and previous management intervals respectively. θ_t, θ_{t-1}: Transformer hot-spot temperatures communicated in the current and previous management intervals respectively.

voltages at each management interval. If a VRDT is currently in use, all entities assume transformer misconduct if a GCP voltage remains critical for more than one management interval. If this occurs, the buildings start implementing reactive-power-based voltage maintenance according to Algorithm 2. Equations 4.33 and 4.34 provide the corresponding conditions, of which at least one has to be met to assume transformer misconduct with regard to switching operation.

$$u_{l(b),t}^{max} > u_Q^{upp} \wedge u_{l(b),t-1}^{max} > u_Q^{upp} \tag{4.33}$$

$$u_{l(b),t}^{min} < u_Q^{low} \wedge u_{l(b),t-1}^{min} < u_Q^{low} \tag{4.34}$$

In Equations 4.33 and 4.34, $u_{l(b),t}^{max}$ and $u_{l(b),t}^{min}$ are the maximum and minimum GCP voltages on the line l feeding building b. u_Q^{upp} and u_Q^{low} are the upper and lower voltage disturbance boundaries, which determine the uncritical voltage range. These boundaries are tighter than the mandated ±10 % around the nominal voltage (see also Section 4.4).

The transformer misconduct is only assumed to be over, when both conditions given in Equations 4.35 and 4.36 are met. If they are, the reactive-power-based voltage maintenance

is gradually scaled back according to Algorithm 2 until the reactive power setpoint reaches zero or transformer misconduct is detected again.

$$u_{l(b),t}^{\max} < u_{\mathrm{Q}}^{\mathrm{upp}} - \Delta u_{\mathrm{Q}}^{\mathrm{dea}} \tag{4.35}$$

$$u_{l(b),t}^{\min} > u_{\mathrm{Q}}^{\mathrm{low}} + \Delta u_{\mathrm{Q}}^{\mathrm{dea}} \tag{4.36}$$

In Equations 4.35 and 4.36, $\Delta u_{\mathrm{Q}}^{\mathrm{dea}}$ is the voltage deadband that has to be overcome before reactive-power-based voltage maintenance can be scaled back.

The described decision processes are summarized in Figure 4.7.

4.6.2.3. Building Misconduct

The misconduct options for buildings taking part in the systems developed in this thesis are analogous to the options for the DSO. A building or a malicious actor in control of the O/C-unit of a building can implement malicious apparent power limits and reactive power setpoints to potentially cause violations of the admissible voltage range, rated line currents, and the admissible transformer hot-spot temperature.

Misconduct with regard to reactive power setpoints requires no dedicated detection method. If a particular building changes its reactive power absorption or injection maliciously, this change is indirectly detected by normally observing the GCP voltages in the grid. Buildings that still behave normally adjust their reactive power setpoints to keep voltages inside the admissible range and thus counteract reactive-power-based misconduct by other buildings automatically.

The same effect applies to apparent-power-based misconduct as well, albeit with a caveat. Since the PV curtailment algorithm for transformer disturbances (Algorithm 5) considers the apparent power limits of all buildings supplied by the transformer, building misconduct has to be explicitly detected in this case. Otherwise, normally acting buildings can not decrease their apparent power limits further in cases where other, maliciously acting buildings do not decrease their limits when commanded to do so by the DSO or when appropriate in the distributed strategy. This is a consequence of the functionality of Algorithm 5, which ensures that buildings that currently implement the highest apparent power limits decrease their limits first, until they reach those of the building group with the second highest limits. If one or more buildings with the highest limits act maliciously and do not decrease their limits in a critical situation, the remaining buildings can not decrease their limits either, since they have to wait for the group with the highest limits. To avoid the described behavior, the buildings and the DSO first check if at least one of the conditions in Equations 4.38 and 4.39 is met, which are derived from the functionality of Algorithm 5. If a condition is met, this indicates that one or more buildings with the highest apparent power limits did not change their limits in response to critical transformer hot-spot temperatures. Consequently, the normally behaving buildings assume the misconduct by other buildings.

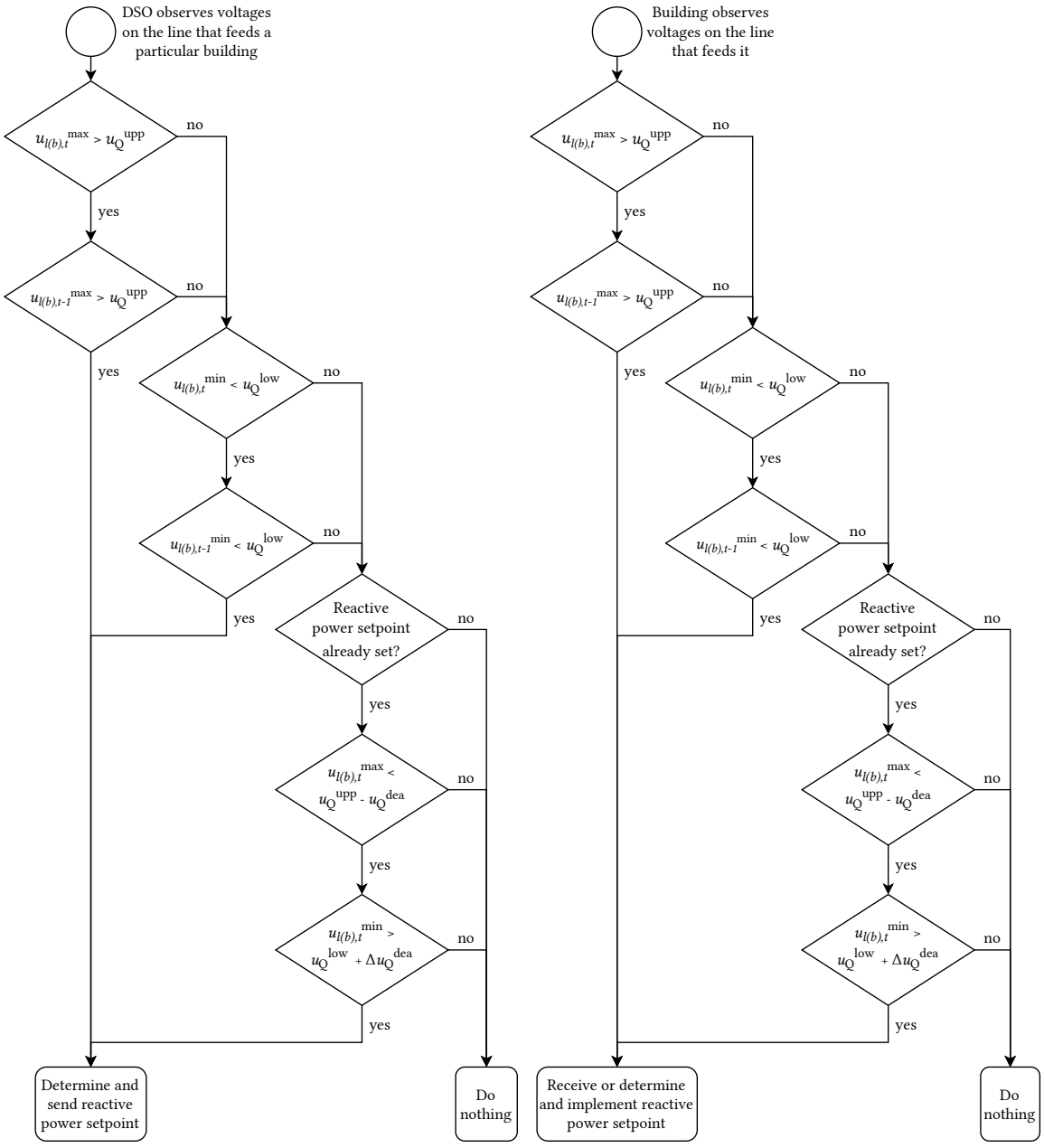

Figure 4.7: Decision processes to determine whether or not reactive-power-based voltage maintenance should be used despite VRDT-based voltage maintenance being active to counter assumed transformer misconduct with regard to switching operations. The perspective of the DSO is shown on the left and the perspective of a building on the right. $u_{l(b),t}^{\max}$, $u_{l(b),t}^{\min}$: Maximum and minimum voltages on the line l feeding building b. u_Q^{upp}, u_Q^{low}: Upper and lower voltage disturbance boundaries for reactive-power-based voltage maintenance. Δu_Q^{dea}: Voltage deadband for reactive-power-based voltage maintenance.

In response, they set all internally saved apparent power limits of the buildings with the highest limits to zero before applying Algorithm 5. This allows the normally acting buildings to decrease their apparent power limits, even if their own limits are currently not the highest. This way, they can compensate for the higher apparent power limits of maliciously acting buildings. While building misconduct is detected, the updating of the learned apparent power limits for the decentralized strategy is paused. Otherwise, the learned limits would become too restrictive for the normally acting buildings.

$$s_t^{\text{lim,max}} = \max_{b \in \mathbf{B}} \left(s_{b,t}^{\text{lim}} \right) \tag{4.37}$$

$$s_{t-1}^{\text{lim,max}} > s_{t-2}^{\text{lim,max}} \wedge \theta_{t-1} \geq \theta^{\text{low}} \tag{4.38}$$

$$s_{t-1}^{\text{lim,max}} = s_{t-2}^{\text{lim,max}} \wedge \left(\theta_{t-1} > \theta^{\text{upp}} \vee \theta_{t-1} > \theta^{\text{mid}} \wedge \theta_{t-1} \geq \theta_{t-2} \right) \tag{4.39}$$

In Equation 4.37, $s_t^{\text{lim,max}}$ is the maximum apparent power limit of all buildings in the grid at management interval t. $\mathbf{B}$ is the set of all buildings in the grid. θ_{t-1} and θ_{t-2} are the previous and penultimate transformer hot-spot temperatures. θ^{low}, θ^{mid}, and θ^{upp} are the lower, mid, and upper transformer hot-spot temperature thresholds for PV curtailment.

The described decision processes are summarized in Figure 4.8.

Another misconduct option for buildings is the communication of false sensor data. This decreases the accuracy of the power-flow studies conducted by the DSO and the buildings, which is already mitigated using the method described in Section 4.6.1. The effects of communicated false sensor data could be further mitigated by explicitly detecting false sensor data and replacing it with values estimated based on historical and/or predicted data. While some of the publications presented in Chapter 3 present corresponding approaches, this is out of scope for this thesis.

4.6.3. Sensor Failure

Sensor failure can present itself in several different ways. With regard to the transformer, the sensor that measures the hot-spot temperature can provide incorrect or no values. The same is true for the smart meters employed by the buildings. The sensors measuring active and reactive power as well as voltages at the GCPs can fail completely or provide incorrect values. All described sensor failure occurrences are already mitigated by deploying the methods described in Sections 4.6.1 to 4.6.2.3.

If sensors fail completely, that is, they stop providing values, the affected transformer or building can not send messages to other buildings or the DSO anymore. This is explicitly detected and mitigated using the methods described in Section 4.6.1.

The maximum deviation between the measured GCP voltages and the corresponding voltages calculated in the power-flow studies defined in Section 4.6.1 allows the implicit detection of incorrect sensor data communicated by a building. If incorrect reactive powers,

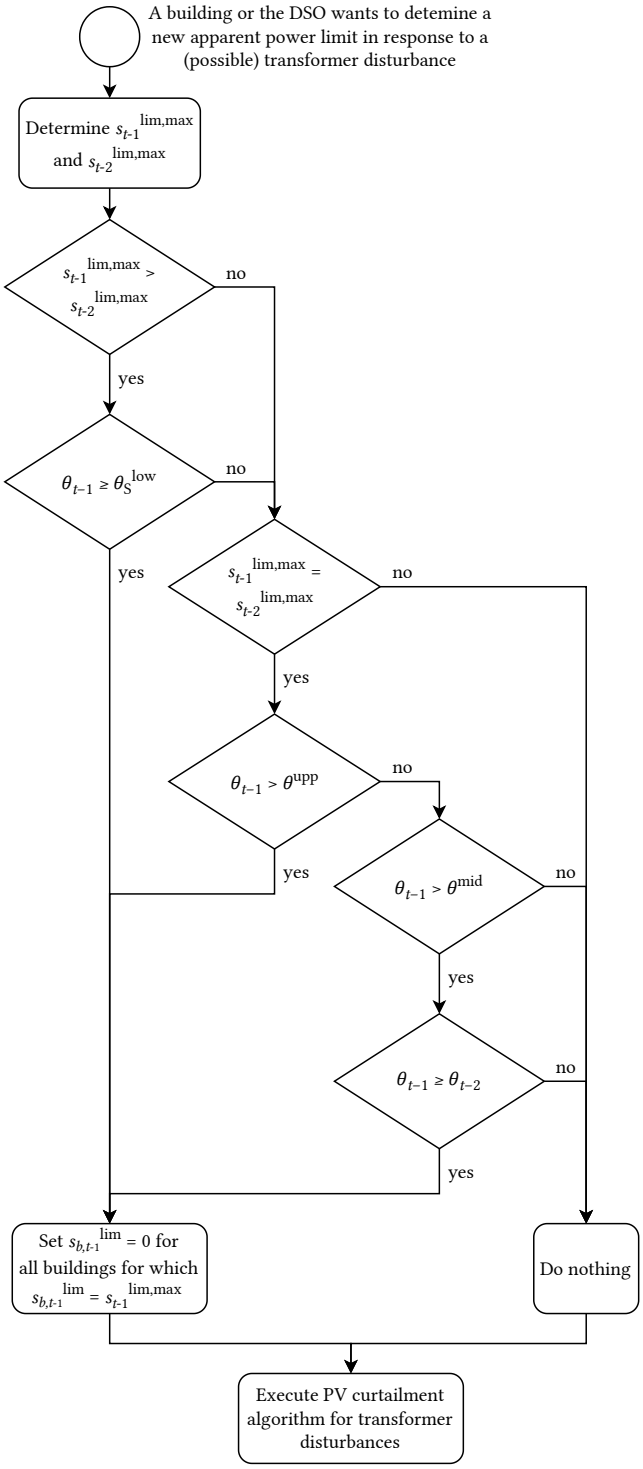

Figure 4.8: Decision processes to determine whether or not the determination of apparent power limits in response to transformer disturbances has to be adjusted in response to building misconduct with regard to apparent power limits. The process is used by the DSO in the centralized strategy or each building in the distributed strategy. The PV curtailment algorithm for transformer disturbances is Algorithm 5. $s_{b,t-1}^{\text{lim,max}}$, $s_{t-2}^{\text{lim,max}}$: Previous and penultimate maximum apparent power limits of all buildings in the grid. θ_{t-1}, θ_{t-2}: Previous and penultimate transformer hot-spot temperatures. θ^{low}, θ^{mid}, θ^{upp}: Lower, mid, and upper transformer hot-spot temperature thresholds for PV curtailment.

active powers, or voltages are communicated by one or more buildings in the grid, this influences the results of the power-flow studies performed by the DSO and each building. If the DSO or a building detects a deviation of more than 0.005 pu between the measured voltage at the GCP of the building and the respective voltage resulting from the power-flow studies, the building switches to the decentralized strategy. Other buildings, for which the deviation is 0.005 pu or lower, can still use the available data to act according to the centralized or distributed strategies. If one or more buildings communicate an excessive deviation and the transformer is a VRDT, the transformer gradually switches to the neutral tap position and gives the buildings clearance to apply reactive-power-based voltage maintenance.

The mitigation methods presented in Section 4.6.2.2, among other things, apply to incorrect communicated transformer hot-spot temperatures. The described methods work, regardless of whether the communicated temperatures are incorrect due to sensor failure or due to misconduct.

Since sensor failure does not require additional detection and mitigation methods that go beyond the ones presented in the previous sections, we do not provide a corresponding decision process diagram.

4.7. Architecture and Implementation

In the following subsections, we detail how we implement the adaptive grid management system on the basis of the OSH building energy management and simulation framework (see also Section 2.4.2). The implementation of the adaptive grid management system is a necessary step for answering Sub-Questions 1.4 and 1.5 of Research Question 1, Sub-Questions 2.1 and 2.2 of Research Question 2, as well as Sub-Question 3.3 of Research Question 3.

Some text passages of this section are transferred verbatim from one of our own publications [33]. For a summary of this publication, its relation to this thesis, and its mapping to our research questions, see Section 1.4.

Since Figures 4.9, 4.10, 4.11, and 4.12 contain a large number of symbols for different quantities, we provide symbol descriptions in Tables 4.8, 4.9, and 4.10. Table 4.8 contains the descriptions of quantities related to the grid status. Table 4.9 gives descriptions of quantities related to grid management measures that are communicated among the DSO, the buildings, and the transformer. Table 4.10 gives descriptions of quantities related to grid management measures that are only internally processed by the DSO, the buildings, or the transformer and are *not* communicated among these participants.

Table 4.8: Symbols used for grid status data in Figures 4.9, 4.10, 4.11, and 4.12.

Symbol	Description
$P_{b,t_{\text{sim}}}$	Simulated active power at the GCP of building b at simulation step t_{sim} [W]
$\boldsymbol{P}_{t_{\text{sim}}}$	Array of simulated active powers at the GCP of each building at simulation step t_{sim} [W]
$P_{b,t}$	Average active power at the GCP of building b in management interval t (calculated from $P_{b,t_{\text{sim}}}$, sensor data in real application) [W]
$\boldsymbol{P}_t$	Array of average active powers at the GCP of each building available in management interval t [W]
$P_{\text{T},t}$	Average active power transferred through the transformer in management interval t (calculated from $\boldsymbol{P}_{t_{\text{sim}}}$, sensor data in real application) [W]
$Q_{b,t_{\text{sim}}}$	Simulated reactive power at the GCP of building b at sim. step t_{sim} [var]
$\boldsymbol{Q}_{t_{\text{sim}}}$	Array of simulated reactive powers at the GCP of each building at simulation step t_{sim} [var]
$Q_{b,t}$	Average reactive power at the GCP of building b in management interval t (calculated from $Q_{b,t_{\text{sim}}}$, sensor data in real application) [var]
$\boldsymbol{Q}_t$	Array of reactive powers at the GCP of each building available in management interval t [var]
$Q_{\text{T},t}$	Reactive power transferred through the transformer in management interval t (calculated from $\boldsymbol{Q}_{t_{\text{sim}}}$, sensor data in real application) [var]
$\boldsymbol{i}_t$	Array of the magnitudes of all normalized line segment currents in the grid in management interval t (result of power-flow studies by buildings and DSO) [-]
$u_{b,t}^{\text{m}}$	Normalized measured GCP voltage of building b in management interval t (result of power-flow studies simulating the actual grid, sensor data in real application) [pu]
$\boldsymbol{u}_t^{\text{m}}$	Array of the normalized measured GCP voltages of each building available in management interval t [pu]
$\boldsymbol{u}_t^{\text{c}}$	Array of normalized calculated GCP voltages available in management interval t (result of power-flow studies by buildings and DSO) [pu]
u_t^{MV}	Normalized voltage at the primary transformer side (medium voltage level) available in management interval t (simulated by functionality from [32], sensor data in real application) [pu]
$u_{t_{\text{sim}}}^{\text{MV}}$	Normalized voltage at primary transformer side (medium voltage level) at simulation step t_{sim} (equals u_t^{MV}, if t_{sim} falls into t) [pu]
θ_t	Transformer hot-spot temperature available in management interval t (simulated by functionality from [32], sensor data in real application) [°C]
k_t	Transformer load factor available in management interval t (calculated from $P_{\text{T},t}$ and $Q_{\text{T},t}$) [-]

Table 4.9: Symbols for quantities related to grid management measures in Figures 4.9, 4.10, 4.11, and 4.12 that are communicated among the DSO, the buildings, and the transformer.

Sym.	Description
$\chi_{\mathrm{C},b}$	Boolean indicating whether reactive power compensation is currently active for building b [-]
$\boldsymbol{\chi}_{\mathrm{C},b}$	Array of Booleans indicating whether reactive power compensation is currently active for each building [-]
$\chi_{\mathrm{P},b}$	Boolean indicating whether active power flexibility use is currently active for building b [-]
$\boldsymbol{\chi}_{\mathrm{P},b}$	Array of Booleans indicating whether active power flexibility use is currently active for each building [-]
$F_{b,t}^{\mathrm{str}}$	Active power flexibility value of building b stored in man. interval t [W²]
$\boldsymbol{F}_{t}^{\mathrm{str}}$	Array of the active power flexibility values for each building stored in management interval t [W²]
calculate $F_{b,t}$	Boolean indicating whether building b should calculate its active power flexibility for the optimization horizon beginning in man. interval t [-]
calculate $\boldsymbol{F}_{t}$	Array of Booleans indicating whether the active power flexibility for the optimization horizon beginning in management interval t should be calculated for each building [-]
$q_{b,t}^{\mathrm{PV,set}}$	Normalized reactive power setpoint determined for/by building b in management interval t [-]
$\boldsymbol{q}_{t}^{\mathrm{PV,set}}$	Array of normalized reactive power setpoints determined for/by each building in management interval t [-]
$s_{b,t}^{\mathrm{lim}}$	Normalized apparent power limit determined for/by building b in management interval t [-]
$\boldsymbol{s}_{t}^{\mathrm{lim}}$	Array of normalized apparent power limits determined for/by each building in management interval t [-]
χ_{b}^{GSR}	Boolean indicating whether the grid simulation is reliable for building b [-]
$\boldsymbol{\chi}^{\mathrm{GSR}}$	Array of Booleans indicating whether the grid simulation is reliable for each building [-]
χ_{b}^{DSO}	Boolean indicating whether the DSO communication is currently assumed to be disrupted or whether DSO misconduct is detected by building b [-]
$\boldsymbol{\chi}^{\mathrm{DSO}}$	Array of Booleans indicating whether the communication to the DSO is currently assumed to be disrupted or whether DSO misconduct is detected by each building [-]
χ_{Q}	Boolean indicating whether a VRDT gives clearance to use reactive-power-based voltage maintenance [-]
r_t	VRDT transmission ratio determined in management interval t [-]

Table 4.10: Symbols for quantities related to grid management measures in Figures 4.9, 4.10, 4.11, and 4.12 that are only internally processed by the DSO, the buildings, or the transformer and *not* communicated among these participants.

Symbol	Description
$\boldsymbol{ED}$	Array of electrical disturbances, that is, information on whether voltage, line, and/or transformer disturbances are currently occurring [-]
$\boldsymbol{IN}$	Array of information on which buildings can influence which electrical disturbance [-]
$r_{t_{\text{sim}}}$	VRDT transmission ratio at simulation step t_{sim} [-]
n_t	Tap position index in management interval t [-]
$P^{\text{PV}}_{b,t_{\text{sim}}}$	Active power generated by the PV system of building b at simulation step t_{sim} [W]
$Q^{\text{PV}}_{b,t_{\text{sim}}}$	Reactive power absorbed or injected by the PV inverter of building b at simulation step t_{sim} [var]
$P^{\text{bat,cha}}_{b,t_{\text{sim}}}$	Active power generated by the PV system of building b at simulation step t_{sim} [-]
$P^{\text{bat,cha}\star}_{b,t_{\text{sim}}}$	Charging power of the BESS of building b at simulation step t_{sim} [-]
$s^{\text{lim}}_{l(b)}$	Learned normalized apparent power limit for line disturbances on the line l feeding building b [-]
$s^{\text{lim}}_{\text{T}}$	Learned normalized apparent power limit for transformer disturbances [-]
$s^{\text{lim,dec}}_{b}$	Learned normalized apparent power limit for the decentralized strategy for building b [-]
$\boldsymbol{OS}$	Array of optimized device operation schedules for each device in a building and two different optimization objectives as well as the two corresponding simulated load profiles at the GCP of the building [-]/[W]

4.7.1. Power-Flow Simulation

For this thesis, the power-flow study capabilities of the OSH are used in two different contexts. On the one hand, they are used to simulate the actual low-voltage grid as a stand-in for a physical grid in the considered evaluation scenarios. On the other hand, they are used by the simulated DSO and buildings. The DSO and each building perform a power-flow study each management interval based on the power data measured and communicated by all buildings (using their smart meter data, which is simulated in this thesis) and the transformer to gather additional data about the grid status. Most importantly these are the line segment currents, which would otherwise have to be measured by a large number of dedicated sensors [327]. Furthermore, the OSH enables additional power-flow studies to determine which buildings are most likely to be able to prevent or improve a critical grid status in grids with ring topologies. However, for the simulated grids in

Chapter 5, this is not relevant, since their topologies are exclusively radial. All performed studies are single-phase as an even load distribution over all three phases is assumed. A detailed description of the implementation of the power-flow study capabilities of the OSH can be found in [32]. A shorter description is given in Section 2.4.2. To decrease the computation time of individual power-flow studies, we reworked the already existing functionality to use the more performant *jblas* library [328] instead of the previously used linear algebra package *JAMA* [329]. This was necessary to accommodate the substantial increase in performed power-flow studies of our system compared to the regional energy management system (REMS) presented in [32]. In the REMS, only one power-flow study per minute is performed by the REMS-O/C-unit, while in our system, each building as well as the DSO perform one power-flow study per minute. The substantial amount of simulations performed for the parameter studies in Section 4.12 and the evaluation in Chapter 5 further exacerbated the need for a substantial reduction in computation time.

4.7.2. Distribution System Operator Grid Management System

In the centralized grid management strategy, the DSO does not solve an optimal power flow problem for the entire grid. All optimization needed to achieve grid supportive behavior is conducted individually by the local BEMS of each building. The DSO is responsible for observing the grid status based on data communicated by the buildings and the transformer as well as determining which buildings should implement which countermeasures (see also Section 4.5) when a critical grid status is detected. We assume that each building in the grid is equipped with a smart meter and a smart meter gateway or similar systems. These devices enable them to measure and communicate the active and reactive powers as well as the voltage at their own GCP to the DSO and receive commands from the DSO (see also Section 2.6.3).

Figure 4.9 shows the architecture and data flows of the DSO grid management system.

As the other figures in this section, Figure 4.9 concentrates on OSH-Java-classes that are directly related to new functionality introduced in this thesis and thus have been reworked or added to the OSH. Naturally, other classes not explicitly mentioned here play a role as well, since they provide the core functionality of the OSH on which our thesis builds. For a more detailed description of the inner workings of the OSH, refer to the publications referenced in Section 2.4.2.

The *GridManagementCommunicationBusDriver*-class handles the communication between the buildings, the DSO, and the transformer using different data objects that are sent and received by these entities. In a real-word scenario, this functionality would for example be handled by a server hosting a publish/subscribe-message broker. The *DSOComDriver*-class receives the data objects relevant for the DSO and passes them to the *DSOComManager*-class. The latter then writes the data to the local O/C-registry to make them available to the *DSOObserver*-class.

The *DSOObserver*-class then performs a power-flow study based on the data communicated by the buildings and the transformer using the *GridSimulation*-class (see also Section 4.7.1).

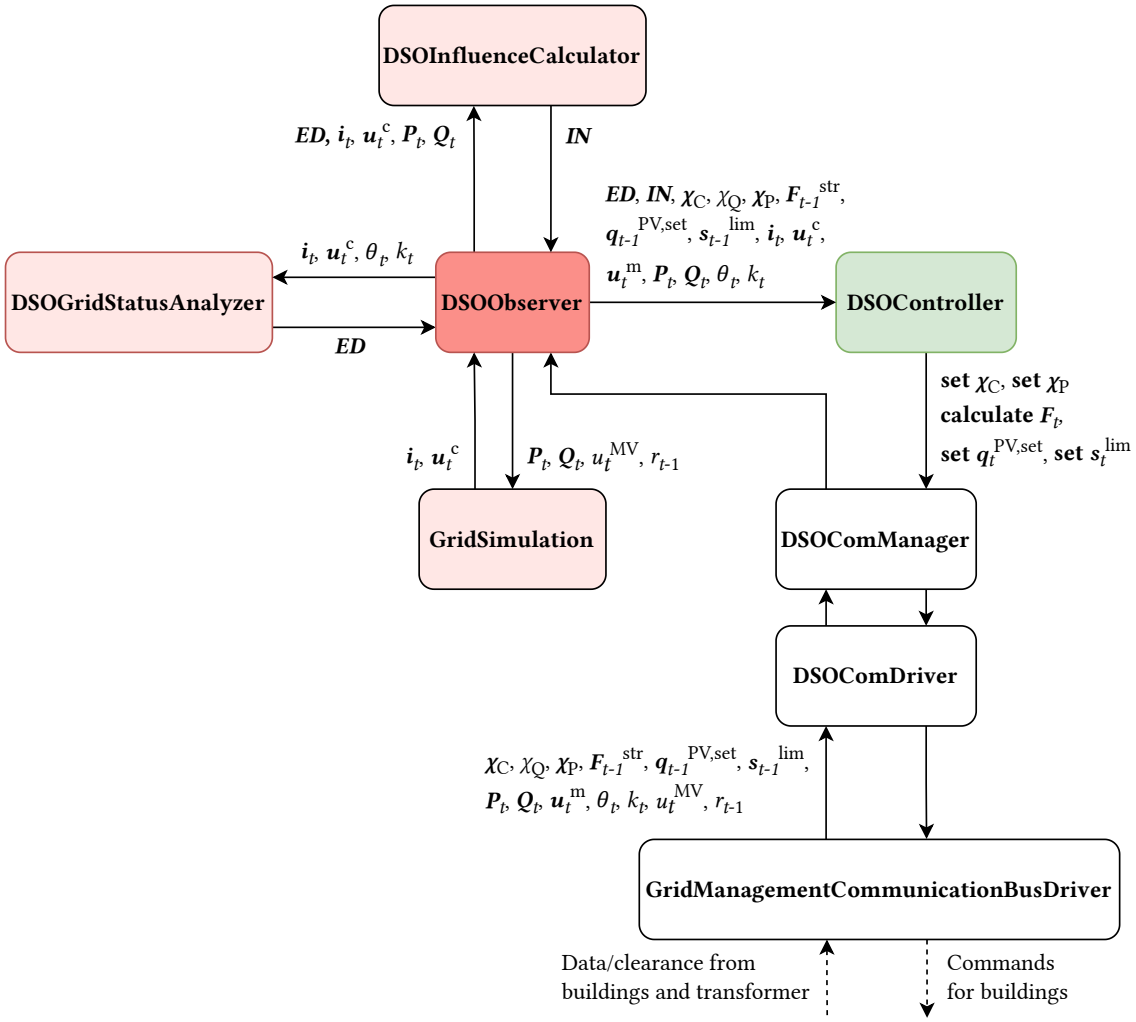

Figure 4.9: Architecture and data flows of the DSO grid management system. Rounded boxes are relevant Java-classes in the OSH. Bold font indicates that the respective data is an array of multiple values. If no data flow is specified on an outgoing arrow, the output data is the same as the input data for the respective class. Dashed arrows indicate communication with other entities not shown in the figure.

This should not be confused with the *GridSimulationBusDriver*-class referenced in the following sections. The *GridSimulationBusDriver* uses the *GridSimulation*-class as well, but to simulate the actual grid and not as a tool to enable the detection of electrical disturbances. The *GridSimulationBusDriver* would be replaced with the physical grid in a real-world scenario, while the *GridSimulation*-class is used as a tool by the DSO and the buildings, regardless of whether the considered scenario is real or simulated. The resulting calculated line segment current and GCP voltage data as well as load factor and temperature data communicated by the transformer are analyzed by the *DSOGridStatusAnalyzer*-class. Here it is determined if voltage, line, or transformer disturbances are currently occurring according to the criteria established in Section 4.4. Occurring electrical disturbances are then saved in an array (called ***ED*** in the figure) and analyzed together with the grid status

data by the *DSOInfluenceCalculator*-class to determine which buildings can influence which occurring disturbance.

The resulting information is saved in an array (called ***IN*** in the figure) and communicated to the *DSOController*-class in addition to the received transformer data, grid status data, and currently implemented grid management measures, such as the reactive power setpoints implemented in the previous management interval. The *DSOController*-class uses this data to determine appropriate countermeasures to the current disturbances, if there are any, using the methods and algorithms presented in Section 4.5. It communicates these countermeasures in the form of commands to the buildings via the *DSOComManager-*, *DSOComDriver-*, and *GridManagementCommunicationBusDriver*-classes.

The *DSOObserver-*, *DSOController-*, and *GridManagementCommunicationBusDriver*-classes are very loosely based on the *REMSGlobalObserver-*, *REMSGlobalController-*, and *BuildingBusDriver*-classes respectively, which were implemented in [32], but retain almost none of their original functionality. Similarly, the *DSOComDriver-* and *DSOComManager*-classes where already implemented in [32] with the same names, but had completely different functionality. The *GridSimulation-*, *DSOGridStatusAnalyzer-* and *DSOInfluenceCalculator*-classes are based on classes implemented in [32] as well, but substantially reworked to accommodate the electrical disturbance and building influence criteria used for the systems developed in this thesis and to achieve substantially shorter computation times (see also Section 4.7.1).

4.7.3. Transformer Grid Management System

The transformer feeding the grid has its own grid management system to analyze, communicate, and, if it is a VRDT, act upon its own sensor data as well as the voltage and grid simulation reliability data provided by the buildings connected to the grid. Figure 4.10 shows the architecture and data flows of this system.

As Figure 4.9, Figure 4.10 only shows OSH-Java-classes that are relevant to the system developed in this thesis.

The transformer uses the *TransformerComDriver* and *TransformerComManager*-classes to receive and communicate relevant data from and to the *GridManagementCommunicationBusDriver*-class. The only data the transformer receives, are the measured GCP voltages of all buildings as well as their determinations of whether the grid simulation is currently reliable or not. The latter indicates whether the communicated data is sufficiently accurate to enable unproblematic transmission ratio switching (see also Section 4.6). The communicated building data is only relevant if the transformer is a VRDT, since a regular transformer can not change its transmission ratio.

In addition to this data, the *TransformerObserver*-class receives the voltage at the primary side of the transformer (voltage at the medium voltage level) from the *GridMeterComDriver*-class as well as the load factor and the hot-spot temperature of the transformer from the *TransformerSimulationDriver*-class. While the primary voltage is calculated by

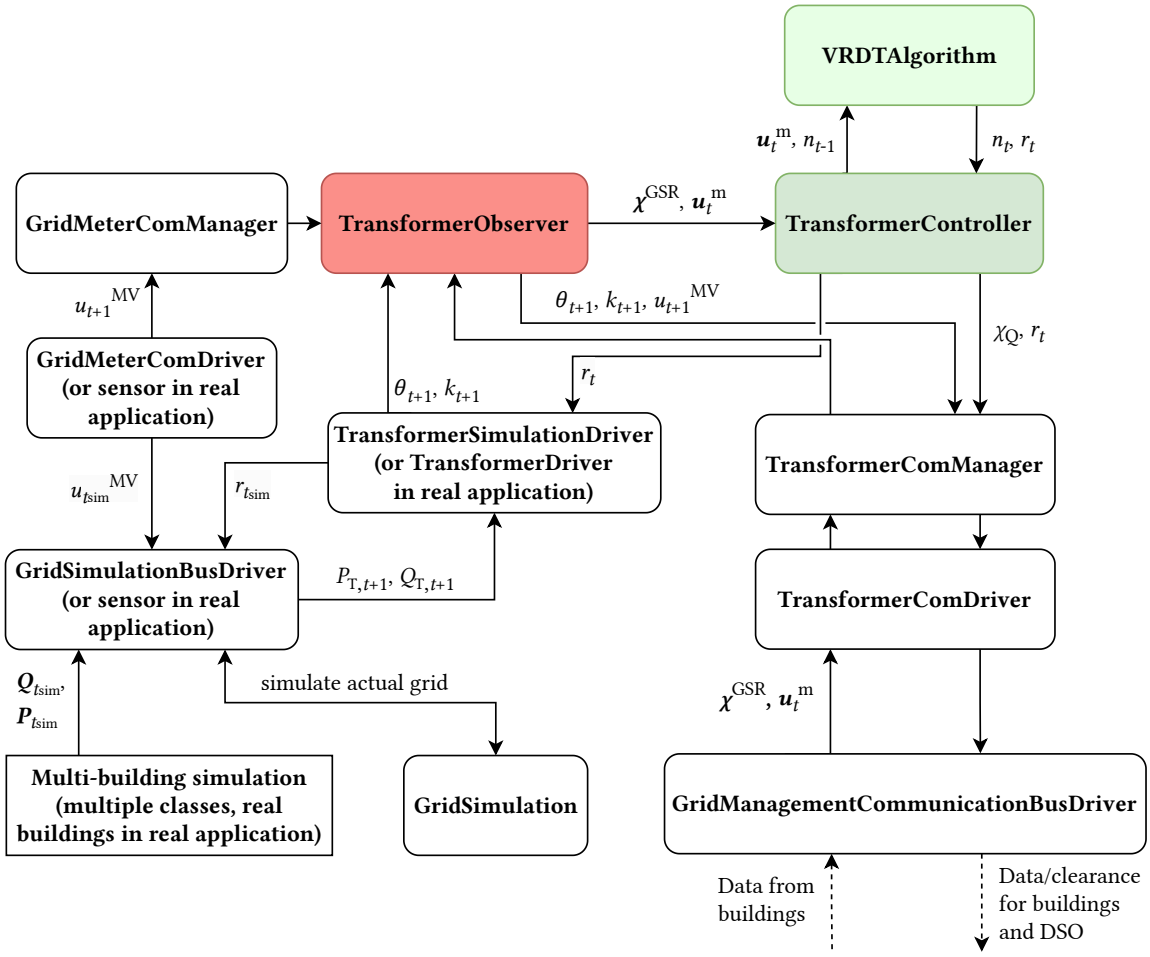

Figure 4.10: Architecture and data flows of the transformer grid management system. Rounded boxes are relevant Java-classes in the OSH. Square boxes encompass multiple OSH classes that are not part of the grid management system itself. Bold font indicates that the respective data is an array of multiple values. If no data flow is specified on an outgoing arrow, the output data is the same as the input data for the respective class. Dashed arrows indicate communication with other entities not shown in the figure.

the *GridMeterComDriver* for the simulations performed in this thesis, this voltage would be measured by a sensor in a real-world application. Similarly, while the *TransformerSimulationDriver* calculates the hot-spot temperature and load factor based on the transformer power data provided by the *GridSimulationBusDriver*-class, in a real-world application, a *TransformerDriver*-class would receive data measured by power and temperature sensors. The *GridSimulationBusDriver* uses the *GridSimulation*-class to simulate the actual electricity grid. This is the same class used by the DSO and the buildings to simulate the grid to detect electrical disturbances based on the data measured and communicated by the buildings and the transformer. However, in this context, it is used to simulate the actual grid based on building power data calculated by aggregating the momentary reactive power absorption or injection and the active power consumption or generation of all devices in a building for each building in the grid. This aggregation process is not shown in Figure 4.9, since it was already implemented in [32] and was not changed for this thesis.

The building power data would be provided by smart meters in a real-world application. The *TransformerObserver* communicates the data provided by the *GridMeterComDriver* and the *TransformerSimulationDriver* to the DSO and the buildings via the *TransformerComManager* and *TransformerComDriver*. It also communicates the received GCP voltage and grid simulation reliability data of the buildings to the *TransformerController*-class.

If the transformer is a VRDT, the *TransformerController* uses the *VRDTAlgorithm*-class to calculate the tap position index and the new transmission ratio based on the old tap position index and the received GCP voltages according to Algorithm 1. If the grid simulation is unreliable according to the conditions given in Section 4.6.1, the *TransformerController* gives the buildings clearance to use reactive-power-based voltage maintenance and gradually switches back to the neutral transmission ratio. This clearance is communicated to the DSO as well, so that it can determine reactive power setpoints for the buildings in the centralized grid management strategy. The new transmission ratio is communicated to the DSO and the buildings as well, since they need it to perform their power-flow studies.

While the *TransformerComDriver*- and *TransformerComManager*-classes are newly implemented to accommodate the communication between the transformer, the buildings, and the DSO, the rest of the classes used by the transformer are based on similar classes implemented in [160] and [32]. The *GridMeterComDriver*- and *GridMeterComManager*-classes are reused for this thesis without changes. The *TransformerSimulationDriver*-, *TransformerObserver*-, and *TransformerController*-classes are based on the *RONTDriver*-, *RONTLocalObserver*-, and *RONTLocalController*-classes. They were substantially reworked to use Algorithm 1, handle data communicated by buildings, and communicate data and clearance information to buildings and the DSO. Only slight changes were made to the *GridSimulationBusDriver*-class itself. However, the latter uses the *GridSimulation*-class to simulate the electricity grid, which was reworked to achieve substantially shorter computation times (see also Section 4.7.1).

4.7.4. Building Grid Management System

The building grid management system is essential for accommodating the three different grid management strategies. In the centralized strategy, it is mainly responsible for implementing the commands received by the DSO and communicating locally measured power and voltage data as well as data on implemented grid management measures to the transformer, the DSO and the other buildings. Additionally, it checks received commands and data for completeness and correctness to mitigate potential communication disruption and misconduct by the DSO, the transformer, or other buildings. If a problem occurs, the building adjusts its behavior and switches to another grid management strategy as appropriate. To enable this mitigation, each building has to perform its own power-flow studies in each management interval using the same input data and methods as the DSO. The power-flow studies are performed regardless of whether the centralized or distributed strategies are used, as they are needed to assume the responsibilities of the DSO in the distributed strategy as well. Only if the decentralized strategy has to be used, the power-flow studies are paused due to insufficient input data. The results of the power-flow studies

itself are checked for accuracy, which can trigger a switch to the decentralized strategy as well. More information on the strategy switching performed on the building level is given in Section 4.6. In the distributed and decentralized strategies, each building uses the appropriate algorithms introduced in Section 4.5 in response to the electrical disturbances defined in Section 4.4.

Figure 4.11 shows the architecture and data flows of the building grid management system. Figure 4.12 shows the architecture and data flows of the modular global controller of a building with regard to grid management. The class *ModularGlobalController* hosts and orchestrates multiple controller modules (subclasses of *GlobalControllerModule*) that take on different tasks.

As Figures 4.9 and 4.10, Figures 4.11 and 4.12 only show OSH-Java-classes that are directly relevant to the functionality developed in this thesis. In contrast to the classes related to the DSO and transformer grid management systems, most of the following classes do not only provide grid management functionality but general building energy management functionality as well, which is not the focus of this thesis and therefore not described in detail. For more information on the energy management capabilities of the OSH, refer to the publications referenced in Section 2.4.2.

The *GlobalObserver*-class receives the data objects containing relevant data from other buildings and the transformer as well as commands from the OSH via the *GridManagement-CommunicationBusDriver*-,*BuildingComDriver*, and *BuildingComManager*-classes. The data received from the other buildings includes information on whether the communication to the DSO is currently disrupted for one or more buildings or if one or more buildings assume DSO misconduct. This enables a building to switch to the distributed strategy in the case of communication disruption or DSO misconduct even before the building detects such a problem itself. For example, this could be the case if a building connected to a particular line detects a critical line current, but does not receive commands from the DSO, while other buildings do not (yet) detect critical currents on their respective lines. Additionally, the received data contains the current active power flexibilities of other buildings if these have recently calculated their flexibilities. Using these flexibilities, the building can determine whether or not its own flexibility puts it in the group of buildings with the highest flexibilities, which implement active power targets first (see also Section 4.5.5). Furthermore, the building receives the current apparent power limits of the other buildings, so that it can perform Algorithm 5. The data received by the transformer includes the possible clearance to implement reactive-power-based voltage maintenance if the transformer is a VRDT, but the grid simulation is currently unreliable according to the conditions introduced in Section 4.6.1.

Based on the received building power data, transformer data, and its own locally measured data from the previous management interval provided by the *GridSimulationBusDriver*-class, the *GlobalObserver* performs power-flow studies using the same *GridSimulation*-class as the DSO. The *GridSimulation*-class is used by the *GridSimulationBusDriver* as well. However, the latter initializes the simulation with different input data. This data is calculated by aggregating the momentary reactive power absorption or injection and the active power consumption or generation of all devices in a building for each building in the grid.

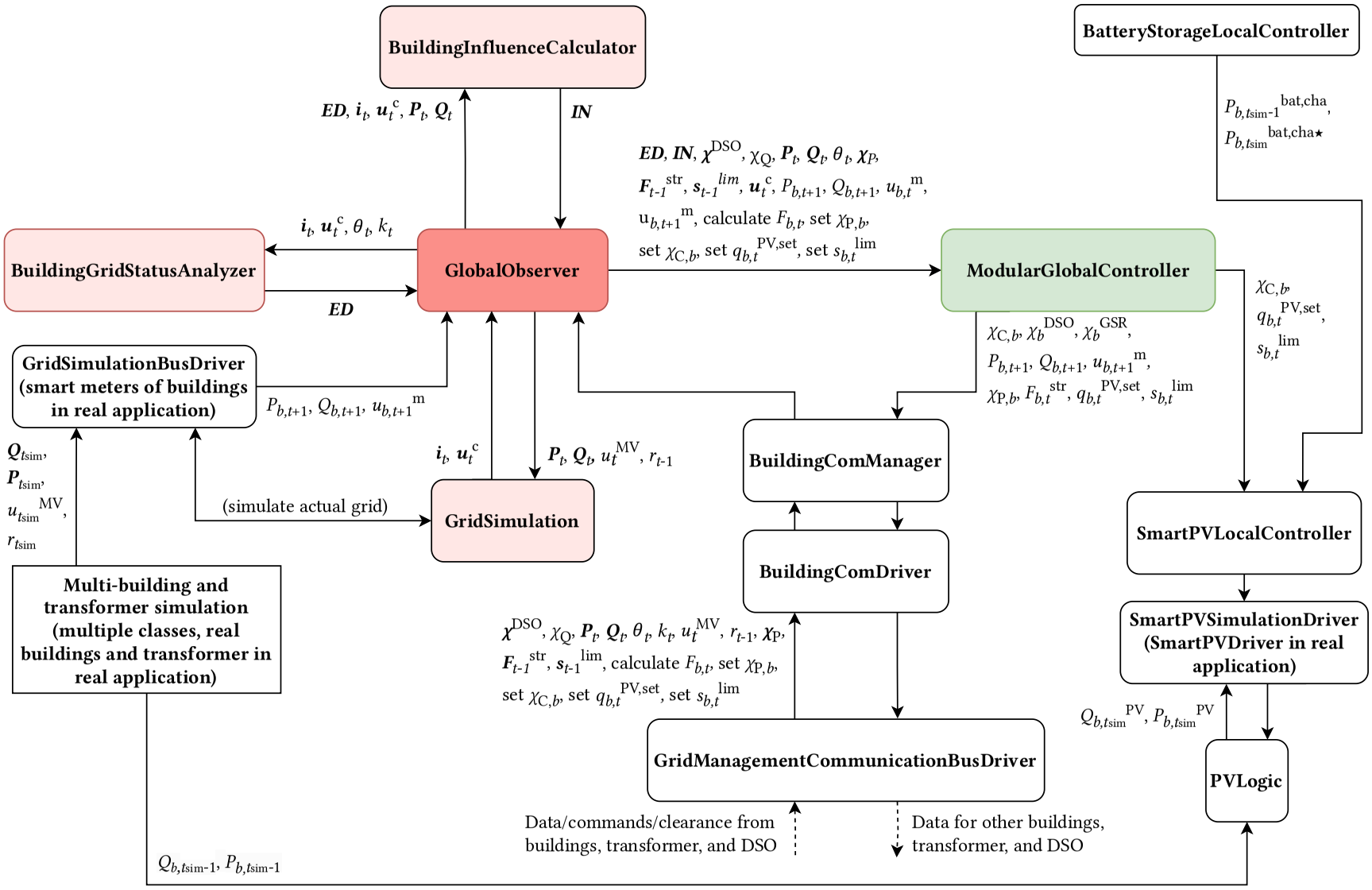

Figure 4.11: Architecture and data flows of the building grid management system. Rounded boxes are relevant Java-classes in the OSH. Square boxes encompass multiple OSH classes that are not part of the grid management system itself. Bold font indicates that the respective data is an array of multiple values. If no data flow is specified on an outgoing arrow, the output data is the same as the input data for the respective class. Dashed arrows indicate communication with other entities not shown in the figure.

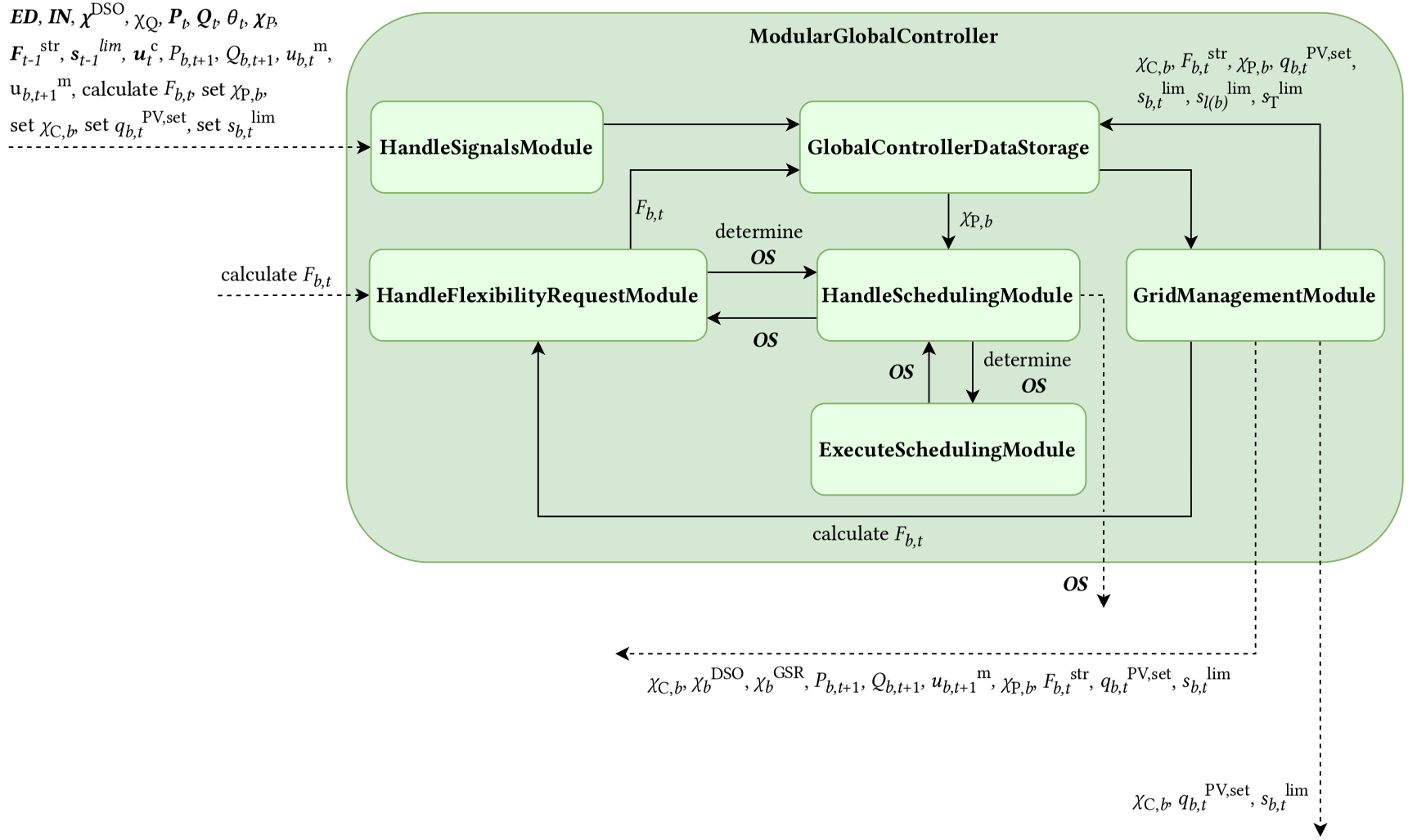

Figure 4.12: Architecture and data flows of the modular global controller of the OSH with regard to grid management. Rounded boxes are relevant Java-classes in the OSH. Bold font indicates that the respective data is an array of multiple values. If no data flow is specified on an outgoing arrow, the output data is the same as the input data for the respective class. Dashed arrows indicate communication with other entities not shown in the figure.

Therefore, the grid simulation initiated by the *GridSimulationBusDriver* represents the actual grid and is not a tool used by a building or the DSO to detect electrical disturbances. In a real-world scenario, the *GridSimulationBusDriver* would be replaced by a smart meter. Analogous to the *DSOObserver*, the *GlobalObserver* checks the current grid status for electrical disturbances using the conditions introduced in Section 4.4 and determines which disturbances the building can influence using the *BuildingGridStatusAnalyzer*- and *BuildingInfluenceCalculator*-classes respectively. It then communicates the array of the occurring electrical disturbances (called ***ED*** in the figure), the corresponding influenceability array (called ***IN*** in the figure), the data received by the buildings and the transformer, as well as the commands from the DSO to the *ModularGlobalController*.

As mentioned earlier, the *ModularGlobalController* hosts several controller modules responsible for different tasks. The *HandleFlexibilityRequestModule*-class handles requests by the DSO in the centralized strategy or the *GridManagementModule*-class in the distributed or decentralized strategies to calculate the current active power flexibility of the building. It uses the *HandleSchedulingModule*- and *ExecuteSchedulingModule*-classes to determine device operation schedules optimized with regard to energy costs and different device operation schedules optimized with regard to an active power target (see also Equation 4.26). The resulting array of device operation schedules (called ***OS*** in the figure) also includes the two load profiles at the GCP of the building, which are simulated based on the two different sets of device operation schedules. The load profiles are used to calculate the current active power flexibility of the building according to Equation 4.27. The calculated flexibility is written to the *GlobalControllerDataStorage*-class and thereby made available to the *GridManagementModule*-class. The *HandleSignalsModule*-class is responsible for receiving all data communicated by the *GlobalObserver*, except flexibility calculation commands, and writing it to the *GlobalControllerDataStorage* for use by the *GridManagementModule*. The *GlobalControllerDataStorage*-class is used for storing data communicated by the controller modules and making this data available to all controller modules on demand. The *HandleSchedulingModule*-class triggers the optimized scheduling of the devices of a building according to the current objective and communicates the schedules to the local O/C-units of the scheduled devices. The optimization objective can either be the minimization of energy costs during undisturbed grid operation or the minimization of the difference between the load profile at the GCP of the building and an active power target set by the DSO or the *GridManagementModule*. The latter is described in Section 4.5.5. When a new scheduling is necessary, the *HandleSchedulingModule* notifies the *ExecuteSchedulingModule*. The latter is responsible for determining the optimized schedules. The optimized device scheduling and schedule implementation involve additional classes that are not mentioned in Figure 4.11, since their functionality is not changed for the new grid management system. For a more detailed explanation of the scheduling process implemented in the OSH refer to the publications referenced in Section 2.4.2. The *GridManagementModule*-class is the centerpiece of the grid management system of a building. It uses the algorithms and methods detailed in Section 4.5 to determine reactive power setpoints and apparent power limits as well as trigger reactive power compensation and active power flexibility use in response to detected and influenceable electrical disturbances. Additionally, it detects possible communication disruption and participant

misconduct and determines whether the centralized, distributed, or decentralized grid management strategies should be used by means of the methods described in Section 4.6. Furthermore, it sends direct commands to the local controller of the PV-system of the building represented by the *SmartPVLocalController*-class, which forwards the commands to the *SmartPVSimulationDriver*-class. These commands can comprise the implementation of reactive power compensation, the implementation of specific reactive power setpoints for reactive-power-based voltage maintenance, and the implementation of apparent power limits for the adaptive curtailment of the PV-system. In a real-world application, the *SmartPVSimulationDriver* would be replaced with a *SmartPVDriver*-class that controls a real PV-inverter. When reactive power compensation is used, the calculation of the reactive power setpoint of the PV-inverter according to Equation 4.15 is performed by the *PVLogic*-class. The latter also performs the calculation of the active power setpoint of the PV-inverter according to Equations 4.21 to 4.24, when an apparent power limit for PV curtailment is used. In contrast, reactive power setpoints for reactive-power-based voltage maintenance are directly implemented by the *SmartPVSimulationDriver*. After the *GridManagementModule* finishes running the mentioned algorithms and methods, it writes the determined setpoints, limits, targets, and other measures to the *GlobalControllerDataStorage* to recall them in the next management interval. Information on whether an active power target should be used is recalled by the *HandleSchedulingModule* as well. The *GridManagementModule* then communicates all data that is relevant for other buildings, the transformer, or the DSO to these entities via the *BuildingComManager*, *BuildingComDriver*, and *GridManagementCommunicationBusDriver*.

The *BuildingComDriver*- and *BuildingComManager*-classes are based on the *CombinedSignalComDriver*- and *CombinedSignalProviderComManager*-classes implemented in [32], but have been extensively reworked to handle the new data objects for the grid management system. The preexisting *GlobalObserver* was substantially enhanced to enable the observation side of the new grid management system of the building. The *GridSimulation*-, *BuildingGridStatusAnalyzer*- and *BuildingInfluenceCalculator*-classes are based on classes implemented in [32] as well, but substantially reworked to support the electrical disturbance and building influence criteria used for the systems developed in this thesis and to achieve substantially shorter computation times (see also Section 4.7.1). The *GridSimulationBusDriver*-class was implemented in [32] as well and could be reused for the systems developed in this thesis without significant modification. However, it uses the new, substantially performance-optimized version of the *GridSimulation*-class implemented for this thesis to simulate the actual electricity grid (see also Section 4.7.1). The *HandleSignalsModule*-, *HandleFlexibilityRequestModule*-, *GlobalControllerDataStorage*-, *HandleSchedulingModule*-, and *ExecuteSchedulingModule*-classes are preexisting classes developed in several of the publications referenced in Section 2.4.2. However, they were extensively revised and enhanced to enable the new functionality introduced by the new grid management system of the building. The majority of the latter was implemented in the newly developed *GridManagementModule*-class. The preexisting *SmartPVLocalController*-, *SmartPVSimulationDriver*-, and *PVLogic*-classes were substantially reworked as well, to allow for the adaptive PV-curtailment, reactive-power-based voltage maintenance, and reactive power compensation algorithms we introduce in this thesis.

4.7.5. Communication Infrastructure

In our evaluation, the communication infrastructure between the DSO, the transformer, and the buildings is simulated by the OSH-Java-class *GridManagementCommunicationBusDriver*. Figure 4.13 shows the architecture and data flows for the communication between the system participants in our simulation.

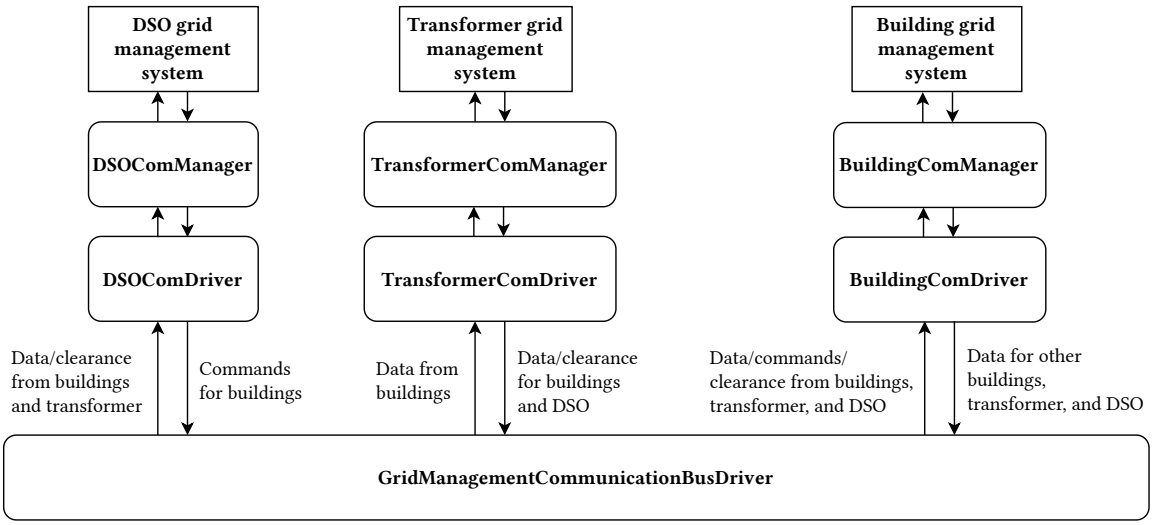

Figure 4.13: Architecture and data flows of the communication system used by the DSO, the transformer, and the buildings. Rounded boxes are relevant Java-classes in the OSH. Square boxes encompass multiple OSH classes that are shown in the other figures in this section. If no data flow is specified on an outgoing arrow, the output data is the same as the input data for the respective class or group of classes.

The classes shown in Figure 4.13 have already been introduced in the previous sections and are therefore not detailed further here. In a real-world application, the *GridManagementCommunicationBusDriver* would be replaced with appropriate physical communication infrastructure, such as fiber optic cable or wireless networks, and one or more servers hosting communication software, such as a publish/subscribe message broker. A peer-to-peer protocol would present a possible more decentralized option than a server. For example, an adjusted version of the peer-to-peer communication system developed in the project *Selbstorganisation und Spontaneität in liberalisierten und harmonisierten Märkten* (SESAM, English: Self-Organization and Spontaneity in Liberalized and Harmonized Markets) [330] may be used as well. We do not recommend a specific communication system for a real-world implementation. The chosen communication system only has to accommodate the required communication for the centralized and distributed strategies to be implementable. Since our presented grid management system is resilient with regard to communication disruption, the chosen communication system is not required to be fail-safe.

4.8. Transferability to Other Energy Management Systems

While we use the OSH as a basis to build our grid management system, the grid management algorithms, methods, and strategies developed in this thesis can be implemented using different BEMSs as well, such as the ones described in Section 2.4.1. A major reason for choosing the OSH for the implementation of our grid management system is its co-simulation capabilities (multi-building and power-flow, see also Section 2.4.2), which we need to develop and evaluate the system. However, the implementation of the system is possible on BEMSs without co-simulation functionality as well. It is also possible to implement only parts of our proposed system, if the particular BEMS is not suited to implement all of the measures we use to mitigate electrical disturbances, communication disruption, participant misconduct, and sensor failure. For example, a particular BEMS might not (yet) provide the same proactive and comprehensive energy flow optimization as the OSH but PV inverter control, power measurement at the GCP, and communication with other entities. In this case, our reactive power compensation, reactive-power-based voltage maintenance, and PV curtailment algorithms can be implemented without the capability of using active power flexibility for grid supportive purposes. The three developed grid management strategies and adaptive grid management via strategy switching could be transferred as well, as long as the BEMS supports bidirectional communication to external entities (DSO, transformer, other buildings), has the capability to perform regular power-flow studies and can decide on appropriate countermeasures to electrical disturbances autonomously. A BEMS that may be suited for the implementation of our grid management system is *OpenEMS* (see also Section 2.4.1). It is open source, uses a modular approach, and has extensive monitoring and control capabilities for a wide range of devices as well as an active community, which would allow extending its functionality to implement at least some, if not all elements of our grid management system. In our assessment, OpenEMS is better suited for this purpose than the other EMSs presented in Section 2.4.1. In contrast to OpenEMS, the latter are either focused on monitoring without comprehensive control capabilities, not specialized on energy management in residential buildings, or partially proprietary. Table 4.11 gives an overview of the prerequisites a BEMS has to fulfill for each developed measure.

4.9. Visual Demonstration

During the software development for the presented grid management system the author of this thesis and a few students created an interactive demonstrator. The demonstrator presents the system at an earlier development stage, but already encompasses the presented countermeasures to electrical disturbances and the three grid management strategies. A screenshot of the graphical user interface of the demonstrator can be seen in Figure 4.14.

The demonstrator does not use prerecorded time series data to show a predefined scenario. The back end of the demonstrator consists of an OSH-based simulation based on an earlier version of the updated *the day after tomorrow* scenario and the village grid (see also

Table 4.11: Prerequisites for the implementation of the different measures encompassed by our grid management system that have to be fulfilled by a BEMS used as a basis for its implementation.

Measure	Prerequisite for BEMS
Countermeasures to electrical disturbances	
Reactive power compensation	Power measurement at GCP, PV inverter control
VRDT-based voltage maintenance	Handled by transformer grid management system, no prerequisites for BEMS
Reactive-power-based voltage maintenance	Power measurement at GCP, PV inverter control
PV curtailment	Power measurement at GCP, PV inverter control
Active power flexibility use	Power measurement at GCP, optimized device operation scheduling
Adaptive grid management to mitigate communication disruption, participant misconduct, and sensor failure	
Centralized grid management strategy	Bidirectional communication, support of at least one of the countermeasures to electrical disturbances
Distributed grid management strategy	Bidirectional communication, capability of running power-flow studies, support of at least one of the countermeasures to electrical disturbances, capability of determining appropriate measures autonomously
Decentralized grid management strategy	Support of at least one of the countermeasures to electrical disturbances, capability of determining appropriate measures autonomously
Adaptive grid management	Support of at least two of the grid management strategies, capability of determining appropriate strategy autonomously

Section 4.10). It simulates 55 buildings, including installed devices and equipment, as well as the surrounding distribution grid bottom-up. The simulation works very similar to the simulations performed for Section 4.12 and Chapter 5. The main difference is that, for the demonstrator, the simulated time is synchronized with the wall clock time, while the simulations performed for this thesis run as fast as the utilized hardware and software allow. The user interface is implemented as an *Angular*-based [331] web application, which enables the visualization of different load and communication scenarios as well as the corresponding grid-supporting reactions of the buildings. Its interactive capabilities allow the manual introduction of electrical disturbances. Furthermore, comprehensive information on the current statuses of lines, the transformer, buildings, and their devices

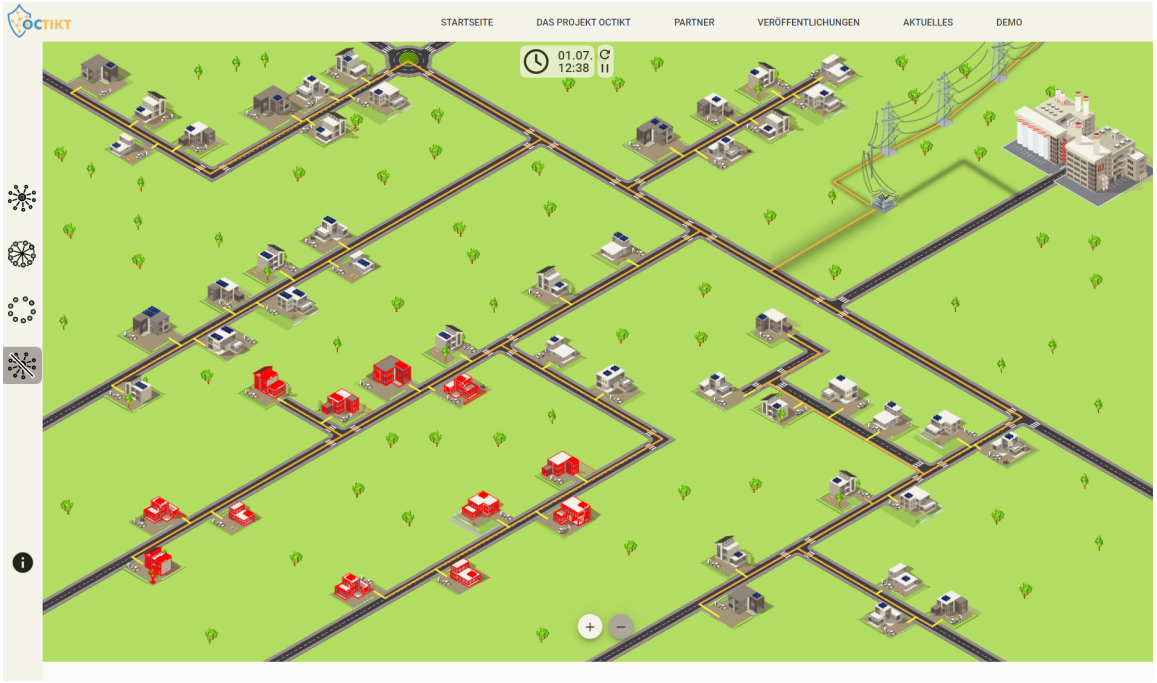

Figure 4.14: Screenshot of the user interface of the interactive demonstrator for the grid management system.

can be gathered by clicking on the respective elements in the user interface. Manual switching between grid management strategies during run time is possible as well. This can be utilized to show how the system reacts if the communication between the participants is partially or fully disrupted. Additionally, the user interface shows the current simulated time and provides buttons to pause, resume, and restart the simulation. A foldout legend provides information on the background and functionality of the demonstrator and explains the elements of the user interface [332]. The demonstrator is available and running at the *FZI Living Lab smartEnergy* of the *FZI House of Living Labs* [30] in Karlsruhe, Germany.

4.10. Simulation, Grid, and Building Configurations

This section establishes the simulation environment used for the parameter studies in Section 4.12 and the evaluation of the developed grid management system in Chapter 5. We thereby provide an answer to Sub-Question 1.3 of Research Question 1 and another prerequisite for answering Sub-Questions 1.4 and 1.5 of Research Question 1, Sub-Questions 2.1 and 2.2 of Research Question 2, as well as Sub-Question 3.3 of Research Question 3.

Since the main purpose of the system is the full prevention of electricity outages, it has to be evaluated in an environment in which such outages occur if no countermeasures are taken. Therefore, the configurations of the simulated buildings and grids are based on the *the day after tomorrow* reference scenario as well as the three low-voltage reference grids developed in [162] and [32]. However, the reference scenario is updated and the reference grids are modified for this thesis, which will be detailed later in this section. Figure 4.15

shows the grid topologies for the rural, village, and suburban reference grids reproduced from [32].

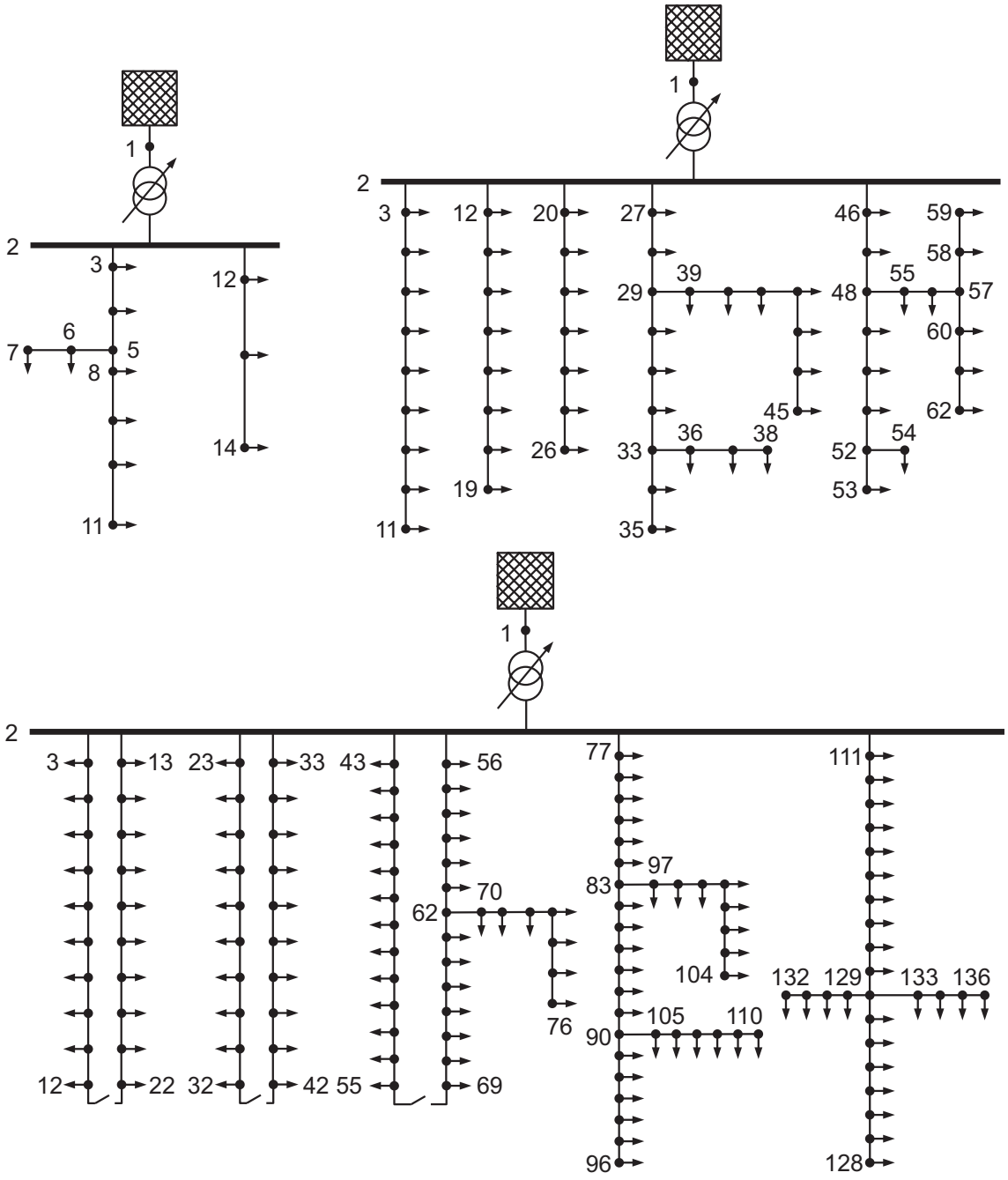

Figure 4.15: Topologies of the reference grids introduced in [162] and used in [32] as well as this thesis. Top left: rural grid, top right: village grid, bottom: suburban grid. Based on a figure in [32].

The configuration of the EA deployed by each building to utilize its active power flexibility by scheduling device operation with regard to different optimization objectives is given in Table 4.12. All parameter studies (see also Section 4.12) that are not directly related to the accuracy of the EA use a different configuration than all other parameter and evaluation

studies. The number of solution candidates as well as the number of generations are reduced to one, respectively, to decrease the computation times for the large number of simulations performed for the parameter studies. Table 4.12 also summarizes the random seed configuration used for all parameter and evaluation studies performed for this thesis. Each building is simulated using a different random seed, which is utilized to simulate the appliance and domestic hot water usage, BEV driving distances associated with the building, and to initialize the EA used by the building. Every evaluation or parameter study is repeated five times using different random seeds for each simulation run. The results of the five simulation runs are then averaged to form a single result to substantially decrease the influence of random effects on the evaluation and parameter studies. Additionally, Table 4.12 specifies the temporal resolutions of the different simulation components. While the building simulations are performed with a one-second resolution, the resolutions of the PV generation and the power-flow studies performed to simulate the grid are set to one minute. In the case of the PV profile, the usable resolution is limited by the resolution at which it was measured. The power-flow study resolution of one minute is a direct result of the latter. Since the PV systems of the buildings represent the highest and most volatile load on the grid compared to the other simulated devices, a higher power-flow study resolution than the one used for the PV systems would not significantly increase their informative value. The power-flow studies and grid management algorithms run by the buildings and the DSO are performed in one-minute intervals as well. These resolutions are limited by the capabilities of the smart meters, which provide the input data for the power-flow studies (see also Section 2.6.3). Furthermore, higher temporal resolutions would entail substantial data traffic and storage requirements, which would lead to substantial hardware cost in real-world implementations as well. The simulations performed by each building to optimally schedule its device usage in advance, use a five-minute resolution, to make the extensive parameter and evaluation studies performed for this thesis feasible with regard to computation time. Despite being very efficient already, the solution times for the EA represent by far the largest share of the simulation duration.

Some of the building and grid configuration parameters and aspects are the same for all simulations performed for this thesis, while others are varied depending on the grid. Table 4.13 contains the parameters and aspects that are used for all three grids. The primary voltage of the transformer is partially randomized according to the mechanism introduced in [32]. The electrical base load of each building is simulated using variations of the H0 [333] standard load profile. A total of nine profiles are used, depending on the simulated season (summer, intermediate, winter) and the current day of the week (weekday, Saturday, Sunday). These profiles are scaled according to the number of inhabitants living in a particular building. Partially flexible appliances are simulated in addition to the base load using measured real-world power profiles of the respective appliance types and probability based starting times as in [67]. The year-long PV generation profile was measured at the *FZI House of Living Labs* in 2013 and is scaled to the peak powers of the respective PV systems of the buildings. We assume that the solar irradiance profile is approximately the same for buildings connected to the same transformer and therefore do not utilize qualitatively different PV generation profiles for individual buildings. Each building is equipped with a PV system and an electric vehicle with a battery capacity of 85 kWh. The

Table 4.12: Configuration of the EA utilized by each building, the random seed configuration for the performed simulations, and the temporal resolutions of the simulation components. The given configurations are the same for all simulated grids and seasons.

Parameter	Value(s)
	EA configuration
Population size	100 solution candidates (1 for non-optimization-related parameter studies)
Stopping criteria	10^7 generations reached (1 for non-optimization-related parameter studies) or fitness delta $\leq 5 \cdot 10^{-5}$ for 20 generations
	Random seed configuration
Given simulation results are always the averages for 5 different random seed configurations, random seeds are different for each building respectively, random seeds are used for appliance and domestic hot water usage, BEV driving distances, and EA initialization	
	Temporal resolutions
Building simulation	1 s (equals the simulation step size Δt_{sim})
PV profile	1 min (equals the management interval duration Δt)
Power-flow studies	1 min (equals the management interval duration Δt)
Grid management algorithms	1 min (equals the management interval duration Δt)
EA	5 min (equals the scheduling time slot duration $\Delta \tau$)

latter corresponds to the electric vehicle type with the largest battery implemented in [334]. This represents a change in comparison to the scenarios evaluated in [32], which is based on the increasing share of BEVs as well as the plans and projections for the future described in Section 2.2.6.

As mentioned before, some building and grid configuration parameters and aspects differ among the considered grids. Consequently, Tables 4.14, 4.15, and 4.16 contain the deviating parameters and aspects for the rural, village, and suburban grids, respectively.

In Tables 4.14 to 4.16, the rated powers of the transformers, the line types, as well as the numbers of feeders, distributing cabinets, secondary lines, grid nodes, and GCPs for each grid correspond to the ones used in [32]. However, the line lengths for all grids are increased by 50 % over the ones in [32] to ensure the occurrence of voltage-related disturbances, as was done in [160] for the village grid.

The numbers of inhabitants of each building, the qualitative distributions of PV systems and BESSs, as well as the configurations of the hot water storage tanks, CHP plants, and HPs for all grids are the same as in [32]. However, the PV system peak active powers, BESS

Table 4.13: Configuration parameters and aspects of the buildings and the grid that are the same for all three simulated grids. Unless stated otherwise, all given building parameters are the same for all buildings. The given configurations are the same for all simulated seasons.

Parameter	Value(s)
Grid configuration	
Voltage on primary side of transformer	Contains a random component as in [32]
Grid topology	Radial
Building configuration	
Base load profile	H0, adjusted for weekday, Saturday, Sunday, season, and number of inhabitants
Simulated appliances (additional to base load)	Dishwasher, washing machine, tumble dryer, induction hob, electric oven (measured real-world power profiles, probability based starting times according to [67])
Flexible appliances	Dishwasher, washing machine, tumble dryer
PV system power profile	Measured at the FZI House of Living Labs in 2013, scaled to respective peak powers
BEV battery capacity	85 kWh
BEV max. active charge power	22 kW ($cos(\varphi) = 0.99$), variable charging, no discharging, usage model developed in [334]

capacities, BESS charge/discharge powers, as well as the distributions of HPs, CHP plants, and BEVs are adjusted for this thesis to account for the developments since the publication of [32] described in Section 2.2. We increase the respective peak powers as well as the BESS capacities and (dis)charge powers according to Table 4.17. Similarly, we reduce the share of buildings equipped with CHP plants and increase the shares of buildings equipped with HPs and BEVs according to Table 4.18. Furthermore, while [32] used three different types of BEVs with different battery capacities (18.8, 24.2, and 85 kWh), we exclusively use the third type, which has the highest battery capacity, since we assume this value to be the most realistic for a future scenario.

4.11. Evaluation Metrics

To conduct the parameter studies and quantify the resilience of the developed adaptive grid management system, we calculate the outage time as well as the aggregated active energy generated by all PV systems in the grid. These metrics relate directly to the resilience

Table 4.14: Deviating configuration parameters of the buildings and the grid specific to the rural grid. Every building uses a PV system, a BESS, a HP, and a hot water storage tank.

Parameter	Value(s)
Grid configuration	
Transformer rated power	250 kVA
Grid line type	70-AL1/11-ST1A, overhead line
Average length of lines between GCPs or line branch points	79.8 m
Feeders	2
Distributing cabinets	1
Secondary lines	1
Grid nodes	14
GCPs (buildings)	11
Building configuration	
Inhabitants per building	2 - 5, average: 3.45
PV system peak active power	15 - 30 kW_p, average: 25.91 kW_p
PV Inverter peak apparent power	16.67 kVA - 33.33 kVA, average: 28.79 kVA
BESS capacity	10 kWh, same for all buildings
BESS max. active charge/discharge power	7 kW ($cos(\varphi) = 1$), same for all buildings, power feed-in to distribution grid temporarily permitted during and after grid-supportive flexibility provision, charging from distribution grid permanently disallowed
Air source HP	6.7 kW_{el} ($cos(\varphi) = 0.95$), coefficient of performance (COP) between 1.2 and 5.1 depending on air and hot water tank temperature, installed in all buildings
Hot water storage tank	750 L, $\theta_{min/max} = 40/60$ °C, used for both domestic and heating hot water

definition we introduce in 4.2. The outage time quantifies the capability of the grid to operate within the technical specifications of the grid equipment and the devices powered by the grid. The aggregated active energy generated by all PV systems in the grid quantifies the invasiveness of the countermeasures used to mitigate electrical disturbances, that is, the extent of the deployed load curtailment. Note that, in the context of our thesis,

Table 4.15: Deviating configuration parameters of the buildings and the grid specific to the village grid. Every building uses a PV system, a BESS, and a hot water storage tank.

Parameter	Value(s)
Grid configuration	
Transformer rated power	400 kVA
Grid line type	NAYY 4x150 SE, buried cable
Average length of lines between GCPs or line branch points	51.41 m
Feeders	5
Distributing cabinets	5
Secondary lines	5
Grid nodes	62
GCPs (buildings)	55
Building configuration	
Inhabitants per building	1 - 5, average: 2.93
PV system peak active power	8 - 30 kW_p, average: 18.84 kW_p
PV Inverter peak apparent power	8.42 kVA - 33.33 kVA, average: 20.78 kVA
BESS capacity	7 - 10 kWh, average: 9.24 kWh
BESS max. active charge/discharge power	4.9 - 7 kW ($cos(\varphi) = 1$), average: 6.47 kW, power feed-in to distribution grid temporarily permitted during and after grid-supportive flexibility provision, charging from distribution grid permanently disallowed
CHP plant (if no HP is used)	1 kW_{el} ($cos(\varphi) = 0.9$), 4 kW_{th}, 5.682 kW_{gas}, installed in 1 of 55 buildings
Air source HP (if no CHP plant is used)	6.7 kW_{el} ($cos(\varphi) = 0.95$), coefficient of performance (COP) between 1.2 and 5.1 depending on air and hot water tank temperature, installed in 54 of 55 buildings
Hot water storage tank	750 L, $\theta_{min/max}$ = 60/80 °C (CHP plant), 40/60 °C (HP), used for both domestic and heating hot water

Table 4.16: Deviating configuration parameters of the buildings and the grid specific to the suburban grid. Every building uses a PV system, a BESS, and a hot water storage tank.

Parameter	Value(s)
Grid configuration	
Transformer rated power	630 kVA
Grid line type	NAYY 4x150 SE, buried cable
Average length of lines between GCPs or line branch points	22.86 m
Feeders	8
Distributing cabinets	4
Secondary lines	5
Grid nodes	136
GCPs (buildings)	130
Building configuration	
Inhabitants per building	1 - 5, average: 2.6
PV system peak active power	6 - 15 kW_p, average: 8.56 kW_p
PV Inverter peak apparent power	6.32 kVA - 16.67 kVA, average: 9.17 kVA
BESS capacity	6 - 10 kWh, average: 7.3 kWh
BESS max. active charge/discharge power	4.2 - 7 kW ($cos(\varphi) = 1$), average: 5.11 kW, power exchange with grid permitted
CHP plant (if no HP is used)	1 kW_{el} ($cos(\varphi) = 0.9$), 4 kW_{th}, 5.682 kW_{gas}, installed in 3 of 130 buildings
Air source HP (if no CHP plant is used)	6.7 kW_{el} ($cos(\varphi) = 0.95$), coefficient of performance (COP) between 1.2 and 5.1 depending on air and hot water tank temperature, installed in 127 of 130 buildings
Hot water storage tank	750 L, $\theta_{min/max}$ = 60/80 °C (CHP plant), 40/60 °C (HP), used for both domestic and heating hot water

Table 4.17: Adjustments made to the PV system peak active powers as well as the BESS capacities and (dis)charge powers in comparison to [32].

Values in [32]		Corresponding values in this thesis	
PV power	**BESS capacity, (dis)charge power**	**PV power**	**BESS capacity, (dis)charge power**
4 kW_p	4 kWh, 3.5 kW	6 kW_p	6 kWh, 4.2 kW
5 kW_p	5 kWh, 3.5 kW	7 kW_p	7 kWh, 4.9 kW
6 kW_p	6 kWh, 3.5 kW	8 kW_p	7 kWh, 4.9 kW
7 kW_p	7 kWh, 3.5 kW	10 kW_p	7 kWh, 4.9 kW
8 kW_p	8 kWh, 3.5 kW	10 kW_p	7 kWh, 4.9 kW
10 kW_p	8 kWh, 3.5 kW	15 kW_p	10 kWh, 7 kW
15 kW_p	8 kWh, 3.5 kW	20 kW_p	10 kWh, 7 kW
20 kW_p	10 kWh, 3.5 kW	30 kW_p	10 kWh, 7 kW
30 kW_p	10 kWh, 3.5 kW	30 kW_p	10 kWh, 7 kW

Table 4.18: Adjustments made to the CHP plant, HP, and BEV shares in comparison to [32].

Shares in [32]					Shares in this thesis				
CHP	**HP**	**BEV model [kWh]**			**CHP**	**HP**	**BEV model [kWh]**		
		18.8	**24.2**	**85**			**18.8**	**24.2**	**85**
Rural grid									
27.27 %	72.73 %	0 %	0 %	36.36 %	0 %	100 %	0 %	0 %	100 %
Village grid									
20 %	80 %	3.64 %	10.91 %	27.27 %	1.82 %	98.18 %	0 %	0 %	100 %
Suburban grid									
21.54 %	78.46 %	6.15 %	11.54 %	21.54 %	2.31 %	97.69 %	0 %	0 %	100 %

we only have to curtail the power feed-in of PV systems. The other considered large loads (BEV charging stations, HPs, BESSs) provide sufficient active power flexibility to enable proactive operation scheduling (see also Section 4.5.5) instead of curtailment. To differentiate between electricity outages caused by voltage range violations, transformer overheating, or violations of rated line currents in the evaluation, we not only calculate the *total outage time*, but also outage times and other metrics specifically ascribable to each of these three causes. We thereby answer Sub-Question 1.2 of Research Question

1 and provide another prerequisite for answering Sub-Questions 1.4 and 1.5 of Research Question 1, Sub-Questions 2.1 and 2.2 of Research Question 2, as well as Sub-Question 3.3 of Research Question 3.

We define *outage time* as the percentage of a reference time period, for example, one week or eight days in Section 5.1, in which electricity outages or equipment damage can potentially occur in the considered grid. For the calculation of the four different outage times, we assume that every violation of the admissible voltage range, maximum transformer hot-spot temperature, or rated line currents directly leads to an electricity outage for at least one building connected to the particular grid. For the simulations performed for this thesis, all management intervals in which one or more of these limits are violated anywhere in the grid are added to the total outage time. Strictly speaking, this is not correct. On the one hand, there may be violations, such as a transformer hot-spot temperature of 121 °C, which are not admissible but will most likely not lead to equipment failure or electricity outages immediately. On the other hand, there may likely be situations, in which an electricity outage lasts much longer than its root cause. We consider this for violations of rated line currents during the learning of appropriate apparent power limits for PV curtailment (see also Section 4.5.4). The fuses used to protect lines against overcurrents allow for well-defined short-term and moderate exceedances of rated currents without blowing, which will be concretized later in this section. However, it is neither feasible nor necessary to consider the highly situation-dependent durability of transformers against excessive temperatures and tolerances of electrical end consumer devices against voltage range violations when comparing the general performance of different parameter combinations or grid management strategies and configurations.

For the following equations, we define the componentwise maximum and minimum of an array $\boldsymbol{a} = (a_j)_{j \in J}$, where $J \neq \emptyset$, according to Equations 4.40 and 4.41:

$$\max(\boldsymbol{a}) := \max_{j \in J} a_j \tag{4.40}$$

$$\min(\boldsymbol{a}) := \min_{j \in J} a_j \tag{4.41}$$

The *total outage time* is calculated according to Equations 4.42, 4.43, and 4.44:

$$N^{\mathrm{ref}} = \frac{T^{\mathrm{ref}}}{\Delta t} \tag{4.42}$$

$$T^{\mathrm{out}} = \frac{\sum_{t=1}^{N^{\mathrm{ref}}} w_t}{T^{\mathrm{ref}}} \cdot 100\,\% \tag{4.43}$$

where

$$w_t = \begin{cases} \Delta t, & \text{if } \max(\boldsymbol{u}_t) > 1.1\,\mathrm{pu} \vee \min(\boldsymbol{u}_t) < 0.9\,\mathrm{pu} \vee \max(\boldsymbol{i}_t) > 1 \vee \theta_t > 120\,^{\circ}\mathrm{C}, \\ 0, & \text{otherwise} \end{cases} \tag{4.44}$$

In Equation 4.42, N^{ref} is the total number of management intervals in the reference time period T^{ref} and Δt the management interval duration. In the evaluation in Section 5, T^{ref} always corresponds to the assessed part of the respective simulated time period. In Equation 4.43, T^{out} is the total outage time (as a percentage of T^{ref}). w_t either equals Δt or zero, depending on Equation 4.44. In Equation 4.44, $\boldsymbol{u}_t$ is the array of all normalized GCP voltages in the grid in management interval t. $\boldsymbol{i}_t$ is the array of the magnitudes of all normalized line segment currents in the grid in management interval t. θ_t is the transformer hot-spot temperature in management interval t.

The outage time related to voltage range violations, simply called *voltage outage time* for brevity in the following sections, is calculated according to Equations 4.45 and 4.46:

$$T_{\mathrm{u}}^{\mathrm{out}} = \frac{\sum_{t=1}^{N^{\mathrm{ref}}} x_t}{T^{\mathrm{ref}}} \cdot 100\,\% \tag{4.45}$$

where

$$x_t = \begin{cases} \Delta t, & \text{if } \max\left(\boldsymbol{u}_t\right) > 1.1\,\mathrm{pu} \vee \min\left(\boldsymbol{u}_t\right) < 0.9\,\mathrm{pu}, \\ 0, & \text{otherwise} \end{cases} \tag{4.46}$$

In Equation 4.45, $T_{\mathrm{u}}^{\mathrm{out}}$ is the voltage outage time (as a percentage of T^{ref}). x_t either equals Δt or zero, depending on Equation 4.46. The other variables and parameters are the same as in Equations 4.42, 4.43, and 4.44.

As a severity measure for voltage range deviations occurring with a particular grid management strategy or configuration, we calculate the maximum GCP voltage in the grid during the reference time period. This voltage, simply called maximum GCP voltage in the following sections for brevity, is calculated according to Equation 4.47:

$$u^{\max} = \max_{1 \le t \le N^{\mathrm{ref}}} \max\left(\boldsymbol{u}_t\right) \tag{4.47}$$

In Equation 4.47, $u^{\max}$ is the maximum GCP voltage (given in pu). The other variables and parameters are the same as in Equations 4.42, 4.43, and 4.44. We do not provide an equation for the minimum GCP voltage, as violations of the minimum admissible voltage do not occur in any of the parameter or evaluation studies performed for this thesis.

The outage time related to exceedances of the maximum admissible transformer hot-spot temperature, simply called *transformer outage time* for brevity in the following sections, is calculated according to Equations 4.48 and 4.49:

$$T_{\theta}^{\mathrm{out}} = \frac{\sum_{t=1}^{N^{\mathrm{ref}}} y_t}{T^{\mathrm{ref}}} \cdot 100\,\% \tag{4.48}$$

where

$$y_t = \begin{cases} \Delta t, & \text{if } \theta_t > 120\,^{\circ}\mathrm{C}, \\ 0, & \text{otherwise} \end{cases} \tag{4.49}$$

In Equation 4.48, T_{θ}^{out} is the transformer outage time (as a percentage of T^{ref}). y_t either equals Δt or zero, depending on Equation 4.49. The other variables and parameters are the same as in Equations 4.42, 4.43, and 4.44.

The PV curtailment algorithm to prevent line-related outages (Algorithm 4) permits short-term and moderate exceedances of rated line currents while learning the appropriate apparent power limits for the buildings connected to a particular line. *Niederspannungs-Hochleistungs* (NH, English: low-voltage-high-performance) fuses, which are predominant in Europe, but also widely used in China, India, the Middle East, Australia and Africa [335], allow such exceedances according to the characteristic curves given in [325]. To determine whether the exceedances during apparent power limit learning are unproblematic, we calculate the maximum duration for which the rated current of at least one line segment is exceeded as well as the maximum normalized line current that occurs. After the appropriate apparent power limit is learned, exceedances of rated currents no longer occur, so the fuses are not strained further.

Since we have to consider these caveats when calculating the outage time related to exceedances of rated line currents, we call this value *potential line outage time*. It is calculated according to Equations 4.50 and 4.51:

$$T_{\text{i}}^{\text{out}} = \frac{\sum_{t=1}^{N^{\text{ref}}} z_t}{T^{\text{ref}}} \cdot 100\,\% \tag{4.50}$$

where

$$z_t = \begin{cases} \Delta t, & \text{if } \max\left(\boldsymbol{i}_t\right) > 1, \\ 0, & \text{otherwise} \end{cases} \tag{4.51}$$

In Equation 4.50, $T_{\text{i}}^{\text{out}}$ is the potential line outage time (as a percentage of T^{ref}). z_t either equals Δt or zero, depending on Equation 4.51. The other variables and parameters are the same as in Equations 4.42, 4.43, and 4.44.

The *maximum potential line outage duration* is calculated according to Equation 4.52:

$$D_{\text{i}}^{\text{out}} = \max_{1 \leq t^{\text{sta}} \leq t^{\text{end}} \leq N^{\text{ref}}} \left\{ \sum_{t=t^{\text{sta}}}^{t^{\text{end}}} \Delta t \;\middle|\; \forall t \in \{t^{\text{sta}}, \ldots, t^{\text{end}}\} : \max\left(\boldsymbol{i}_t\right) > 1 \right\} \tag{4.52}$$

In Equation 4.52, $D_{\text{i}}^{\text{out}}$ is the maximum potential line outage duration (given in minutes). t^{sta} and t^{end} are the first and last management intervals of periods during which the rated current of at least one line segment in the grid is exceeded in each management interval. The other variables and parameters are the same as in Equations 4.42, 4.43, and 4.44. If there are no exceedances of rated currents during the reference period, $D_{\text{i}}^{\text{out}}$ is set to zero.

The *maximum normalized line current* is calculated according to Equation 4.53:

$$i^{\max} = \max_{1 \leq t \leq N^{\mathrm{ref}}} \max\left(\boldsymbol{i}_t\right) \tag{4.53}$$

In Equation 4.53, $i^{\max}$ is the maximum normalized line current. The other variables and parameters are the same as in Equations 4.42, 4.43, and 4.44.

Based on the characteristic curves for NH fuses given in [325], we define $D_{\mathrm{i}}^{\mathrm{out}} \leq 4\,\mathrm{min}$ and $i^{\max} \leq 1.4$ as acceptable during the process of learning the appropriate apparent power limits for line disturbances. Note that these criteria are conservative, since $D_{\mathrm{i}}^{\mathrm{out}}$ is calculated grid-wide and not for specific line segments, and $D_{\mathrm{i}}^{\mathrm{out}}$ and $i^{\max}$ might not occur on the same line segment. Although this simplification can overestimate the maximum potential line outage duration in some scenarios, we use it for the following reasons. First, a grid-wide evaluation substantially reduces the amount of data that has to be logged for the extensive parameter and evaluation studies, since only the maximum line segment current in each management interval has to be stored instead of all line segment currents. Second, in the scenarios considered in this thesis, overloads of different lines occur with substantial time intervals in between if PV curtailment is used. If no PV curtailment is used, overloads of additional lines occur only within already ongoing longer overload periods of other lines. This prevents an artificial concatenation of the overload periods of different lines when using a grid-wide evaluation. Third, consecutive but alternating rated current exceedances of different line segments of the same line indicate a continuous critical status of the affected line. A line-segment-specific evaluation would assign these alternating exceedances to different line segments and would therefore not capture the full duration of the line-level disturbance. In the context of this thesis, the considered grids are radial, all line segments have the same rated current, and the line overloads are exclusively caused by the feed-in of PV generation. In these scenarios, the most heavily loaded segments of an affected line are generally the neighboring segments closest to the transformer, because they carry the aggregated feed-in of all downstream PV systems. This means that, even if the rated current is not exceeded on the same line segment in every management interval under the realized load conditions, slightly different but still plausible local load conditions could lead to a continuous rated current exceedance of similar duration on one specific line segment as well. A grid-wide evaluation accounts for this possibility, while a line-segment-specific evaluation does not. For scenarios other than those considered in this thesis, such as non-radial grids, grids with different rated currents per line segment, or consumption-induced line overloads, a line-segment-specific evaluation may be more appropriate to avoid a significant overestimation of the maximum potential line outage duration. Note that the established criteria assume that the employed fuses behave like the ones considered in [325] and have not been subjected to significant overcurrents previously. Already excessively worn fuses or different fuse types may require stricter or allow more relaxed criteria.

Different parameter combinations in the parameter studies as well as grid management strategies and configurations in the evaluation have to be compared with respect to the losses of potentially generatable active energy by PV systems due to PV curtailment as well. Consequently, we calculate the aggregated active energy generated by all PV systems

in the grid during the reference time period, simply called *PV active energy* for brevity in the following sections, according to Equation 4.54:

$$E^{\mathrm{PV}} = \sum_{b \in \mathbf{B}} \sum_{t=1}^{N^{\mathrm{ref}}} \left| P_{b,t}^{\mathrm{PV}} \right| \cdot \Delta t \tag{4.54}$$

In Equation 4.54, E^{PV} is the PV active energy. $P_{b,t}^{\mathrm{PV}}$ is the average active power generated by the PV system of building b in management interval t. We use the magnitude of $P_{b,t}^{\mathrm{PV}}$, since we define generated powers as negative. $\mathbf{B}$ is the set of buildings equipped with PV systems in the grid, which corresponds to all buildings in the grid in the context of this thesis. The other variables and parameters are the same as in Equations 4.42, 4.43, and 4.44. For brevity, we refer to the curtailed portion of the potentially generatable PV active energy as *losses of PV active energy* in the following sections. In Section 5, we express these losses as percentages of the potentially generatable PV active energy.

4.12. Parameter Studies

The grid management strategies and methods described in the previous sections utilize various parameters for which adequate values have to be determined with appropriate parameter studies. These parameter studies are another prerequisite for answering Sub-Questions 1.4 and 1.5 of Research Question 1, Sub-Questions 2.1 and 2.2 of Research Question 2, as well as Sub-Question 3.3 of Research Question 3.

The tested value ranges are based on an initial parameter configuration. This configuration was incrementally established during development and is, depending on the particular parameter, based on technical specifications, estimates, experience, as well as trial and error.

Unless stated otherwise, each test is performed by simulating the first week of July using the updated *the day after tomorrow* scenario and the village grid described in Section 4.10. The village grid in summer experiences the highest load relative to the utilized grid equipment of all scenarios evaluated in Chapter 5. If a parameter value combination performs well for this scenario, it is highly likely that it will perform well in less demanding scenarios. Furthermore, the studies are mostly performed using the distributed strategy, since the used parameters are the same for the distributed and the centralized strategy. Parameters that are only relevant for the decentralized strategy are tested using the decentralized strategy. For each test, five simulations are performed, each using different random seeds for the building behavior and the EA used by each building. While the PV active energy is averaged over the seed-specific results, we always use the maximum of all seed-specific results when it comes to worst-case metrics, such as the maximum occurring transformer hot-spot temperature.

To avoid a combinatorial explosion, we split the parameters into groups, each containing only parameters that are strongly interdependent. The first six tested groups contain parameters related to the VRDT- and reactive-power-based voltage maintenance algorithms (Algorithms 1, 2, and 3) as well as the PV curtailment algorithms for line and transformer disturbances (Algorithms 4 and 5). For each of these groups, we test all parameters in a group in combination with two to five different values per parameter. The number of values tested for a particular parameter depends on the number of parameters in its group and the possibility of reasonable cutbacks. We avoid unreasonable value combinations as well. As an example, we use two different step sizes to decrease the apparent power limit in the PV curtailment algorithms, depending on the previous apparent power limit. It would be unreasonable to test combinations that use an apparent power level for step size switching that is larger than the initial apparent power limit that is used when a line or transformer disturbance first occurs. Each of the first six parameter groups is tested while only the countermeasure it relates to is active. We do this to prevent other countermeasures from influencing the determination of appropriate parameter values for a specific countermeasure. For example, the parameter studies for the group related to the PV curtailment algorithm for line disturbances are performed while only this algorithm is used. Using the PV curtailment algorithm for transformer disturbances at the same time would decrease the load on lines as well, so that line-related outages, which would otherwise occur, would be, at least partially, masked. For the first six parameter groups, we deactivate the energy flow optimization usually performed by each building completely. We do this, because the computation time required for one simulation is mainly determined by the solution times of the EA. In the scenario chosen for the parameter studies, 55 buildings are simulated at the same time, with each performing multiple optimization runs during one simulated day. For parameters related to the provision of active power flexibility, running the optimizations is feasible and necessary. However, parameters unrelated to flexibility have no or negligible dependencies to the building optimization, so that we can avoid the large time expenditure that testing them with active optimization would incur.

We test the group containing parameters related to the VRDT-based voltage maintenance algorithm first. To determine the best parameter value combination, we calculate the voltage outage time according to Equations 4.45 and 4.46 and the maximum occurring GCP voltage according to Equation 4.47. Only a small number of tested parameter combinations prevents all voltage-related outages and we only consider combinations incurring maximum GCP voltages below 1.098 pu further. For these combinations, we calculate the transformer outage time according to Equations 4.48 and 4.49, because calculating the generatable energy lost due to PV curtailment is not possible, since the latter is not active for the tests of this parameter group. We prefer lower transformer outage times when deciding on the final parameter combination for this group, since lower transformer outage time indicates less additional load on the grid introduced by the VRDT. The tested values for each parameter in the group are given in Table 4.19. The best performing parameter value combination with regard to the transformer outage time is indicated by bold font. We use this value combination for the evaluation in Section 5. If a parameter value corresponds to the value in the initial parameter configuration, this is indicated by italic font.

Table 4.19: Results for parameter group 1: Parameters used in the VRDT control algorithm (Algorithm 1). The parameter values of the best performing parameter value combination are indicated by **bold** font. This parameter value combination achieves the lowest transformer outage time, while still preventing all voltage-related outages and corresponds to the parameter value combination used in the evaluation in Section 5. Parameter values also contained in the initial parameter configuration are indicated by *italic* font. Parameter values contained in both the initial as well as the best performing parameter configuration are indicated by ***bold and italic*** font.

Parameter [unit] {value set}	**Description**
T_{V} [min] {*5*, 10, **15**}	Delay before switching to a more neutral transmission ratio
$u_{\mathrm{V}}^{\mathrm{upp}}$ [pu] {***1.07***, 1.08, 1.09}	Upper voltage boundary for VRDT switching (always tied to lower voltage disturbance boundary (symmetry around nominal voltage))
$u_{\mathrm{V}}^{\mathrm{low}}$ [pu] {***0.93***, 0.92, 0.91}	Lower voltage boundary for VRDT switching (always tied to upper voltage disturbance boundary (symmetry around nominal voltage))
$\Delta u_{\mathrm{V}}^{\mathrm{dea}}$ [pu] {*0.03*, 0.04, **0.05**}	Voltage deadband for VRDT-based voltage maintenance
$\Delta u_{\mathrm{V}}^{\mathrm{jum}}$ [pu] {**0.01**, *0.02*, 0.03}	Minimum voltage jump for VRDT-based voltage maintenance
$u_{\mathrm{V}}^{\mathrm{jum,min}}$ [pu] {1.04, *1.05*, **1.06**}	Minimum voltage to consider voltage jumps for VRDT-based voltage maintenance

We conduct the study for the second parameter group, which contains the parameters related to the reactive-power-based voltage maintenance algorithms, in the same manner. See Table 4.20 for the results.

The third tested group contains the parameters related to the PV curtailment algorithm for line disturbances. For this group, we calculate the potential line outage time according to Equations 4.50 and 4.51, the maximum potential line outage duration according to Equation 4.52, and the maximum normalized line current according to Equation 4.53. We only consider parameter combinations with maximum potential line outage durations below five minutes and maximum normalized line currents smaller than or equal to 1.4 further. For these combinations, we calculate the PV active energy according to Equation 4.54 and prefer higher values over lower ones to determine the final parameter combination. We provide the results for this group in Table 4.21.

We test the fourth group, which contains the parameters related to the PV curtailment algorithm for transformer disturbances, next. To evaluate the studies for this group, we consider the maximum occurring transformer hot-spot temperature and calculate the transformer outage time using Equations 4.48 and 4.49. Only parameter combinations that incur no transformer outages with a maximum transformer hot-spot temperature below

Table 4.20: Results for parameter group 2: Parameters used in the reactive-power-based voltage maintenance algorithms (Algorithms 2 and 3). The parameter values of the best performing parameter value combination are indicated by **bold** font. This parameter value combination achieves the lowest transformer outage time, while still preventing all voltage-related outages and corresponds to the parameter value combination used in the evaluation in Section 5. Parameter values also contained in the initial parameter configuration are indicated by *italic* font. Parameter values contained in both the initial as well as the best performing parameter configuration are indicated by ***bold and italic*** font.

Parameter [unit] {value set}	**Description**
$u_{\mathrm{Q}}^{\mathrm{upp}}$ [pu] {**1.075**, *1.08*}	Upper voltage boundary for reactive-power-based voltage maintenance. Always tied to lower voltage disturbance boundary (symmetry around nominal voltage)
$u_{\mathrm{Q}}^{\mathrm{low}}$ [pu] {**0.925**, *0.92*}	Lower voltage boundary for reactive-power-based voltage maintenance. Always tied to upper voltage disturbance boundary (symmetry around nominal voltage)
$\Delta u_{\mathrm{Q}}^{\mathrm{dea}}$ [pu] {*0.005*, **0.01**}	Voltage deadband for reactive-power-based voltage maintenance
T_{Q} [min] {10, 20, ***30***}	Delay for the reduction of reactive power absorption or injection
$\Delta u_{\mathrm{Q}}^{\mathrm{jum}}$ [pu] {**0.01**, *0.02*}	Minimum voltage jump for reactive-power-based voltage maintenance
$u_{\mathrm{Q}}^{\mathrm{jum,min}}$ [pu] {1.03, ***1.04***, 1.05}	Minimum voltage for reactive-power-based voltage maintenance due to voltage jumps
Δq^{lar} [-] {*0.3*, **0.4**}	Normalized reactive power large step
Δq^{sma} [-] {***0.01***, 0.02, 0.03}	Normalized reactive power small step
$q^{\mathrm{lar\|sma}}$ [-] {*0.5*, 0.6, **0.7**}	Normalized reactive power threshold for step size switching

118 °C are considered further. Among these combinations, we chose the one achieving the highest PV active energy as the final combination. The results can be viewed in Table 4.22.

The fifth group contains parameters related to the algorithm for reactive-power-based voltage maintenance specific to the decentralized strategy (Algorithm 3). Since these parameters are unrelated to flexibility use, the general testing procedure is the same as for the first two groups. However, we test ten different values for this parameter, because the time expenditure is low for a single parameter, which allows evaluating a larger range. Since a part of the parameters is shared between the reactive-power-based voltage maintenance algorithms for the different strategies and has already been determined for

Table 4.21: Results for parameter group 3: Parameters used in the PV curtailment algorithm for line disturbances (Algorithm 4). The parameter values of the best performing parameter value combination are indicated by **bold** font. This parameter value combination achieves the highest PV active energy, while still preventing all line-related outages and corresponds to the parameter value combination used in the evaluation in Section 5. Parameter values also contained in the initial parameter configuration are indicated by *italic* font. Parameter values contained in both the initial as well as the best performing parameter configuration are indicated by ***bold and italic*** font.

Parameter [unit] {value set}	**Description**
i_{S} [-] {*0.98*, 0.99, **1.0**}	Normalized line current threshold for PV curtailment
$s_{\mathrm{L}}^{\mathrm{ini}}$ [-] {*0.7*, **0.8**, 0.9}	Initial normalized apparent power limit for line disturbances
$s_{\mathrm{L}}^{\mathrm{lar\|sma}}$ [-] {***0.5***, 0.6}	Normalized apparent power level for step size switching for line disturbances
$\Delta s_{\mathrm{L}}^{\mathrm{lar}}$ [-] {*0.05*, **0.1**}	Normalized apparent power large step for line disturbances
$\Delta s_{\mathrm{L}}^{\mathrm{sma}}$ [-] {**0.01**, *0.02*}	Normalized apparent power small step for line disturbances

the second group, these parameters are set to their previously determined final values before testing. For the results, see Table 4.23.

The sixth group is specific to the decentralized strategy as well and contains only one parameter, the normalized apparent power offset for the learned normalized apparent power limit for transformer disturbances. The procedure is the same as for the parameter groups containing parameters related to the PV curtailment algorithms. However, for the same reasons as for the fifth group, we test ten different values for this parameter. The results are given in Table 4.24.

After the test series for the first six parameter groups are finished, the parameters in these groups are set to their respective best values, while the other parameters remain at their values from the initial parameter configuration. We then test this partially updated parameter configuration for all grid management configurations and strategies tested in the evaluation in Chapter 5 with the rural and village grid in the summer time period. To decrease the time expenditure for these tests, we only use one generation and a population size of one for the EA, which essentially equates to random building behavior with regard to active power flexibility use. If outages occur in this test series, the management, strategy, and grid configuration for which the outages occur is tested again, but with the second best parameter value combination for the parameter group associated with the particular problem. An example would be a voltage range violation occurring when both PV curtailment and reactive-power-based voltage maintenance are used at the same time, despite using the best previously determined parameter value combination for group 2. In

Table 4.22: Results for parameter group 4: Parameters used in the PV curtailment algorithm for transformer disturbances (Algorithm 5). The parameter values of the best performing parameter value combination are indicated by **bold** font. This parameter value combination achieves the highest PV active energy, while still preventing all transformer-related outages and corresponds to the parameter value combination used in the evaluation in Section 5. Parameter values also contained in the initial parameter configuration are indicated by *italic* font. Parameter values contained in both the initial as well as the best performing parameter configuration are indicated by ***bold and italic*** font.

Parameter [unit] {value set}	**Description**
θ^{upp} [°C] {*110*, 112, **114**}	Upper transformer hot-spot temperature for PV curtailment
θ^{mid} [°C] {θ^{upp}−**7**, θ^{upp}−*5*, θ^{upp}−3}	Mid transformer hot-spot temperature for PV curtailment. For the parameter studies, this parameter is loosely tied to the upper transformer hot-spot temperature threshold for PV curtailment and always 3, 5, or 7 °C below the latter
θ^{low} [°C] {θ^{mid}−**7**, θ^{mid}−*5*, θ^{mid}−3}	Lower transformer hot-spot temperature for PV curtailment. For the parameter studies, this parameter is loosely tied to the mid transformer hot-spot temperature threshold for PV curtailment and always 3, 5, or 7 °C below the latter
$s_{\text{T}}^{\text{ini}}$ [-] {***0.7***, 0.8, 0.9}	Initial normalized apparent power limit for transformer disturbances
$s_{\text{T}}^{\text{lar\|sma}}$ [-] {***0.5***, 0.6}	Normalized apparent power level for step size switching for transformer disturbances
$\Delta s_{\text{T}}^{\text{lar}}$ [-] {***0.15***, 0.2}	Normalized apparent power large step for transformer disturbances
$\Delta s_{\text{T}}^{\text{sma}}$ [-] {**0.01**, *0.02*}	Normalized apparent power small step for transformer disturbances

Table 4.23: Results for parameter group 5: Parameter used in the algorithm for reactive-power-based voltage maintenance specific to the decentralized strategy (Algorithm 3). The best performing parameter value is indicated by **bold** font. This parameter value achieves the lowest transformer outage time, while still preventing all voltage-related outages and corresponds to the parameter value used in the evaluation in Section 5. The parameter value in the initial parameter configuration is indicated by *italic* font.

Parameter [unit] {value set}	**Description**
$\Delta u_{\text{Q}}^{\text{coe}}$ [pu] {0.02, 0.025, **0.03**, 0.035, 0.04, 0.045, 0.05, *0.055*, 0.06, 0.065}	Voltage coefficient used in the position-based voltage disturbance criteria for the decentralized strategy

Table 4.24: Results for parameter group 6: Parameter used as an offset for the learned normalized apparent power limit for transformer disturbances (Algorithm 5). The best performing parameter value is indicated by **bold** font. This parameter value achieves the highest PV active energy, while still preventing all transformer-related outages and corresponds to the parameter value used in the evaluation in Section 5. The parameter value in the initial parameter configuration is indicated by *italic* font.

Parameter [unit] {value set}	**Description**
$\Delta s_{\mathrm{T}}^{\mathrm{off}}$ [-] {*0.0*, 0.01, 0.02, 0.03, 0.04, **0.05**, 0.06, 0.07, 0.08, 0.1}	Normalized apparent power offset for the learned normalized apparent power limit for transformer disturbances

this case, the problematic test series is repeated with the second best value combination for group 2. If the second best value combination of a parameter group associated with a particular problem still leads to problems in the retest, this process is repeated with the respective next best value combinations until the problems do not occur anymore. The best and final value combinations indicated by bold font in the tables in this section are the best combinations that do not incur outages in any test series.

The seventh group of tested parameters contains parameters related to grid-supportive active power flexibility use (see also Section 4.5.5). For the studies concerning this group, we activate the building energy flow optimization and use the same maximum number of generations per optimization run for the EA as in the evaluation in Chapter 5. This is necessary to minimize the influence of insufficient EA accuracy on active power flexibility use. To make testing the flexibility-related parameters with full EA accuracy feasible, we test the parameters in this group individually. Testing them in combination would lead to extreme time expenditure and we assume these parameters to not be as closely interdependent as the ones in the other parameter groups. However, two of the parameters in this group are closely related to an ancillary parameter respectively. These parameters are tested in combination with their ancillary parameters. We restrict the value range of the ancillary parameters to two values each to make these studies feasible. In contrast to the tests performed for the parameters unrelated to active power flexibility, we enable all countermeasures to electrical disturbances for the studies performed for this group. The main use case for active power flexibility in our grid management system is the reduction of the losses of generatable energy caused by PV curtailment. For one, appropriate flexibility use reduces the active power transmitted via the grid. Furthermore, active power flexibility use lessens the need for reactive-power-based voltage maintenance to keep voltages under control, which reduces the reactive power that lines and the transformer have to carry as well. Both of these effects lessen the need for PV curtailment. To effectively evaluate how well a specific flexibility-related parameter contributes to these effects, the corresponding countermeasures have to be active. The parameters related to the other countermeasures are set to their previously determined final values. When testing a specific parameter from the group, the values for the other flexibility-related parameters are set to their values from the initial parameter configuration. We determine the best value for each parameter according to the PV active energy, preferring higher values. We provide the results in

Table 4.25. When problems related to other parameter groups occur during the test series for group 7, we use a similar process as for the intermediate tests after the tests for groups 1 to 6. The most problematic combination of flexibility-related parameters is repeatedly tested using the next best parameter combinations for the group the problem relates to, until the problems are resolved. For these tests, we use the full accuracy for the EA as well, so that the occurring problems can be reproduced.

Table 4.25: Parameter group 7: Parameters related to grid-supportive active power flexibility use (Algorithms 6 and 7). The best performing parameter values are indicated by **bold** font. These parameter values achieve the highest PV active energy and correspond to the parameter values used in the evaluation in Section 5. Parameter values also contained in the initial parameter configuration are indicated by *italic* font. Parameter values contained in both the initial as well as the best performing parameter configuration are indicated by ***bold and italic*** font.

Parameter [unit] {value set}	**Description**
T^{opt} [min] {120, 240, *360*, 480, **600**}	Active power target optimization horizon
T^{cal} [min] {5, **10**, *15*, 20, 25}	Delay between flexibility calculations
i_{P} [-] {0.5, 0.6, **0.7**, *0.8*, 0.9}	Normalized line current threshold for active power flexibility
Δi^{dea} [-] {0.05, ***0.1***}	Normalized line current deadband for flexibility
k_{P} [-] {0.6, ***0.7***, 0.8, 0.9, 1.0}	Transformer load factor threshold for active power flexibility
$\Delta k_{\mathrm{P}}^{\mathrm{dea}}$ [-] {**0.05**, *0.1*}	Transformer load factor deadband for active power flexibility
T^{unc} [min] {**5**, *30*, 60, 90, 120}	Minimum uncritical duration for active power flexibility deactivation
g [-] {*0.1*, 0.2, 0.3, **0.4**, 0.5}	Building group size for active power flexibility (fraction of total number of grid nodes)

After the process for group 7 is finished, we repeat the same test series as after the first six groups with the updated parameter configuration. If any outages occur, the parameter configuration is updated again until all problems are resolved. The latter was possible in all cases.

The eighth and last group contains parameters related to active power flexibility use specific to the decentralized strategy. Since the same conditions apply as for the tests of the flexibility-related parameters in group 7, the general procedure is the same as for those parameters. However, here we test the parameters in combination, as they are all too closely related to be tested individually. To keep the time expenditure manageable despite using full evolution algorithm accuracy, we reduce the number of tested values

per parameter to two. While this represents a relatively small number of different tested values, the range of sensible values for the parameters in this group is very limited already. Since the parameters are used to indicate the necessity of active power flexibility use against potential transformer- or line-related disturbances, without available data on the actual load on this equipment, they have to be set very conservatively. This means that the values have to be chosen such that the resulting voltage at which a building decides to use active power flexibility is neither too low nor too high. The voltage must be higher than the nominal voltage (1.0 pu). Otherwise, the buildings would almost always use active power flexibility in the decentralized strategy, which is unnecessary and substantially restricts the freedom of the buildings to use their flexibility for other purposes, such as energy cost reduction. The voltage must also be lower than the upper voltage boundary for reactive-power-based voltage maintenance (1.075 pu). Otherwise, reactive-power-based voltage maintenance would be activated, consequently decreasing the voltage again, before active power flexibility use could ever be activated. Furthermore, the values of $\Delta u^{\mathrm{off,Q}}$ and $\Delta u_{\mathrm{P}}^{\mathrm{coe,Q}}$ have to be equal to or lower than the values of Δu^{off} and $\Delta u_{\mathrm{P}}^{\mathrm{coe}}$, respectively, as activated reactive-power-based voltage maintenance decreases the general voltage level, potentially masking the necessity for active power flexibility use. $\Delta u_{\mathrm{P}}^{\mathrm{dea}}$ has to have an even smaller value to ensure that active power flexibility use is deactivated in a timely manner when it is not needed anymore. We are therefore confident that the relatively low number of tested parameter values is sufficient for this particular parameter group. We show the results for group 8 in Table 4.26.

The final test series is the evaluation of the grid management system shown in Chapter 5 itself. If problems such as voltage range deviations occur during the test series performed for the evaluation, the parameter value combination for the parameter group associated with the particular problem is updated using the previously described method as well.

4.13. Summary

After a brief explanation of the typographic conventions and time scales used in this thesis, we provided a resilience definition for smart electricity distribution grids based on the existing definitions from the literature presented in the previous chapter. Subsequently, we introduced the centralized, distributed, and decentralized grid management strategies our adaptive grid management system can use to adapt its operation in the case of ICT disturbances entailing communication disruption, participant misconduct, or sensor failure. We then presented the criteria we use to decide on countermeasures in response to electrical disturbances, namely voltage-, line-, and transformer-related disturbances. Afterwards, we detailed the corresponding countermeasures themselves. These countermeasures encompass voltage maintenance, either using a voltage regulated distribution transformer or the reactive power provided by the photovoltaic (PV) inverters present in residential buildings, as well as reactive power compensation, adaptive PV curtailment, and active power flexibility use in response to impending line or transformer congestion. Following that, we described the way in which our grid management system adapts its strategies in

Table 4.26: Parameter group 8: Parameters related to grid-supportive active power flexibility use specific to the decentralized strategy (Algorithm 7). The parameter values of the best performing parameter value combination are indicated by **bold** font. This parameter value combination achieves the highest PV active energy and corresponds to the parameter value combination used in the evaluation in Section 5. Parameter values also contained in the initial parameter configuration are indicated by *italic* font. Parameter values contained in both the initial as well as the best performing parameter configuration are indicated by ***bold and italic*** font.

Parameter [unit] {value set}	**Description**
$\Delta u^{\mathrm{off,Q}}$ [pu] {0.005, ***0.01***}	Voltage offset used in the voltage- and position-based transformer/line disturbance criteria for the decentralized strategy if reactive-power-based voltage maintenance is currently active
Δu^{off} [pu] {***0.01***, 0.015}	Voltage offset used in the voltage- and position-based transformer/line disturbance criteria for the decentralized strategy if reactive-power-based voltage maintenance is currently inactive
$\Delta u_{\mathrm{P}}^{\mathrm{coe,Q}}$ [pu] {**0.02**, *0.03*}	Voltage coefficient used in the voltage- and position-based transformer/line disturbance criteria for the decentralized strategy if reactive-power-based voltage maintenance is currently active
$\Delta u_{\mathrm{P}}^{\mathrm{coe}}$ [pu] {**0.03**, *0.04*}	Voltage coefficient used in the voltage- and position-based transformer/line disturbance criteria for the decentralized strategy if reactive-power-based voltage maintenance is currently inactive
$\Delta u_{\mathrm{P}}^{\mathrm{dea}}$ [pu] {*0.005*, **0.01**}	Voltage deadband for active power flexibility

response to communication disruption, participant misconduct, or sensor failure. We then detailed the concrete implementation and architecture of the developed system with the *Organic Smart Home* building energy management system (BEMS) as a foundation. After briefly discussing the transferability of the developed grid management system to other BEMSs and presenting an interactive demonstrator developed in the context of this thesis, we presented the scenarios and metrics used to evaluate the grid management system in the following chapter. We concluded the chapter by detailing the parameter studies we performed to approximately maximize the performance of the system and substantiate our choices of parameter values.

5. Evaluation and Discussion

In this chapter, we present and discuss our evaluation results. The chapter starts with a comparative evaluation of the three grid management strategies available to the adaptive grid management system and an array of different grid management configurations. We compare the strategies and configurations with respect to their ability to prevent electricity outages and equipment damage as well as the resulting losses of potentially generatable active energy from photovoltaic (PV) systems due to curtailment. For brevity, the latter will be referred to as *losses of PV active energy* in this chapter. All strategies and configurations are evaluated for three different distribution grids and three seasons, covering a wide range of possible scenarios. Subsequently, we evaluate the ability of the system to adapt to communication disruption and participant misconduct, which implicitly covers sensor failure as well. We evaluate different scenarios to isolate the responses of the system to different types of problems that can be introduced by the dependence of a smart electricity distribution grid on information and communication technology (ICT) infrastructure. The chapter concludes with a summary of the evaluations results.

5.1. Comparative Evaluation of Grid Management Strategies and Configurations

The developed grid management system is evaluated using the simulation environment established in Section 4.10. We use the evaluation metrics introduced in Section 4.11 to compare the performance of different grid management strategies and configurations. We thereby answer Sub-Questions 1.4 and 1.5 of Research Question 1 as well as Sub-Questions 2.1 and 2.2 of Research Question 2. Is it important to note that the centralized and distributed grid management strategies yield identical results in the absence of ICT disturbances. Since the comparative evaluation presented in this section assumes undisturbed ICT infrastructure, the corresponding evaluation results are given under the joint descriptor *centralized or distributed* throughout this section.

5.1.1. Village Grid

In the following, the simulation results for the village grid (see also Section 4.10) are shown for exemplary time periods in summer, the intermediate seasons, and winter. Due to time constraints imposed by the operator of the server cluster used to perform the

simulations, the respective simulated time frame is limited to eight days. For the analyses of voltage-, line-, and transformer-related disturbances or electricity outages, the results for the full eight-day time period are utilized. This is done to show the influence of the learning process of the apparent power limits by the PV curtailment algorithms on potential electrical disturbances or electricity outages. For the performance evaluation with regard to the total outage times as well as the losses of PV active energy if applicable, only the last seven days are used. This is done to provide more realistic initial states of charge (SoCs) for the battery electric vehicles (BEVs) and the battery energy storage systems (BESSs), as the initial SoCs for the eight-day period are 100 % for all BEVs and 0 % for all BESSs.

5.1.1.1. Summer

The voltage-related results for the eight-day time period from June 30 to July 7 are given in Table 5.1.

Table 5.1: Outage times due to violations of the admissible voltage range at one or more grid connection points (GCPs) in the grid and maximum GCP voltages for all grid management strategies and selected management configurations. The simulated time period is the last day of June and the first week of July. The simulations use the village grid introduced in [162] and [32] and modified in Section 4.10. None = no grid management, * = no energy cost optimization, Conv. = static $\cos(\varphi)$ and 70 % PV curtailment, Q = reactive-power-based voltage maintenance, P_1 = active power flexibility use through active power targets, c = reactive power compensation, V = voltage-regulated-distribution-transformer-based (VRDT-based) voltage maintenance.

Management configuration	**Management strategy**			
	Centralized or distributed		**Decentralized**	
	Voltages outside of admissible range (±10 %)			
	Voltage outage time	**Maximum GCP voltage**	**Voltage outage time**	**Maximum GCP voltage**
None*	14.83 %	1.1354 pu	14.83 %	1.1354 pu
None	12.84 %	1.1339 pu	12.84 %	1.1339 pu
Conv.	0.0 %	1.0791 pu	0.0 %	1.0791 pu
Q*	0.0 %	1.0978 pu	0.0 %	1.0977 pu
Q	0.0 %	1.0988 pu	0.0 %	1.0965 pu
P_1c	9.98 %	1.1307 pu	10.23 %	1.1359 pu
V*	0.0 %	1.0968 pu	VRDT unsupported	
V	0.0 %	1.0938 pu	VRDT unsupported	

The results in Table 5.1 indicate that the optimization with regard to energy costs (**None**) already significantly reduces the voltage outage time compared to a configuration without any optimization of the energy flows inside the buildings (**None***). This can be explained

by the default behavior of the building energy management system (BEMS) if no optimization is used. BESSs are fully charged as soon as the PV systems generate active power. Regardless of the current PV generation, BEVs are always charged at the maximum charge powers the respective charging stations support as soon as they are plugged in. Heat pumps are only run when the lower temperature limits of the hot water storage tanks are reached. Similarly, household appliances are started immediately after they are programmed. In contrast, when the device schedules are optimized with regard to energy costs, the predicted PV generation profiles are considered, since it is cheaper to use locally generated active power rather than drawing active power from the grid. This reduces the amount of active energy drawn from and fed into the grid, which consequently reduces the voltage outage time. However, the 1.99 percentage point improvement resulting from the optimization of energy costs is by far not sufficient to prevent all voltage-related outages in this scenario.

The optimization with regard to active power targets ($\mathbf{P_1}$, see also Section 4.5.5), combined with the use of reactive power compensation (**c**, see also Section 4.5.2), further reduces the voltage outage time by a more substantial 2.86 percentage points. This is mainly achieved by the optimization to an active power target of 0 W and a preferably flat load profile for the duration of the active power target optimization horizon as well as the incentives to discharge the BESSs again after the optimization horizon is over. However, this is still not sufficient to prevent all voltage-related outages in this scenario. It should be noted that the active power targets are not explicitly used to prevent voltage-related outages, but to prevent transformer- and line-related outages. The decrease in voltage-related outages is just a side effect of the resulting lower and flatter active power feed-in profiles.

Only the use of reactive power (**Q**, see also Section 4.5.3) or a VRDT (**V**, see also Section 4.5.1) for voltage maintenance can reliably keep the voltages inside the admissible range for all GCPs in the grid. This means that the voltage maintenance algorithms presented in Section 4.5, with the parameterizations determined in Section 4.12, work well, even in a high load scenario, such as the one shown here. The results for the decentralized strategy are very similar to the results for the centralized and distributed strategies. This indicates that voltage-related outages can be effectively prevented even during ICT disturbances if the grid management strategy adaptation (see also Section 4.6) works as intended.

The conventional management configuration (**Conv.**) statically curtails the active powers of all PV systems to 70 % of their respective peak active powers, while the PV inverters absorb reactive power at a fixed $\cos(\varphi)$. This strategy prevents all voltage-related outages as well and lowers the maximum GCP voltage occurring during the simulated time period. However, it entails significant disadvantages with regard to the other types of electrical disturbance, which are detailed in the following.

Table 5.2 contains the transformer-related results for the same time period.

The results in Table 5.2 show that the optimization of energy costs by itself leads to a 2.52 percentage point reduction in the transformer outage time and a 12.12 °C reduction in the maximum transformer hot-spot temperature. The reasons for this are the same as for voltage-related disturbances.

Table 5.2: Outage times due to violations of the maximum admissible transformer hot-spot temperature and maximum transformer hot-spot temperatures for all grid management strategies and selected management configurations. The simulated time period is the last day of June and the first week of July. The simulations use the village grid introduced in [162] and [32] and modified in Section 4.10. None = no grid management, * = no energy cost optimization, Conv. = static cos(φ) and 70 % PV curtailment, Q = reactive-power-based voltage maintenance, P_1 = active power flexibility use through active power targets, c = reactive power compensation, C = adaptive PV curtailment, V = VRDT-based voltage maintenance.

Management configuration	**Management strategy**			
	Centralized or distributed		**Decentralized**	
	Admissible transformer hot-spot temperature (120 °C) exceeded			
	Transformer outage time	**Maximum temperature**	**Transformer outage time**	**Maximum temperature**
None*	21.79 %	233.57 °C	21.79 %	233.57 °C
None	19.27 %	221.45 °C	19.27 %	221.45 °C
Conv.	24.69 %	234.8 °C	24.69 %	234.8 °C
Q*	26.89 %	267.8 °C	27.18 %	268.9 °C
Q	25.14 %	252.45 °C	25.38 %	255.38 °C
c	19.22 %	221.21 °C	19.22 %	221.21 °C
P_1c	17.59 %	206.48 °C	17.58 %	205.96 °C
QC*	0.0 %	115.49 °C	0.0 %	114.86 °C
QC	0.0 %	115.19 °C	0.0 %	112.83 °C
V*	24.38 %	260.28 °C	VRDT unsupported	
V	21.44 %	242.79 °C	VRDT unsupported	
VC*	0.0 %	114.86 °C	VRDT unsupported	
VC	0.0 %	117.71 °C	VRDT unsupported	

The use of the conventional management configuration increases the transformer outage time instead of reducing it. The additional reactive power absorbed by the PV systems, although it reduces the voltages, puts more load on the transformer, which leads to higher heat generation. Without further measures to reduce the load on the transformer, the same can be observed when applying the reactive-power- or VRDT-based voltage maintenance algorithms developed in this thesis. The load on the transformer and the resulting outage time are increased more when reactive power is used instead of a VRDT, since the additional reactive power generally increases the current on the transformer windings more significantly than running a VRDT with a higher transmission ratio than the default. The reason for the lower increase in transformer outage time with the conventional management configuration compared to the exclusive use of the reactive-power-based voltage maintenance algorithm is the additional static PV curtailment the conventional management configuration employs. Without this, the transformer outage time would be higher than with the reactive-power-based voltage maintenance algorithm, since the

latter uses reactive power only when it is necessary and only as much as is needed to keep the voltages inside the admissible range.

Compared to a standalone optimization of energy costs, additionally applying reactive power compensation only very slightly reduces transformer-related outages. At least in this scenario, the fraction of the load on the transformer caused by reactive power absorption or injection of devices other than PV inverters can thus be assumed to be almost irrelevant compared to the load fraction related to the active power generation by PV systems.

The optimization with regard to active power targets in combination with reactive power compensation reduces the transformer outage time and the maximum transformer hot-spot temperature by a more significant 1.68 percentage points and 14.97 °C respectively compared to the exclusive energy cost optimization. However, the still substantial remaining outage time emphasizes the need for additional measures.

When adaptive PV curtailment (**C**, see also Section 4.5.4) is used, the transformer outage time reduces to 0 % and the transformer hot-spot temperature stays below 120 °C at all times. This is the case for any management configuration using adaptive PV curtailment, regardless of whether reactive power, a VRDT, no optimization at all, or energy cost optimization is used. This indicates that the PV curtailment algorithm for transformer disturbances (Algorithm 5) and its parameterization determined in Section 4.12 work as intended. However, the curtailment entails losses of generatable energy, which will be further considered in the analysis of the aggregated evaluation results later in this section.

As with voltage-related disturbances, the results for transformer-related disturbances are very similar for the centralized, distributed, and decentralized strategies. This indicates that the transformer hot-spot temperature can be reliably kept below the maximum admissible temperature even when ICT disturbances occur, assuming the buildings switch to the decentralized strategy in a timely fashion.

Table 5.3 shows the line-related results for the previously established time period.

The results in Table 5.3 show similar qualitative effects as the transformer-related results. The potential line outage time and the maximum potential line outage duration are already reduced by employing standalone energy cost optimization instead of no optimization at all. The conventional management configuration as well as the standalone deployment of voltage maintenance, either via reactive power or via a VRDT, increase the potential line outage time, since they increase the currents on lines.

Reactive power compensation can only decrease the potential line outage time slightly, while the addition of active power flexibility use reduces it more substantially.

Only adaptive PV curtailment can reduce the maximum potential line outage duration and the maximum normalized line current below five minutes and 1.4 respectively. These results are sufficient to prevent the blowing of employed fuses under the assumptions made in Section 4.11 and thus line-related outages as well. This shows that Algorithm 4 and its parameterization determined in Section 4.12 perform as intended.

Table 5.3: Potential outage times due to violations of the rated line current of one or more lines in the grid and maximum potential line outage durations for all grid management strategies and selected management configurations. The simulated time period is the last day of June and the first week of July. The simulations use the village grid introduced in [162] and [32] and modified in Section 4.10. None = no grid management, * = no energy cost optimization, Conv. = static cos(φ) and 70 % PV curtailment, Q = reactive-power-based voltage maintenance, P_1 = active power flexibility use through active power targets, c = reactive power compensation, C = adaptive PV curtailment, V = VRDT-based voltage maintenance.

Man. config.	**Management strategy**					
	Centralized or distributed			**Decentralized**		
	Rated current of one or more lines exceeded					
	Potential line outage time	**Max. pot. line outage duration**	**Maximum normalized line current**	**Potential line outage time**	**Max. pot. line outage duration**	**Maximum normalized line current**
None*	16.11 %	293 min	1.4	16.11 %	293 min	1.4
None	14.18 %	274 min	1.38	14.18 %	274 min	1.38
Conv.	18.34 %	322 min	1.34	18.34 %	322 min	1.34
Q*	21.76 %	471 min	1.66	22.05 %	483 min	1.65
Q	20.34 %	453 min	1.62	20.47 %	460 min	1.62
c	14.16 %	273 min	1.38	14.16 %	273 min	1.38
P_1c	11.96 %	172 min	1.4	12.19 %	174 min	1.4
QC*	0.05 %	3 min	1.24	0.0 %	0 min	0.74
QC	0.05 %	4 min	1.14	0.0 %	0 min	0.77
V*	17.41 %	301 min	1.52			VRDT unsupported
V	15.47 %	282 min	1.49			VRDT unsupported
VC*	0.05 %	3 min	1.38			VRDT unsupported
VC	0.05 %	3 min	1.39			VRDT unsupported

The results for the decentralized strategy deviate from the results for the centralized and distributed strategies if PV curtailment is used. The decentralized strategy uses fixed apparent power limits, which are learned during the prior use of the centralized or distributed strategies (see also Section 4.5.4). The lowest learned limits applicable for each building are continuously upheld by the respective buildings until the centralized or distributed strategies are usable again. In this scenario, the learned apparent power limits for transformer disturbances are substantially lower than the respective learned apparent power limits for line disturbances. As a consequence, the maximum occurring currents are substantially lower when using PV curtailment in the decentralized strategy. This leads to a greater loss of generatable energy as well, which is further discussed in the following.

The total outage times, which contain voltage-, transformer-, and line-related outages, as well as the PV active energies and corresponding losses for all simulated management configurations and strategies are given in Table 5.4.

Table 5.4: Total outage times and PV active energies for all grid management strategies and selected management configurations. The simulated time period is the first week of July. The simulations use the village grid introduced in [162] and [32] and modified in Section 4.10. None = no grid management, * = no energy cost optimization, Conv. = fixed cos(φ) and static 70 % PV curtailment, Q = reactive-power-based voltage maintenance, P_1 = active power flexibility use through active power targets, P_2 = curtailment based active power flexibility, c = reactive power compensation, C = adaptive PV curtailment, perf. = perfect PV generation prediction, V = VRDT-based voltage maintenance.

Man. config.	**Management strategy**			
	Centralized or distributed		**Decentralized**	
	Total outage time and PV active energy (loss)			
	Total outage time	**PV active energy (loss)**	**Total outage time**	**PV active energy (loss)**
None*	25.12 %	41.8 MWh (0.0 %)	25.12 %	41.8 MWh (0.0 %)
None	22.47 %	41.8 MWh (0.0 %)	22.47 %	41.8 MWh (0.0 %)
Conv.	27.52 %	40.2 MWh (-3.83 %)	27.52 %	40.2 MWh (-3.83 %)
Q*	29.36 %	41.8 MWh (0.0 %)	29.77 %	41.8 MWh (0.0 %)
Q	27.31 %	41.8 MWh (0.0 %)	27.64 %	41.8 MWh (0.0 %)
c	22.44 %	41.8 MWh (0.0 %)	22.44 %	41.8 MWh (0.0 %)
P_1c	21.01 %	41.8 MWh (0.0 %)	21.07 %	41.8 MWh (0.0 %)
QC*	0.0 %	31.89 MWh (-23.71 %)	0.0 %	30.63 MWh (-26.72 %)
QC	0.0 %	33.28 MWh (-20.38 %)	0.0 %	31.82 MWh (-23.87 %)
QP_1c	0.0 %	35.01 MWh (-16.24 %)	0.0 %	33.48 MWh (-19.9 %)
QP_1c-p	0.0 %	35.2 MWh (-15.79 %)	0.0 %	33.9 MWh (-18.9 %)
QP_2c	0.0 %	34.67 MWh (-17.06 %)	0.0 %	33.3 MWh (-20.33 %)
QP_2c-p	0.0 %	35.14 MWh (-15.92 %)	0.0 %	34.02 MWh (-18.6 %)
V*	26.89 %	41.8 MWh (0.0 %)		VRDT unsupported
V	24.06 %	41.8 MWh (0.0 %)		VRDT unsupported
VC*	0.0 %	32.14 MWh (-23.1 %)		VRDT unsupported
VC	0.0 %	33.54 MWh (-19.76 %)		VRDT unsupported
VP_1c	0.0 %	35.26 MWh (-15.64 %)		VRDT unsupported
VP_1c-p	0.0 %	35.42 MWh (-15.27 %)		VRDT unsupported
VP_2c	0.0 %	35.14 MWh (-15.92 %)		VRDT unsupported
VP_2c-p	0.0 %	35.4 MWh (-15.3 %)		VRDT unsupported

As expected, Table 5.4 shows that only management configurations using both voltage maintenance as well as adaptive PV curtailment can reliably prevent all occurring outages during the simulated time period. In this scenario, these management configurations always entail some losses of PV active energy, which vary depending on the specific countermeasures to electrical disturbances used in the particular management configuration. However, it should be noted that other management configurations would entail more substantial losses in reality, since the occurring outages would fully prevent the feed-in of

PV-generated active energy until the grid is physically strengthened or a different solution is found.

Although the use of the conventional management configuration entails energy losses due to the employed static PV curtailment, it still increases the total outage time instead of reducing it. This is due to the intensive use of reactive power for voltage maintenance, which, while it keeps voltages in the admissible range, can congest lines as well as the transformer. No countermeasures to disturbances and no optimization at all already lead to a 2.4 percentage point lower total outage time than the conventional management configuration, as this does not put additional stress on the grid through increased reactive power use. The optimization of energy costs achieves a further reduction by 2.65 percentage points, due to the reasons stated previously in this section. The optimization with regard to active power targets further reduces the total outage time by 1.46 percentage points. This indicates that in less extreme load and grid scenarios, the optimization with regard to active power targets may be able to prevent all outages even without additional countermeasures such as PV curtailment.

Although the reactive power algorithms for voltage maintenance introduced in Section 4.5.3 use reactive power more cautiously than the conventional management configuration, they still lead to higher outage times, as the conventional management configuration also employs PV curtailment. However, if a VRDT can be used for voltage maintenance, the total outage time decreases significantly, as the currents on lines and the transformer windings are reduced compared to reactive-power-based voltage maintenance.

There are significant differences in the losses of PV active energy among the management configurations that use the PV curtailment algorithms introduced in Section 4.5.4. The exclusive use of reactive power for voltage maintenance and PV curtailment against line and transformer congestion leads to a relatively high energy loss of 23.71 %. The additional optimization of energy costs can already reduce this loss by 3.33 percentage points. The reasons for this are the same as for the reduction in total outage time resulting from the energy cost optimization, when no PV curtailment is used. The optimization with regard to active power targets further reduces the energy loss by a substantial 4.14 percentage points. The standard PV generation prediction method utilized by the *Organic Smart Home* (OSH) calculates predicted generation profiles by averaging the generation profiles of the preceding 14 days. Even a perfect PV generation prediction (**...-p**), where the predicted PV power generation profile is the same as the following actual PV power generation profile, can only reduce the energy loss by an additional 0.45 percentage points. This indicates that the optimization with regard to active power targets is relatively robust with regard to uncertainty in predicting the future PV generation. This is different for the second active power flexibility use method ($\mathbf{P}_2$) introduced in Section 4.5.5, in which no active power targets are used, but the apparent power limit for PV curtailment is considered during the energy cost optimization. With the standard PV generation prediction method, the second active power flexibility use method entails a 0.82 percentage point higher energy loss than the optimization to active power targets. If perfect PV generation prediction is simulated, the two methods perform significantly more similar with a 0.13 percentage point difference. This indicates that the second active power flexibility use method needs a

more accurate PV generation prediction than the first method to approach the optimal use of available flexibility. Using VRDT- instead of reactive-power-based voltage maintenance reduces the losses of PV active energy further, as the former entails less additional load on the grid that has to be mitigated by PV curtailment.

In contrast to most of the results shown in the previous tables, here, the decentralized strategy shows a somewhat different behavior than the centralized and distributed strategies. The general PV active energy loss level when using the decentralized strategy is higher for all management configurations using PV curtailment due to the constant application of the lowest, previously learned apparent power limits. The centralized and distributed strategies have more leeway when it comes to setting apparent power limits. When using these strategies, only the learned apparent power limit for line disturbances is kept indefinitely, while the apparent power limit for transformer disturbances is dynamically adjusted depending on the temperature of the transformer, which is unknown when using the decentralized strategy.

Another difference between the decentralized strategy and the centralized and distributed strategies can be observed with regard to the active power flexibility use methods. The two different methods perform significantly more similar to each other in the decentralized strategy. When using perfect PV generation prediction, the second method even performs slightly better than the first one, which is the opposite of what can be observed in the centralized and distributed strategies. This may be explained by the uncertainty introduced by the voltage- and position-based transformer and line disturbance criteria utilized in the decentralized strategy (see also Section 4.4), which can only provide an indirect approximation of the current grid status based on the locally measured voltage. Unlike the first active power flexibility use method, the second method does not use these criteria. This means that it can perform better in certain situations if the quality of the PV generation predictions is sufficiently high.

To visualize the evaluation results for this scenario, Figure 5.1 shows the profiles of the previously analyzed aspects for an exemplary day of the summer time period. July 1 is chosen for this scenario because it exhibits the highest amount of active energy potentially generatable by PV systems in the simulated time period.

Figure 5.1 shows that all management configurations employing at least voltage maintenance as well as adaptive PV curtailment are able to reliably keep voltages, transformer hot-spot temperatures, and line currents within their respective admissible ranges. However, there are differences between the configurations shown in the figure as well, which have already been partly indicated in the analyses of the result tables.

The voltage profile for the decentralized strategy is slightly lower than the ones for the other strategies when reactive power is used for voltage maintenance. The reason for this is the lower amount of information available to the buildings in the decentralized strategy. Since they can only rely on their position in the grid and the voltage at their own GCP to decide on appropriate reactive power setpoints, they deploy a modified version of the reactive-power-based voltage maintenance algorithm (see also Section 4.5.3). The differences between the respective reactive-power-based voltage maintenance algorithms as well as

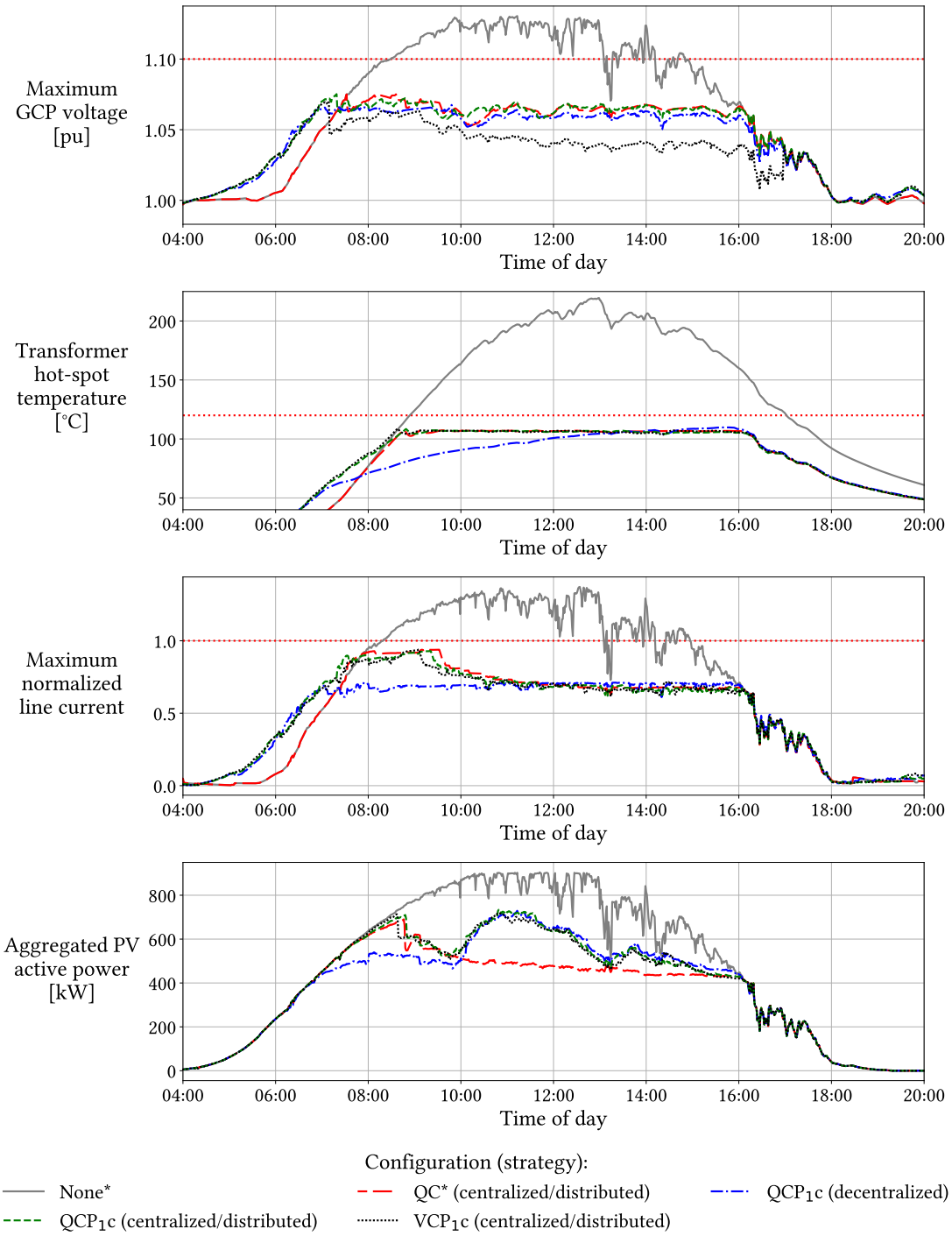

Figure 5.1: Profiles of the maximum GCP voltage in the grid, the transformer hot-spot temperature, the maximum normalized line current in the grid, and the active power generated by PV systems for July 1 and the village grid. Maximum admissible values are indicated by red dotted lines. None = no grid management, * = no energy cost optimization, Q = reactive-power-based voltage maintenance, P_1 = active power flexibility use through active power targets, c = reactive power compensation, C = adaptive PV curtailment, V = VRDT-based voltage maintenance.

their parameterizations determined in Section 4.12 lead to the observed discrepancies in the voltage profiles for the different management strategies.

The voltage profile when using a VRDT for voltage maintenance is substantially lower on average than even the profile for the decentralized strategy. This is due to the functionality of the VRDT. It switches the transmission ratio down when the voltage reaches the upper voltage boundary and only switches up again, when the voltage drops below the voltage deadband (see also Sections 4.4, 4.5.1, and 4.12). When reactive power is used for voltage maintenance, the deadband is substantially narrower, since the amount of reactive power can be adjusted with much finer granularity. A narrower deadband for a VRDT would entail frequent switching operations and overcorrections as well as possibly introduce new voltage disturbances, since a single switching operation changes all voltages in the grid substantially.

When using adaptive PV curtailment, the transformer hot-spot temperature profile for the decentralized strategy deviates from those for the other strategies. As mentioned before, the decentralized strategy indefinitely uses the lowest apparent power limit previously learned when using the centralized or distributed strategies. In contrast, the centralized and distributed strategies adjust the apparent power limit for transformer disturbances dynamically, since the current transformer hot-spot temperature is always known when using these strategies. This means that, with the decentralized strategy, the transformer heats up more slowly throughout the day, which can be observed in the figure.

The same effect can be observed in the maximum normalized line current profiles. Since the decentralized strategy always upholds the lowest learned apparent power limit, the PV curtailment caps the line current at a lower level than in the other strategies. Later in the day, when the apparent power limit for transformer disturbances drops below the apparent power limit for line disturbances when using the centralized and distributed strategies, all strategies show similar maximum normalized line currents.

This effect is seen in the aggregated PV active power profiles as well, where the feed-in of active power is curtailed earlier with the decentralized strategy than with the other strategies. As mentioned before, this explains the generally higher energy losses with the decentralized strategy in this scenario.

The aggregated PV active power profiles also show the way active power flexibility is used to limit the curtailment of PV systems. While the management configuration that does not use optimization incurs high losses of PV active energy especially around noon, the configurations using optimization with regard to active power targets compensate for a part of the energy that would otherwise be lost due to curtailment. When no optimization is used, the BESSs start charging as soon as PV-generated active power is available. This can also be observed in the voltage, line current, and transformer hot-spot temperature profiles. These profiles ramp up later but more sharply, because the first fraction of the active energy generated by the PV systems throughout the day is directly transferred into the local BESSs instead of being fed into the grid.

5.1.1.2. Intermediate

The voltage-related results for the eight-day time period from March 31 to April 7 are given in Table 5.5.

Table 5.5: Outage times due to violations of the admissible voltage range at one or more GCPs in the grid and maximum GCP voltages for all grid management strategies and selected management configurations. The simulated time period is the last day of March and the first week of April. The simulations use the village grid introduced in [162] and [32] and modified in Section 4.10. None = no grid management, * = no energy cost optimization, Conv. = static cos(φ) and 70 % PV curtailment, Q = reactive-power-based voltage maintenance, P_1 = active power flexibility use through active power targets, c = reactive power compensation, V = VRDT-based voltage maintenance.

Management configuration	**Management strategy**			
	Centralized or distributed		**Decentralized**	
	Voltages outside of admissible range (±10 %)			
	Voltage outage time	**Maximum GCP voltage**	**Voltage outage time**	**Maximum GCP voltage**
None*	4.4 %	1.1385 pu	4.4 %	1.1385 pu
None	3.34 %	1.1306 pu	3.34 %	1.1306 pu
Conv.	0.0 %	1.073 pu	0.0 %	1.073 pu
Q*	0.0 %	1.095 pu	0.0 %	1.0963 pu
Q	0.0 %	1.0917 pu	0.0 %	1.0902 pu
P_1c	2.32 %	1.1294 pu	2.29 %	1.1269 pu
V*	0.0 %	1.0926 pu	VRDT unsupported	
V	0.0 %	1.0829 pu	VRDT unsupported	

The results in Table 5.5 show the same qualitative behaviors as the ones in Table 5.1 for the summer time period, but with generally lower voltage outage times. The latter are caused by the lower amount of active energy generated by PV systems in the intermediate seasons compared to the high amount generated in summer. Although the voltage outage times are lower in the intermediate time period, explicit voltage maintenance is still necessary to prevent all violations of the admissible voltage range for this grid.

Table 5.6 contains the transformer-related results for the same time period.

As with the voltages, the transformer-related results in Table 5.6 show the same relative behaviors of the different tested management configurations, but on a generally lower level with regard to transformer outage times and maximum transformer hot-spot temperatures. Adaptive PV curtailment is still necessary to prevent transformer hot-spot temperatures from exceeding the admissible limit.

However, the maximum transformer hot-spot temperatures for the decentralized strategy are significantly lower than the temperatures resulting from the use of the other strategies if PV curtailment is used. The reason for this is the use of constant apparent power

Table 5.6: Outage times due to violations of the maximum admissible transformer hot-spot temperature and maximum transformer hot-spot temperatures for all grid management strategies and selected management configurations. The simulated time period is the last day of March and the first week of April. The simulations use the village grid introduced in [162] and [32] and modified in Section 4.10. None = no grid management, * = no energy cost optimization, Conv. = static cos(φ) and 70 % PV curtailment, Q = reactive-power-based voltage maintenance, P_1 = active power flexibility use through active power targets, c = reactive power compensation, C = adaptive PV curtailment, V = VRDT-based voltage maintenance.

Management configuration	**Management strategy**			
	Centralized or distributed		**Decentralized**	
	Admissible transformer hot-spot temperature (120 °C) exceeded			
	Transformer outage time	**Maximum temperature**	**Transformer outage time**	**Maximum temperature**
None*	6.83 %	197.06 °C	6.83 %	197.06 °C
None	4.76 %	183.29 °C	4.76 %	183.29 °C
Conv.	7.88 %	205.66 °C	7.88 %	205.66 °C
Q*	8.9 %	238.69 °C	8.9 %	235.83 °C
Q	7.0 %	217.25 °C	7.26 %	217.31 °C
c	4.7 %	183.05 °C	4.7 %	183.05 °C
P_1c	2.92 %	168.03 °C	2.8 %	169.2 °C
QC*	0.0 %	113.31 °C	0.0 %	103.0 °C
QC	0.0 %	113.73 °C	0.0 %	100.71 °C
V*	7.81 %	224.57 °C	VRDT unsupported	
V	5.98 %	202.16 °C	VRDT unsupported	
VC*	0.0 %	114.86 °C	VRDT unsupported	
VC	0.0 %	113.05 °C	VRDT unsupported	

limits in the decentralized strategy, learned during the use of the other strategies. Since these apparent power limits are learned over the course of a year, limits learned during summer can be more restrictive than necessary for different seasons. For the simulations performed in this chapter, the learned apparent power limits for the decentralized strategy are preset at the start of the simulation and based on the limits learned when simulating the centralized and distributed strategies in the summer time period.

Table 5.7 shows the line-related results for the intermediate time period.

Again, the results in Table 5.7 indicate the same qualitative differences between the tested management configurations as in the summer time period, while the potential line outage times and maximum potential line outage durations are substantially lower on average. As with transformer-related outages, adaptive PV curtailment is still necessary to prevent line currents from exceeding the respective rated currents of any line for longer and with a higher magnitude than the utilized fuses can handle.

Table 5.7: Potential outage times due to violations of the rated line current of one or more lines in the grid and maximum potential line outage durations for all grid management strategies and selected management configurations. The simulated time period is the last day of March and the first week of April. The simulations use the village grid introduced in [162] and [32] and modified in Section 4.10. None = no grid management, * = no energy cost optimization, Conv. = static cos(φ) and 70 % PV curtailment, Q = reactive-power-based voltage maintenance, P_1 = active power flexibility use through active power targets, c = reactive power compensation, C = adaptive PV curtailment, V = VRDT-based voltage maintenance.

Man. config.	**Management strategy**					
	Centralized or distributed			**Decentralized**		
	Rated current of one or more lines exceeded					
	Potential line outage time	**Max. pot. line outage duration**	**Maximum normalized line current**	**Potential line outage time**	**Max. pot. line outage duration**	**Maximum normalized line current**
None*	4.85 %	133 min	1.45	4.85 %	133 min	1.45
None	4.25 %	109 min	1.39	4.25 %	109 min	1.39
Conv.	6.3 %	143 min	1.34	6.3 %	143 min	1.34
Q*	8.24 %	285 min	1.69	8.31 %	288 min	1.68
Q	7.56 %	209 min	1.63	7.44 %	214 min	1.63
c	4.23 %	109 min	1.39	4.23 %	109 min	1.39
P_1c	3.2 %	100 min	1.33	3.07 %	104 min	1.31
QC*	0.05 %	4 min	1.19	0.0 %	0 min	0.78
QC	0.05 %	4 min	1.18	0.0 %	0 min	0.77
V*	5.46 %	141 min	1.56		VRDT unsupported	
V	4.81 %	124 min	1.48		VRDT unsupported	
VC*	0.05 %	4 min	1.15		VRDT unsupported	
VC	0.05 %	4 min	1.08		VRDT unsupported	

The total outage times, which contain voltage-, transformer-, and line-related outages, as well as the PV active energies and corresponding losses for the intermediate time period are given in Table 5.8.

As in the previous tables for the intermediate time period, the behaviors indicated by the results in Table 5.8 are similar to the behaviors in the summer time period, but total outage times and losses of PV active energy are substantially lower in general. Only management configurations employing adaptive PV curtailment as well as explicit voltage maintenance are able to reliably avoid all outages during the simulated time period.

A notable difference between the results for the summer time period and the intermediate time period lies in the behavior of the two different active power flexibility use methods. While the performance of the two methods differs significantly if the default PV generation prediction is used during the summer time period, the performance gap closes substantially if a perfect PV generation prediction is used. In contrast, in the intermediate time period,

Table 5.8: Total outage times and PV active energies for all grid management strategies and selected management configurations. The simulated time period is the first week of April. The simulations use the village grid introduced in [162] and [32] and modified in Section 4.10. None = no grid management, * = no energy cost optimization, Conv. = fixed cos(φ) and static 70 % PV curtailment, Q = reactive-power-based voltage maintenance, P_1 = active power flexibility use through active power targets, P_2 = curtailment based active power flexibility, c = reactive power compensation, C = adaptive PV curtailment, perf. = perfect PV generation prediction, V = VRDT-based voltage maintenance.

Man. config.	**Management strategy**			
	Centralized or distributed		**Decentralized**	
	Total outage time and PV active energy (loss)			
	Total outage time	**PV active energy (loss)**	**Total outage time**	**PV active energy (loss)**
None*	9.41 %	24.49 MWh (0.0 %)	9.41 %	24.49 MWh (0.0 %)
None	7.27 %	24.49 MWh (0.0 %)	7.27 %	24.49 MWh (0.0 %)
Conv.	11.17 %	24.02 MWh (-1.89 %)	11.17 %	24.02 MWh (-1.89 %)
Q*	12.43 %	24.49 MWh (0.0 %)	12.33 %	24.49 MWh (0.0 %)
Q	10.91 %	24.49 MWh (0.0 %)	11.02 %	24.49 MWh (0.0 %)
c	7.23 %	24.49 MWh (0.0 %)	7.23 %	24.49 MWh (0.0 %)
P_1c	5.14 %	24.49 MWh (0.0 %)	4.94 %	24.49 MWh (0.0 %)
QC*	0.0 %	21.45 MWh (-12.39 %)	0.0 %	20.42 MWh (-16.59 %)
QC	0.0 %	22.22 MWh (-9.26 %)	0.0 %	20.89 MWh (-14.67 %)
QP_1c	0.0 %	22.71 MWh (-7.25 %)	0.0 %	21.41 MWh (-12.57 %)
QP_1c-p	0.0 %	22.97 MWh (-6.18 %)	0.0 %	21.78 MWh (-11.07 %)
QP_2c	0.0 %	22.66 MWh (-7.46 %)	0.0 %	21.37 MWh (-12.73 %)
QP_2c-p	0.0 %	22.86 MWh (-6.65 %)	0.0 %	21.81 MWh (-10.93 %)
V*	10.34 %	24.49 MWh (0.0 %)		VRDT unsupported
V	8.62 %	24.49 MWh (0.0 %)		VRDT unsupported
VC*	0.0 %	21.83 MWh (-10.85 %)		VRDT unsupported
VC	0.0 %	22.61 MWh (-7.64 %)		VRDT unsupported
VP_1c	0.0 %	23.15 MWh (-5.44 %)		VRDT unsupported
VP_1c-p	0.0 %	23.35 MWh (-4.63 %)		VRDT unsupported
VP_2c	0.0 %	23.15 MWh (-5.45 %)		VRDT unsupported
VP_2c-p	0.0 %	23.33 MWh (-4.71 %)		VRDT unsupported

the performance gap between the two methods widens if a perfect PV generation prediction is used instead of the default one. Consequently, the exact behavior observed in the summer period can not be generalized. However, the optimization according to active power targets still performs better than the consideration of PV curtailment during the energy cost optimization, regardless of which PV generation prediction method is used.

Another difference in comparison with the summer time period can be observed for the decentralized strategy. As mentioned previously, the learned apparent power limits the

decentralized strategy uses to curtail PV generation can be more restrictive than necessary during time periods with lower amounts of potentially generatable active energy, such as the intermediate seasons. This does not only lead to the previously observed lower transformer hot-spot temperatures compared to the other strategies, but to higher losses of PV active energy as well. Since the centralized and distributed strategies dynamically adapt the apparent power limits for transformer disturbances, they are not affected by this behavior. As a consequence, the differences in losses of PV active energy between the strategies are larger in the intermediate time period than in the summer time period.

A subtler difference to the results of the summer time period can be observed when comparing reactive-power- and VRDT-based voltage maintenance. The relative advantage with respect to losses of PV active energy when using a VRDT for voltage maintenance is significantly higher in the intermediate time period. This can be explained by the additional reactive power used to proactively react to voltage jumps (see also Section 4.5.3). Voltage jumps are more frequent in the intermediate time period, due to higher cloud coverage and movement and the resulting jumps in PV generation. The algorithm for VRDT-based voltage maintenance (Algorithm 1) is less susceptible to such voltage jumps, as the minimum voltage that has to be reached after a jump is significantly higher than for the reactive-power-based voltage maintenance algorithms (Algorithms 2 and 3) as a result of the parameter studies performed in Section 4.12.

To visualize the evaluation results for this scenario, Figure 5.2 shows the profiles of the previously analyzed aspects for an exemplary day of the intermediate time period. April 7 is chosen for this scenario because it exhibits the highest amount of active energy potentially generatable by PV systems in the simulated time period.

Most of the aforementioned differences between the intermediate and the summer time periods can be seen in Figure 5.1 as well. The voltage profile for the management configuration using VRDT-based voltage maintenance is close to the profiles of the configurations using reactive-power-based voltage maintenance in the time period before noon, in which frequent voltage drops and subsequent jumps occur. These voltage jumps trigger a more substantial use of reactive power compared to a steadier voltage, which results in generally lower voltages. This also entails a higher load on lines and the transformer, which results in more substantial PV curtailment. The latter is also visible in the aggregated PV active power profiles. Here, the profiles of the management configurations using reactive-power-based voltage maintenance are lower on average than the profile for the configuration using VRDT-based voltage maintenance.

The lower maximum transformer hot-spot temperatures when using the decentralized strategy, which are caused by the previously explained differences between the management strategies with regard to PV curtailment, can be observed in the transformer hot-spot temperature profiles as well.

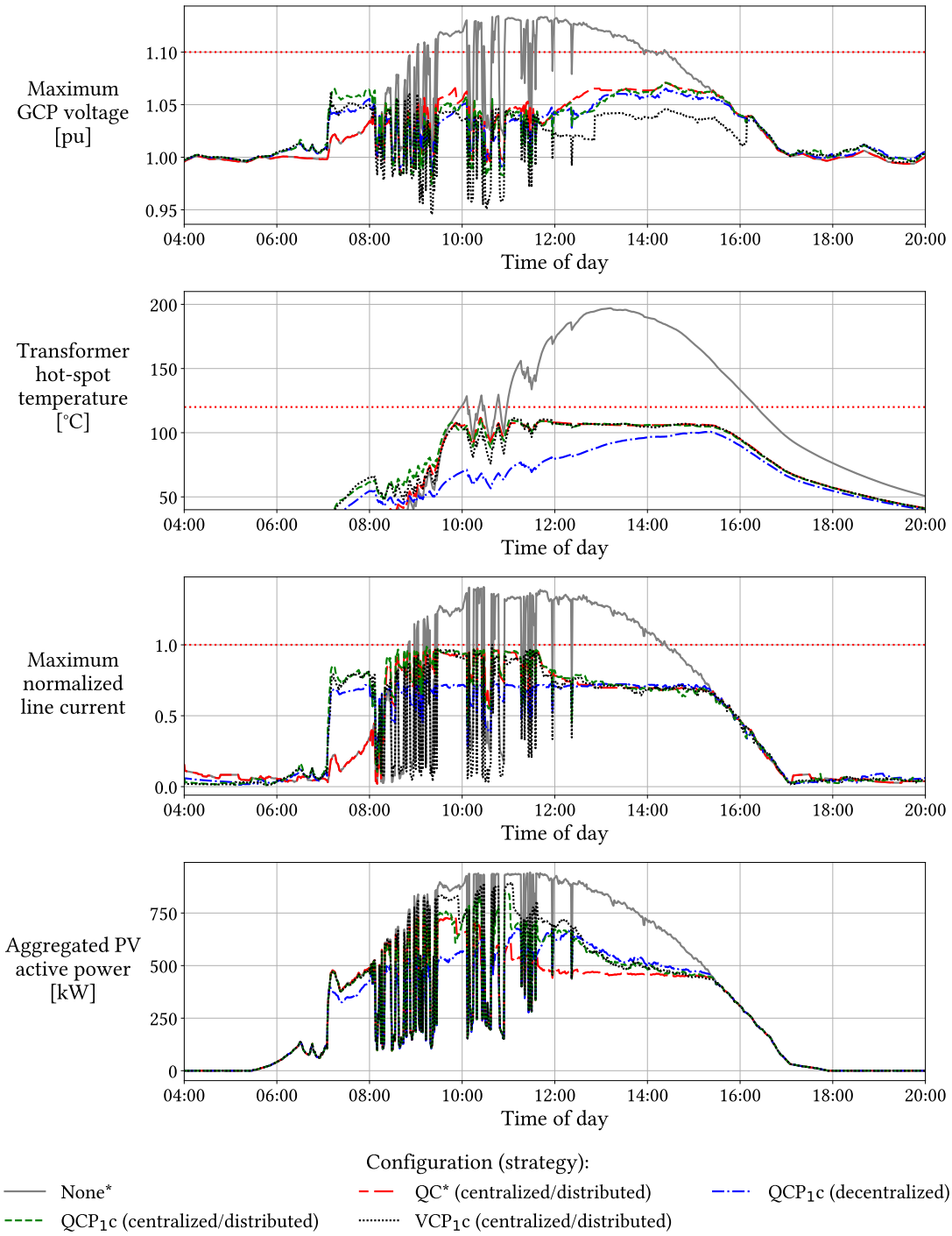

Figure 5.2: Profiles of the maximum GCP voltage in the grid, the transformer hot-spot temperature, the maximum normalized line current in the grid, and the active power generated by PV systems for April 7 and the village grid. Maximum admissible values are indicated by red dotted lines. None = no grid management, * = no energy cost optimization, Q = reactive-power-based voltage maintenance, P_1 = active power flexibility use through active power targets, c = reactive power compensation, C = adaptive PV curtailment, V = VRDT-based voltage maintenance.

5.1.1.3. Winter

The total outage times, which contain voltage-, transformer-, and line-related outages, as well as the PV active energies and corresponding losses for the time period from January 1 to January 7 are given in Table 5.9. As there are no outages during this time period, we forgo the presentation and discussion of specific voltage-, transformer-, and line-related results.

Table 5.9: Total outage times and PV active energies for all grid management strategies and selected management configurations. The simulated time period is the first week of January. The simulations use the village grid introduced in [162] and [32] and modified in Section 4.10. None = no grid management, * = no energy cost optimization, Conv. = fixed cos(φ) and static 70 % PV curtailment, Q = reactive-power-based voltage maintenance, P_1 = active power flexibility use through active power targets, P_2 = curtailment based active power flexibility, c = reactive power compensation, C = adaptive PV curtailment, perf. = perfect PV generation prediction, V = VRDT-based voltage maintenance.

Man. config.	**Management strategy**			
	Centralized or distributed		**Decentralized**	
	Total outage time and PV active energy (loss)			
	Total outage time	**PV active energy (loss)**	**Total outage time**	**PV active energy (loss)**
None*	0.0 %	3.12 MWh (0.0 %)	0.0 %	3.12 MWh (0.0 %)
None	0.0 %	3.12 MWh (0.0 %)	0.0 %	3.12 MWh (0.0 %)
Conv.	0.0 %	3.12 MWh (0.0 %)	0.0 %	3.12 MWh (0.0 %)
Q*	0.0 %	3.12 MWh (0.0 %)	0.0 %	3.12 MWh (0.0 %)
Q	0.0 %	3.12 MWh (0.0 %)	0.0 %	3.12 MWh (0.0 %)
c	0.0 %	3.12 MWh (0.0 %)	0.0 %	3.12 MWh (0.0 %)
P_1c	0.0 %	3.12 MWh (0.0 %)	0.0 %	3.12 MWh (0.0 %)
QC*	0.0 %	3.12 MWh (0.0 %)	0.0 %	3.12 MWh (-0.0 %)
QC	0.0 %	3.12 MWh (0.0 %)	0.0 %	3.12 MWh (-0.0 %)
QP_1c	0.0 %	3.12 MWh (0.0 %)	0.0 %	3.12 MWh (-0.01 %)
QP_1c-p	0.0 %	3.12 MWh (0.0 %)	0.0 %	3.12 MWh (-0.0 %)
QP_2c	0.0 %	3.12 MWh (0.0 %)	0.0 %	3.12 MWh (-0.03 %)
QP_2c-p	0.0 %	3.12 MWh (0.0 %)	0.0 %	3.12 MWh (-0.02 %)
V*	0.0 %	3.12 MWh (0.0 %)		VRDT unsupported
V	0.0 %	3.12 MWh (0.0 %)		VRDT unsupported
VC*	0.0 %	3.12 MWh (0.0 %)		VRDT unsupported
VC	0.0 %	3.12 MWh (0.0 %)		VRDT unsupported
VP_1c	0.0 %	3.12 MWh (0.0 %)		VRDT unsupported
VP_1c-p	0.0 %	3.12 MWh (0.0 %)		VRDT unsupported
VP_2c	0.0 %	3.12 MWh (0.0 %)		VRDT unsupported
VP_2c-p	0.0 %	3.12 MWh (0.0 %)		VRDT unsupported

The results in Table 5.9 indicate that there are no outages during the winter time period, even if no measures are taken. As a consequence, there are no relevant differences between the tested management configurations and strategies. However, in contrast to the other strategies, the decentralized strategy shows very minor losses of PV active energy if PV curtailment is used. Since the decentralized strategy uses constant apparent power limits for PV curtailment, which have been learned when using the centralized and distributed strategies during summer, some curtailment can occur even during the winter time period. The incurred losses are nevertheless negligible, which shows that the developed methods and strategies are not overly restrictive.

5.1.2. Rural Grid

In the following, we present and discuss the simulation results for the rural grid (see also Section 4.10). The general procedure is the same as in Section 5.1.1.

5.1.2.1. Summer

The voltage-related results for the eight-day time period from June 30 to July 7 are given in Table 5.10.

Table 5.10: Outage times due to violations of the admissible voltage range at one or more GCPs in the grid and maximum GCP voltages for all grid management strategies and selected management configurations. The simulated time period is the last day of June and the first week of July. The simulations use the rural grid introduced in [162] and [32] and modified in Section 4.10. None = no grid management, * = no energy cost optimization, Conv. = static $\cos(\varphi)$ and 70 % PV curtailment, Q = reactive-power-based voltage maintenance, P_1 = active power flexibility use through active power targets, c = reactive power compensation, V = VRDT-based voltage maintenance.

Management configuration	**Management strategy**			
	Centralized or distributed		**Decentralized**	
	Voltages outside of admissible range (±10 %)			
	Voltage outage time	**Maximum GCP voltage**	**Voltage outage time**	**Maximum GCP voltage**
None*	13.23 %	1.1305 pu	13.23 %	1.1305 pu
None	11.32 %	1.1287 pu	11.32 %	1.1287 pu
Conv.	0.0 %	1.0673 pu	0.0 %	1.0673 pu
Q*	0.0 %	1.0975 pu	0.0 %	1.0956 pu
Q	0.0 %	1.0973 pu	0.0 %	1.0944 pu
P_1c	8.64 %	1.1394 pu	8.47 %	1.1263 pu
V*	0.0 %	1.0962 pu	VRDT unsupported	
V	0.0 %	1.0904 pu	VRDT unsupported	

The results in Table 5.10 are very similar to the results for the village grid and the summer time period. The explanations for the behaviors indicated by these results are the same as for the village grid and thus not repeated at this point (see also Section 5.1.1.1).

Table 5.11 contains the transformer-related results for the same time period.

Table 5.11: Outage times due to violations of the maximum admissible transformer hot-spot temperature and maximum transformer hot-spot temperatures for all grid management strategies and selected management configurations. The simulated time period is the last day of June and the first week of July. The simulations use the rural grid introduced in [162] and [32] and modified in Section 4.10. None = no grid management, * = no energy cost optimization, Conv. = static cos(φ) and 70 % PV curtailment, Q = reactive-power-based voltage maintenance, P_1 = active power flexibility use through active power targets, c = reactive power compensation, C = adaptive PV curtailment, V = VRDT-based voltage maintenance.

Management configuration	**Management strategy**			
	Centralized or distributed		**Decentralized**	
	Admissible transformer hot-spot temperature (120 °C) exceeded			
	Transformer outage time	**Maximum temperature**	**Transformer outage time**	**Maximum temperature**
None*	0.0 %	83.51 °C	0.0 %	83.51 °C
None	0.0 %	82.8 °C	0.0 %	82.8 °C
Conv.	0.0 %	84.81 °C	0.0 %	84.81 °C
Q*	0.0 %	93.18 °C	0.0 %	91.4 °C
Q	0.0 %	92.4 °C	0.0 %	91.09 °C
c	0.0 %	82.78 °C	0.0 %	82.78 °C
P_1c	0.0 %	79.66 °C	0.0 %	78.1 °C
QC*	0.0 %	93.18 °C	0.0 %	91.4 °C
QC	0.0 %	92.4 °C	0.0 %	91.09 °C
V*	0.0 %	89.18 °C	VRDT unsupported	
V	0.0 %	88.08 °C	VRDT unsupported	
VC*	0.0 %	89.18 °C	VRDT unsupported	
VC	0.0 %	88.08 °C	VRDT unsupported	

The results in Table 5.11 indicate that the transformer of the rural grid can handle all potentially generatable PV active energy without the need for PV curtailment. This is still true when voltage maintenance is used, regardless of whether it is achieved using a VRDT or reactive power. As a consequence, the results for the management configurations utilizing PV curtailment do not differ from those of the otherwise identical management configurations that do not use PV curtailment. The qualitative differences between the maximum transformer hot-spot temperatures of management configurations that do not use PV curtailment are very similar to the ones observed in the village grid and can be explained in the same way (see also Section 5.1.1.1).

The maximum transformer hot-spot temperatures are slightly lower for the decentralized strategy compared to the other strategies if reactive-power-based voltage maintenance or optimization with regard to active power targets are used. Both differences can be explained by the different functionality of the decentralized strategy. In this scenario, the reactive-power-based voltage maintenance algorithm utilized in the decentralized strategy (Algorithm 3) results in lower reactive power use on average. This lessens the load on the transformer and consequently reduces its temperature. The optimization with regard to active power targets is used more often in the decentralized strategy as in the other strategies, since the criterion that triggers active power flexibility use in the former is voltage-based. In the rural grid, voltages are relatively high, while the load on lines and the transformer is relatively low. This leads to the frequent use of active power flexibility in the decentralized strategy, although this is not necessary to prevent transformer- and line-related outages. However, it does increase the longevity of the grid equipment.

Table 5.12 shows the line-related results.

Table 5.12: Potential outage times due to violations of the rated line current of one or more lines in the grid and maximum potential line outage durations for all grid management strategies and selected management configurations. The simulated time period is the last day of June and the first week of July. The simulations use the rural grid introduced in [162] and [32] and modified in Section 4.10. None = no grid management, * = no energy cost optimization, Conv. = static cos(φ) and 70 % PV curtailment, Q = reactive-power-based voltage maintenance, P_1 = active power flexibility use through active power targets, c = reactive power compensation, C = adaptive PV curtailment, V = VRDT-based voltage maintenance.

Man. config.	**Management strategy**					
	Centralized or distributed			**Decentralized**		
	Rated current of one or more lines exceeded					
	Potential line outage time	**Max. pot. line outage duration**	**Maximum normalized line current**	**Potential line outage time**	**Max. pot. line outage duration**	**Maximum normalized line current**
None*	0.0 %	0 min	0.68	0.0 %	0 min	0.68
None	0.0 %	0 min	0.68	0.0 %	0 min	0.68
Conv.	0.0 %	0 min	0.67	0.0 %	0 min	0.67
Q*	0.0 %	0 min	0.82	0.0 %	0 min	0.81
Q	0.0 %	0 min	0.82	0.0 %	0 min	0.81
c	0.0 %	0 min	0.68	0.0 %	0 min	0.68
P_1c	0.0 %	0 min	0.73	0.0 %	0 min	0.67
QC*	0.0 %	0 min	0.82	0.0 %	0 min	0.81
QC	0.0 %	0 min	0.82	0.0 %	0 min	0.81
V*	0.0 %	0 min	0.73		VRDT unsupported	
V	0.0 %	0 min	0.73		VRDT unsupported	
VC*	0.0 %	0 min	0.73		VRDT unsupported	
VC	0.0 %	0 min	0.73		VRDT unsupported	

As the results in Table 5.12 show, the lines of the rural grid can handle all potentially generatable PV active energy without PV curtailment, even if voltage maintenance is used, just like the transformer. Consequently, the maximum normalized line currents of management configurations that include PV curtailment do not differ from their otherwise identical counterparts without PV curtailment. As expected, the maximum line currents for management configurations utilizing voltage maintenance are somewhat higher than those observed for the other management configurations, but nevertheless entirely unproblematic.

The total outage times, which contain voltage-, transformer-, and line-related outages, as well as the PV active energies and corresponding losses for all simulated management configurations and strategies are given in Table 5.13.

Table 5.13: Total outage times and PV active energies for all grid management strategies and selected management configurations. The simulated time period is the first week of July. The simulations use the rural grid introduced in [162] and [32] and modified in Section 4.10. None = no grid management, * = no energy cost optimization, Conv. = fixed cos(φ) and static 70 % PV curtailment, Q = reactive-power-based voltage maintenance, P_1 = active power flexibility use through active power targets, P_2 = curtailment based active power flexibility, c = reactive power compensation, C = adaptive PV curtailment, V = VRDT-based voltage maintenance.

Man. config.	**Management strategy**			
	Centralized or distributed		**Decentralized**	
	Total outage time and PV active energy (loss)			
	Total outage time	**PV active energy (loss)**	**Total outage time**	**PV active energy (loss)**
None*	13.59 %	11.5 MWh (0.0 %)	13.59 %	11.5 MWh (0.0 %)
None	11.63 %	11.5 MWh (0.0 %)	11.63 %	11.5 MWh (0.0 %)
Conv.	0.0 %	11.01 MWh (-4.24 %)	0.0 %	11.01 MWh (-4.24 %)
Q*	0.0 %	11.5 MWh (0.0 %)	0.0 %	11.5 MWh (0.0 %)
Q	0.0 %	11.5 MWh (0.0 %)	0.0 %	11.5 MWh (0.0 %)
c	11.89 %	11.5 MWh (0.0 %)	11.91 %	11.5 MWh (0.0 %)
P_1c	8.9 %	11.5 MWh (0.0 %)	8.52 %	11.5 MWh (0.0 %)
QC*	0.0 %	11.5 MWh (0.0 %)	0.0 %	11.5 MWh (0.0 %)
QC	0.0 %	11.5 MWh (0.0 %)	0.0 %	11.5 MWh (0.0 %)
QCP_1c	0.0 %	11.5 MWh (0.0 %)	0.0 %	11.5 MWh (0.0 %)
QCP_2c	0.0 %	11.5 MWh (0.0 %)	0.0 %	11.5 MWh (0.0 %)
V*	0.0 %	11.5 MWh (0.0 %)		VRDT unsupported
V	0.0 %	11.5 MWh (0.0 %)		VRDT unsupported
VC*	0.0 %	11.5 MWh (0.0 %)		VRDT unsupported
VC	0.0 %	11.5 MWh (0.0 %)		VRDT unsupported
VCP_1c	0.0 %	11.5 MWh (0.0 %)		VRDT unsupported
VCP_2c	0.0 %	11.5 MWh (0.0 %)		VRDT unsupported

The results in Table 5.13 again indicate that only voltage maintenance is needed to avoid all outages for the rural grid. The standalone use of active power flexibility and reactive power compensation can reduce the total outage time significantly, but not prevent it entirely. However, all management configurations employing some form of voltage maintenance reduce the total outage time to 0 %.

The total outage time increases slightly when reactive power compensation is used in addition to the normal energy cost optimization. This is caused by the slightly different GCP voltages that result from the changes in reactive power absorption or injection.

Due to the static PV curtailment, which is unnecessary in this scenario, employed in the conventional management configuration, the latter incurs significant losses of PV active energy. This is not the case for the management configurations employing the adaptive PV curtailment algorithms introduced in Section 4.5.4. In contrast to the static PV curtailment employed in the conventional management configuration, the adaptive curtailment algorithms only curtail the PV generation if and when necessary.

As PV curtailment is unnecessary in this scenario, the results for the decentralized strategy are very similar to the results for the other strategies. Since PV curtailment is never triggered when using the centralized and distributed strategies, no apparent power limits are learned and thus the decentralized strategy does not employ PV curtailment either.

To visualize the evaluation results for this scenario, Figure 5.3 shows the profiles of the previously analyzed aspects for an exemplary day of the summer time period. July 1 is chosen for this scenario because it exhibits the highest amount of active energy potentially generatable by PV systems in the simulated time period.

In Figure 5.3, the voltage profiles for the management configurations utilizing reactive-power-based voltage maintenance are very similar. The profile for the management configuration using VRDT-based voltage maintenance is lower on average, due to the reasons already given for the village grid in Section 5.1.1.1.

The transformer hot-spot temperature and maximum normalized line current profiles for management configurations employing active power flexibility are lower around noon than those of the management configuration utilizing reactive-power-based voltage maintenance and adaptive PV curtailment but no optimization at all. This is caused by the parameter values determined in the parameter studies in Section 4.12. The determined minimum transformer load factor as well as the normalized line current threshold at which the use of active power flexibility is triggered are low enough to trigger the use of active power flexibility even in this scenario. While not explicitly necessary to prevent outages or losses of PV active energy in this scenario, this behavior is still beneficial in terms of grid equipment longevity. If the latter is not of concern, the use of active power flexibility can also be deactivated for this scenario.

The aggregated PV active power profiles show no differences between the different management configurations, which is expected as PV curtailment is not necessary in this scenario.

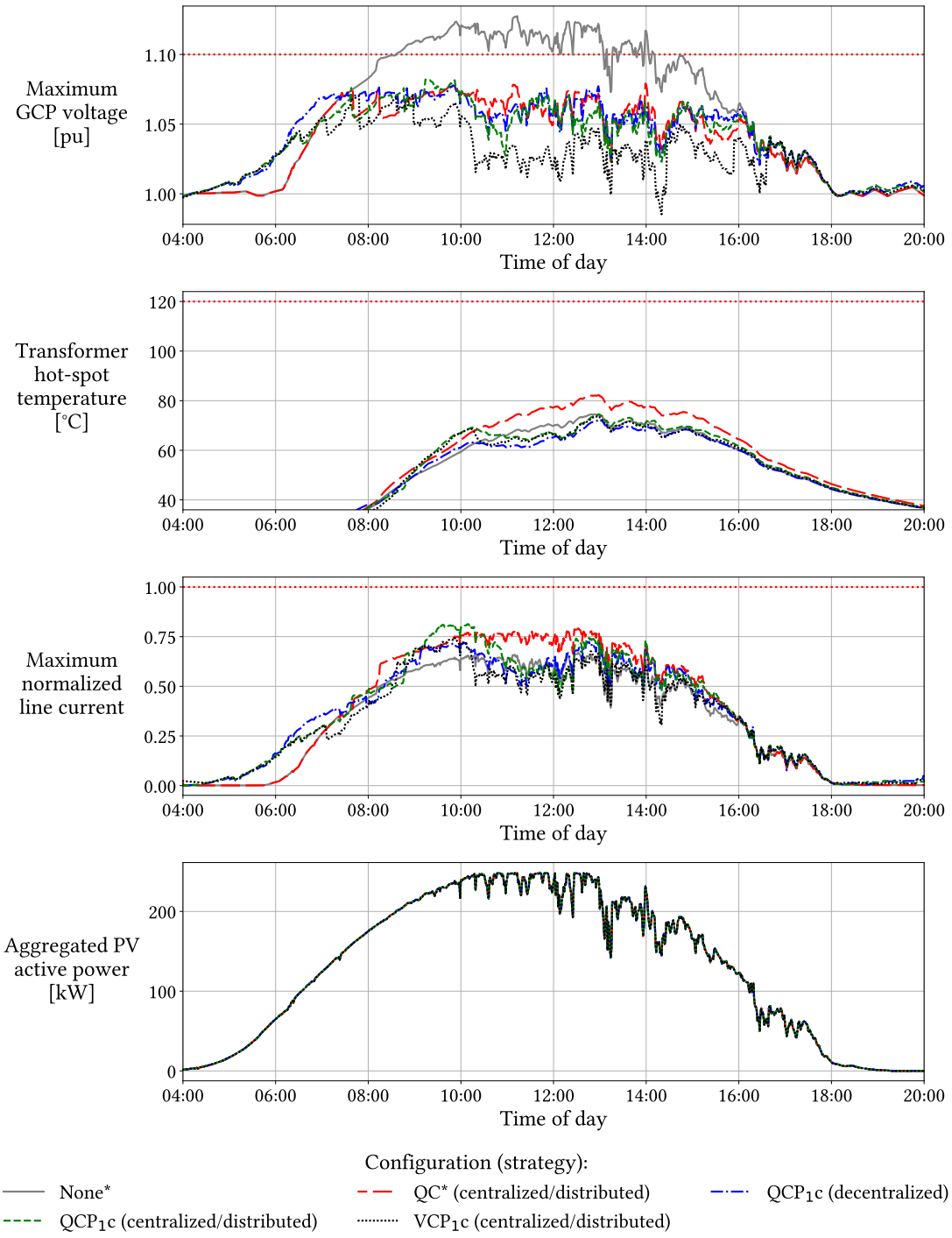

Figure 5.3: Profiles of the maximum GCP voltage in the grid, the transformer hot-spot temperature, the maximum normalized line current in the grid, and the active power generated by PV systems for July 1 and the rural grid. Maximum admissible values are indicated by red dotted lines. None = no grid management, * = no energy cost optimization, Q = reactive-power-based voltage maintenance, P_1 = active power flexibility use through active power targets, c = reactive power compensation, C = adaptive PV curtailment, V = VRDT-based voltage maintenance.

5.1.2.2. Intermediate

The voltage-, transformer-, and line-related results for March 31 to April 7 as well as the aggregated results for April 1 to April 7 are given in Tables 5.14 to 5.17, respectively. A visualization of the evaluation results for the exemplary day of April 7 is given in Figure 5.4. April 7 is chosen for this scenario because it exhibits the highest amount of active energy potentially generatable by PV systems in the simulated time period.

The qualitative behaviors that can be observed in the intermediate time period are the same as in the summer time period, but on a generally lower outage time level, due to the lower amount of potentially generatable PV active energy. Consequently, the results for the intermediate time period are not discussed further at this point (see also Section 5.1.2.1).

Table 5.14: Outage times due to violations of the admissible voltage range at one or more GCPs in the grid and maximum GCP voltages for all grid management strategies and selected management configurations. The simulated time period is the last day of March and the first week of April. The simulations use the rural grid introduced in [162] and [32] and modified in Section 4.10. None = no grid management, * = no energy cost optimization, Conv. = static cos(φ) and 70 % PV curtailment, Q = reactive-power-based voltage maintenance, P_1 = active power flexibility use through active power targets, c = reactive power compensation, V = VRDT-based voltage maintenance.

Management configuration	**Management strategy**			
	Centralized or distributed		**Decentralized**	
	Admissible transformer hot-spot temperature (120 °C) exceeded			
	Transformer outage time	**Maximum temperature**	**Transformer outage time**	**Maximum temperature**
None*	3.96 %	1.1327 pu	3.96 %	1.1327 pu
None	3.08 %	1.1308 pu	3.08 %	1.1308 pu
Conv.	0.0 %	1.0647 pu	0.0 %	1.0647 pu
Q*	0.0 %	1.0878 pu	0.0 %	1.0868 pu
Q	0.0 %	1.0872 pu	0.0 %	1.0876 pu
P_1c	2.48 %	1.1347 pu	2.15 %	1.1293 pu
V*	0.0 %	1.0908 pu		VRDT unsupported
V	0.0 %	1.096 pu		VRDT unsupported

5.1.2.3. Winter

The total outage times, which contain voltage-, transformer-, and line-related outages, as well as the PV active energies and corresponding losses for the time period from January 1 to January 7 are given in Table 5.18. As there are no outages during this time period, we forgo the presentation and discussion of specific voltage-, transformer-, and line-related results.

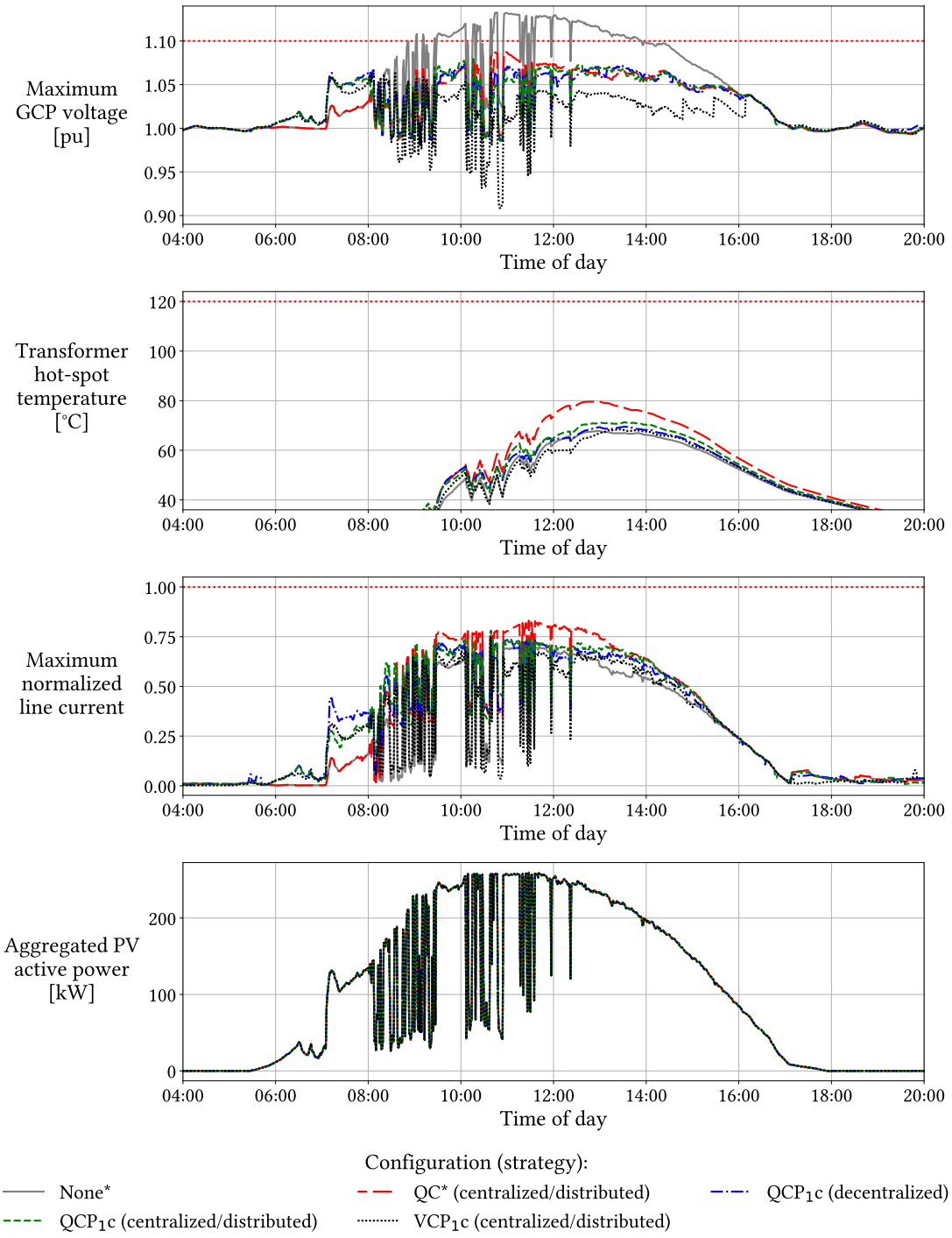

Figure 5.4: Profiles of the maximum GCP voltage in the grid, the transformer hot-spot temperature, the maximum normalized line current in the grid, and the active power generated by PV systems for April 7 and the rural grid. Maximum admissible values are indicated by red dotted lines. None = no grid management, * = no energy cost optimization, Q = reactive-power-based voltage maintenance, P_1 = active power flexibility use through active power targets, c = reactive power compensation, C = adaptive PV curtailment, V = VRDT-based voltage maintenance.

Table 5.15: Outage times due to violations of the maximum admissible transformer hot-spot temperature and maximum transformer hot-spot temperatures for all grid management strategies and selected management configurations. The simulated time period is the last day of March and the first week of April. The simulations use the rural grid introduced in [162] and [32] and modified in Section 4.10. None = no grid management, * = no energy cost optimization, Conv. = static cos(φ) and 70 % PV curtailment, Q = reactive-power-based voltage maintenance, P_1 = active power flexibility use through active power targets, c = reactive power compensation, C = adaptive PV curtailment, V = VRDT-based voltage maintenance.

Management configuration	**Management strategy**			
	Centralized or distributed		**Decentralized**	
	Admissible transformer hot-spot temperature (120 °C) exceeded			
	Transformer outage time	**Maximum temperature**	**Transformer outage time**	**Maximum temperature**
None*	0.0 %	67.89 °C	0.0 %	67.89 °C
None	0.0 %	65.97 °C	0.0 %	65.97 °C
Conv.	0.0 %	70.97 °C	0.0 %	70.97 °C
Q*	0.0 %	79.73 °C	0.0 %	78.53 °C
Q	0.0 %	76.98 °C	0.0 %	75.47 °C
c	0.0 %	65.94 °C	0.0 %	65.94 °C
P_1c	0.0 %	64.48 °C	0.0 %	62.87 °C
QC*	0.0 %	79.73 °C	0.0 %	78.53 °C
QC	0.0 %	76.98 °C	0.0 %	75.47 °C
V*	0.0 %	73.1 °C	VRDT unsupported	
V	0.0 %	70.92 °C	VRDT unsupported	
VC*	0.0 %	73.1 °C	VRDT unsupported	
VC	0.0 %	70.92 °C	VRDT unsupported	

As in the village grid, the results in Table 5.18 show that there are no outages during the winter time period, even if no measures are taken. However, in contrast to the very minor losses of PV active energy observed in the village grid when using the decentralized strategy, no losses occur in the rural grid. As mentioned before, PV curtailment is not necessary for the rural grid. Consequently, no apparent power limits for PV curtailment are learned during the use of the centralized or distributed strategies, so that the decentralized strategy does not curtail PV systems either.

5.1.3. Suburban Grid

In the following, we present and discuss the simulation results for the suburban grid (see also Section 4.10). The general procedure is the same as in Sections 5.1.1 and 5.1.2.

Table 5.16: Potential outage times due to violations of the rated line current of one or more lines in the grid and maximum potential line outage durations for all grid management strategies and selected management configurations. The simulated time period is the last day of March and the first week of April. The simulations use the rural grid introduced in [162] and [32] and modified in Section 4.10. None = no grid management, * = no energy cost optimization, Conv. = static cos(φ) and 70 % PV curtailment, Q = reactive-power-based voltage maintenance, P_1 = active power flexibility use through active power targets, c = reactive power compensation, C = adaptive PV curtailment, V = VRDT-based voltage maintenance.

Man. config.	**Management strategy**					
	Centralized or distributed			**Decentralized**		
	Rated current of one or more lines exceeded					
	Potential line outage time	**Max. pot. line outage duration**	**Maximum normalized line current**	**Potential line outage time**	**Max. pot. line outage duration**	**Maximum normalized line current**
None*	0.0 %	0 min	0.71	0.0 %	0 min	0.71
None	0.0 %	0 min	0.7	0.0 %	0 min	0.7
Conv.	0.0 %	0 min	0.67	0.0 %	0 min	0.67
Q*	0.0 %	0 min	0.84	0.0 %	0 min	0.83
Q	0.0 %	0 min	0.81	0.0 %	0 min	0.81
c	0.0 %	0 min	0.7	0.0 %	0 min	0.7
P_1c	0.0 %	0 min	0.72	0.0 %	0 min	0.7
QC*	0.0 %	0 min	0.84	0.0 %	0 min	0.83
QC	0.0 %	0 min	0.81	0.0 %	0 min	0.81
V*	0.0 %	0 min	0.76		VRDT unsupported	
V	0.0 %	0 min	0.74		VRDT unsupported	
VC*	0.0 %	0 min	0.76		VRDT unsupported	
VC	0.0 %	0 min	0.74		VRDT unsupported	

5.1.3.1. Summer

The voltage-related results for the eight-day time period from June 30 to July 7 are given in Table 5.19.

Table 5.19 shows that dedicated voltage maintenance is not needed to keep voltages in the admissible range for the suburban grid. Short violations of the maximum admissible voltage only occur if no optimization is used at all. Since the conventional management configuration employs a fixed cos(φ) regardless of the current grid status, it nevertheless lowers the maximum GCP voltage substantially. The VRDT- and reactive-power-based voltage maintenance algorithms introduced in Sections 4.5.1 and 4.5.3 lower the maximum voltages significantly as well, since they engage before the admissible voltage range is violated. There are no notable differences between the decentralized and the other strategies with regard to voltages in this scenario.

Table 5.17: Total outage times and PV active energies for all grid management strategies and selected management configurations. The simulated time period is the first week of April. The simulations use the rural grid introduced in [162] and [32] and modified in Section 4.10. None = no grid management, * = no energy cost optimization, Conv. = fixed cos(φ) and static 70 % PV curtailment, Q = reactive-power-based voltage maintenance, P_1 = active power flexibility use through active power targets, P_2 = curtailment based active power flexibility, c = reactive power compensation, C = adaptive PV curtailment, V = VRDT-based voltage maintenance.

Manag. config.	**Management strategy**			
	Centralized or distributed		**Decentralized**	
	Total outage time and PV active energy (loss)			
	Total outage time	**PV active energy (loss)**	**Total outage time**	**PV active energy (loss)**
None*	4.31 %	6.74 MWh (0.0 %)	4.31 %	6.74 MWh (0.0 %)
None	3.4 %	6.74 MWh (0.0 %)	3.4 %	6.74 MWh (0.0 %)
Conv.	0.0 %	6.59 MWh (-2.15 %)	0.0 %	6.59 MWh (-2.15 %)
Q*	0.0 %	6.74 MWh (0.0 %)	0.0 %	6.74 MWh (0.0 %)
Q	0.0 %	6.74 MWh (0.0 %)	0.0 %	6.74 MWh (0.0 %)
c	3.59 %	6.74 MWh (0.0 %)	3.6 %	6.74 MWh (0.0 %)
P_1c	2.76 %	6.74 MWh (0.0 %)	2.45 %	6.74 MWh (0.0 %)
QC*	0.0 %	6.74 MWh (0.0 %)	0.0 %	6.74 MWh (0.0 %)
QC	0.0 %	6.74 MWh (0.0 %)	0.0 %	6.74 MWh (0.0 %)
QP_1c	0.0 %	6.74 MWh (0.0 %)	0.0 %	6.74 MWh (0.0 %)
QP_2c	0.0 %	6.74 MWh (0.0 %)	0.0 %	6.74 MWh (0.0 %)
V*	0.0 %	6.74 MWh (0.0 %)		VRDT unsupported
V	0.0 %	6.74 MWh (0.0 %)		VRDT unsupported
VC*	0.0 %	6.74 MWh (0.0 %)		VRDT unsupported
VC	0.0 %	6.74 MWh (0.0 %)		VRDT unsupported
VP_1c	0.0 %	6.74 MWh (0.0 %)		VRDT unsupported
VP_2c	0.0 %	6.74 MWh (0.0 %)		VRDT unsupported

Table 5.20 contains the transformer-related results for the same time period.

While explicit countermeasures are not needed to keep voltages inside the admissible range for the suburban grid, Table 5.20 indicates that they are needed to keep the transformer hot-spot temperature below the 120 °C limit. If only energy cost optimization is used, there are short periods in which the temperature still exceeds 120 °C. These violations are exacerbated by the use of VRDT- or reactive-power-based voltage maintenance as well as the conventional management configuration, which increase the currents on the transformer windings.

As in the other grids, reactive power compensation reduces the transformer outage time and maximum transformer hot-spot temperature slightly, but not significantly. This suggests

Table 5.18: Total outage times and PV active energies for all grid management strategies and selected management configurations. The simulated time period is the first week of January. The simulations use the rural grid introduced in [162] and [32] and modified in Section 4.10. None = no grid management, * = no energy cost optimization, Conv. = fixed cos(φ) and static 70 % PV curtailment, Q = reactive-power-based voltage maintenance, P_1 = active power flexibility use through active power targets, P_2 = curtailment based active power flexibility, c = reactive power compensation, C = adaptive PV curtailment, perf. = perfect PV generation prediction, V = VRDT-based voltage maintenance.

Manag. config.	**Management strategy**			
	Centralized or distributed		**Decentralized**	
	Total outage time and PV active energy (loss)			
	Total outage time	**PV active energy (loss)**	**Total outage time**	**PV active energy (loss)**
None*	0.0 %	0.86 MWh (0.0 %)	0.0 %	0.86 MWh (0.0 %)
None	0.0 %	0.86 MWh (0.0 %)	0.0 %	0.86 MWh (0.0 %)
Conv.	0.0 %	0.86 MWh (0.0 %)	0.0 %	0.86 MWh (0.0 %)
Q*	0.0 %	0.86 MWh (0.0 %)	0.0 %	0.86 MWh (0.0 %)
Q	0.0 %	0.86 MWh (0.0 %)	0.0 %	0.86 MWh (0.0 %)
c	0.0 %	0.86 MWh (0.0 %)	0.0 %	0.86 MWh (0.0 %)
P_1c	0.0 %	0.86 MWh (0.0 %)	0.0 %	0.86 MWh (0.0 %)
QC*	0.0 %	0.86 MWh (0.0 %)	0.0 %	0.86 MWh (0.0 %)
QC	0.0 %	0.86 MWh (0.0 %)	0.0 %	0.86 MWh (0.0 %)
QCP_1c	0.0 %	0.86 MWh (0.0 %)	0.0 %	0.86 MWh (0.0 %)
QCP_2c	0.0 %	0.86 MWh (0.0 %)	0.0 %	0.86 MWh (0.0 %)
V*	0.0 %	0.86 MWh (0.0 %)	VRDT unsupported	
V	0.0 %	0.86 MWh (0.0 %)	VRDT unsupported	
VC*	0.0 %	0.86 MWh (0.0 %)	VRDT unsupported	
VC	0.0 %	0.86 MWh (0.0 %)	VRDT unsupported	
VCP_1c	0.0 %	0.86 MWh (0.0 %)	VRDT unsupported	
VCP_2c	0.0 %	0.86 MWh (0.0 %)	VRDT unsupported	

that the reactive power absorbed or injected by devices other than PV inverters may not relevant with regard to the electrical disturbances considered in this thesis, regardless of the considered grid type.

If active power flexibility via active power targets is used without voltage maintenance, the maximum transformer hot-spot temperature remains significantly below the 120 °C limit, despite not using PV curtailment. As expected, adaptive PV curtailment is able to keep temperatures well below the limit as well, even if voltage maintenance is applied.

Management configurations that do not comprise PV curtailment perform relatively similarly for all management strategies. However, for configurations that do use PV curtailment, the decentralized strategy produces different results than the other strategies.

Table 5.19: Outage times due to violations of the admissible voltage range at one or more GCPs in the grid and maximum GCP voltages for all grid management strategies and selected management configurations. The simulated time period is the last day of June and the first week of July. The simulations use the suburban grid introduced in [162] and [32] and modified in Section 4.10. None = no grid management, * = no energy cost optimization, Conv. = static $\cos(\varphi)$ and 70 % PV curtailment, Q = reactive-power-based voltage maintenance, P_1 = active power flexibility use through active power targets, c = reactive power compensation, V = VRDT-based voltage maintenance.

Management configuration	**Management strategy**			
	Centralized or distributed		**Decentralized**	
	Voltages outside of admissible range (±10 %)			
	Voltage outage time	**Maximum GCP voltage**	**Voltage outage time**	**Maximum GCP voltage**
None*	0.71 %	1.1064 pu	0.71 %	1.1064 pu
None	0.0 %	1.0969 pu	0.0 %	1.0969 pu
Conv.	0.0 %	1.0583 pu	0.0 %	1.0583 pu
Q*	0.0 %	1.0872 pu	0.0 %	1.0836 pu
Q	0.0 %	1.078 pu	0.0 %	1.0773 pu
P_1c	0.0 %	1.0981 pu	0.0 %	1.0927 pu
V*	0.0 %	1.0833 pu	VRDT unsupported	
V	0.0 %	1.0833 pu	VRDT unsupported	

This is caused by the learned apparent power limits the decentralized strategy uses to curtail the PV systems. Since they are applied continuously, as opposed to the dynamic limits used in the other strategies, the transformer does not heat up to the same extent. While this is beneficial with regard to transformer longevity, it entails losses of PV active energy. This behavior can also be observed in the village grid to some extent, but it is more pronounced in the suburban grid.

Table 5.21 shows the line-related results.

Table 5.21 indicates that line-related outages constitute the main challenge for the suburban grid. As with transformer-related outages, voltage maintenance measures increase the magnitude and duration of line-related outages due to the higher line currents they entail.

While reactive power compensation alone does not significantly decrease the potential line outage time and maximum potential line outage duration, the use of active power flexibility is able to reduce both values substantially. However, the achieved reduction in the maximum potential line outage duration is not quite sufficient to comply with the four-minute limit chosen in Section 4.11. Furthermore, if no PV curtailment is used, the observed exceedances of the rated line current will occur recurrently, which wears down the utilized fuses over time. Only management configurations utilizing the adaptive PV curtailment algorithms introduced in Section 4.5.4 are able to keep the maximum potential line outage duration below the previously defined limit while learning the appropriate

Table 5.20: Outage times due to violations of the maximum admissible transformer hot-spot temperature and maximum transformer hot-spot temperatures for all grid management strategies and selected management configurations. The simulated time period is the last day of June and the first week of July. The simulations use the suburban grid introduced in [162] and [32] and modified in Section 4.10. None = no grid management, * = no energy cost optimization, Conv. = static cos(φ) and 70 % PV curtailment, Q = reactive-power-based voltage maintenance, P_1 = active power flexibility use through active power targets, c = reactive power compensation, C = adaptive PV curtailment, V = VRDT-based voltage maintenance.

Management configuration	**Management strategy**			
	Centralized or distributed		**Decentralized**	
	Admissible transformer hot-spot temperature (120 °C) exceeded			
	Transformer outage time	**Maximum temperature**	**Transformer outage time**	**Maximum temperature**
None*	2.11 %	136.39 °C	2.11 %	136.39 °C
None	0.13 %	120.98 °C	0.13 %	120.98 °C
Conv.	0.86 %	127.84 °C	0.86 %	127.84 °C
Q*	5.32 %	145.5 °C	6.08 %	147.05 °C
Q	0.7 %	127.49 °C	0.88 %	129.34 °C
c	0.1 %	120.78 °C	0.1 %	120.77 °C
P_1c	0.0 %	110.44 °C	0.0 %	109.97 °C
QC*	0.0 %	108.15 °C	0.0 %	94.39 °C
QC	0.0 %	107.35 °C	0.0 %	90.02 °C
V*	5.44 %	143.91 °C	VRDT unsupported	
V	0.66 %	126.51 °C	VRDT unsupported	
VC*	0.0 %	107.89 °C	VRDT unsupported	
VC	0.0 %	107.49 °C	VRDT unsupported	

apparent power limits. Once the learning process is finished and the learned limits are continuously upheld, repeated exceedances of the rated line current are prevented.

The decentralized strategy again yields results similar to those for the other strategies, except for lower maximum line currents when PV curtailment is used. The latter are caused by the same functionality that leads to the previously observed lower maximum transformer hot-spot temperatures when using the decentralized strategy.

The total outage times, which contain voltage-, transformer-, and line-related outages, as well as the PV active energies and corresponding losses for all simulated management configurations and strategies are given in Table 5.22.

As in the village grid, Table 5.22 shows that only management configurations using adaptive PV curtailment prevent all outages. The resulting losses of PV active energy vary substantially depending on the other measures used. As already mentioned in Section 5.1.1.1, management configurations that do not apply PV curtailment would incur

Table 5.21: Potential outage times due to violations of the rated line current of one or more lines in the grid and maximum potential line outage durations for all grid management strategies and selected management configurations. The simulated time period is the last day of June and the first week of July. The simulations use the suburban grid introduced in [162] and [32] and modified in Section 4.10. None = no grid management, * = no energy cost optimization, Conv. = static cos(φ) and 70 % PV curtailment, Q = reactive-power-based voltage maintenance, P_1 = active power flexibility use through active power targets, c = reactive power compensation, C = adaptive PV curtailment, V = VRDT-based voltage maintenance.

Man. config.	**Management strategy**					
	Centralized or distributed			**Decentralized**		
	Rated current of one or more lines exceeded					
	Potential line outage time	**Max. pot. line outage duration**	**Maximum normalized line current**	**Potential line outage time**	**Max. pot. line outage duration**	**Maximum normalized line current**
None*	8.21 %	100 min	1.18	8.21 %	100 min	1.18
None	1.68 %	49 min	1.12	1.68 %	49 min	1.12
Conv.	3.43 %	61 min	1.07	3.43 %	61 min	1.07
Q*	12.23 %	237 min	1.31	12.43 %	238 min	1.33
Q	7.16 %	121 min	1.25	7.59 %	100 min	1.25
c	1.61 %	48 min	1.12	1.61 %	48 min	1.12
P_1c	0.11 %	6 min	1.18	0.09 %	5 min	1.11
QC*	0.03 %	2 min	1.02	0.0 %	0 min	0.78
QC	0.03 %	2 min	1.17	0.0 %	0 min	0.77
V*	9.82 %	159 min	1.23			VRDT unsupported
V	2.9 %	62 min	1.18			VRDT unsupported
VC*	0.03 %	3 min	1.02			VRDT unsupported
VC	0.03 %	1 min	1.08			VRDT unsupported

even higher losses in reality, because the occurring outages would prevent the feed-in of PV-generated active energy for extended time periods.

The relative reduction in total outage time achieved by each building independently optimizing its energy costs, as opposed to using simple control algorithms, is far more substantial for the suburban grid than for the village grid. This is because the violations of the admissible voltage, transformer hot-spot temperature, and line current ranges are less severe in the suburban grid. When using the same measures to reduce violation magnitudes in both grids, grid components remain overloaded more often in the village grid, which makes the relative reduction in total outage time less significant.

The use of active power flexibility via the optimization with regard to active power targets further reduces the total outage time substantially compared to the optimization of energy costs. However, as mentioned earlier, this can not completely prevent all outages in this scenario, since the maximum potential line outage duration is slightly too long.

Table 5.22: Total outage times and PV active energies for all grid management strategies and selected management configurations. The simulated time period is the first week of July. The simulations use the suburban grid introduced in [162] and [32] and modified in Section 4.10. None = no grid management, * = no energy cost optimization, Conv. = fixed cos(φ) and static 70 % PV curtailment, Q = reactive-power-based voltage maintenance, P_1 = active power flexibility use through active power targets, P_2 = curtailment based active power flexibility, c = reactive power compensation, C = adaptive PV curtailment, V = VRDT-based voltage maintenance.

Man. config.	**Management strategy**			
	Centralized or distributed		**Decentralized**	
	Total outage time and PV active energy (loss)			
	Total outage time	**PV active energy (loss)**	**Total outage time**	**PV active energy (loss)**
None*	9.15 %	44.9 MWh (0.0 %)	9.15 %	44.9 MWh (0.0 %)
None	1.88 %	44.9 MWh (0.0 %)	1.88 %	44.9 MWh (0.0 %)
Conv.	3.94 %	43.75 MWh (-2.57 %)	3.94 %	43.75 MWh (-2.57 %)
Q*	13.52 %	44.9 MWh (0.0 %)	14.05 %	44.9 MWh (0.0 %)
Q	7.22 %	44.9 MWh (0.0 %)	7.64 %	44.9 MWh (0.0 %)
c	1.79 %	44.9 MWh (0.0 %)	1.79 %	44.9 MWh (0.0 %)
P_1c	0.06 %	44.9 MWh (0.0 %)	0.06 %	44.9 MWh (0.0 %)
QC*	0.0 %	42.65 MWh (-5.02 %)	0.0 %	38.69 MWh (-13.84 %)
QC	0.0 %	43.98 MWh (-2.07 %)	0.0 %	40.16 MWh (-10.58 %)
QCP_1c	0.0 %	44.49 MWh (-0.93 %)	0.0 %	42.04 MWh (-6.38 %)
QCP_1c-p	0.0 %	44.48 MWh (-0.94 %)	0.0 %	42.31 MWh (-5.78 %)
QCP_2c	0.0 %	44.48 MWh (-0.94 %)	0.0 %	41.73 MWh (-7.08 %)
QCP_2c-p	0.0 %	44.55 MWh (-0.8 %)	0.0 %	42.51 MWh (-5.34 %)
V*	12.28 %	44.9 MWh (0.0 %)		VRDT unsupported
V	3.47 %	44.9 MWh (0.0 %)		VRDT unsupported
VC*	0.0 %	42.65 MWh (-5.01 %)		VRDT unsupported
VC	0.0 %	44.17 MWh (-1.64 %)		VRDT unsupported
VCP_1c	0.0 %	44.68 MWh (-0.5 %)		VRDT unsupported
VCP_1c-p	0.0 %	44.6 MWh (-0.67 %)		VRDT unsupported
VCP_2c	0.0 %	44.62 MWh (-0.64 %)		VRDT unsupported
VCP_2c-p	0.0 %	44.71 MWh (-0.44 %)		VRDT unsupported

While voltage maintenance increases the total outage time if no PV curtailment is used, the increase is substantially lower when using VRDT-based instead of reactive-power-based voltage maintenance in this scenario. This can be explained in the same way as the substantial reductions in the total outage time when using energy cost optimization instead of simple control algorithms. Since the violations that lead to outages are less severe in the suburban grid than in the village grid, the moderately lower currents incurred

when using a VRDT instead of reactive power lead to a more substantial reduction in total outage time for the suburban grid.

If adaptive PV curtailment is used, the first active power flexibility use method performs better than the second method, when the standard PV generation prediction method is used. However, this situation is reversed, when presupposing a perfect PV generation prediction, where the performance of the first active power flexibility use method is slightly decreased, while the performance of the second method is increased. This can be understood by recalling the observations for the village grid, which already show that the first method does not benefit as much from perfect PV generation prediction as the second method. In this case, this circumstance even leads to a very slight performance decrease when using the first method in combination with perfect PV generation prediction in the centralized or distributed strategies. However, the outcomes can be different for other time periods, grids, and management strategies. This can be observed for the decentralized strategy, in which the first method benefits moderately from the perfect prediction, both in this scenario and in the intermediate time period discussed in the following section.

It is noteworthy that the conventional management configuration incurs substantially higher losses of PV active energy than the combination of adaptive PV curtailment and active power flexibility use in the centralized and distributed strategies, while still not being able to prevent outages. This shows the high precision of the measures developed in this thesis when it comes to avoiding both outages as well as losses of PV active energy.

The losses of PV active energy incurred when using PV curtailment are substantially higher for the decentralized strategy than for the other strategies. The reasons for this are the same as for the substantially lower maximum transformer hot-spot temperatures and line currents discussed earlier as well as the more moderate increases in losses of PV active energy observed when using the decentralized strategy in the village grid.

To visualize the evaluation results for this scenario, Figure 5.5 shows the profiles of the previously analyzed aspects for an exemplary day of the summer time period. July 1 is chosen for this scenario because it exhibits the highest amount of active energy potentially generatable by PV systems in the simulated time period.

Figure 5.5 shows some of the previously observed behaviors of the different management configurations.

The voltage profiles for the management configurations employing active power flexibility use show substantially lower voltages in the two hours before noon. This indicates again that voltage maintenance is not strictly necessary for the suburban grid, as long as some form of energy flow optimization, preferably with regard to active power targets, is used.

When observing the transformer hot-spot temperature profiles, it is evident that PV curtailment would only be necessary for the management configuration that neither employs grid management measures nor energy flow optimization. All other management configurations keep the transformer hot-spot temperatures well below the minimum temperature that triggers the use of PV curtailment for transformer disturbances (107 °C,

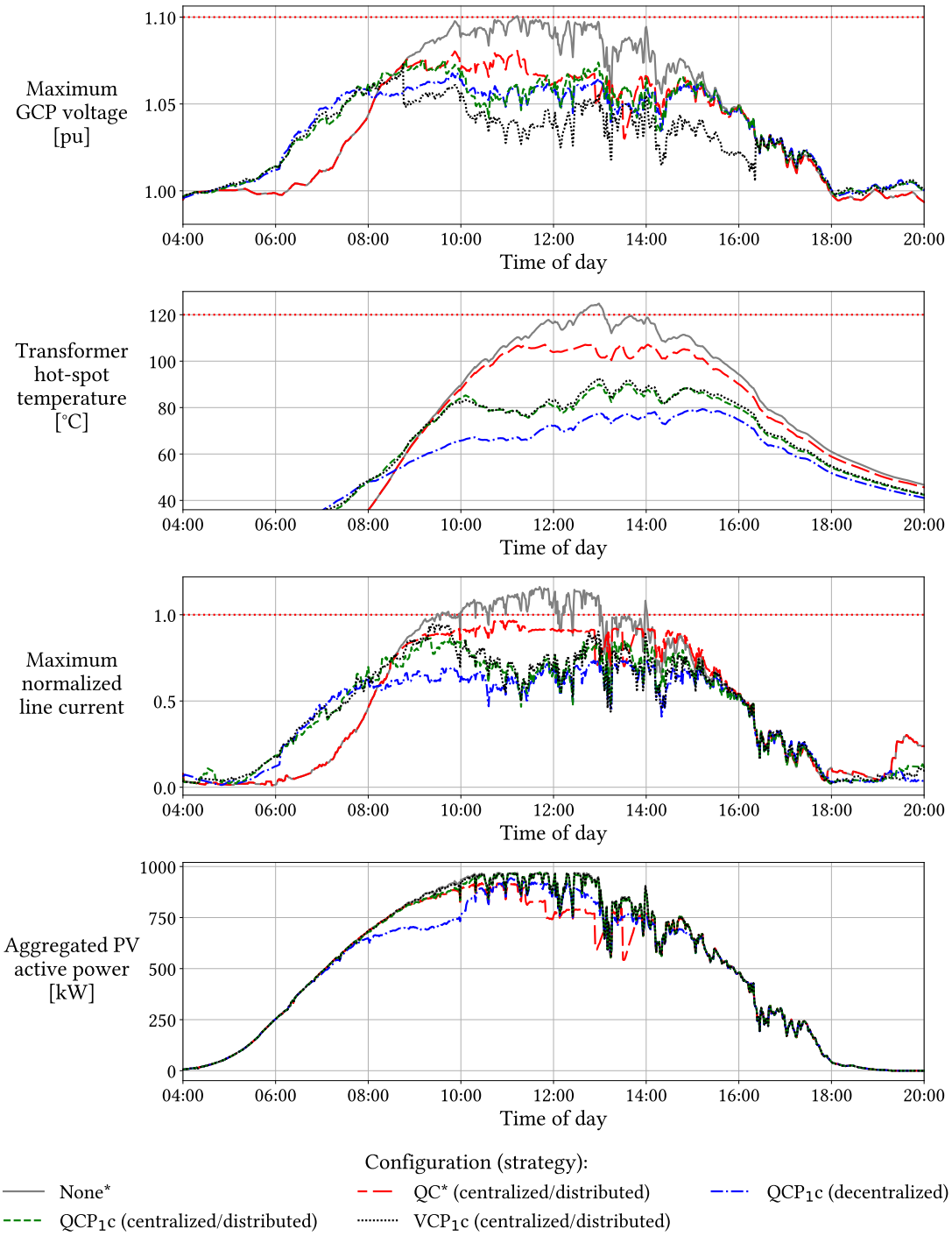

Figure 5.5: Profiles of the maximum GCP voltage in the grid, the transformer hot-spot temperature, the maximum normalized line current in the grid, and the active power generated by PV systems for July 1 and the suburban grid. Maximum admissible values are indicated by red dotted lines. None = no grid management, * = no energy cost optimization, Q = reactive-power-based voltage maintenance, P_1 = active power flexibility use through active power targets, c = reactive power compensation, C = adaptive PV curtailment, V = VRDT-based voltage maintenance.

see also Section 4.12). The temperature profile is the lowest for the decentralized strategy due to the reasons stated previously in this section.

The line current profile for the decentralized strategy is substantially lower before noon than the other profiles. This is caused by the continuous application of the learned apparent power limit for transformer disturbances, as opposed to the adaptive application of apparent power limits in the other strategies.

The aggregated PV active power profiles of the management configurations utilizing optimization with regard to active power targets and the centralized or distributed strategies follow the base profile without any grid management measures almost exactly, since these configurations use PV curtailment very sparsely. The profile for the management configuration that only uses reactive-power-based voltage maintenance and PV curtailment is considerably lower from approximately 11:30 to 14:00, since the lines as well as the transformer require substantial PV curtailment during this time period. The profile for the decentralized strategy is lower on average as well, especially before 10:00, again due to the continuous application of the learned apparent power limit for PV curtailment.

5.1.3.2. Intermediate

The voltage-related results for the eight-day time period from March 31 to April 7 are given in Table 5.23.

Since the results in Table 5.23 show the same qualitative behaviors as the results for the summer time period, only on lower voltage outage time and maximum GCP voltage levels, they are not analyzed further at this point (see also Section 5.1.3.1).

Table 5.24 contains the transformer-related results for the same time period.

While the results in Table 5.24 show the same qualitative behaviors as the results for the summer time period, it is noteworthy that, in this scenario, no measures are needed to keep the transformer hot-spot temperature below the maximum admissible value of 120 °C.

Table 5.25 shows the line-related results for the intermediate time period.

Again, the results in Table 5.25 indicate the same qualitative behaviors that can be observed in the summer time period. Due to the lower amount of potentially generatable PV active energy in the intermediate time period, the use of reactive power compensation and the optimization with regard to active power targets without further measures achieves a potential line outage time of 0.0 % in this scenario. However, the values in the table are rounded to two decimal places and the maximum normalized line current is still above the rated current at 1.03. This means that if no PV curtailment is used, recurrent exceedances of the rated line current could still wear down the utilized fuses over time in the intermediate time period. This is why the value for this configuration is given in square brackets. When using the same management configuration in the decentralized strategy, the maximum normalized line current is lower than 1.0. However, this can be assumed to be a coincidence due to the different criteria used to trigger the use of active power

Table 5.23: Outage times due to violations of the admissible voltage range at one or more GCPs in the grid and maximum GCP voltages for all grid management strategies and selected management configurations. The simulated time period is the last day of March and the first week of April. The simulations use the suburban grid introduced in [162] and [32] and modified in Section 4.10. None = no grid management, * = no energy cost optimization, Conv. = static cos(φ) and 70 % PV curtailment, Q = reactive-power-based voltage maintenance, P_1 = active power flexibility use through active power targets, c = reactive power compensation, V = VRDT-based voltage maintenance.

Management configuration	**Management strategy**			
	Centralized or distributed		**Decentralized**	
	Voltages outside of admissible range (±10 %)			
	Voltage outage time	**Maximum GCP voltage**	**Voltage outage time**	**Maximum GCP voltage**
None*	0.01 %	1.1004 pu	0.01 %	1.1004 pu
None	0.0 %	1.0872 pu	0.0 %	1.0872 pu
Conv.	0.0 %	1.0504 pu	0.0 %	1.0504 pu
Q*	0.0 %	1.0769 pu	0.0 %	1.0755 pu
Q	0.0 %	1.0756 pu	0.0 %	1.0717 pu
P_1c	0.0 %	1.0857 pu	0.0 %	1.083 pu
V*	0.0 %	1.0758 pu	VRDT unsupported	
V	0.0 %	1.0716 pu	VRDT unsupported	

flexibility in the decentralized strategy, which lead to deviating building load profiles. For longer durations and different time periods, the active power flexibility use in the decentralized strategy is not expected to keep line currents below the respective rated currents at all times.

The total outage times, which contain voltage-, transformer-, and line-related outages, as well as the PV active energies and corresponding losses for the intermediate time period are given in Table 5.26.

While the results in Table 5.26 are very similar to those for the summer time period, there is a noteworthy observation with regard to the use of the perfect PV generation prediction. For the centralized and distributed strategies, the latter causes increased losses of PV active energy compared to the standard PV generation prediction method. This can be explained by the already very small losses achieved using the standard method. Differences in the results of the optimization of energy costs or with regard to active power targets resulting from the different PV generation prediction methods, produce different building load profiles. Since the total outage time is very low in this scenario, even small load profile variations can lead to substantial relative differences in the losses of PV active energy. The evolutionary algorithm (EA) utilized for this thesis (see also Sections 2.1.4 and 2.4.2) is employed to find good solutions with low computational time rather than optimal solutions. Furthermore, the prediction of other quantities than the

Table 5.24: Outage times due to violations of the maximum admissible transformer hot-spot temperature and maximum transformer hot-spot temperatures for all grid management strategies and selected management configurations. The simulated time period is the last day of March and the first week of April. The simulations use the suburban grid introduced in [162] and [32] and modified in Section 4.10. None = no grid management, * = no energy cost optimization, Conv. = static cos(φ) and 70 % PV curtailment, Q = reactive-power-based voltage maintenance, P_1 = active power flexibility use through active power targets, c = reactive power compensation, C = adaptive PV curtailment, V = VRDT-based voltage maintenance.

Management configuration	**Management strategy**			
	Centralized or distributed		**Decentralized**	
	Admissible transformer hot-spot temperature (120 °C) exceeded			
	Transformer outage time	**Maximum temperature**	**Transformer outage time**	**Maximum temperature**
None*	0.0 %	107.12 °C	0.0 %	107.12 °C
None	0.0 %	88.06 °C	0.0 %	88.06 °C
Conv.	0.0 %	102.84 °C	0.0 %	102.84 °C
Q*	0.0 %	114.95 °C	0.0 %	118.59 °C
Q	0.0 %	92.77 °C	0.0 %	93.3 °C
c	0.0 %	87.71 °C	0.0 %	87.71 °C
P_1c	0.0 %	83.02 °C	0.0 %	81.19 °C
QC*	0.0 %	106.78 °C	0.0 %	79.3 °C
QC	0.0 %	91.69 °C	0.0 %	72.41 °C
V*	0.0 %	113.51 °C	VRDT unsupported	
V	0.0 %	90.5 °C	VRDT unsupported	
VC*	0.0 %	107.16 °C	VRDT unsupported	
VC	0.0 %	90.6 °C	VRDT unsupported	

PV generation, such as the hot water tank temperature, are not perfectly predicted when using the perfect PV generation prediction. The imperfections in both the optimization algorithm as well as the prediction of relevant quantities can lead to situations in which one PV generation peak can randomly be slightly higher when using the perfect instead of the standard PV generation prediction. This slightly higher peak can then trigger PV curtailment and consequently increase losses of PV active energy, while a slightly lower peak does not. For the decentralized strategy, where the PV active energy loss level is substantially higher, such effects are not as prominent. As a consequence, the perfect PV generation prediction performs better than the standard prediction method when using the decentralized strategy in this scenario.

To visualize the evaluation results for this scenario, Figure 5.6 shows the profiles of the previously analyzed aspects for an exemplary day of the intermediate time period. April 7 is chosen for this scenario because it exhibits the highest amount of active energy potentially generatable by PV systems in the simulated time period.

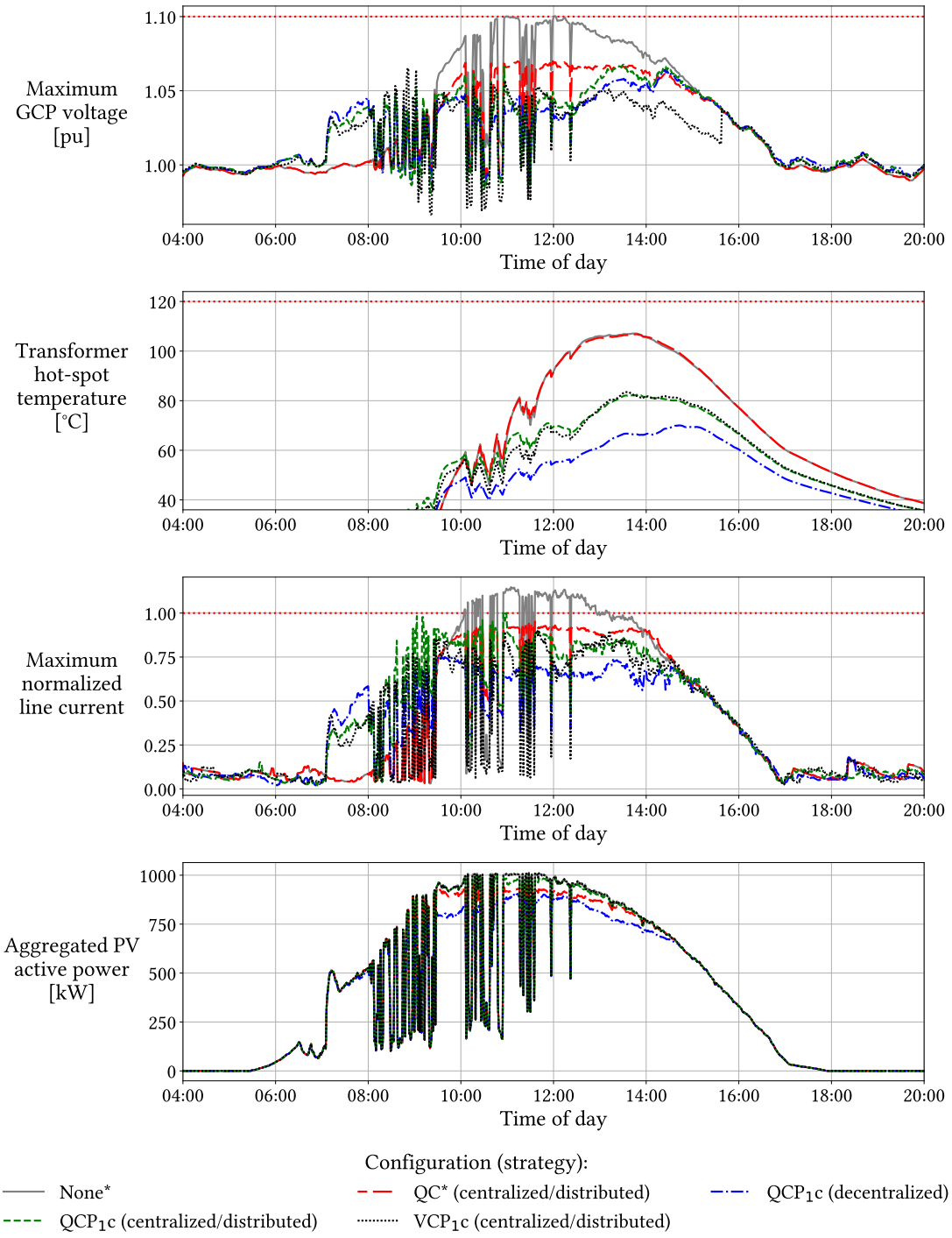

Figure 5.6: Profiles of the maximum GCP voltage in the grid, the transformer hot-spot temperature, the maximum normalized line current in the grid, and the active power generated by PV systems for April 7 and the suburban grid. Maximum admissible values are indicated by red dotted lines. None = no grid management, * = no energy cost optimization, Q = reactive-power-based voltage maintenance, P_1 = active power flexibility use through active power targets, c = reactive power compensation, C = adaptive PV curtailment, V = VRDT-based voltage maintenance.

Table 5.25: Potential outage times due to violations of the rated line current of one or more lines in the grid and maximum potential line outage durations for all grid management strategies and selected management configurations. The simulated time period is the last day of March and the first week of April. The simulations use the suburban grid introduced in [162] and [32] and modified in Section 4.10. None = no grid management, * = no energy cost optimization, Conv. = static cos(φ) and 70 % PV curtailment, Q = reactive-power-based voltage maintenance, P_1 = active power flexibility use through active power targets, c = reactive power compensation, C = adaptive PV curtailment, V = VRDT-based voltage maintenance.

Man. config.	**Management strategy**					
	Centralized or distributed			**Decentralized**		
	Rated current of one or more lines exceeded					
	Potential line outage time	**Max. pot. line outage duration**	**Maximum normalized line current**	**Potential line outage time**	**Max. pot. line outage duration**	**Maximum normalized line current**
None*	1.41 %	52 min	1.16	1.41 %	52 min	1.16
None	0.01 %	2 min	1.01	0.01 %	2 min	1.01
Conv.	0.2 %	33 min	1.05	0.2 %	33 min	1.05
Q*	2.75 %	116 min	1.3	2.76 %	92 min	1.28
Q	0.59 %	39 min	1.16	0.55 %	39 min	1.13
c	0.01 %	2 min	1.0	0.01 %	2 min	1.0
P_1c	[0.0 %]	1 min	1.03	0.0 %	0 min	0.94
QC*	0.03 %	2 min	1.15	0.0 %	0 min	0.77
QC	0.02 %	2 min	1.06	0.0 %	0 min	0.76
V*	1.85 %	82 min	1.21		VRDT unsupported	
V	0.03 %	4 min	1.03		VRDT unsupported	
VC*	0.03 %	2 min	1.1		VRDT unsupported	
VC	0.01 %	2 min	1.03		VRDT unsupported	

While the maximum GCP voltage and maximum normalized line current profiles show very similar behaviors as the profiles for the exemplary day in the summer time period, there are some notable differences in the transformer hot-spot temperature and aggregated PV active power profiles.

The transformer hot-spot temperature profile for the management configuration that uses only reactive-power-based voltage maintenance and adaptive PV curtailment follows the baseline profile for the management configuration without any grid management measures very closely. This visualizes the previously observed circumstance that no measures, such as PV curtailment, are needed to keep the transformer hot-spot temperature below the maximum admissible value in this scenario. This can also be observed in the respective aggregated PV active power profile, which is closer to the baseline profile as well.

The aggregated PV active power profile for the decentralized strategy is flatter in the intermediate than in the summer time period. This can be explained when taking the

Table 5.26: Total outage times and PV active energies for all grid management strategies and selected management configurations. The simulated time period is the first week of April. The simulations use the suburban grid introduced in [162] and [32] and modified in Section 4.10. None = no grid management, * = no energy cost optimization, Conv. = fixed cos(φ) and static 70 % PV curtailment, Q = reactive-power-based voltage maintenance, P_1 = active power flexibility use through active power targets, P_2 = curtailment based active power flexibility, c = reactive power compensation, C = adaptive PV curtailment, V = VRDT-based voltage maintenance.

Man. config.	**Management strategy**			
	Centralized or distributed		**Decentralized**	
	Total outage time and PV active energy (loss)			
	Total outage time	**PV active energy (loss)**	**Total outage time**	**PV active energy (loss)**
None*	1.62 %	26.31 MWh (0.0 %)	1.62 %	26.31 MWh (0.0 %)
None	0.01 %	26.31 MWh (0.0 %)	0.01 %	26.31 MWh (0.0 %)
Conv.	0.23 %	26.04 MWh (-1.0 %)	0.23 %	26.04 MWh (-1.0 %)
Q*	3.14 %	26.31 MWh (0.0 %)	3.15 %	26.31 MWh (0.0 %)
Q	0.67 %	26.31 MWh (0.0 %)	0.63 %	26.31 MWh (0.0 %)
c	0.01 %	26.31 MWh (0.0 %)	0.01 %	26.31 MWh (0.0 %)
P_1c	[0.0 %]	26.31 MWh (0.0 %)	0.0 %	26.31 MWh (0.0 %)
QC*	0.0 %	26.04 MWh (-1.0 %)	0.0 %	24.58 MWh (-6.55 %)
QC	0.0 %	26.22 MWh (-0.34 %)	0.0 %	25.05 MWh (-4.76 %)
QCP_1c	0.0 %	26.26 MWh (-0.18 %)	0.0 %	25.4 MWh (-3.46 %)
QCP_1c-p	0.0 %	26.19 MWh (-0.44 %)	0.0 %	25.49 MWh (-3.11 %)
QCP_2c	0.0 %	26.24 MWh (-0.25 %)	0.0 %	25.36 MWh (-3.58 %)
QCP_2c-p	0.0 %	26.18 MWh (-0.48 %)	0.0 %	25.46 MWh (-3.2 %)
V*	2.12 %	26.31 MWh (0.0 %)		VRDT unsupported
V	0.03 %	26.31 MWh (0.0 %)		VRDT unsupported
VC*	0.0 %	26.12 MWh (-0.69 %)		VRDT unsupported
VC	0.0 %	26.29 MWh (-0.04 %)		VRDT unsupported
VCP_1c	0.0 %	26.31 MWh (0.0 %)		VRDT unsupported
VCP_1c-p	0.0 %	26.24 MWh (-0.24 %)		VRDT unsupported
VCP_2c	0.0 %	26.31 MWh (0.0 %)		VRDT unsupported
VCP_2c-p	0.0 %	26.24 MWh (-0.24 %)		VRDT unsupported

deviating weather conditions in the different seasons into account. As mentioned earlier, the standard PV generation prediction method of the OSH calculates predicted generation profiles by averaging the generation profiles of the preceding 14 days. In the intermediate time period, the PV generation profiles are more strongly linked to weather conditions such as cloudy skies or rain and less strongly linked to the actual sun path than they are in summer. As a consequence, the predicted generation profiles are flatter in the intermediate than in the summer time period. Since the predicted generation profiles are part of

the inputs for the optimization with regard to active power targets, the corresponding optimized device schedules result in a more temporally distributed active power flexibility use that produces flatter curtailed aggregated PV active power profiles.

5.1.3.3. Winter

The total outage times, which contain voltage-, transformer-, and line-related outages, as well as the PV active energies and corresponding losses for the time period from January 1 to January 7 are given in Table 5.27. As there are no outages during this time period, we forgo the presentation and discussion of specific voltage-, transformer-, and line-related results.

As in the previously analyzed grids, the results in Table 5.27 show that there are no outages in the winter time period, even if no measures are taken. As a consequence, there are no relevant differences between the tested management configurations and strategies. However, as in the village grid, in contrast to the other strategies, the decentralized strategy shows very minor losses of PV active energy if PV curtailment is used. The reasons for this are the same as in the village grid and thus not discussed again at this point. In the suburban grid, the conventional management configuration incurs very minor losses as well, since the static 70 % PV curtailment utilized in this configuration slightly curtails the highest occurring PV generation peaks.

5.2. Communication Disruption

Some text passages of this section are transferred verbatim from one of our own publications [34]. For a summary of this publication, its relation to this thesis, and its mapping to our research questions, see Section 1.4.

In this section, the ability of the developed grid management system to maintain reliable grid operation during communication disruption is evaluated. We thereby answer a part of Sub-Question 3.3 of Research Question 3.

In the chosen evaluation scenario, different communication disruptions occur at different times of the day. July 1 is chosen as the basis for this scenario, as it is the day with the highest amount of potentially generatable PV active energy among the time periods simulated for the comparative evaluation in the previous section and consequently the highest potential for electricity outages. We only use the village grid for the following evaluation, as the results in Section 5.1 show that this grid incurs the most electricity outages out of the three evaluated grids if no countermeasures are applied. In contrast to the simulations in Section 5.1, we already apply the appropriate learned apparent power limits for PV curtailment at the beginning of the simulated time period. This is because the learning process is not the focus of the communication disruption and participant misconduct scenarios. Furthermore, the learning process starts with the activation of the grid management system, and the time spent learning the appropriate limits is very short

Table 5.27: Total outage times and PV active energies for all grid management strategies and selected management configurations. The simulated time period is the first week of January. The simulations use the suburban grid introduced in [162] and [32] and modified in Section 4.10. None = no grid management, * = no energy cost optimization, Conv. = fixed cos(φ) and static 70 % PV curtailment, Q = reactive-power-based voltage maintenance, P_1 = active power flexibility use through active power targets, P_2 = curtailment based active power flexibility, c = reactive power compensation, C = adaptive PV curtailment, perf. = perfect PV generation prediction, V = VRDT-based voltage maintenance.

Man. config.	**Management strategy**			
	Centralized or distributed		**Decentralized**	
	Total outage time and PV active energy (loss)			
	Total outage time	**PV active energy (loss)**	**Total outage time**	**PV active energy (loss)**
None*	0.0 %	3.35 MWh (0.0 %)	0.0 %	3.35 MWh (0.0 %)
None	0.0 %	3.35 MWh (0.0 %)	0.0 %	3.35 MWh (0.0 %)
Conv.	0.0 %	3.35 MWh (-0.0 %)	0.0 %	3.35 MWh (-0.0 %)
Q*	0.0 %	3.35 MWh (0.0 %)	0.0 %	3.35 MWh (0.0 %)
Q	0.0 %	3.35 MWh (0.0 %)	0.0 %	3.35 MWh (0.0 %)
c	0.0 %	3.35 MWh (0.0 %)	0.0 %	3.35 MWh (0.0 %)
P_1c	0.0 %	3.35 MWh (0.0 %)	0.0 %	3.35 MWh (0.0 %)
QC*	0.0 %	3.35 MWh (0.0 %)	0.0 %	3.35 MWh (-0.0 %)
QC	0.0 %	3.35 MWh (0.0 %)	0.0 %	3.35 MWh (-0.0 %)
QCP_1c	0.0 %	3.35 MWh (0.0 %)	0.0 %	3.35 MWh (-0.02 %)
QCP_1c-p	0.0 %	3.35 MWh (0.0 %)	0.0 %	3.35 MWh (-0.01 %)
QCP_2c	0.0 %	3.35 MWh (0.0 %)	0.0 %	3.35 MWh (-0.04 %)
QCP_2c-p	0.0 %	3.35 MWh (0.0 %)	0.0 %	3.35 MWh (-0.02 %)
V*	0.0 %	3.35 MWh (0.0 %)		VRDT unsupported
V	0.0 %	3.35 MWh (0.0 %)		VRDT unsupported
VC*	0.0 %	3.35 MWh (0.0 %)		VRDT unsupported
VC	0.0 %	3.35 MWh (0.0 %)		VRDT unsupported
VCP_1c	0.0 %	3.35 MWh (0.0 %)		VRDT unsupported
VCP_1c-p	0.0 %	3.35 MWh (0.0 %)		VRDT unsupported
VCP_2c	0.0 %	3.35 MWh (0.0 %)		VRDT unsupported
VCP_2c-p	0.0 %	3.35 MWh (0.0 %)		VRDT unsupported

compared to the total operating time of the system. We therefore consider scenarios in which ICT disturbances occur after the learning process is completed more representative of real-world conditions.

The default grid management strategy for this scenario is the centralized strategy. The first communication disruption occurs at 08:00, when the distribution system operator (DSO) can not communicate anymore. This means that the buildings stop receiving new commands. Additionally, at 09:00, the first building stops to communicate. After that,

every three minutes an additional building ceases to communicate. This goes on until 10:57. At 11:00, the communication between the buildings is restored, but the transformer stops to communicate, and the communication to the DSO stays disrupted. At 12:00 the communication between all participants is fully restored.

Figure 5.7 shows the voltage, transformer hot-spot temperature, line current, and aggregated PV active power profiles for different communication disruption mitigation configurations when applying reactive-power-based voltage maintenance, adaptive PV curtailment, active power flexibility use via active power targets, and reactive power compensation. The profiles for a management configuration with no measures to combat electrical disturbances and no occurring communication disruptions (grey profiles) are given as a reference.

As can be gathered from Figure 5.7, the occurring communication disruptions lead to intense violations of the maximum admissible transformer hot-spot temperature if no communication disruption mitigation measures are implemented (red profiles). This occurs because the apparent power limits for PV curtailment last communicated by the DSO before it stops communicating are insufficiently restrictive to prevent violations of the maximum admissible transformer hot-spot temperature. However, since the apparent power limits for line disturbances are already sufficiently restrictive before the first communication disruption occurs, all line currents stay below the rated line current. The maximum GCP voltage stays inside the admissible voltage range as well, as the DSO already communicates reactive power setpoints before 08:00 in this scenario. However, since these setpoints are not updated after the communication disruption to the DSO, the highest maximum GCP voltage is higher than it would be if the reactive power setpoints were updated as usual. Only after the communication between all participants is fully restored, the DSO heavily decreases the apparent power limits of all buildings, such that the transformer hot-spot temperature decreases back below its admissible maximum value.

If the communication disruption mitigation measures presented in Section 4.6 are implemented (green profiles), all grid status indicators stay inside their respective acceptable ranges, regardless of the occurring communication disruptions. When the communication to the DSO starts to be disrupted, this is detected by the buildings, which consequently switch to the distributed grid management strategy and thus determine appropriate measures against electrical disturbances on their own, based on the data communicated by the other buildings and the transformer. When the buildings cease to communicate one by one, all buildings that can not communicate anymore switch to the decentralized strategy. Buildings that still communicate and receive data from other communicating buildings keep using the distributed strategy, as long as the voltages measured at their GCPs do not deviate too far from the voltages calculated in the power-flow studies based on the data communicated by the other still communicating buildings (see also Section 4.6). If a building detects that its measured GCP voltage deviates too far from the corresponding calculated voltage, it switches to the decentralized strategy, regardless of whether it and other buildings can still communicate. The described behaviors can not be reliably observed in the presented profiles, since the buildings that still use the distributed strategy adjust their reactive power and apparent power limits for PV curtailment to compensate for potentially

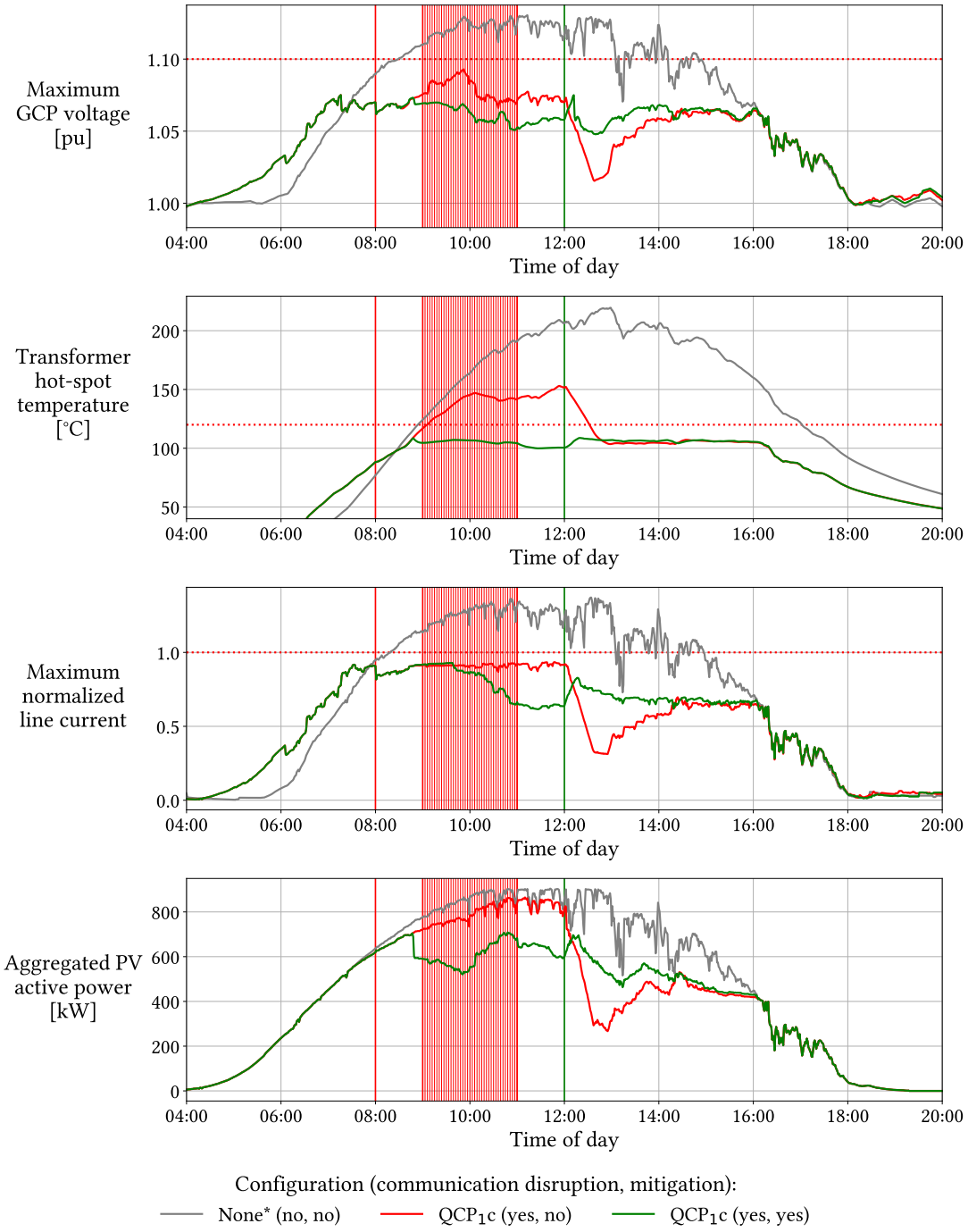

Figure 5.7: Profiles of the maximum GCP voltage in the grid, the transformer hot-spot temperature, the maximum normalized line current in the grid, and the active power generated by PV systems for July 1 and the village grid. The initial grid management strategy applied before any communication disruption occurs is the centralized strategy presented in Section 4.3.1. Red line at 08:00: DSO stops to communicate. Red lines between 09:00 and 10:57: buildings stop to communicate one after the other in three-minute intervals. Red line at 11:00: transformer stops to communicate, but all buildings communicate again. Green line at 12:00: all participants communicate again. Maximum admissible values are indicated by red dotted lines. None = no grid management, * = no energy cost optimization, Q = reactive-power-based voltage maintenance, C = adaptive PV curtailment, P_1 = active power flexibility use through active power targets, c = reactive power compensation. Based on a figure published by the author of this thesis in [336].

differing implemented limits determined by buildings using the decentralized strategy. When the transformer ceases to communicate, all buildings switch to the decentralized strategy. This can be observed in the transformer hot-spot temperature profile, which drops to a lower level, as the decentralized strategy uses the previously learned apparent power limit to prevent transformer disturbances, which is slightly lower than the limit actually needed for this particular time period. When the communication is fully restored, the buildings switch back to the centralized strategy and the DSO increases the apparent power limits again until the lower transformer hot-spot temperature threshold for PV curtailment (see also Algorithm 5) is reached. As a consequence, the maximum GCP voltage and line current increase as well.

Figure 5.8 shows the same scenarios, but using the distributed instead of the centralized grid management strategy as a starting point. In this case, communication disruption concerning the DSO is irrelevant.

While the grid status data profiles in Figure 5.8 are very similar to the ones in Figure 5.7 if communication disruption mitigation measures are used (green profiles), the profiles without those measures (red profiles) differ substantially. Since the distributed strategy is the default for the management configuration without communication disruption mitigation measures as well, the apparent power limits for PV curtailment can still be decreased by all buildings that still regularly receive updated data from the transformer. As a consequence, the transformer hot-spot temperature increases more slowly than in the previously shown scenario, where the centralized strategy is the default and the DSO fails to communicate. This leads to a situation where the admissible ranges for the different grid status data are not violated despite the occurrence of communication disruptions without mitigation measures. This shows that by using the distributed strategy by default, a significant point of failure would already be eliminated. However, when the communication to the transformer is disrupted at 11:00, but the buildings can communicate again, the buildings do not switch to the decentralized strategy in this case and still assume they can use the distributed strategy. Since the buildings do not receive updated transformer hot-spot temperatures anymore, they use the last communicated temperature to adjust their apparent power limits for PV curtailment. Consequently, as the temperature known to the buildings is too high and does not react to limit decreases, the limits are gradually decreased further until the transformer can communicate again. This can be observed as substantial dips in all status data profiles from 11:00 to approximately 13:00. This behavior is fully prevented by the communication disruption mitigation measures.

Figures 5.9 and 5.10 show the same scenarios as Figures 5.7 and 5.8, but using VRDT-based voltage maintenance instead of reactive-power-based voltage maintenance.

Figures 5.9 and 5.10 show very similar behaviors as Figures 5.7 and 5.8 respectively. However, there are notable differences in the voltage profiles due to the different voltage maintenance methods.

If the communication disruption mitigation measures are used (green profiles), the transformer switches its transmission ratio to the neutral position if it considers the voltages calculated in the power-flow studies by the DSO and the buildings unreliable. This is the

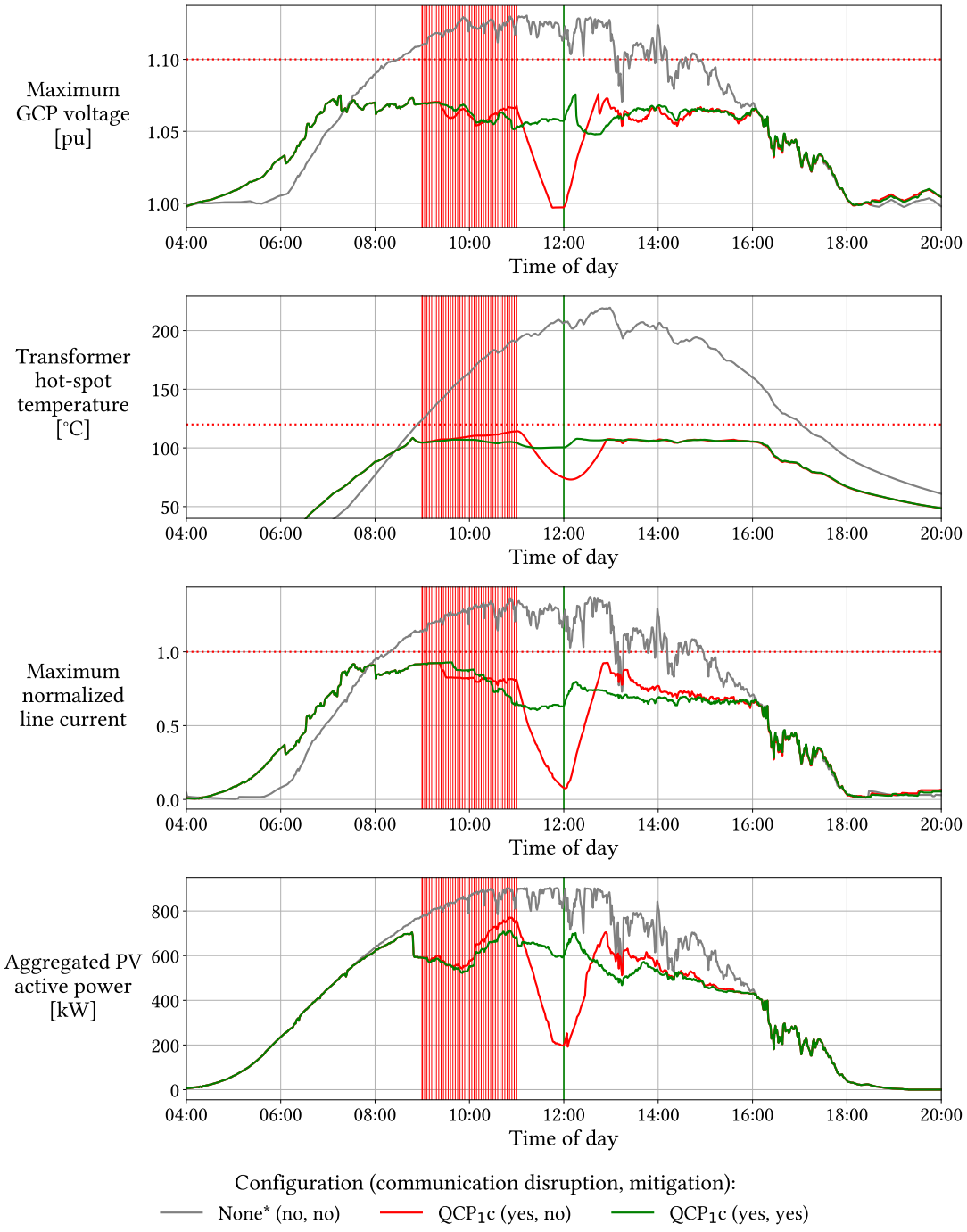

Figure 5.8: Profiles of the maximum GCP voltage in the grid, the transformer hot-spot temperature, the maximum normalized line current in the grid, and the active power generated by PV systems for July 1 and the village grid. The initial grid management strategy applied before any communication disruption occurs is the distributed strategy presented in Section 4.3.2. Red lines between 09:00 and 10:57: buildings stop to communicate one after the other in three-minute intervals. Red line at 11:00: transformer stops to communicate, but all buildings communicate again. Green line at 12:00: all participants communicate again. Maximum admissible values are indicated by red dotted lines. None = no grid management, * = no energy cost optimization, Q = reactive-power-based voltage maintenance, C = adaptive PV curtailment, P_1 = active power flexibility use through active power targets, c = reactive power compensation.

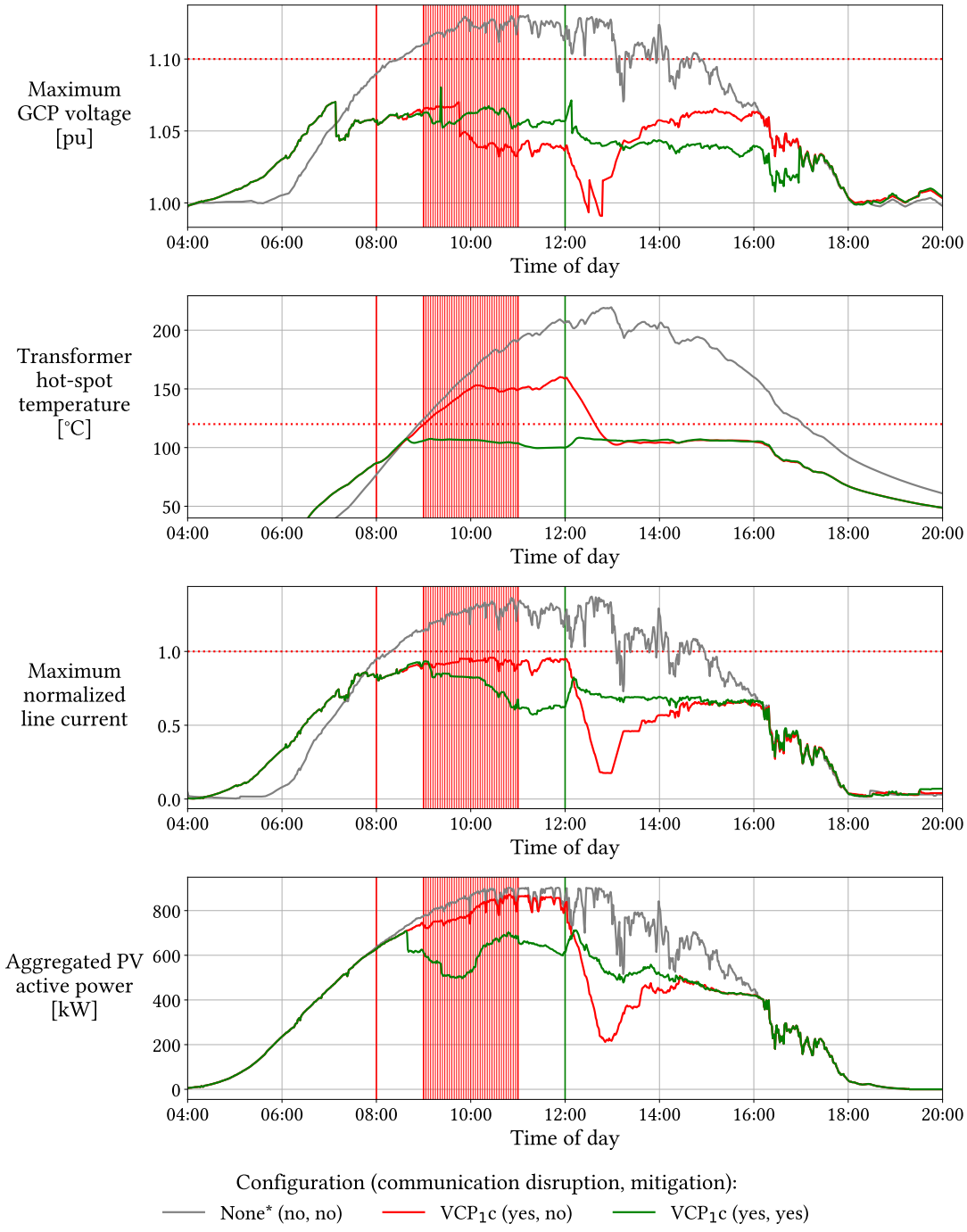

Figure 5.9: Profiles of the maximum GCP voltage in the grid, the transformer hot-spot temperature, the maximum normalized line current in the grid, and the active power generated by PV systems for July 1 and the village grid. The initial grid management strategy applied before any communication disruption occurs is the centralized strategy presented in Section 4.3.1. Red line at 08:00: DSO stops to communicate. Red lines between 09:00 and 10:57: buildings stop to communicate one after the other in three-minute intervals. Red line at 11:00: transformer stops to communicate, but all buildings communicate again. Green line at 12:00: all participants communicate again. Maximum admissible values are indicated by red dotted lines. None = no grid management, * = no energy cost optimization, V = VRDT-based voltage maintenance, C = adaptive PV curtailment, P_1 = active power flexibility use through active power targets, c = reactive power compensation.

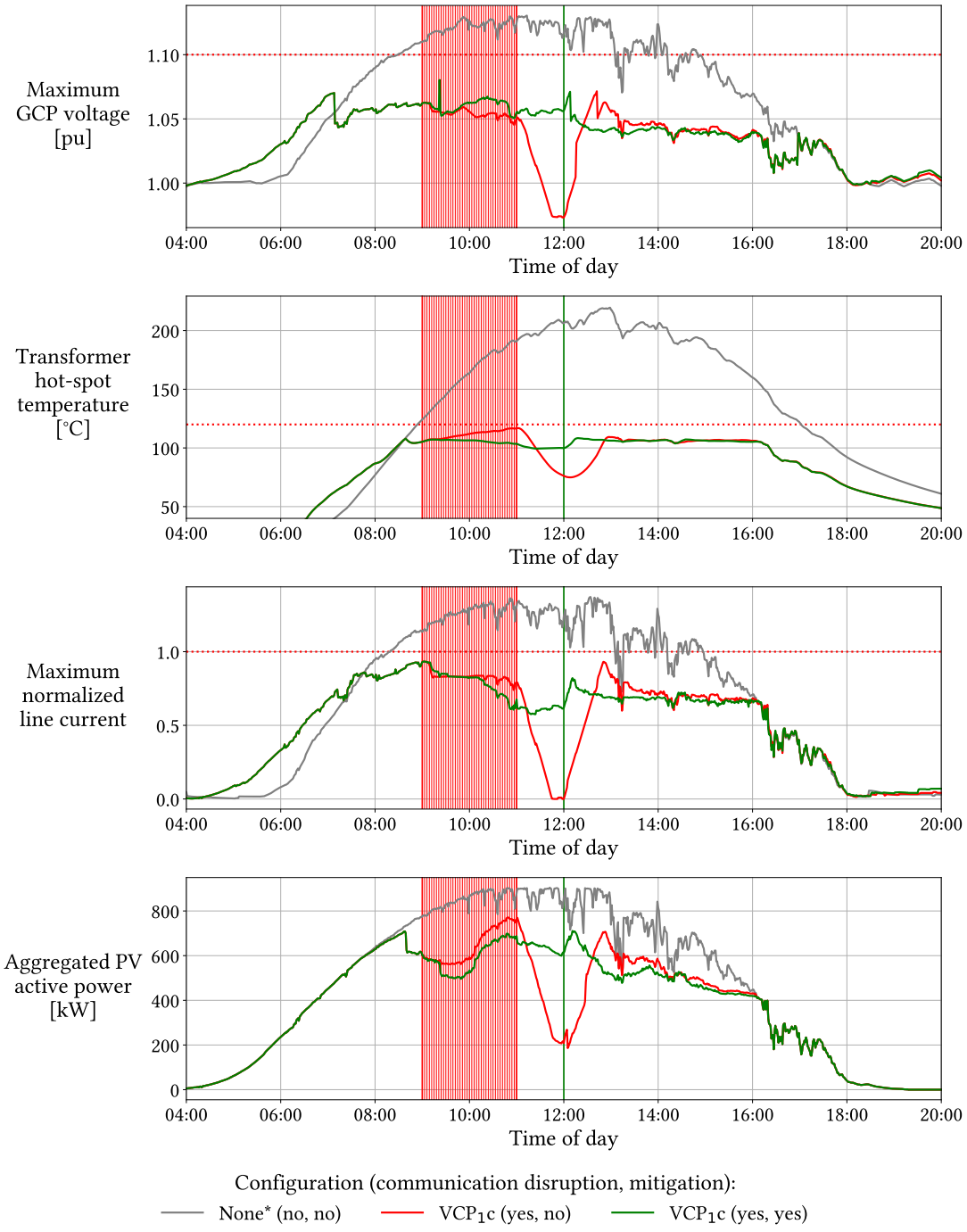

Figure 5.10: Profiles of the maximum GCP voltage in the grid, the transformer hot-spot temperature, the maximum normalized line current in the grid, and the active power generated by PV systems for July 1 and the village grid. The initial grid management strategy applied before any communication disruption occurs is the distributed strategy presented in Section 4.3.2. Red lines between 09:00 and 10:57: buildings stop to communicate one after the other in three-minute intervals. Red line at 11:00: transformer stops to communicate, but all buildings communicate again. Green line at 12:00: all participants communicate again. Maximum admissible values are indicated by red dotted lines. None = no grid management, * = no energy cost optimization, V = VRDT-based voltage maintenance, C = adaptive PV curtailment, P_1 = active power flexibility use through active power targets, c = reactive power compensation.

case if one or more buildings communicate that their measured GCP voltage deviates too far from the voltage calculated in their own power-flow studies or if less than 80 % of all buildings are still communicating updated GCP voltages. This behavior can be observed via the voltage peak at 09:24, when the transformer switches to its neutral position, because two buildings communicate that their calculated voltages are unreliable. This transformer switching operation is then quickly counteracted by the buildings, which receive clearance from the transformer to use reactive-power-based voltage maintenance and implement appropriate reactive power setpoints as soon as possible.

The described behavior does not occur if no communication disruption mitigation measures are used (red profiles). Here, the transformer acts as if the data communicated by the buildings is reliable and uses the last communicated GCP voltages of buildings that can not communicate anymore to decide on switching operations. In this particular scenario, this does not cause violations of the admissible voltage range. However, in different scenarios, such violations may occur.

5.3. Participant Misconduct

In this section, the performance of the participant misconduct mitigation measures introduced in Section 4.6.2 is evaluated using appropriate evaluation scenarios. We thereby answer another part of Sub-Question 3.3 of Research Question 3.

For the same reasons as in Section 5.2, July 1 and the village grid are chosen as the basis for the following scenarios. As in the simulation of the communication disruption scenarios, the appropriate learned apparent power limits for PV curtailment are already applied from the beginning of the simulated time period. The misconduct, either by the DSO, the transformer, or the buildings, occurs between 10:00 and 14:00, which is the time period with the highest amount of potentially generatable PV active energy in the chosen scenario. Such misconduct could be caused by internal actors, such as employees of the DSO or building inhabitants, or external actors, such as terrorists or agents of hostile governments performing cyberattacks. While the behaviors considered in this section are assumed to be intentional, the same or similar behaviors could occur unintentionally as well, for example due to hardware or software failure. The implemented mitigation measures work independently of the particular cause of the occurring misconduct.

5.3.1. Distribution System Operator Misconduct

The first participant misconduct scenario considers misconduct by the DSO. Starting at 10:00, the DSO continuously communicates apparent power limits for PV curtailment that allow for the full feed-in of PV-generated active power by all buildings regardless of the current grid status. Furthermore, the DSO communicates reactive power setpoints that increase all GCP voltages as far as possible.

Figure 5.11 shows the voltage, transformer hot-spot temperature, line current, and aggregated PV active power profiles for different participant misconduct mitigation configurations when applying reactive-power-based voltage maintenance, adaptive PV curtailment, active power flexibility use via active power targets, and reactive power compensation as well as the centralized grid management strategy. The profiles for a management configuration with no measures to combat electrical disturbances and no occurring participant misconduct (grey profiles) are given as a reference.

As can be gathered from Figure 5.11, the misconduct by the DSO leads to intense violations of the admissible ranges for all considered grid status indicators if no participant misconduct mitigation measures are implemented (red profiles). After the misconduct is stopped at 14:00, the DSO drastically decreases the apparent power limits for PV curtailment to bring the line currents and the transformer hot-spot temperature back below their respective admissible maxima. Furthermore, it scales back the reactive power setpoints to bring the GCP voltages back inside the admissible range as well. It should be noted that if this scenario occurred in the real world, grid operation would be highly compromised after 10:00. Protective equipment would be triggered by excessive voltages, which could entail electricity outages for at least some of the buildings. Furthermore, the excessive line currents would eventually cause the fuses protecting the lines to blow. Even if these problems did not occur, the transformer would likely fail after some time due to excessive hot-spot and oil temperatures.

The implemented misconduct mitigation measures introduced in Section 4.6.2.1 fully prevent these violations and thus electricity outages and equipment failure (green profiles). When the buildings receive the first malicious commands from the DSO, they detect this immediately and switch to the distributed grid management strategy, ignoring further commands from the DSO, until the commands are considered appropriate again at 14:00.

Figure 5.12 shows the same scenario as Figure 5.11, but using VRDT-based voltage maintenance instead of reactive-power-based voltage maintenance.

The transformer hot-spot temperature, line current, and aggregated PV active power profiles in Figure 5.12 are similar to the ones in Figure 5.11. However, the voltage profile differs substantially, especially if no misconduct mitigation measures are used (red profile). This is caused by the transformer, which counteracts the malicious reactive power setpoints communicated by the DSO by switching its transmission ratio to direct all GCP voltages back inside the admissible range. However, at 10:00, the transformer can not react quickly enough to prevent a short exceedance of the maximum admissible voltage.

The distributed grid management strategy is not separately tested as the default strategy for this misconduct scenario, as misconduct by the DSO would have no effect in that case. This shows that using the distributed strategy by default would already eliminate a significant attack vector.

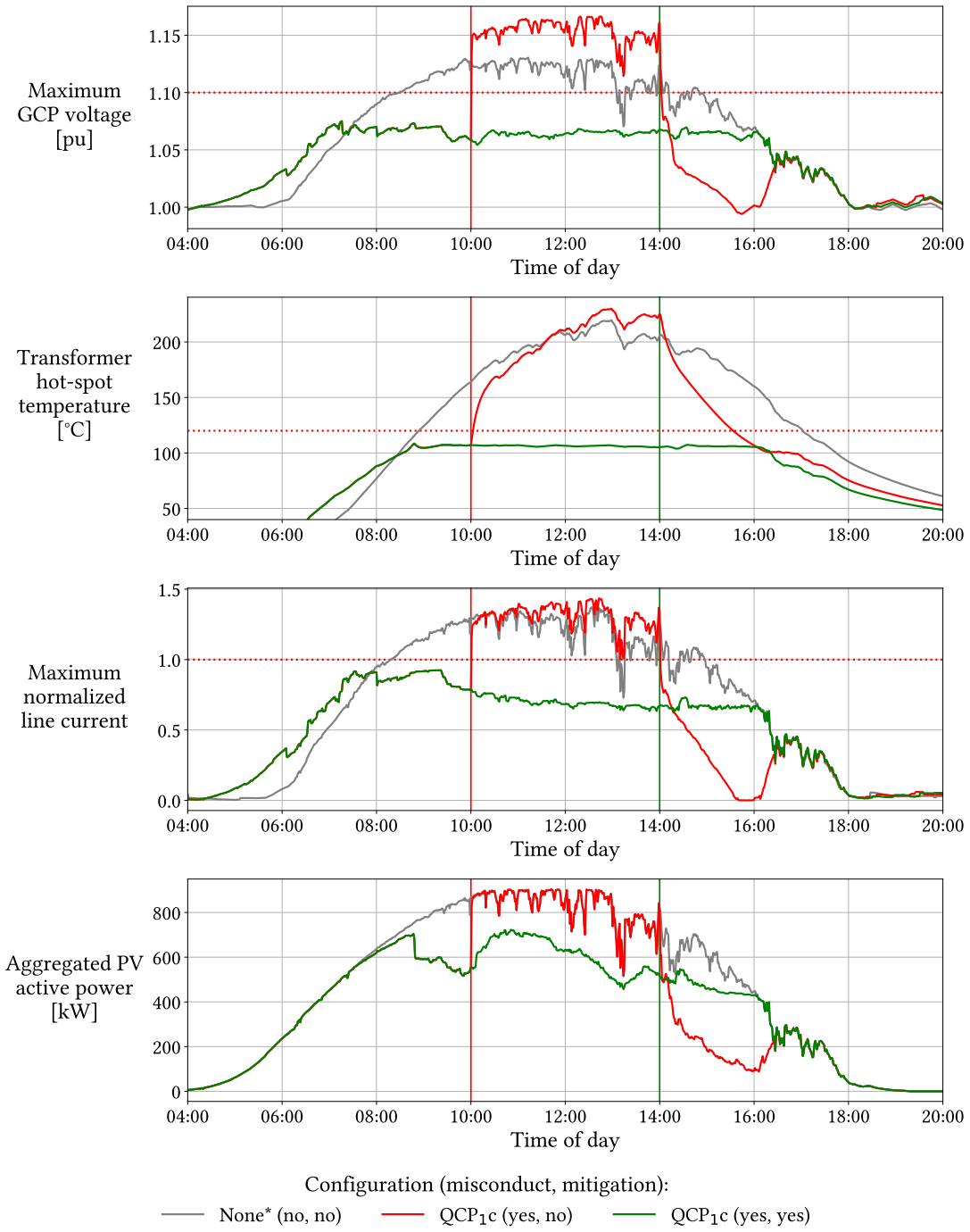

Figure 5.11: Profiles of the maximum GCP voltage in the grid, the transformer hot-spot temperature, the maximum normalized line current in the grid, and the active power generated by PV systems for July 1 and the village grid. The initial grid management strategy applied before any misconduct occurs is the centralized strategy presented in Section 4.3.1. Red line at 10:00: DSO maliciously starts to communicate false apparent power limits for PV curtailment and reactive power setpoints. Green line at 14:00: DSO stops misconduct. Maximum admissible values are indicated by red dotted lines. None = no grid management, * = no energy cost optimization, Q = reactive-power-based voltage maintenance, C = adaptive PV curtailment, P_1 = active power flexibility use through active power targets, c = reactive power compensation.

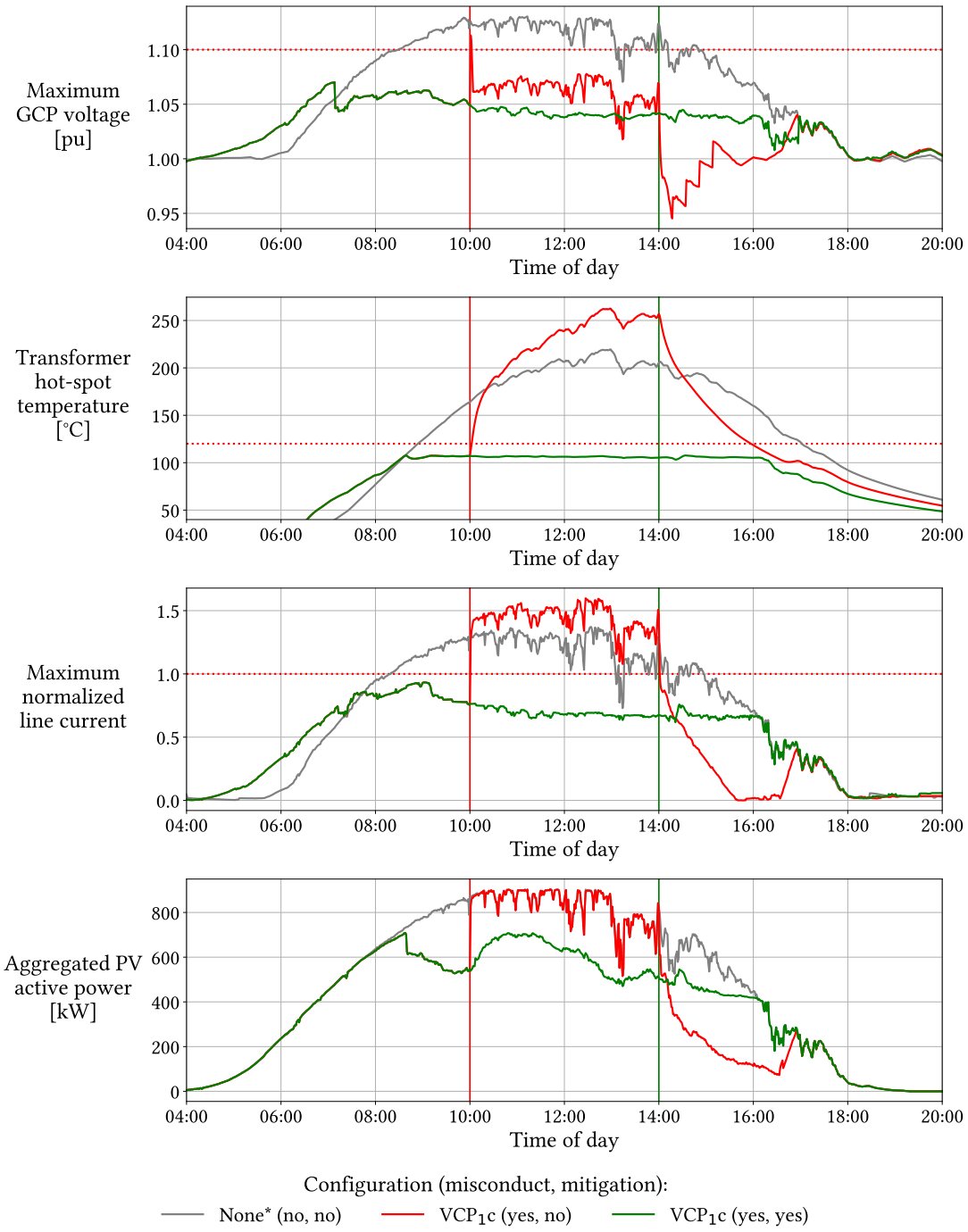

Figure 5.12: Profiles of the maximum GCP voltage in the grid, the transformer hot-spot temperature, the maximum normalized line current in the grid, and the active power generated by PV systems for July 1 and the village grid. The initial grid management strategy applied before any misconduct occurs is the centralized strategy presented in Section 4.3.1. Red line at 10:00: DSO maliciously starts to communicate false apparent power limits for PV curtailment and reactive power setpoints. Green line at 14:00: DSO stops misconduct. Maximum admissible values are indicated by red dotted lines. None = no grid management, * = no energy cost optimization, V = VRDT-based voltage maintenance, C = adaptive PV curtailment, P_1 = active power flexibility use through active power targets, c = reactive power compensation.

5.3.2. Transformer Misconduct

The second participant misconduct scenario considers misconduct by the transformer. Starting at 10:00, the transformer continuously communicates a hot-spot temperature of 20 °C, regardless of the currently measured temperature. It is important to note that the specific value of the incorrectly communicated temperature is not relevant as long as it is below the temperature thresholds that trigger PV curtailment (see also Sections 4.4 and 4.6.2.2).

Figure 5.13 shows the voltage, transformer hot-spot temperature, line current, and aggregated PV active power profiles for different participant misconduct mitigation configurations when applying reactive-power-based voltage maintenance, adaptive PV curtailment, active power flexibility use via active power targets, and reactive power compensation as well as the centralized grid management strategy. The profiles for a management configuration with no measures to combat electrical disturbances and no occurring participant misconduct (grey profiles) are given as a reference.

As can be gathered from Figure 5.13, the occurring misconduct by the transformer leads to substantial violations of the admissible maximum transformer hot-spot temperature if no participant misconduct mitigation measures are implemented (red profile). Since neither the DSO nor the buildings know the actual transformer hot-spot temperature after 10:00, they can not adjust the apparent power limits for PV curtailment accordingly. To the contrary, as they continuously receive a temperature of 20 °C, the DSO even scales back PV curtailment until the respective learned apparent power limits for line disturbances are reached. After the misconduct is stopped at 14:00, the DSO drastically decreases the apparent power limits to bring the transformer hot-spot temperature back below its admissible maximum value. The occurring exceedances of the latter between 10:00 and 14:00 would lead to substantially accelerated aging of the transformer oil at the least and to transformer failure as well as an electrical outage affecting the entire grid at the worst.

The participant misconduct mitigation measures introduced in Section 4.6.2.2 fully prevent these exceedances of the maximum admissible transformer hot-spot temperature (green profile). As soon as the DSO detects the implausibility of the temperature communicated by the transformer, it lets the buildings switch to the decentralized strategy, which does not decide on grid management measures based on the transformer hot-spot temperature. This can be observed in the transformer hot-spot temperature and line current profiles, which drop slightly after 10:00 and then stay relatively constant, due to the continuous application of the learned apparent power limits for PV curtailment in the decentralized strategy.

Figure 5.14 shows a scenario that is modified compared to the one shown in Figure 5.13. Here, VRDT-based voltage maintenance is used instead of reactive-power-based voltage maintenance. Furthermore, an additional type of misconduct by the transformer is introduced. At 10:00, the transformer not only starts to communicate false temperatures, but also switches its transmission ratio to increase voltages as far as possible. In the figure, four different misconduct and respective mitigation measure configurations are shown. In

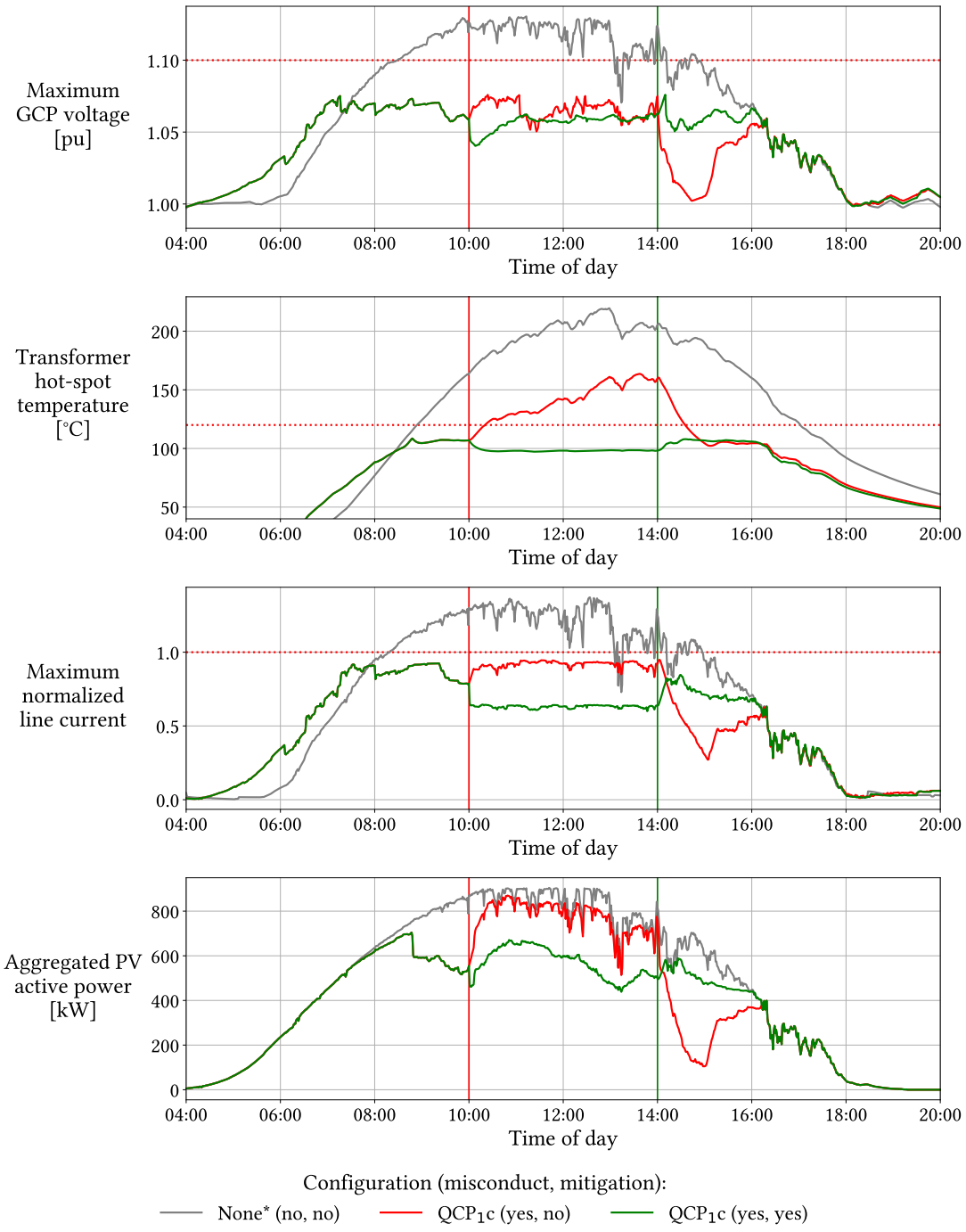

Figure 5.13: Profiles of the maximum GCP voltage in the grid, the transformer hot-spot temperature, the maximum normalized line current in the grid, and the active power generated by PV systems for July 1 and the village grid. The initial grid management strategy applied before any misconduct occurs is the centralized strategy presented in Section 4.3.1. Red line at 10:00: transformer maliciously starts to communicate a false transformer hot-spot temperature (20 °C). Green line at 14:00: transformer stops misconduct. Maximum admissible values are indicated by red dotted lines. None = no grid management, * = no energy cost optimization, Q = reactive-power-based voltage maintenance, C = adaptive PV curtailment, P_1 = active power flexibility use through active power targets, c = reactive power compensation.

the first configuration, the transformer only switches its transmission ratio to maximally increase all GCP voltages and no mitigation measures are used (black profiles). In the second configuration, the transformer additionally continuously communicates a hot-spot temperature of 20 °C (red profiles). In the third configuration, mitigation measures are used against the malicious transmission ratio switching, but not against the false temperatures (blue profiles). In the fourth configuration, mitigation measures against both types of misconduct are used (green profiles).

As shown in Figure 5.14, the malicious switching by the transformer results in very high maximum GCP voltages if no mitigation measures are implemented (black profiles). These voltages would likely cause electricity outages for at least some of the buildings in the grid. Voltages increase even further, when the transformer additionally communicates a hot-spot temperature of 20 °C, while the real temperature is substantially higher (red profile), since the DSO can not adjust the apparent power limits for PV curtailment according to the real temperature anymore. This results in violations of the maximum admissible transformer hot-spot temperature as well. However, line currents still stay below their respective rated values, as the learned apparent power limits for line disturbances are upheld indefinitely unless otherwise specified.

If only measures against malicious transmission ratio switching are used but the transformer performs both types of misconduct (blue profiles), the maximum GCP voltages are reduced substantially, but not sufficiently to keep voltages inside the admissible range and consequently prevent electricity outages. The transformer hot-spot temperatures and line currents are even higher in this case, due to the additional reactive power used to counteract the increased voltages. Only if mitigation measures against both misconduct types are used (green profiles), voltages and transformer hot-spot temperatures stay inside their admissible ranges in this scenario. In this case, the buildings not only use reactive-power-based voltage maintenance to counteract the malicious transmission ratio switching, but also switch to the decentralized strategy and consequently curtail their PV systems according to the learned apparent power limits for PV curtailment. This can be well observed in the aggregated PV active power profile, which drops substantially as soon as the misconduct by the transformer starts. It should be noted that the drop is not only caused by the changes of the apparent power limits for PV curtailment at 10:00, but also by the increased use of reactive power, which is considered when determining the maximum admissible PV active power according to Equations 4.21 to 4.24. If the duration of the transformer misconduct would be even longer, the maximum admissible transformer hot-spot temperature would be slightly violated even in this configuration, since the previously learned apparent power limits do not fully account for the extremely high use of reactive power in response to the malicious switching by the transformer. However, a duration of more than four hours of misconduct would already be very long and a slight violation of the maximum admissible transformer hot-spot temperature in such a situation would most likely not lead to equipment failure if the misconduct itself is stopped through administrative measures within a reasonable time frame.

The distributed grid management strategy is not separately tested as the default strategy for this misconduct scenario, as the corresponding grid status data profiles would look

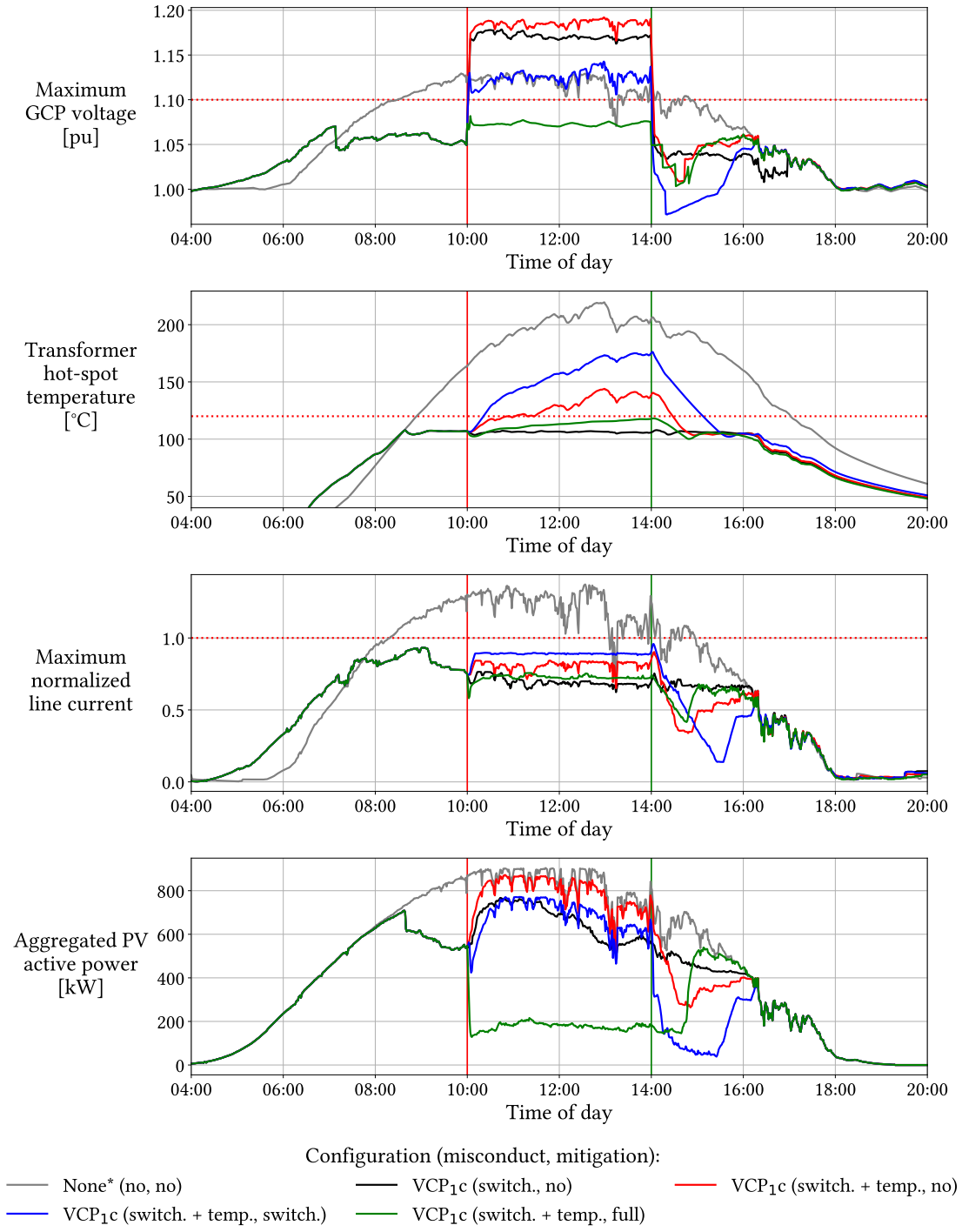

Figure 5.14: Profiles of the maximum GCP voltage in the grid, the transformer hot-spot temperature, the maximum normalized line current in the grid, and the active power generated by PV systems for July 1 and the village grid. The initial grid management strategy applied before any misconduct occurs is the centralized strategy presented in Section 4.3.1. Red line at 10:00: transformer maliciously starts to communicate a false transformer hot-spot temperature (20 °C) and to decrease the transmission ratio in one-minute time intervals until the lowest possible ratio is reached. Green line at 14:00: transformer stops misconduct. Maximum admissible values are indicated by red dotted lines. None = no grid management, * = no energy cost optimization, V = VRDT-based voltage maintenance, C = adaptive PV curtailment, P_1 = active power flexibility use through active power targets, c = reactive power compensation. switch. = malicious transmission ratio switching. temp. = malicious communication of incorrect transformer hot spot temperatures.

the same as for the centralized strategy. Whether the switch to the decentralized strategy at 10:00 is initiated by the DSO coming from the centralized strategy or by the buildings themselves coming from the distributed strategy, has no effect on the resulting building behavior after 10:00.

5.3.3. Building Misconduct

The third participant misconduct scenario considers misconduct by the buildings. Starting at 10:00, one group of five buildings (one building per feeder) after the other starts misconduct in ten-minute intervals. The misconduct comprises the disregard of apparent power limits for PV curtailment to allow for the full feed-in of PV-generated active power, regardless of the current grid status, as well as the implementation of reactive power setpoints that increase voltages in the grid as far as possible.

Figure 5.15 shows the voltage, transformer hot-spot temperature, line current, and aggregated PV active power profiles for different misconduct and respective mitigation configurations when applying reactive-power-based voltage maintenance, adaptive PV curtailment, active power flexibility use via active power targets, and reactive power compensation as well as the centralized grid management strategy. The profiles for a management configuration with no measures to combat electrical disturbances and no occurring misconduct (grey profiles) are given as a reference. In the figure, four different misconduct and respective mitigation measure configurations are shown. In the first configuration, up to five groups of five buildings (one building per feeder) start the previously described misconduct in ten-minute intervals, starting at 10:00 (black profiles). In the second configuration, the group-wise start of misconduct goes on until all buildings exhibit misconduct (red profiles). The third configuration is based on the first configuration, but mitigation measures are used by buildings that do not (yet) exhibit misconduct (green profiles). This configuration is presented because it represents the highest number of misbehaving buildings per feeder for which the remaining, normally behaving buildings can sufficiently compensate. The fourth configuration is based on the second configuration, but mitigation measures are used by buildings that do not (yet) exhibit misconduct (blue profiles).

As can be gathered from Figure 5.15, the occurring misconduct by up to five buildings per feeder leads to significant violations of the admissible maximum transformer hot-spot temperature if no participant misconduct mitigation measures are implemented (black profiles). The PV curtailment algorithm for transformer disturbances (Algorithm 5) only allows decreasing the apparent power limit of a particular building if no other building is currently implementing a higher limit or no limit at all. Since none of the buildings exhibiting misconduct implement apparent power limits at all, the DSO only commands these buildings to decrease their limits. Due to the misconduct, these commands are not followed by the misbehaving buildings, while the other buildings receive no updated limits. This allows the transformer hot-spot temperature to rise above its admissible maximum value. However, this does not affect line currents, as the PV curtailment algorithm for line disturbances (Algorithm 4) does not require that other buildings currently implement the

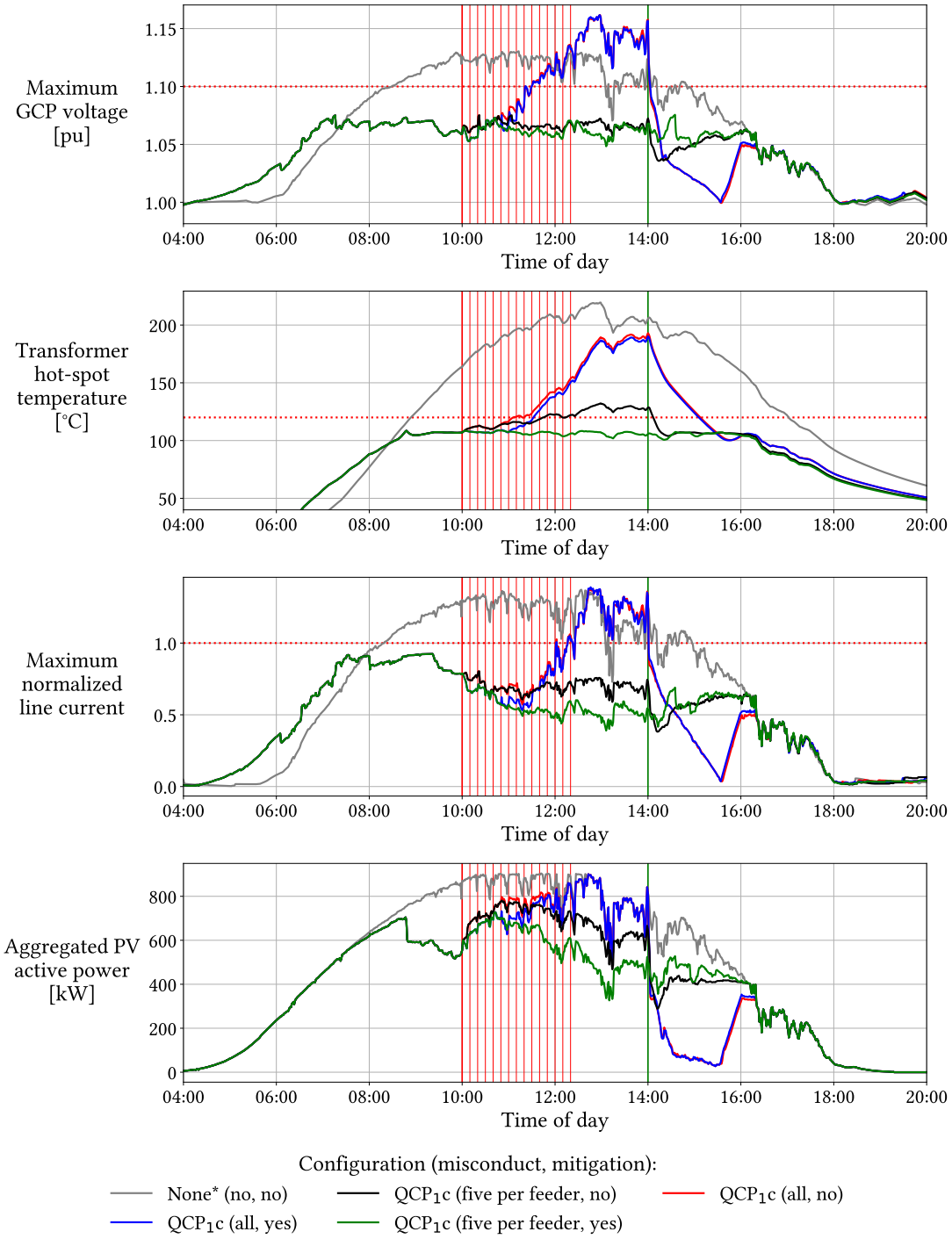

Figure 5.15: Profiles of the maximum GCP voltage in the grid, the transformer hot-spot temperature, the maximum normalized line current in the grid, and the active power generated by PV systems for July 1 and the village grid. The grid management strategy applied is the centralized strategy presented in Section 4.3.1. Red lines between 10:00 and 12:20: buildings start to maliciously implement false PV curtailment and reactive power setpoints, one group of five buildings (one building per feeder) after the other in ten-minute intervals. In the "five per feeder" configuration, only up to five buildings per feeder start acting maliciously. Green line at 14:00: all buildings stop their misconduct. Maximum admissible values are indicated by red dotted lines. None = no grid management, * = no energy cost optimization, Q = reactive-power-based voltage maintenance, C = adaptive PV curtailment, P_1 = active power flexibility use through active power targets, c = reactive power compensation.

same or lower apparent power limits to decrease the limit of a particular building. If this was a requirement for a limit decrease in response to critical line currents, the implementation of different apparent power limits depending on the line feeding a particular building would not be possible. As a consequence, buildings that do not (yet) exhibit misconduct can compensate for the misconduct by other buildings on the same line by lowering their own apparent power limits further. The same is true when considering the GCP voltages. Normally behaving buildings compensate for the misconduct by other buildings in the grid by adjusting their reactive power setpoints.

As should be expected, if all buildings are exhibiting misconduct (red profiles) eventually, the line currents and voltages rise above the respective admissible ranges as well, since there are no buildings left to compensate for the misconduct by other buildings. As a consequence, the transformer hot-spot temperature rises substantially higher in this case as well.

If explicit mitigation measures against the misconduct by buildings (see also Section 4.6.2.3) are used and only up to five buildings per feeder exhibit misconduct (green profiles), which corresponds to 25 out of 55 buildings in this scenario, the occurring misconduct can be fully compensated for by the other buildings. In this case, the DSO detects that the misbehaving buildings do not respond to commands and lowers the apparent power limits of the still normally behaving buildings instead.

If all buildings exhibit misconduct eventually, the mitigation measures only work up to this point and with gradually decreasing effectiveness (blue profiles). This can be best observed in the transformer hot-spot temperature profile. Here, the profile matches that for the configuration in which up to five buildings per feeder exhibit misconduct, until the sixth building per feeder starts to exhibit misconduct. After that, the temperature gradually rises and approaches the temperature profile for the configuration in which no misconduct mitigation measures are used (red profiles). This illustrates the limits of what can be achieved through misconduct mitigation measures. If too many buildings start misbehaving in a particular grid or on a particular line, the grid status becomes compromised and electricity outages as well as equipment damage may occur, even when using the strategies and methods developed in this thesis. This could de facto only be prevented if the DSO could selectively and remotely disconnect buildings from the grid. Furthermore, if enough buildings started misbehaving at once, the other buildings might not be able to react sufficiently quickly enough. The strategies and methods developed in this thesis can not fully prevent this and we expect it to only be preventable by implementing hardware-based restrictions on the rates of change of relevant control variables.

Figure 5.16 shows the same scenarios as Figure 5.15, but using VRDT-based voltage maintenance instead of reactive-power-based voltage maintenance.

The transformer hot-spot temperature, line current, and aggregated PV active power profiles in Figure 5.16 are similar to the ones in Figure 5.15. However, the voltage profiles differ substantially if all buildings exhibit misconduct after a certain point in time (red and blue profiles). This is caused by the transformer, which counteracts the malicious reactive power setpoints implemented by the buildings by switching its transmission ratio

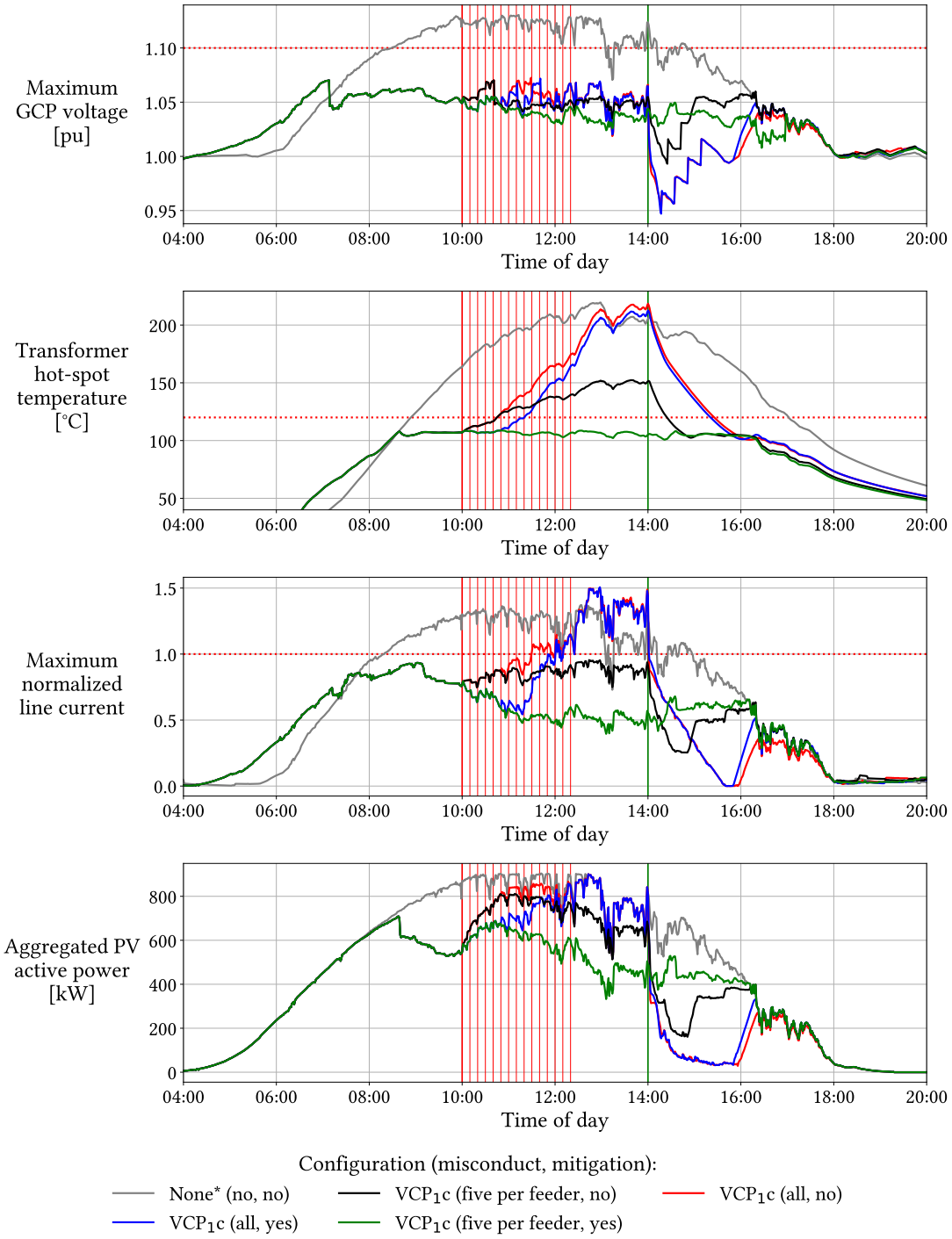

Figure 5.16: Profiles of the maximum GCP voltage in the grid, the transformer hot-spot temperature, the maximum normalized line current in the grid, and the active power generated by PV systems for July 1 and the village grid. The grid management strategy applied is the centralized strategy presented in Section 4.3.1. Red lines between 10:00 and 12:20: buildings start to maliciously implement false PV curtailment and reactive power setpoints, one group of five buildings (one building per feeder) after the other in ten-minute intervals. In the "five per feeder" configuration, only up to five buildings per feeder start acting maliciously. Green line at 14:00: all buildings stop their misconduct. Maximum admissible values are indicated by red dotted lines. None = no grid management, * = no energy cost optimization, V = VRDT-based voltage maintenance, C = adaptive PV curtailment, P_1 = active power flexibility use through active power targets, c = reactive power compensation.

to direct all GCP voltages back inside the admissible range. In contrast to the scenario presented in Section 5.3.1, where misconduct is exhibited by the DSO, the transformer reacts quickly enough to prevent exceedances of the maximum admissible voltage. This is because the buildings start to exhibit misconduct group-wise in this scenario, while in the DSO misconduct scenario, the DSO commands the implementation of malicious reactive power setpoints for all buildings simultaneously. This gives the transformer sufficient time to react appropriately. If all building were starting their misconduct at once, the same behavior as in the DSO misconduct scenario would be observed in this scenario as well.

The distributed grid management strategy is not separately tested as the default strategy for this misconduct scenario, as the corresponding grid status data profiles would look the same as for the centralized strategy. Whether the compensation for the misconduct by buildings by other buildings is initiated by the DSO coming from the centralized strategy or by the buildings themselves coming from the distributed strategy has no effect on the resulting building behavior.

5.4. Summary

Table 5.28 summarizes the results of the comparative evaluation of the grid management strategies and configurations (see also Section 5.1). For clarity, only selected grid management configurations are considered in the summary table. Among these are two full grid management configurations (**QCP$_1$c/VCP$_1$c**), where all countermeasures to electrical disturbances are used. These configurations employ adaptive PV curtailment (**C**), active power flexibility use (**P$_1$**), reactive power compensation (**c**), and reactive-power- (**Q**) or VRDT-based (**V**) voltage maintenance. Since the evaluation showed that the first method of active power flexibility use (**P$_1$**) is more robust with respect to lower PV generation prediction accuracy than the second method (see also Section 4.5.5), only the first method is considered in the table. The full configurations are compared to a configuration with no grid management measures or energy flow optimization at all (**None***), a configuration that only enables an energy cost optimization (**None**), and a conventional reference configuration (**Conv.**). The latter employs static PV curtailment, which curtails each PV system in the grid to 70 % of its respective peak power, and a constant power factor $\cos(\varphi)$ for reactive-power-based voltage maintenance. The results for two additional configurations (**QC***/**QC**) are given as comparison points for the effects of the active power flexibility use on the losses of active energy potentially generatable by PV systems due to PV curtailment. For brevity, we refer to the latter as *losses of PV active energy* in the following. The **QC***- and **QC**-configurations use adaptive PV curtailment and reactive-power-based voltage maintenance, but forego active power flexibility use and reactive power compensation. In the **QC***-configuration, no energy-cost-based optimizations are performed by the buildings, similar to the **None***-configuration.

The results in Table 5.28 show that the developed grid management measures prevent all electricity outages, which would otherwise occur, as is evident from the outage times of the **None***-, **None**-, and **Conv.**-configurations. However, this often comes with losses

Table 5.28: Summary of the results of the comparative evaluation of the grid management strategies and configurations (see also Section 5.1). T^{out}: Total outage time in % of the considered simulated time period (see also Section 5.1), E^{PV} loss: loss of potentially generatable PV active energy due to PV curtailment.

	Village Grid				**Rural Grid**				**Suburban Grid**			
	Centralized/ Distributed		**Decentralized**		**Centralized/ Distributed**		**Decentralized**		**Centralized/ Distributed**		**Decentralized**	
	T^{out}	E^{PV} **loss**	T^{out}	E^{PV} **loss**	T^{out}	E^{PV} **loss**	T^{out}	E^{PV} **loss**	T^{out}	E^{PV} **loss**	T^{out}	E^{PV} **loss**
Summer												
None*	25.12 %	-	25.12 %	-	13.59 %	-	13.59 %	-	9.15 %	-	9.15 %	-
None	22.47 %	-	22.47 %	-	11.63 %	-	11.63 %	-	1.88 %	-	1.88 %	-
Conv.	27.52 %	-3.83 %	27.52 %	-3.83 %	0.0 %	-4.24 %	0.0 %	-4.24 %	3.94 %	-2.57 %	3.94 %	-2.57 %
QC*	0.0 %	-23.71 %	0.0 %	-26.72 %	0.0 %	0.0 %	0.0 %	0.0 %	0.0 %	-5.02 %	0.0 %	-13.84 %
QC	0.0 %	-20.38 %	0.0 %	-23.87 %	0.0 %	0.0 %	0.0 %	0.0 %	0.0 %	-2.07 %	0.0 %	-10.58 %
QCP$_1$c	0.0 %	-16.24 %	0.0 %	-19.9 %	0.0 %	0.0 %	0.0 %	0.0 %	0.0 %	-0.93 %	0.0 %	-6.38 %
VCP$_1$c	0.0 %	-15.64 %	VRDT unsupported		0.0 %	0.0 %	VRDT unsupported		0.0 %	-0.5 %	VRDT unsupported	
Intermediate												
None*	9.41 %	-	9.41 %	-	4.31 %	-	4.31 %	-	1.62 %	-	1.62 %	-
None	7.27 %	-	7.27 %	-	3.4 %	-	3.4 %	-	0.01 %	-	0.01 %	-
Conv.	11.17 %	-1.89 %	11.17 %	-1.89 %	0.0 %	-2.15 %	0.0 %	-2.15 %	0.23 %	-1.0 %	0.23 %	-1.0 %
QC*	0.0 %	-12.39 %	0.0 %	-16.59 %	0.0 %	0.0 %	0.0 %	0.0 %	0.0 %	-1.0 %	0.0 %	-6.55 %
QC	0.0 %	-9.26 %	0.0 %	-14.67 %	0.0 %	0.0 %	0.0 %	0.0 %	0.0 %	-0.34 %	0.0 %	-4.76 %
QCP$_1$c	0.0 %	-7.25 %	0.0 %	-12.57 %	0.0 %	0.0 %	0.0 %	0.0 %	0.0 %	-0.18 %	0.0 %	-3.46 %
VCP$_1$c	0.0 %	-5.44 %	VRDT unsupported		0.0 %	0.0 %	VRDT unsupported		0.0 %	0.0 %	VRDT unsupported	
Winter												
No electrical disturbances occur during the evaluated winter time period												

of PV active energy. These losses can be partially mitigated by using the active power flexibility of the buildings and reactive power compensation. The default energy flow optimization to minimize energy costs already reduces the energy losses significantly, despite not considering the current grid status, as can be seen when comparing the results of the **QC***- and **QC**-configurations. However, the grid-supportive active power flexibility use reduces the energy losses significantly again, as can be gathered from the results of the $\mathbf{QCP_1c}$- and $\mathbf{VCP_1c}$-configurations. Using a VRDT instead of reactive power for voltage maintenance reduces the losses further, as the reactive power transmitted by the transformer and lines is greatly reduced, lessening the need for PV curtailment to decrease grid equipment utilization. The highest losses occur during the summer time period, due to the large amounts of energy that are potentially generated by the PV systems. The losses are lower in the intermediate season, due to the reduced PV generation during this time period. There are almost no losses in winter, since no electrical disturbances that would have to be mitigated occur during this time period. The slight losses incurred in the winter time period when using the decentralized strategy (see also Tables 5.9 and 5.27) are due to the conservative and continuously upheld apparent power limits for PV curtailment used in this strategy. The stable grid operation in the winter also indicates excessive PV generation as the primary reason for the outages occurring in the evaluated scenarios. BEV charging and HP use, which are equally or more pronounced and less offset by local PV generation during the colder seasons, evidently do not introduce electrical disturbances, even in the relatively weak grids evaluated in this thesis. This can be explained by the substantially lower simultaneity of power consumption by these devices across the grid compared to the highly synchronized PV generation. The losses of PV active energy are highest in the village grid, since its transformer and lines are more strongly undersized in relation to the installed PV capacity compared to the other two grids.

The results of the evaluation with respect to communication disruption (see also Section 5.2) show that the developed grid management system can handle any communication disruption between the participating buildings, the DSO, and the transformer. This is achieved by adequately adapting the utilized grid management strategies when disruptions occur, as described in Section 4.6. The adaptations are performed automatically at the building level, depending on the data or commands the buildings receive and they are effective in mitigating sensor failure as well (see also Section 4.6.3). The system response to sensor failure is not evaluated explicitly, since the evaluated communication disruption and participant misconduct scenarios already include the disruption of sensor data communication as well as the communication of incorrect sensor data.

The evaluation of the resilience of the system against misconduct by the participants (see also Section 5.3) shows very promising results as well. Misconduct by the DSO is fully mitigated by the developed grid management system. This is achieved by allowing each building to switch to the distributed strategy if it detects an inappropriate command. Misconduct by the transformer is fully mitigated by the system as well, at least in the evaluated scenario. However, there may be elaborate transformer misconduct strategies, which the system can not detect, unless it is extended, for example, by machine learning based anomaly detection, which is out of scope for this thesis. Misconduct by a part of the buildings can be fully mitigated by the other buildings for up to five misbehaving

buildings per feeder in the evaluated scenario, which corresponds to 25 of 55 buildings. After that, increasing the number of misbehaving buildings per feeder and consequently decreasing the number of correctly behaving buildings further makes it impossible to compensate for the misconduct. This means that, in a situation where too many buildings misbehave at the same time, more drastic countermeasures would be necessary, such as forcibly disconnecting the GCPs of misbehaving buildings. However, such measures are out of scope for the grid management system developed in this thesis.

6. Conclusion and Outlook

In this chapter, we summarize the developments and results of this thesis, concretely answer the research questions posed in Section 1.2, and give an outlook to future work.

6.1. Summary

In this thesis, we developed and evaluated an adaptive grid management system that leverages the energy flexibility of smart buildings to increase the resilience of electricity distribution grids with regard to both electrical as well as information and communication technology (ICT) disturbances. Thereby, the system provides solutions to the grid operation challenges introduced by the growing share of renewable, distributed energy generation and the electrification of the heating and transportation sectors, without neglecting the additional challenges arising from the use of the required ICT infrastructure.

We developed the grid management system based on the building energy management system *Organic Smart Home*, which is based on the Observer/Controller architecture stemming from the research initiative Organic Computing. This allows for the hierarchical self-organization of the system participants. The latter comprise the observation and control units of the distribution system operator (DSO) and the transformer as well as the building energy management systems of the smart residential buildings connected to the distribution grid. Another, major reason for using the OSH was its co-simulation capabilities (multi-building and power-flow), which we needed to develop and evaluate the system.

We introduced the relevant distributed energy resources (DERs) in residential buildings, the concept of energy flexibility, and the principles of building energy management. We provided an overview of electricity grid operation, smart grids, resilience definitions for technical systems and electricity grids, as well as typical electrical and ICT disturbances.

Based on the scope of our grid management system, we analyzed the literature related to our thesis and found that none of the publications we became aware of presented approaches as comprehensive as ours. Additionally, we summarized the existing research on the impacts of cyberattacks and communication disruption on grid operation and found that the impacts are generally significant and sometimes catastrophic. Furthermore, we gave an overview of different methods for detecting cyberattacks in the context of distribution grid operation.

With the introduced basic concepts as a foundation, we developed a resilience definition for smart electricity distribution grids as well as appropriate countermeasures to electrical as well as ICT disturbances. To provide resilience against voltage-related disturbances, we developed voltage regulated distribution transformer (VRDT)- as well as reactive-power-based voltage maintenance algorithms. These algorithms are designed in a way that the additional load placed on the grid by voltage maintenance is as limited as possible. Resilience against line- and transformer-related disturbances is provided through adaptive photovoltaic (PV) curtailment algorithms, reactive power compensation, and grid-supportive active power flexibility use via optimized device operation scheduling. To achieve resilience against ICT disturbances comprising or entailing communication disruption, participant misconduct (either system-internal or externally induced through cyberattacks), and sensor failure, we developed centralized, distributed, and decentralized grid management strategies. The grid management system switches between these strategies to adapt to and mitigate the mentioned effects of ICT disturbances.

After establishing appropriate evaluation scenarios and metrics as well as optimizing our grid management system by conducting comprehensive parameter studies, we evaluated the system through detailed simulation studies. This includes a comparative evaluation of the different grid management measures and strategies as well as individual studies evaluating the performance of the system with regard to mitigating communication disruption and participant misconduct.

Our evaluation results show that the developed grid management system fully prevents electricity outages and equipment damage even in extreme scenarios if undisturbed ICT infrastructure is assumed. However, this often comes with losses of active energy potentially generatable by PV systems due to PV curtailment. To keep these losses low, we utilize adaptive curtailment instead of fixed curtailment levels, so that curtailment is applied only as much as a particular situation requires. The remaining losses can be further reduced by using the active power flexibility of the buildings and reactive power compensation. The default energy flow optimization the buildings perform to minimize energy costs already reduces the energy losses significantly, despite not considering the current grid status. However, grid-supportive active power flexibility use reduces the energy losses significantly again. Using a VRDT for voltage maintenance instead of reactive power decreases the losses further, as the reactive power transferred by the transformer and lines is greatly reduced, lessening the need for PV curtailment to decrease grid equipment utilization. When tested separately, all three grid management strategies prevent all electricity outages and equipment damage due to electrical disturbances in the evaluated scenarios if undisturbed ICT infrastructure is assumed. The centralized and distributed grid management strategies achieve the exact same results, since the utilized algorithms are the same for both strategies. The algorithms are executed by the DSO in the centralized and by each building in the distributed strategy. However, the decentralized strategy incurs higher losses of PV active energy, since it utilizes fixed apparent power limits for PV curtailment, learned during the use of the centralized or distributed strategies. In contrast, the centralized and distributed strategies can adjust these limits dynamically, since the application of these strategies includes and requires comprehensive knowledge of the current grid status, which is not available in the decentralized strategy.

Through strategy adaptation, that is, by appropriately switching between the three strategies, the grid management system prevents electricity outages and equipment damage for almost all evaluated communication disruption and participant misconduct scenarios as well, which also implicitly cover sensor failure. However, our evaluation shows that misconduct by multiple buildings can only be compensated for by the remaining, correctly acting buildings up to a certain point. If too many buildings per feeder misbehave, the flexibility provided by the other buildings is not sufficient to reduce the overall load on the grid far enough to maintain grid operation. In the evaluated scenario, this occurred for more than five misbehaving buildings per feeder. However, the number of buildings per feeder that can misbehave without deteriorating the grid status can not be generalized, as it depends on many different factors. The latter comprise the time of day, the season, the weather, the grid topology and equipment, the number and available flexibility of unaffected buildings, as well as the concrete manifestation of the misconduct. These and potentially other factors could provide the basis for developing estimation methods in future research, which could aid in electrical and ICT infrastructure planning. Furthermore, the mitigation of misconduct by the transformer is limited to behaviors, which can be detected by the current version of the system. More sophisticated misconduct can potentially circumvent the deployment of countermeasures, especially if an attacker is aware of the conditions that trigger them. This could only be mitigated by using more sophisticated detection methods, which are outside the scope of this thesis.

Another notable finding is that no electricity outages or equipment damage occur during the evaluated winter period, even if no grid management measures are used at all. This shows that the primary reason for grid overloading, at least in the evaluated scenarios, is the excessive feed-in of PV-generated active energy. Heat pump use, which is more prevalent in winter, and battery electric vehicle (BEV) charging do not lead to overloading, even in the relatively weak grids and with the high penetrations of electric vehicles and heat pumps simulated for our evaluation. This can be explained by the substantially higher simultaneity and load peaks associated with PV feed-in.

6.2. Answers to the Posed Research Questions

In the following, we answer the research questions posed in Section 1.2 based on the methods, definitions, metrics, and scenarios developed in Chapter 4 and evaluated in Chapter 5.

Research Question 1 Can the use of energy flexibility provided by smart buildings improve the resilience of distribution grids?

This research question is addressed by answering the sub-questions defined in Section 1.2:

Sub-Question 1.1 How can resilience be defined in the context of smart electricity distribution grids?

Based on the existing definitions introduced in Section 2.7, we developed the following resilience definition (see also Section 4.2). In contrast to the definitions proposed in the literature, it applies specifically to smart electricity distribution grids and incorporates the aspect of the invasiveness of the utilized countermeasures to electrical disturbances.

The resilience of a smart electricity distribution grid can be defined as the capability of the grid to operate within the technical specifications of the grid equipment and the devices powered by the grid even in the presence of electrical disturbances as well as disturbances of the utilized information and communication technology and without curtailing connected loads (that is, power generation or consumption) more than necessary.

Sub-Question 1.2 How can the resilience of a smart electricity distribution grid be quantified?

The first aspect noted in our developed resilience definition for smart electricity distribution grids is the capability of the grid to operate within the technical specifications of the grid equipment and the devices powered by the grid. To quantify this resilience aspect, we calculate the total duration in which electricity outages or equipment damage can potentially occur in the considered grid, as a percentage of a reference time period. We call this the *total outage time*. The lower it is, the higher is the resilience of the considered grid with regard to the first resilience aspect. For the calculation of the total outage time, we assume that every violation of the minimum or maximum admissible voltages, maximum transformer hot-spot temperature, or rated line currents directly results in an electricity outage for the duration of the respective violation and at least one of the buildings connected to the grid. Strictly speaking, this is not correct. On the one hand, there may likely be situations, in which an electricity outage lasts much longer than its root cause. On the other hand, there may be violations, such as a transformer hot-spot temperature of 121 °C, which are not admissible but will most likely not lead to equipment failure or electricity outages immediately. We consider this for violations of rated line currents during the learning of appropriate apparent power limits for PV curtailment (see also Section 4.5.4). Commonly used fuses that protect lines against overcurrents allow for well-defined short-term and moderate exceedances of rated currents without blowing. However, it is neither feasible nor necessary to consider the highly situation-dependent durability of transformers against excessive temperatures and tolerances of electrical end consumer devices against voltage range violations when comparing the general performance of grid management strategies and configurations. The total outage time is calculated according to Equations 6.1, 6.2, and 6.3:

$$N^{\mathrm{ref}} = \frac{T^{\mathrm{ref}}}{\Delta t} \tag{6.1}$$

$$T^{\text{out}} = \frac{\sum_{t=1}^{N^{\text{ref}}} w_t}{T^{\text{ref}}} \cdot 100\,\% \tag{6.2}$$

where

$$w_t = \begin{cases} \Delta t, & \text{if } \max(\boldsymbol{u}_t) > 1.1\,\text{pu} \vee \min(\boldsymbol{u}_t) < 0.9\,\text{pu} \vee \max(\boldsymbol{i}_t) > 1 \vee \theta_t > 120\,^{\circ}\text{C}, \\ 0, & \text{otherwise} \end{cases} \tag{6.3}$$

In Equation 6.1, N^{ref} is the total number of management intervals in the reference time period T^{ref} and Δt the management interval duration. In the evaluation in Section 5, T^{ref} always corresponds to the assessed part of the respective simulated time period. In Equation 6.2, T^{out} is the total outage time (as a percentage of T^{ref}). w_t either equals Δt or zero, depending on Equation 6.3. In Equation 6.3, $\boldsymbol{u}_t$ is the array of all normalized GCP voltages in the grid in management interval t. $\boldsymbol{i}_t$ is the array of the magnitudes of all normalized line segment currents in the grid in management interval t. θ_t is the transformer hot-spot temperature in management interval t.

The second aspect noted in our developed resilience definition for smart electricity distribution grids is the invasiveness of the deployed countermeasures to electrical disturbances, that is, the extent of the deployed load curtailment. The aggregated active energy generated by all PV systems in the grid quantifies this aspect. Note that, in the context of our thesis, we only have to curtail the power feed-in of PV systems. The other considered large loads (BEV charging stations, heat pumps, battery energy storage systems) provide sufficient active power flexibility to enable proactive operation scheduling (see also Section 4.5.5) instead of curtailment. We calculate the aggregated active energy generated by all PV systems in the grid during the reference time period according to Equation 6.4:

$$E^{\text{PV}} = \sum_{b \in \mathbf{B}} \sum_{t=1}^{N^{\text{ref}}} \left| P_{b,t}^{\text{PV}} \right| \cdot \Delta t \tag{6.4}$$

In Equation 6.4, E^{PV} is the aggregated active energy generated by all PV systems in the grid during the reference time period. $P_{b,t}^{\text{PV}}$ is the average active power generated by the PV system of building b in management interval t. We use the magnitude of $P_{b,t}^{\text{PV}}$, since we define generated powers as negative. $\mathbf{B}$ is the set of buildings equipped with PV systems in the grid, which corresponds to all buildings in the grid in the context of this thesis. The other variables and parameters are the same as in Equations 6.1, 6.2, and 6.3.

Sub-Question 1.3 Which evaluation scenarios are representative of realistic situations that require an increase in distribution grid resilience?

Since the main purpose of the developed grid management system is the full prevention of electricity outages and equipment damage, it has to be evaluated in an environment in

which such outages and equipment damage occur if no countermeasures are taken. Therefore, the configurations of the simulated buildings and grids used to evaluate the system are based on the *the day after tomorrow* reference scenario as well as the three low-voltage reference grids developed in [162] and [32]. However, the reference scenario is updated and the reference grids are modified for this thesis, which is detailed in Section 4.10.

Sub-Question 1.4 To what extent can electrical disturbances be mitigated by smart buildings in the chosen evaluation scenarios, assuming undisturbed ICT infrastructure?

By leveraging the energy flexibility of smart buildings, which includes adaptive PV curtailment, to mitigate voltage-, line-, and transformer-related disturbances, the developed grid management system fully prevents electricity outages and potential equipment damage in all evaluated scenarios that assume undisturbed ICT infrastructure. Consequently, the substantial outage times and potential equipment damage occurring in these scenarios if no countermeasures are taken are reduced by 100 % (see also Section 5.1).

Sub-Question 1.5 To what extent can the necessity of load curtailment be reduced in the chosen evaluation scenarios by utilizing adaptive and less invasive measures for achieving grid-supportive operation of smart buildings, assuming undisturbed ICT infrastructure?

As mentioned in the answer to Sub-Question 1.4, the evaluation results show that the developed grid management measures prevent all electricity outages and potential equipment damage in the considered evaluation scenarios that assume undisturbed ICT infrastructure. However, this often comes with losses of active energy potentially generatable by PV systems due to PV curtailment. To prevent unnecessary losses, we use adaptive PV curtailment, which only curtails PV systems as much as is necessary in a given situation (see also Section 4.5.4). Additionally, the remaining losses are reduced further by using the active power flexibility of the smart buildings (see also Section 4.5.5) and reactive power compensation (see also Section 4.5.2). The default energy flow optimization the buildings perform to minimize energy costs already reduces the curtailment-induced losses significantly, despite not considering the current grid status. However, grid-status-aware active power flexibility use reduces these losses even more. Compared to active power flexibility use, the loss reduction achieved through reactive power compensation is very small. Using a voltage regulated distribution transformer (VRDT, see also Section 4.5.1) instead of reactive-power-based voltage maintenance (see also Section 4.5.3) reduces the losses further, as the reactive power transmitted by the transformer and lines is greatly reduced, lessening the need for PV curtailment to decrease grid equipment utilization. The exact results for the evaluated scenarios are given in Section 5.1.

Research Question 2 How do distributed or decentralized grid management strategies compare to a centralized grid management strategy?

This research question is addressed by answering the sub-questions defined in Section 1.2:

Sub-Question 2.1 How do the different strategies compare with regard to mitigating electrical disturbances in the chosen evaluation scenarios, assuming undisturbed ICT infrastructure?

All developed grid management strategies (see also Section 4.3) fully prevent electricity outages and potential equipment failure in the evaluated scenarios that assume undisturbed ICT infrastructure (see also Section 5.1).

Sub-Question 2.2 How do the different strategies compare with regard to the invasiveness of the deployed countermeasures to electrical disturbances, assuming undisturbed ICT infrastructure?

The developed centralized and distributed grid management strategies achieve the exact same results in the evaluation scenarios that assume undisturbed ICT infrastructure, since the utilized algorithms are the same for both strategies. The algorithms are executed by the DSO for each building in the centralized strategy and by each building in the distributed strategy.

However, the developed decentralized grid management strategy incurs higher losses of active energy potentially generatable by PV systems, since it utilizes fixed apparent power limits for PV curtailment learned during the use of the centralized or distributed strategies. In contrast, the centralized and distributed strategies can adjust these limits dynamically, since these strategies include and require comprehensive knowledge of the current grid status, which is not available in the decentralized strategy.

The exact results for each grid management strategy are given in Section 5.1.

Sub-Question 2.3 Are there additional advantages or disadvantages to each strategy?

The centralized grid management strategy has the advantage that the DSO has full control over the grid, which may be required depending on the applicable regulations. The major disadvantage of this strategy is that it introduces a single point of failure. If the DSO is subject to a physical attack or cyberattack or if the communication between the DSO and the buildings and/or transformer is disrupted, stand-alone use of the centralized strategy is impossible.

The distributed grid management strategy removes this single point of failure and is usable, even if some of the buildings can not communicate anymore or are behaving maliciously, as long as the available grid status data are sufficiently accurate. A disadvantage could be that stand-alone use of this strategy takes away control from the DSO, which may not be permissible depending on the applicable regulations.

The decentralized grid management strategy removes the necessity of a functioning communication infrastructure as well, since each building only uses the data it measures at its own GCP and previously learned apparent power limits for PV curtailment. However, it is important to note that the decentralized strategy is a backup strategy that can only be used after the appropriate apparent power limits for PV curtailment are learned during the

application of the centralized or distributed strategies. Stand-alone use of the decentralized strategy is potentially possible, but only if the appropriate apparent power limits for PV curtailment for each building are known beforehand, for example, by simulating the given grid before deploying the grid management system.

By combining the strategies, the respective disadvantages of each strategy can be mitigated while keeping its advantages. The developed adaptive grid management system uses the centralized strategy by default and switches to the other strategies depending on whether communication disruption, participant misconduct, or sensor failure occurs. It is important to note that the strategy adaptation is a self-organized process initiated mainly by the buildings themselves based on their local view of the current status of the electrical and ICT infrastructures. This also allows the hybrid use of different strategies on a per building basis when appropriate.

Research Question 3 Can grid operation be upheld during communication disruption, sensor failure, or participant misconduct?

This research question is addressed by answering the sub-questions defined in Section 1.2:

Sub-Question 3.1 Which communication disruption, participant misconduct, and sensor failure scenarios should be considered?

To evaluate the ability of the developed grid management system to adapt in response to communication disruption, participant misconduct, and sensor failure, we simulate several different scenarios. These scenarios are designed to cover different types and magnitudes of problems potentially introduced by utilizing an ICT infrastructure for grid management.

We evaluate different communication disruption scenarios affecting the DSO, the transformer, and the smart buildings connected to the grid in Section 5.2.

Furthermore, the effects and mitigation of participant misconduct by the DSO, the transformer, or the buildings are evaluated in Section 5.3 using appropriate scenarios as well. Note that the participant misconduct can either be system-internal and willingly performed by the participants or introduced externally through cyberattacks. Our grid management system covers both cases. Misconduct by the DSO comprises the communication of inappropriate apparent power limits for PV curtailment and reactive power setpoints, which is aimed at causing electricity outages and equipment damage. Misconduct by the transformer comprises the communication of incorrect transformer hot-spot temperature values to provoke transformer overheating and, if the transformer is a VRDT, malicious transmission ratio switching to induce violations of the admissible voltage range. A building has similar misconduct options as the DSO, just on a scale that is limited to the individual maliciously acting building. It can set its own apparent power limit for PV curtailment and reactive power setpoint to inappropriate values to negatively influence grid operation.

Sensor failure can manifest in two different ways, a sensor can (temporarily) provide incorrect values or no values at all. We do not evaluate our system in dedicated sensor failure scenarios, since the communication disruption scenarios already include the occurrence of missing sensor data, while the participant misconduct scenarios already include the communication of false sensor data by the transformer. Incorrect sensor data communicated by buildings, either maliciously or due to sensor failure, are mitigated in the same way as sensor data that are missing, for example due to communication disruption, which is explained in the answer to Sub-Question 3.2. The effectiveness of this mechanism is evaluated in the communication disruption scenarios in Section 5.2 and therefore not separately evaluated for incorrect sensor data.

It is important to note that the considered ICT disturbance scenarios are non-exhaustive, since it is impossible to cover all potentially occurring scenarios. The considered scenarios are chosen to evaluate whether the developed grid management system can handle diverse and severe effects of ICT disturbances as well as to identify potential limitations.

Sub-Question 3.2 How can communication disruption, participant misconduct, and sensor failure be mitigated?

In the centralized grid management strategy, the buildings detect communication disruption to the DSO by continuously monitoring the grid status based on the data received from other buildings and the transformer. If they detect an electrical disturbance but do not receive an appropriate command from the DSO, they assume the communication to the latter to be disrupted and autonomously switch to the distributed strategy.

If the buildings stop receiving hot-spot temperature, load factor, and voltage data from the transformer, they assume the communication to the latter to be disrupted and switch to the decentralized strategy.

If the buildings stop receiving any data, or receive insufficient data from other buildings to estimate their local grid status with the required accuracy, they switch to the decentralized strategy as well. Note that this may not affect all buildings at the same time. If a building does not communicate sensor data anymore, either due to communication disruption or due to sensor failure, while the centralized or distributed strategies are currently in use, the last communicated data of this building is reused by the other buildings and the DSO. This reduces the accuracy of the power-flow studies, which the DSO and the buildings regularly conduct. However, the accuracy reduction does not necessarily affect all parts of the grid evenly. Therefore, the results of the power-flow studies are cross-checked with the measured voltages communicated by the still communicating buildings. If the voltage measured at the grid connection point of a particular building deviates too far from the corresponding voltage calculated in the power-flow studies, this building switches from the centralized or distributed strategy to the decentralized strategy. The latter takes only locally measured data and previously learned apparent power limits for PV curtailment into account and is therefore not dependent on the accuracy or topicality of data communicated by other participants. Buildings for which the locally measured voltage is still close to the corresponding calculated voltage keep using the centralized or distributed strategy. The

transformer, if it is a VRDT and receives insufficient data from the buildings, gradually switches back to the neutral tap position. This changes the voltages in the grid, which prompts the buildings to implement reactive-power-based voltage maintenance.

Misconduct by the DSO is detected by the buildings through checking every received command for correctness. This is possible, since the buildings use the same algorithms to determine appropriate measures in the distributed strategy as the DSO uses in the centralized strategy. If a building detects an inappropriate command, it assumes the DSO to be compromised, switches to the distributed strategy, and informs all other buildings.

In our simulation studies, the buildings (and the DSO) detect transformer misconduct with regard to the communication of incorrect hot-spot temperature values by observing the received values over the course of time. If the communicated temperature has not changed to the fourth decimal place over three consecutive measurements, or if it changes by more than 7 °C between two measurements, the buildings assume the transformer to be compromised and switch to the decentralized strategy. Since this method of detecting false hot-spot temperatures requires the communication of temperatures with a very high accuracy, it may be unsuitable for a real-world application. We therefore propose a more practical method as well, which is based on estimating the current transformer load factor from the power data communicated among the buildings and the DSO. If the progression of the estimated load factor over time contradicts the progression of the hot-spot temperatures communicated by the transformer, the buildings (and the DSO) assume the transformer to be compromised. As the first method, this second method can be circumvented by a sophisticated attacker that is aware of the conditions used to detect false hot-spot temperatures and adjusts the communicated temperatures accordingly. This could only be mitigated by deploying more sophisticated detection methods. The cyberattack detection methods presented in Section 3.2 can provide possible courses of action, but are outside the scope of this thesis.

If a VRDT switches its transmission ratio maliciously to provoke deviations from the admissible voltage range, the buildings and the DSO can mitigate this as well, since they observe the voltages in the grid. If voltages threaten to rise or fall outside the admissible range, they start deploying reactive-power-based voltage maintenance to counteract this effect. In this case, any of the three grid management strategies can be used.

Correctly acting buildings (or the DSO) mitigate misconduct by other buildings implicitly. If a building sets its apparent power limit for PV curtailment and reactive power setpoint to inappropriate values, the grid status changes in response. This is observed by the other buildings (and the DSO), which then adjust their own apparent power limits for PV curtailment and reactive power setpoints accordingly. Naturally, this is only feasible up to a certain number of maliciously acting buildings. The latter depends on the time of day, the season, the weather, the grid topology and equipment, the number and available flexibility of unaffected buildings, as well as the concrete manifestation of the misconduct. As with the malicious switching of the transmission ratio by a VRDT, any of the three grid management strategies can be used here as well.

If a building communicates incorrect sensor data, either maliciously or due to sensor failure, when the centralized or distributed strategies are currently in use, this reduces the accuracy of the power-flow studies conducted by the DSO and the buildings. This is very similar to the accuracy reduction resulting from missing sensor data due to communication disruption, which we described earlier. Consequently, the strategy switching mechanism is the same, regardless of whether sensor data is missing or incorrect.

As already indicated above, sensor failure does not have to be detected explicitly for the grid management system to mitigate its impacts on grid operation. If a sensor in a building stops providing data, the building stops applying the algorithms to determine and implement appropriate countermeasures to electrical disturbances and stops communicating its locally measured data. This triggers the same reactions by the other buildings, the DSO, and the transformer as if the building stopped communicating due to communication disruption. Similarly, if the transformer stops communicating new hot-spot temperature or load factor data due to sensor failure, the buildings react in the same way as they would if the communication to the transformer was disrupted. If a sensor provides incorrect data, which is communicated to the other participants, the same mitigation measures are triggered as if incorrect sensor data is communicated maliciously.

For more detailed information on the described detection and mitigation measures, see Section 4.6.

Sub-Question 3.3 Is the adaptive grid management system able to handle the considered communication disruption, participant misconduct, and sensor failure scenarios?

The evaluation results presented in Sections 5.2 and 5.3 show that the developed grid management system prevents electricity outages and equipment damage for almost all evaluated communication disruption and participant misconduct scenarios, which implicitly cover sensor failure as well. The only exception is a scenario, in which more than five buildings per feeder act maliciously by maximizing their reactive power setpoints in the opposite direction of what the current grid status would require and letting their PV systems feed energy into the grid without curtailment. This corresponds to more than 25 of the 55 buildings connected to the grid in the considered scenario. In this scenario, the misconduct by these buildings can not be fully compensated for by the correctly acting buildings anymore and drastic measures, such as remote-controlled load shedding, would be necessary to uphold grid operation. Such measures are out of scope for the developed grid management system. Nevertheless, for up to five maliciously acting buildings per feeder, the system can leverage sufficient energy flexibility (which includes more restrictive PV curtailment) from the remaining buildings to prevent electricity outages and equipment damage in the evaluated scenario. However, the misbehaving buildings could additionally communicate severely incorrect sensor data to provoke a switch to the decentralized strategy by the still correctly acting buildings. This would decrease the maximum number of buildings per feeder for which misconduct can still be compensated for, since the decentralized strategy does not support adaptive PV curtailment. This could be a topic for future research. Some of the publications analyzed in Chapter 3 address this

by explicitly detecting incorrect power and voltage data and replacing it with estimated values based on historical and/or predicted data. However, this is out of scope for this thesis.

As already mentioned in the answer to Sub-Question 3.2, there are more sophisticated methods to maliciously communicate false transformer hot-spot temperatures that can circumvent the conditions that trigger the countermeasures to transformer misconduct (see also Section 4.6.2.2). Such methods could only be mitigated by using more sophisticated detection methods as well. As with incorrect building sensor data, some of the publications presented in Chapter 3 provide approaches for future research in this direction.

6.3. Outlook

While the developed adaptive grid management system provides extensive resilience with regard to both electrical as well as ICT disturbances, there are several options for extending and improving its functionality in future research.

In its current form, the system can not react to sub-minute fluctuations of the grid status and does not consider problems related to harmonics, an unequal load distribution across the three phases, or the physical destruction of grid equipment. To accommodate reactions to sub-minute fluctuations, the temporal resolution of the utilized power-flow studies could be increased. However, this would require transformer sensors and smart meters capable of measuring power and voltage data with a sub-minute resolution as well. Considering problems related to harmonics would require even more sophisticated sensor and actor infrastructure. To cover unequal load distributions across phases, the measurements and power-flow studies would have to accommodate differentiating between the three phases. While physical destruction itself may be impossible to mitigate with a software system, the incorporation of alert functionality could accelerate detection and repair.

The system could be further developed to include functionality for predictive maintenance and physical load shedding as well, which would however require dedicated sensor and actor infrastructure. Frequency control and islanded operation are currently not covered by the system, which would be advantageous in the context of microgrid operation. While the system is designed to manage low-voltage distribution grids, future work could extend its functionality to manage or provide flexibility to higher grid levels. Furthermore, the system could be extended to consider bidirectional BEV charging and grid topologies other than radial ones without substantial development effort.

Although the system is able to mitigate sensor failure and participant misconduct with regard to the communication of false sensor data to a large extent, the mitigation measures could be further enhanced in future work by explicitly detecting false sensor data and replacing the affected measurements with estimated values based on historical and/or predicted data. Some of the publications discussed in Chapter 3 provide potential approaches that could be incorporated into our system.

Future work could provide estimation methods for the time-, weather-, grid-, building-configuration-, and misconduct-dependent compensation potential for participant misconduct by buildings. Such methods could aid in the planning and dimensioning of distribution grids and adjacent ICT infrastructure.

Last but not least, the system should be evaluated in real-world environments. While Hardware-in-the-Loop-studies in controlled laboratory environments would be a possible course of action, field tests with realistic and diverse smart buildings could provide even more detailed insights with regard to the performance and limitations of the system.

Bibliography

[1] Mischa Ahrens. “Increasing Power Grid Resilience with a Multi-Agent System of Smart Buildings”. In: *Organic Computing - Doctoral Dissertation Colloquium 2021*. Ed. by Sven Tomforde and Christian Krupitzer. kassel university press, 2022, pp. 15–31. DOI: 10.17170/kobra-202202215780.

[2] Ali Ipakchi and Farrokh Albuyeh. “Grid of the future”. In: *IEEE Power and Energy Magazine* 7.2 (2009), pp. 52–62. DOI: 10.1109/MPE.2008.931384.

[3] Binghui Han et al. “Home Energy Management Systems: A Review of the Concept, Architecture, and Scheduling Strategies”. In: *IEEE Access* 11 (2023), pp. 19999–20025. DOI: 10.1109/ACCESS.2023.3248502.

[4] Bernd M. Buchholz and Zbigniew A. Styczynski. *Smart Grids: Fundamentals and Technologies in Electric Power Systems of the Future*. Berlin, Heidelberg: Springer, 2020. ISBN: 978-3-662-60930-9. DOI: 10.1007/978-3-662-60930-9.

[5] Hassan Farhangi. “The path of the smart grid”. In: *IEEE Power and Energy Magazine* 8.1 (2010), pp. 18–28. DOI: 10.1109/MPE.2009.934876.

[6] George W. Arnold. “Challenges and Opportunities in Smart Grid: A Position Article”. In: *Proceedings of the IEEE* 99.6 (2011), pp. 922–927. DOI: 10.1109/JPROC.2011.2125930.

[7] Adolf J. Schwab. *Elektroenergiesysteme: Smarte Stromversorgung im Zeitalter der Energiewende (English: Electrical Energy Systems: Smart Electricity Supply in the Age of the Energy Transition)*. Berlin, Heidelberg: Springer, 2022. ISBN: 978-3-662-64774-5. DOI: 10.1007/978-3-662-64774-5.

[8] Ishan Srivastava, Sunil Bhat, and Arvind R. Singh. “Smart Grid Communication: Recent Trends and Challenges”. In: *Next Generation Smart Grids: Modeling, Control and Optimization*. Ed. by Surender Reddy Salkuti and Papia Ray. Singapore: Springer Nature Singapore, 2022, pp. 49–75. ISBN: 978-981-16-7794-6. DOI: 10.1007/978-981-16-7794-6_3.

[9] Qi Wang et al. “Framework for vulnerability assessment of communication systems for electric power grids”. In: *IET Generation, Transmission & Distribution* 10.2 (2016), pp. 477–486. DOI: 10.1049/iet-gtd.2015.0857.

[10] V. S. G. Thadikemalla, Ishan Srivastava, S. S. Bhat, and A. S. Gandhi. “Data Loss Mitigation Mechanism using Compressive Sensing for Smart Grids”. In: *2020 IEEE International Conference on Power Electronics, Smart Grid and Renewable Energy (PESGRE2020)*. 2020, pp. 1–6. DOI: 10.1109/PESGRE45664.2020.9070414.

[11] Ren Liu, Ceeman Vellaithurai, Saugata S. Biswas, Thoshitha T. Gamage, and Anurag K. Srivastava. "Analyzing the Cyber-Physical Impact of Cyber Events on the Power Grid". In: *IEEE Transactions on Smart Grid* 6.5 (2015), pp. 2444–2453. DOI: 10.1109/TSG.2015.2432013.

[12] Bilkisu Jimada-Ojuolape and Jiashen Teh. "Impact of the Integration of Information and Communication Technology on Power System Reliability: A Review". In: *IEEE Access* 8 (2020), pp. 24600–24615. DOI: 10.1109/ACCESS.2020.2970598.

[13] Katerina Simou, Friederike Berger, and Anastasiia Komshakova. *Smart grids in Germany: Current situation*. Technical report. Sino-German Energy Partnership. Commissioned by the German Federal Ministry for Economic Affairs and Climate Action (BMWK) and implemented by Deutsche Gesellschaft für Internationale Zusammenarbeit GmbH (GIZ, English: German Society for International Cooperation). Available online: https://www.dena.de/fileadmin/dena/Dokumente/Projektportrait/Projektarchiv/Entrans/Smart_Grids_in_Germany_Current_Situation_EN.pdf (accessed on July 23, 2025). Beijing and Berlin: Deutsche Energie-Agentur GmbH (dena, English: German Energy Agency), Aug. 2022.

[14] Zakaria El Mrabet, Naima Kaabouch, Hassan El Ghazi, and Hamid El Ghazi. "Cyber-security in smart grid: Survey and challenges". In: *Computers & Electrical Engineering* 67 (2018), pp. 469–482. ISSN: 0045-7906. DOI: 10.1016/j.compeleceng.2018.01.015.

[15] Hanko Ipach, Leonard Fisser, Christian Becker, and Andreas Timm-Giel. "Distributed Utility-Based Real-Time Power Flow Optimization in ICT-enabled Low Voltage Distribution Grids". In: *IET Generation, Transmission & Distribution* 17.13 (2023), pp. 2900–2925. ISSN: 1751-8695. DOI: 10.1049/gtd2.12653.

[16] S. Iacovella et al. "Distributed Voltage Control Mechanism in Low-Voltage Distribution Grid Field Test". In: *IEEE PES ISGT Europe 2013*. Oct. 2013, pp. 1–5. DOI: 10.1109/ISGTEurope.2013.6695393.

[17] Meisam Ansari and Arash Asrari. "Reaction to Detected Cyberattacks in Smart Distribution Systems". In: *2020 IEEE Power & Energy Society Innovative Smart Grid Technologies Conference (ISGT)*. Feb. 2020, pp. 1–5. DOI: 10.1109/ISGT45199.2020.9087771.

[18] Erdem Gümrükcü et al. "Dynamic Capacity Sharing for Cyber–Physical Resilience of EV Charging". In: *Energies* 17.24 (Dec. 2024). ISSN: 1996-1073. DOI: 10.3390/en17246277.

[19] Akshay Kumar Jain, Nitasha Sahani, and Chen-Ching Liu. "Detection of Falsified Commands on a DER Management System". In: *IEEE Transactions on Smart Grid* 13.2 (Mar. 2022), pp. 1322–1334. ISSN: 1949-3061. DOI: 10.1109/TSG.2021.3132848.

[20] Ehsan Naderi, Arash Asrari, and Benito Ramos. "Moving Target Defense Strategy to Protect a PV/Wind Lab-Scale Microgrid Against False Data Injection Cyberattacks: Experimental Validation". In: *2023 IEEE Power & Energy Society General Meeting (PESGM)*. July 2023, pp. 1–5. DOI: 10.1109/PESGM52003.2023.10252369.

[21] Baosen Zhang, Albert Y.S. Lam, Alejandro D. Domínguez-García, and David Tse. "An Optimal and Distributed Method for Voltage Regulation in Power Distribution Systems". In: *IEEE Transactions on Power Systems* 30.4 (July 2015), pp. 1714–1726. ISSN: 1558-0679. DOI: 10.1109/TPWRS.2014.2347281.

[22] Cen Yuan, Zhiyi Li, and Huanhai Xin. "Cyber-Resilient Distributed Operation of Active Distribution Networks Based on Relaxed Alternating Direction Method of Multipliers". In: *2021 4th International Conference on Energy, Electrical and Power Engineering (CEEPE)*. Apr. 2021, pp. 415–421. DOI: 10.1109/CEEPE51765.2021.9475721.

[23] Ramon Zamora and Anurag K. Srivastava. "Multi-Layer Architecture for Voltage and Frequency Control in Networked Microgrids". In: *IEEE Transactions on Smart Grid* 9.3 (May 2018), pp. 2076–2085. ISSN: 1949-3061. DOI: 10.1109/TSG.2016.2606460.

[24] Wenxia Liu, Yu Lu, Mengyao Yang, Mengdi Fu, and Lingfeng Wang. "Differentiated Local Controls for Distributed Generators in Active Distribution Networks Considering Cyber Failures". In: *International Journal of Electrical Power & Energy Systems* 135, 107569 (Feb. 2022). ISSN: 0142-0615. DOI: 10.1016/j.ijepes.2021.107569.

[25] Ankur Majumdar, Yashodhan P. Agalgaonkar, Bikash C. Pal, and Ralph Gottschalg. "Centralized Volt–Var Optimization Strategy Considering Malicious Attack on Distributed Energy Resources Control". In: *IEEE Transactions on Sustainable Energy* 9.1 (Jan. 2018), pp. 148–156. ISSN: 1949-3037. DOI: 10.1109/TSTE.2017.2706965.

[26] Hartmut Schmeck, Antonello Monti, and Veit Hagenmeyer. "Energy Informatics: Key Elements for Tomorrow's Energy System". In: *Commun. ACM* 65.4 (Mar. 2022), pp. 58–63. ISSN: 0001-0782. DOI: 10.1145/3511666.

[27] *Erneuerbare-Energien-Gesetz - EEG 2021 (English: Renewable Energy Sources Act 2021)*. Available online: https://www.gesetze-im-internet.de/eeg_2014/__4.html (accessed on October 18, 2022). German law.

[28] Energieversum. *70-Prozent-Regelung bei Photovoltaikanlagen: Mit den richtigen Tools kein Problem (English: 70-Percent-Rule for Photovoltaic Systems: No problem with the right tools)*. Available online: https://www.energieversum.de/70-prozent-regelung-pv/ (accessed on October 20, 2022). Website article. 2022.

[29] Karlsruher Institut für Technologie (KIT, English: Karlsruhe Institute of Technology). *The Energy Smart Home Lab (ESHL)*. https://www.elab.kit.edu/english/eshl.php (accessed on January 29, 2026). Website article.

[30] FZI Forschungszentrum Informatik (FZI, English: FZI Research Center for Information Technology). *FZI House of Living Labs*. Available online: https://www.fzi.de/en/experience/house-of-living-labs/ (accessed on November 7, 2025). Website article.

[31] David Wölfle et al. "Open energy services: forecasting and optimization as a service for energy management applications at scale". In: *Data-Centric Engineering* 6, e35 (2025). 37.12.02; LK 01. ISSN: 2632-6736. DOI: 10.1017/dce.2025.14.

[32] Sebastian Kochanneck. “Systemdienstleistungserbringung durch intelligente Gebäude (English: Provision of System Services by Intelligent Buildings)”. German. 37.06.01; LK 01. PhD thesis. Karlsruher Institut für Technologie (KIT, English: Karlsruhe Institute of Technology), 2019. DOI: 10.5445/IR/1000089171.

[33] Mischa Ahrens, Fabian Kern, and Hartmut Schmeck. “Strategies for an Adaptive Control System to Improve Power Grid Resilience with Smart Buildings”. In: *Energies* 14.15, 4472 (2021). ISSN: 1996-1073. DOI: 10.3390/en14154472.

[34] Mischa Ahrens and Hartmut Schmeck. “Organic Computing for Adaptive and Resilient Electricity Grid Management”. In: *Go Where the Bugs Are: Essays Dedicated to Wolfgang Reif on the Occasion of His 65th Birthday*. Ed. by Gidon Ernst et al. Cham: Springer Nature Switzerland, 2025, pp. 242–261. ISBN: 978-3-031-92196-4. DOI: 10.1007/978-3-031-92196-4_12.

[35] Benito van der Zander. *TeXstudio website*. Available online: https://www.texstudio.org/ (accessed on February 9, 2026).

[36] Christian Schenk. *MiKTeX website*. Available online: https://miktex.org/ (accessed on February 9, 2026).

[37] Software Design and Quality (SDQ). *Templates website of the research group Software Design and Quality at the Karlsruhe Institute of Technology (KIT)*. Available online: https://sdq.kastel.kit.edu/wiki/Dokumentvorlagen (accessed on February 9, 2026).

[38] Corporation for Digital Scholarship. *Zotero website*. Available online: https://www.zotero.org/ (accessed on February 9, 2026).

[39] Adobe Systems Software Ireland Limited. *Adobe Acrobat Reader website*. Available online: https://www.adobe.com/de/acrobat/pdf-reader.html (accessed on February 9, 2026).

[40] *Briss 0.9 website*. Available online: https://sourceforge.net/projects/briss/ (accessed on February 10, 2026).

[41] Microsoft Corporation. *Microsoft Word website*. Available online: https://www.microsoft.com/de-de/microsoft-365/word?market=de (accessed on February 9, 2026).

[42] Microsoft Corporation. *Microsoft Excel website*. Available online: https://www.microsoft.com/de-de/microsoft-365/excel?market=de (accessed on February 9, 2026).

[43] Microsoft Corporation. *Microsoft PowerPoint website*. Available online: https://www.microsoft.com/de-de/microsoft-365/powerpoint?market=de (accessed on February 9, 2026).

[44] Microsoft Corporation. *Microsoft Windows Snipping Tool website*. Available online: https://www.microsoft.com/de-de/windows/tips/snipping-tool (accessed on February 9, 2026).

[45] The Apache Software Foundation. *OpenOffice Calc website*. Available online: https://www.openoffice.org/ (accessed on February 9, 2026).

[46] draw.io Ltd. *Draw.io desktop GitHub repository*. Available online: https://github.com/jgraph/drawio-desktop/releases/tag/v29.3.6 (accessed on February 9, 2026).

[47] Eclipse Foundation AISBL. *Eclipse IDE website*. Available online: https://eclipse ide.org/ (accessed on February 9, 2026).

[48] JetBrains s.r.o. *PyCharm website*. Available online: https://www.jetbrains.com/pycharm/ (accessed on February 9, 2026).

[49] OpenAI. *OpenAI website*. Available online: https://openai.com/ (accessed on February 9, 2026).

[50] OpenAI. *ChatGPT website*. Available online: https://chatgpt.com/ (accessed on February 9, 2026).

[51] Google. *Google Gemini website*. Available online: https://gemini.google.com/ (accessed on February 9, 2026).

[52] DeepL SE. *DeepL translator website*. Available online: https://www.deepl.com/de/translator (accessed on February 9, 2026).

[53] Christian Müller-Schloer and Sven Tomforde. *Organic Computing – Technical Systems for Survival in the Real World*. Autonomic Systems. Cham: Springer International Publishing, 2017. ISBN: 978-3-319-68477-2. DOI: 10.1007/978-3-319-68477-2.

[54] Sven Tomforde, Bernhard Sick, and Christian Müller-Schloer. *Organic Computing in the Spotlight*. 2017. DOI: 10.48550/arXiv.1701.08125. arXiv: 1701.08125 [cs.MA].

[55] Christian Müller-Schloer, Hartmut Schmeck, and Theo Ungerer, eds. *Organic Computing — A Paradigm Shift for Complex Systems*. Basel: Springer, 2011. ISBN: 978-3-0348-0130-0. DOI: 10.1007/978-3-0348-0130-0.

[56] Sven Tomforde, Jan Kantert, and Bernard Sick. "Measuring Self-organisation at Runtime - A Quantification Method based on Divergence Measures". In: *Proceedings of the 9th International Conference on Agents and Artificial Intelligence - Volume 2: ICAART*. INSTICC. SciTePress, 2017, pp. 96–106. ISBN: 978-989-758-219-6. DOI: 10.5220/0006240400960106.

[57] Urban Maximilian Richter. "Controlled self-organisation using learning classifier systems". PhD thesis. Karlsruher Institut für Technologie (KIT, English: Karlsruhe Institute of Technology), 2009. ISBN: 978-3-86644-431-7. DOI: 10.5445/KSP/1000013138.

[58] J.O. Kephart and D.M. Chess. "The vision of autonomic computing". In: *Computer* 36.1 (2003), pp. 41–50. DOI: 10.1109/MC.2003.1160055.

[59] Hartmut Schmeck, Christian Müller-Schloer, Emre Çakar, Moez Mnif, and Urban Richter. "Adaptivity and Self-Organization in Organic Computing Systems". In: *ACM Transactions on Autonomous and Adaptive Systems* 5.3 (Sept. 2010). ISSN: 1556-4665. DOI: 10.1145/1837909.1837911.

[60] Sven Tomforde. *Runtime Adaptation of Technical Systems: An Architectural Framework for Self-Configuration and Self-Improvement at Runtime*. Saarbrücken, Germany: Südwestdeutscher Verlag für Hochschulschriften, Feb. 2012. ISBN: 978-3-8381-3133-7.

[61] Christian Becker, Jörg Hähner, and Sven Tomforde. "Flexibility in Organic Systems - Remarks on Mechanisms for Adapting System Goals at Runtime". In: *Proceedings of the 9th International Conference on Informatics in Control, Automation and Robotics - Volume 1: ICINCO*. INSTICC. SciTePress, 2012, pp. 287–292. ISBN: 978-989-8565-21-1. DOI: 10.5220/0004121002870292.

[62] Jan Kantert, Sven Tomforde, Christian Müller-Schloer, Sarah Edenhofer, and Bernard Sick. "Quantitative Robustness – A Generalised Approach to Compare the Impact of Disturbances in Self-organising Systems". In: *Proceedings of the 9th International Conference on Agents and Artificial Intelligence - Volume 2: ICAART*. INSTICC. SciTePress, 2017, pp. 39–50. ISBN: 978-989-758-219-6. DOI: 10.5220/0006137300390050.

[63] Sven Tomforde, Jan Kantert, Christian Müller-Schloer, Sebastian Bödelt, and Bernhard Sick. "Comparing the Effects of Disturbances in Self-adaptive Systems - A Generalised Approach for the Quantification of Robustness". In: *Transactions on Computational Collective Intelligence XXVIII*. Ed. by Ngoc Thanh Nguyen, Ryszard Kowalczyk, Jaap van den Herik, Ana Paula Rocha, and Joaquim Filipe. Cham: Springer International Publishing, 2018, pp. 193–220. ISBN: 978-3-319-78301-7. DOI: 10.1007/978-3-319-78301-7_9.

[64] Dominik Fisch, Martin Jänicke, Bernhard Sick, and Christian Müller-Schloer. "Quantitative Emergence – A Refined Approach Based on Divergence Measures". In: *2010 Fourth IEEE International Conference on Self-Adaptive and Self-Organizing Systems*. 2010, pp. 94–103. DOI: 10.1109/SASO.2010.31.

[65] C. Müller-Schloer. "Organic computing: on the feasibility of controlled emergence". In: *Proceedings of the 2nd IEEE/ACM/IFIP International Conference on Hardware/Software Codesign and System Synthesis*. CODES+ISSS '04. Stockholm, Sweden: Association for Computing Machinery, 2004, pp. 2–5. ISBN: 158113 9373. DOI: 10.1145/1016720.1016724.

[66] Urban Richter, Moez Mnif, Jürgen Branke, Christian Müller-Schloer, and Hartmut Schmeck. "Towards a generic observer/controller architecture for organic computing". In: *INFORMATIK 2006 – Informatik für Menschen, Band 1*. Bonn: Gesellschaft für Informatik e. V. (English: German Informatics Society), 2006, pp. 112–119. ISBN: 978-3-88579-187-4.

[67] Ingo Mauser. "Multi-modal Building Energy Management". 37.06.01; LK 01. PhD thesis. Karlsruher Institut für Technologie (KIT, English: Karlsruhe Institute of Technology), 2017. DOI: 10.5445/IR/1000070625.

[68] Sven Tomforde et al. “Observation and Control of Organic Systems”. In: *Organic Computing — A Paradigm Shift for Complex Systems*. Ed. by Christian Müller-Schloer, Hartmut Schmeck, and Theo Ungerer. Basel: Springer Basel, 2011, pp. 325–338. ISBN: 978-3-0348-0130-0. DOI: 10.1007/978-3-0348-0130-0_21.

[69] Karsten Weicker. *Evolutionäre Algorithmen*. Wiesbaden: Springer Fachmedien, 2015. ISBN: 978-3-658-09958-9. DOI: 10.1007/978-3-658-09958-9.

[70] Florian Allerding. “Organic Smart Home - Energiemanagement für Intelligente Gebäude (English: Organic Smart Home - Energy Management for Intelligent Buildings)”. PhD thesis. Karlsruher Institut für Technologie (KIT, English: Karlsruhe Institute of Technology), 2013. ISBN: 978-3-7315-0181-7. DOI: 10.5445/KSP/1000038928.

[71] Jürgen Quentin. *Status des Windenergieausbaus an Land in Deutschland – Jahr 2024 (English: Status of the Onshore Wind Energy Expansion in Germany – Year 2024)*. Statistic. Available online: https://www.wind-energie.de/fileadmin/redaktion/dokumente/publikationen-oeffentlich/themen/06-zahlen-und-fakten/20250115_Status_des_Windenergieausbaus_an_Land_Jahr_2024.pdf (accessed on May 15, 2025). Fachagentur Wind und Solar e. V. (English: Specialist agency for wind and solar energy), 2025.

[72] Konrad Mertens. *Photovoltaik – Lehrbuch zu Grundlagen, Technologie und Praxis (English: Photovoltaics – Textbook on Fundamentals, Technology, and Practice)*. 5th ed. München: Carl Hanser Verlag GmbH & Co. KG, 2020. ISBN: 978-3-446-46506-0. DOI: 10.3139/9783446465060.

[73] Geschäftsstelle der Arbeitsgruppe Erneuerbare Energien-Statistik (AGEE-Stat) am Umweltbundesamt (English: Office of the Working Group on Renewable Energy Statistics (AGEE-Stat) at the German Federal Environment Agency). *Erneuerbare Energien in Deutschland 2024 – Daten zur Entwicklung im Jahr 2024 (English: Renewable Energies in Germany - Data on Development in 2024)*. Statistic. Available online: https://www.umweltbundesamt.de/publikationen/erneuerbare-energien-in-deutschland-2024 (accessed on November 17, 2025). Umweltbundesamt (UBA, English: German Environment Agency), 2025.

[74] *Statistische Zahlen der deutschen Solarstrombranche (Photovoltaik) (English: Statistical figures of the German solar energy industry (photovoltaics)*. Fact sheet. Available online: https://www.solarwirtschaft.de/datawall/uploads/2025/10/BSW-Solar_Faktenblatt_Photovoltaik.pdf (accessed on November 17, 2025). Berlin: Bundesverband Solarwirtschaft e. V. (BSW, English: German Solar Industry Association), Sept. 2025.

[75] *Prosumer-Report 2025: Ausbau statt Stillstand – Prosumer trotzen schwierigem Marktumfeld (English: Prosumer Report 2025: Expansion instead of stagnation – prosumers defy difficult market conditions)*. Market report. Available online: https://www.lichtblick.de/presse/prosumer2025/ (accessed on November 17, 2025). LichtBlick SE and EuPD Research Sustainable Management GmbH, 2025.

[76] Gaëtan Masson, Adrien Van Rechem, Melodie de l'Epine, and Arnulf Jäger-Waldau. *Snapshot 2025*. Market report. Available online: https://iea-pvps.org/snapshot-reports/snapshot-2025/ (accessed on May 15, 2025). International Energy Agency Photovoltaic Power Systems Programme (IEA PVPS), 2025. DOI: 10.69766/PBHV9141.

[77] *Gesetz zu Sofortmaßnahmen für einen beschleunigten Ausbau der erneuerbaren Energien und weiteren Maßnahmen im Stromsektor (English: Law on Immediate Measures for the Accelerated Expansion of Renewable Energies and Further Measures in the Electricity Sector)*. Bundesministerium der Justiz und für Verbraucherschutz (English: German Federal Ministry of Justice and Consumer Protection). Available online: http://www.bgbl.de/xaver/bgbl/start.xav?startbk=Bundesanzeiger_BGBl&jumpTo=bgbl122s1237.pdf (accessed on October 20, 2022). German law. 2022.

[78] *Erneuerbare-Energien-Gesetz - EEG 2023 (English: Renewable Energy Sources Act 2023)*. Available online: https://datenbank.nwb.de/Dokument/514174_DBLw1220ab3b1b1ac23b1/ (accessed on October 18, 2022). German law.

[79] Harry Wirth. *Aktuelle Fakten zur Photovoltaik in Deutschland (English: Current facts about photovoltaics in Germany)*. Statistic. Available online: https://www.ise.fraunhofer.de/de/veroeffentlichungen/studien/aktuelle-fakten-zur-photovoltaik-in-deutschland.html (accessed on November 17, 2025). Fraunhofer-Institut für Solare Energiesysteme (ISE, English: Fraunhofer Institute for Solar Energy Systems), 2025.

[80] Bundesministerium für Wirtschaft und Klimaschutz (BMWK, English: German Federal Ministry for Economic Affairs and Climate Action). *Habeck: "Further strengthening preparedness by temporarily increasing electricity generation from renewables and via further measures to cut gas consumption"*. Available online: https://www.bmwk.de/Redaktion/EN/Pressemitteilungen/2022/09/20220914-habeck-further-strengthening-preparedness-by-temporarily-increasing-electricity-generation-from-renewables-and-via-further-measures-to-cut-gas-consumption.html (accessed on November 10, 2022). Press release. 2022.

[81] Hartmut Frey. *Energieautarke Gebäude – Auf dem Weg zu Smart Energy Systems (English: Energy self-sufficient buildings – On the way to smart energy systems)*. Springer eBook Collection. Berlin, Heidelberg: Springer Vieweg, 2019. ISBN: 978-3-662-57874-2. DOI: 10.1007/978-3-662-57874-2.

[82] *Zeitreihen zur Entwicklung der erneuerbaren Energien in Deutschland (English: Time series for the development of renewable energy sources in Germany*. Statistic. Available online: https://www.umweltbundesamt.de/themen/klima-energie/erneuerbare-energien/erneuerbare-energien-in-zahlen (accessed on November 19, 2025). Arbeitsgruppe Erneuerbare Energien-Statistik (AGEE-Stat) am Umweltbundesamt (English: Working Group on Renewable Energy Statistics (AGEE-Stat) at the German Federal Environment Agency), 2025.

[83] Umweltbundesamt (English: German Environment Agency). *Umgebungswärme und Wärmepumpen (English: Ambient heat and heat pumps)*. Available online: https://www.umweltbundesamt.de/themen/klima-energie/erneuerbare-energien/umgebungswaerme-waermepumpen#kennzahlen (accessed on November 19, 2025). Website article. 2025.

[84] Deutsche Energie-Agentur GmbH (dena, English: German Energy Agency). *dena-Gebäudereport 2024: Zahlen, Daten, Fakten zum Klimaschutz im Gebäudebestand (English: dena-Building-Report 2024: Facts, figures, and data on climate protection in existing buildings)*. Statistic. Available online: https://www.gebaeudeforum.de/gebaeudereport2024 (accessed on November 19, 2025). Berlin, 2023.

[85] Statistisches Bundesamt (Destatis, English: Federal Statistical Office of Germany). *Mehr als zwei Drittel der im Jahr 2024 errichteten Wohngebäude heizen mit Wärmepumpen (English: More than two-thirds of residential buildings constructed in 2024 are heated with heat pumps)*. Available online: https://www.destatis.de/DE/Presse/Pressemitteilungen/2025/06/PD25_N031_31_51.html (accessed on November 19, 2025). Press release. 2025.

[86] Bundesministerium für Wirtschaft und Klimaschutz (BMWK, English: German Federal Ministry for Economic Affairs and Climate Action) and Bundesministerium für Wohnen, Stadtentwicklung und Bauwesen (BMWSB, English: Federal Ministry for Housing, Urban Development and Building). *Breites Bündnis will mindestens 500.000 neue Wärmepumpen pro Jahr (English: Broad alliance wants at least 500,000 new heat pumps per year)*. Available online: https://www.bmwk.de/Redaktion/DE/Pressemitteilungen/2022/06/20220629-breites-buendnis-will-mindestens-500000-neue-waermepumpen-pro-jahr.html (accessed on November 8, 2022). Press release. 2022.

[87] *Branchenstudie 2025 – Marktentwicklung, Prognosen & Handlungsempfehlungen (English: Industry study 2025 – Market development, forecasts, and recommendations for action)*. Market report. Available online: https://www.waermepumpe.de/fileadmin/user_upload/Branchenstudie_2025_final.pdf (accessed on November 19, 2025). Berlin: Bundesverband Wärmepumpe (BWP) e. V. (English: German Heat Pump Association), 2025.

[88] International Energy Agency (IEA). *Heat pumps*. Available online: https://www.iea.org/energy-system/buildings/heat-pumps (accessed on November 20, 2025). Website article. 2024.

[89] Gunter Schaumann and Karl W. Schmitz, eds. *Kraft-Wärme-Kopplung*. Berlin, Heidelberg: Springer, 2010. ISBN: 978-3-642-01425-3. DOI: 10.1007/978-3-642-01425-3.

[90] *Auswertungstabellen zur Energiebilanz 1990 bis 2024 (English: Evaluation tables for the energy balance sheet of Germany 1990 to 2024)*. Statistic. Available online: https://ag-energiebilanzen.de/daten-und-fakten/auswertungstabellen/ (accessed on November 20, 2025). AG Energiebilanzen e. V. (AGEB, English: Working Group Energy Balance Sheets), 2025.

[91] Sebastian Briem et al. *Status quo der Kraft-Wärme-Kopplung in Deutschland – Sachstandspapier (English: Status quo of cogeneration of heat and power in Germany – status report.* Report. Available online: https://www.umweltbundesamt.de/publikationen/status-quo-der-kraft-waerme-kopplung-in-deutschland (accessed on October 28, 2022). Umweltbundesamt (UBA, English: German Federal Environmental Agency), 2020.

[92] *Statistik: Zulassung von KWK-Anlagen nach dem Kraft-Wärme-Kopplungsgesetz (KWKG) (English: Statistics: Approval of CHP plants according to the Combined Heat and Power Act (KWKG).* Statistic. Available online: https://www.bafa.de/SharedDocs/Downloads/DE/Energie/kwk_statistik_zulassungen_kwk_anlagen.html (accessed on November 20, 2025). Bundesamt für Wirtschaft und Ausfuhrkontrolle (BAFA, English: German Federal Office for Economic Affairs and Export Control), 2025.

[93] *Evaluierung der Kraft-Wärme-Kopplung – Analysen zur Entwicklung der Kraft-Wärme-Kopplung in einem Energiesystem mit hohem Anteil erneuerbarer Energien (English: Evaluation of cogeneration – Analyses on the development of cogeneration in an energy system with a high share of renewable energies).* Study. Available online: https://www.bmwk.de/Redaktion/DE/Publikationen/Studien/evaluierung-der-kraft-waerme-kopplung.html (accessed on November 11, 2022). Bundesministerium für Wirtschaft und Klimaschutz (BMWK, English: German Federal Ministry for Economic Affairs and Climate Action), 2019.

[94] *Positionspapier – Aktuelle Hemmnisse und Maßnahmen zur Weiterentwicklung der KWK und des KWKG (English: Position paper – Current obstacles and measures for the further development of CHP and the CHP Act).* Report. Available online: https://www.bdew.de/media/documents/2024-02-01_Positionspapier_aktueller_Stand_KWK_KWKG_oA.pdf (accessed on November 20, 2025). Berlin: Bundesverband der Energie- und Wasserwirtschaft e. V. (BDEW, English: Federal Association of the Energy and Water Industry), 2024.

[95] Matthias Koch and Sabine Gores. *Welche Rolle spielt die Kraft-Wärme-Kopplung im künftigen Energiesystem? (English: What role will combined heat and power play in the energy system of the future?)* Available online: https://www.oeko.de/publikation/welche-rolle-spielt-die-kraft-waerme-kopplung-im-kuenftigen-energiesystem/ (accessed on November 20, 2025). Talk. 2022.

[96] *Residential Micro CHP Systems - Global Market Share and Ranking, Overall Sales and Demand Forecast 2025–2031.* Market report. Available online: https://www.qyresearch.com/reports/4604148/residential-micro-chp-systems (accessed on November 20, 2025). QYResearch, Inc., 2025.

[97] V. Cigolotti and M. Genovese. *Stationary Fuel Cell Applications – Tracking Market Trends.* Market report. Available online: https://ieafuelcell.com/wp-content/uploads/2024/11/stationary-fuel-cell-applications-market-trends-2021.pdf (accessed on November 20, 2025). International Energy Agency (IEA) Technology Collaboration Programme Advanced Fuel Cells, 2021.

[98] Statistisches Bundesamt (Destatis, English: Federal Statistical Office of Germany). *Jeder zehnte Haushalt verfügt über smarte Energiemanagement-Systeme (English: One in ten households have smart energy management systems)*. Available online: https://www.destatis.de/DE/Presse/Pressemitteilungen/2022/10/PD22_455_63.html (accessed on November 14, 2022). Press release. 2022.

[99] Bernhard Rohleder. *Smart Home 2024*. Statistic. Available online: https://www.bitkom.org/sites/main/files/2024-08/240822-Bitkom-Charts-Smart-Home-2024.pdf (accessed on November 21, 2025). Bitkom, 2024.

[100] *Consumer Tech & Durables – Outlook 2024*. Market report. Available online: https://www.gfk.com/hubfs/State%20of%20T%20and%20D%20report%20Outlook%202024/Consumer-Technology-%26-Durables-Outlook-2024_3.pdf (accessed on November 21, 2025). NielsenIQ (NIQ) and Gesellschaft für Konsumforschung (GfK, English: Society for Consumer Research), 2024.

[101] Nevin Francis. *Smart home outlook: The demand and price dynamics shaping the market into 2025*. Market report. Available online: https://nielseniq.com/global/en/insights/analysis/2024/smart-home-2024-the-demand-and-price-dynamics-shaping-the-market/ (accessed on November 21, 2025). NielsenIQ (NIQ) and Gesellschaft für Konsumforschung (GfK, English: Society for Consumer Research), 2024.

[102] *Smart Dishwashers Global Market Report 2025*. Market report. Available online: https://www.thebusinessresearchcompany.com/report/smart-dishwashers-global-market-report (accessed on November 21, 2025). The Business Research Company, 2025.

[103] *Ownership of smart home products doubles in the UK in five years*. Statistic. Available online: https://nielseniq.com/global/en/insights/analysis/2024/ownership-of-smart-home-products-doubles-in-the-uk-in-five-years/ (accessed on November 21, 2025). NielsenIQ (NIQ) and Gesellschaft für Konsumforschung (GfK, English: Society for Consumer Research), 2024.

[104] Lutz Hillemacher. "Lastmanagement mittels dynamischer Strompreissignale bei Haushaltskunden (English: Load Management Through Dynamic Electricity Price Signals for Household Customers)". PhD thesis. Karlsruher Institut für Technologie (KIT, English: Karlsruhe Institute of Technology), 2014. DOI: 10.5445/IR/1000044670.

[105] Adrian Tantau, András Puskás-Tompos, Laurentiu Fratila, and Costel Stanciu. "Acceptance of Demand Response and Aggregators as a Solution to Optimize the Relation between Energy Producers and Consumers in order to Increase the Amount of Renewable Energy in the Grid". In: *Energies* 14.12, 3441 (2021). ISSN: 1996-1073. DOI: 10.3390/en14123441.

[106] Araavind Sridhar et al. "Toward residential flexibility - Consumer willingness to enroll household loads in demand response". In: *Applied Energy* 342, 121204 (2023). ISSN: 0306-2619. DOI: 10.1016/j.apenergy.2023.121204.

[107] Milan Robert Wanek. *The State of Development of Residential Demand-Side Flexibility in France – Report on the Research Visit*. Report. Available online: https://future-energy-lab.de/app/uploads/2024/12/Wanek_Bericht.pdf (accessed on November 21, 2025). Deutsche Energie-Agentur GmbH (dena, English: German Energy Agency) and Future Energy Lab Berlin, 2024.

[108] Reiner Korthauer, ed. *Lithium-Ion Batteries: Basics and Applications*. Berlin, Heidelberg: Springer, 2018. ISBN: 978-3-662-53071-9. DOI: 10.1007/978-3-662-53071-9.

[109] BloombergNEF. *Lithium-Ion Battery Pack Prices See Largest Drop Since 2017, Falling to $115 per Kilowatt-Hour: BloombergNEF*. Available online: https://about.bnef.com/blog/lithium-ion-battery-pack-prices-see-largest-drop-since-2017-falling-to-115-per-kilowatt-hour-bloombergnef/ (accessed on November 24, 2025). Press release. 2024.

[110] Romain Zissler. *Solar PV Significantly Grew Globally in 2024, Bolstered by Cheaper Batteries*. Report. Available online: https://www.renewable-ei.org/en/activities/column/REupdate/20250507.php (accessed on November 24, 2025). Renewable Energy Institute, 2025.

[111] Tobias Reuther and Christoph Kost. *Photovoltaik- und Batteriespeicherzubau in Deutschland in Zahlen: Auswertung des Marktstammdatenregisters – Stand Februar 2024 (English: Photovoltaic and battery storage expansion in Germany in figures: Evaluation of the market master data register as of February 2024)*. Statistic. Available online: https://www.ise.fraunhofer.de/content/dam/ise/de/documents/publications/studies/2024-02-photovoltaik-und-batteriespeicherzubau-in-deutschland.pdf (accessed on November 24, 2025). Fraunhofer-Institut für Solare Energiesysteme ISE (English: Fraunhofer Institute for Solar Energy Systems ISE), 2024.

[112] *Statistische Zahlen der deutschen Solarstrombranche (Speicher/Mobilität) (English: Statistical figures for the German solar power industry (storage/mobility)*. Fact sheet. Available online: https://www.solarwirtschaft.de/datawall/uploads/2022/08/bsw_faktenblatt_stromspeicher.pdf (accessed on November 24, 2025). Bundesverband Solarwirtschaft e. V. (BSW, English: German Solar Industry Association), 2025.

[113] Netze BW GmbH. *Stromeinspeisung – Wissenswertes zu Photovoltaik – Einspeisevergütung für Neuanlagen nach EEG 2023 (English: Electricity feed-in – Things to know about photovoltaics – Feed-in tariff for new installations according to EEG 2023)*. Available online: https://www.netze-bw.de/stromeinspeisung/wissenswertes-zu-photovoltaik (accessed on November 24, 2025). Website article.

[114] Bundesnetzagentur (English: German Federal Network Agency). *EEG-Förderung und -Fördersätze (English: EEG subsidies and subsidy rates)*. Available online: https://www.bundesnetzagentur.de/DE/Fachthemen/ElektrizitaetundGas/ErneuerbareEnergien/EEG_Foerderung/start.html (accessed on November 24, 2025). Website article. 2025.

[115] J. v. G. technology GmbH. *Die EEG-Umlage auf Eigenverbrauch: 2024 ersatzlos gestrichen – Was jetzt für Sie gilt (English: The EEG surcharge on self-consumption: abolished without replacement in 2024 – What applies to you now)*. Available online: https://www.photovoltaik.info/eeg-umlage-eigenverbrauch-2024/ (accessed on November 24, 2025). Website article. 2024.

[116] *Scaling the Residential Energy Storage Market*. Market report. Available online: https://assets.bbhub.io/professional/sites/24/Scaling-the-Residential-Energy-Storage-Market.pdf (accessed on November 24, 2025). BloombergNEF and Pylontech, 2023.

[117] *Nationaler Entwicklungsplan Elektromobilität der Bundesregierung (NEP, English: National Electromobility Development Plan of the German Federal Government)*. Available online: https://www.erneuerbar-mobil.de/sites/default/files/2016-08/nep_09_bmu_bf.pdf (accessed on October 21, 2022). 2009.

[118] Anton Karle. *Elektromobilität – Grundlagen und Praxis (English: Electromobility – Fundamentals and Practice)*. 6th ed. Hanser eLibrary. München: Carl Hanser Verlag GmbH & Co. KG, 2022. ISBN: 978-3-446-47509-0. DOI: 10.3139/9783446475090.

[119] *Neuzulassungen von Personenkraftwagen (Pkw) im Jahresverlauf 2025 nach Marken und alternativen Antrieben (English: New registrations of passenger cars in the course of the year 2025 by brands and alternative drives)*. Statistic. Available online: https://www.kba.de/DE/Presse/Pressemitteilungen/AlternativeAntriebe/2025/pm48_2025_Antriebe_10_25_komplett.html (accessed on November 24, 2025). Kraftfahrt-Bundesamt (KBA, English: German Federal Motor Transport Authority), 2025.

[120] *Bestand an Kraftfahrzeugen und Kraftfahrzeuganhängern nach Bundesländern, Fahrzeugklassen und ausgewählten Merkmalen, 1. Juli 2025 (English: Stock of motor vehicles and motor vehicle trailers by federal states, vehicle classes and selected characteristics, July 1, 2025)*. Statistic. Available online: https://www.kba.de/DE/Statistik/Produktkatalog/produkte/Fahrzeuge/fz27_b_uebersicht.html?nn=835828 (accessed on November 24, 2025). Kraftfahrt-Bundesamt (KBA, English: German Federal Motor Transport Authority), 2025.

[121] Umweltbundesamt (UBA, English: German Environment Agency). *Klimaschutz im Verkehr (English: Climate protection in transportation)*. Available online: https://www.umweltbundesamt.de/themen/verkehr/klimaschutz-im-verkehr (accessed on November 24, 2025). Website article. 2025.

[122] International Energy Agency (IEA). *Global EV Outlook 2025 – Expanding sales in diverse markets*. Available online: https://www.iea.org/reports/global-ev-outlook-2025 (accessed on November 24, 2025). Website article. 2025.

[123] C.W. Gellings. "The concept of demand-side management for electric utilities". In: *Proceedings of the IEEE* 73.10 (1985), pp. 1468–1470. DOI: 10.1109/PROC.1985.13318.

[124] Rongling Li, ed. *Energy Flexible Buildings Towards Resilient Low Carbon Energy Systems (Annex 82): Summary report*. Technical report. Available online: https://www.iea-ebc.org/Data/publications/Energy%20Flexible%20Buildings%20Towards%20Resilient%20Low%20Carbon%20Energy%20Systems%20%28Annex%2082%29%20Summary%20report.pdf (accessed on November 25, 2025). Kongens Lyngby, Denmark: Technical University of Denmark and International Energy Agency (IEA), May 2025.

[125] SMA Solar Technology AG. *SMA shifts the phase - Why reactive power is important - and no problem with SMA technology*. https://www.sma.de/en/partners/knowledgebase/sma-shifts-the-phase.html (accessed on November, 14 2022). Website article.

[126] SMA Solar Technology AG. *Configuring Limitation of Active Power Feed-In*. Available online: https://manuals.sma.de/EDMM-10/en-US/1071201163.html (accessed on November 16, 2022). User manual.

[127] Jun Hong, N. Kelly, Ian Richardson, and Murray Thomson. "Assessing heat pumps as flexible load". In: *Proceedings of the Institution of Mechanical Engineers, Part A: Journal of Power and Energy* 227.1 (Feb. 2013), pp. 30–42. DOI: 10.1177/0957650912454830.

[128] Jan Müller, Matthias März, Ingo Mauser, and Hartmut Schmeck. "Optimization of Operation and Control Strategies for Battery Energy Storage Systems by Evolutionary Algorithms". In: *Applications of Evolutionary Computation*. Ed. by Giovanni Squillero and Paolo Burelli. Cham: Springer International Publishing, 2016, pp. 507–522. ISBN: 978-3-319-31204-0. DOI: 10.1007/978-3-319-31204-0_33.

[129] FZI Forschungszentrum Informatik (FZI, English: FZI Research Center for Information Technology). *Organic Smart Home website*. Available online: https://organicsmarthome.fzi.de/ (accessed on August 29, 2025). Karlsruhe, Germany.

[130] *Organic Smart Home GitHub repository*. Available online: https://github.com/organicsmarthome/OSHv4 (accessed on August 29, 2025). 2016.

[131] *Energy management systems – Requirements with guidance for use (ISO 50001:2018)*. Standard. DIN Deutsches Institut für Normung (English: DIN German Institute for Standardization) and International Organization for Standardization, Dec. 2018.

[132] Sumit K. Rathor and D. Saxena. "Energy management system for smart grid: An overview and key issues". In: *International Journal of Energy Research* 44.6 (2020), pp. 4067–4109. DOI: 10.1002/er.4883.

[133] Khawla Ettalbi, Hanan Elabd, Mohammed Ouassaid, and Mohamed Maaroufi. "A comparative study of energy management systems for PV self-consumption". In: *2016 International Renewable and Sustainable Energy Conference (IRSEC)*. 2016, pp. 1086–1091. DOI: 10.1109/IRSEC.2016.7983966.

[134] Manuel Lösch. "Utilization of Electric Prosumer Flexibility Incentivized by Spot and Balancing Markets". PhD thesis. Karlsruher Institut für Technologie (KIT, English: Karlsruhe Institute of Technology), 2022. DOI: 10.5445/IR/1000152126.

[135] Alessandra De Paola, Marco Ortolani, Giuseppe Lo Re, Giuseppe Anastasi, and Sajal K. Das. "Intelligent Management Systems for Energy Efficiency in Buildings: A Survey". In: *ACM Comput. Surv.* 47.1 (June 2014). ISSN: 0360-0300. DOI: 10.1145/2611779.

[136] Sara Barja-Martinez et al. "A Novel Hybrid Home Energy Management System Considering Electricity Cost and Greenhouse Gas Emissions Minimization". In: *IEEE Transactions on Industry Applications* 57.3 (2021), pp. 2782–2790. DOI: 10.1109/TIA.2021.3057014.

[137] Peter Palensky and Dietmar Dietrich. "Demand Side Management: Demand Response, Intelligent Energy Systems, and Smart Loads". In: *IEEE Transactions on Industrial Informatics* 7.3 (2011), pp. 381–388. DOI: 10.1109/TII.2011.2158841.

[138] W. Khamphanchai et al. "Conceptual architecture of building energy management open source software (BEMOSS)". In: *IEEE PES Innovative Smart Grid Technologies, Europe*. 2014, pp. 1–6. DOI: 10.1109/ISGTEurope.2014.7028784.

[139] *BEMOSS3.5 GitHub repository*. Available online: https://github.com/bemoss/BEMOSS3.5 (accessed on November 27, 2025).

[140] OpenEMS Association e. V. *OpenEMS Website*. Available online: https://openems.io/ (accessed on November 5, 2025).

[141] *OpenEMS GitHub repository*. Available online: https://github.com/OpenEMS/openems/blob/develop/README.md (accessed on November 27, 2025).

[142] Fraunhofer Institute for Integrated Circuits IIS. *OGEMA 2.0 – Open Gateway Energy Management – Secure and Flexible Framework for Energy Management Systems*. Available online: https://www.iis.fraunhofer.de/content/dam/iis/de/doc/lv/nsa/Flyer/OGEMA2_Open_Gateway_for_Energy_Managemen_d.pdf (accessed on November 27, 2025).

[143] *OGEMA GitHub repository*. Available online: https://github.com/ogema (accessed on November 27, 2025).

[144] U.S. Department of Energy. *VOLTTRON*. Available online: https://www.energy.gov/eere/buildings/volttron (accessed on November 27, 2025). Website article.

[145] Eclipse Foundation. *VOLTTRON project website*. Available online: https://projects.eclipse.org/projects/iot.volttron (accessed on November 27, 2025).

[146] The VOLTTRON Community. *VOLTTRON documentation!* Available online: https://volttron.readthedocs.io/en/main/index.html (accessed on November 27, 2025).

[147] *VOLTTRON GitHub repository*. Available online: https://github.com/VOLTTRON/volttron (accessed on November 27, 2025).

[148] NOBATEK/INEF4. *BEMServer website*. Available online: https://www.bemserver.org/ (accessed on November 27, 2025).

[149] *BEMServer GitHub repository*. Available online: https://github.com/bemserver (accessed on November 27, 2025).

[150] Arduino. *Arduino website*. Available online: https://www.arduino.cc/ (accessed on November 27, 2025).

[151] Raspberry Pi Foundation. *Raspberry Pi website*. Available online: https://www.raspberrypi.org/ (accessed on November 27, 2025).

[152] OpenEnergyMonitor. *OpenEnergyMonitor website*. Available online: https://openenergymonitor.org/ (accessed on November 27, 2025).

[153] openHAB Community and openHAB Foundation e. V. *openHAB website*. Available online: https://www.openhab.org/ (accessed on November 27, 2025).

[154] Open Home Foundation. *Home Assistant website*. Available online: https://www.home-assistant.io/ (accessed on November 27, 2025).

[155] *MyEMS website*. Available online: https://myems.io/en/ (accessed on November 27, 2025).

[156] *MyEMS GitHub repository*. Available online: https://github.com/MyEMS/myems (accessed on November 27, 2025).

[157] Ingo Mauser, Christian Hirsch, Sebastian Kochanneck, and Hartmut Schmeck. "Organic Architecture for Energy Management and Smart Grids". In: *2015 IEEE International Conference on Autonomic Computing*. 2015, pp. 101–108. DOI: 10.1109/ICAC.2015.10.

[158] Ingo Mauser, Jan Müller, Florian Allerding, and Hartmut Schmeck. "Adaptive building energy management with multiple commodities and flexible evolutionary optimization". In: *Renewable Energy* 87 (2016). Optimization Methods in Renewable Energy Systems Design, pp. 911–921. ISSN: 0960-1481. DOI: 10.1016/j.renene.2015.09.003.

[159] Jan Müller, Mischa Ahrens, Ingo Mauser, and Hartmut Schmeck. "Achieving Optimized Decisions on Battery Operating Strategies in Smart Buildings". In: *Applications of Evolutionary Computation*. Ed. by Kevin Sim and Paul Kaufmann. Cham: Springer International Publishing, 2018, pp. 205–221. ISBN: 978-3-319-77538-8. DOI: 10.1007/978-3-319-77538-8_15.

[160] Johanna Geis-Schroer. "Integration eines regelbaren Ortsnetztransformators in Multi-Haushalt-Simulationen mit dem Organic Smart Home (English: Integration of a voltage regulated distribution transformer in multi-household simulations with the Organic Smart Home)". Bachelor thesis. Karlsruher Institut für Technologie (KIT, English: Karlsruhe Institute of Technology), 2017.

[161] *Smart Grid Traffic Light Concept – Design of the Amber Phase*. Technical report. Available online: https://www.bdew.de/media/documents/Stn_20150310_Smart-Grids-Traffic-Light-Concept_english.pdf (accessed on August 27, 2025). Berlin, Germany: Bundesverband der Energie- und Wasserwirtschaft e. V. (BDEW, English: Federal Association of the Energy and Water Industry), Mar. 2015.

[162] Sebastian Kochanneck, Johanna Geis-Schroer, Ingo Mauser, and Hartmut Schmeck. "Reference Scenarios for the Evaluation of the Traffic Light Concept in Low-voltage Power Systems". In: *ETG Congress 2017*. ETG-Fachberichte (English: ETG technical reports). Berlin: VDE, Nov. 2017, pp. 330–335. ISBN: 978-3-8007-4505-0.

[163] Abdulrahman Alassi, Santiago Bañales, Omar Ellabban, Grain Adam, and Callum MacIver. "HVDC Transmission: Technology Review, Market Trends and Future Outlook". In: *Renewable and Sustainable Energy Reviews* 112 (2019), pp. 530–554. ISSN: 1364-0321. DOI: https://doi.org/10.1016/j.rser.2019.04.062.

[164] Statkraft Germany GmbH. *NordLink: Das grüne Kabel ist am Netz (English: The green cable is connected to the grid)*. https://www.statkraft.de/presse/2021/nordlink-feierliche-inbetriebnahme/ (accessed on January 16, 2025). Press release. 2021.

[165] Bundesnetzagentur (English: German Federal Network Agency). *Brunsbüttel – Großgartach (SuedLink)*. https://www.netzausbau.de/Vorhaben/ansicht/de.html?gruppe=bbplg&nummer=3 (accessed on January 16, 2025). Website article.

[166] *DIN IEC 60076-7 (VDE 0532-76-7): 2008-02, Power transformers – Part 7: Loading guide for oil-immersed power transformers (DIN IEC 60076-7:2005)*. Standard. DIN Deutsches Institut für Normung (English: DIN German Institute for Standardization) and International Electrotechnical Commission (IEC), Feb. 2008.

[167] *IEC 60038:2009, IEC standard voltages*. Standard. International Electrotechnical Commission, June 2009.

[168] *VDE-AR-N 4105:2018-11 – Erzeugungsanlagen am Niederspannungsnetz - Technische Mindestanforderungen für Anschluss und Parallelbetrieb von Erzeugungsanlagen am Niederspannungsnetz (English: Generation plants in the low-voltage grid - Minimum Technical Requirements for Connection and Parallel Operation of Generation Plants in the Low-Voltage Grid)*. Standard. VDE Verband der Elektrotechnik Elektronik Informationstechnik e. V. (English: VDE Association for Electrical Engineering Electronics Information Technology), VDE-Verlag (English: VDE Publishing House), Nov. 2018.

[169] Nikos Hatziargyriou, Hiroshi Asano, Reza Iravani, and Chris Marnay. "Microgrids". In: *IEEE Power and Energy Magazine* 5.4 (2007), pp. 78–94. DOI: 10.1109/MPAE.2007.376583.

[170] Daniel Burmester, Ramesh Rayudu, Winston Seah, and Daniel Akinyele. "A review of nanogrid topologies and technologies". In: *Renewable and Sustainable Energy Reviews* 67 (2017), pp. 760–775. ISSN: 1364-0321. DOI: 10.1016/j.rser.2016.09.073.

[171] *Technology Roadmap – Smart Grids*. Technical report. Available online: https://iea.blob.core.windows.net/assets/fe14d871-ebcb-47d3-8582-b3a6be3662ba/smartgrids_roadmap.pdf (accessed on August 1, 2025). International Energy Agency (IEA), 2011.

[172] *The Integrated Energy and Communication Systems Architecture – Volume I: User Guidelines and Recommendations*. Technical report. Available online: https://xanthus-consulting.com/IntelliGrid_Architecture/IECSA_Volumes/IECSA_VolumeI.pdf (accessed on August 5, 2025). Palo Alto, CA: Electric Power Research Institute (EPRI) and Electricity Innovation Institute, 2003.

[173] *The Integrated Energy and Communication Systems Architecture – Volume II: Functional Requirements*. Technical report. Available online: https://xanthus-consulting.com/IntelliGrid_Architecture/IECSA_Volumes/IECSA_VolumeII.pdf (accessed on August 5, 2025). Palo Alto, CA: Electric Power Research Institute (EPRI) and Electricity Innovation Institute, 2003.

[174] *The Integrated Energy and Communication Systems Architecture – Volume III: Models*. Technical report. Available online: https://xanthus-consulting.com/IntelliGrid_Architecture/IECSA_Volumes/IECSA_VolumeIII.pdf (accessed on August 5, 2025). Palo Alto, CA: Electric Power Research Institute (EPRI) and Electricity Innovation Institute, 2003.

[175] *The Integrated Energy and Communication Systems Architecture – Volume IV: Technical Analysis*. Technical report. Available online: https://xanthus-consulting.com/IntelliGrid_Architecture/IECSA_Volumes/IECSA_VolumeIV.pdf (accessed on August 5, 2025). Palo Alto, CA: Electric Power Research Institute (EPRI) and Electricity Innovation Institute, 2003.

[176] The GridWise Architecture Council. *GridWise Interoperability Context-Setting Framework*. Technical report. Available online: https://gridwiseac.org/pdfs/GridWise_Interoperability_Context_Setting_Framework.pdf (accessed on August 5, 2025). Mar. 2008.

[177] "IEEE Guide for Smart Grid Interoperability of Energy Technology and Information Technology Operation with the Electric Power System (EPS), End-Use Applications, and Loads". In: *IEEE Std 2030-2011* (2011), pp. 1–126. DOI: 10.1109/IEEESTD.2011.6018239.

[178] *Modern Distribution Grid (DSPx) – Volume I: Objective Driven Functionality*. Technical report. Version 2.0. Available online: https://gridarchitecture.pnnl.gov/media/Modern-Distribution-Grid_Volume_I_v2_0.pdf (accessed on August 5, 2025). U.S. Department of Energy, Nov. 2019.

[179] *Modern Distribution Grid (DSPx) – Volume II: Advanced Technology Maturity Assessment*. Technical report. Version 2.0. Available online: https://gridarchitecture.pnnl.gov/media/Modern-Distribution-Grid_Volume_II_v2_0.pdf (accessed on August 5, 2025). U.S. Department of Energy, Nov. 2019.

[180] *Modern Distribution Grid – Decision Guide – Volume III*. Technical report. Available online: https://gridarchitecture.pnnl.gov/media/Modern-Distribution-Grid-Volume-III.pdf (accessed on August 5, 2025). U.S. Department of Energy, June 2017.

[181] *Modern Distribution Grid DSPx – Strategy & Implementation Planning Guidebook*. Technical report. Available online: https://gridarchitecture.pnnl.gov/media/Modern-Distribution-Grid_Volume_IV_v1_0_draft.pdf (accessed on August 5, 2025). U.S. Department of Energy, June 2020.

[182] *NIST Framework and Roadmap for Smart Grid Interoperability Standards, Release 1.0*. Technical report. NIST Special Publication 1108. National Institute of Standards and Technology (NIST), Jan. 2010. DOI: 10.6028/NIST.sp.1108.

[183] Avi Gopstein, Cuong Nguyen, Cheyney O'Fallon, Nelson Hastings, and David A. Wollman. *NIST Framework and Roadmap for Smart Grid Interoperability Standards, Release 4.0*. Technical report. NIST Special Publication 1108r4. National Institute of Standards and Technology (NIST), 2021. DOI: 10.6028/NIST.SP.1108r4.

[184] *Guidelines on the promotion of smart grids development*. Technical report. Available online: https://chinaenergyportal.org/guidelines-on-the-promotion-of-smart-grids-development/ (accessed on August 6, 2025). National Development and Reform Commission and National Energy Administration, July 2015.

[185] *Guidelines for promoting internet+ smart energy development*. Technical report. Available online: https://chinaenergyportal.org/guidelines-for-promoting-internet-smart-energy-development/ (accessed on August 6, 2025). National Development and Reform Commission and National Energy Administration and Ministry of Industry and Information Technology, Feb. 2016.

[186] Licheng Li et al. "Theoretical Framework and Key Technologies of Transparent Power Grid". In: *Strategic Study of CAE* 24.4 (2022), pp. 32–43. DOI: 10.15302/J-SSCAE-2022.04.025.

[187] *Smart Grid Reference Architecture*. Technical report SG-CG/M490/C. Available online: https://www.cencenelec.eu/media/CEN-CENELEC/AreasOfWork/CEN-CENELEC_Topics/Smart%20Grids%20and%20Meters/Smart%20Grids/reference_architecture_smartgrids.pdf (accessed on August 6, 2025). CEN-CENELEC-ETSI Smart Grid Coordination Group, Nov. 2012.

[188] *CEN-CENELEC-ETSI Smart Grid Coordination Group – Sustainable Processes*. Technical report SG-CG/M490/E. Available online: https://www.cencenelec.eu/media/CEN-CENELEC/AreasOfWork/CEN-CENELEC_Topics/Smart%20Grids%20and%20Meters/Smart%20Grids/smartgrids_sustainableprocesses.pdf (accessed on August 6, 2025). CEN-CENELEC-ETSI Smart Grid Coordination Group, Nov. 2012.

[189] *Overview of SG-CG Methodologies*. Technical report SG-CG/M490/F. Available online: https://www.cencenelec.eu/media/CEN-CENELEC/AreasOfWork/CEN-CENELEC_Topics/Smart%20Grids%20and%20Meters/Smart%20Grids/2_sgcg_methodology_overview.pdf (accessed on August 6, 2025). CEN-CENELEC-ETSI Smart Grid Coordination Group, Nov. 2014.

[190] *Smart Grid Set of Standards – Version 3.1.* Technical report SG-CG/M490/G. Available online: https://www.cencenelec.eu/media/CEN-CENELEC/AreasOfWork/CEN-CENELEC_Topics/Smart%20Grids%20and%20Meters/Smart%20Grids/1_sgcg_standards_report.pdf (accessed on August 6, 2025). CEN-CENELEC-ETSI Smart Grid Coordination Group, Oct. 2014.

[191] *Smart Grid Information Security.* Technical report SG-CG/M490/H. Available online: https://www.cencenelec.eu/media/CEN-CENELEC/AreasOfWork/CEN-CENELEC_Topics/Smart%20Grids%20and%20Meters/Smart%20Grids/7_sgcg_sgis_report.pdf (accessed on August 6, 2025). CEN-CENELEC-ETSI Smart Grid Coordination Group, Dec. 2014.

[192] *Smart Grid Interoperability – Methodologies to facilitate Smart Grid system interoperability through standardization, system design and testing.* Technical report SG-CG/M490/I. Available online: https://www.cencenelec.eu/media/CEN-CENELEC/AreasOfWork/CEN-CENELEC_Topics/Smart%20Grids%20and%20Meters/Smart%20Grids/6_sgcg_interoperability_report.pdf (accessed on August 6, 2025). CEN-CENELEC-ETSI Smart Grid Coordination Group, Oct. 2014.

[193] *SGAM User Manual — Applying, testing & refining the Smart Grid Architecture Model (SGAM).* Manual SG-CG/M490/K. Available online: https://www.cencenelec.eu/media/CEN-CENELEC/AreasOfWork/CEN-CENELEC_Topics/Smart%20Grids%20and%20Meters/Smart%20Grids/4_sgcg_methodology_sgamusermanual.pdf (accessed on August 6, 2025). CEN-CENELEC-ETSI Smart Grid Coordination Group, Nov. 2014.

[194] *Flexibility Management – Overview of the main concepts of flexibility management – Version 3.0.* Technical report SG-CG/M490/L. Available online: https://www.cencenelec.eu/media/CEN-CENELEC/AreasOfWork/CEN-CENELEC_Topics/Smart%20Grids%20and%20Meters/Smart%20Grids/5_sgcg_methodology_flexibilitymanagement.pdf (accessed on August 6, 2025). CEN-CENELEC-ETSI Smart Grid Coordination Group, Nov. 2014.

[195] EU DSO Entity. *EU DSO Entity website.* Available online: https://eudsoentity.eu/ (accessed on August 26, 2025).

[196] European Network of Transmission System Operators for Electricity (ENTSO-E). *ENTSO-E website.* Available online: https://www.entsoe.eu/ (accessed on August 26, 2025). Website.

[197] European Network of Transmission System Operators for Electricity (ENTSO-E). *DSO Entity and ENTSO-E Submit Joint Network Code on Demand Response.* Available online: https://www.entsoe.eu/news/2024/05/08/dso-entity-and-entso-e-submit-joint-network-code-on-demand-response/ (accessed on August 26, 2025). Website article. May 2024.

[198] European Network of Transmission System Operators for Electricity (ENTSO-E). *ENTSO-E and DSO Entity launch JWG Data Interoperability Repository to support transparent and harmonised data access across Europe.* Available online: https://www.entsoe.eu/news/2025/07/07/entso-e-and-dso-entity-launch-jwg-data-

interoperability-repository-to-support-transparent-and-harmonised-data-access-across-europe/ (accessed on August 26, 2025). Website article. July 2025.

[199] *BDEW Roadmap – Realistic Steps for the Implementation of Smart Grids in Germany*. Technical report. Available online: https://www.bdew.de/media/documents/Pub_20130211_Roadmap-Smart-Grids_english.pdf (accessed on August 27, 2025). Berlin, Germany: Bundesverband der Energie- und Wasserwirtschaft e. V. (BDEW, English: Federal Association of the Energy and Water Industry), Feb. 2013.

[200] *USEF: The Framework Explained*. Technical report. Available online: https://www.usef.energy/app/uploads/2016/12/USEF_TheFrameworkExplained-18nov15.pdf (accessed on August 27, 2025). Universal Smart Energy Framework (USEF) Foundation, Nov. 2015.

[201] *Gesetz über die Elektrizitäts- und Gasversorgung (Energiewirtschaftsgesetz — EnWG) (English: Law on Electricity and Gas Supply (Energy Industry Act — EnWG))*. Available online: https://www.gesetze-im-internet.de/enwg_2005/ (accessed on August 27, 2025). German law. Bundesministerium der Justiz und für Verbraucherschutz und Bundesamt für Justiz (English: German Federal Ministry of Justice and Consumer Protection and German Federal Office of Justice). 2005.

[202] *Roll-out intelligente Messsysteme: Quartalsweise Erhebungen (English: Roll-out of smart metering systems: quarterly inquiries)*. Statistic. Available online: https://www.bundesnetzagentur.de/DE/Fachthemen/ElektrizitaetundGas/NetzzugangMesswesen/Mess-undZaehlwesen/iMSys/artikel.html (accessed on February 10, 2026). Bundesnetzagentur (English: German Federal Network Agency).

[203] Greta Drasti. "The deployment of electricity smart meters in Italy: an econometric analysis on Italian municipalities". In: *Economia Marche Journal of Applied Economics* 43.3 (2024). ISSN: 3034-8234. DOI: 10.57638/3034-8234DEPSMARTCITY.

[204] *Estonia 2023 – Energy Policy Review*. Report. Available online: https://www.oecd.org/content/dam/oecd/en/publications/reports/2023/11/estonia-2023_60624cc7/9e91fe6a-en.pdf (accessed on December 1, 2025). International Energy Agency (IEA), 2023.

[205] Adarsh Krishnan. *Smart electricity meter market 2024: Global adoption landscape*. Market report. Available online: https://iot-analytics.com/wp-content/uploads/2024/02/INSIGHTS-RELEASE-Smart-electricity-meter-market-2024-Global-adoption-landscape.pdf (accessed on December 1, 2025). IoT Analytics, Feb. 2024.

[206] Felix Linderum. *Smart Metering in Europe – 19th Edition*. Market report. Available online: https://media.berginsight.com/2025/03/20120551/bi-sm19-ps.pdf (accessed on December 1, 2025). Berg Insight, 2025.

[207] Mattias Carlsson. *Smart Metering in North America – 6th Edition*. Market report. Available online: https://media.berginsight.com/2024/06/07124747/bi-smna6-ps.pdf (accessed on December 1, 2025). Berg Insight, 2024.

[208] *Gesetz über den Messstellenbetrieb und die Datenkommunikation in intelligenten Energienetzen (Messstellenbetriebsgesetz - MsbG) (English: German Act on Metering Point Operation and Data Communication in Smart Energy Networks (Metering Point Operation Act - MsbG))*. Available online: https://www.gesetze-im-internet.de/messbg/MsbG.pdf (accessed on February 11, 2026). German law. Bundesministerium der Justiz und für Verbraucherschutz und Bundesamt für Justiz (English: German Federal Ministry of Justice and Consumer Protection and German Federal Office of Justice). 2016.

[209] *Technische Richtlinie BSI-TR-03109-1: Anforderungen an die Interoperabilität der Kommunikationseinheit eines intelligenten Messsystems (English: Technical Guideline BSI-TR-03109-1: Requirements for the Interoperability of the Communication Unit of a Smart Metering System), Version 2.0*. Technical guideline. Available online: https://www.bsi.bund.de/DE/Themen/Unternehmen-und-Organisationen/Standards-und-Zertifizierung/Smart-metering/Smart-Meter-Gateway/TechnRichtlinie/TR_03109-1_node.html (accessed on July 31, 2025). Bundesamt für Sicherheit in der Informationstechnik (BSI, English: German Federal Office for Information Security), Dec. 2024.

[210] Kevin Förderer, Manuel Lösch, Ralf Növer, Marilen Ronczka, and Hartmut Schmeck. "Smart Meter Gateways: Options for a BSI-Compliant Integration of Energy Management Systems". In: *Applied Sciences* 9.8, 1634 (2019). ISSN: 2076-3417. DOI: 10.3390/app9081634.

[211] *Technische Richtlinie BSI-TR-03109-1: Anforderungen an die Interoperabilität der Kommunikationseinheit eines intelligenten Messsystems (English: Technical Guideline BSI-TR-03109-1: Requirements for the Interoperability of the Communication Unit of a Smart Metering System)*. Technical guideline. Available online: https://www.bsi.bund.de/SharedDocs/Downloads/DE/BSI/Publikationen/TechnischeRichtlinien/TR03109/TR03109-1.pdf (accessed on July 28, 2025). Bundesamt für Sicherheit in der Informationstechnik (BSI, English: German Federal Office for Information Security), Jan. 2019.

[212] *Technische Richtlinie BSI-TR-03109-1 – Anlage VII: Interoperabilitätsmodell und Geräteprofile für Smart-Meter-Gateways (English: Technical Guideline BSI-TR-03109-1 – Annex VII: Interoperability Model and Device Profiles for Smart Meter Gateways)*. Technical guideline. Version 1.0. Available online: https://www.bsi.bund.de/SharedDocs/Downloads/DE/BSI/Publikationen/TechnischeRichtlinien/TR03109/TR-03109-1_Anlage_Interop-Modell-Geraeteprofile.pdf (accessed on July 31, 2025). Bundesamt für Sicherheit in der Informationstechnik (BSI, English: German Federal Office for Information Security), Jan. 2019.

[213] *FNN-Hinweis – Lastenheft – Basiszähler – Funktionale Merkmale (English: FNN-note – Functional Specification – Basic Meter – Functional Characteristics)*. Technical specification. Version 1.4.1. Available online: https://www.vde.com/resource/blob/2345790/e6c822aa22d51592aba388f6a5ceaed2/fnn-hinweis--lastenheft-basiszaehler---funktionale-merkmale---2018--data.pdf (accessed on July

31, 2025). Forum Netztechnik/Netzbetrieb im VDE (FNN, English: Forum Network Technology/Network Operation in the VDE), May 2018.

[214] Siri Wiig and Babette Fahlbruch, eds. *Exploring Resilience: A Scientific Journey from Practice to Theory*. SpringerBriefs in Applied Sciences and Technology. Cham: Springer International Publishing, 2019. ISBN: 978-3-030-03189-3. DOI: 10.1007/978-3-030-03189-3.

[215] Xiaolong Xue, Liang Wang, and Rebecca J. Yang. "Exploring the science of resilience: critical review and bibliometric analysis". In: *Natural Hazards* 90 (2018), pp. 477–510. ISSN: 1573-0840. DOI: 10.1007/s11069-017-3040-y.

[216] Seyedmohsen Hosseini, Kash Barker, and Jose E. Ramirez-Marquez. "A review of definitions and measures of system resilience". In: *Reliability Engineering & System Safety* 145 (2016), pp. 47–61. ISSN: 0951-8320. DOI: 10.1016/j.ress.2015.08.006.

[217] Ran Bhamra, Samir Dani, and Kevin Burnard. "Resilience: the concept, a literature review and future directions". In: *International Journal of Production Research* 49.18 (2011), pp. 5375–5393. DOI: 10.1080/00207543.2011.563826.

[218] Angela Weber Righi, Tarcisio Abreu Saurin, and Priscila Wachs. "A systematic literature review of resilience engineering: Research areas and a research agenda proposal". In: *Reliability Engineering & System Safety* 141 (2015). Special Issue on Resilience Engineering, pp. 142–152. ISSN: 0951-8320. DOI: 10.1016/j.ress.2015.03.007.

[219] Alessandro Annarelli and Fabio Nonino. "Strategic and operational management of organizational resilience: Current state of research and future directions". In: *Omega* 62 (2016), pp. 1–18. ISSN: 0305-0483. DOI: 10.1016/j.omega.2015.08.004.

[220] Erik Hollnagel. *Resilience Engineering*. Available online: https://erikhollnagel.com/ideas/resilience-engineering.html (accessed on January 18, 2023). Website article.

[221] Yezhou Wang, Chen Chen, Jianhui Wang, and Ross Baldick. "Research on Resilience of Power Systems Under Natural Disasters—A Review". In: *IEEE Transactions on Power Systems* 31.2 (2016), pp. 1604–1613. DOI: 10.1109/TPWRS.2015.2429656.

[222] Mostafa Nazemi, Moein Moeini-Aghtaie, Mahmud Fotuhi-Firuzabad, and Payman Dehghanian. "Energy Storage Planning for Enhanced Resilience of Power Distribution Networks Against Earthquakes". In: *IEEE Transactions on Sustainable Energy* 11.2 (2020), pp. 795–806. DOI: 10.1109/TSTE.2019.2907613.

[223] Fauzan Hanif Jufri, Victor Widiputra, and Jaesung Jung. "State-of-the-art review on power grid resilience to extreme weather events: Definitions, frameworks, quantitative assessment methodologies, and enhancement strategies". In: *Applied Energy* 239 (2019), pp. 1049–1065. ISSN: 0306-2619. DOI: 10.1016/j.apenergy.2019.02.017.

[224] Sarmad Mehrdad, Seyedamirabbas Mousavian, Golshan Madraki, and Yury Dvorkin. "Cyber-Physical Resilience of Electrical Power Systems Against Malicious Attacks: a Review". In: *Current Sustainable/Renewable Energy Reports* 5 (2018), pp. 14–22. ISSN: 2196-3010. DOI: 10.1007/s40518-018-0094-8.

[225] Hamzeh Davarikia and Masoud Barati. "A tri-level programming model for attack-resilient control of power grids". In: *Journal of Modern Power Systems and Clean Energy* 6 (2018), pp. 918–929. DOI: 10.1007/s40565-018-0436-y.

[226] Tien Nguyen et al. "Electric Power Grid Resilience to Cyber Adversaries: State of the Art". In: *IEEE Access* 8 (2020), pp. 87592–87608. DOI: 10.1109/ACCESS.2020.2993233.

[227] Reza Arghandeh, Alexandra von Meier, Laura Mehrmanesh, and Lamine Mili. "On the definition of cyber-physical resilience in power systems". In: *Renewable and Sustainable Energy Reviews* 58 (2016), pp. 1060–1069. DOI: 10.1016/j.rser.2015.12.193.

[228] Richard E. Brown. *Electric power distribution reliability*. Power engineering 14. Marcel Dekker Inc, 2002. ISBN: 0824707982.

[229] Julie G Osborn and Cornelia Kawann. *Reliability of the U.S. Electricity System: Recent Trends and Current Issues*. Technical report. Available online: https://emp.lbl.gov/publications/reliability-us-electricity-system (accessed on February 10, 2026). Ernest Orlando Lawrence Berkeley National Laboratory, University of Califonia, Aug. 2001.

[230] P. Kundur et al. "Definition and classification of power system stability IEEE/CIGRE joint task force on stability terms and definitions". In: *IEEE Transactions on Power Systems* 19.3 (2004), pp. 1387–1401. DOI: 10.1109/TPWRS.2004.825981.

[231] Helge Seljeseth, Thomas Rump, and Krister Haugen. "Overvoltage Immunity of Electrical Appliances Laboratory Test Results from 60 Appliances". In: *Proceedings of the 21st International Conference on Electric Power Distribution (CIRED)*. June 2011.

[232] *Investigation Report into the Loss of Supply Incident affecting parts of the West Midlands at 10:10 on the morning of Friday, 5 September 2003*. Report. Available online: http://www.g4jnt.com/hams_hall_investigation_report.pdf (accessed on February 3, 2023). National Grid Company plc, 2003.

[233] Xiaofan Shen, Zhihuai Shu, Yu Liu, Pengfei Lü, and Lie Zhang. "Statistics and analysis on operation situation of protective relayings of State Grid Corporation of China in 2009". In: *Power System Technology* 35.2 (2011), pp. 189–193.

[234] G. Andersson et al. "Causes of the 2003 major grid blackouts in North America and Europe, and recommended means to improve system dynamic performance". In: *IEEE Transactions on Power Systems* 20.4 (2005), pp. 1922–1928. DOI: 10.1109/TPWRS.2005.857942.

[235] Giuseppe Aceto, Alessio Botta, Pietro Marchetta, Valerio Persico, and Antonio Pescapé. "A comprehensive survey on internet outages". In: *Journal of Network and Computer Applications* 113 (2018), pp. 36–63. ISSN: 1084-8045. DOI: 10.1016/j.jnca.2018.03.026.

[236] The European Parliament and the Council of the European Union. *Directive (EU) 2016/1148 of the European Parliament and of the Council of 6 July 2016 concerning measures for a high common level of security of network and information systems across the Union*. Available online: https://eur-lex.europa.eu/eli/dir/2016/1148/oj/eng (accessed on December 2, 2025). EU directive. 2016.

[237] *Gesetz zur Erhöhung der Sicherheit informationstechnischer Systeme (IT-Sicherheitsgesetz) (English: Act on Enhancing the Security of Information Technology Systems (IT Security Act))*. Bundesministerium der Justiz und für Verbraucherschutz (English: German Federal Ministry of Justice and Consumer Protection). Available online: https://www.bgbl.de/xaver/bgbl/start.xav?start=%2F%2F%2A%5B%40attr_id%3D%27bgbl115031.pdf%27%5D (accessed on December 2, 2025). German law. 2015.

[238] Gu Chaojun and Panida Jirutitijaroen. "Impacts of communication failure on power system operations". In: *2013 IEEE PES Asia-Pacific Power and Energy Engineering Conference (APPEEC)*. Dec. 2013, pp. 1–5. DOI: 10.1109/APPEEC.2013.6837209.

[239] Spencer Dutton, Chris Marnay, Wei Feng, Matthew Robinson, and Andrea Mammoli. "Moore vs. Murphy: Tradeoffs between complexity and reliability in distributed energy system scheduling using software-as-a-service". In: *Applied Energy* 238 (Mar. 2019), pp. 1126–1137. ISSN: 0306-2619. DOI: 10.1016/j.apenergy.2019.01.067.

[240] João E. R. Baptista, Anselmo B. Rodrigues, and Maria G. da Silva. "Voltage profile assessment in smart distribution grids considering BESS and communication network failures". In: *Electric Power Systems Research* 213, 108660 (Dec. 2022). ISSN: 0378-7796. DOI: 10.1016/j.epsr.2022.108660.

[241] Mingxiao Ma, André M. H. Teixeira, Jan van den Berg, and Peter Palensky. "Voltage Control in Distributed Generation under Measurement Falsification Attacks". In: *IFAC-PapersOnLine*. 20th IFAC World Congress 50.1 (July 2017), pp. 8379–8384. ISSN: 2405-8963. DOI: 10.1016/j.ifacol.2017.08.1562.

[242] Omniyah Gul M Khan, Ehab El-Saadany, Khaled Saleh, Mostafa Shaaban, and Amr Youssef. "Cyber Attacks On Distributed Congestion Management Methods". In: *2019 IEEE Power & Energy Society General Meeting (PESGM)*. Aug. 2019, pp. 1–5. DOI: 10.1109/PESGM40551.2019.8973458.

[243] Temitayo O. Olowu, Shamini Dharmasena, Hassan Jafari, and Arif. Sarwat. "Investigation of False Data Injection Attacks on Smart Inverter Settings". In: *2020 IEEE CyberPELS (CyberPELS)*. Oct. 2020, pp. 1–6. DOI: 10.1109/CyberPELS49534.2020.9311541.

[244] Ehsan Naderi and Arash Asrari. "Hardware-in-the-Loop Experimental Validation for a Lab-Scale Microgrid Targeted by Cyberattacks". In: *2021 9th International Conference on Smart Grid (icSmartGrid)*. June 2021, pp. 57–62. DOI: 10.1109/icSmartGrid52357.2021.9551023.

[245] Samrat Acharya, Yury Dvorkin, and Ramesh Karri. "Causative Cyberattacks on Online Learning-Based Automated Demand Response Systems". In: *IEEE Transactions on Smart Grid* 12.4 (July 2021), pp. 3548–3559. ISSN: 1949-3061. DOI: 10.1109/TSG.2021.3067896.

[246] Bo Tu, Wen-Tai Li, and Chau Yuen. "Vulnerability of Distributed Inverter VAR Control in PV Distributed Energy System". In: *2022 IEEE International Conference on Communications, Control, and Computing Technologies for Smart Grids (SmartGridComm)*. Oct. 2022, pp. 47–52. DOI: 10.1109/SmartGridComm52983.2022.9960972.

[247] Tommaso Bragatto et al. "False Data Injection Impact on High RES Power Systems with Centralized Voltage Regulation Architecture". In: *Sensors* 23.5, 2557 (Jan. 2023). ISSN: 1424-8220. DOI: 10.3390/s23052557.

[248] Mohd Asim Aftab, Astha Chawla, Pedro P. Vergara, Shehab Ahmed, and Charalambos Konstantinou. "Volt/VAR Optimization in the Presence of Attacks: A Real-Time Co-Simulation Study". In: *2023 IEEE International Conference on Communications, Control, and Computing Technologies for Smart Grids (SmartGridComm)*. Oct. 2023, pp. 1–7. DOI: 10.1109/SmartGridComm57358.2023.10333952.

[249] Xu Tang, Jing Wang, Xiaohong Ran, Kaipei Liu, and Liang Qin. "False Data Injection Attack Diminishing the Performance of Controllable Devices in Active Distribution Networks". In: *2023 3rd International Conference on Energy, Power and Electrical Engineering (EPEE)*. Sept. 2023, pp. 1379–1384. DOI: 10.1109/EPEE59859.2023.10351849.

[250] Amirhossein Akbarian, Mahdi Bahrami, Mehdi Vakilian, and Matti Lehtonen. "Vulnerability of EV Charging Stations to Cyber Attacks Manipulating Prices". In: *2023 International Conference on Future Energy Solutions (FES)*. June 2023, pp. 1–6. DOI: 10.1109/FES57669.2023.10183070.

[251] Yang Liu et al. "CFDI: Coordinated false data injection attack in active distribution network". In: *IET Generation, Transmission & Distribution* 18.15 (2024), pp. 2556–2569. ISSN: 1751-8695. DOI: 10.1049/gtd2.13217.

[252] Amin Rezaeizadeh, Roy S. Smith, and Silvia Mastellone. "Stealthy Cyber Attack Filter and its Impact on Control of Grid-forming Inverter". In: *2024 IEEE 63rd Conference on Decision and Control (CDC)*. Dec. 2024, pp. 2367–2372. DOI: 10.1109/CDC56724.2024.10886227.

[253] Gelli Ravikumar, Burhan Hyder, and Manimaran Govindarasu. "Hardware-in-the-Loop CPS Security Architecture for DER Monitoring and Control Applications". In: *2020 IEEE Texas Power and Energy Conference (TPEC)*. Feb. 2020, pp. 1–5. DOI: 10.1109/TPEC48276.2020.9042578.

[254] Subham Sahoo, Tomislav Dragičević, and Frede Blaabjerg. "Cyber Security in Control of Grid-Tied Power Electronic Converters—Challenges and Vulnerabilities". In: *IEEE Journal of Emerging and Selected Topics in Power Electronics* 9.5 (Oct. 2021), pp. 5326–5340. ISSN: 2168-6785. DOI: 10.1109/JESTPE.2019.2953480.

[255] Omniyah Gul M. Khan, Ehab F. El-Saadany, Amr Youssef, and Mostafa F. Shaaban. "Cyber Security of Market-Based Congestion Management Methods in Power Distribution Systems". In: *IEEE Transactions on Industrial Informatics* 17.12 (Dec. 2021), pp. 8142–8153. ISSN: 1941-0050. DOI: 10.1109/TII.2021.3065714.

[256] Yangyang Fu et al. "Modeling and evaluation of cyber-attacks on grid-interactive efficient buildings". In: *Applied Energy* 303, 117639 (Dec. 2021). ISSN: 0306-2619. DOI: 10.1016/j.apenergy.2021.117639.

[257] Juanwei Chen, Jun Yan, Hang Du, Mourad Debbabi, and Marthe Kassouf. "Vulnerability Analysis of Virtual Power Plant Voltage Support under Denial-of-Service Attacks". In: *2023 IEEE Power & Energy Society Innovative Smart Grid Technologies Conference (ISGT)*. Jan. 2023, pp. 1–5. DOI: 10.1109/ISGT51731.2023.10066361.

[258] Vineet Kumar, Adlin Jebakumari S, and Mansingh Meena. "Cybersecurity Challenges In Grid-Tied Power Converters". In: *2023 International Conference on Power Energy, Environment & Intelligent Control (PEEIC)*. Dec. 2023, pp. 1310–1314. DOI: 10.1109/PEEIC59336.2023.10450745.

[259] Diptendu Pal and Sameer Singh. "Cyber-Physical Power System Implementation using HYPERSIM and EXata to Examine the Impact of Cyber-Attack on Microgrid Controller". In: *2023 IEEE International Conference on Power Electronics, Smart Grid, and Renewable Energy (PESGRE)*. Dec. 2023, pp. 1–6. DOI: 10.1109/PESGRE58662.2023.10405332.

[260] Yunan Zhang, Yixin Jiang, Aidong Xu, Chao Hong, and Jiaqi Chen. "Method to Evaluate the Impact of Cyberattacks Against Charging Piles on Distribution Network". In: *2020 12th IEEE PES Asia-Pacific Power and Energy Engineering Conference (APPEEC)*. Sept. 2020, pp. 1–5. DOI: 10.1109/APPEEC48164.2020.9220574.

[261] Afroz Mokarim, Giovanni Battista Gaggero, and Mario Marchese. "Evaluation of the Impact of Cyber-Attacks Against Electric Vehicle Charging Stations in a Low Voltage Distribution Grid". In: *2023 IEEE International Conference on Communications, Control, and Computing Technologies for Smart Grids (SmartGridComm)*. Oct. 2023, pp. 1–7. DOI: 10.1109/SmartGridComm57358.2023.10333896.

[262] Omniyah Gul M Khan, Ehab El-Saadany, Amr Youssef, and Mostafa Shaaban. "Impact of Electric Vehicles Botnets on the Power Grid". In: *2019 IEEE Electrical Power and Energy Conference (EPEC)*. Oct. 2019, pp. 1–5. DOI: 10.1109/EPEC47565.2019.9074822.

[263] Armin Teymouri, Ali Mehrizi-Sani, and Chen-Ching Liu. "Cyber Security Risk Assessment of Solar PV Units with Reactive Power Capability". In: *IECON 2018 - 44th Annual Conference of the IEEE Industrial Electronics Society*. Oct. 2018, pp. 2872–2877. DOI: 10.1109/IECON.2018.8591583.

[264] Georgios Tertytchny et al. "Demonstration of Man in the Middle Attack on a Commercial Photovoltaic Inverter Providing Ancillary Services". In: *2020 IEEE CyberPELS (CyberPELS)*. Oct. 2020, pp. 1–7. DOI: 10.1109/CyberPELS49534.2020.9311531.

[265] Sai Chandana Vallam Kondu, Gelli Ravikumar, and Sathya Narayana Mohan. "CPS-DERMS: Cyber-Physical Security and Impact Analysis of DERMS Against MITM Attacks". In: *2025 IEEE Green Technologies Conference (GreenTech)*. Mar. 2025, pp. 1–5. DOI: 10.1109/GreenTech62170.2025.10977697.

[266] Erdem Gumrukcu et al. "Impact of Cyber-attacks on EV Charging Coordination: The Case of Single Point of Failure". In: *2022 4th Global Power, Energy and Communication Conference (GPECOM)*. June 2022, pp. 506–511. DOI: 10.1109/GPECOM55404.2022.9815727.

[267] Ahmed S. Musleh, Guo Chen, and Zhao Yang Dong. "A Survey on the Detection Algorithms for False Data Injection Attacks in Smart Grids". In: *IEEE Transactions on Smart Grid* 11.3 (May 2020), pp. 2218–2234. ISSN: 1949-3061. DOI: 10.1109/TSG.2019.2949998.

[268] Lei Cui, Youyang Qu, Longxiang Gao, Gang Xie, and Shui Yu. "Detecting False Data Attacks Using Machine Learning Techniques in Smart Grid: A Survey". In: *Journal of Network and Computer Applications* 170, 102808 (Nov. 2020). ISSN: 1084-8045. DOI: 10.1016/j.jnca.2020.102808.

[269] Mengxiang Liu et al. "Enhancing Cyber-Resiliency of DER-Based Smart Grid: A Survey". In: *IEEE Transactions on Smart Grid* 15.5 (Sept. 2024), pp. 4998–5030. ISSN: 1949-3061. DOI: 10.1109/TSG.2024.3373008.

[270] Kumarsinh Jhala, Parth Pradhan, and Balasubramaniam Natarajan. "Perturbation-Based Diagnosis of False Data Injection Attack Using Distributed Energy Resources". In: *IEEE Transactions on Smart Grid* 12.2 (Mar. 2021), pp. 1589–1601. ISSN: 1949-3061. DOI: 10.1109/TSG.2020.3029954.

[271] Kumarsinh Jhala, Parth Pradhan, Bo Chen, and Ravindra Singh. "Sequential Perturbation-based Attack Detection Using DERs for Unbalanced Distribution System". In: *2021 IEEE Power & Energy Society Innovative Smart Grid Technologies Conference (ISGT)*. Feb. 2021, pp. 1–5. DOI: 10.1109/ISGT49243.2021.9372180.

[272] Tong Huang et al. "Detection of Cyber Attacks in Renewable-rich Microgrids Using Dynamic Watermarking". In: *2020 IEEE Power & Energy Society General Meeting (PESGM)*. Aug. 2020, pp. 1–5. DOI: 10.1109/PESGM41954.2020.9282071.

[273] Hasan Ibrahim et al. "An Active Detection Scheme for Sensor Spoofing in Grid-tied PV Systems". In: *2021 IEEE Energy Conversion Congress and Exposition (ECCE)*. Oct. 2021, pp. 1433–1439. DOI: 10.1109/ECCE47101.2021.9595733.

[274] Abdulmohsen Almalawi, Xinghuo Yu, Zahir Tari, Adil Fahad, and Ibrahim Khalil. "An Unsupervised Anomaly-Based Detection Approach for Integrity Attacks on SCADA Systems". In: *Computers & Security* 46 (Oct. 2014), pp. 94–110. ISSN: 0167-4048. DOI: 10.1016/j.cose.2014.07.005.

[275] Mohammed S. Kemal, Wissam Aoudi, Rasus L. Olsen, Magnus Almgren, and Hans-Peter Schwefel. "Model-Free Detection of Cyberattacks on Voltage Control in Distribution Grids". In: *2019 15th European Dependable Computing Conference (EDCC)*. Sept. 2019, pp. 171–176. DOI: 10.1109/EDCC.2019.00041.

[276] Habila Basumatary, Manas Khatua, and Shabari Nath. "False Data Injection Attack Detection in EV Charging Network Using NARX Neural Network". In: *IEEE Transactions on Transportation Electrification* 11.4 (Aug. 2025), pp. 9686–9700. ISSN: 2332-7782. DOI: 10.1109/TTE.2025.3553391.

[277] Leen Al Homoud et al. "Cyber-Physical Defense in Smart Distribution Networks". In: *2021 North American Power Symposium (NAPS)*. Nov. 2021, pp. 1–6. DOI: 10.1109/NAPS52732.2021.9654478.

[278] Mostafa Mohammadpourfard, Yang Weng, and Mohsen Tajdinian. "Benchmark of Machine Learning Algorithms on Capturing Future Distribution Network Anomalies". In: *IET Generation, Transmission & Distribution* 13.8 (2019), pp. 1441–1455. ISSN: 1751-8695. DOI: 10.1049/iet-gtd.2018.6801.

[279] Omniyah Gul M Khan, Amr Youssef, Ehab El-Saadany, and Magdy Salama. "LSTM-based Approach to Detect Cyber Attacks on Market-Based Congestion Management Methods". In: *2021 IEEE Power & Energy Society General Meeting (PESGM)*. July 2021, pp. 1–5. DOI: 10.1109/PESGM46819.2021.9637976.

[280] Suman Sourav, Partha P. Biswas, Binbin Chen, and Daisuke Mashima. "Detecting Hidden Attackers in Photovoltaic Systems Using Machine Learning". In: *2022 IEEE International Conference on Communications, Control, and Computing Technologies for Smart Grids (SmartGridComm)*. Oct. 2022, pp. 360–366. DOI: 10.1109/SmartGridComm52983.2022.9960965.

[281] Ahmad Mohammad Saber, Amr Youssef, Davor Svetinovic, Hatem Zeineldin, and Ehab El-Saadany. "Learning-Based Detection of Malicious Volt-VAr Control Parameters in Smart Inverters". In: *IECON 2023- 49th Annual Conference of the IEEE Industrial Electronics Society*. Oct. 2023, pp. 1–6. DOI: 10.1109/IECON51785.2023.10312615.

[282] Haopeng An et al. "Cluster Partition-Fuzzy Broad Learning-Based Fast Detection and Localization Framework for False Data Injection Attack in Smart Distribution Networks". In: *Sustainable Energy, Grids and Networks* 40, 101534 (Dec. 2024). ISSN: 2352-4677. DOI: 10.1016/j.segan.2024.101534.

[283] Xinrui Liu et al. "Modeling and Detection of False Data Injection Attacks in Cyber-Physical Distribution System with Load Aggregator Interaction". In: *Sustainable Energy, Grids and Networks* 40, 101533 (Dec. 2024). ISSN: 2352-4677. DOI: 10.1016/j.segan.2024.101533.

[284] Xin Ge and Minnan Yue. "A Detection Strategy Based on Deep Learning against Sequential Outages Induced by False Data Injection Attacks". In: *Electrical Engineering* 106.4 (Aug. 2024), pp. 5201–5217. ISSN: 1432-0487. DOI: 10.1007/s00202-024-02277-z.

[285] Vijaykumar Kamble, Vandana Navale, Varsha Dange, and Archana Chaudhari. "An Analysis of Cyber Threats in Distributed Energy Power Networks". In: *International Journal of Basic and Applied Sciences* 14.2 (June 2025), pp. 49–57. ISSN: 2227-5053. DOI: 10.14419/0cz1w646.

[286] A. Ananda Kumar, Dr. K. Srikumar, and Dr. G. Nageswara Rao. "A high-dimensional data-driven approach for enhancing cyber-physical attack detection in PV-connected distribution power grids using deep Q-networks". In: *Computers and Electrical Engineering* 129, 110814 (2026). ISSN: 0045-7906. DOI: 10.1016/j.compeleceng.2025.110814.

[287] Quan Liu et al. "Cyber-Attack Detection Approach In Photovoltaic Microgrids Using LSTM-based Autoencoders". In: *2023 4th International Conference on Power Engineering (ICPE)*. Dec. 2023, pp. 183–188. DOI: 10.1109/ICPE59729.2023.10469652.

[288] Ahmed S. Musleh, Guo Chen, Zhao Yang Dong, Chen Wang, and Shiping Chen. "Spatio-Temporal Data-Driven Detection of False Data Injection Attacks in Power Distribution Systems". In: *International Journal of Electrical Power & Energy Systems* 145, 108612 (Feb. 2023). ISSN: 0142-0615. DOI: 10.1016/j.ijepes.2022.108612.

[289] Mehdi Jabbari Zideh, Mohammad Reza Khalghani, and Sarika Khushalani Solanki. "An Unsupervised Adversarial Autoencoder for Cyber Attack Detection in Power Distribution Grids". In: *Electric Power Systems Research* 232, 110407 (July 2024). ISSN: 0378-7796. DOI: 10.1016/j.epsr.2024.110407.

[290] Yang Liu, Shiyan Hu, and Albert Y. Zomaya. "The Hierarchical Smart Home Cyberattack Detection Considering Power Overloading and Frequency Disturbance". In: *IEEE Transactions on Industrial Informatics* 12.5 (Oct. 2016), pp. 1973–1983. ISSN: 1941-0050. DOI: 10.1109/TII.2016.2591911.

[291] Sajjad Abedi, Ata Arvani, and Reza Jamalzadeh. "Cyber Security of Plug-in Electric Vehicles in Smart Grids: Application of Intrusion Detection Methods". In: *Plug In Electric Vehicles in Smart Grids: Integration Techniques*. Ed. by Sumedha Rajakaruna, Farhad Shahnia, and Arindam Ghosh. Singapore: Springer, 2015, pp. 129–147. ISBN: 978-981-287-299-9. DOI: 10.1007/978-981-287-299-9_5.

[292] El-Nasser S. Youssef, Fabrice Labeau, and Marthe Kassouf. "Detection of Load-Altering Cyberattacks Targeting Peak Shaving Using Residential Electric Water Heaters". In: *Energies* 15.20, 7807 (2022). ISSN: 1996-1073. DOI: 10.3390/en15207807.

[293] Z. S. Warraich and W. G. Morsi. "Early Detection of Cyber–Physical Attacks on Fast Charging Stations Using Machine Learning Considering Vehicle-to-Grid Operation in Microgrids". In: *Sustainable Energy, Grids and Networks* 34, 101027 (June 2023). ISSN: 2352-4677. DOI: 10.1016/j.segan.2023.101027.

[294] Jianbo Yi et al. "A Cyber Attack Detection Strategy for Plug-in Electric Vehicles during Charging Based on CEEMDAN and Broad Learning System". In: *Energy Reports*. 2022 The 3rd International Conference on Power, Energy and Electrical Engineering 9 (May 2023), pp. 80–88. ISSN: 2352-4847. DOI: 10.1016/j.egyr.2022.12.094.

[295] Elsevier. *Scopus website*. https://www.scopus.com/ (accessed on January 12, 2025).

[296] Juanwei Chen et al. "An SDN-Based Framework for Cyber-Physically Coordinated Voltage Support of Virtual Power Plants Against DoS Attacks". In: *IEEE Transactions on Smart Grid* 17.1 (2026), pp. 617–633. DOI: 10.1109/TSG.2025.3614650.

[297] Wenqian Zhang, Rui Song, Jun Han, Han Guo, and Yutong Liu. "Distributed Voltage Control Strategy for High Proportion Photovoltaic Distribution Network Considering Abnormal Communication". In: *2024 21st International Conference on Harmonics and Quality of Power (ICHQP)*. Oct. 2024, pp. 259–264. DOI: 10.1109/ICHQP61174.2024.10768722.

[298] Mohammad Panahazari et al. "A Hybrid Optimization and Deep Learning Algorithm for Cyber-resilient DER Control". In: *2023 IEEE Power & Energy Society Innovative Smart Grid Technologies Conference (ISGT)*. Jan. 2023, pp. 1–5. DOI: 10.1109/ISGT51731.2023.10066345.

[299] Alaa Selim, Junbo Zhao, Fei Ding, Fei Miao, and Sung-Yeul Park. "Adaptive Deep Reinforcement Learning Algorithm for Distribution System Cyber Attack Defense With High Penetration of DERs". In: *IEEE Transactions on Smart Grid* 15.4 (July 2024), pp. 4077–4089. ISSN: 1949-3061. DOI: 10.1109/TSG.2023.3345314.

[300] Daniel Arnold et al. "Adaptive Control of Distributed Energy Resources for Distribution Grid Voltage Stability". In: *IEEE Transactions on Power Systems* 38.1 (Jan. 2023), pp. 129–141. ISSN: 1558-0679. DOI: 10.1109/TPWRS.2022.3157558.

[301] Alaa Selim, Junbo Zhao, Fei Ding, Fei Miao, and Sung-Yeul Park. "Deep Reinforcement Learning for Distribution System Cyber Attack Defense with DERs". In: *2023 IEEE Power & Energy Society Innovative Smart Grid Technologies Conference (ISGT)*. Jan. 2023, pp. 1–5. DOI: 10.1109/ISGT51731.2023.10066375.

[302] Faeza Hafiz and Dmitry Ishchenko. "Security Enhancement of Network Constraint Grid-Edge Energy Management System". In: *2022 IEEE Industry Applications Society Annual Meeting (IAS)*. Oct. 2022, pp. 1–8. DOI: 10.1109/IAS54023.2022.9940067.

[303] Nanduni Nimalsiri and Elizabeth Ratnam. "Network-Aware EV Charging and Discharging in Unbalanced Distribution Grids: A Distributed, Robust Approach against Communication Failures". In: *2023 IEEE International Conference on Energy Technologies for Future Grids (ETFG)*. Dec. 2023, pp. 1–6. DOI: 10.1109/ETFG55873.2023.10408529.

[304] F. Tangerding, I. A. M. Varenhorst, G. Hoogsteen, M. E. T. Gerards, and J. L. Hurink. "GridShield: A Robust Fall-Back Control Mechanism for Congestion Management in Distribution Grids". In: *2022 IEEE PES Innovative Smart Grid Technologies Conference Europe (ISGT-Europe)*. Oct. 2022, pp. 1–5. DOI: 10.1109/ISGT-Europe54678.2022.9960301.

[305] Shammya Shananda Saha et al. "Lyapunov Stability of Smart Inverters Using Linearized Distflow Approximation". In: *IET Renewable Power Generation* 15.1 (2021), pp. 114–126. ISSN: 1752-1424. DOI: 10.1049/rpg2.12009.

[306] Asma Farooq, Kamal Shahid, Yonghao Gui, and Rasmus Løvenstein Olsen. "Impact of Cyber-Attack on Coordinated Voltage Control in Low Voltage Grids". In: *IET Renewable Power Generation* 17.11 (2023), pp. 2887–2894. ISSN: 1752-1424. DOI: 10.1049/rpg2.12571.

[307] Daniel Arnold et al. "Adam-Based Augmented Random Search for Control Policies for Distributed Energy Resource Cyber Attack Mitigation". In: *2022 American Control Conference (ACC)*. June 2022, pp. 4559–4566. DOI: 10.23919/ACC53348.2022.9867545.

[308] Ciaran Roberts et al. "Deep Reinforcement Learning for Mitigating Cyber-Physical DER Voltage Unbalance Attacks". In: *2021 American Control Conference (ACC)*. May 2021, pp. 2861–2867. DOI: 10.23919/ACC50511.2021.9482815.

[309] Partha S. Sarker, Md Fazley Rafy, and Anurag K. Srivastava. "Enabling Cyber-Resilient Distribution Systems With DERs: Distributed vs. Centralized Control". In: *IEEE Transactions on Power Delivery* 40.6 (Dec. 2025), pp. 3710–3720. ISSN: 1937-4208. DOI: 10.1109/TPWRD.2025.3626271.

[310] Partha S. Sarker, Md. Fazley Rafy, Anurag K. Srivastava, and R. K. Singh. "Cyber Anomaly-Aware Distributed Voltage Control With Active Power Curtailment and DERs". In: *IEEE Transactions on Industry Applications* 60.1 (Jan. 2024), pp. 1622–1633. ISSN: 1939-9367. DOI: 10.1109/TIA.2023.3328850.

[311] Azwirman Gusrialdi, Ying Xu, Zhihua Qu, and Marwan A. Simaan. "Resilient Cooperative Voltage Control for Distribution Network with High Penetration Distributed Energy Resources". In: *2020 European Control Conference (ECC)*. 2020, pp. 1533–1539. DOI: 10.23919/ECC51009.2020.9143684.

[312] Darcy Reeves, Ghavameddin Nourbakhsh, Ghassem Mokhtari, and Arindam Ghosh. "A Distributed Control Based Coordination Scheme of Household PV Systems for Overvoltage Prevention". In: *2013 IEEE Power & Energy Society General Meeting*. July 2013, pp. 1–5. DOI: 10.1109/PESMG.2013.6672774.

[313] Alejandro D. Dominguez-Garcia, Christoforos N. Hadjicostis, and Nitin H. Vaidya. "Resilient Networked Control of Distributed Energy Resources". In: *IEEE Journal on Selected Areas in Communications* 30.6 (July 2012), pp. 1137–1148. ISSN: 1558-0008. DOI: 10.1109/JSAC.2012.120711.

[314] Mohammad Panahazari, Guangming Yao, and Jianhua Zhang. "Distribution Grid Services Performance Analysis for Cyber-resilient Online Feedback-based DER Control". In: *2023 IEEE International Conference on Communications, Control, and Computing Technologies for Smart Grids (SmartGridComm)*. Oct. 2023, pp. 1–6. DOI: 10.1109/SmartGridComm57358.2023.10333955.

[315] Hanko Ipach, Leonard Fisser, Christian Becker, and Andreas Timm-Giel. "Utility-Based Operation Management for Low Voltage Distribution Grids Using Online Optimization". In: *e & i Elektrotechnik und Informationstechnik* 138.8 (Dec. 2021), pp. 495–504. ISSN: 1613-7620. DOI: 10.1007/s00502-021-00931-z.

[316] Ankur Majumdar and Bikash C. Pal. "Bad Data Detection in the Context of Leverage Point Attacks in Modern Power Networks". In: *IEEE Transactions on Smart Grid* 9.3 (2018), pp. 2042–2054. DOI: 10.1109/TSG.2016.2605923.

[317] J. Cappelle et al. “Introducing small storage capacity at residential PV installations to prevent overvoltages”. In: *2011 IEEE International Conference on Smart Grid Communications (SmartGridComm)*. 2011, pp. 534–539. DOI: 10.1109/SmartGridComm.2011.6102380.

[318] Lukas Held et al. “Impact of Electric Vehicle Charging on Low-Voltage Grids and the Potential of Battery Storage as Temporary Equipment during Grid Reinforcement”. In: *Proceedings of the E-Mobility Integration Symposium, Berlin, Germany*. Vol. 23. Available online: https://mobilityintegrationsymposium.org/wp-content/uploads/sites/7/2017/11/2A_5_EMob17_139_paper_Held_Lukas.pdf (accessed on February 11, 2026). 2017.

[319] German Federal Ministry for Economic Affairs and Energy (BMWi). *What exactly is “grid congestion”?* Available online: https://www.bmwi-energiewende.de/EWD/Redaktion/EN/Newsletter/2018/03/Meldung/direkt-account.html (accessed on July 5, 2021). Website article. Mar. 2018.

[320] *VDE-AR-N 4105:2011-08, Erzeugungsanlagen am Niederspannungsnetz - Technische Mindestanforderungen für Anschluss und Parallelbetrieb von Erzeugungsanlagen am Niederspannungsnetz (English: Generation plants in the low-voltage grid - Minimum Technical Requirements for Connection and Parallel Operation of Generation Plants in the Low-Voltage Grid)*. Standard. VDE Verband der Elektrotechnik Elektronik Informationstechnik e. V. (English: VDE Association for Electrical Engineering Electronics Information Technology), VDE-Verlag (English: VDE Publishing House), Aug. 2011.

[321] *Technische Anschlussbedingungen Niederspannung (English: Technical Connection Conditions for Low Voltage)*. Technical specification. Available online: https://www.westnetz.de/content/dam/revu-global/westnetz/documents/bauen/ihr-weg-zum-netzanschluss/niederspannung/tab-niederspannung-01022025.pdf (accessed on October 10, 2025). Westnetz GmbH, Feb. 2025.

[322] *Technische Anschlussbedingungen für den Anschluss an das Niederspannungsnetz der Regionetz GmbH (TAB Niederspannung, English: Technical connection conditions for connection to the low-voltage grid of Regionetz GmbH)*. Technical specification. Available online: https://www.regionetz.de/de/Privatkunden/Elektromobilitaet/Technische-Anforderungen/TAB-NS-2024.pdf (accessed on February 10, 2026). Regionetz GmbH, Mar. 2024.

[323] Yi Yang, Ronald G. Harley, Deepak Divan, and Thomas G. Habetler. “Thermal modeling and real time overload capacity prediction of overhead power lines”. In: *2009 IEEE International Symposium on Diagnostics for Electric Machines, Power Electronics and Drives*. 2009, pp. 1–7. DOI: 10.1109/DEMPED.2009.5292772.

[324] Philip Ochs. “Dezentrale Spannungshaltung in Stromverteilnetzen durch intelligente Gebäude (English: Decentralized Voltage Maintenance in Electricity Distribution Grids by Intelligent Buildings)”. Bachelor thesis. Karlsruher Institut für Technologie (KIT, English: Karlsruhe Institute of Technology), 2020.

[325] Klaus Heuck, Klaus-Dieter Dettmann, and Detlef Schulz. *Elektrische Energieversorgung – Erzeugung, Übertragung und Verteilung elektrischer Energie für Studium und Praxis (English: Electrical power supply – Generation, transmission, and distribution of electrical energy for study and practice)*. Wiesbaden: Springer Fachmedien, 2013. ISBN: 978-3-8348-2174-4. DOI: 10.1007/978-3-8348-2174-4.

[326] Jan Müller. "Optimization Under Uncertainty in Building Energy Management". 37.06.01; LK 01. PhD thesis. Karlsruher Institut für Technologie (KIT, English: Karlsruhe Institute of Technology), 2019. DOI: 10.5445/IR/1000098441.

[327] A. G. Phadke, J. S. Thorp, and M G. Adamiak. "A New Measurement Technique for Tracking Voltage Phasors, Local System Frequency, and Rate of Change of Frequency". In: *IEEE Transactions on Power Apparatus and Systems* PAS-102.5 (1983), pp. 1025–1038. DOI: 10.1109/TPAS.1983.318043.

[328] Mikio L. Braun. *jblas website*. Available online: https://jblas.org/ (accessed on September 12, 2024).

[329] National Institute of Standards and Technology (NIST). *JAMA website*. Available online: https://math.nist.gov/javanumerics/jama/ (accessed on September 12, 2024).

[330] *Selbstorganisation und Spontaneität in liberalisierten und harmonisierten Märkten : SESAM ; Abschlussbericht (English: Self-Organization and Spontaneity in Liberalized and Harmonized Markets : SESAM ; Final Report)*. Project report. Karlsruhe: Universität Karlsruhe (TH), 2008. DOI: 10.2314/GBV:592179478.

[331] Google. *What is Angular?* Available online: https://angular.dev/overview (accessed on November 7, 2025). Website article.

[332] Samed Rouven Elias Oktay Voßberg. "Entwicklung und Implementierung einer Benutzeroberfläche zur Visualisierung von Methoden zur Steigerung der Resilienz eines Stromverteilnetzes (English: Development and Implementation of a User Interface for Visualizing Methods for Increasing the Resilience of an Electricity Distribution Grid)". Bachelor thesis. Karlsruher Institut für Technologie (KIT, English: Karlsruhe Institute of Technology), 2021.

[333] Hermann Meier, Christian Fünfgeld, Thomas Adam, and Bernd Schieferdecker. *Repräsentative VDEW-Lastprofile (English: Representative VDEW Load Profiles)*. VDEW Materialien M-32/99. Available online: https://www.bdew.de/media/documents/1999_Repraesentative-VDEW-Lastprofile.pdf (accessed on August 11, 2025). Frankfurt am Main: Verband der Elektrizitätswirtschaft e. V. (VdEW, English: German Electricity Industry Association), 1999.

[334] Gabi Hummel. "Integration von Elektrofahrzeugen in ein Gebäudeenergiemanagementsystem (English: Integration of Electric Vehicles into a Building Energy Management System)". Bachelor thesis. Karlsruher Institut für Technologie (KIT, English: Karlsruhe Institute of Technology), 2016.

[335] Fuseco. *Learn more about Low Voltage Fuses*. Available online: https://www.fuseco.com.au/fuses/resources/articles/learn-more-about-low-voltage-fuses-bff56589-1d16-4864-9411-af59fe41b3fb (accessed on August 12, 2025). Website article.

[336] Mischa Ahrens and Hartmut Schmeck. "Organic Computing for Adaptive and Resilient Electricity Grid Management". In: *Go Where the Bugs Are: Essays Dedicated to Wolfgang Reif on the Occasion of His 65th Birthday*. Ed. by Gidon Ernst et al. Cham: Springer Nature Switzerland, 2025, pp. 242–261. ISBN: 978-3-031-92196-4. DOI: 10.1007/978-3-031-92196-4_12.

[337] Jan Müller, Mischa Ahrens, Ingo Mauser, and Hartmut Schmeck. "Achieving Optimized Decisions on Battery Operating Strategies in Smart Buildings". In: *Applications of Evolutionary Computation*. Ed. by Kevin Sim and Paul Kaufmann. Cham: Springer International Publishing, 2018, pp. 205–221. ISBN: 978-3-319-77538-8. DOI: 10.1007/978-3-319-77538-8_15.

[338] Mischa Ahrens and Hartmut Schmeck. "Generation of Time-of-Use Tariffs for Demand Side Management using Artificial Neural Networks". In: *Proceedings of the Ninth International Conference on Future Energy Systems*. e-Energy '18. Karlsruhe, Germany: Association for Computing Machinery, 2018, pp. 396–398. ISBN: 9781450357678. DOI: 10.1145/3208903.3212037.

[339] Kevin Förderer, Mischa Ahrens, Kaibin Bao, Ingo Mauser, and Hartmut Schmeck. "Towards the Modeling of Flexibility Using Artificial Neural Networks in Energy Management and Smart Grids: Note". In: *Proceedings of the Ninth International Conference on Future Energy Systems*. e-Energy '18. Karlsruhe, Germany: Association for Computing Machinery, 2018, pp. 85–90. ISBN: 9781450357678. DOI: 10.1145/3208903.3208915.

[340] Kevin Förderer, Mischa Ahrens, Kaibin Bao, Ingo Mauser, and Hartmut Schmeck. "Modeling flexibility using artificial neural networks". In: *Energy Informatics* 1.1, 21 (Oct. 2018). ISSN: 2520-8942. DOI: 10.1186/s42162-018-0024-4.

[341] Mischa Ahrens. "Towards Price Based Demand Side Management Using Machine Learning". In: *Abstracts from the 8th DACH+ Conference on Energy Informatics*. Energy Informatics 2 (Suppl 2), 31. Poster abstract P2. Sept. 2019. DOI: 10.1186/s42162-019-0098-7.

[342] Hendro Wicaksono et al. "Artificial-intelligence-enabled dynamic demand response system for maximizing the use of renewable electricity in production processes". In: *The International Journal of Advanced Manufacturing Technology* 138.1 (May 2025), pp. 247–271. ISSN: 1433-3015. DOI: 10.1007/s00170-024-13372-7.

A. Appendix

A.1. Own Publications

Table A.1 gives an overview of the scientific publications of the author of this thesis and describes their relation to this thesis. The given abstracts are quoted verbatim from the respective publications.

Table A.1: Overview of the publications by the author of this thesis. Some are directly related to this thesis, others are not directly related but touch the broader context of energy management and energy flexibility use. The given abstracts are quoted verbatim from the respective publications.

2018	Jan Müller, Mischa Ahrens, Ingo Mauser, and Hartmut Schmeck. "Achieving Optimized Decisions on Battery Operating Strategies in Smart Buildings". In: *Applications of Evolutionary Computation.* Edited by Kevin Sim and Paul Kaufmann. Cham: Springer International Publishing, 2018, pp. 205–221. ISBN: 978-3-319-77538-8. DOI: 10.1007/978-3-319-77538-8_15.	[337]

Abstract

Battery energy storage systems are a key to the utilization of renewable energies, allowing for short-term storage of electricity and balancing of energy generation and consumption. However, the optimal operation of these systems is still an area of research. This paper presents operating strategies and their optimization with respect to total operational energy costs in buildings that are equipped with automated building energy management systems. The presented approach uses an evolutionary algorithm to set the parameters of the battery system controller for a rolling horizon. The combination of scheduling and control is chosen to aim at robustness against deviations of local loads from predictions. Scenarios comprising different electricity tariffs and the optimization of three operating strategies are simulated and evaluated. The results show that the operating strategies and their optimization lead to significantly different results, reflecting their ability to cope with uncertainty of future consumption and generation.

Relation to this thesis

The simulation, control, and optimization functionality for battery energy storage systems introduced in the cited publication is one of the prerequisites for the grid-supportive active power flexibility use presented in this thesis.

Continued on next page

Table A.1: Overview of the publications by the author of this thesis. Some are directly related to this thesis, others are not directly related but touch the broader context of energy management and energy flexibility use. The given abstracts are quoted verbatim from the respective publications (continued).

2018	Mischa Ahrens and Hartmut Schmeck. "Generation of Time-of-Use Tariffs for Demand Side Management using Artificial Neural Networks". In: *Proceedings of the Ninth International Conference on Future Energy Systems*. e-Energy '18. Karlsruhe, Germany: Association for Computing Machinery, 2018, pp. 396–398. ISBN: 9781450357678. DOI: 10.1145/3208903.3212037.	[338]

Abstract

This poster proposes a new method to generate individual time-of-use electricity tariffs to exploit the flexibility of energy prosumers while preserving privacy and minimizing communication effort as well as computational cost. Since an employed tariff structure may be impossible to derive analytically from a particular behavior of a prosumer, artificial neural networks may be used to learn the underlying mechanisms implicitly based on simulated household data. Using the acquired knowledge, such a network could be able to generate suitable tariffs to achieve a desired behavior.

Relation to this thesis

The poster relates to this thesis in that the proposed process of flexibility extraction from smart buildings could be used for grid-supportive purposes as well. However, we ultimately developed a more direct and decentralized approach for the adaptive grid management system.

Continued on next page

Table A.1: Overview of the publications by the author of this thesis. Some are directly related to this thesis, others are not directly related but touch the broader context of energy management and energy flexibility use. The given abstracts are quoted verbatim from the respective publications (continued).

2018	Kevin Förderer, Mischa Ahrens, Kaibin Bao, Ingo Mauser, and Hartmut Schmeck. "Towards the Modeling of Flexibility Using Artificial Neural Networks in Energy Management and Smart Grids: Note". In: *Proceedings of the Ninth International Conference on Future Energy Systems*. e-Energy '18. Karlsruhe, Germany: Association for Computing Machinery, 2018, pp. 85–90. ISBN: 9781450357678. DOI: 10.1145/3208903.3208915.	[339]

Abstract

This paper presents a novel approach to the representation and communication of the energy flexibility of distributed energy resources. The approach uses artificial neural networks (ANNs) to represent the devices and act as surrogate models. The main benefit of this approach is its potential to represent arbitrary energy flexibilities and the resulting universal applicability in various usage patterns, some of which are presented in detail in this paper. Furthermore, the flexibility represented by an ANN can be conditioned on the state of the corresponding devices and their environment, such that only a small state update needs to be communicated to construct feasible load profiles by a third party. Therefore, in contrast to other approaches, such as support vector data description, new ANNs only need to be constructed once the device configuration changes.

Relation to this thesis

The paper presents a different approach to representing energy flexibility than the one ultimately used in this thesis.

Continued on next page

Table A.1: Overview of the publications by the author of this thesis. Some are directly related to this thesis, others are not directly related but touch the broader context of energy management and energy flexibility use. The given abstracts are quoted verbatim from the respective publications (continued).

2018	Kevin Förderer, Mischa Ahrens, Kaibin Bao, Ingo Mauser, and Hartmut Schmeck. "Modeling flexibility using artificial neural networks". In: *Energy Informatics* 1.1, 21 (Oct. 2018). ISSN: 2520-8942. DOI: 10.1186/s42162-018-0024-4.	[340]

Abstract

The flexibility of distributed energy resources (DERs) can be modeled in various ways. Each model that can be used for creating feasible load profiles of a DER represents a potential model for the flexibility of that particular DER. Based on previous work, this paper presents generalized patterns for exploiting such models. Subsequently, the idea of using artificial neural networks (ANNs) in such patterns is evaluated. We studied different types and topologies of ANNs for the presented realization patterns and multiple device configurations, achieving a remarkably precise representation of the given devices in most of the cases. Overall, there was no single best ANN topology. Instead, a suitable individual topology had to be found for every pattern and device configuration. In addition to the best performing ANNs for each pattern and configuration that is presented in this paper all data from our experiments is published online. The paper is concluded with an evaluation of a classification based pattern using data of a real combined heat and power plant in a smart building.

Relation to this thesis

The paper evaluates the approach to representing energy flexibility introduced in the previous publication, which still differs from the one ultimately used in this thesis.

Continued on next page

Table A.1: Overview of the publications by the author of this thesis. Some are directly related to this thesis, others are not directly related but touch the broader context of energy management and energy flexibility use. The given abstracts are quoted verbatim from the respective publications (continued).

2019 Mischa Ahrens. "Towards Price Based Demand Side Management Using Machine Learning". In: *Abstracts from the 8th DACH+ Conference on Energy Informatics*. Energy Informatics 2 (Suppl 2), 31. Poster abstract P2. Sept. 2019. DOI: 10.1186/s42162-019-0098-7. [341]

Abstract

In demand side management, variable electricity pricing is often used to shape the load of electricity consumers and producers. The task of finding the right price profile to realize a target load profile is a bilevel optimization problem that varies in complexity depending on the considered distributed energy resources. Solutions to this problem proposed in the literature usually rely on extensive simplifications and often consider only specific device types or load shaping methods. Simple pricing schemes often fail to induce specific target load profiles due to effects like load synchronization. This poster abstract extends a machine learning based electricity pricing scheme proposed in previous work. Its objective is to generate price profiles based on knowledge about the behavior of energy resources in response to different price profiles and in various situations. Principally, the presented pricing scheme can be used for any device configuration under the assumption that it offers exploitable flexibility and is governed by an automated energy management system aimed at minimizing energy costs.

Relation to this thesis

Since the approach and results presented in this poster represent a continuation of the preliminary work presented on the 2018 poster "Generation of Time-of-Use Tariffs for Demand Side Management using Artificial Neural Networks" listed above, they relate to this thesis in the same way.

Continued on next page

Table A.1: Overview of the publications by the author of this thesis. Some are directly related to this thesis, others are not directly related but touch the broader context of energy management and energy flexibility use. The given abstracts are quoted verbatim from the respective publications (continued).

2021 — Mischa Ahrens, Fabian Kern, and Hartmut Schmeck. "Strategies for an Adaptive Control System to Improve Power Grid Resilience with Smart Buildings". In: *Energies* 14.15 (2021). ISSN: 1996-1073. DOI: 10.3390/en14154472. [33]

Abstract

Low-voltage distribution grids face new challenges through the expansion of decentralized, renewable energy generation and the electrification of the heat and mobility sectors. We present a multi-agent system consisting of the energy management systems of smart buildings, a central grid controller, and the local controller of a transformer. It can coordinate the provision of ancillary services for the local grid in a centralized way, coordinated by the central controller, and in a decentralized way, where each building makes independent control decisions based on locally measurable data. The presented system and the different control strategies provide the foundation for a fully adaptive grid control system we plan to implement in the future, which does not only provide resilience against electricity outages but also against communication failures by appropriate switching of strategies. The decentralized strategy, meant to be used during communication failures, could also be used exclusively if communication infrastructure is generally unavailable. The strategies are evaluated in a simulated scenario designed to represent the most extreme load conditions that might occur in low-voltage grids in the future. In the tested scenario, they can substantially reduce voltage range deviations, transformer temperatures, and line congestions.

Relation to this thesis

This publication presents some of the preliminary work for this thesis in that it introduces the centralized and decentralized grid management strategies, early versions of the reactive-power-based voltage maintenance algorithms and active power flexibility use approach, as well as some preliminary evaluation results comparing the two strategies.

Continued on next page

Table A.1: Overview of the publications by the author of this thesis. Some are directly related to this thesis, others are not directly related but touch the broader context of energy management and energy flexibility use. The given abstracts are quoted verbatim from the respective publications (continued).

2022	Mischa Ahrens. "Increasing Power Grid Resilience with a Multi-Agent System of Smart Buildings". In: *Organic Computing - Doctoral Dissertation Colloquium 2021*. Edited by Sven Tomforde and Christian Krupitzer. kassel university press, 2022, pp. 15–31. DOI: 10.17170/kobra-202202215780.	[1]

Abstract

The flexibility of buildings with energy generation and storage capacities, intelligent appliances, and energy management systems can be utilized to prevent or reduce critical situations in electricity grids arising from the ongoing adaptation of decentralized energy generation and electric vehicles. This work outlines a multi-agent system that determines and coordinates the responses of multiple buildings to such situations to increase the resilience of the local grid. The utilized methods are designed to be resilient against communication failures as well. The energy management systems used to facilitate the proposed methods are based on the Observer/Controller-architecture. This enables them to work adaptively using centralized, cooperative, or autonomous control schemes depending on the availability of communication infrastructure.

Relation to this thesis

This book chapter lays out the planned functionality of the adaptive grid management system presented in this thesis, presents an approach to answer earlier versions of the corresponding research questions, and provides some evaluation results for earlier versions of the centralized and distributed strategies. Resilience against participant misconduct and sensor failure as well as adaptive PV curtailment are not considered yet.

Continued on next page

Table A.1: Overview of the publications by the author of this thesis. Some are directly related to this thesis, others are not directly related but touch the broader context of energy management and energy flexibility use. The given abstracts are quoted verbatim from the respective publications (continued).

2025	Hendro Wicaksono, Martin Trat, Atit Bashyal, Tina Boroukhian, Mine Felder, Mischa Ahrens, Janek Bender, Sebastian Groß, Daniel Steiner, Christoph July, Christoph Dorus, and Thorsten Zoerner. "Artificial-intelligence-enabled dynamic demand response system for maximizing the use of renewable electricity in production processes". In: *The International Journal of Advanced Manufacturing Technology* 138.1 (May 2025), pp. 247–271. ISSN: 1433-3015. DOI: 10.1007/s00170-024-13372-7.	[342]

Abstract

The transition towards renewable electricity provides opportunities for manufacturing companies to save electricity costs through participating in demand response programs. End-to-end implementation of demand response systems focusing on manufacturing power consumers is still challenging due to multiple stakeholders and subsystems that generate a heterogeneous and large amount of data. This work develops an approach utilizing artificial intelligence for a demand response system that optimizes industrial consumers' and prosumers' production-related electricity costs according to time-variable electricity tariffs. It also proposes a semantic middleware architecture that utilizes an ontology as the semantic integration model for handling heterogeneous data models between the system's modules. This paper reports on developing and evaluating multiple machine learning models for power generation forecasting and load prediction, and also mixed-integer linear programming as well as reinforcement learning for production optimization considering dynamic electricity pricing represented as Green Electricity Index (GEI). The experiments show that the hybrid auto-regressive long-short-term-memory model performs best for solar and convolutional neural networks for wind power generation forecasting. Random forest, k-nearest neighbors, ridge, and gradient-boosting regression models perform best in load prediction in the considered use cases. Furthermore, this research found that the reinforcement-learning-based approach can provide generic and scalable solutions for complex and dynamic production environments. Additionally, this paper presents the validation of the developed system in the German industrial environment, involving a utility company and two small to medium-sized manufacturing companies. It shows that the developed system benefits the manufacturing company that implements fine-grained process scheduling most due to its flexible rescheduling capacities.

Continued on next page

Table A.1: Overview of the publications by the author of this thesis. Some are directly related to this thesis, others are not directly related but touch the broader context of energy management and energy flexibility use. The given abstracts are quoted verbatim from the respective publications (continued).

Relation to this thesis
This publication is only loosely related to this thesis in that it tackles the use of energy flexibility for different purposes, albeit not in the context of residential buildings but rather industrial production facilities.

Continued on next page

Table A.1: Overview of the publications by the author of this thesis. Some are directly related to this thesis, others are not directly related but touch the broader context of energy management and energy flexibility use. The given abstracts are quoted verbatim from the respective publications (continued).

2025 Mischa Ahrens and Hartmut Schmeck. “Organic Computing for Adaptive and Resilient Electricity Grid Management”. In: *Go Where the Bugs Are: Essays Dedicated to Wolfgang Reif on the Occasion of His 65th Birthday*. Edited by Gidon Ernst et al. Cham: Springer Nature Switzerland, 2025, pp. 242–261. ISBN: 978-3-031-92196-4. DOI: 10.1007/978-3-031-92196-4_12. [34]

Abstract

The motivation behind the research initiative "Organic Computing” has been the need for system architectures supporting the self-organized response of decentralized technical application systems to changing requirements and disturbances in their operational environment, while respecting functional objectives as defined by their users. Such a property is strongly resembling the notion of system resilience. In this paper, we report some results on the achievement of resilience in energy systems by an adaptive system for regional management of electricity grids. This system mitigates physical disturbances of the grid in different ways, depending on the availability of information on the current status of the relevant entities, such as the distribution system operator, grid equipment, and (active) buildings. Our approach is based on an extension of the Organic Smart Home, a software framework for energy system management, simulation, and optimization, which has been strongly influenced by the observer/controller architecture, which emerged as a core generic architectural concept for organic computing systems. Depending on the current availability of communication infrastructure, the adaptive grid management switches between centralized, distributed, and completely decentralized derivation of control decisions in response to undesired deviations of voltages at grid connection points, high transformer temperatures, or high line currents. Based on power profiles from real-life studies and simulation models, our evaluation shows that even the completely decentralized strategy is still capable of guaranteeing the desired resilience.

Relation to this thesis

This publication provides a substantially updated overview of the adaptive grid management system presented in this thesis and first evaluation results for the management strategy adaptation in response to communication disruption.